

# Hydrogeology and water quality of wetlands in East Africa

case studies  
of a floodplain and a valley bottom wetland

---

## Dissertation

zur

Erlangung des Doktorgrades (Dr. rer. nat.)

der

Mathematisch-Naturwissenschaftlichen Fakultät

der

Rheinischen Friedrich-Wilhelms-Universität Bonn

vorgelegt von

**Sonja Burghof** (geb. Beuel)

aus

Euskirchen

Bonn, Mai 2017



Angefertigt mit Genehmigung der Mathematisch-Naturwissenschaftlichen Fakultät der  
Rheinischen Friedrich-Wilhelms-Universität Bonn

1. Gutachter: Prof. Dr. Barbara Reichert  
2. Gutachter: Prof. Dr. Romain Chesnaux  
Tag der Promotion: 22.08.2017  
Erscheinungsjahr: 2017



I declare that this thesis was composed by myself, that the work contained herein is my own except where explicitly stated otherwise in the text, and that this work has not been submitted for any other degree or professional qualification.

---



## Acknowledgements

This study was funded and supported by the German Federal Ministry of Education and Research (BMBF) as a part of the project “GlobE – Wetlands in East Africa” under grant No. 031A250 C.

First of all, I would like to thank my first supervisor Prof. Dr. Barbara Reichert for the opportunity to work in the GlobE project and for all her scientific and personal support. I convey my thanks to my second supervisor Prof. Dr. Romain Chesnaux for his interest in my work and his great support.

I warmly thank Dr. Sven-Oliver Franz and the laboratory team of the Steinmann Institute (University of Bonn) for their work and help and their technical as well as personal support, namely Bettina Schultevan Berkum, Camilla Kurth, and Beate Dahlhausen. Furthermore, I thank Dr. Christine Stumpp and the laboratory team of the Helmholtz Zentrum in Munich for the experienced support regarding stable water isotopes and their evaluation.

My additional thanks go to the Rufiji Basin Water Board (RBWB), the NGO Maji Safi Kwa Afya Bora Ifakara (MSABI), and the Ministry of Water and Environment, Uganda (MWE) for the provision of secondary data. Namely I would like to thank David Munkyaala (RBWB), Kate Hyland (MSABI), Elisa Urbinati (MSABI), Alphonsina Kanyeto (MSABI), Nancy Pule (MWE), and Francis Kisitu (MWE).

Furthermore, I thank all colleagues of the GlobE project. I thank Prof. Dr. Salome Misana, Dr. Michael Ugen, and Dr. Mathias Behangana for their help and support regarding my field visits. I also thank Dr. Constanze Leemhuis for her scientific input, her personal support, and her amazing administrative work. I thank Geoffrey Gabiri for the successful collaboration, the exchange of data, and all the discussions in the field and in the office. My special thanks go to all colleagues, who provided data and support for this thesis, namely Dr. Andrea Rechenburg, Kristian Näschen, Esther Amler, Susanne Ziegler, Kristina Grotelüschen, Kai Behn, Björn Glasner, Katrin Wagner, Claudia Schepp, Julius Kwesiga, Fridah Kirimi, Dr. Miguel Alvarez, Matian van Soest, Dr. Daniel Kyalo Willy, Bisrat Haile Gebrekidan, Dr. Michael Schmidt, Sophie-Bo Heinkel, Viviane Umulisa, Dr. Volker Ermert, Dr. Carlos Angulo, Prof. Dr. Gunter Menz, Prof. Dr. Bernd Diekkrüger, and Prof. Dr. Mathias Becker. Furthermore, I would like to thank the GlobE head office, especially Eike Kiene for his tireless administrative work.

The completion of this thesis would have not been possible without the great work of all field assistants, namely Robert Mutebi, Sissiria Akoth, Ivan Lyatumi, Abdul Tarik Kawere, Francis Kimaru, John Sama, Novatus Mwangeta, and Dittrick Mwingira. I also thank all drivers, guards, and housekeepers for all their hospitality and assistance. Asante sana! Webale nyo!

I express my thanks to our current and former working group members for discussions, proofreading, and help in the lab, especially to Laura Heiß, Isa Görlich, Layla Hashweh, Jana Schneider, Fabian Klein, Kim Hußmann, and Dr. Stephan Klose. Furthermore, I would like to thank all master students, who contributed to this work, namely Tina Geißler, Katharina Liedtke, Laura Heiß, Kim Hußmann, and Max Wieczorek.

My deep thanks go to my family and friends for their support, especially my husband for his pure honesty during proofreading and for discussing every single sentence of this thesis.

## Abstract

This thesis is embedded in the interdisciplinary BMBF-funded project “GlobE – Wetlands in East Africa”, which focuses on reconciling future food production in East African wetlands with the concurrent environmental protection of these valuable ecosystems. In this context, the aim of the work presented here was to characterize and evaluate the hydrogeological situation of those wetlands. To this end, two study sites were selected, which represent the major wetland types prevalent in East Africa, floodplains and valley bottom wetlands.

The Ifakara study site is located in the northeastern Kilombero Catchment in southcentral Tanzania, which comprises a huge floodplain wetland. The Namulonge study site is represented by a small valley bottom wetland that is part of a huge system of wetlands in southcentral Uganda. Both wetlands are agriculturally used, and an intensification of crop production is expected in future. As agricultural production and other ecosystem services in wetlands highly depend on water quantity and quality, the assessment of hydrological processes within wetlands is mandatory. Wetlands are open systems, which interact with other water components in their catchments. Groundwater has been recognized as one important component, interacting with wetlands on different temporal and spatial scales.

This thesis provides the first hydrogeological characterization of the two study sites, focusing on the analysis of hydrogeological and hydrochemical processes. Considering the lack of reliable data about both sites, in a comprehensive approach aquifer structure, water dynamics, and water composition were assessed thoroughly. A combination of geological, hydraulic, and tracer-based methods was applied, to provide an overview of all processes and to outline the systems’ interconnections. The results were summarized and visualized in hydrogeological conceptual models. Hydrochemical modeling was performed to quantify the processes and to enhance the conceptual models. These models help scientists and stakeholders as information and decision tools. They are furthermore necessary for other research activities within the GlobE project in terms of boundary conditions and general hydrogeological conclusions. The status quo of the water quality was evaluated for its suitability as drinking water, for domestic use, and irrigation. Additionally, current as well as future mutual effects between agricultural production and water quality were identified and discussed.

Both studied wetlands are located on alluvial sediments that are variable in terms of geological and hydraulic properties. The sediments are derived from a saprolite weathering profile of crystalline rocks. However, deposition environments, sedimentological features, and geomorphology are highly different between the two study sites. The Ifakara wetland is located on thick sediments south of an escarpment made up of crystalline rocks. The weathering profile above these rocks has been extensively eroded. At Namulonge, the sediments are thinner and cover the weathering profile of crystalline rocks only in valley bottoms. Here, the weathering profile is much thicker due to prolonged weathering with minor tectonic movement. Hydrochemistry at both study sites is mainly influenced by silicate weathering, which occurs within each lithological unit. Groundwater level measurements and tracer-based assessments revealed that both wetlands interact with groundwater, though these interactions are highly variable in space and time.

At Ifakara, groundwater flows from a fractured rock aquifer in the mountains north of the wetland through an unconfined sedimentary aquifer to the wetland in the south most of the year. Finally, it discharges into the wetland, made up of stream and flooding water. Wetland water does not contribute significantly to groundwater recharge. Main recharge occurs due to direct infiltration of precipitation in the mountains and in an alluvial fan north of the floodplain. Stream water is derived from precipitation



of the entire catchment and groundwater discharge. Flooding water near the main stream is in direct contact to the stream and originates from over-bank flow and little groundwater discharge. In contrast, flooding water at a greater distance to the stream comprises precipitation and slight groundwater discharge. Evaporation rates of flooding water increase with greater distance to the stream.

In the Namulonge area, regional groundwater flows through a weathering profile aquifer from the upper to the lower catchment as well as from the hilltops to the valley bottoms. This regional aquifer mainly receives direct recharge from heavy rainfall events on top of the hills and at the slopes. Local groundwater flow within a smaller confined porous aquifer of valley sediments follows the same flow pattern from the upper to the lower catchment and from the valley fringes to the valley bottoms. This local groundwater is recharged by infiltrating precipitation and surface runoff in the valley of the upper catchment. Moreover, it receives inflow from groundwater of the weathering profile aquifer by upwards discharge below the valley and subsurface runoff from the slopes. Groundwater discharges to the main stream of the wetland in the upper catchment. In the lower catchment, groundwater is separated from wetland water by an impermeable clay layer. Percolation of soil water to groundwater is hampered by the clay layer here, inducing confined conditions, which can be of an artesian character during rainy seasons. Flooding water mainly originates from over-bank flow and precipitation.

Inorganic chemical groundwater quality in terms of drinking water is comparatively good at both study sites. However, at Ifakara, a geogenic contamination with manganese was detected. Based on the spatial analysis of this contamination, it is highly recommended to inform local population about associated hazards and possible solution strategies. Currently, groundwater in the study sites is not significantly influenced by the input of agrochemicals. For example, only few groundwater samples showed elevated concentrations of nitrate and nitrite. In the Ifakara study site, such elevated concentrations either originate from waste water discharge of Ifakara City or from leaching of nitrogen from agriculturally used soils in the uplands surrounding the wetland. The latter one is also true for the Namulonge study site, indicating that upland agriculture is more hazardous to groundwater quality than wetland agriculture in both study sites. Regarding irrigation, many water components showed low electrical conductivities combined with high sodium concentrations, inducing a decrease in the infiltration capacity of the soil. In terms of big scale irrigation schemes, which are planned for Ifakara, the irrigation water needs to be chosen with precaution, considering water quality aspects, to ensure a sustainable crop production.

Based on the developed conceptual models and the evaluation of water quality, recommendations are given for stakeholders, in order to develop a first framework for a sustainable management of wetlands. Until now, only a small influence of agricultural production on water quality was found and water purification of both wetlands is considered as good. Nevertheless, the planned intensification of agricultural production in the wetlands will most probably include an increased amount of applied agrochemicals and maybe lower the groundwater table due to water consumption for irrigation. This might in the future lead to degradation of water quality within and in the vicinity of the wetlands.

This thesis emphasizes the need for more case studies about groundwater in East African wetlands, due to the high variability of hydrogeological and hydrochemical settings and processes. The applied methods can be transferred to other East African wetlands, as it was proven that a combination of quantity and quality related assessments yields reliable results in regions with very limited data.

## Kurzfassung

Die vorliegende Arbeit ist in das interdisziplinäre, BMBF-finanzierte Projekt „GlobE – Wetlands in East Africa“ eingebettet. Ziel des Projektes ist die zukünftig steigende Nahrungsmittelproduktion in ostafrikanischen Feuchtgebieten mit einem gleichzeitigen Schutz dieser wertvollen Ökosysteme in Einklang zu bringen. Diese Arbeit hatte in diesem Zusammenhang zum Ziel, die hydrogeologischen Bedingungen dieser Gebiete näher zu charakterisieren und zu bewerten.

Hierfür wurden zwei Feuchtgebiete als Haupttypen ostafrikanischer Feuchtgebiete, Überflutungsebenen und Talgrund-Feuchtgebiete, ausgewählt. Das Untersuchungsgebiet Ifakara liegt in Süd-Zentral-Tansania im nordöstlichen Kilombero Einzugsgebiet, das eine große Überflutungsebene umfasst. Das Untersuchungsgebiet Namulonge, ein kleines Talgrund-Feuchtgebiet, ist Teil eines großen Systems von Feuchtgebieten in Süd-Zentral-Uganda. Beide Untersuchungsgebiete werden landwirtschaftlich genutzt und eine Intensivierung des landwirtschaftlichen Anbaus wird in Zukunft erwartet. Da sowohl landwirtschaftliche Produktion als auch weitere Ökosystemdienstleistungen in Feuchtgebieten stark von Quantität und Qualität des verfügbaren Wassers abhängen, ist eine Untersuchung hydrologischer Prozesse zwingend notwendig. Feuchtgebiete sind offene Systeme, die mit anderen Wasserkomponenten in ihren Einzugsgebieten interagieren. Grundwasser wurde hierbei als eine wichtige Komponente erkannt, die auf unterschiedlichen räumlichen und zeitlichen Skalen mit Feuchtgebieten in Wechselwirkung steht.

Vor diesem Hintergrund liefert die vorliegende Arbeit die erste hydrogeologische Charakterisierung der beiden Untersuchungsgebiete mit einem Fokus auf der Analyse von hydrogeologischen und hydrochemischen Prozessen. Aufgrund der sehr geringen Datengrundlage beider Untersuchungsgebiete, wurde ein umfassender Ansatz gewählt, der Untersuchungen von Aquiferaufbau, Wasserdynamik und Wasserzusammensetzung beinhaltet. Eine Kombination von geologischen, hydraulischen und tracerbasierten Methoden wurde angewandt, um einen fundierten Überblick aller Prozesse zu geben und die Verbindungen dieser Prozesse im System Feuchtgebiet zu umreißen. Die gewonnenen Ergebnisse wurden in hydrogeologischen konzeptionellen Modellen zusammengefasst und visualisiert. Mithilfe hydrochemischer Modellierung konnten die Prozesse quantifiziert und die konzeptionellen Modelle verbessert und erweitert werden. Diese Modelle dienen Wissenschaftlern und Interessenvertretern als Informations- und Entscheidungshilfe und sind für weitere Forschungsaktivitäten innerhalb des GlobE Projektes von Bedeutung. So liefern sie zum Beispiel Randbedingungen und geben einen Einblick in die Hydrogeologie der Gebiete. Der aktuelle Zustand der Wasserqualität wurde in Bezug auf Trink-, Haushalts- und Bewässerungswasser bewertet. Des Weiteren wurden aktuelle sowie zukünftige wechselseitige Beeinflussungen zwischen Landwirtschaft und Wasserqualität identifiziert und diskutiert.

Beide untersuchten Feuchtgebiete liegen auf alluvialen Sedimenten mit variablen geologischen und hydraulischen Eigenschaften. Die Sedimente entstammen einem Verwitterungsprofil, das im oberen Bereich von kristallinem Gestein entstanden ist. Ablagerungsmilieu, sedimentologische Eigenschaften und Geomorphologie sind jedoch in beiden Untersuchungsgebieten grundverschieden. Das Untersuchungsgebiet Ifakara befindet sich auf mächtigen Sedimenten südlich einer Abbruchkante aus kristallinem Gestein. Das Verwitterungsprofil dieser Gesteine ist größtenteils erodiert. Im Untersuchungsgebiet Namulonge sind die Sedimente geringmächtiger und überlagern das Verwitterungsprofil, das aufgrund von langanhaltender Verwitterung und geringer tektonischer Aktivität wesentlich mächtiger ist als in Ifakara, lediglich in den Tälern. Die Hydrochemie in beiden Untersuchungsgebieten ist maßgeblich von Silikatverwitterung geprägt, die in allen lithologischen Einheiten auftritt. Grundwasserstandsmessungen und tracerbasierte Untersuchungen zeigten, dass beide Feuchtgebiete mit Grundwasser interagieren, obwohl diese Interaktion sowohl räumlich als auch zeitlich variabel ist.

Im Untersuchungsgebiet Ifakara fließt das Grundwasser ganzjährig von einem geklüfteten Festgesteinsaquifer in den Bergen nördlich des Feuchtgebietes durch einen freien Porenaquifer in das Feuchtgebiet im Süden, wo es letztendlich in das Feuchtgebietwasser, dargestellt durch Fluss- und Überflutungswasser, exfiltriert. Feuchtgebietwasser trägt nicht signifikant zur Grundwasserneubildung bei. Ein Großteil der Grundwasserneubildung findet in Form von direkt infiltrierendem Niederschlag in den Bergen und in einem alluvialen Fächer nördlich der Überflutungsebene statt. Flusswasser setzt sich aus Niederschlag des gesamten Einzugsgebietes und Grundwasserabfluss zusammen. Überflutungswasser in der Nähe des Hauptvorfluters befindet sich in direktem Kontakt zu diesem Vorfluter und besteht aus über die Ufer getretenem Flusswasser und zu geringen Teilen aus Grundwasser. Im Gegensatz dazu, beinhaltet Überflutungswasser in größerer Entfernung zum Vorfluter hauptsächlich Niederschlag und wenig Grundwasser. Evaporationsraten des Überflutungswassers steigen mit zunehmender Entfernung zum Vorfluter an.

Im Untersuchungsgebiet Namulonge strömt Grundwasser im Verwitterungsprofil auf regionaler Ebene vom oberen zum unteren Einzugsgebiet und von den Hügelkuppen zu den Tälern. Grundwasser in diesem regionalen Aquifer wird durch direkte Grundwasserneubildung, die hauptsächlich während starker Niederschläge auf den Hügelkuppen und Hängen stattfindet, gespeist. Lokaler Grundwasserfluss in einem kleineren gespannten Porenaquifer, der aus Talsedimenten besteht, folgt dem gleichen Fließmuster vom oberen zum unteren Einzugsgebiet und von den Talrändern zur Talmitte. Grundwasserneubildung in diesem Aquifer findet durch infiltrierenden Niederschlag und Oberflächenabfluss im Tal des oberen Einzugsgebietes statt. Des Weiteren erfährt der Aquifer einen Zufluss aus dem Grundwasser des Verwitterungsprofils durch einen aufwärts gerichteten hydraulischen Gradienten im Bereich der Täler und durch unterirdischen Abfluss entlang der Hänge. Im oberen Einzugsgebiet exfiltriert Grundwasser in den Hauptvorfluter des Feuchtgebietes. Im Gegensatz dazu, ist das Grundwasser des unteren Einzugsgebietes durch eine undurchlässige Tonschicht hydraulisch vom Feuchtgebietwasser getrennt. Diese Tonschicht verhindert die Perkolation von Bodenwasser ins Grundwasser und erzeugt gespannte Bedingungen, die während der Regenzeiten artesisch sein können. Überflutungswasser besteht hauptsächlich aus über die Ufer getretenem Flusswasser und Niederschlag.

Die anorganische chemische Grundwasserqualität beider Untersuchungsgebiete in Bezug auf Trinkwasser ist vergleichsweise gut. Nichtsdestotrotz wurde in Ifakara eine geogene Verunreinigung durch Mangan nachgewiesen. Basierend auf der räumlichen Analyse dieser Kontamination wird dringend empfohlen, die lokale Bevölkerung über die damit einhergehenden Risiken und möglichen Lösungsansätze zu informieren. Grundsätzlich ist das Grundwasser in den Untersuchungsgebieten derzeit nicht wesentlich von Düngemittelsatz beeinflusst. Nur wenige Grundwasserproben zeigten zum Beispiel erhöhte Konzentrationen von Nitrat und Nitrit. Diese Erhöhung ist in Ifakara auf den Zufluss von ungereinigten Abwässern der Stadt und auf die Auswaschung von Stickstoff aus landwirtschaftlich genutzten Böden in den Trockengebieten, die das Feuchtgebiet umgeben, zurückzuführen. Da Letzteres auch in Namulonge als Hauptquelle von Nitrat und Nitrit angesehen werden kann, wird deutlich, dass Landwirtschaft in den umgebenden Trockengebieten ein größeres Gefährdungspotential der Grundwasserqualität darstellt als Landwirtschaft in den Feuchtgebieten. Bezüglich des Einsatzes von Bewässerungswasser weisen viele Wasserkomponenten geringe elektrische Leitfähigkeiten zusammen mit hohen Natriumkonzentrationen auf, was zu einer Verringerung der Infiltrationskapazität des Bodens führen kann. Daher sollte bei der Planung großskaliger Bewässerungssysteme, wie sie in Ifakara geplant sind, die Wahl des Bewässerungswassers unter Berücksichtigung von Wasserqualitätsaspekten mit Bedacht erfolgen, um eine nachhaltige Bestellung der Böden zu gewährleisten.

Auf Grundlage der entwickelten konzeptionellen Modelle und der Bewertung der Wasserqualität, wurden Empfehlungen für Interessenvertreter ausgesprochen, um ein erstes Rahmenkonzept hinsichtlich der nachhaltigen Bewirtschaftung von Feuchtgebieten zu entwickeln. Bis heute ist nur ein geringfügiger Einfluss der landwirtschaftlichen Produktion auf die Wasserqualität erkennbar und die Gewässerreinigungsfunktionen beider Feuchtgebiete sind intakt. Dahingegen wird die geplante Intensivierung der landwirtschaftlichen Nutzung wahrscheinlich auch einen erhöhten Eintrag von Düngemitteln und möglicherweise eine Absenkung des Grundwasserspiegels aufgrund der Entnahme von Bewässerungswasser mit sich bringen. Diese Umstände könnten in Zukunft zu einer Degradierung der Wasserqualität in den Feuchtgebieten und ihrer Umgebung führen.

Die Ergebnisse dieser Arbeit zeigten deutlich, dass aufgrund der starken Variabilität von hydrogeologischen und hydrochemischen Gegebenheiten mehr Fallstudien zur Grundwasserforschung in ostafrikanischen Feuchtgebieten notwendig sind. Die angewandten Methoden lassen sich auf andere ostafrikanische Feuchtgebiete übertragen, da gezeigt wurde, dass die verwendete Kombination aus Untersuchungen von quantitativen und qualitativen Aspekten des Grundwassers in Gebieten mit geringer Datengrundlage zuverlässige Ergebnisse liefert.

## Table of Contents

<b>Acknowledgements</b> .....	<b>I</b>
<b>Abstract</b> .....	<b>II</b>
<b>Kurzfassung</b> .....	<b>IV</b>
<b>Table of Contents</b> .....	<b>VII</b>
<b>List of Figures</b> .....	<b>XI</b>
<b>List of Tables</b> .....	<b>XVII</b>
<b>List of Appendices</b> .....	<b>XIX</b>
<b>List of Abbreviations</b> .....	<b>XX</b>
<b>List of Units</b> .....	<b>XXI</b>
<b>1 Introduction</b> .....	<b>1</b>
1.1 Project “GlobE – Wetlands in East Africa”.....	2
1.2 Aim and research approach.....	3
<b>2 Study sites</b> .....	<b>6</b>
2.1 Climate of East Africa.....	7
2.2 Geology of East Africa.....	7
2.2.1 Geodynamic evolution.....	7
2.2.2 Deep weathering of crystalline rocks.....	9
2.3 The Ifakara study site.....	10
2.3.1 Climate (IF).....	12
2.3.2 Geology (IF).....	12
2.3.3 Soils (IF).....	15
2.3.4 Hydrogeology and hydrology (IF).....	16
2.3.5 Vegetation, land cover, and land use (IF).....	17
2.4 The Namulonge study site.....	18
2.4.1 Climate (NA).....	20
2.4.2 Geology (NA).....	20
2.4.3 Soils (NA).....	22
2.4.4 Hydrogeology and hydrology (NA).....	23
2.4.5 Vegetation, land cover, and land use (NA).....	24
<b>3 Current state of research</b> .....	<b>26</b>
3.1 Hydrogeology and wetlands.....	26
3.1.1 Floodplains.....	27
3.1.2 Valley bottom wetlands.....	28
3.2 Water quality and wetlands.....	31
3.2.1 Nitrogen.....	32

3.2.2	Phosphorous .....	32
3.2.3	Sulfur .....	32
3.2.4	Iron, manganese, and other heavy metals .....	33
3.3	Hydrogeology of weathering profiles above crystalline rocks.....	33
3.3.1	Silicate weathering.....	34
<b>4</b>	<b>Methods.....</b>	<b>37</b>
4.1	Analysis of aquifer structure and properties .....	38
4.1.1	Drilling surveys, rock and sediment sampling, and installation of piezometers.....	39
4.1.2	Determination of hydraulic conductivities .....	39
4.1.3	Mineralogical and geochemical analyses .....	41
4.2	Analysis of water dynamics.....	42
4.2.1	Groundwater level measurements.....	42
4.2.2	Data processing.....	42
4.2.3	Creation of piezometric maps.....	43
4.3	Analyses of water composition.....	43
4.3.1	Water sampling.....	43
4.3.2	Water analyses.....	45
4.3.3	Plausibility tests and data processing.....	46
4.3.4	Hydrochemical evaluation methods.....	47
4.3.5	Stable water isotopes evaluation methods .....	49
4.3.6	Water quality assessment.....	50
4.4	Inverse geochemical modeling .....	52
<b>5</b>	<b>Data base .....</b>	<b>53</b>
5.1	Data base of the Ifakara study site .....	53
5.1.1	Data of aquifer structure and properties (IF) .....	53
5.1.2	Groundwater level data (IF).....	57
5.1.3	Hydrochemical and isotopic data (IF) .....	57
5.1.4	Precipitation data (IF) .....	59
5.2	Data base of the Namulonge study site.....	59
5.2.1	Data of aquifer structure and properties (NA) .....	59
5.2.2	Groundwater level data (NA).....	63
5.2.3	Hydrochemical and isotopic data (NA) .....	64
5.2.4	Precipitation data (NA) .....	67
<b>6</b>	<b>Case study of the Ifakara study site .....</b>	<b>68</b>
6.1	Aquifer structure and properties (IF).....	68
6.1.1	Crystalline rocks (Aqf1 <sub>IF</sub> ) .....	69

6.1.2	Non-alluvial sediments (Aqp2 <sub>IF</sub> ).....	70
6.1.3	Alluvial sediments (Aqp1 <sub>IF</sub> ) .....	70
6.1.4	Spatial distribution of aquifers and hydraulic connections (IF).....	77
6.2	Water dynamics (IF).....	78
6.2.1	Groundwater flow direction (IF).....	79
6.2.2	Groundwater table fluctuations (IF).....	79
6.3	Water composition (IF).....	82
6.3.1	Hydrochemistry (IF) .....	82
6.3.2	Stable water isotopes (IF).....	96
6.3.3	Water quality (IF).....	98
6.4	Conceptual model (IF).....	102
6.4.1	Groundwater flow paths (IF) .....	103
6.4.2	Hydrochemical evolution (IF).....	104
6.4.3	Groundwater-surface water interaction and recharge processes (IF) .....	105
6.4.4	Current mutual effects between agricultural production and water quality (IF).....	108
6.5	Hydrochemical modeling of origin and evolution of flooding water (IF) .....	108
<b>7</b>	<b>Case study of the Namulonge study site .....</b>	<b>112</b>
7.1	Aquifer structure and properties (NA).....	112
7.1.1	Crystalline rocks (Atf1 <sub>NA</sub> ) .....	113
7.1.2	Weathering profile of crystalline rocks (Aqp2 <sub>NA</sub> ).....	113
7.1.3	Valley sediments (Aqp1 <sub>NA</sub> , Aqt1 <sub>NA</sub> ) .....	116
7.1.4	Spatial distribution of aquifers and hydraulic connections (NA).....	121
7.2	Water dynamics (NA).....	123
7.2.1	Groundwater flow in the regional aquifer (NA) .....	124
7.2.2	Groundwater flow in the valley sediment aquifer (NA) .....	124
7.3	Water composition (NA).....	127
7.3.1	Hydrochemistry (NA) .....	127
7.3.2	Stable water isotopes (NA) .....	144
7.3.3	Water quality (NA).....	147
7.4	Conceptual model (NA).....	152
7.4.1	Groundwater flow paths (NA) .....	153
7.4.2	Hydrochemical evolution (NA) .....	153
7.4.3	Groundwater-surface water interaction and recharge processes (NA) .....	155
7.4.4	Current mutual effects between agricultural production and water quality (NA).....	157
7.5	Hydrochemical modeling of origin and evolution of flooding water (NA) .....	158

<b>8</b>	<b>Conclusions and recommendations .....</b>	<b>160</b>
8.1	Characterization of hydrogeological setting and processes .....	160
8.2	Evaluation of status quo of water quality .....	163
8.3	Identification of current and future mutual effects between agricultural production and water quality .....	165
8.4	Integration of the two study sites into a regional context .....	167
<b>9</b>	<b>References .....</b>	<b>168</b>
	<b>Appendix .....</b>	



## List of Figures

Fig. 1.1:	Research clusters of the project “GlobE – Wetlands in East Africa” and their interrelationships (wetlands-africa.de). .....	2
Fig. 2.1:	Topographic map of East Africa showing the locations of the two study sites Ifakara (Tanzania) and Namulonge (Uganda). Data sources: earthexplorer.usgs.gov (elevation), Lehner and Döll (2004) (lakes), gadm.org (country borders). .....	6
Fig. 2.2:	Typical weathering profile above crystalline rocks in tropical Africa (modified after Chilton and Foster 1995). .....	9
Fig. 2.3:	Topographic map of the Kilombero Valley and its surroundings showing the location of the Ifakara study site. Data sources: earthexplorer.usgs.gov (elevation), Lehner and Döll (2004) (lakes), gadm.org (country borders), openlayers.org (streams) (IF). .....	11
Fig. 2.4:	Shading map of the Ifakara study site. Data sources: earthexplorer.usgs.gov (elevation), Geological Survey of Tanganyika (1962) (streams), google.com/earth (Ifakara city), Beuel et al. (2016) (wetland), personal communication with E. Amler (2016) (floodplain) (IF). .....	11
Fig. 2.5:	Climate diagram showing annual temperature (red), precipitation (blue), and rainy and dry seasons in the Ifakara study site (modified after climate-data.org) (IF). .....	12
Fig. 2.6:	Geological map of the Ifakara study site. Data sources: Geological Survey of Tanganyika (1962) (geology, streams), Jätzold and Baum (1968) (alluvial fan) (IF). .....	15
Fig. 2.7:	Soil map of the Ifakara study site. Data sources: esdac.jrc.ec.europa.eu (soil), Geological Survey of Tanganyika (1962) (streams) (IF). .....	16
Fig. 2.8:	Topographic map of the area around Kampala showing the location of the Namulonge study site. Data sources: earthexplorer.usgs.gov (elevation), Lehner and Döll (2004) (lakes), gadm.org (country borders), hydrosheds.cr.usgs.gov (streams) (NA). .....	19
Fig. 2.9:	Shading map of the Namulonge study site. Data sources: earthexplorer.usgs.gov (elevation), GTK Consortium (2012) (streams), Beuel et al. (2016) (wetland), Gabiri (unpublished) (Nasiry Stream) (NA). .....	19
Fig. 2.10:	Climate diagram showing annual temperature (red), precipitation (blue), and rainy and dry seasons in the Namulonge study site (modified after climate-data.org) (NA). .....	20
Fig. 2.11:	Geological map of the Namulonge study site. Data sources: GTK Consortium (2012) (geology, streams), Heiß (2016) (alluvium), Gabiri (unpublished) (Nasiry Stream) (NA). .....	22
Fig. 2.12:	Soil map of the Nasiry Catchment within the Namulonge study site. Data sources: Gabiri (unpublished) (soil, Nasiry Stream), GTK Consortium (2012) (streams) (NA). .....	23
Fig. 3.1:	Relations between groundwater and wetlands (Seelig and DeKeyser 2006). .....	26
Fig. 3.2:	Groundwater-surface water interactions in floodplains, showing channel cross sections with a) gaining stream, b) and c) losing stream, and d) groundwater through-flow (modified after Woessner 2000). .....	28
Fig. 3.3:	Schematic cross section of a valley bottom wetland that developed on granite in West Africa (Rodenburg 2013). .....	29
Fig. 3.4:	Schematic cross sections of a valley bottom wetland referring to two different formation models, a) pediplanation model (stripping) and b) etchplanation model (deep weathering) (modified after McFarlane 1992). .....	30
Fig. 3.5:	Hydrogeological properties of weathering profiles above crystalline rocks in tropical Africa (modified after Chilton and Foster 1995). .....	34
Fig. 3.6:	Weatherability (susceptibility to chemical weathering) of silicate minerals (modified after Goldich 1938). .....	35
Fig. 4.1:	Color scheme for hydrostratigraphic units according to their type of porosity and hydraulic conductivities (modified after Struckmeier and Margat 1995). .....	39
Fig. 4.2:	Schematic overview of a falling-head permeability test and important parameters. ....	40
Fig. 4.3:	Installation of pressure data loggers in a pumping well in the Ifakara study site (pictures: G. Gabiri). .....	43

Fig. 4.4: Impressions of sampling points, showing a deep pumping well and a shallow draw well in the Ifakara study site, and a deep pumping well in the Namulonge study site (pictures: A. Rechenburg, L. Hei).	44
Fig. 4.5: Scheme of the used precipitation collector (upgmbh.com) and picture of the installed precipitation collector in the Namulonge study site.	44
Fig. 5.1: Map section of the south central study site showing locations of piezometers and central field trials. Data sources: Geological Survey of Tanganyika (1962) (geology, streams), Jtzold and Baum (1968) (alluvial fan), personal communication with E. Amler (2016) (floodplain) (IF).	55
Fig. 5.2: Locations of deep drilling log descriptions, crystalline rock outcrops, and pumping test data. Data sources: Geological Survey of Tanganyika (1962) (geology, streams), Jtzold and Baum (1968) (alluvial fan), personal communication with E. Amler (2016) (floodplain) (IF).	56
Fig. 5.3: Locations of sampling points related to groundwater level data. Data sources: Geological Survey of Tanganyika (1962) (geology, streams), Jtzold and Baum (1968) (alluvial fan), personal communication with E. Amler (2016) (floodplain) (IF).	57
Fig. 5.4: Locations of sampling points related to hydrochemical and isotopic data. Data sources: Geological Survey of Tanganyika (1962) (geology, streams), Jtzold and Baum (1968) (alluvial fan), personal communication with E. Amler (2016) (floodplain) (IF).	58
Fig. 5.5: Map section of the south eastern study site showing the three transects A, C, and D including locations of piezometers and central field trials. Data sources: GTK Consortium (2012) (geology, streams), Hei (2016) (alluvium), Gabiri (unpublished) (Nasirye Stream) (NA).	61
Fig. 5.6: Locations of sampling points related to data of aquifer structure and properties, including a schematic overview of the three transects. Data sources: GTK Consortium (2012) (geology, streams), Hei (2016) (alluvium), Gabiri (unpublished) (Nasirye Stream) (NA).	62
Fig. 5.7: Locations of sampling points related to groundwater level data. Data sources: GTK Consortium (2012) (geology, streams), Hei (2016) (alluvium), Gabiri (unpublished) (Nasirye Stream) (NA).	64
Fig. 5.8: Locations of sampling points related to hydrochemical and isotopic data. Data sources: GTK Consortium (2012) (geology, streams), Hei (2016) (alluvium), Gabiri (unpublished) (Nasirye Stream) (NA).	65
Fig. 6.1: Lithological and hydrostratigraphic standard section of the study site showing hydrogeological properties of the different units. Hydraulic conductivities were assigned based on <sup>a</sup> Geological Survey of Tanganyika (1962), <sup>b</sup> own data, and <sup>c</sup> data provided by Rufiji Basin Water Board (RBWB) (IF).	68
Fig. 6.2: Mineralogical compositions of a) gneisses (OC2 <sub>IF</sub> , OC1 <sub>IF</sub> ), b) leucosome (left) and melanosome (right) of migmatite (OC4 <sub>IF</sub> ), and c) pegmatite (OC6 <sub>IF</sub> ) (IF).	69
Fig. 6.3: Drilling logs of the two piezometers in the central field trial <i>center</i> (left: PZ02 <sub>IF</sub> , right: PZ04 <sub>IF</sub> ). Hydraulic conductivities were derived from falling-head permeability tests (hydraulic conductivity <sub>1</sub> ) and grain size distribution analyses (hydraulic conductivity <sub>2</sub> ) (IF).	72
Fig. 6.4: Drilling logs of the two piezometers in the central field trial <i>middle</i> (left: PZ06 <sub>IF</sub> , right: PZ07 <sub>IF</sub> ). Hydraulic conductivities were derived from falling-head permeability tests (hydraulic conductivity <sub>1</sub> ) and grain size distribution analyses (hydraulic conductivity <sub>2</sub> ) (IF).	73
Fig. 6.5: Drilling logs of the two piezometers in the central field trial <i>fringe</i> (left: PZ09 <sub>IF</sub> , right: PZ10 <sub>IF</sub> ). Hydraulic conductivities were derived from falling-head permeability tests (hydraulic conductivity <sub>1</sub> ) and grain size distribution analyses (hydraulic conductivity <sub>2</sub> ) (IF).	74
Fig. 6.6: Distribution of the crystalline rock and alluvial sediment samples in a ternary diagram of the trace elements lanthanum (La), scandium (Sc), and thorium (Th) (IF).	75
Fig. 6.7: Boxplots of hydraulic conductivities of the alluvial sediments determined on three different scales (IF).	76
Fig. 6.8: Hydrogeological map of the study site. Units are labeled and colored according to Figure 6.1. Data sources: Geological Survey of Tanganyika (1962) (geology, streams) (IF).	77
Fig. 6.9: Schematic hydrogeological cross section, crossing the study site from north to south. Units are labeled and colored according to Figure 6.1 (IF).	77

Fig. 6.10: Spatial distribution of the groups of piezometers and wells based on correlation analyses of hydrographs within the southern study site. Data sources: Geological Survey of Tanganyika (1962) (geology, streams), Jätzold and Baum (1968) (alluvial fan) (IF). .....	80
Fig. 6.11: Comparison of daily precipitation (above) and hydrographs of the representative piezometers and wells that were selected based on correlation analyses (below) (IF). .....	81
Fig. 6.12: Boxplots of measured <i>in-situ</i> parameters (electrical conductivity (EC), pH, O <sub>2</sub> -content (O <sub>2</sub> <sup>con</sup> ), redox potential (Eh)) of deep and shallow groundwater, stream water, and flooding water (IF). .....	83
Fig. 6.13: Schoeller diagram of the main stream water samples (Kilombero and Lumemo rivers) and flooding water samples (center and fringe) for 2014 and 2015 (IF). .....	84
Fig. 6.14: Piper diagrams of a) deep groundwater samples and b) shallow groundwater samples (IF). .....	85
Fig. 6.15: Histograms showing the distribution of differences in electrical conductivities (ECs) for shallow and deep groundwater between rainy and dry seasons (IF). .....	85
Fig. 6.16: Spatial distribution of electrical conductivities of groundwater samples in dry season 2015. Data sources: Geological Survey of Tanganyika (1962) (geology, streams), Jätzold and Baum (1968) (alluvial fan) (IF). .....	86
Fig. 6.17: Spatial distribution of differences in electrical conductivity of groundwater samples between rainy and dry season 2015. Data sources: Geological Survey of Tanganyika (1962) (geology, streams), Jätzold and Baum (1968) (alluvial fan) (IF). .....	87
Fig. 6.18: Dendrogram of the Hierarchical Cluster Analysis, performed for 165 water samples using the variables logEC, pH, logNa <sup>+</sup> , logK <sup>+</sup> , logMg <sup>2+</sup> , logCa <sup>2+</sup> , logCl <sup>-</sup> , logSO <sub>4</sub> <sup>2-</sup> , logHCO <sub>3</sub> <sup>-</sup> , logFe <sup>2+</sup> , logMn <sup>2+</sup> , and SiO <sub>2</sub> showing the different cluster groups of water samples and their characteristic names (IF). .....	89
Fig. 6.19: Barcharts of mean hydrochemical compositions of the four groups identified by Hierarchical Cluster Analysis (IF). .....	90
Fig. 6.20: Spatial distribution of the four cluster groups. Data sources: Geological Survey of Tanganyika (1962) (geology, streams), Jätzold and Baum (1968) (alluvial fan), google.com/earth (Ifakara city) (IF). .....	90
Fig. 6.21: Scatterplot of the two principal components (PC1 <sub>IF</sub> and PC2 <sub>IF</sub> ) showing the distribution of water samples. Samples of wells PW30 <sub>IF</sub> and DW36 <sub>IF</sub> , which are located in the non-alluvial sediments, are encircled (IF). .....	92
Fig. 6.22: Selected ratios of different hydrochemical parameters for the four cluster groups. Specific ion ratios are illustrated as lines (IF). .....	94
Fig. 6.23: Distribution of saturation indices of primary silicate minerals (feldspars), secondary clay minerals, and secondary iron-(hydr)oxides for the four cluster groups (IF). .....	95
Fig. 6.24: Stability diagrams of anorthite, albite, k-feldspar (microcline), and their respective weathering products for the four cluster groups (following Tardy 1971) (IF). .....	96
Fig. 6.25: Scatterplot of δ <sup>2</sup> H against δ <sup>18</sup> O for deep and shallow groundwater, stream water (Kilombero and Lumemo rivers), flooding water, and precipitation samples (IF). .....	97
Fig. 6.26: Monthly weighted averages of δ <sup>18</sup> O in precipitation (red points) and monthly amount of precipitation (blue bars) as a) time series (June 2014 to November 2015), and b) correlation graph. The regression line in b) was calculated excluding the three outliers ( <i>black points</i> ) (IF). .....	97
Fig. 6.27: Histograms showing the distribution of differences in δ <sup>18</sup> O for shallow and deep groundwater, and stream water of Kilombero and Lumemo rivers between rainy and dry seasons (IF). .....	98
Fig. 6.28: Stacked bar charts of the percentage amount of all samples exceeding the guideline values (WHO 2011) of nitrate (NO <sub>3</sub> <sup>-</sup> ), nitrite (NO <sub>2</sub> <sup>-</sup> ), and manganese (Mn <sup>2+</sup> ) for the four snapshot samplings, and of fluoride (F) for rainy season 2014 (IF). .....	99
Fig. 6.29: Groundwater quality related to human health displayed as Degree of Health related Water Quality (DHWQ). Drinking water quality decreases from 0 (no guideline value exceeded) to 3 (guideline values of three constituents exceeded). Data sources: Geological Survey of Tanganyika (1962) (geology, streams), Jätzold and Baum (1968) (alluvial fan), google.com/earth (Ifakara city) (IF). .....	100
Fig. 6.30: Stacked bar charts of the percentage amount of all samples exceeding the acceptability thresholds (WHO 2011) of manganese (Mn <sup>2+</sup> ) and iron (Fe <sup>2+</sup> ) for the four snapshot samplings (IF). .....	101

Fig. 6.31: Stacked bar charts of the percentage amount of all samples showing Degrees of Restriction on Use (Ayers and Westcot 1985) related to salinity and infiltration for the four snapshot samplings (IF).....	102
Fig. 6.32: Conceptual hydrogeological wetland model of the Ifakara study site for dry and rainy seasons. Hydrostratigraphic units are colored according to Figure 6.1 (p.68). Water fluxes and compositions are displayed in blue, while hydrochemical processes are displayed in brown. Red texts refer to anthropogenic influences (IF).....	103
Fig. 6.33: Schematic composition and evolution of flooding water at <i>center</i> and <i>fringe</i> based on hydrochemical modeling (IF).....	111
Fig. 7.1: Lithological and hydrostratigraphic standard section of the study site showing hydrogeological properties of the different units. Hydraulic conductivities were assigned based on <sup>a)</sup> personal communication with B. Glasner (2016), <sup>b)</sup> own data, <sup>c)</sup> McFarlane (1992), Taylor and Howard (1996), and <sup>d)</sup> Howard et al. (1992) (NA).....	112
Fig. 7.2: Drilling log of saprolite weathering profile (SA1 <sub>NA</sub> ). Typical weathering profile was assigned based on Chilton and Foster (1995) (NA).....	115
Fig. 7.3: Drilling logs of the piezometer in the central field trial <i>fringe</i> (PZ40 <sub>NA</sub> ) and the drilling log next to it (SD15 <sub>NA</sub> ). Screened parts refer to short and long piezometers (PZ40S <sub>NA</sub> , PZ40L <sub>NA</sub> ). Hydraulic conductivities were derived from falling-head permeability tests (hydraulic conductivity <sub>1</sub> ) and grain size distribution analyses (hydraulic conductivity <sub>2</sub> ) (NA).....	117
Fig. 7.4: Drilling logs of the piezometer in the central field trial <i>middle</i> (PZ42 <sub>NA</sub> ) and the drilling log next to it (SD14 <sub>NA</sub> ). Screened parts refer to short and long piezometers (PZ42S <sub>NA</sub> , PZ42L <sub>NA</sub> ). Hydraulic conductivities were derived from falling-head permeability tests (hydraulic conductivity <sub>1</sub> ) and grain size distribution analyses (hydraulic conductivity <sub>2</sub> ) (NA).....	118
Fig. 7.5: Drilling logs of the piezometer in the central field trial <i>center</i> (PZ46 <sub>NA</sub> ) and the drilling log next to it (SD13 <sub>NA</sub> ). Screened parts refer to short and long piezometers (PZ46S <sub>NA</sub> , PZ46L <sub>NA</sub> ). Hydraulic conductivities were derived from falling-head permeability tests (hydraulic conductivity <sub>1</sub> ) and grain size distribution analyses (hydraulic conductivity <sub>2</sub> ) (NA).....	119
Fig. 7.6: Characteristic grey clay layer (left) and grey sand layer with interbedded orange zones (right) (NA).....	119
Fig. 7.7: Ternary diagram of the trace elements lanthanum (La), scandium (Sc), and thorium (Th) showing crystalline rock (Westerhof et al. 2014) and valley sediment samples (NA).....	120
Fig. 7.8: Hydrogeological map of the study site. Units are labeled and colored according to Figure 7.1. Data sources: GTK Consortium (2012) (geology, streams), Heiß (2016) (alluvium), Gabiri (unpublished) (Nasirye Stream) (NA).....	122
Fig. 7.9: Scatterplots of a) elevation against depth to fresh crystalline rock and b) elevation against top of fresh crystalline rock.....	122
Fig. 7.10: Schematic hydrogeological cross section, crossing the study site from southwest to northeast. Units are labeled and colored according to Figure 7.1 (NA).....	123
Fig. 7.11: Piezometric map of groundwater in the weathering profile aquifer and crystalline rock aquitard (Aqp2 <sub>NA</sub> and Aqf1 <sub>NA</sub> ), showing isolines of hydraulic heads and point data of static groundwater levels. Data sources: earthexplorer.usgs.gov (elevation), GTK Consortium (2012) (streams), Gabiri (unpublished) (Nasirye Stream) (NA).....	124
Fig. 7.12: Hydrographs of the piezometers at the three transects. Daily precipitation and the two representative points of time for dry (03/01/15) and rainy seasons (12/01/15) are shown above (NA).....	125
Fig. 7.13: Hydraulic heads of long piezometers at transect C during dry (01.03.15) and rainy (01.12.15) seasons and stream water level during rainy season (01.12.15).....	127
Fig. 7.14: Hydraulic heads of piezometers at transect C in the central field trials <i>center</i> , <i>middle</i> , and <i>fringe</i> (NA).....	127
Fig. 7.15: Boxplots of measured <i>in-situ</i> parameters (electrical conductivity (EC), pH, O <sub>2</sub> -content (O <sub>2</sub> <sup>con</sup> ), redox potential (Eh)) of deep and shallow groundwater, soil water, stream water, and flooding water (NA).....	128

Fig. 7.16: Schoeller diagram of flooding water and stream water of Nasirye stream (both sampled at transect C in autumn 2014) (NA). .....	129
Fig. 7.17: Time series of electrical conductivity (EC), sodium ( $\text{Na}^+$ ) concentrations (indicator of silicate weathering), and cumulative chloride, sulfate, and nitrate ( $\text{Cl}^-$ , $\text{SO}_4^{2-}$ , $\text{NO}_3^-$ ) concentrations (indicators of anthropogenic influence) of stream water, sampled at the inflow ( $\text{ST1}_{\text{NA}}$ ) and outflow ( $\text{ST7}_{\text{NA}}$ ) of lower Nasirye Catchment. Daily precipitation is shown, and rainy and dry seasons are marked (NA). .....	130
Fig. 7.18: Piper diagrams of a) deep groundwater samples and b) shallow groundwater samples (NA). .....	131
Fig. 7.19: Distribution of a) electrical conductivity (EC) and b) sodium ( $\text{Na}^+$ ) concentrations for different $\text{HCO}_3^-$ water types of deep groundwater (NA). .....	131
Fig. 7.20: Spatial distribution of electrical conductivities and water types of deep groundwater (spring 2015). Data sources: GTK Consortium (2012) (geology, streams), Heiß (2016) (alluvium), Gabiri (unpublished) (Nasirye Stream) (NA). .....	132
Fig. 7.21: Time series of electrical conductivity (EC), sodium ( $\text{Na}^+$ ) concentrations (indicator of silicate weathering), and cumulative chloride, sulfate, and nitrate ( $\text{Cl}^-$ , $\text{SO}_4^{2-}$ , $\text{NO}_3^-$ ) concentrations (indicators of anthropogenic influence) of deep groundwater at $\text{PW07}_{\text{NA}}$ and $\text{PW36}_{\text{NA}}$ . Daily precipitation is shown, and rainy and dry seasons are marked (NA). .....	133
Fig. 7.22: Distribution of electrical conductivity (EC) in shallow groundwater of the valley sediments for the three different transects (NA). .....	134
Fig. 7.23: Time series of electrical conductivity (EC) for shallow groundwater from piezometers and the spring at transect C. Daily precipitation is shown and rainy and dry seasons are marked (NA). .....	134
Fig. 7.24: Schoeller diagram of the three fully analyzed soil water samples (NA). .....	135
Fig. 7.25: Dendrogram of the Hierarchical Cluster Analysis, performed for 104 water samples using the variables $\log\text{EC}$ , $\text{pH}$ , $\log\text{Na}^+$ , $\log\text{K}^+$ , $\log\text{Mg}^{2+}$ , $\log\text{Ca}^{2+}$ , $\log\text{Cl}^-$ , $\log\text{SO}_4^{2-}$ , $\log\text{HCO}_3^-$ , $\log\text{Fe}^{2+}$ , $\log\text{Mn}^{2+}$ , and $\text{SiO}_2$ showing the different sub-cluster groups of water samples and their characteristic names (NA). .....	137
Fig. 7.26: Barcharts of mean hydrochemical compositions of the six sub-cluster groups identified by Hierarchical Cluster Analysis (NA). .....	138
Fig. 7.27: Scatterplot of the two principal components ( $\text{PC1}_{\text{NA}}$ and $\text{PC2}_{\text{NA}}$ ) showing the distribution of water samples (NA). .....	140
Fig. 7.28: Selected ratios of different hydrochemical parameters for the six sub-cluster groups. Specific ion ratios are illustrated as lines (NA). .....	141
Fig. 7.29: Selected ratios of different hydrochemical parameters for the six sub-cluster groups. Redox potential needed for transformation processes are illustrated as lines (NA). .....	142
Fig. 7.30: Distribution of saturation indices of primary silicate minerals (feldspars), secondary clay minerals, and secondary iron (hydr)oxides for the six sub-cluster groups (NA). .....	143
Fig. 7.31: Stability diagrams of anorthite, albite, k-feldspar (microcline), and their respective weathering products for the six sub-cluster groups (following Tardy 1971) (NA). .....	144
Fig. 7.32: Scatterplot of $\delta^2\text{H}$ against $\delta^{18}\text{O}$ for a) precipitation samples and b) deep and shallow groundwater, soil water, stream water, and flooding water (NA). .....	145
Fig. 7.33: Monthly weighted averages of $\delta^{18}\text{O}$ in precipitation (red points) and monthly amount of precipitation (blue bars) as a) time series (June 2014 to June 2016), and b) correlation graph (NA). ....	145
Fig. 7.34: Time series of $\delta^{18}\text{O}$ for monthly weighted averages of precipitation, monthly samples of shallow (piezometers, spring) and deep groundwater, and monthly samples of stream water. Daily precipitation is shown and rainy and dry seasons are marked above. Periods with very little precipitation are shaded in grey (NA). .....	146
Fig. 7.35: Time series of the D-Excess for monthly samples of stream water. Periods with very little precipitation are shaded in grey (NA). .....	147
Fig. 7.36: Stacked bar charts of the percentage amount of all samples exceeding the guideline values (WHO 2011) of nitrate ( $\text{NO}_3^-$ ), nitrite ( $\text{NO}_2^-$ ), and manganese ( $\text{Mn}^{2+}$ ) for the four snapshot samplings, and of fluoride (F) for spring 2016 (IF). .....	148

---

Fig. 7.37: Time series of nitrate ( $\text{NO}_3^-$ ) concentrations for spring water ( $\text{SP1}_{\text{NA}}$ ) and deep groundwater ( $\text{PW07}_{\text{NA}}$ , $\text{PW36}_{\text{NA}}$ ). Daily precipitation is shown and rainy and dry seasons are marked (NA).....	149
Fig. 7.38: Groundwater quality related to human health displayed as Degree of Health related Water Quality (DHWQ). Drinking water quality decreases from 0 (no guideline value exceeded) to 3 (guideline values of three constituents exceeded). Data sources: GTK Consortium (2012) (geology, streams), Hei (2016) (alluvium), Gabiri (unpublished) (Nasirye Stream) (NA). .....	149
Fig. 7.39: Stacked bar charts of the percentage amount of all samples showing Degrees of Restriction on Use (Ayers and Westcot 1985) related to salinity and infiltration for the four snapshot samplings (NA).....	150
Fig. 7.40: Concentrations of four indicator ions of fertilizer application, potassium ( $\text{K}^+$ ), phosphate ( $\text{PO}_4^{3-}$ ), chloride ( $\text{Cl}^-$ ), and sulfate ( $\text{SO}_4^{2-}$ ) in soil water samples extracted from the four different treatment plots (NA).....	151
Fig. 7.41: Conceptual hydrogeological model of the Namulonge study site on a) catchment scale and b) wetland scale. Hydrostratigraphic units are colored according to Figure 7.1 (p.112). Water fluxes and compositions are displayed in blue, while hydrochemical processes are displayed in brown. Red texts refer to anthropogenic influences (NA). .....	152
Fig. 7.42: Schematic composition and evolution of flooding water at <i>center</i> based on hydrochemical modeling (NA).....	159

## List of Tables

Tab. 3.1: Oxidized and reduced forms of several elements and approximate redox potentials for transformation (Mitsch and Gosselink 2007).....	32
Tab. 4.1: Classification of hydraulic conductivity following Hannappel et al. (2003) (Klose 2012). .....	38
Tab. 4.2: Analytes determined during hydrochemical analyses, respective analysis and conservation methods, limit of detection (LOD), and limit of quantification (LOQ). If LOD or LOQ varied between different sampling periods, ranges are displayed. ....	46
Tab. 4.3: Health-related guideline values and acceptability thresholds for selected inorganic constituents in drinking water (WHO 2011). ....	50
Tab. 4.4: Guidelines for the interpretation of water quality for irrigation based on the Degree of Restriction on Use (DRU) in terms of salinity and infiltration (Ayers and Westcot 1985). ....	51
Tab. 4.5: Different treatment plots, where soil water was sampled, in order to assess the influence of different agricultural management options on water quality. ....	52
Tab. 5.1: Data used in the case study of the Ifakara study site (IF). ....	54
Tab. 5.2: Detailed descriptions of all used data of aquifer structure and properties (IF). ....	55
Tab. 5.3: Depths and locations of sediment samples and respective available data (IF). ....	56
Tab. 5.4: Number of water samples analyzed for hydrochemistry and stable water isotopes during the four snapshot samplings. For the analysis of hydrochemistry, only samples with ion charge balance errors below 10 % are listed (IF). ....	59
Tab. 5.5: Number of precipitation samples out of 33 samples in total and respective data availability of different analytes (IF). ....	59
Tab. 5.6: Data used in the case study of the Namulonge study site (NA). ....	60
Tab. 5.7: Detailed descriptions of all used data of aquifer structure and properties (NA). ....	61
Tab. 5.8: Depths and locations of saprolite and sediment samples and respective available data (NA). ....	63
Tab. 5.9: Number of water samples analyzed for hydrochemistry and stable water isotopes during the four snapshot samplings. For the analysis of hydrochemistry, only samples with ion charge balance errors below 10 % are listed (NA). ....	66
Tab. 5.10: Sampling points that were monthly sampled and analyzed for selected ions and stable water isotopes (NA). ....	66
Tab. 5.11: Number of precipitation samples out of 83 samples in total and respective data availability of different analytes (NA). ....	67
Tab. 6.1: Pearson’s correlation coefficients of hydrographs of different piezometers and wells. Coefficients equal or higher than 0.95 are marked as bold. Sampling points are sorted and signed to groups based on correlation analyses. Representative hydrographs are marked as bold (IF). ....	80
Tab. 6.2: Measured <i>in-situ</i> parameters of flooding water at <i>center</i> and <i>fringe</i> during rainy seasons 2014 and 2015 (IF). ....	84
Tab. 6.3: Minimum, maximum, and median concentrations of different analytes measured in weekly precipitation samples. Median values for East Africa were adopted from Rodhe et al. (1981) (In Johnson 1996) (IF). ....	87
Tab. 6.4: Loadings of variables on the first two principal components (PC1 <sub>IF</sub> , PC2 <sub>IF</sub> ) and the respective explained variance. High factor loadings are marked in grey (IF). ....	88
Tab. 6.5: Means and standard deviations (in brackets) of each variable for all four cluster groups. The amount of samples per group (n) is displayed below the group name (IF). ....	89
Tab. 6.6: P-values of multiple comparison tests, following Kruskal-Wallis-tests, for different pairs of cluster groups. Those p-values that indicated a rejection of the null-hypothesis that both cluster groups come from one distribution with respect to a certain variable are marked in grey (level of significance = 1 %) (IF). ....	92
Tab. 6.7: Results of inverse modeling of the origin and hydrochemical evolution of flooding water at <i>center</i> for rainy season 2014 (IF). ....	109

---

Tab. 6.8: Results of inverse modeling of the origin and hydrochemical evolution of flooding water at <i>fringe</i> for rainy season 2014 (IF). .....	111
Tab. 7.1: Assignment of drilling log descriptions to lithological units of the typical weathering profile of Chilton and Foster (1995) and thicknesses of the respective units. ....	114
Tab. 7.2: Mean values of electrical conductivity (EC), pH value, sodium ( $\text{Na}^+$ ), and nitrate ( $\text{NO}_3^-$ ) concentrations of monthly shallow groundwater samples from spring ( $\text{SP1}_{\text{NA}}$ ) and piezometers at transect C (November 2014 – June 2016). For the second spring ( $\text{SP2}_{\text{NA}}$ ) values of the snapshot sampling in autumn 2015 are displayed (LOD = limit of detection) (NA). ....	135
Tab. 7.3: Minimum, maximum, and median concentrations of different analytes measured in weekly precipitation samples. Median values for East Africa were adopted from Rodhe et al. (1981) (In Johnson 1996) (NA). ....	136
Tab. 7.4: Loadings of variables on the first two principal components ( $\text{PC1}_{\text{NA}}$ , $\text{PC2}_{\text{NA}}$ ) and the respective explained variance. High factor loadings are marked in grey (NA). ....	137
Tab. 7.5: Means and standard deviations (in brackets) of each variable for all six sub-cluster groups. Nitrate ( $\text{NO}_3^-$ ) was added for consistency. The amount of samples per group (n) is displayed below the group name (NA). ....	139
Tab. 7.6: P-values of multiple comparison tests, following Kruskal-Wallis-tests, for different pairs of sub-cluster groups. Those p-values that indicated a rejection of the null-hypothesis that both sub-cluster groups come from one distribution with respect to a certain variable are marked in grey (level of significance = 1 %) (NA). ....	139
Tab. 7.7: Results of inverse modeling of the origin and hydrochemical evolution of flooding water at <i>center</i> for autumn 2014 (NA). ....	159



## List of Appendices

### Appendix A – Data of aquifer structure and properties

#### A<sub>IF</sub> – Ifakara study site

- A<sub>IF</sub>1 – Deep drilling log descriptions
- A<sub>IF</sub>2 – Shallow drilling log descriptions of piezometers
- A<sub>IF</sub>3 – Hydraulic conductivities of sediments derived from grain size analysis
- A<sub>IF</sub>4 – Hydraulic conductivities of sediments derived from falling-head permeability tests
- A<sub>IF</sub>5 – Hydraulic conductivities of sediments derived from pumping tests
- A<sub>IF</sub>6 – Geochemical compositions (major oxides) of rock and sediments samples

#### A<sub>NA</sub> – Namulonge study site

- A<sub>NA</sub>1 – Deep drilling log descriptions
- A<sub>NA</sub>2 – Shallow drilling log descriptions of piezometers and additional drilling logs
- A<sub>NA</sub>3 – Hydraulic conductivities of sediments derived from grain size analysis
- A<sub>NA</sub>4 – Hydraulic conductivities of sediments derived from falling-head permeability tests
- A<sub>NA</sub>5 – Geochemical compositions (major oxides) of saprolite and sediment samples

### Appendix B – Groundwater level data

#### B<sub>IF</sub> – Ifakara study site

- B<sub>IF</sub>1 – Hydrographs of groundwater levels

#### B<sub>NA</sub> – Namulonge study site

- B<sub>NA</sub>1 – Pearson's correlation coefficients of hydrographs of different piezometers

### Appendix C – Hydrochemical and isotopic data

#### C<sub>IF</sub> – Ifakara study site

- C<sub>IF</sub>1 – *In-situ* parameters and HCO<sub>3</sub><sup>-</sup> and CO<sub>2</sub> concentrations of the four snapshot samplings
- C<sub>IF</sub>2 – Hydrochemical data of the four snapshot samplings
- C<sub>IF</sub>3 – PO<sub>4</sub><sup>3-</sup> and trace heavy metal concentrations of the first snapshot sampling
- C<sub>IF</sub>4 – Stable water isotope data of the four snapshot samplings
- C<sub>IF</sub>5 – Stable water isotope and hydrochemical data of weekly sampled precipitation

#### C<sub>NA</sub> – Namulonge study site

- C<sub>NA</sub>1 – *In-situ* parameters and HCO<sub>3</sub><sup>-</sup> and CO<sub>2</sub> concentrations of the four snapshot samplings
- C<sub>NA</sub>2 – Hydrochemical data of the four snapshot samplings
- C<sub>NA</sub>3 – PO<sub>4</sub><sup>3-</sup> and trace heavy metal concentrations of the fourth snapshot sampling
- C<sub>NA</sub>4 – Stable water isotope data of the four snapshot samplings
- C<sub>NA</sub>5 – Stable water isotope and hydrochemical data of weekly sampled precipitation
- C<sub>NA</sub>6 – *In-situ* parameters and hydrochemical data of monthly samplings
- C<sub>NA</sub>7 – Stable water isotope data of monthly samplings
- C<sub>NA</sub>8 – *In-situ* parameters and hydrochemical data of soil water from suction cups
- C<sub>NA</sub>9 – Stable water isotope data of soil water from suction cups

### Appendix D – Sampling point locations

#### D<sub>IF</sub> – Ifakara study site

- D<sub>IF</sub>1 – Geographic coordinates (WGS84) of all sampling points in the Ifakara study site

#### D<sub>NA</sub> – Namulonge study site

- D<sub>NA</sub>1 – Geographic coordinates (WGS84) of all sampling points in the Namulonge study site

## List of Abbreviations

AAS	Atomic Absorption Spectrometry
CFT	Central field trial
DEM	Digital Elevation Model
DHWQ	Degree of Health related Water Quality
DRU	Degree of Restriction on Use
EARS	East African Rift System
EC	Electrical Conductivity
GMWL	Global Meteoric Water Line
GNSS	Global Navigation Satellite System
HCA	Hierarchical Cluster Analysis
IC	Ion Chromatography
IF	Ifakara study site
ITCZ	Inter-Tropical Convergence Zone
LMWL	Local Meteoric Water Line
LOD	Limit of Detection
LOI	Loss on Ignition
LOQ	Limit of Quantification
MSABI	Maji Safi Kwa Afya Bora Ifakara
MWE	Ministry of Water and Environment, Uganda
NA	Namulonge study site
NACRRI	National Crop Resources Research Institute
PC	Principal Component
PCA	Principal Component Analysis
RBWB	Rufiji Basin Water Board
SAGCOT	Southern Agricultural Growth Corridor of Tanzania
SAR	Sodium Adsorption Ratio
SI	Saturation Index
UAV	Unmanned Aerial Vehicle
VSMOW	Vienna Standard Mean Ocean Water
WTT	West Tanzanian Terrain
XRD	X-Ray Diffraction Analysis
XRF	X-Ray Fluorescence Analysis

## List of Units

cm	centimeter
°C	degree Celsius
d	day
g	gram
kg	kilogram
km	kilometer
L	litre
m	meter
mg	milligram
mL	millilitre
mm	millimeter
mmol	millimol
mmol(eq)	millimol equivalent
mol	mol
mV	millivolt
m.a.s.l.	meter above sea level
m.a.s.	meter above surface
m.b.s.	meter below surface
μS	microsiemens
ppm	parts per million
s	second



## 1 Introduction

Although the worldwide progress in the fight against hunger continues, today still 795 million people are suffering from undernourishment (FAO et al. 2015). Worldwide, the percentage amount of undernourished people in East Africa is higher, with a percentage of 31.5 %, than on a global scale (10.9 %) (FAO et al. 2015). The increase in food demand will continue for at least another 40 years, due to population and consumption growth (Godfray et al. 2010). Furthermore, access to clean drinking water in Sub-Saharan Africa is limited for a huge part of the population (Wright 1992). This limitation could be met by groundwater, providing a reliable water source, due to its perennial nature and often good water quality (Pavelic et al. 2012). In developing countries, a huge proportion of the peri-urban population is already depending on groundwater for drinking water purposes (Cronin et al. 2006).

In recent times, wetlands worldwide have been recognized as “new” areas of agricultural production, outlining their potential as a solution to food security challenges (Frenken and Mharapara 2002, Turya-habwe et al. 2013). Wetlands enable smallholder farmers to produce crops all year-round, due to their nutrient rich soils and high moisture availability throughout the whole year (Sakané et al. 2011). At global scale, wetlands cover about 9.2 million km<sup>2</sup>, with 1.3 million km<sup>2</sup> being located in Africa (Lehner and Döll 2004). In the East African countries Uganda, Rwanda, Tanzania, and Kenya, wetlands cover an estimated area of about 0.15 million km<sup>2</sup> (Amler et al. 2015). Global change processes involving land use change, climate change, and globalization effects are leading to an overuse and degradation of upland soils and hence to a shift from upland to wetland agriculture (Dixon and Wood 2003). At the same time, wetlands provide a wide range of ecosystem services, such as the regulation of floods, the removal of pollutants, the supply of drinking water, and the provision of habitats for wildlife (Dixon and Wood 2003, Cui et al. 2012, Johnston et al. 2013). The major challenge of agricultural production in wetlands is to balance the benefits of food production and the protection of the wetlands’ other ecosystem functions (McCartney et al. 2010). On a long term, agricultural production in wetlands often alters its ecological character, for example by increasing the input of pollutants (McCartney et al. 2010). For instance, crop cultivation and drainage in wetlands of Ethiopia has led to extreme spatial and temporal variations in groundwater levels below the wetlands (Dixon 2002). Thus, a sustainable increase in food production from wetlands needs to be reconciled with environmental protection.

The primary force creating and altering wetland ecosystems is hydrology. Consequently, agricultural production and other ecosystem services highly depend on quantity and quality of water within the wetlands. Most wetlands interact with other water components and are thus strongly related to hydrological processes in their catchments (Acreman and Miller 2007). Therefore, they cannot be seen as isolated systems. One of the components interacting with wetlands is groundwater (von der Heyden 2004). Spatial and temporal variable groundwater inflows and outflows in wetland systems and their effects on the ecosystem have been recognized by many authors worldwide (e.g. McCarthy 2006, Hunt et al. 2006). Moreover, a lot of studies showed that hydrological assessments of wetlands will only be valid, if groundwater and its interactions with surface water are addressed as well (e.g. Devito et al. 1996, von der Heyden 2004). Investigating groundwater-surface water interactions within wetlands is also known to be important, for a better understanding of the effects of wetland hydrology on water quality (Kazezyilmaz-Alhan et al. 2007).

In order to identify and quantify interactions between groundwater and surface water, a sound understanding of the groundwater system in terms of flow paths and hydrochemical processes is required. However, hydrogeological conditions and processes of wetland systems are complex (Woessner 2000, Lazareva and Pichler 2011) and can be highly diverse for specific wetlands (Hollands 1987). Bullock

(1992b) outlined the need for (hydro)geological background data to support conclusions about wetland hydrology. Hence, site specific hydrogeological conceptual models of wetlands are required as tools for stakeholders and non-hydrogeologists, helping them to integrate groundwater related aspects into agricultural management decisions.

### 1.1 Project “GlobE – Wetlands in East Africa”

The comprehensive topic of reconciling future food production and environmental protection in wetlands is addressed by the BMBF-funded project “GlobE – Wetlands in East Africa”, providing the framework for this study (wetlands-africa.de). In the context of this project, an interdisciplinary team assesses the impacts of agricultural production on wetland ecosystems in four different wetland study sites within East Africa. Two study sites, namely Ifakara (Tanzania) and Namulonge (Uganda), were declared as super test sites. These super test sites represent the two main wetland types of East Africa in terms of national priority, floodplains, and inland valley wetlands (Leemhuis et al. 2016). It is hypothesized that the biophysical differences of the selected floodplain and inland valley wetlands cover the diversity of many floodplains and inland valleys in East Africa (wetlands-africa.de).

The two super test sites are studied by all scientific disciplines integrated in GlobE. Research activities are divided into five clusters (Fig. 1.1). These clusters all interact and build on one another. The study at hand is embedded in clusters A and B, focusing on status quo and processes within the wetlands as well as on agricultural management options.

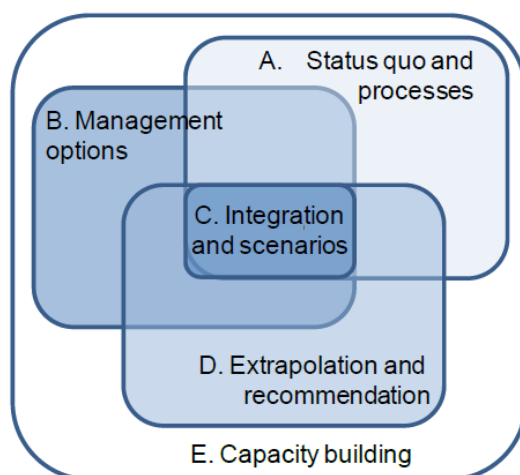


Fig. 1.1: Research clusters of the project “GlobE – Wetlands in East Africa” and their interrelationships (wetlands-africa.de).

The overall aim of the GlobE project is to assess how wetlands can be agriculturally used to improve food security, on one side, without destroying their ecological functionality, on the other side. Science-based guidelines, tools, and policy devices will be provided, to facilitate the process of increasing food production in agricultural used wetlands. In order to assess the threats of agricultural production on wetlands, a sound understanding of the physical environment of the wetland is essential (Cools et al. 2013). In this context, the main aim of this study is to provide the first characterization of the two super test sites, in terms of hydrogeology and water quality. Therefore, conceptual hydrogeological models of the study sites need to be developed, describing and visualizing groundwater related processes in the wetlands and their surroundings. This background knowledge is crucial for a range of further research activities. For instance, physically based hydrological models, simulating hydrological processes and the water balance at various scales and dimensions, are calibrated and validated to assess climate change, land use, and agricultural management scenarios (Gabiri unpublished, Näschen unpublished). In a first

step, such numerical models require conceptual models of the study sites in terms of water flow and mixing processes. These are needed to define boundary conditions regarding recharge and interactions between different water components. The same is true for transport models, seeking to determine the fluxes of nutrients to the wetland (Schepp unpublished). Furthermore, information about groundwater levels and fluctuations are used in dynamic crop growth models to estimate potential yields and quantify yield limiting factors under varying hydrogeological conditions within the wetland (Grotelüschen unpublished). Overall, the project is described by a strong interdisciplinary research concept at various scales.

In the two super test sites, agricultural experiments were set up, in order to assess different agricultural management options for the cultivation of rice and maize (Ziegler unpublished, Kwesiga unpublished, Alibu unpublished). These experimental set ups allow the direct measurements of influences of management options on biophysical indicators.

The floodplain wetland, namely Ifakara study site, is located in southcentral Tanzania within the Kilombero Catchment. On the one hand, the Kilombero Valley is part of the Southern Agricultural Growth Corridor, being a region in Tanzania that was declared by the government to produce cash crops and enhance food as well as livelihood security, by increasing the area of agriculturally used land (Paul and Steinbrecher 2013). Here, especially upland irrigation is planned. However, also huge parts of the wetland itself are already used for agricultural production, namely rice cultivation. On the other hand, the Kilombero Valley Wetland was designated as a Ramsar-Site, which designs an area of high ecological sensitivity (Kangalawe and Liwenga 2005), comprising a rare and unique ecosystem and providing a major source of drinking water (McCartney et al. 2010). Ministry of Water URT (2012a) already stated that more focused groundwater studies should be undertaken in the region to assess agricultural management options, such as large scale irrigation.

The inland valley wetland located in southcentral Uganda north of Kampala, namely Namulonge study site, is part of a huge system comprising small wetlands in an undulating topography. Those wetlands are located along a gradient from urban to rural areas. During the last decades, these wetlands have become increasingly important for agricultural production, but also for settlements, industrial waste dumping, and brick making (NEMA 2004). The studied wetland is located in rural areas, with parts of it being located in an agricultural research station (Nsubuga et al. 2011). It is mainly used for agriculture by smallholder farmers and scientists. Although it is known that wetlands in Uganda are valuable ecosystems and several management plans seek to protect them, they become more and more degraded and scientific biophysical and socio-economic monitoring systems are lacking (NEMA 2008).

In terms of terminology, floodplains are inland valleys as well, and no clear definitions are given regarding the term inland valley wetland. Thus, in this study, this term will be replaced by the term channeled valley bottom wetland, following the hydrogeomorphic wetlands classification scheme provided by Kotze et al. (2012). Both wetland types, floodplains and channeled valley bottoms, are represented by valley bottom areas with a well-defined stream channel. Floodplains are generally gently sloped and show several characteristic floodplain features, such as oxbow depressions and natural levees (Kotze et al. 2012). In contrast, channeled valley bottoms can be gently or steeper sloped and show no floodplain features (Kotze et al. 2012).

## **1.2 Aim and research approach**

Although the hydrogeology and water quality of wetlands have been studied by many authors worldwide, comparatively few hydrogeological studies exist for East African wetlands (Owor et al. 2011). In

the two selected study sites, almost no hydrogeological studies have been conducted so far. Additionally, the study sites are data scarce in terms of geology, hydrogeology, and water quality, as common for East African wetlands. Consequently, this study aims at the collection of a sound hydrogeological data set as well as on the interpretation of these data, in order to achieve the three research aims

1. Characterization of hydrogeological setting and processes,
2. Evaluation of status quo of water quality, and
3. Identification of current and future mutual effects between agricultural production and water quality.

The achievement of the third research aim strongly relies on results gained for the first two research aims. The hydrogeological characterizations of the study sites focus on the analyses of hydrogeological and hydrochemical processes and their interrelationships in the system (first research aim). The combination of these processes and relations in the system results in the development of hydrogeological conceptual models. These models are intended to describe and visualize

- Groundwater flow paths,
- Hydrochemical evolution of groundwater and surface water,
- Groundwater-surface water interactions, and
- Recharge processes.

In order to assess these processes, with respect to spatial and temporal variations, a comprehensive methodological approach has to be conducted. This approach includes the review of literature data, the collection of data during field campaigns and laboratory analyses, and the interpretation of those data. Thereby, the study follows a classical hydrogeological investigation approach (Kovalevsky et al. 2004), addressing the three different aspects of the groundwater system

- Aquifer structure,
- Water dynamics, and
- Water composition.

Flooding water is one of the major water components in wetlands and highly important as a water source for agricultural production. Hence, its origin and evolution are verified and quantified using hydrochemical modeling, based on the conceptual models. This modeling is assumed to outline the amount of groundwater and other water components contributing to flooding water as well as the hydrochemical evolution of flooding water. The conceptual models as well as the quantified origin of flooding water provide the first hydrogeological characterization of the two wetlands. Thus, they are important for scientists from other disciplines and stakeholders as information tools, and build the base for any further hydrogeological investigations.

The status quo of inorganic, chemical water quality of the different water components is evaluated in terms of drinking water, domestic use, and irrigation purposes (second research aim). In terms of drinking water quality, the focus is given to groundwater, providing the major source of drinking water in both study sites. All water components in the wetlands are assessed in terms of irrigation purposes.

The conclusions of the first two research aims are finally combined to identify current and future mutual effects between agricultural production and water quality (third research aim). On the one hand, understanding groundwater inflow to wetlands is important, in terms of quantity and quality of available water for agriculture. On the other hand, knowledge about recharge processes from wetlands to ground-



water is important, in terms of drinking water quality assurance. If anthropogenic contaminated wetland water recharges the aquifer below the wetland, the drinking water source groundwater will maybe become degraded. Geogenic background concentrations of water quality indicators as well as the influence of different agricultural management options on water quality need to be assessed. In this context, the influence of different management options is investigated by the analysis of soil water in the agricultural experiments. Finally, the results regarding the third research aim can enhance the conceptual models.

In general, this study intends to give a sound overview of all processes and outline the systems' interconnections. In a final step, based on the conceptual models, recommendations are given for stakeholders and non-hydrogeologists, in order to develop a first framework regarding a sustainable management of wetlands.

## 2 Study sites

The two selected study sites are located in the subtropical region of East Africa (Fig. 2.1). Considering that delineation of wetlands strongly depends on the respective definition of wetlands, the actual area of the wetlands in the study sites was adopted from Beuel et al. (2016). This delineation is a first estimation of the wetland areas, based on digital elevation models (DEMs) and satellite data. Nevertheless, it was not verified by ground-truthing and should thus be regarded with caution. While the focus of the GlobE project is given to wetland and plot scale, in terms of hydrogeology it is furthermore necessary to assess the boundary conditions of the wetlands. Therefore, this study focusses on extended study sites that cover the wetlands as well as their surroundings.

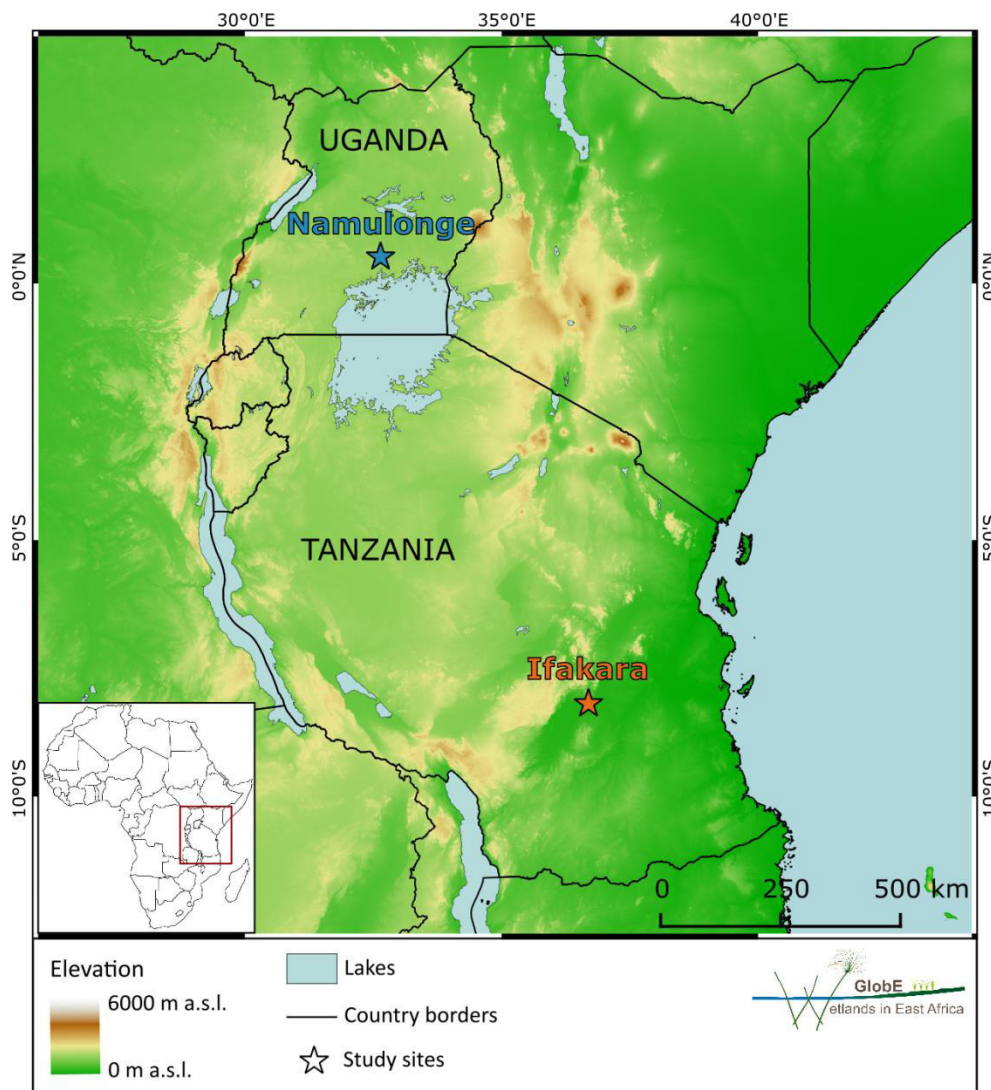


**Fig. 2.1:** Topographic map of East Africa showing the locations of the two study sites Ifakara (Tanzania) and Namulonge (Uganda). Data sources: earthexplorer.usgs.gov (elevation), Lehner and Döll (2004) (lakes), gadm.org (country borders).

The Ifakara study site (IF) is located in the northeast of the Kilombero Valley in southcentral Tanzania and represents a part of a huge lowland floodplain wetland. Due to the large size of this wetland and the catchment of its draining stream (Kilombero River), the study site solely comprises a small part of the whole catchment. The Namulonge study site (NA) is situated in the Namulonge Valley in southcentral

Uganda and represents a small channeled valley-bottom wetland. Here, the study site covers the whole wetland, the catchment of its draining stream (Nasirye Stream), and the surroundings of this catchment.

## 2.1 Climate of East Africa

In East Africa, large-scale tropical controls, such as convergence zones, interfere with several regional factors associated with lakes, topography, and maritime influence (Nicholson 1996). Thus, the climatic conditions vary highly in their spatial distribution (Hecklau 1989). For example, Nicholson (1996) stated that seasonality of East African rainfall “changes significantly within distances on the order of tens of kilometers; within Eastern Africa are regions with one, two and three rainfall maxima in the seasonal cycle”.

One important factor influencing the climate of East Africa is the so-called Inter-Tropical Convergence Zone (ITCZ) (Hecklau 1989). This zone of low air-pressure, where the monsoons coming from the north and south converge, emerges due to the heating of air masses by vertical solar radiation and their subsequent rising (McClanahan and Young 1996). As air rises, it cools and thus its water vapor capacity is lowered, which leads to fast condensation and subsequently heavy rainfalls directly under the ITCZ (McClanahan and Young 1996). The ITCZ crosses the equator twice a year and lies in the north of East Africa during northern hemisphere summer and in the south during northern hemisphere winter (Hecklau 1989). This should usually lead to two precipitation maxima at the equator throughout the year (Hecklau 1989). Nevertheless, the pattern of the ITCZ is disturbed and superimposed due to the topography of East Africa. This change in location and movement of the convergence zone in combination with the influence of the great lakes leads to a change in climatic patterns, such that the seasons do not follow the classical pattern of the ITCZ (Griffiths 1972). Accordingly, annual maximum and minimum temperatures are highly depending on elevation and thus strongly vary over the whole region (Griffiths 1972).

Following the Köppen-Geiger classification, major parts of East Africa fall within tropical climate types (Peel et al. 2007). However, some regions in northern Kenya and Uganda and in central Tanzania belong to arid climate types and one region covering southern Kenya and northern Tanzania belongs to temperate climate types.

## 2.2 Geology of East Africa

East Africa’s geology includes rocks of Archaean to Cenozoic age (Schlüter 1997). While large parts of the region are made up of crystalline rocks, some parts are covered with sedimentary and volcanic rocks or unconsolidated sediments (Key 1992). Due to the long term tectonic stability of East Africa and the tropical climate, huge parts of the crystalline rocks developed deep weathering profiles (Chilton and Foster 1995). Section 2.2.1 gives an overview of the geodynamic evolution of East Africa, with a special focus on Tanzania and Uganda, and section 2.2.2 outlines the processes and products of deep weathering.

### 2.2.1 Geodynamic evolution

The geodynamic evolution of East Africa has lasted from Archaean to recent times. The oldest rocks are found in the Tanzanian Craton, representing the fourth largest of 13 Archaean cratons throughout the African continent (Cloutier et al. 2005). Archaean cratons or Archaean Cratonic nuclei are “stable remnants of the Earth’s earliest continental lithosphere” (Westerhof et al. 2014). They are mainly composed of low-grade greenstone belts, high-grade gneisses, granite series, and late minor intrusions (Key 1992). These Archaean cratons and their surrounding orogenic provinces or mobile belts present the main part

of East Africa's crystalline basement (Schlüter 2006). The mobile belts developed during several orogenic cycles of Precambrian age that reworked the primordial Archaean cratons (Key 1992).

Schlüter (1997) stated that "a tectonostratigraphic synopsis of the whole region of East Africa is to a large extent unresolved in spite of much important mapping in critical sections". This is mainly reasoned by the widespread and repeated tectonic activity during Precambrian times that has imposed a superficial uniformity of rocks of differing characters and ages (Pallister 1971). Nevertheless, geodynamic evolution of East Africa is addressed by several authors (Pallister 1971, Schlüter 1997, Westerhof et al. 2014). The first crustal assemblies generating greenstone belts around the Tanzanian Craton formed during the Archaean (Westerhof et al. 2014). After Key (1992), the Tanzanian Craton consists of 80 % granitoids and gneisses and 20 % greenstone belts mostly found in the northern half of the craton. The ancient Tanzanian Craton, including its greenstone belts, can be subdivided into granitoid terranes and the schist belts of the Dodoman, Nyanzian, and Kavirondian System. The Dodoman System represents the largest part of the Tanzanian Craton, mainly consisting of granitoid rocks (Schlüter 1997).

During Proterozoic times, several Supercontinent Cycles gave rise to formations of mobile belts around the Tanzanian Craton (Condie 1998). These cycles include the break-ups and re-assemblies of supercontinents resulting in the production of new crust (Westerhof et al. 2014). The first Supercontinent Cycle recorded took place during the Palaeoproterozoic and is widely known as the "Eburnian Orogenic Cycle" (Westerhof et al. 2014). Mobile belts laid down during that time are the Ubendian and Usagaran belts in Tanzania and the Buganda-Toro System in Uganda (Schlüter 1997). Those belts are lithologically similar to the Archaean greenstone belts (Key 1992).

The second Supercontinent Cycle occurred in the Mesoproterozoic and resulted in the Rodinia Supercontinent (Westerhof et al. 2014). During that cycle, orogenic activities in East Africa were less pronounced as during the Palaeoproterozoic (Key 1992). One major structure that originated during that time is the Kibaran Belt or Karagwe Ankolean System (Schlüter 1997). The last Supercontinent Cycle of Proterozoic age occurred during the Neoproterozoic and led to the development of Gondwana (Westerhof et al. 2014). This cycle is also known as the Pan-African Cycle and resulted in the formation of the Bukoban System and the Mozambique Belt (Schlüter 1997).

The crystalline basement rocks of East Africa are extensively overlain by essentially unmetamorphosed cover rocks (Key 1992). While East Africa appeared to be a region of denudation during most of the Palaeozoic, the break-up of Gondwana induced several phases of crustal extension and basin development along Pan-African and older structures (Westerhof et al. 2014). A huge sequence of sediments was deposited during a Permo-Triassic megacycle, referred to as Karoo deposits (Schlüter 1997). Karoo sediments are mainly composed of continental quartz-rich deposits (Pallister 1971). They can be found all over the African continent, and in East Africa they were mainly deposited in NNE-SSW trending fault controlled basins. The sedimentological sequences can reach thicknesses higher than 7,000 m (Schlüter 1997). These basins are believed to represent the precursors of Tertiary rift depressions, which were probably formed on Pre-Cambrian lines of weakness (Pallister 1971). During Jurassic and Cretaceous times, marine sedimentation took place along the coasts of East Africa (Schlüter 1997). These marine sediments are lithologically clearly separated from the underlying terrestrial Karoo rocks (Schlüter 1997). During Tertiary and Quaternary, additional deposition of mainly marine sediments occurred along the East African coast (Schlüter 1997).

A very important structural feature of East Africa's geology is the East African Rift System (EARS). Rifting mainly took place between the Late Eocene and Early Miocene and continues until recent times (Westerhof et al. 2014). The EARS developed two branches. The eastern branch is known as Gregory rift

and stretches from the Kenian-Ethiopian border in the north to northern Tanzania in the south. The western branch runs from northern Uganda along the western borders of Uganda and Tanzania. Several minor branches splay out from these two major rifts (Schlüter 1997). The eastern branch developed already in Early Miocene times, with the deposition of Cenozoic volcanic rocks during rifting in a band along the rift system (McConnell 1972). These volcanic rocks are much more widespread in Ethiopia. The western branch represents a typical rift structure and was developed in Late Miocene times. McConnell (1972) stated that the Cenozoic rift faults of the EARS are often aligned parallel to Karoo basins or Precambrian structures.

### 2.2.2 Deep weathering of crystalline rocks

The land surface of tropical Africa has been exposed to prolonged weathering, which has led to the formation of a weathered mantle of alteration products. This weathering profile has developed over very long periods, due to the infiltration of rainfall and the subsequent leaching of more soluble and mobile components and the reprecipitation of secondary, less mobile, minerals (Chilton and Foster 1995). Several authors have described the weathering profile above crystalline rocks in tropical regions suggesting different zonal groupings (Chilton and Smith-Carington 1984, Ollier and Galloway 1990, McFarlane 1992, Wright 1992, Chilton and Foster 1995). The present study adopts the zonal grouping suggested by Chilton and Foster (1995), because these authors focused on the region of tropical Africa and had a closer look at hydraulic properties.

Chilton and Foster (1995) divided the weathering profile into saprock, saprolite, and residual soil (Fig. 2.2). The latter two can be subsumed to the so-called regolith. The saprock represents a fractured zone of gradual transition between regolith and fresh crystalline rock showing remnants of fresh crystalline rocks in a deeply weathered matrix. While the saprolite was derived from *in-situ* weathering, the residual soil developed from the saprolite by further leaching and bioturbation (Chilton and Foster 1995). Wright (1992) described the residual soil as a collapsed zone, which is typically sandy on watershed areas and changes to sandy clays and clays in valley bottoms. At slopes, colluvial material accumulates (Wright 1992).

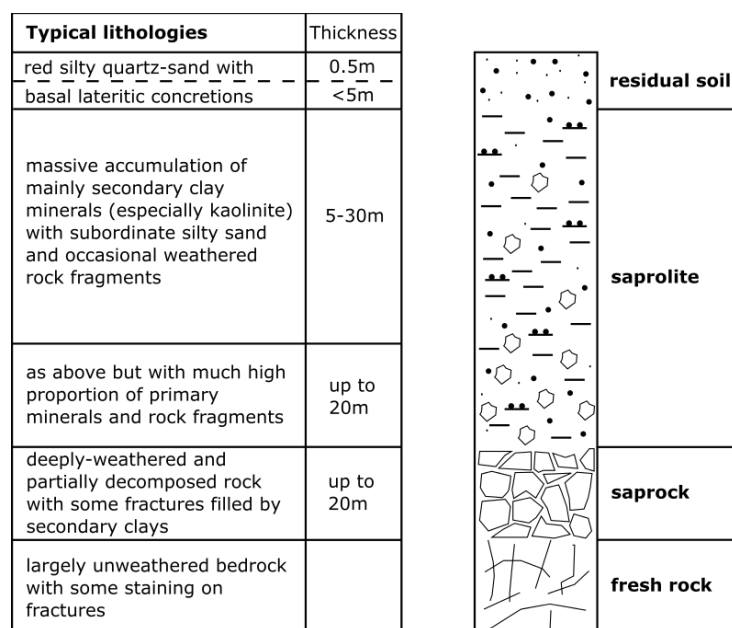


Fig. 2.2: Typical weathering profile above crystalline rocks in tropical Africa (modified after Chilton and Foster 1995).

Weathering profiles as well as fractured crystalline rocks in East Africa represent important aquifers in terms of drinking water supply for rural populations (Wright 1992). Due to the prolonged destruction of primary minerals during weathering, weathered crystalline rock aquifers are usually porous in character (Fass 2004).

### 2.3 The Ifakara study site

The Ifakara study site is located in the northeast Kilombero Valley, which forms the basin floor of the catchment of Kilombero River (Fig. 2.3). The Kilombero Catchment is part of the Rufiji Catchment, the biggest river catchment in Tanzania. The valley is located at the foot of the Great Escarpment of East Africa in the Morogoro region in southcentral Tanzania at around 8°S and 36°E and covers an area of about 11,700 km<sup>2</sup> (Jätzold and Baum 1968). The topographical depression, with a length of 257 km and a width of 64 km at its maximum, shows an average elevation of 274 m.a.s.l. (Jätzold and Baum 1968). The level gradient in longitudinal direction from southwest to northeast is about 0.4 ‰ (Bonarius 1975). The valley is drained by the Kilombero River along this gradient and lies within the districts Kilombero and Ulanga (Mombo et al. 2011). It is bounded by the Udzungwa Mountains in the northwest and the Mahenge Hills in the southeast with a maximum elevation of 2,200 and 1,400 m.a.s.l., respectively (earthexplorer.usgs.gov). With an area of 7,967 km<sup>2</sup> (Mombo et al. 2011), the floodplain of the Kilombero Valley presents the largest freshwater wetland at low altitude in East Africa and has been designated as a Ramsar Site (Kangalawe and Liwenga 2005).

The actual study site is located around the city of Ifakara in the northeast of the Kilombero Catchment (Fig. 2.4). It is about 30 x 20 km in size and comprises the southern fringe of the Udzungwa Mountains, the urban areas of Ifakara, and the surrounding rural areas including the floodplain north of Kilombero River. Kilombero River drains the study site from west to east, and is joined by Lumemo River coming from the north. The elevation decreases from a maximum of around 1,050 m.a.s.l. in the mountain fringe in the north to a minimum of around 250 m.a.s.l. at Kilombero River in the south (earthexplorer.usgs.gov). The wetland area covers the entire study site south of the mountain fringe (Beuel et al. 2016) (Fig. 2.4). The seasonal flooded area (floodplain) is located around the Kilombero River. This area was delineated based on the normalized difference water index, calculated from data of the Landsat satellite mission (personal communication with E. Amler 2016).

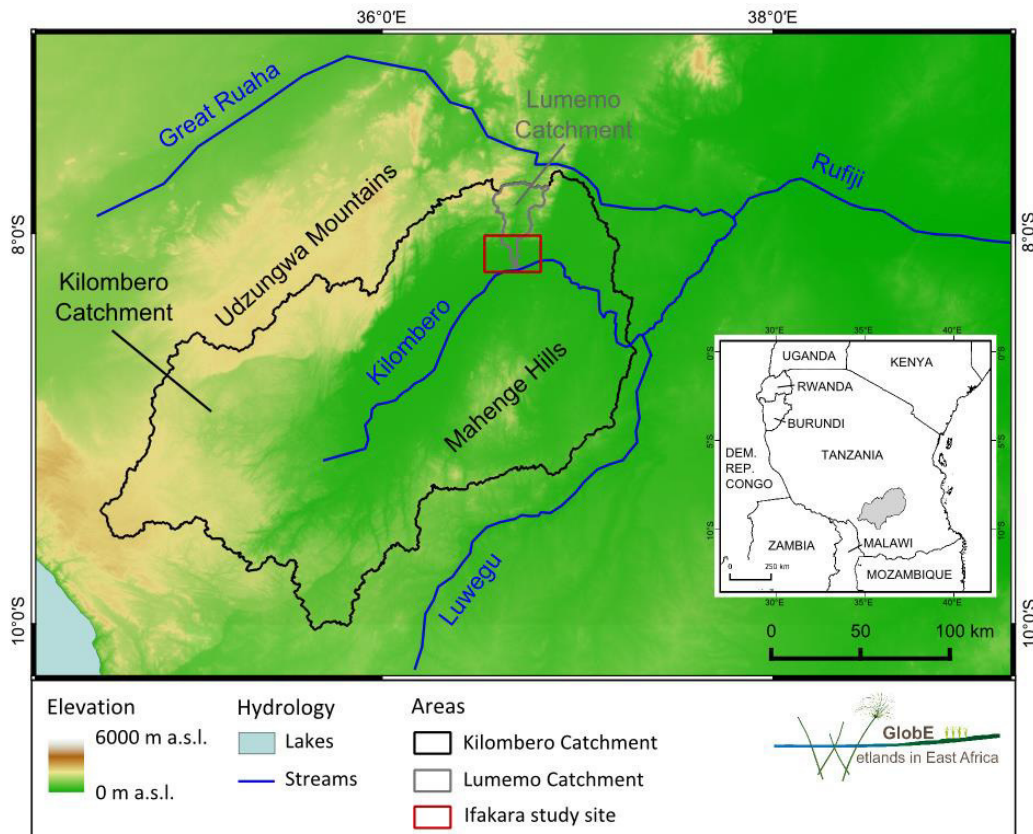


**Fig. 2.3:** Topographic map of the Kilombero Valley and its surroundings showing the location of the Ifakara study site. Data sources: earthexplorer.usgs.gov (elevation), Lehner and Döll (2004) (lakes), gadm.org (country borders), openlayers.org (streams) (IF).

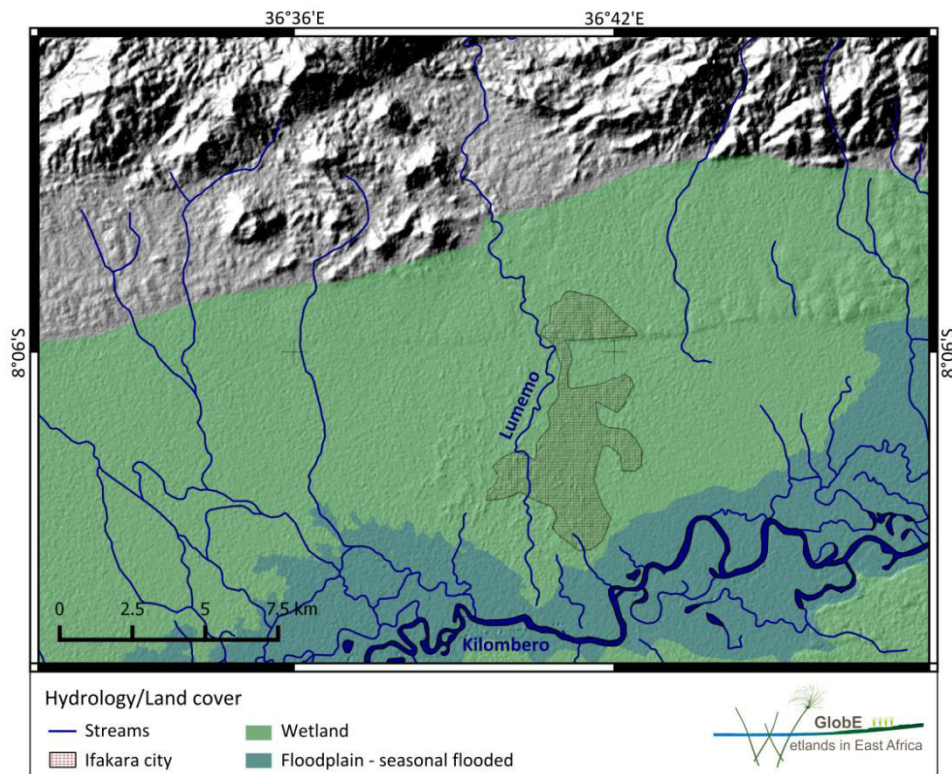


**Fig. 2.4:** Shading map of the Ifakara study site. Data sources: earthexplorer.usgs.gov (elevation), Geological Survey of Tanganyika (1962) (streams), google.com/earth (Ifakara city), Beuel et al. (2016) (wetland), personal communication with E. Amler (2016) (floodplain) (IF).

### 2.3.1 Climate (IF)

According to the Köppen-Geiger classification, the climate of the Ifakara study site and the whole Kilombero Catchment belong to the “Tropical Savannah” type (Aw) (Peel et al. 2007). The average annual temperature is 25°C around Ifakara (Hijmans et al. 2005) and does not vary much throughout the year (Fig. 2.5). Annual precipitation sums up to around 1,000 mm in the Kilombero Valley and increases towards the edges of the valley up to 2,000 mm (Beck 1964). The windward site of the Great Escarpment receives higher rainfall amounts than the valley plains and the leeward site of Mahenge Hills (Jätzold and Baum 1968). Around Ifakara, Hijmans et al. (2005) proposed a mean annual precipitation of 1,427 mm. Most of the precipitation falls in the rainy season between the end of November and the end of May, though beginning and ending of this season are highly variable (Jätzold and Baum 1968). The rainy season can be subdivided into a small and a big rainy season, intermittent by a decrease of rainfall in January and February (Jätzold and Baum 1968). During that time, the ITCZ moves too far to the south and causes even dry periods lasting several weeks in some years (Jätzold and Baum 1968).

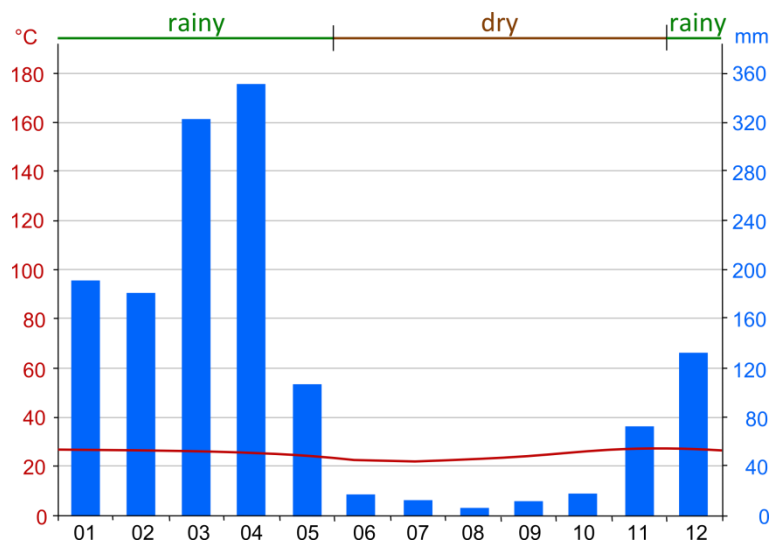


Fig. 2.5: Climate diagram showing annual temperature (red), precipitation (blue), and rainy and dry seasons in the Ifakara study site (modified after climate-data.org) (IF).

### 2.3.2 Geology (IF)

The Kilombero Valley is a SW-NE trending trough-like depression, covered with Cenozoic sediments between crystalline rocks of the Precambrian Mozambique Belt (Beck 1964, Mruma 2002). This depression is a southern extension of the EARS (McConnell 1972). Mruma (2002) described the Kilombero Valley as a part of the northeast-trending Kilombero Rift, where the Udzungwa scarp forms the uplifted and the Kilombero Valley the down-thrown block of the rift fault. Nevertheless, the term “Kilombero Valley” or “Kilombero Rift” is often used for the north-trending rift to the east of the study site (Nilsen et al. 1999, Dypvik et al. 2001, Dypvik and Nilsen 2002, Le Gall et al. 2004). The Kilombero Valley as described by Beck (1964), Jätzold and Baum (1968), and Mruma (2002) comprising the study site, is a southwestern extension of this north-trending rift. In terms of consistency, the terms “Kilombero Valley” and “Kilombero Rift” will henceforth refer to the northeast-trending valley, while the north-trending rift structure described by Nilsen et al. (1999), Dypvik et al. (2001), Dypvik and Nilsen (2002), and Le Gall et al. (2004) will be called Kidodi-Mkata Rift following Mruma (2002).

As the eastern branch of the EARS crosses the Tanzanian Craton, it splits up into “ill-defined” arms (Mruma 2002). One of these arms forms the Kilombero Rift, which is a northeastern continuation of the Ruhuhu Rift and joins the Kidodi-Mkata Rift in the north (Mruma 2002). To the northwest, the Kil-



ombero Valley is bounded by the so-called Udzungwa scarp, the escarpment of the Udzungwa Mountains that was formed by large-scale faulting and tilting of the Kilombero Rift System (Geological Survey of Tanganyika 1962). To the southeast, the valley is bounded by the northern foothills of the Mahenge Mountain block (Geological Survey of Tanganyika 1962). In the northeast, it ends at the Haldemann sills, rocky outcrops crossing the river bed, which act as weirs (Jätzold and Baum 1968). The valley itself is filled with a sedimentary basin infilling (Beck 1964).

The Udzungwa Mountains belong to the Neoproterozoic Mozambique Belt, which is located to the east of the Tanzanian Craton (Schlüter, 1997). It was strongly affected by the Neoproterozoic (Pan-African) metamorphic event from 650 to 615 Ma (Möller et al. 1998). In former studies, some authors assigned the rocks of the Udzungwa Mountains to the Usagaran System (Geological Survey of Tanganyika 1962), maybe due to the ambiguous usage of the term Usagaran, which was sometimes applied to both Palaeoproterozoic and Neoproterozoic rocks (Schlüter 1997). However, this belt represents a zone of Neoproterozoic orogenies associated with the collision of East and West Gondwana (Reddy et al. 2003). The rocks were formed and metamorphosed during Archaean and Palaeoproterozoic times and have been actively reworked during the Pan-African tectonothermal event in the Neoproterozoic (Schlüter 1997). The belt exhibits mainly paragneisses and orthogneisses representing amphibolite to granulite facies (Schlüter 1997). The part of the Mozambique Belt being exposed at the northwestern flank of the Kilombero Valley is referred to as Western Granulites and comprises gneisses with greenschist to lower amphibolite facies in the west and granulite facies rocks in the east (Tenczer et al. 2007).

The existence of a weathering profile (section 2.2.2) overlying crystalline rocks in Tanzania was proven in several studies (e.g. Little and Lee 2006, Kashaigili 2010). Ministry of Water URT (2012a) mentioned this weathering profile to occur in the Rufiji Catchment as well. However, no information about depths and characteristics of this profile exist so far and no publication mentions the weathering profile to exist within the Kilombero Catchment. Nevertheless, it is most likely that the crystalline rocks surrounding Kilombero Valley have been exposed to weathering.

Only little information is available regarding the age of the normal fault structure, which separates the Udzungwa Mountains from the sedimentary basin infilling of the Kilombero Valley (Le Gall et al. 2004). Fracture investigations of Mruma (2002) revealed three different sets of fractures trending in different directions (WNW-ESE, E-W, NE-SW, NW-SE). All fractures showed relatively steep dips and most of them showed a reverse sense. While the striking directions of fractures fit with those of the fault system of the Udzungwa scarp, the reverse sense contradicts with the normal sense of the scarp faults. Mruma (2002) gives two possible explanations. Firstly, it could be that the reverse faults are older than the normal faults, with the latter being reactivated structures of Permo-Triassic age. Secondly, both faults could be of the same age either Permo-Triassic (with reactivations in Cenozoic) or Cenozoic. For the Kidodi-Mkata Rift located north of the study site, Le Gall et al. (2004) assumed a first rifting phase during Karoo times and a subsequent reactivation of the fault system in Neogene-Holocene times. Consequently, it is most likely that the Kilombero Rift belongs to the EARS, but first movements already took place in Karoo or even earlier times.

During Karoo times, huge formations of continental sediments were deposited in the tectonic depression. These formations are mainly made up of sandstones and conglomerates (Geological Survey of Tanganyika 1962). Le Gall et al. (2004) described 4,000 to 5,000 m thick Karoo rocks within the Kidodi-Mkata rift north of Kilombero Valley. After Geological Survey of Tanganyika (1962), it is most likely that these rocks underlie huge parts of the Kilombero Valley as well.

Comparatively little information about the unconsolidated sediments deposited in the Kilombero Valley exists. No geological publications are available regarding the sedimentary basin infilling. Following Beck (1964), the Kilombero Valley is covered with “Pliocene and Pleistocene deposits and alluvial material of recent age”. Bonarius (1975) classified the sediments in terms of soil forming processes into i) braided and meandering river zone in the widespread central alluvial plain, ii) alluvial fans laid down by streams entering the valley, and iii) marginal colluvial sand-flats or miombo plains.

Information about geological units and structures within the Ifakara study site is solely available from the geological map by Geological Survey of Tanganyika (1962). The Precambrian metamorphic rocks of the southern hills of the Udzungwa Mountains are exposed in the north of the study site (Fig. 2.6). These hills, building the mountain fringe of the Udzungwa Mountains, are referred to as Itula range of hills. They are made up of Neoproterozoic migmatitic, quartzo-feldspathic gneisses and pyroxene granulites. In the very northwest of the study site, garnetiferous biotite gneisses occur. These metamorphic rocks of the Mozambique Belt are separated from a sedimentary basin infilling via the normal fault system, which developed during rifting. Two major faults cross the study site in west-eastern direction building a tilted block faulting structure with tilting in northern direction.

The sedimentary basin infilling is divided into non alluvial sediments, covering the mountain fringe and the tilted block between the two major faults, and alluvial sediments in the south. The non-alluvial sediments in the central and western part of the basin between the two normal faults are made up of pale locally ferruginous sands. Red-brown and light sandy earths are found in the east of the basin and as overlays of the hard rocks in the depressions of the mountain fringe. Ferruginized cemented sands and gravels occur in small parts along the southern fault. These non-alluvial sediments are of Neogene age and once covered the whole Kilombero Valley, but have been eroded away in huge parts. They might represent the zone of marginal colluvial sand-flats described by Bonarius (1975). The Quaternary alluvial sediments are described as alluvial sands, silts, and clays, without any further description. However, based on the suggested classification of Bonarius (1975), it is most likely that these sediments are made up of river deposits, alluvial fans, and maybe colluvial sediments.

The alluvial fan within the study site was described by Jätzold and Baum (1968) and is clearly visible in topographic elevation. The fan is located around Lumemo River (Fig. 2.6). The higher elevated areas of this fan underlie the city of Ifakara. These areas do not become flooded by over-bank flow of Kilombero River and thus result in a bottleneck structure of the floodplain south of the fan. River and floodplain deposits are located near Kilombero River, which has a meandering character in the study site, and in potentially former river or floodplain locations. Colluvial sediments were probably deposited by smaller rivers along the southern normal fault, east and west of the alluvial fan. Nevertheless, a differentiation of these depositional environments is not possible based on the geological map. The delineation of the alluvial fan was adopted from Jätzold and Baum (1968). However, it is not clear which criteria they used for the delineation. As all of these sediments were deposited in Quaternary to recent times, it is most likely that they interfinger with each other. Recently, Kilombero River is cutting into the alluvial sediments, maybe due to further fault movement or tilting (Geological Survey of Tanganyika 1962). Although it is most likely that sedimentary rocks of Karoo age underlie parts of the Kilombero Valley, Geological Survey of Tanganyika (1962) supposed no Karoo rocks around Ifakara. They rather described a ridge of Proterozoic gneisses between Ifakara and Kivukoni, which is located south of Kilombero River.

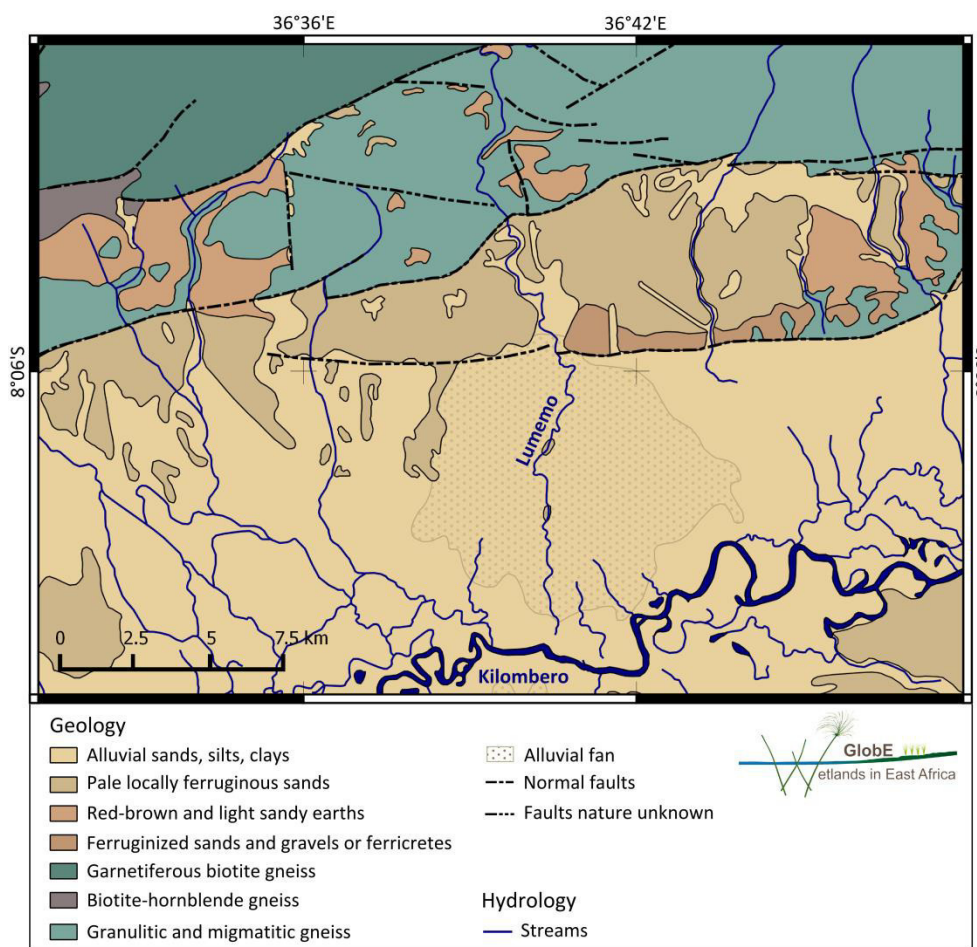


Fig. 2.6: Geological map of the Ifakara study site. Data sources: Geological Survey of Tanganyika (1962) (geology, streams), Jätzold and Baum (1968) (alluvial fan) (IF).

### 2.3.3 Soils (IF)

Following the Soil Atlas of Africa (Jones et al. 2013), the main soil type covering the Kilombero Valley is a eutric fluvisol. Typically for floodplains, it is characterized by a base saturation of 50 % or more in its major parts between 20 and 100 cm depth (Jones et al. 2013). This soil type can contain all types of grain sizes, depending on the velocity of water during deposition. It is usually very suitable for agricultural production, especially for wetland rice, due to its fertility and proximity to fresh water (Jones et al. 2013). The surroundings of the valley within the Kilombero Catchment are covered by several other soil types, such as nitisols, acrisols, ferrasols, cambisols, and lixisols (Jones et al. 2013). At the edges of the valley, some patches of arenosols occur as well (Jones et al. 2013). However, this Soil Atlas has a low resolution and does therefore not give detailed information about the spatial distribution of soils within the study site. A higher resolved soil map of the Morogoro region is available from the European Soil Data Centre ([esdac.jrc.ec.europa.eu](http://esdac.jrc.ec.europa.eu)). Compared to the Soil Atlas, this map does not follow the same soil classification scheme, but describes the soils based on geomorphology, texture, color, and drainage conditions (Fig. 2.7).

The spatial distribution of soil types clearly correlates with that of geological units. While the floodplain is covered with deep imperfectly drained sand and loam (Fig. 2.7: A2), the alluvial fan is covered with deep well-drained sandy loam including sand patches (C12). The soil covering the colluvium west of the alluvial fan is described as deep poorly drained sandy clays and clays (C3), and the soil east of the alluvial fan is described as deep poorly drained low-lying sandy soils (C24). Soils covering the non-alluvial sedi-

ments and the mountain fringe are represented by deep well-drained loamy coarse sand, sandy loam, and sandy clay (F21). The hard rocks are covered with shallow well-drained loam and sandy loam being stony and rocky (M11). According to Figure 2.7, all kind of textures occur in the soils of the study site. Good drainage is solely given at the mountain fringe and in the higher elevated parts of the alluvial fan.

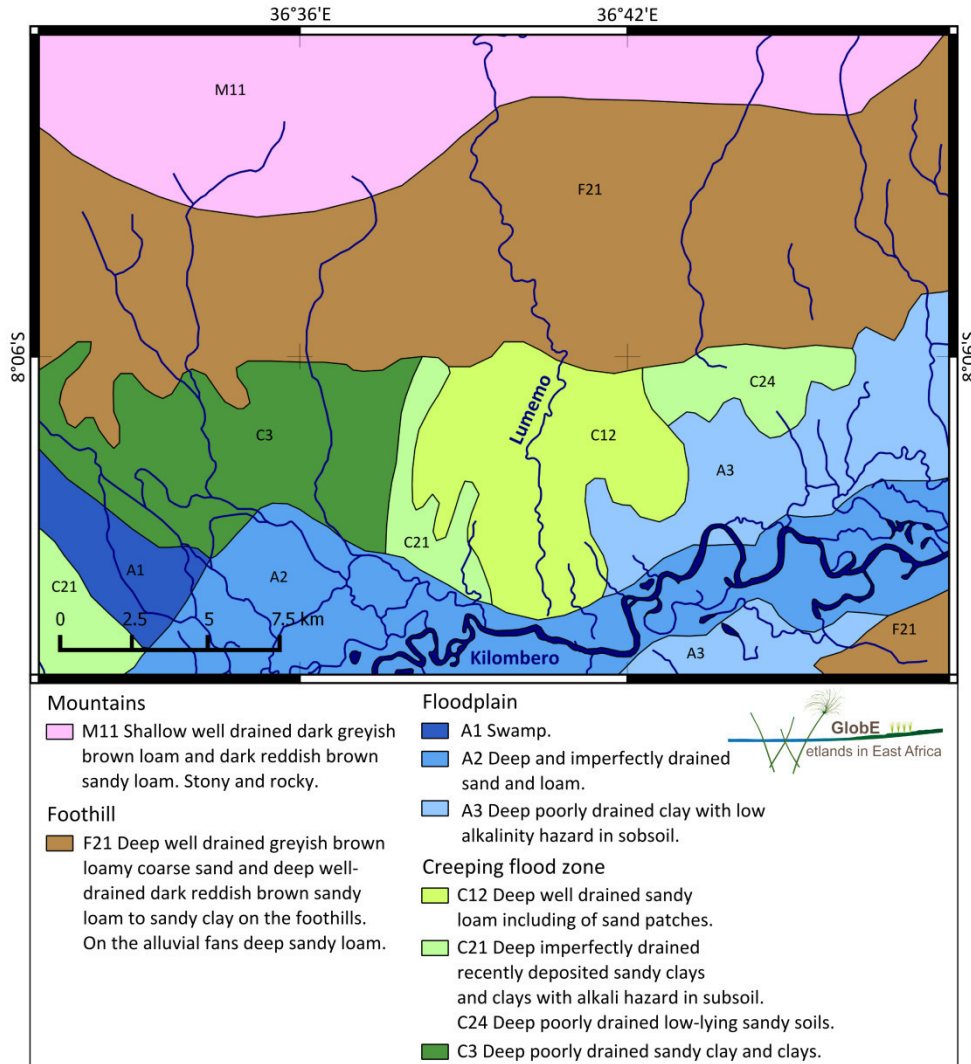


Fig. 2.7: Soil map of the Ifakara study site. Data sources: esdac.jrc.ec.europa.eu (soil), Geological Survey of Tanganyika (1962) (streams) (IF).

### 2.3.4 Hydrogeology and hydrology (IF)

The whole Kilombero Catchment is about 40,000 km<sup>2</sup> in size (Mombo et al. 2011). Kilombero River's main tributary, Ruhudji River, flows through a steep and narrow valley in the southwestern catchment and subsequently reaches the valley bottom. There, it is joined by the Pitu River from the south and the Mnyera River from the west. FAO (1960) state this junction point as the beginning of the Kilombero River itself. Within the valley, Kilombero River bifurcates several times building a typical braided river system, which later on turns into a meandering river system due to the decreasing gradient (Jätzold and Baum 1968). The river is joined by many perennial tributaries coming from the west and northwest (FAO 1960). The biggest tributary draining the study area from north to south is the Lumemo River. However, a huge number of smaller seasonal streams are found as well. Furthermore, a lot of smaller streams join Kilombero River from south and southeast. Within the study site south of Ifakara, Kilombero River leaves

the valley through a bottleneck structure, where it flows south and finally joins Luwegu River, which then forms Rufiji River.

In general, runoff in the Kilombero Catchment is very high (FAO 1960). The average runoff of Kilombero River at its downstream part is 520 m<sup>3</sup>/s (Yawson et al. 2005). Runoff contribution from the valley plains is smaller than from the hills and escarpments, and the upper half of the catchment produces less runoff than the lower half (FAO 1960). However, discharge data of Kilombero River are scarce and a huge variability is observed within one year as well as between different years. During rainy season, huge amounts of runoff, the bottle neck character of the valley near Ifakara, and the geomorphology of the Haldemann sills induce inundation in one third of the plain (Jätzold and Baum 1968, Mombo et al. 2011). The central part of the plain even turns into a lake like swamp, during the period from January to May (Jätzold and Baum 1968). Flood levels can reach up to three meters above ground (Bonarius 1975). Near Ifakara, the width of the flooded area is about 3.4 km, which is relatively small compared to a width of 24 km in the central portion of the extensive braided river zone (Bonarius 1975). During dry seasons, the area completely dries up except for the rivers, river margins, and some permanent patches of swamps (Hughes and Hughes 1992).

Groundwater represents the major source of drinking water within the study site. A huge amount of small hand pumping wells is found within the city of Ifakara and its surroundings. Within the whole Kilombero Catchment, groundwater is used for domestic and livestock water supply, irrigation, hydropower generation, fishing, wildlife water supply, and transport (Ministry of Water URT 2012a). Nevertheless, only very little research was conducted regarding groundwater in the study site and the whole Kilombero Catchment so far, and national groundwater monitoring is only carried out in very few locations (Ministry of Water URT 2012a). In this context, Lyon et al. (2015) as well as Koutsouris et al. (2016) already outlined the hydrological and hydrogeological data scarcity and its influence on hydrological research within the Kilombero Catchment. For instance, no long time groundwater level records (> two months) are available for the Kilombero Catchment (Ministry of Water URT 2012a).

The analyses of groundwater depletion, based on stream discharge hydrographs, showed that 85 % of the total groundwater supply within the Rufiji Catchment is provided by the Kilombero Catchment (FAO 1960). In terms of water quality, Ministry of Water URT (2012a) state that surface water in the Kilombero Catchment has good chemical, but poor physical and bacteriological quality. Mean values of electrical conductivity are 57 µS/cm for surface water, and 70 µS/cm for groundwater (Ministry of Water URT 2012a). However, no generalizations can be made regarding water quality in the Kilombero Catchment, as only few water samples have been analyzed (Ministry of Water URT 2012a).

### **2.3.5 Vegetation, land cover, and land use (IF)**

The Kilombero Catchment falls within the Greater Selous Ecosystem, a World Heritage Site (Kangalawe and Liwenga 2005). Moreover, the wetland within the Kilombero Valley has been designated as a Ramsar Site, due to its rare and unique ecosystem (rsis.ramsar.org). In contrast, the Kilombero Valley is part of the Southern Agricultural Growth Corridor (SAGCOT), being a region in Tanzania that was declared by the government to produce cash crops and enhance food as well as livelihood security by increasing the area of agriculturally used land (Paul and Steinbrecher 2013). In the context of this development program, dry land irrigation derived from wetland water is planned, and the areas around Ifakara fall within an area with medium irrigation potential (Ministry of Water URT 2012b).

Natural vegetation of the floodplain in the Kilombero Valley is represented by patches of papyrus swamps, flood grasslands, and flood savannahs with very high grasses (Jätzold and Baum 1968). To-

wards the edges of the valley, the vegetation turns into woodlands and forests (Jätzold and Baum 1968). In terms of land use, the Kilombero Valley provides a huge potential for agricultural production (Beck 1964) and recently there is only little unused land (ERM 2013). Jätzold and Baum (1968) state that vegetation as well as agricultural activities are mainly depending on the annual flooding of Kilombero River and its tributaries. Agriculture in the Kilombero Valley is dominated by rainfed and irrigated agriculture that is undertaken by both small- and large-scale farmers (Kangalawe and Liwenga 2005). In the wetter parts towards the valley, mainly rice is cultivated, while several crops, such as maize and sugarcane, are cultivated in the dryer areas towards the mountains (Kato 2007). Furthermore, the floodplain and its surroundings are used for fishery and cattle grazing (Hughes and Hughes 1992).

The northern parts of the study site are covered with forests of the Udzungwa Mountains. The southern parts fall within the areas of flood grasslands and flood savannahs. Ifakara city covers the major parts of the alluvial fan and smaller settlements are found in the surroundings as well. According to the land use of the whole valley, the study site is used for cultivation of different crops, and fishery is conducted within the flooded parts. Most agricultural fields are cultivated by small-scale farmers. However, large-scale teak plantations are found as well (Kilombero Valley Teak Company).

## **2.4 The Namulonge study site**

The Namulonge study site is located within a huge wetland system comprising a number of small valleys north of Lake Victoria in southcentral Uganda (Fig. 2.8). This area is characterized by undulating topography, where gently, wavy slopes alternate with wetlands in the shallow valley bottoms (Myamoto et al. 2012). The Namulonge study site covers the whole catchment of Nasirye Stream and its surroundings and has a size of approximately 14 x 10 km. It is located 25 km north of Kampala in Wakiso district at around 0.5°N and 33°E (Fig. 2.9).

The studied wetland lies in the Namulonge Valley, the main valley of Nasirye Catchment. Several side-valleys occur within the catchment draining into the main valley. The Namulonge wetland is drained by the small stream Nasirye from northwest to southeast (GTK Consortium 2012). The catchment is divided by the Gayaza-Zirobwe road crossing the eponymous village Namulonge. The focus is given to the lower catchment located east of the road, which covers an area of 10.5 km<sup>2</sup>. The elevation of the study site decreases from west to east, with values ranging between 1,250 m.a.s.l. and 1,100 m.a.s.l. (earthexplorer.usgs.gov). Within the catchment, elevation also decreases from the outer boundaries of the catchment to the inner valley.

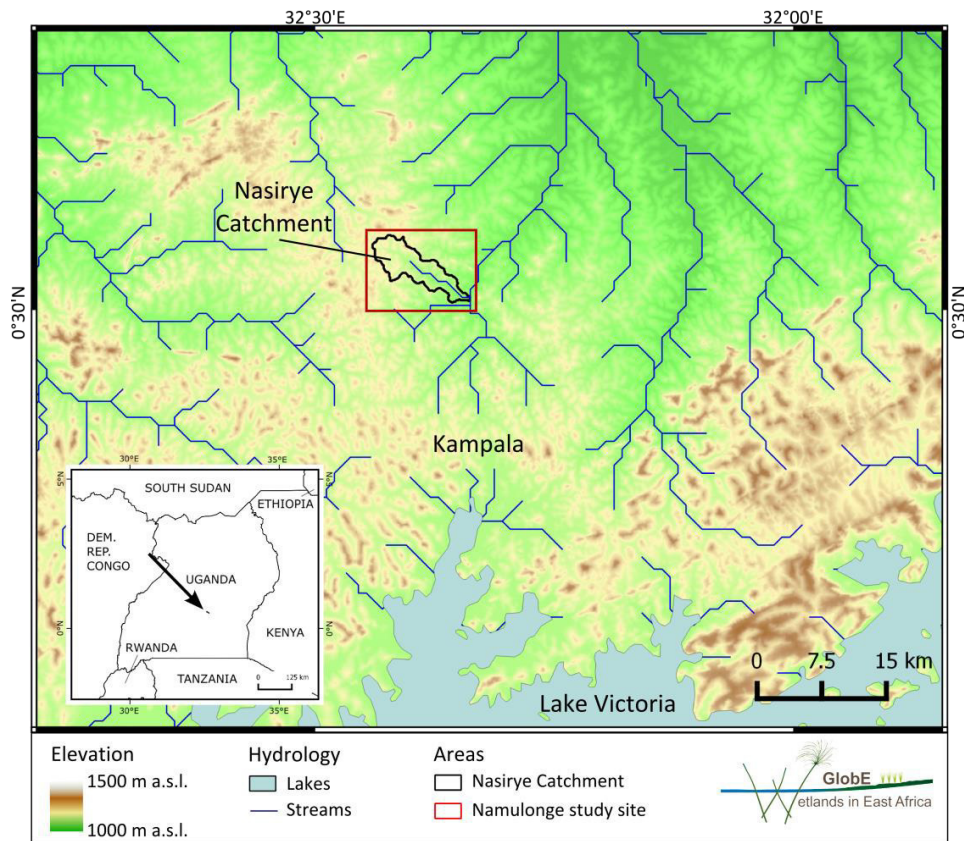


**Fig. 2.8:** Topographic map of the area around Kampala showing the location of the Namulonge study site. Data sources: earthexplorer.usgs.gov (elevation), Lehner and Döll (2004) (lakes), gadm.org (country borders), hydrosheds.cr.usgs.gov (streams) (NA).

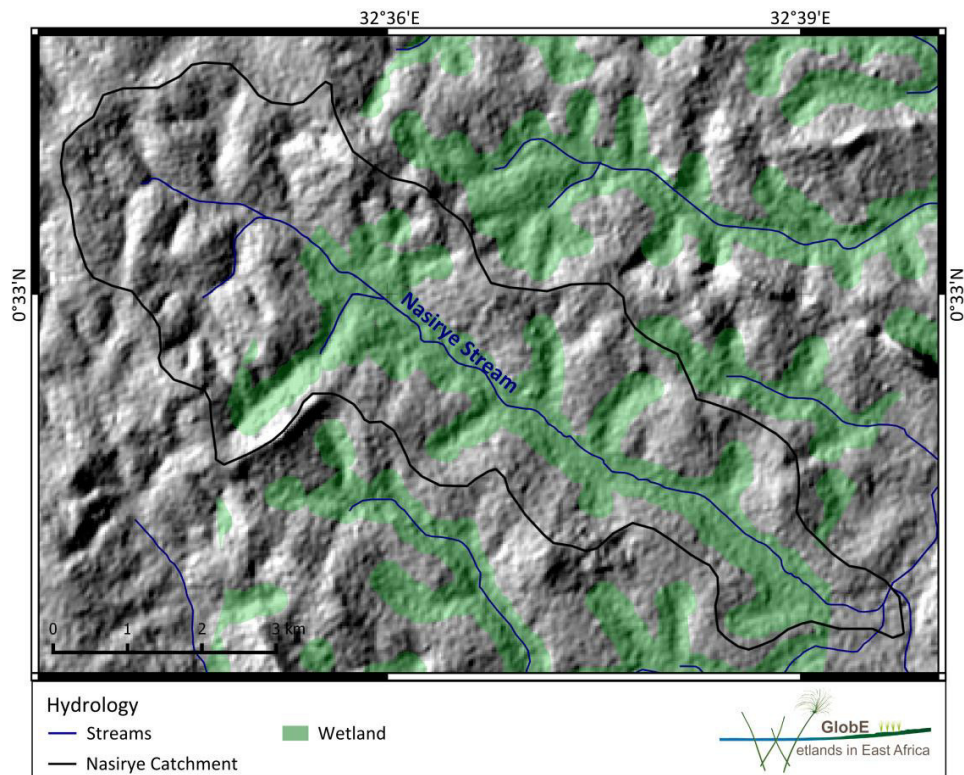


**Fig. 2.9:** Shading map of the Namulonge study site. Data sources: earthexplorer.usgs.gov (elevation), GTK Consortium (2012) (streams), Beuel et al. (2016) (wetland), Gabiri (unpublished) (Nasirye Stream) (NA).

### 2.4.1 Climate (NA)

The lower catchment of Nasirye Stream belongs to the Köppen-Geiger classification “Tropical savannah” type (Aw) (Peel et al. 2007). The upper catchment belongs to the “Tropical monsoon” type (Am), indicating more rainfall in dry seasons compared to the lower catchment. The mean annual precipitation in Namulonge amounts around 1,170 mm (Nsubuga et al. 2011). Two wet seasons occur during the year from March to May and from September to November (Fig. 2.10). However, transitions between rainy and dry seasons are not well marked and rainfall occurs all over the year. Average temperature is around 22°C with highest values in February and lowest values in July (Nsubuga et al. 2011).

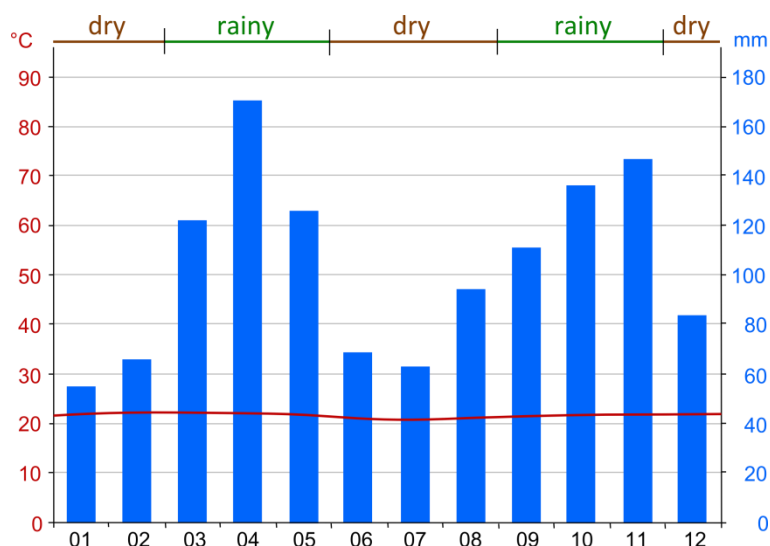


Fig. 2.10: Climate diagram showing annual temperature (red), precipitation (blue), and rainy and dry seasons in the Namulonge study site (modified after climate-data.org) (NA).

### 2.4.2 Geology (NA)

Southcentral Uganda is dominated by Archean and Proterozoic rocks. The Archean rocks are represented by the so-called Basement Complex, which outcrops in huge parts of Uganda (Westerhof et al. 2014). This complex is believed to be a part of the Tanzanian Craton (Schlüter 1997). However, no clear definition of the term Basement Complex exists and synonyms such as Western Gneiss-Granulite Complex (Schlüter 1997) or Western Granitic Complex (Westerhof et al. 2014) are commonly used. Most formations of the Basement Complex are represented by high grade metamorphic rocks of amphibolite or granulite facies (Schlüter 1997). Compositions of granulites usually range from acid to intermediate, with basic compositions occurring occasionally (Schlüter 1997). Furthermore, synorogenic acid gneisses and granites are found in wide areas of the Basement Complex. Following Westerhof et al. (2014) the Basement Complex in southcentral Uganda is called West Tanzanian Terrane (WTT). This domain is bounded by Lake Victoria in the south and by the North Uganda Terrane in the north. It is covered with rocks of the Rwenzori Fold Belt in the west. The WTT can be subdivided into the three units i) TTG gneisses, ii) Tororo Suite, and iii) Kampala Suite (Westerhof et al. 2014).

Further crystalline rocks in southcentral Uganda are of Proterozoic age. They are represented by the Buganda-Toro System, a formation of two lithostratigraphic units, which are rather difficult to separate (Schlüter 1997). The system is sometimes correlated with Neoproterozoic systems, such as Nyanzian and Kavirondian Systems, but this correlation was rejected by Tanner (1973), who suggested a Paleoproterozoic age. Most recent studies defined the Buganda-Toro System as a part of the Rwenzori Fold Belt (Westerhof et al. 2014), which developed during the Eburnian Orogeny. While Toro formations mainly occur in the west of the Buganda-Toro-System, southcentral Uganda is dominated by Buganda for-



mations (Schlüter 1997). The Buganda Group is represented by a metasedimentary succession of mica schists, phyllites, quartzites, and rare marbles and calc-silicates overlain by a succession of amphibolites and mafic metavolcanic rocks (Master et al. 2013). The thickness of this group is highly speculative, with estimates ranging from 1,000 to 7,000 m (Schlüter 1997). The Buganda Group can be subdivided into the Victoria Formation and the Nile Formation. The Victoria Formation is represented by orthoquartzites and conglomerates (Westerhof et al. 2014). In contrast, the Nile Formation is mainly composed of very fine grained slates (Westerhof et al. 2014). However, several other lithologies, such as quartzites and gneisses, are found within this formation as well.

Most crystalline rocks in Uganda are overlain by a weathering profile, as described in section 2.2.2 (Taylor and Howard 1996, Owor et al. 2011). As outlined by Taylor and Howard (1998), the surface of Uganda has been formed by cycles of deep weathering and stripping. The formation of a weathered mantle is known as deep weathering (section 2.2.2), while the removal of this mantle due to surface runoff is known as stripping. Both processes usually operate contemporaneously. In Uganda, a long period of deep weathering occurred during the Mesozoic followed by a period of stripping from Palaeocene to Oligocene (Taylor and Howard 1998). From Miocene to recent times, eastern Uganda was mainly influenced by deep weathering, while western Uganda was influenced by short cycles of deep weathering and stripping (Taylor and Howard 1998). Southcentral Uganda, and thus the study site, is located in that part, where deep weathering dominated since the Miocene (Taylor and Howard 1998). This period of deep weathering was proven by drilling logs in the Aroca Catchment, a catchment located in central Uganda underlain by crystalline rocks of the Basement Complex. Here, no outcrops of fresh crystalline rocks were observed and the weathered mantle showed a thickness of 26 m (geometric mean) (Taylor and Howard 1999).

The Namulonge study site is located at the boundary between the Basement Complex, or rather the WTT, and the Buganda-Toro System (Fig. 2.11). Thus, both rock formations are present in the study site. The WTT is represented by the Kampala granitoids and orthogneisses (A3KAgr) of the Kampala Suite (iii) (GTK Consortium 2012). These rocks are composed of heterogeneous granitoids and banded gneisses of mainly plutonic origin (Westerhof et al. 2014). Grain sizes and mineral compositions are distinctive variable and granitic and pegmatitic patches occur commonly (Westerhof et al. 2014). The Buganda-Toro System in the study site is represented by rocks of the Buganda Group. Both, Victoria and Nile formations are found (GTK Consortium 2012). The orthoquartzites and conglomerates (P1BVqc) of the Victoria Formation are present as small patches distributed over the whole study site (Fig. 2.11). Westerhof et al. (2014) describes these rocks as strongly metamorphosed and deformed orthoquartzites, sericite quartzites, and quartz rocks. The Nile Formation is represented by slates, shales, and phyllites (P1BNsh), and by porphyroblastic phyllites (P1BNamp) (Fig. 2.11). The unit of slates, shales, and phyllites (P1BNsh) is mainly composed of slate with vertical cleavage that locally grades into laminar shale with graded bedding (Westerhof et al. 2014). Regional increased metamorphism resulted in the formation of phyllites as well. The slates are dominated by fine grained quartz and sericite, with minor amounts of goethite, hematite, and ilmenite. The porphyroblastic phyllites comprise about 50 % muscovite, locally appearing as coarse flakes (Westerhof et al 2014). Additionally, they contain chlorite, hematite, and goethite. The porphyroblasts are made up of andalusite and cordierite (Westerhof et al 2014). According to Taylor and Howard (1999), the crystalline rocks are overlain by a weathering profile.

The valleys in the study site are filled with Quaternary sediments, which are described as alluvium, swamps, and lacustrine deposits (GTK Consortium 2012). No further description of these sediments is given in literature. The geological map by GTK Consortium (2012) shows that the Namulonge Valley fol-

lows a covered fault line. Another parallel covered fault is located in a small valley north of Nasirye Catchment (Fig. 2.11). However, no type of fault is given in the map legend.

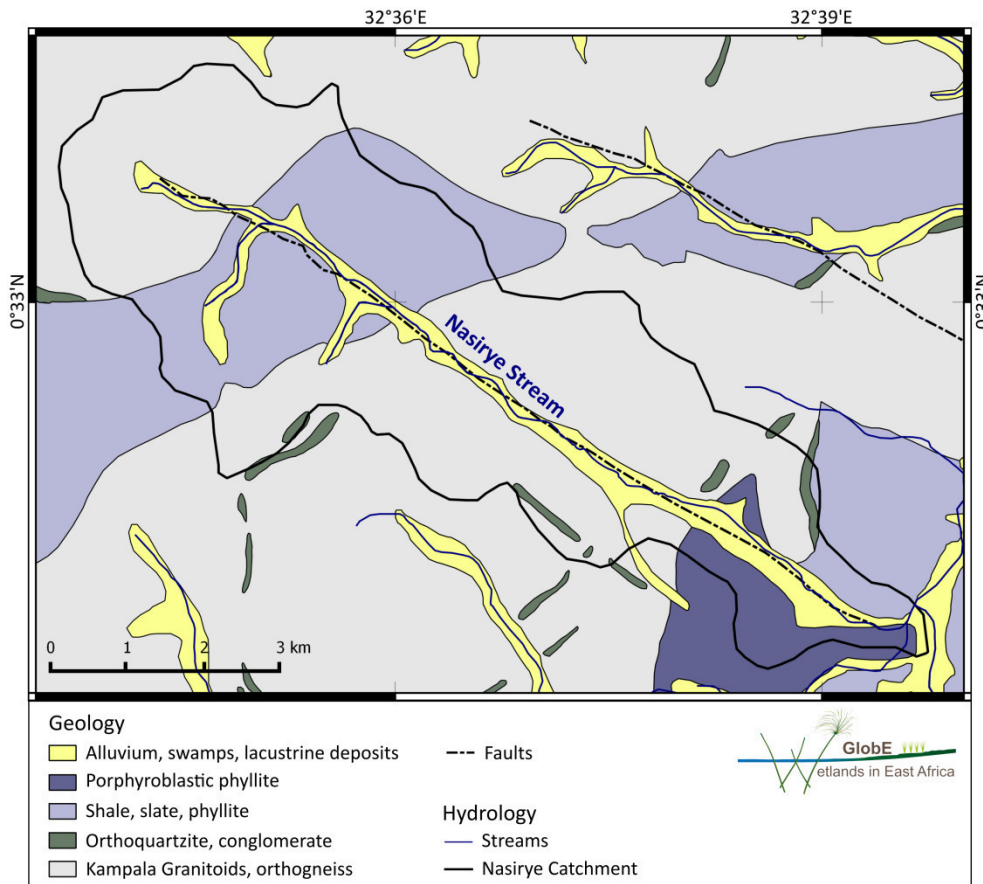
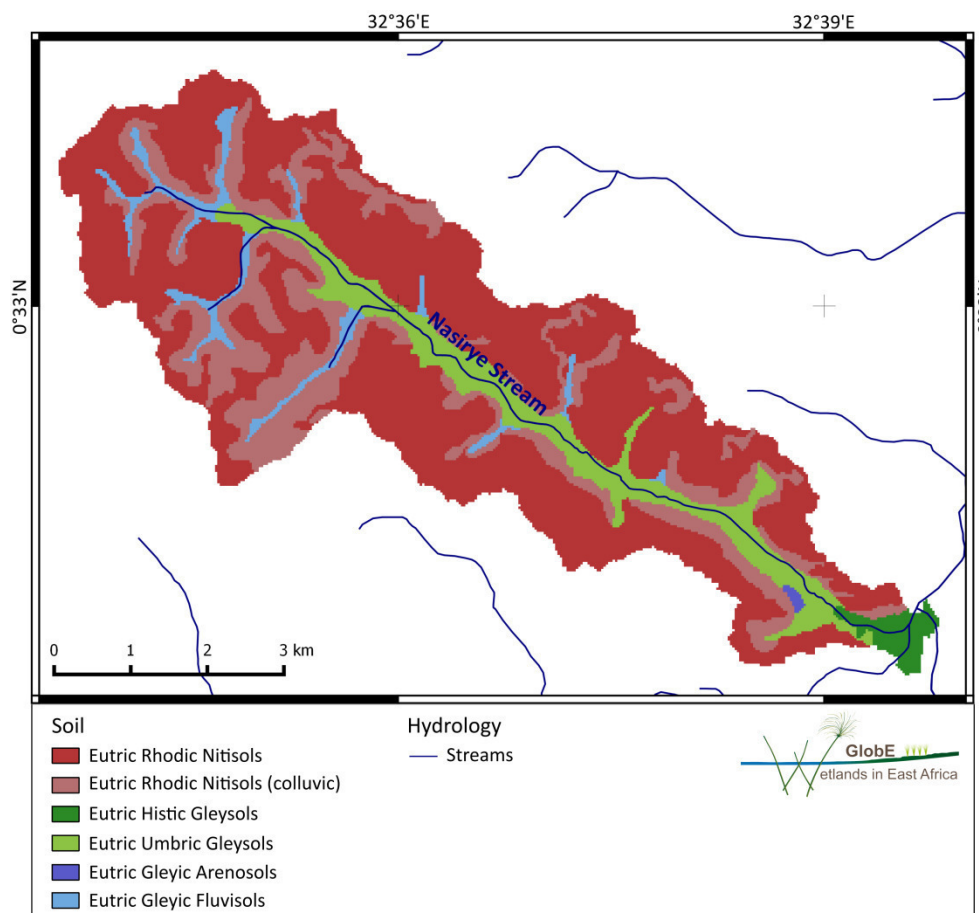


Fig. 2.11: Geological map of the Namulonge study site. Data sources: GTK Consortium (2012) (geology, streams), Heiß (2016) (alluvium), Gabiri (unpublished) (Nasirye Stream) (NA).

### 2.4.3 Soils (NA)

The Namulonge study site and its surroundings are covered with undifferentiated nitisols (Jones et al. 2013). These soils show a deep red color with a well-developed nut-shaped structure and are suitable for the cultivation of a wide range of crops, such as coffee, due to their high potential water content. However, fertilizer application is necessary to make this soil productive in terms of agriculture and it is likely to be eroded quickly on slopes (Jones et al. 2013). Furthermore, the high amount of iron in this soil leads to phosphate-fixation problems with retention rates of 80 % or more (Jones et al. 2013).

A detailed soil survey within the Namulonge study site was conducted by Yost and Eswaran (1990). They stated that the soils around Namulonge are formed in residuum from different types of bedrock depending on the geomorphological location. While soil on side slopes and hill tops is formed from quartzite, gneiss, and laterite, soil in valleys is formed from alluvium (Yost and Eswaran 1990). According to Jones et al. (2013), the soil map of the Nasirye Catchment (Gabiri unpublished) shows mainly eutric rhodic nitisols, which are of colluvial character at the slopes (Fig. 2.12). Within the valley bottom wetland, eutric umbric gleysols are found, while the side-valleys are covered with eutric gleyic fluvisols.



**Fig. 2.12:** Soil map of the Nasirye Catchment within the Namulonge study site. Data sources: Gabiri (unpublished) (soil, Nasirye Stream), GTK Consortium (2012) (streams) (NA).

#### 2.4.4 Hydrogeology and hydrology (NA)

The region north of Kampala belongs to the Kyoga Basin, the second biggest drainage sub-basin in Uganda (Nsubuga et al. 2014). Lake Kyoga is the third biggest lake in Uganda and is drained by the Kyoga Nile flowing into Lake Albert (Nsubuga et al. 2014). Wetlands cover around 13 % of Uganda's surface (NEMA 2004), with highest densities in the Kyoga Basin. However, wetland coverage in Kyoga Basin declined by 27 % from 1994 to 2008 (Nsubuga et al. 2014). Although it is known that wetlands in Uganda hold an important amount of freshwater and their coverage is decreasing, the hydrology of wetlands in Uganda is not well documented and understood (NEMA 2008).

All streams in the study site drain into Lwajali River, a tributary of a huge floodplain wetland being connected to Lake Kyoga in the north. The Nasirye Catchment covers an area of 33.2 km<sup>2</sup> (earthexplorer.usgs.gov). The valley of Nasirye Catchment is characterized as a seasonal wetland (WRI 2009). This wetland is drained by the Nasirye Stream. The straight course of the stream indicates that it is an artificial stream, dug to drain the wetland. Nasirye Stream originates in the northwest of the catchment and flows to the southeast, where it finally flows into Lwajali River. All other streams in the study site drain valley bottom wetlands as well. Nasirye Stream is perennial, with variable discharge volumes. Within the lower catchment, the stream shows a maximum width of 3 m and a maximum depth of 2 m (personal communication with local population 2015). Stream water is used to irrigate surrounding fields in the valley bottom. Due to changing field positions, artificial tributaries are regularly constructed by small-holder farmers (personal communication with local population 2015).

Groundwater development in Uganda started in the 1930s and currently, groundwater is the main drinking water source (Tindimugaya 2005, Nsubuga et al. 2014). It is planned to increase the amount of people being supplied by groundwater in future (Tindimugaya 2005). Nevertheless, hydrogeological knowledge is often missing, making sustainable groundwater management difficult (Nsubuga et al. 2014). Within Wakiso District, approximately 33 % of the population is served by five groundwater based pumped piped water supply schemes, while the other 67 % is served by point water sources (MWE 2010). Those point water sources are represented by more than 3,500 shallow hand pumping wells (MWE 2010). Within the study site, hand pumping wells are found as well as electrical pumping wells.

No hydrogeological studies exist for the study site in particular. However, the hydrogeology of Uganda has been studied on regional and local scales by several authors (Taylor and Howard 1999, Kulabako et al. 2007, Owor et al. 2011). As Uganda is mainly located on crystalline rocks, groundwater resources are in general poor and limited to fractured areas (NEMA 2008). However, these crystalline rock aquifers are usually suitable for small scale water supplies (Howard et al. 1992). Moreover, the weathering profile, covering wide areas of crystalline rocks in Uganda, represents an aquifer as well (Chilton and Foster 1995). Additionally, with annual rates between 90 and 220 mm, groundwater recharge in Uganda is quite high compared to abstraction rates (NEMA 2008).

Water quality of both, surface water and groundwater, have been deteriorating in many parts of Uganda, due to increasing urbanization, population growth, and anthropogenic activities (NEMA 2008). While groundwater quality is still acceptable in general, especially with respect to inorganic water quality, it shows sometimes high amounts of aluminum, chloride, iron, manganese, nitrate, and zinc (NEMA 2008). High concentrations of iron, manganese, and zinc are often related to corroded pipes, but they can also be derived from aquifer weathering. With that regard, quality of saprolite aquifers is usually better than that in the fractured crystalline rocks (NEMA 2008). Increased concentrations of chloride and nitrate are often related to sewage influence. If water has objectionable characteristics, such as discoloration due to iron, users often reject the water and resort to unprotected sources such as surface water (NEMA 2008). Another important factor regarding groundwater quality is organic contamination, because during a national water quality survey in 2007 only 41 % of all sampled water points were free of faecal bacteria (NEMA 2008).

#### **2.4.5 Vegetation, land cover, and land use (NA)**

The area north of Kampala is characterized by a gradient from urban to rural areas. Today, the study site is located in the rural areas, but the big settlement agglomeration of Kampala grows continuously. In the study site itself, only small villages are found, with Namulonge Village being the main trading center. Some areas of the study site, especially the lower Nasirye Catchment, are part of a research site of the National Crop Resources Research Institute (NACRRI), which seeks to develop varieties and agricultural management options to improve Uganda's food security (Nsubuga et al. 2011). Most of the people living around Namulonge Village are either current or past employees of the research institute.

Potential natural vegetation in the region around the study site is dominated by rainforests and woodlands (Lind and Morrison 1974, Lillesø et al. 2011). In the valley bottoms, the wetlands, swamp forests and papyrus marshes are common (Lind and Morrison 1974, Denny 1993). However, actual vegetation is governed by agricultural use and natural vegetation solely occurs in small patches. Huge parts of the study site are used for agricultural production. In the uplands, vegetables such as maize, cassava, and sweet potatoes are grown, while in the wetlands, mainly rice, taro, and sugarcane are cultivated. Never-

theless, the variety of agricultural crops is high and several other crops are found as well. Agricultural fields often belong to the NACRRI research site, but outside the station also smallholder farmers cultivate fields for subsistence farming. An additional use of wetlands in the area north of Kampala is the production of bricks from wetland clay.

### 3 Current state of research

This section gives an overview of the current state of research. Firstly, an overview of previous research activities and outcomes about hydrogeology and water quality in wetlands is outlined. The focus is given to floodplains and valley bottom wetlands. Secondly, the general hydrogeology of weathered crystalline rock aquifers in tropical Africa is addressed, including processes of silicate weathering. A basic understanding of silicate weathering is necessary to interpret collected data in this study.

#### 3.1 Hydrogeology and wetlands

The important role of hydrogeology in wetland research has been recognized by many authors (e.g. Hollands 1987, Winter and Llamas 1993, Woessner 2000, Seelig and DeKeyser 2006, Acreman and Miller 2007, Lazareva and Pichler 2011, Fig. 3.1). Hollands (1987) summarized that groundwater may

- be recharged by wetlands,
- discharge to wetlands,
- flow through wetlands, and
- evaporate from wetlands.

Many wetlands are mainly groundwater fed and their wetness results from constant groundwater influxes (Winter and Llamas 1993). Other wetlands are only little or not influenced by groundwater, as their soils are almost impermeable, preventing groundwater recharge or discharge (Mitsch and Gosselink 2007). Interaction processes between groundwater and surface water in wetlands have been assessed by many authors worldwide (e.g. Siegel 1988, Kehew et al. 1998, McCarthy 2006, Sikdar and Sahu 2009). Most of these studies showed that recharge and discharge zones of groundwater within wetlands are very variable in space and time (Shedlock et al. 1993, Hunt et al. 1996). Furthermore, it was shown that interactions between wetlands and groundwater strongly influence structure and functions of wetlands' ecosystems (McCarthy 2006, Hunt et al. 2006).

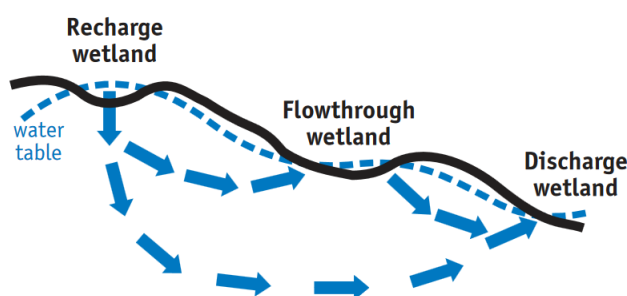


Fig. 3.1: Relations between groundwater and wetlands (Seelig and DeKeyser 2006).

A wide range of methods has been conducted including water balance estimations (Hunt et al. 1996), hydrochemistry (Kehew et al. 1998, Nasir and Harikumar 2012), stable water isotopes (Clay et al. 2004, Sikdar and Sahu 2009), water level measurements (Devito et al. 1996, Hunt et al. 2006), and numerical modeling (Kazezyilmaz-Alhan et al. 2007). It is widely accepted that a combination of different methods is required in order to obtain valuable results. For instance, King et al. (2014) outlined the importance of linking three-dimensional geological models with multivariate statistical analyses of hydrochemical data. In wetlands, hydrochemical analyses should be used to supplement water table measurements, in order to delineate areas of groundwater recharge and discharge (Kehew et al. 1998). Additionally, tracer-based assessments should integrate isotopes as well as hydrochemistry, because most hydrogeological situations are too complex to be easily explained with single-tracer approaches (Herczeg and Edmunds

2000). In any case, it becomes clear that the hydrogeology of wetlands is never simple and should always be assessed site specific, even for wetlands with similar vegetation (Devito et al. 1996). Hollands (1987) emphasized that many data from multi-disciplinary investigations are required to accurately predict groundwater processes within a wetland. If these data are lacking, it will be necessary to collect a sound dataset, in order to describe the groundwater flow regime and its interaction processes with wetland water.

Comparatively few studies exist for East African wetlands (e.g. Owor et al. 2011). Moreover, the lack of hydrogeological data for most East African regions impedes general conclusions about wetland hydrogeology, and the variety of open research questions is large. Several wetland classification schemes are based on groundwater related decision schemes (e.g. Acreman and Miller 2007). Classifying wetlands based on their hydrogeology is important to understand the effects of hydrology on wetland functions (Hollands 1987). For instance, Acreman and Miller (2007) classified wetlands primarily based on landscape locations and secondarily based on water transfer mechanisms. They stated that secondary types are difficult to determine, because knowledge about the contribution of groundwater to wetlands is often lacking and hard to obtain. A more simplified classification scheme was provided by Kotze et al. (2012), as it solely refers to hydrogeomorphic characteristics that are easy to identify.

The variety of classification schemes makes it difficult to review research studies related to floodplains and valley bottom wetlands, as those types can include almost all freshwater wetlands. Thus, the following differentiation between research on floodplains and valley bottom wetlands should be regarded with caution and some information are valid for both wetland types.

### **3.1.1 Floodplains**

Due to their high ecological importance, floodplains are of great interest in research. A lot of ecological and hydrological functions of floodplains strongly rely on interaction processes between groundwater and surface water (Stanford and Ward 1993, Butturini et al. 2002, Hayashi and Rosenberry 2002). Surface water in wetlands includes stream water as well as flooding water. In general, groundwater in floodplains flows downstream (Woessner 2000). This flow direction is interrupted by flows perpendicular to the stream, induced by interaction processes between groundwater and stream or flooding water (Fig. 3.2). Those interactions occur on floodplain scale as well as on stream scale (Woessner 2000). The part of the floodplain, where interaction processes occur and thus, where water originates from both the aquifer and the stream channel, is called hyporheic zone (Hinkle et al. 2001). However, no clear definition of this zone exists between different disciplines, such as hydrogeology, biology, and geochemistry (Woessner 2000). As it was proposed that the size of the hyporheic zone increases with increasing stream order (White 1993), hyporheic zones play an important role in large floodplains (Hinkle et al. 2001).

The stream of a floodplain may show gaining as well as losing or even through-flow conditions (Fig. 3.2). Interaction processes are related to connectivities between stream bed and aquifer. These are determined by the geology of the respective aquifer including its hydraulic properties in the vicinity of the stream (Winter 1999, Woessner 2000). Additional important factors are the geometry of the stream channel during low flow conditions and the geometry of the floodplain during flooding events. Furthermore, the degree to which interaction processes occur depends on hydraulic head gradients between surface water and groundwater (Sophocleous 2002). Inundation of floodplains results from different water sources (Mertes 1997). Flooding events are often induced by overland flow, which is defined as water flowing over the ground as laminar sheet flow (Rassam et al. 2009). This overland flow, which

results from over-bank flow of stream water, may become important for groundwater recharge, when filling depression storages (Rassam et al. 2009). While in some cases over-bank flow inundates dry floodplains, in other cases the floodplain is already saturated before over-bank flow occurs (Mertes 1997). This saturation may be induced by precipitation, hillslope seepage, or rising groundwater levels (Mertes 1997). Hence, flooding water can be derived from several sources, such as groundwater, stream water, or precipitation.

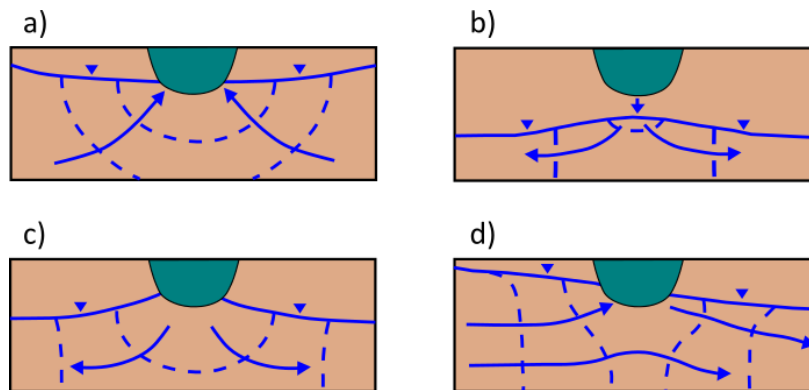


Fig. 3.2: Groundwater-surface water interactions in floodplains, showing channel cross sections with a) gaining stream, b) and c) losing stream, and d) groundwater through-flow (modified after Woessner 2000).

A wide range of studies has been conducted on floodplains all over the world. Measurement and evaluation of water levels are widely accepted methods to assess interactions in floodplains (Jung et al. 2004, Kaplan et al. 2010). Hydrochemical and isotopic methods have been conducted as well (Königer et al. 2001, Lambs 2004, Nyarko et al. 2010). A combination of both methods was applied by Lamontagne et al. (2005). Furthermore, numerical modeling has been used to understand flow processes between streams, flooding water, and groundwater in floodplains (Bates et al. 2000, Krause et al. 2007, Rassam et al. 2009).

Bates et al. (2000) and Jung et al. (2004) studied interactions between groundwater and surface water in a floodplain in the United Kingdom. They showed that interaction processes in floodplains are influenced by flooding events as well as by hillslope seepage. During flooding events, a groundwater ridge is formed below the floodplain, which hampers the inflow of groundwater from the hillslope for some time (Jung et al. 2004). However, during low flow conditions, hillslope groundwater flows into the floodplain and discharges to the stream. Bates et al. (2000) set up a numerical model of the flow within the floodplain during a flooding event. It was concluded that unsaturated zone hydrology is relatively insignificant, and that groundwater movement during flooding events is mainly a two-dimensional lateral process, perpendicular to the river.

Krause et al. (2007) showed that interactions in floodplains are variable in space and time. The hydraulic gradient between surface water and groundwater of the floodplain changes, due to fluctuations of surface water levels or the higher water retention capacity in some parts of the floodplain. They stated that it is not appropriate to evaluate exchange fluxes by annual net balances, because temporal and spatial dynamics of interactions need to be considered as well. This variability is also necessary to be displayed, when assessing the impact of interactions on the ecosystem.

### 3.1.2 Valley bottom wetlands

Valley bottom wetlands are found all over the world and their hydrogeology has been assessed by several authors (e.g. Devito et al. 1996, Clay et al. 2004). In Sub-Saharan Africa, several local names for valley bottom wetlands exist, such as *dambos*, *mbugas*, *bas-fonds*, and *vleis* (Rodenburg 2013, von der



Heyden 2004). Following Rodenburg (2013), there are three major morphological types of valley bottom wetlands depending on the rainfall intensity in the respective region. The Namulonge study site belongs to the type of concave valleys, which are mainly found in zones with intermediate rainfall between 1100 and 1400 mm (Fig. 3.3). Those valley bottom wetlands are usually located between adjacent side slopes, which are often referred to as interfluves.

In literature, the most frequent term for valley bottom wetlands of tropical and subtropical Africa is *dambo*. *Dambos* are defined as seasonally saturated channel-less valley floors, and are found throughout central and southern Africa (Mahan and Brown 2007). They often retain marginal seepage zones in dry seasons, when the central valley is already no longer waterlogged (McFarlane 1989). *Dambos* are usually associated with crystalline rocks and their characteristic weathering profiles (von der Heyden 2004). However, they may also develop on carbonate rocks, as observed in Zambia (Smith 1985). Hence, they are not strongly related to lithology. Although many authors stick to the definition that *dambos* are stream-less, McFarlane (1989) stated that some of them might have streams, indicating a first stage of *dambo* destruction. Considering different definitions and descriptions of *dambos*, the wetland in the Namulonge study site might be considered a *dambo*-like wetland as well. This is confirmed by the proposed spatial distribution of *dambos* covering huge parts of Uganda (Acres et al. 1985).

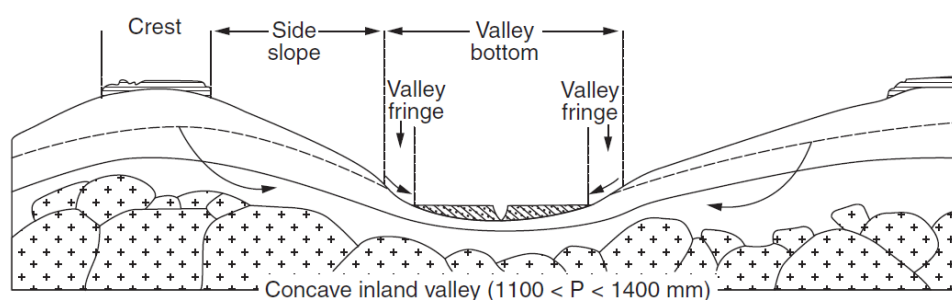


**Fig. 3.3:** Schematic cross section of a valley bottom wetland that developed on granite in West Africa (Rodenburg 2013).

The hydrology of *dambos* has been assessed in many African regions (e.g. Balek and Perry 1973, Faulkner and Lambert 1991, Bullock 1992a, McCartney et al. 1998). Nevertheless, little consensus has been reached so far on the hydrological functions of *dambos*, as outlined in several review studies of *dambos* and their hydrology (Boast 1990, Bullock 1992b, von der Heyden 2004). Although some authors assessed and reviewed the hydrogeology of *dambos* as well (McFarlane 1989, McFarlane 1992, McCartney and Neil 1999, von der Heyden 2004), it becomes obvious that only little is known about the contribution of groundwater to *dambos* in terms of groundwater-surface water interactions (von der Heyden 2004). Several studies determined major sources of water input to *dambos*. Thereby, four primary sources have been identified so far (Bullock 1992b),

- direct precipitation onto the *dambo* surface,
- subsurface flow from the interfluves,
- overland flow from the interfluves, and
- over-bank flow from stream channels.

Some studies tried to identify one of these sources as the major contribution to *dambo* water. For example, McCartney (2000) identified direct precipitation onto the *dambo* surface as the major water source in a *dambo* of Zimbabwe based on water budget estimations. Those inputs of precipitation are usually proportional to the size of the *dambo* within the catchment. In contrast, McFarlane (1992) considered subsurface flow as the dominant water input to the *dambo*. Surface and subsurface runoff are

related to relief and soil characteristics (von der Heyden 2004). The contribution of groundwater to dry season flows is determined by aquifer structure and properties (von der Heyden 2004). Bullock (1992b) stated that most of the studies about *dambo* hydrology did not present geological background or hydrogeological data to support their conclusions. In addition, comparatively few studies on *dambos* and *dambo*-like wetlands have been conducted in Uganda (Taylor and Howard 1996, Mahan and Brown 2007).

In former times, *dambos* in general were believed to act as regulators or “sponges”, storing water collected in rainy seasons and releasing it slowly during dry seasons (e.g. Debenham 1948, von der Heyden 2004). This was shown in different studies by an increase in dry season flows induced by *dambos* (Balek and Perry 1973). Nevertheless, this hydrological function has been questioned during the last decades (Bullock 1992b). It was rather proposed that dry season stream discharge in *dambos* is mainly derived by groundwater of the saprolite beneath the *dambo* (McFarlane 1989). Bullock (1992a) showed that *dambos* in Zimbabwe did not significantly affect stream flows. Again, this outlines the lack of comparable data and hints at different hydrological behaviors in different sites due to variable factors, such as climate, geology, and vegetation (von der Heyden 2004). Furthermore, *dambos* vary in terms of morphology, soil, and channel characteristics, leading to different hydrological characteristics (Bullock 1992b). Conclusions about *dambo* hydrology often rely on the assumed hydrogeological conceptual model, which strongly varies depending on the considered literature (von der Heyden 2004).

Most hydrogeological model concepts of *dambos* assume a low permeability layer close to the *dambo* soil surface. *Dambo* soils themselves usually show low permeabilities as well, due to the accumulation of clays (Bullock 1992b). Therefore, they often form an impermeable barrier layer, preventing vertical exchange of water between the *dambo* and the underlying saprolite. This feature is responsible for the waterlogged conditions of *dambo* soils (Bullock 1992b). Following McFarlane (1992), the geological formation of *dambos* is strongly related to the two processes of deep weathering and stripping on weathered crystalline rocks (section 2.4.2, Taylor and Howard 1998). McFarlane (1992) outlined two formation models of *dambos* in Malawi, based on two different hypotheses concerning the origin of the African erosion surface (Fig. 3.4).

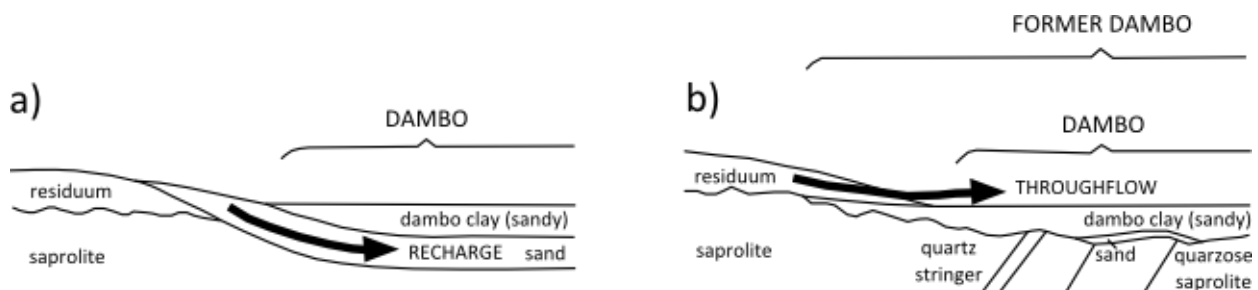


Fig. 3.4: Schematic cross sections of a valley bottom wetland referring to two different formation models, a) pediplanation model (stripping) and b) etchplanation model (deep weathering) (modified after McFarlane 1992).

The first hypothesis suggests that the relief developed due to erosion caused by surface runoff. This process is known as stripping and associated with the process of pediplanation. The second hypothesis explains the relief by differential leaching or etchplanation, which is mainly induced by infiltrating water. The weathered crystalline rock collapses and forms a blanket that is locally redistributed to even out the irregularly lowered surface. The residual material migrates downslope towards the bottomlands. The pediplanation model defines *dambos* as ancient river systems that were excavated, due to surface runoff, and filled with alluvial sediments. Those sediments usually show a fining-upwards sequence, due to progressively reduced flow energy. The etchplanation model defines *dambos* as bottomlands of the

surface, which was irregularly lowered by differential leaching. In this case, fining-upwards is induced by groundwater flow below the *dambo* clay. Both models evoke different hydrogeological scenarios (Fig. 3.4). The pediplanation model allows direct surface runoff from the slopes to recharge the groundwater in the *dambo* sediments. This recharge is prevented in the etchplianation model. However, a combination of both processes in the formation of *dambos* is possible as well.

### 3.2 Water quality and wetlands

Wetlands in general provide water purification functions being efficient at removing nutrients from surface water (Fisher and Acreman 2004, Verhoeven et al. 2006). This is of major concern, because today many river basins are highly impacted by nutrient enrichment due to agricultural production (Verhoeven et al. 2006). Furthermore, other anthropogenic sources, such as waste water discharges, and even natural sources result in inflows of pollutants to wetlands (Hemond and Benoit 1988). Several inorganic water constituents may be affected by agricultural activities, such as nitrogen, phosphorous, and sulfur (Böhlke 2002). However, other elements, such as iron, manganese, and other heavy metals, are of concern regarding water quality as well (Seelig and DeKeyser 2006).

Water purification functions of wetlands include many different biogeochemical processes (Hemond and Benoit 1988). These processes are complex and wetlands cannot be considered as pollutants sinks, in general. They rather act as short- or long-term storage reservoirs and sometimes even as sources for pollutants (Hemond and Benoit 1988). Additionally, wetlands can act as transformers of chemicals (Mitsch and Gosselink 2007). The most important processes of water quality improvement in wetlands include high sedimentation rates, uptake of nutrients by plants, retention of nutrients in soil, and removal of nitrate ( $\text{NO}_3^-$ ) due to enhanced denitrification (Hemond and Benoit 1988, Johnston 1991, Fisher and Acreman 2004). However, these processes vary in magnitude and reversibility, depending on the wetland type (Johnston 1991). In terms of groundwater, low permeable wetland soils can additionally prevent polluted surface water from entering aquifers below wetlands (Hollands 1987).

A lot of research has been conducted on the issue of water purification in wetlands (Fisher and Acreman 2004, Seelig and DeKeyser 2006). The focus was given to artificial or natural treatment wetlands that are constructed and/or used to remove pollutants from wastewater (e.g. Schreijer et al. 1996, Spieles and Mitsch 2000, Nahlik and Mitsch 2006, Khan et al. 2009). Many authors focused on nitrogen and phosphorous, as these are of major concern regarding agricultural pollution and eutrophication of surface waters (Phipps 1997, Spieles and Mitsch 2000, Hogan et al. 2004, Nahlik and Mitsch 2006). The removal of heavy metals by wetlands was studied as well (Cheng et al. 2002, Khan et al. 2009, Laing et al. 2009). The status quo of water quality in wetlands depends on much more factors than water purification, such as the water quality of inflows, water-rock interactions, and others (Mitsch and Gosselink 2007).

The use of wetlands for water treatment can lead to drastic changes in ecosystem functions and biodiversity, if a critical threshold of nutrient inflow is surpassed (Verhoeven et al. 2006). In extreme cases, the wetland may even lose its water purification functions (Osbourne and Totome 1994, Verhoeven et al. 2006). Another disadvantage related to nutrient removals by wetlands is the enhanced emission of the greenhouse gas  $\text{N}_2\text{O}$  due to incomplete denitrification (Verhoeven et al. 2006). Hemond and Benoit (1988) stated that negative impacts of water quality functions in wetlands are often cumulative and interact with each other.

A lot of water purification functions are related to anaerobic conditions, which prevail in wetlands due to waterlogged conditions of the soil (Fisher and Acreman 2004). Wetland soils and their solution usually become depleted in oxygen, leading to reduced conditions several hours to a few days after inundation

started (Mitsch and Gosselink 2007). However, a small layer on top of the soil often remains oxidized. Several elements become reduced with decreasing redox potential (Tab. 3.1). Regarding redox-sensitive species, it needs to be considered that measured redox potentials in the field do often not reflect the real redox state of a system (Appelo and Postma 2005).

**Tab. 3.1: Oxidized and reduced forms of several elements and approximate redox potentials for transformation (Mitsch and Gosselink 2007).**

Element	Oxidized Form	Reduced Form	Approximate Redox Potential for transformation (mV)
Nitrogen	NO <sub>3</sub> <sup>-</sup> (nitrate)	N <sub>2</sub> O, N <sub>2</sub> , NH <sub>4</sub> <sup>+</sup>	250
Manganese	Mn <sup>4+</sup> (manganic)	Mn <sup>2+</sup> (manganous)	225
Iron	Fe <sup>3+</sup> (ferric)	Fe <sup>2+</sup> (ferrous)	-100 – 100
Sulfur	SO <sub>4</sub> <sup>2-</sup> (sulfate)	S <sup>2-</sup> (sulfide)	-200 – -100
Carbon	CO <sub>2</sub> (carbon dioxide)	CH <sub>4</sub> (methane)	< -200

In order to outline water purification functions as well as transformation processes in wetlands, the most important elements and their cycles in wetlands are outlined in the following sections. Furthermore, general dissolution and precipitation processes of the elements are discussed.

### 3.2.1 Nitrogen

Nitrogen (N) is one of the most important elements in terms of agriculture and water quality. In wetlands, it can be removed during the accumulation by plants, sedimentation, and denitrification (Hemond and Benoit 1988). Thereby, denitrification is the only process, which completely removes N from the system, while the other two processes only have a temporal effect (Hemond and Benoit 1988). During denitrification, anaerobic bacteria use nitrate (NO<sub>3</sub><sup>-</sup>) as an electron acceptor in respiration. This leads to a reduction of NO<sub>3</sub><sup>-</sup> to gaseous N<sub>2</sub>O or N, which is released to the atmosphere (Hemond and Benoit 1988). This process occurs at redox conditions below 250 mV (Mitsch and Gosselink 2007). In contrast, the accumulation of N by plants is not limitless and only temporary, because N may be returned to solution when plants decompose again (Hemond and Benoit 1988).

### 3.2.2 Phosphorous

Comparable to nitrogen, phosphorous (P) is added to water by agricultural production. Wetlands were found to remove P from water during sedimentation, plant uptake, microbial immobilization, and adsorption or precipitation (Hogan et al. 2004). In general, the retention of soluble P is less efficient than the retention of particulate P (Fisher and Acreman 2004). Dissolved phosphate (PO<sub>4</sub><sup>3-</sup>) is adsorbed by hydrous iron- and aluminum-oxides or clays by ion exchange (Hemond and Benoit 1988). Thereby, aluminum may be more efficient in removing P than iron, because iron-bound P may be released under anoxic conditions (Hogan et al. 2004). Additionally, P can also precipitate as iron-, aluminum-, or calcium-phosphate (Hemond and Benoit 1988).

### 3.2.3 Sulfur

Transformation processes within the sulfur cycle in wetlands are usually biologically mediated and depend on pH and redox conditions (Faulkner and Richardson 1989). Under oxidizing conditions, assimilatory sulfate (SO<sub>4</sub><sup>2-</sup>) reduction, inorganic sulfide (S<sup>2-</sup>) and elemental sulfur (S) oxidization, and mineralization of organic S to inorganic SO<sub>4</sub><sup>2-</sup> occur. In contrast, under reducing conditions, dissimilatory SO<sub>4</sub><sup>2-</sup> reduction is the dominant process. Assimilatory SO<sub>4</sub><sup>2-</sup> reduction can occur under aerobic and anaerobic conditions. During this process, SO<sub>4</sub><sup>2-</sup> is reduced to S<sup>2-</sup>, which is needed for the biosynthesis of sulfur-containing amino acids (Schiff and Fankhauser 1981). This type of SO<sub>4</sub><sup>2-</sup> reduction can be induced by

plants and nearly all bacteria. For instance, assimilatory  $\text{SO}_4^{2-}$  reduction is known to be of great importance for rice nutrition (Lefroy et al. 1992). During dissimilatory  $\text{SO}_4^{2-}$  reduction, which is induced by strictly anaerobic bacteria,  $\text{SO}_4^{2-}$  is reduced to hydrogen sulfide ( $\text{H}_2\text{S}$ ). Conditions with redox potentials below -100 mV are necessary for the dissimilatory reduction of  $\text{SO}_4^{2-}$  (Mitsch and Gosselink 2007). In wetlands, this process mainly occurs in the soil and subsoil, where reducing conditions are dominant, induced by soil saturation and flooding (Faulkner and Richardson 1989). However, redox conditions of wetland soils are highly variable ranging from aerobic to anaerobic (Faulkner and Richardson 1989). Furthermore, the identity of  $\text{SO}_4^{2-}$ -reducing bacteria in wetlands is largely unknown (Pester et al. 2012). According to Faulkner and Richardson (1989), many wetlands act as S sinks. However, the long-term removal of S by wetlands depends on anaerobic, reduced conditions, storage in organic forms, and volatilization as S gases. If, for instance, the soil becomes aerobic during dry seasons, reduced S will be oxidized to  $\text{SO}_4^{2-}$ , which might then be flushed away from the wetland system by rainfall events.

### 3.2.4 Iron, manganese, and other heavy metals

The dissolution of iron-bearing minerals, such as amphiboles and pyroxenes, occurs under reducing conditions (Hem 1985). Under oxidizing conditions the dissolved iron precipitates as iron (hydr)oxides (Appelo and Postma 2005). Moreover, iron will be precipitated as pyrite or marcasite under reducing conditions, if sulfur is available (Hem 1985). Manganese acts similar to iron (Hem 1985). However, it is more stable towards oxidation than iron (Tab. 3.1).

In general, wetlands are assumed to act as sinks for heavy metals by removing them from water, due to adsorption on organic or mineral matter (Hemond and Benoit 1988). This capacity is strongly related to the respective element and the type of wetland. The sorption of heavy metals is enhanced by high pH values and oxidizing conditions (Hemond and Benoit 1988). For instance, iron and manganese precipitate as hydr(oxides) under oxidizing conditions, removing these elements from solution. Under reducing conditions, these metals become reduced and get into solution (Tab. 3.1). Dissolved organic material can increase the solubility of iron. Furthermore, most heavy metals are removed from water and sediments by the uptake of wetlands plants (Khan et al. 2009).

### 3.3 Hydrogeology of weathering profiles above crystalline rocks

Hydrogeology and water quality of wetlands in East Africa are impacted by the hydrogeology of weathered crystalline rock aquifers (section 2.2.2). In general, the process of weathering in crystalline rocks leads to a change in their hydraulic properties, such as hydraulic conductivity, porosity, and specific yield (Chilton and Foster 1995). While the weathering of primary minerals tends to increase hydraulic conductivity and specific yield, the subsequent formation of secondary clay minerals tends to reduce them by sealing fractures and pores (Wright 1992). Sometimes, even dissociation of kaolinite can occur, again leading to an increase of hydraulic properties. In this case, solely quartz sand is left after weathering (Chilton and Foster 1995). As the matrix of the crystalline rock is completely destroyed during weathering, the whole weathering profile shows rather a porous character than a fractured (Fass 2004). Recharge to weathered crystalline rock aquifers in tropical Africa usually occurs after heavy rainfall events, exceeding a certain threshold (Jasechko and Taylor 2015). Thus, small rainfall events during dry seasons do not contribute to recharge.

A differentiation of upper and lower saprolite is suggested in terms of hydraulic properties (Fig. 3.5, Chilton and Foster 1995). As the proportion of secondary clay minerals is often higher in the upper part compared to the lower part, the upper part has a lower hydraulic conductivity (Chilton and Foster 1995). This differentiation combined with the high hydraulic conductivity of the underlying saprock shows that

lower saprolite together with saprock make up the most permeable part of the weathering profile. This permeable part represents an important aquifer in terms of drinking water supply for rural populations (Wright 1992). However, the fractured crystalline rocks themselves locally represent aquifers as well. One of the major factors controlling permeability development is the type of crystalline rock. Coarse-grained, quartz-rich, crystalline rocks develop weathering profiles with highest permeabilities, whereas schistose, metamorphic rocks and tectonic disturbed zones cause thickest regoliths (Chilton and Foster 1995).

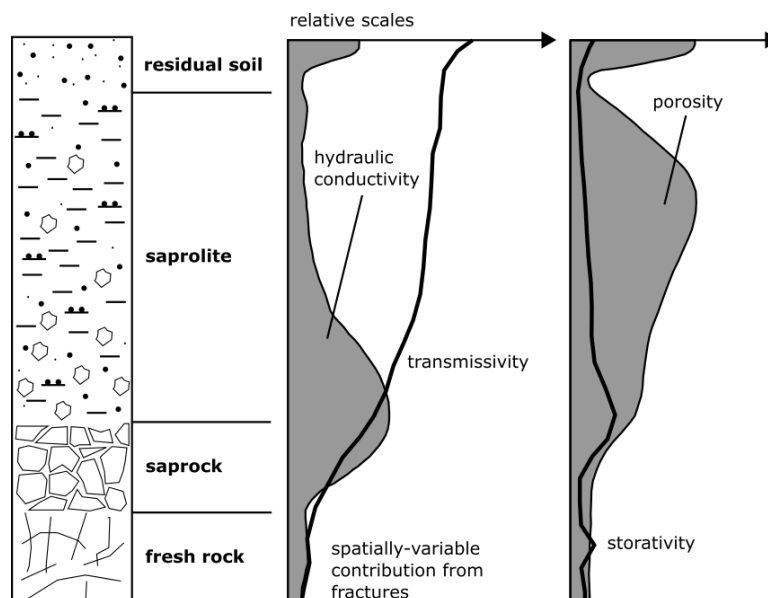


Fig. 3.5: Hydrogeological properties of weathering profiles above crystalline rocks in tropical Africa (modified after Chilton and Foster 1995).

### 3.3.1 Silicate weathering

In tropical Africa, the development of weathering profiles above crystalline rocks and the chemistry of groundwater within these aquifers are both strongly linked to silicate weathering. This chemical weathering of silicate minerals is related to the thermodynamic conditions at the earth's surface, which differ from those conditions that existed during the formation of such minerals (White and Brantley 1995). Higher temperatures and the abundance of water in tropical regions enhance silicate weathering processes (Tardy et al. 1973). Silicate weathering on a global scale is of concern, as it controls global climate over long time scales acting as a sink of atmospheric  $\text{CO}_2$  (West et al. 2005).

Although all silicate weathering reactions consume  $\text{H}^+$  and thus provide a pH-buffer, groundwater in silicate aquifers is vulnerable to acidification due to the slow dissolution rates of silicate minerals (Appelo and Postma 2005). Compared to carbonate weathering, silicate weathering is a very slow process resulting in gradual changes in hydrochemistry. The process of silicate weathering leads to incongruent dissolution, meaning that the ratio of elements in the solution is not consistent with the ratio of elements in the dissolved mineral (Appelo and Postma 2005). This is caused by slow dissolution of primary minerals and by precipitation of secondary minerals. Those secondary minerals, represented by clay minerals and iron (hydr)oxides, form during silicate weathering, due to the insolubility of aluminum and iron (Appelo and Postma 2005). Their formation leads to an accumulation of iron and aluminum in the weathering profile.

Different silicate minerals show different susceptibilities to chemical weathering following the weathering sequence of Goldich (1938) (Fig. 3.6). This sequence is the reverse sequence of the Bowen reaction

series, predicting the precipitation of minerals cooling from basaltic magma. The differences in weatherability are directly linked to number and weakness of cation links between silicate tetrahedras in minerals (Okrusch and Matthes 2014). Weatherabilities decrease with higher charges and increase with bigger sizes of cations (Scheffer and Schachtschabel 2010). Quartz is relatively unaffected by chemical weathering. While K-feldspars and muscovites are also quite resistant to weathering, plagioclases, biotites, amphiboles, pyroxene, and olivines react readily.

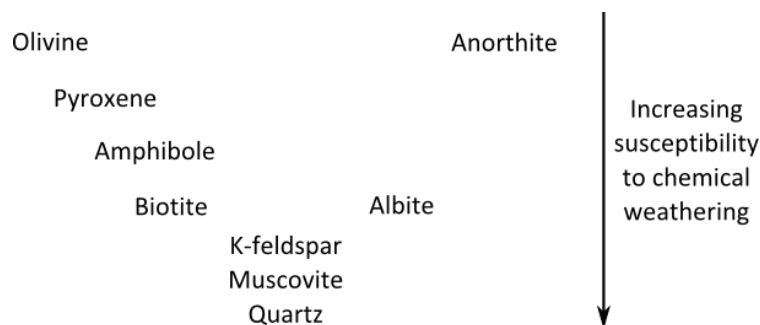
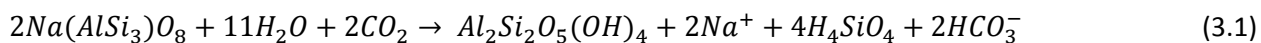


**Fig. 3.6: Weatherability (susceptibility to chemical weathering) of silicate minerals (modified after Goldich 1938).**

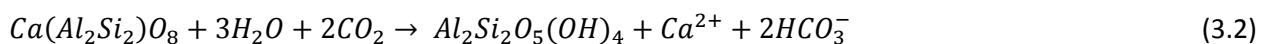
The dissociation of primary silicate minerals to weathering products is usually irreversible at temperatures less than 50°C (Steffánsson and Arnórsson 2000). Thus, primary silicate minerals are dissolved, while secondary clay minerals precipitate at the same time. While primary silicate minerals dissolve quite slowly limited by kinetics, the precipitation of secondary weathering products is faster and often approaches equilibrium (Helgeson et al. 1969). This shows that the dissolution kinetics of the primary silicate minerals are overall rate limiting in the weathering process. The most common secondary clay minerals that form during silicate weathering are kaolinite, illite, montmorillonite, and gibbsite (Appelo and Postma 2005). Which clay mineral precipitates depends on hydrological conditions and on the type of rock (Appelo and Postma 2005). Montmorillonite is more likely formed in dry climates, where water has longer residence times and thus becomes higher concentrated. In contrast, gibbsite forms preferentially under tropical conditions, where leaching is intense due to high amounts of rainfall. Here, gibbsite and other aluminum-hydroxides may even form bauxites (Scheffer and Schachtschabel 2010). Furthermore, basic rocks are more reactive than granitic rocks and thus support the formation of montmorillonite compared to gibbsite and kaolinite (Appelo and Postma 2005). The secondary clay minerals remain quite stable during erosion and transport and are often deposited as coatings on sand grains. Those coatings are often intermingled with iron (hydr)oxides and are important for the ion exchange capacity of the aquifer (Appelo and Postma 2005).

The weathering of silicate minerals usually results in increased concentrations of major cations ( $\text{Na}^+$ ,  $\text{K}^+$ ,  $\text{Mg}^{2+}$ ,  $\text{Ca}^{2+}$ ), silica ( $\text{SiO}_2$ ), and bicarbonate ( $\text{HCO}_3^-$ ) in the solution (Appelo and Postma 2005). Sodium ( $\text{Na}^+$ ) predominantly indicates the weathering of plagioclase (albite). In this case,  $\text{Na}^+$  is not balanced by chloride ( $\text{Cl}^-$ ), as it would be the case, if seawater or evaporates were the sources of  $\text{Na}^+$  (Appelo and Postma 2005). Calcium ( $\text{Ca}^{2+}$ ) is released during the weathering of plagioclase (anorthite), amphiboles, and pyroxenes, and magnesium ( $\text{Mg}^{2+}$ ) is released during the weathering of amphiboles, pyroxenes, and biotite (Appelo and Postma 2005). Potassium ( $\text{K}^+$ ) is usually only present in small amounts, although it is released during the weathering of k-feldspars (Appelo and Postma 2005). The increase of  $\text{HCO}_3^-$  in the solution sometimes even induces precipitation of carbonates (Appelo and Postma 2005). Iron, being present in some silicate minerals, usually forms iron-oxides due to its low solubility (Appelo and Postma 2005). The occurrence of aluminium in the solution is controlled by the solubility of secondary minerals, such as gibbsite and kaolinite.

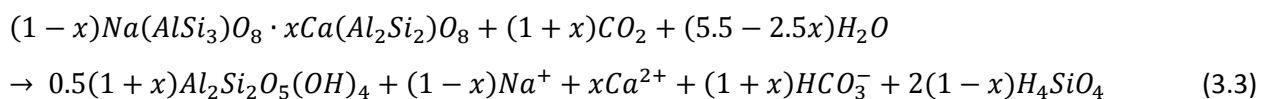
Several specific ion ratios can be deduced from weathering equations of silicate minerals. If, for instance, a pure albite weathers to kaolinite, 1 mol  $\text{Na}^+$ , 1 mol  $\text{HCO}_3^-$ , and 2 mols  $\text{SiO}_2$  will be released to the solution (Appelo and Postma 2005) (Eq. 3.1).



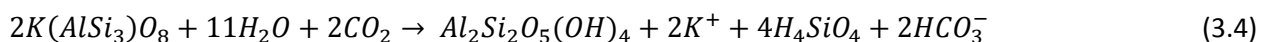
Thus, specific ion ratios in solution are 1 for  $\text{HCO}_3^-/\text{Na}^+$ , and 2 for  $\text{SiO}_2/\text{Na}^+$  and  $\text{SiO}_2/\text{HCO}_3^-$ . During weathering of pure anorthite, 0.5 mol  $\text{Ca}^{2+}$  and 1 mol  $\text{HCO}_3^-$  get into solution, leading to a specific ion ratio of 2 for  $\text{HCO}_3^-/\text{Ca}^{2+}$  (Eq. 3.2).



However, pure end members of plagioclases are usually not present in nature, but solid solutions occur. The reaction equation of a plagioclase, composed of anorthite ( $x$ ) and albite ( $1 - x$ ), that weathers to kaolinite shows that the ratio of  $\text{SiO}_2/\text{Na}^+$  in the solution is 2, while the ratio of  $\text{HCO}_3^-/(\text{Na}^+ + 2\text{Ca}^{2+})$  is 1 regardless of the exact plagioclase composition (Van der Weijden and Pacheco 2007) (Eq. 3.3).



Weathering of Alkali-feldspars, being solid solutions of albite and orthoclase (k-feldspar), leads to specific ion ratios of 1 for  $\text{HCO}_3^-/(\text{Na}^+ + \text{K}^+)$  and 2 for  $\text{SiO}_2/(\text{Na}^+ + \text{K}^+)$  (Eq. 3.1, 3.4) (Appelo and Postma 2005).





## 4 Methods

Available hydrogeological data of the two study sites are very scarce. Hence, a comprehensive methodological approach was applied, in order to answer the introduced research questions (section 1.2). This methodological approach can be divided into four steps:

- 1) Data collection in the field and laboratory analyses
- 2) Interpretation and evaluation of collected data using classical hydrogeological approaches
- 3) Development of hydrogeological conceptual wetland models visualizing and describing the groundwater system, its interactions with surface water, and the mutual effects between agriculture and water quality
- 4) Quantification of origin and hydrochemical evolution processes of flooding water, based on hydrogeochemical modeling

Steps 1 and 2 followed a classical hydrogeological investigation concept (Kovalevsky et al. 2004), including the assessment of three different aspects of the groundwater system:

- a) Aquifer structure
- b) Water dynamics
- c) Water composition

Gained results were summarized in conceptual models (Step 3). In the context of Step 4, mixing and evolution processes of flooding water, described in the conceptual models, were implemented in the hydrogeochemical modeling code *PhreeqC*, in order to verify and quantify these processes.

Throughout the GlobE project, focus is given to the so-called central field trials (CFTs) within the wetlands of both study sites. These CFTs represent the main cropping experiments and are located in three different positions (Ziegler unpublished, Kwesiga unpublished). The three positions are referred to as *center*, *middle*, and *fringe*, and are located along a hydrological gradient across the respective wetland. This gradient is positioned orthogonal to the respective stream draining the wetland. The general assumption is that water availability decreases with distance to the stream from *center* over *middle* to *fringe*. In each CFT, different rice plots with different management options (treatment plots) were set up and cropped throughout the whole project period. Each treatment plot is replicated four times in each CFT. In the context of this study, bigger study sites were assessed to get an overview of the whole wetland system and its boundary conditions. However, some methods were conducted with a focus on the CFTs.

Field work included the installation of piezometers in collaboration with the hydrology research group (Gabiri unpublished). Piezometers were installed along the hydrological gradients of the CFTs in both study sites. Additional piezometers were placed in different locations, depending on the on-site conditions of the respective study site. Several methods, such as drilling surveys, sediment sampling, water level measurements, hydraulic tests, and hydrochemical sampling, were applied at the installed piezometers. Hence, piezometers played a major role in data collection.

In terms of data provision for future research, the spatial distribution of geological and hydrogeological information was summarized and visualized in a GIS-data base (Quantum GIS). Data that were collected as point information were georeferenced in a geographic coordinate system (WGS84). Therefore, locations of sampling points were registered using a GPS device (Garmin Etrex 30). All statistical and mathematical methods were performed using the software MATLAB (Trauth 2015).

#### 4.1 Analysis of aquifer structure and properties

Understanding the geological setting of a study site is the basis for aquifer structure analysis. Therefore, information about the geological settings of the two study sites were gained from a comprehensive literature review, including descriptions of geology and lithology, geological maps, and drilling logs. Subsequently, several geological mappings including drilling surveys were carried out in the context of this study and different master theses (Liedtke 2015, Geißler 2015, Heiß 2016).

Field observations and literature review were used to verify or improve existing geological and geomorphological maps. Additionally, collected information resulted in a closer description of lithological units. Drilling logs were digitized, interpreted, and correlated, in order to understand the three-dimensional geological setting.

In a second step, lithological units were classified into hydrostratigraphic units, based on the type of porosity (porous, fractured) and the respective hydraulic conductivity. Differentiation between aquifer and aquitard was adopted from Fetter (1994), who defined an aquifer as a hydrogeological unit with a lumped hydraulic conductivity greater or equal  $10^{-7}$  m/s. Classification of hydraulic conductivities was assigned based on Hannappel et al. (2003) (Tab. 4.1). Hydraulic conductivities of lithological units were either determined by *in-situ* and laboratory measurements or assigned in comparison with described values of similar rocks in similar environments. According to the three-dimensional geological setting, horizontal aquifer extension was determined based on geological maps and drilling logs. Thicknesses were gained from drilling log analyzes.

All results were visualized in geological and hydrogeological maps, cross sections, and standard sections. Colors of the different geological and hydrostratigraphic units were assigned according to USGS (2005) and Struckmeier and Margat (1995), respectively (Fig. 4.1). Signatures and colors in the digitized drilling logs were assigned according to DIN 4023 (2006).

Tab. 4.1: Classification of hydraulic conductivity following Hannappel et al. (2003) (Klose 2012).

Class of hydraulic conductivity	Hydraulic conductivity [m/s]
very high	$> 10^{-2}$
high	$> 10^{-3} - 10^{-2}$
medium	$> 10^{-4} - 10^{-3}$
moderate	$> 10^{-5} - 10^{-4}$
moderate to low	$> 10^{-6} - 10^{-4}$
low	$> 10^{-7} - 10^{-5}$
very low	$> 10^{-9} - 10^{-7}$
ultralow	$< 10^{-9}$
low to ultralow	$< 10^{-5}$
highly variable	if range of hydraulic conductivities does not fit the other classes

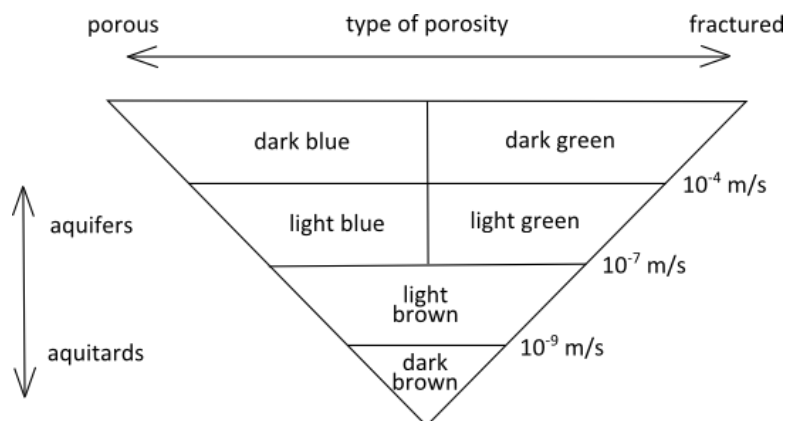


Fig. 4.1: Color scheme for hydrostratigraphic units according to their type of porosity and hydraulic conductivities (modified after Struckmeier and Margat 1995).

#### 4.1.1 Drilling surveys, rock and sediment sampling, and installation of piezometers

Locations of drilling survey points were selected according to the different lithological units within the respective study site, focusing on units that underlie the respective wetland. In order to gain information about the wetlands' underground structure, drilling points were localized along different transects across the wetlands in orthogonal direction to the respective stream. Drilling was conducted with an Edlmann-driller driven by hand. During drilling, depths, thicknesses, textures, colors, and other features of the different layers were determined and documented. Sediment samples were taken during drilling. Hard rocks were described at outcrops and rock samples were taken as well. If possible, all different lithological units were sampled.

Drilling was also conducted in order to install piezometers. Locations and target depths of piezometers were identified by prior drilling, which gave information about the geological structure and texture of layers. Piezometers were placed in all CFTs (*center*, *middle*, and *fringe*) in order to gain results that can be set in a wider context within the GlobE project. Drilling procedures were the same as described above, but protective tubes were used to ensure the stability of drilling logs. Piezometers, which composed of 10 cm diameter PVC pipes with a 1 m filter section at the end covered with filter cloth, were installed in these logs. PVC pipes were put in the log and afterwards fixed with filter sand in the lower part and sealed with bentonite in the upper part. The bentonite is supposed to avoid infiltration of surface or precipitation water along the pipes and hydraulic connections between different aquifers.

#### 4.1.2 Determination of hydraulic conductivities

Hydraulic conductivities of lithological units were determined using different methods. For fractured hard rocks, fracture aperture and spacing were measured in a 1 m<sup>2</sup> scan window at outcrops. Hydraulic conductivity was then calculated following the cubic law (e.g. Cook 2003) (Eq. 4.1).

$$k_f = \frac{(2b)^3}{2B} * \frac{\rho g}{12\mu} \quad (4.1)$$

$k_f$	Hydraulic conductivity [m/s]
$2b$	Fracture aperture [m]
$2B$	Fracture spacing [m]
$\rho$	Density of water [kg/m <sup>3</sup> ]
$g$	Acceleration due to gravity [m <sup>2</sup> /s]
$\mu$	Viscosity of water [kg/ms]

The calculated hydraulic conductivity represents the hydraulic conductivity in fracture direction. For the calculation, a system of separated, identical, plane, and parallel fractures within an impermeable matrix is assumed (Cook 2003).

Hydraulic conductivities of porous unconsolidated sediments were determined at three different scales using grain size distribution analyses (cm-scale), falling-head permeability tests (m-scale), and pumping tests (10 m-scale). Grain size distribution analyses were conducted for several sediment samples that were taken during drilling. The sediment samples were dried for 24 hours at a temperature of 105°C in a drying oven. Subsequently, grain size distribution analysis was performed using dry sieves and laser particle sizer (*Horiba Particia LA-950V2*). Sieving was conducted at the laboratory of the Steinmann-Institute and laser particle sizer measurements were carried out at the laboratory of the Department of Geography, University of Bonn. Hydraulic conductivities were then calculated using the software HydroGeoSieveXL (Devlin 2015). This software calculates hydraulic conductivities based on grain size distributions using several methods. The applicability of each method requires certain restrictions. Hydraulic conductivities based on those methods, for which restrictions were fulfilled, were chosen. For the Ifakara study site values calculated after Hazen (1892) and Beyer (1964) were averaged, while for the Namulonge study site values calculated after Sauerbrey (1932) (In Devlin 2015) were used.

Falling-head permeability tests were conducted at the installed piezometers. These tests are based on the recovery of the water table in a piezometer after changing this water table due to the injection of a volume of water (Chesnaux et al. 2011). Water was injected into the piezometers using a bucket. Afterwards, the change in water level was recorded in certain time steps using an electric contact gauge (Fig. 4.2). Time steps were chosen in relation to the velocity of water level change. The calculated hydraulic conductivity is only valid for the screened part of the aquifer and for the close proximity of the piezometer (Langguth and Voigt 2004).

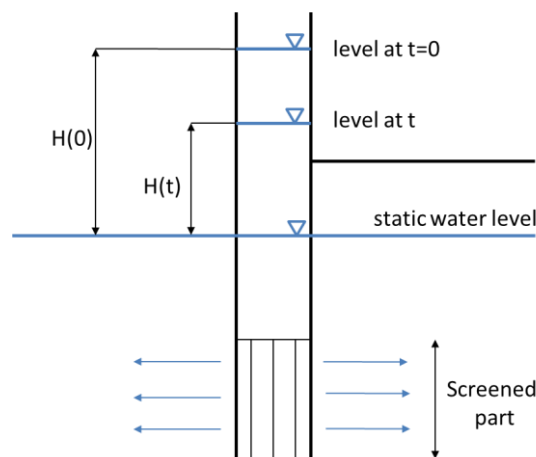


**Fig. 4.2:** Schematic overview of a falling-head permeability test and important parameters.

Hydraulic conductivities were calculated after Hvorslev (1951) (Eq. 4.2).

$$-\frac{Ck_f}{S_{inj}} t = \ln\left(\frac{H(t)}{H(0)}\right) \quad (4.2)$$

C	Shape factor [m]
$k_f$	Hydraulic conductivity [m/s]
$S_{inj}$	Surface of injection (inner surface of the well) [m <sup>2</sup> ]
t	Time [s]
H(t)	Difference of hydraulic head between the water level at time t and the static water level [m]
H(0)	Difference of hydraulic head between the water level at time 0 and the static water level [m]

Therefore, the right side of equation 4.2 was plotted against the time (t) and the slope of the resulting regression line was determined. If the slope (m) is known, hydraulic conductivity can be calculated based on equation 4.3.

$$k_f = -\frac{mS_{inj}}{C} \quad (4.3)$$

$k_f$	Hydraulic conductivity [m/s]
$m$	Slope of the regression line [1/s]
$S_{inj}$	Surface of injection (inner surface of the well) [m <sup>2</sup> ]
$C$	Shape factor [m]

Solely those tests were evaluated, where Pearson's correlation coefficient was 0.95 or higher. The shape factor (C) depends on the shape of the piezometer and its connection to the aquifer. As the piezometers installed in this study have a filter section filled with highly permeable sand, the shape factor of Bouwer and Rice (1976) was used (Eq. 4.4). The radius of influence of the injection was set to 5 m.

$$C = \frac{2\pi L}{\ln\left(\frac{R_0}{r_w}\right)} \quad (4.4)$$

$C$	Shape factor [m]
$L$	Length of the piezometer screen [m]
$R_0$	Radius of influence of the injection [m]
$r_w$	Radius of the piezometer [m]

Transmissivities derived from pumping tests according to Cooper and Jacob (1946) were available for some deep wells (e.g. Krusemann and de Ridder 2000). Hydraulic conductivities of the underground surrounding these wells were calculated based on equation 4.5. Aquifer thickness was adopted from created cross and standard sections and evaluated drilling log data.

$$k = \frac{T}{M} \quad (4.5)$$

$k$	Hydraulic conductivity [m/s]
$T$	Transmissivity [m <sup>2</sup> /s]
$M$	Saturated aquifer thickness [m]

### 4.1.3 Mineralogical and geochemical analyses

Rock and sediment samples were analyzed for their mineralogical and chemical compositions using X-Ray Diffraction Analysis (XRD) and X-Ray Fluorescence Analysis (XRF), respectively. Theoretical descriptions of both methods are given in Moore and Reynolds (1997) and Brouwer (2003). Both methods were carried out at the laboratory of the Steinmann Institute in Bonn. As a first preparation step for both methods, samples were dried at 105°C for 24 hours and grinded using a vibratory disk mill (T250 *Siebtechnik GmbH*) or an agate mortar depending on the available sample volume.

XRD was carried out using a *Bruker AXS D8 Advance* device and the software *MacDiff 4.2.5*. This method is semi-quantitative and allows a determination of the relative mineral content of bulk samples in vol%. Thus, a limit of detection is not given, but values below 5 to 10 vol%, depending on the amount of organic matter and iron, are assumed to be not reliable (personal communication with Dr. S.O. Franz 2015). Some minerals showed similar diffraction patterns, which reflect similar structures. Therefore, they were evaluated in groups (e.g. plagioclases, and k-feldspars).

XRF was carried out using a *PANalytical Axios 3kW* device. This method is quantitative and analyzes the wt%-amount of major and trace elements of a bulk sample. Melted pellets (0.4 g sample + 4 g  $\text{Li}_2\text{B}_4\text{O}_7$ ) were prepared to measure major elements expressed as oxide concentrations and powder pellets (5 g sample + 1 g  $\text{C}_{38}\text{H}_{76}\text{N}_2\text{O}_2$ ) were prepared to measure trace element concentrations. Generally, valid limits of detection are 100 ppm for Na, Mg, Al, Si, and P, 10 ppm for S, K, Ca, Ti, Mn, Fe, and Cl, and 1 ppm for Sc, V, Cr, Co, Ni, Cu, Zn, Ga, Ge, As, Rb, and Sr (Hahn-Weinheimer et al. 1995).

The Loss On Ignition (LOI) was calculated in double determination. The LOI describes the loss of high vulnerable components during the process of ignition. It is determined by measuring the loss in weight of 5 g sample after igniting it for 2 hours at 1100°C. The measured value defines the mass of organic matter, captured water, C, Cl,  $\text{CO}_2$ , F, and S (Heiri et al. 2001).

## 4.2 Analysis of water dynamics

Groundwater dynamics were interpreted based on groundwater level measurements conducted in this study and on historical groundwater level measurements derived from different organizations. Groundwater level measurements were displayed as time series, and piezometric maps were created for different time steps.

### 4.2.1 Groundwater level measurements

Groundwater pressure values were measured on an hourly time resolution by pressure data loggers that were installed in piezometers and hand pumping wells (Fig. 4.3). Based on measured pressure, groundwater level below surface was calculated using equation 4.6.

$$gwI_{bs} = d_s - \frac{(p_m - p_{atm})}{\rho g} \quad (4.6)$$

$gwI_{bs}$	Groundwater level below surface [m]
$d_s$	Depth of sensor below surface [m]
$p_m$	Measured piezometric pressure
$p_{atm}$	Measured atmospheric pressure
$\rho$	Density of water [ $\text{kg}/\text{m}^3$ ]
$g$	Acceleration due to gravity [ $\text{m}^2/\text{s}$ ]

Manual measurements were carried out at different time steps within the measurement period using an electric contact gauge. Atmospheric pressure was measured using the same pressure data logger located in the atmosphere at each study site.

### 4.2.2 Data processing

Sensor measurements were compared to manual measurements in order to verify the data. Sensors with deviations exceeding a certain threshold were discarded from further analyses. These thresholds were chosen depending on conditions of the respective piezometer or pumping well and are addressed in section 5. If deviations between sensor measurements and manual measurements were obviously due to errors in sensor depth, sensor values were adjusted. In addition, piezometer sensors that showed no movement of groundwater level at all were discarded. These behaviors are assumed to result from connection problems between aquifer and piezometer. Subsequently, outliers that occurred due to sensor removals were removed manually.

Groundwater levels below surface were displayed over time as hydrographs. For pumping wells, only values between 3:00 and 4:00 am were considered, in order to avoid influences of pumping activities during daytime. Interrelationships between different hydrographs were identified using correlation

analysis. Following Jung et al. (2004), the results of correlation analyses were used to classify piezometers and pumping wells into groups with similar hydraulic behavior. However, this method does not incorporate absolute depths of groundwater tables. Pearson's correlation coefficients were calculated for each pair of sensors considering those timeframes where both hydrographs overlapped. Subsequently, those pairs showing correlation coefficients of 0.95 or higher were grouped together. Here, piezometers and wells were separated from each other. The different groups will be represented by one hydrograph each, reducing the complexity of different hydrographs. Thereby, sensors with smallest or no data gaps were preferred.



Fig. 4.3: Installation of pressure data loggers in a pumping well in the Ifakara study site (pictures: G. Gabiri).

#### 4.2.3 Creation of piezometric maps

In order to gain information about groundwater flow direction, piezometric maps were created for certain time steps based on groundwater level measurements. Those maps show isolines of hydraulic heads above a certain reference level (e.g. sea level). Time steps were chosen considering climatic and technical conditions. Hydraulic heads (piezometric levels) were calculated by subtracting the measured groundwater levels below surface from elevation values derived from digital elevation models (DEMs).

### 4.3 Analyses of water composition

Water composition data was gathered during water sampling in the field and subsequent analysis in the laboratory. The analysis of water composition followed a classical approach of hydrochemical mapping (Kovalevsky et al. 2004, Glynn and Plummer 2005) including the analysis of physico-chemical parameters, inorganic hydrochemistry, and stable water isotopes. Therefore, several methods were used to describe and evaluate water composition, such as water classifications, multivariate statistical analyses, saturation indices, stability calculations, and threshold inquiries.

#### 4.3.1 Water sampling

Water samples were taken at different sampling points (Fig. 4.4). Groundwater was sampled at pumping wells, draw wells, piezometers, and springs. Surface water was sampled at streams and flooded areas. In the Namulonge study site, soil water was sampled in different depths of 20, 30, and 50 cm using suction cups. Soil water was sampled as mixed samples. The volumetric amount that accumulated in the suction cups over 24 hours was too small for analyses. However, it seemed unrewarding to mix water during more than four consecutive days. Therefore, most soil samples could not be analyzed for all analytes.

Four snapshot samplings of all sampling points were carried out in both study sites. If possible, two of those snapshot samplings were conducted at the end of rainy season, while the other two were conducted at the end of dry season, in order to monitor states of lowest and highest water levels. In the Namulonge study site, monthly sampling of selected points was carried out in addition, as rainy and dry seasons were not well marked there. Furthermore, soil water samples were taken from different treatment plots in the Namulonge study site, in order to assess the influence of different agricultural management options.



**Fig. 4.4:** Impressions of sampling points, showing a deep pumping well and a shallow draw well in the Ifakara study site, and a deep pumping well in the Namulonge study site (pictures: A. Rechenburg, L. Heiß).

In general, water sampling included the measurements of *in-situ* parameters, titration, and collection of water samples, which were transported to different laboratories in Germany. The *in-situ* parameters specific electrical conductivity (EC), pH value, redox potential (Eh), oxygen saturation ( $O_2^{\text{sat}}$ ) and content ( $O_2^{\text{con}}$ ), as well as temperature of water ( $T_w$ ) and air ( $T_a$ ) were measured using a multi-meter (WTW Multi 342). Measurements were conducted in flowing medium at streams and springs, while flow was imitated by moving the probes at the other sampling points.

Precipitation was sampled in both study sites in a location next to the respective GlobE weather station, in order to ensure consistency between precipitation samples and the amount of rainfall. Sampling was carried out each week, when enough rainfall occurred. Rainfall was collected with a funnel installed in 1 m above surface and stored in a bottle placed 30 cm below surface to prevent evaporation (Fig. 4.5).

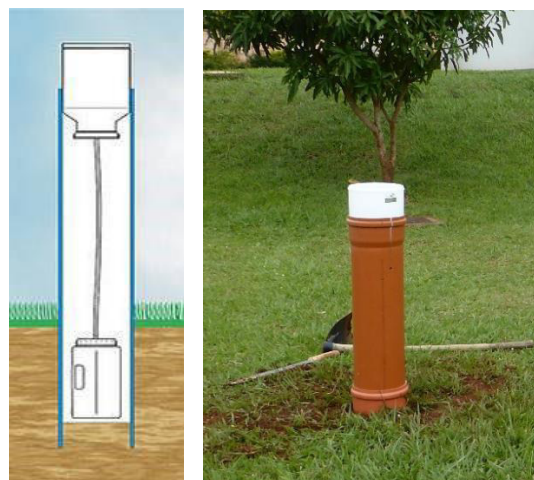


**Fig. 4.5:** Scheme of the used precipitation collector (upgmbh.com) and picture of the installed precipitation collector in the Namulonge study site.



### 4.3.2 Water analyses

Titration was directly conducted at the sampling location with hydrochloric acid (HCl) to a pH of 4.3 and with sodium hydroxide solution (NaOH) to a pH of 8.2. Assuming pH-values between 4.5 and 8.3, concentrations of bicarbonate ( $\text{HCO}_3^-$ ) and carbon dioxide ( $\text{CO}_2$ ) were calculated based on equations 4.7 and 4.8 (Hütter 1988). If the ionic strength of a water sample was smaller than 4 mmol/L, concentration of bicarbonate was adjusted by subtracting 0.05 mmol/L from alkalinity (DEV 2009).

$$c_{\text{HCO}_3^-} = \underbrace{V * c * f}_{\text{Alkalinity}} * M_{\text{HCO}_3^-} \quad (4.7)$$

$c_{\text{HCO}_3^-}$	Concentration of $\text{HCO}_3^-$ [mg/L]
V	Volumetric acid amount to reach pH of 4.3 [mL]
c	Concentration of NaOH [0.02 mol/L]
f	Factor (sample amount 100 ml: f = 10) [10 mmol/mol mL]
$M_{\text{HCO}_3^-}$	Molar mass of $\text{HCO}_3^-$ [61.02 g/mol]

$$c_{\text{CO}_2} = V * c * f * M_{\text{CO}_2} \quad (4.8)$$

$c_{\text{CO}_2}$	Concentration of $\text{CO}_2$ [mg/L]
V	Volumetric base amount to reach pH of 8.2 [mL]
c	Concentration of NaOH [0.02 mol/L]
f	Factor (sample amount 100 ml: f = 10) [10 mmol/mol mL]
$M_{\text{CO}_2}$	Molar mass of $\text{CO}_2$ [44.01 g/mol]

Water samples were filtered (0.45  $\mu\text{m}$ ) and filled in bottles. Depending on further analyses, some samples were acidified with nitric ( $\text{HNO}_3$ ) or sulfuric acid ( $\text{H}_2\text{SO}_4$ ) (Tab. 4.2). Due to the transport to Germany, the water samples were exposed to changing temperature and pressure conditions. Storage times were often longer than one month due to logistical issues. Hydrochemical measurements were carried out at the laboratory of the Steinmann-Institute Geology of the University of Bonn. Concentrations of major, minor, and trace anions were determined using Ion Chromatography (IC) (*Shimadzu HIC-A6*) and concentrations of major, minor, and trace cations were determined using Atomic Absorption Spectrometry (AAS) (*Perkin Elmer AAnalyst 700*) (Tab. 4.2). The concentrations of phosphate ( $\text{PO}_4^{3-}$ ) and silica ( $\text{SiO}_2$ ) were determined using photometry (*Analytik Jena Specord 50 plus*) (Tab. 4.2). Detailed descriptions of those methods can be found in Weiss (1995), Isaac and Kerber (1971), and Welz (1976).

Analyses of stable water isotopes  $^{18}\text{O}$  and  $^2\text{H}$  were carried out at the laboratory of the Institute for Groundwater Ecology at the Helmholtz Zentrum in Munich using a cavity ring-down spectrometer (*Picarro Isotopic Analyzer L2120-i*). Measured values were documented as  $\delta$ -values in ‰ with reference to the Vienna Standard Mean Ocean Water (VSMOW). Accuracy was 0.1 ‰ for  $\delta^{18}\text{O}$  and 0.5 ‰ for  $\delta^2\text{H}$ .

All samples taken during the four snapshot samplings were usually analyzed for all *in-situ* parameters (section 4.3.1), all major ions ( $\text{HCO}_3^-$ ,  $\text{Cl}^-$ ,  $\text{SO}_4^{2-}$ ,  $\text{NO}_3^-$ ,  $\text{Na}^+$ ,  $\text{K}^+$ ,  $\text{Ca}^{2+}$ ,  $\text{Mg}^{2+}$ ),  $\text{NO}_2^-$ ,  $\text{Fe}^{2+}$ ,  $\text{Mn}^{2+}$ ,  $\text{Al}^{3+}$ ,  $\text{SiO}_2$ ,  $\text{CO}_2$ , and stable water isotopes ( $\delta^{18}\text{O}$ ,  $\delta^2\text{H}$ ). Furthermore, all samples of at least one snapshot sampling were additionally analyzed for  $\text{F}^-$ ,  $\text{PO}_4^{3-}$ , and trace cations (As, Cd, Cr, Cu, Ni, Pb, Zn). Monthly samples in the Namulonge study site were analyzed for EC, pH,  $T_w$ ,  $\text{Cl}^-$ ,  $\text{SO}_4^{2-}$ ,  $\text{NO}_3^-$ ,  $\text{Na}^+$ ,  $\text{K}^+$ ,  $\text{Ca}^{2+}$ ,  $\text{Mg}^{2+}$ ,  $\text{Fe}^{2+}$ ,  $\text{Mn}^{2+}$ ,  $\text{Al}^{3+}$ ,  $\text{SiO}_2$ ,  $\delta^{18}\text{O}$ , and  $\delta^2\text{H}$ . Soil water samples were analyzed for selected analytes according to the sampled amount of water. Priority was given to stable water isotopes and agricultural related constituents, such as  $\text{NO}_3^-$ ,  $\text{K}^+$ , and  $\text{PO}_4^{3-}$ . Precipitation samples were analyzed for  $\text{Cl}^-$ ,  $\text{SO}_4^{2-}$ ,  $\text{NO}_3^-$ ,  $\text{Na}^+$ ,  $\text{K}^+$ ,  $\text{Ca}^{2+}$ ,  $\text{Mg}^{2+}$ ,  $\text{SiO}_2$ , and stable water isotopes, if the amount of sampled water was sufficient. If the amount of sampled water was not sufficient, priority was given to the analysis of stable water isotopes.

**Tab. 4.2:** Analytes determined during hydrochemical analyses, respective analysis and conservation methods, limit of detection (LOD), and limit of quantification (LOQ). If LOD or LOQ varied between different sampling periods, ranges are displayed.

Method	Analytes	Conservation	LOD [mg/L]	LOQ [mg/L]
Atomic Absorption Spectrometry (AAS)	Sodium (Na <sup>+</sup> )	HNO <sub>3</sub> (3 drops)	-	0.1-0.5
	Potassium (K <sup>+</sup> )		-	0.1-0.5
	Calcium (Ca <sup>2+</sup> )		-	0.5
	Magnesium (Mg <sup>2+</sup> )		-	0.05-0.5
	Iron (Fe <sup>2+</sup> )		-	0.005
	Manganese (Mn <sup>2+</sup> )		-	0.005
	Aluminum (Al <sup>3+</sup> )		-	0.005
	Arsenic (As)		-	0.005
	Cadmium (Cd)		-	0.005
	Chromium (Cr)		-	0.005
	Copper (Cu)		-	0.005
	Nickel (Ni)		-	0.005
	Lead (Pb)		-	0.005
Zinc (Zn)	-	0.005		
Ion-Chromatography (IC)	Chloride (Cl <sup>-</sup> )	none	0.07-0.43	0.24-1.23
	Sulfate (SO <sub>4</sub> <sup>2-</sup> )		0.12-0.30	0.39-0.89
	Nitrate (NO <sub>3</sub> <sup>-</sup> )		0.09-0.13	0.34-0.43
	Nitrite (NO <sub>2</sub> <sup>-</sup> )		0.07-0.08	0.26-0.27
	Fluoride (F <sup>-</sup> )		0.09-0.40	0.34-1.39
Photometry	Silica (SiO <sub>2</sub> )	H <sub>2</sub> SO <sub>4</sub> (3 drops)	0.06-0.88	0.47-2.94
	Phosphate (PO <sub>4</sub> <sup>3-</sup> )		0.01-0.03	0.03-0.11

### 4.3.3 Plausibility tests and data processing

Several measured data were processed and tested for plausibility prior to interpretation. Redox potentials, measured with an *ORP Sentix* probe, were referenced to a normal hydrogen probe by adding 210 mV to the measured value (WTW 2009). In order to test plausibility of hydrochemical data, ion charge balance errors were calculated for each sample (Eq. 4.9) (Freeze and Cherry 1979). Following Güler et al. (2002) and Moya et al. (2015), samples with ion charge balance errors higher than  $|10\%|$  were discarded from further analyses.

$$\text{ion charge balance error [\%]} = \frac{\sum(\text{cations}) - \sum(\text{anions})}{\sum(\text{cations}) + \sum(\text{anions})} * 100 \quad (4.9)$$

$\sum(\text{cations})$       Sum of cations [mmol(eq)/L]  
 $\sum(\text{anions})$       Sum of anions [mmol(eq)/L]

As hydrochemical concentration values below the limit of detection (LOD) or limit of quantification (LOQ) cannot be handled, if numerical calculations are applied, these values were replaced by numerical values. For concentrations detected with IC and photometry, values below the LOD were replaced by half LOD as recommended by Farnham et al. (2002) for hydrochemical data. Values below LOQ were replaced by the actual measured value. For concentrations detected with AAS, solely values above the LOQ were quantified. Thus, values below the LOQ were replaced by half LOQ.

In terms of multivariate statistical analyses, several steps of data base editing were necessary. For multivariate statistical analyses of chemical or isotopic data, usually normal distributed data are assumed (Güler et al. 2002, Belkhir et al. 2011). Therefore, data were tested for normality based on histograms. Data that were not normally distributed were log-transformed and again tested for normality. Depending on the respective distribution, data were log-transformed or not prior to the multivariate statistical analysis. Subsequently, data were standardized to ensure that each variable is equally weighted in the

analysis. Standardization was carried out by calculating the standard score (z-score) according to Güler et al. (2002) (Eq. 4.10).

$$z_i = \frac{(x_i - \bar{x})}{\sigma} * 100 \quad (4.10)$$

$z_i$	Standard score of the sample
$x_i$	Value of sample
$\bar{x}$	Mean of all samples
$\sigma$	Standard deviation of sample

Variables that showed more than 15 % of values below the LOD were discarded from the analysis (Montcoudiol et al. 2015).

#### 4.3.4 Hydrochemical evaluation methods

Several methods were applied to hydrochemical data in order to gain information about the groundwater system and related processes. These methods include calculations of characteristic values, graphical tools, and statistical analyses.

##### 4.3.4.1 Characteristic values and graphical tools

Graphical tools following Piper (1944) and Schoeller (1955) were applied in order to display and describe the hydrochemical composition of different sampling points at different points of time (Fetter 1994, Güler et al. 2002, Kovalevsky et al. 2004).

Water samples were classified based on their hydrochemical composition. The classification by dominant cation and anion was used. The most abundant cation and the most abundant anion comparing mmol(eq)/L values represent the respective water type.

Hydrochemical evolution processes of groundwater along its flowpaths and during mixing with other water components, such as flooding water, were identified using ion ratios, saturation indices, and stability diagrams. Selected ion ratios, referring to characteristic mineral phases or hydrochemical evolution processes (Hem 1985), were calculated and displayed in scatter plots. Ion ratios were selected considering silicate weathering (section 3.3.1) and redox processes within wetlands (section 3.2). Saturation indices were calculated using the software PhreeqC and the data base phreeqc.dat (Appelo and Postma 2005, Merkel and Planer-Friedrich 2008). The focus was given to silicate minerals, which were identified during mineralogical analysis. The saturation index (SI) expresses the state of saturation of a water sample with respect to certain minerals (Eq. 4.11) (Merkel and Planer-Friedrich 2008).

$$SI = \log\left(\frac{IAP}{K}\right) \quad (4.11)$$

SI	Saturation index
IAP	Ion activity product
K	Solubility product

If the SI is 0, the solution is in equilibrium with the respective mineral. A SI greater than 0 indicates supersaturation leading to precipitation and a SI lower than 0 indicates subsaturation leading to dissolution (Appelo and Postma 2005). Water samples were displayed in stability diagrams of different feldspars and their weathering products, in order to evaluate silicate weathering processes (Tardy 1971). Those diagrams show stability fields of minerals based on the assumption that all  $Al^{3+}$  is preserved in the weathering product (Appelo and Postma 2005). Activities used for the development of stability diagrams were calculated using PhreeqC.

Furthermore, major cations,  $\text{HCO}_3^-$ , and  $\text{SiO}_2$  were used as indicators of silicate weathering (Appelo and Postma 2005), while  $\text{NO}_3^-$ ,  $\text{Cl}^-$ , and  $\text{SO}_4^{2-}$  were used as indicators of anthropogenic influences (van der Weijden and Pacheco 2007), such as fertilizer input, waste water discharge, and washing activities.

#### 4.3.4.2 Statistical analyses

In order to identify differences and similarities in hydrochemical composition between different kinds of groups, statistical tests were applied. Grouping was assigned based on different classification parameters, such as type of sampling point or season of sampling. As most hydrochemical datasets show no normal distribution, non-parametric tests were selected.

The non-parametric Kruskal-Wallis-test compares distributions of more than two independent groups differentiated by one explanatory variable (Helsel and Hirsch 2002). This method tests the null hypothesis that all of the groups come from the same distribution of data in terms of the respective variable. However, the rejection of the null hypothesis does not allow telling which group or groups are different. Therefore a multiple comparison test was conducted subsequently.

If two groups with logically paired objects were compared, for instance samples taken during rainy and dry season at the same sampling points, the non-parametric sign-test was applied (Helsel and Hirsch 2002).

Multivariate statistical analyses are common tools to evaluate groundwater samples in terms of their hydrochemical evolution (King et al. 2014, Belkhiri et al. 2011, Farnham et al. 2003, Güler et al. 2002, Meng and Maynard 2001, Ashley and Lloyd 1978). Two of the most common methods, Principal Component Analysis (PCA) and Hierarchical Cluster Analysis (HCA), were applied in this study.

PCA is widely used in hydrochemistry to identify major sources of variation in hydrochemistry (Belkhiri et al. 2011, Moya et al. 2015). The dimensions of the hydrochemical dataset are reduced by calculating principal components (PCs). These components represent the eigenvectors of the covariance-variance matrix of the data. They can help to interpret the datasets by identifying interrelationships between different hydrochemical variables (Wold et al. 1987, Brown 1998). Thereby, each PC corresponds to one or more hydrogeochemical processes affecting the variation of the dataset.

HCA is a technique to group objects (Q-mode) or variables (R-mode) into unknown groups (Hötzl and Witthüser 1999). As for this method the number and characteristics of the groups are not known prior to the analysis, it is not a true classification technique (Brown 1998). Based on a matrix of distances, objects or variables are mathematically grouped using a linkage algorithm (Hötzl and Witthüser 1999). Results can be visualized in dendrograms showing the clustering of groups and their relations to each other. Variables are usually represented by hydrochemical constituents or *in-situ* parameters and objects are represented by water samples. In this study, Q-mode-HCA using ward's linkage method was applied and the calculated grouping of objects was verified based on geological and other features (Hötzl and Witthüser 1999).

Several authors recommend statistical tests to test the significance of differences between groups. However, no clear recommendation is given in terms of which test should be used (Hötzl and Witthüser 1999, Güler et al. 2002). As most cluster groups usually show distributions of variables that are not normal distributed, Kruskal-Wallis-tests and subsequent multiple comparisons tests were performed to test for differences between groups.

#### 4.3.5 Stable water isotopes evaluation methods

As outlined by Herczeg and Edmunds (2000), most hydrogeological situations require a multi-parameter approach combining hydrochemistry and stable water isotopes. Therefore, stable water isotope signatures of samples were used to evaluate origin and mixing processes of water components and to verify or disprove conclusions gained from hydrochemical results.

Stable water isotopes are documented as  $\delta^{18}\text{O}$  and  $\delta^2\text{H}$ . These terms express the differences between the measured isotope ratios of the sample and an international standard reference (Eq. 4.12) (Clark and Fritz 1997). Isotope ratios are defined as the ratio of the two most abundant isotopes of the respective element. These are  $^{18}\text{O}/^{16}\text{O}$  for oxygen and  $^2\text{H}/^1\text{H}$  for hydrogen (Clark and Fritz 1997). For stable water isotopes, the Vienna Standard Mean Ocean Water (VSMOW) is used as standard reference. Positive  $\delta^{18}\text{O}$  and  $\delta^2\text{H}$  values signify enrichment in heavy isotopes of the sample compared to the standard, while negative values signify depletion (Clark and Fritz 1997).

$$\delta^{18}\text{O}_{\text{sample}} = \left( \frac{(^{18}\text{O}/^{16}\text{O})_{\text{sample}}}{(^{18}\text{O}/^{16}\text{O})_{\text{reference}}} - 1 \right) * 1000 \text{‰ VSMOW} \quad (4.12)$$

Isotope fractionation, describing processes that affect the relative abundance of heavy isotopes, occurs due to several causes in nature, such as biological activity and exchange with other materials (Dansgaard 1964). Furthermore, fractionation occurs during state transformations of water within the hydrological cycle (Dansgaard 1964). Thus, stable water isotopes are helpful in tracking the origin and evolution of a water sample.

On a global scale,  $\delta^{18}\text{O}$  and  $\delta^2\text{H}$  of precipitation correlate with each other. This correlation is expressed by the Global Meteoric Water Line (GMWL:  $\delta^2\text{H} = 8 * \delta^{18}\text{O} + 10$ ; Craig 1961). In general, isotopically depleted waters are rather found in cold regions, while enriched waters are found in warm regions (Clark and Fritz 1997). Thus, in temperate regions with seasonal variations in temperature, a seasonal variation in isotopes of precipitation is observed with isotopically lighter rain in colder seasons (Rozanski et al. 1993). In tropical regions, where temperatures stay stable throughout the year,  $\delta^{18}\text{O}$  and  $\delta^2\text{H}$  in precipitation are strongly related to precipitation intensities (Jasechko and Taylor 2015). Low intensity rainfall events are relatively enriched in stable water isotopes, while high intensity rainfall events are relatively depleted. This phenomenon is known as the amount effect, and generally leads to a change in  $\delta^{18}\text{O}$  of -1 to -1.5 promille per 100 mm monthly precipitation (Moser 1998). Based on this knowledge, those rainfall intensities that lead to groundwater recharge can be identified by comparing isotopic signatures of precipitation and groundwater (Jasechko and Taylor 2015). Furthermore, isotopes in precipitation are influenced by the altitude effect, meaning that precipitation becomes depleted in heavy isotopes due to the rising of a moist air mass caused by orographic elevation. This effect leads to a change in  $\delta^{18}\text{O}$  of -0.1 to -0.5 promille per 100 m increasing elevation (Moser 1998). Evaporation of water leads to an enrichment of heavy isotopes in the residual water, while the vapour becomes depleted (Clark and Fritz 1997). Thus, evaporated waters plot below the GMWL showing slopes below 8 (Moser 1998).

Signatures of precipitation samples were used to develop a Local Meteoric Water Line (LMWL) using linear regression. For local investigations a LMWL is important to compare surface water and groundwater data with local precipitation patterns (Clark and Fritz 1997). Those patterns may deviate from the global pattern expressed by the GMWL. The relation of water samples to the LMWL was used to evaluate evaporation effects.

Information about recharge in the study sites was obtained from average values and variations in precipitation isotopes (Jasechko and Taylor 2015). Moreover, groundwater-surface water interactions and mixing processes between different water components were identified based on isotopic signatures (e.g. Geyh 2000, Königer et al. 2001). Krukall-Wallis-tests as well as sign-tests were applied to isotopic data as well.

#### 4.3.6 Water quality assessment

Groundwater is the major drinking source for the local population in both study sites. Additionally, groundwater and surface water are used for other domestic or irrigation purposes. Therefore, in this study a) the status quo of water quality related to human health, acceptability, and irrigation purposes is assessed, b) the origin of contaminants as well as the water quality functions of the wetlands is discussed, and c) the influence of agriculture, different management options, and settlements on water quality is evaluated. Different methods were used to address these issues.

Guideline values of WHO (2011) were consulted, in order to evaluate the inorganic water quality in terms of domestic water (Tab. 4.3). In terms of aluminum and manganese, WHO (2011) did not establish health related guideline values as those are high above the acceptability threshold. However, they recommend health-based values of 0.9 mg/L for aluminum and 0.4 mg/L for manganese. Those values were treated as health related guideline values in this study.

**Tab. 4.3: Health-related guideline values and acceptability thresholds for selected inorganic constituents in drinking water (WHO 2011).**

Constituent	Guideline value [mg/L]	Acceptability threshold [mg/L]	Remarks
Aluminum	(0.9)	0.2	Deposition of aluminium hydroxide floc and exacerbation of discoloration of water by iron above 0.2 mg/L
Arsenic	0.01		
Cadmium	0.003		
Chromium	0.05		
Chloride	-	250	Taste threshold of 250 mg/L
Copper	2	1	Stains laundry above 0.1 mg/L; taste threshold of 5mg/L
Fluoride	1.5		Volume of water consumed and intake from other sources should be considered when setting national standards
Iron	-	0.3	Stains laundry and leads to deposits in pipes above 0.3 mg/L
Lead	0.01		
Manganese	(0.4)	0.1	Stains laundry, leads to deposits in pipes and causes an undesirable taste above 0.1 mg/L; health-based value of 0.4 mg/L is higher than that acceptability threshold
Nickel	0.07		
Nitrate	50		Short-term exposure
Nitrite	3		Short-term exposure
pH	-	6.5-8.5	Optimum range to avoid corrosion of pipes
Sodium	-	200	Average taste threshold at room temperature of 200 mg/L
Sulfate	-	250	Taste threshold of 250 mg/L
Zinc		4	Taste threshold of 4 mg/L

To display water quality related to public health, an assessment scheme was developed introducing the Degree of Health related Water Quality (DHWQ). This DHWQ was calculated for each sampling point based on the amount of exceeded guideline values. It is the sum of all exceeded guideline values. Thereby, a guideline value was considered as exceeded, if the respective sampling point exceeded that guideline value in one of the four snapshot samplings.

In terms of water quality related to irrigation purposes, the guideline of Ayers and Westcot (1985) was consulted. This guideline is a tool that helps to interpret water quality for irrigation from different points of view. The suitability of water for irrigation purposes can be expressed by the Degree of Restriction on Use (DRU). This DRU can be calculated for different potential irrigation problems. The problems of salinity and infiltration are of concern for all kinds of crops, while other problems are only related to sensitive or susceptible crops (Ayers and Westcot 1985). Thus, the two DRUs regarding salinity and infiltration were calculated for each water sample (Tab. 4.4). Salinity can cause a loss in yield, if salt accumulates in the crop root zone and can be expressed by EC. Infiltration of irrigation water might be limited by a) low salinity and b) high sodium content. This problem is quantified by EC and Sodium Adsorption Ratio (SAR) (Eq. 4.13).

$$SAR = \frac{Na^+}{\sqrt{\frac{Ca^{2+} + Mg^{2+}}{2}}} \quad (4.13)$$

SAR      Sodium adsorption ratio  
 Na<sup>+</sup>      Concentration of sodium [mmol(eq)/L]  
 Ca<sup>2+</sup>      Concentration of calcium [mmol(eq)/L]  
 Mg<sup>2+</sup>      Concentration of magnesium [mmol(eq)/L]

Additionally, Ayers and Westcot (1985) give guideline values for several trace elements that can be toxic to crops. These values were evaluated qualitatively. The guideline was developed for crops in semi-arid to arid climatic areas and values are considered as too strict under more humid conditions (Ayers and Westcot 1985). Furthermore, a DRU of 0 indicating no restriction on use means that full production capability of all crops is possible without the use of special practices. Thus, a restriction on use does not directly indicate that the water is unsuitable for irrigation.

In order to assess the influence of different agricultural management options on water quality, the soil water samples taken from different treatment plots were evaluated in terms of indicators of fertilizer input. Four different treatment plots were sampled (Tab. 4.5). As the main nutrients provided by fertilizer, either inorganic or organic, are nitrogen, phosphorous, and potassium, chosen indicators were NO<sub>3</sub><sup>-</sup>, PO<sub>4</sub><sup>3-</sup>, and K<sup>+</sup>. If possible, soil water was also analyzed for Cl<sup>-</sup>, Ca<sup>2+</sup>, and SO<sub>4</sub><sup>2-</sup>, because these elements are part of the applied fertilizers as well (sdnotill.com).

**Tab. 4.4: Guidelines for the interpretation of water quality for irrigation based on the Degree of Restriction on Use (DRU) in terms of salinity and infiltration (Ayers and Westcot 1985).**

Potential Irrigation Problem	Degree of Restriction on Use (DRU)		
	None (0)	Slight to Moderate (1)	Severe (2)
Salinity (affects crop water availability)	EC [μS/cm]	EC [μS/cm]	EC [μS/cm]
	< 700	700 – 3,000	> 3,000
Infiltration (affects infiltration rate of water into the soil)	SAR	EC [μS/cm]	EC [μS/cm]
	0 – 3	> 700	200 – 700
	3 – 6	> 1,200	300 – 1,200
	6 – 9	> 1,900	500 – 1,900
	9 – 12	> 2,900	1,300 – 2,900
12 -20	> 5,000	2,900 – 5,000	< 2,900

**Tab. 4.5: Different treatment plots, where soil water was sampled, in order to assess the influence of different agricultural management options on water quality.**

<b>Treatment</b>	<b>Characteristic name</b>	<b>Management option</b>
T01	Natural vegetation	No management
T02	Rice - unbunded	Rice cultivation twice a year, field is not banded
T09	Rice – inorganic NPK fertilizer	Rice cultivation four times a year, field is banded, 120 kg/ha mineral N, 60 kg/ha PK, irrigated
T10	Rice – organic manure	Rice cultivation four times a year, field is banded, pre-crop green manure, farmyard manure

#### 4.4 Inverse geochemical modeling

Inverse geochemical modeling with PhreeqC was applied, in order to verify and quantify mixing ratios and hydrochemical evolution processes of flooding water within the wetlands of both study sites. As a sound numerical model always requires a reliable conceptual model of the system, the implementation was based on the developed conceptual models.

The inverse modeling code of PhreeqC allows the quantification of known processes in a hydrochemical system (Parkhurst and Appelo 1999). It calculates the processes occurring during hydrochemical evolution of an initial solution to an end solution. It is possible to include more solutions, which can be mixed with the initial solution, in order to result in the end solution. The model calculates mixing fractions of the initial solutions and mol transfers of gases and minerals producing the composition of the end solution (Parkhurst and Appelo 1999). All mixing, dissolution, and precipitation reactions must be implemented by the user.

Therefore, an input file was generated including the chemical compositions of initial and end solutions as well as those mineral and gas phases that were identified to react with the solutions. Furthermore, uncertainties of chemical analyses and those elements, for which mass-balances are required, were defined. All implemented solutions, phases, uncertainties, and elements are described in the respective sections. All models were run based on the data base phreeqc.dat.

Hydrochemical compositions of initial and end solutions were usually adopted from water samples. Nevertheless, in some cases it was not easy to identify a certain sample as the respective solution. Then, HCA groups or parts of these groups were used as solutions based on the assumption that water samples, which fall within one cluster group have a similar evolution history (Kebede et al. 2005).



## 5 Data base

In general, data used in this study can be divided into primary data and secondary data. Primary data were collected during the period from 2014 to 2016. Data collection included hydrogeological mappings, drilling surveys, and water level measurements. Furthermore, water, rocks, and sediments were sampled during field campaigns and analyzed in the laboratory. Some primary data were collected in the context of different master theses (Geißler 2015, Liedtke 2015, Heiß 2016). Those data related to the piezometers were collected in collaboration with the hydrology research group of GlobE (Gabiri unpublished). Secondary data were either acquired from literature or provided by external organizations and other research groups within GlobE. Additionally, personal communications with stakeholders and people from local communities helped to gain knowledge about the study sites.

Piezometer and sampling point locations were selected aiming to cover the whole study sites with a focus on the CFTs. However, selection was sometimes restricted due to accessibility issues. Data availability of primary data varies from one study site to the other, due to different on-site conditions in the two study sites. In terms of temporal coverage of water sampling, four snapshot samplings were conducted in both study sites seeking to cover rainy and dry seasons. In the Namulonge study site, the four snapshot samplings were enhanced with monthly water samples of selected sampling points (section 4.3.1). Soil water was solely sampled in the Namulonge study site, as the installation of suction cups was not possible in the Ifakara study site, due to flooding conditions. Furthermore, no outcrops of crystalline rocks were found in the Namulonge study site. Hence, chemical data of crystalline rocks were gained from literature. It was tried to acquire as much secondary data as possible. However, as both study sites are located in data scarce regions, valuable data were often lacking.

In the following section, a detailed overview of data used in the two case studies, referring to their locations, is given.

### 5.1 Data base of the Ifakara study site

A list of all available data for the case study of the Ifakara study site is given in Table 5.1. Collection of primary data took place between May 2014 and November 2015. Two piezometers each were placed in the CFTs *center*, *middle*, and *fringe* (Fig. 5.1). Additional piezometers were placed in selected positions along the hydrological gradient of CFTs. Following the delineation of the floodplain based on satellite images (personal communication with E. Amler 2016), seven piezometers are located in the floodplain, while other seven are located further north within the alluvial fan and colluvial deposits.

#### 5.1.1 Data of aquifer structure and properties (IF)

Primary data of aquifer structure and properties were collected during field mappings, piezometer installation, and laboratory analyses (Tab. 5.2). Rock samples and fracture measurements were collected at outcrops in the northern study site (Fig. 5.2). For all of them, mineralogical and geochemical data are available. Shallow drilling log descriptions are available for all piezometers (Fig. 5.1). Sediment samples were taken from drilling logs of piezometers in the CFTs. Depths of sampling points were selected based on layering and texture of the drilling logs. Selected samples were analyzed for mineralogy and geochemistry as well as for grain size distributions (Tab. 5.3). Moreover, falling-head permeability tests were conducted at all piezometers except for PZ05<sub>IF</sub> and PZ08<sub>IF</sub> (Fig. 5.1).

Secondary data were provided by the organizations Rufiji Basin Water Board (RBWB) and Maji Safi kwa Afya Bora Ifakara (MSABI). These data include descriptions of deep drilling logs and pumping test evaluations (Fig. 5.2).

**Tab. 5.1: Data used in the case study of the Ifakara study site (IF).**

<b>Data description</b>	<b>Primary/Secondary</b>	<b>Further description/Source</b>
Altitude	Secondary	SRTM 1 Arc-Second Global Digital Elevation Model (30 m spatial resolution) – data available from the U.S. Geological Survey ( <a href="http://earthexplorer.usgs.gov">earthexplorer.usgs.gov</a> )
Geology and lithology	Primary/Secondary	Geological map of Ifakara 1:125,000 – Geological Survey of Tanganyika (1962) Outcrop descriptions and fracture measurements – Liedtke (2015) Description of deep drilling logs – data provided by Rufiji Basin Water Board (RBWB) and Maji Safi kwa Afya Bora Ifakara (MSABI) Description of shallow drilling logs – this study, collected in collaboration with the hydrology research group (Gabiri unpublished)
Geomorphology	Secondary	Geomorphological map of Ifakara – Jätzold and Baum (1968)
Catchment	Secondary	Delineation of Kilombero Catchment – personal communication with K. Näschen (2014)
Wetland	Secondary	Delineation of wetland – Beuel et al. (2016) Delineation of floodplain – personal communication with E. Amler (2016), based on Landsat satellite data
Land use	Secondary	Delineation of Ifakara city – this study, based on <a href="http://google.com/earth">google.com/earth</a>
Weather	Secondary	Precipitation, temperature (GlobE weather station) – personal communication with V. Ermert (2016) Precipitation – Gabiri (unpublished)
Aquifer properties	Primary/Secondary	Fracture scan windows – Liedtke (2015) Pumping test data – data provided by RBWB, processed by Liedtke (2015) Falling head permeability tests, grain size analyses – this study
Mineralogy and Geochemistry	Primary	Geochemical and mineralogical data of rock and sediment samples – Liedtke (2015) (rock samples), this study (sediment samples)
Groundwater level	Primary	Hourly groundwater level data of piezometers and wells – this study, collected in collaboration with the hydrology research group (Gabiri unpublished)
Hydrochemistry and stable water isotopes	Primary	Hydrochemistry and stable water isotope data of groundwater and surface water samples taken during four snapshot samplings – Geißler (2015) (first sampling), this study (all samplings) Weekly stable water isotope data of precipitation – this study

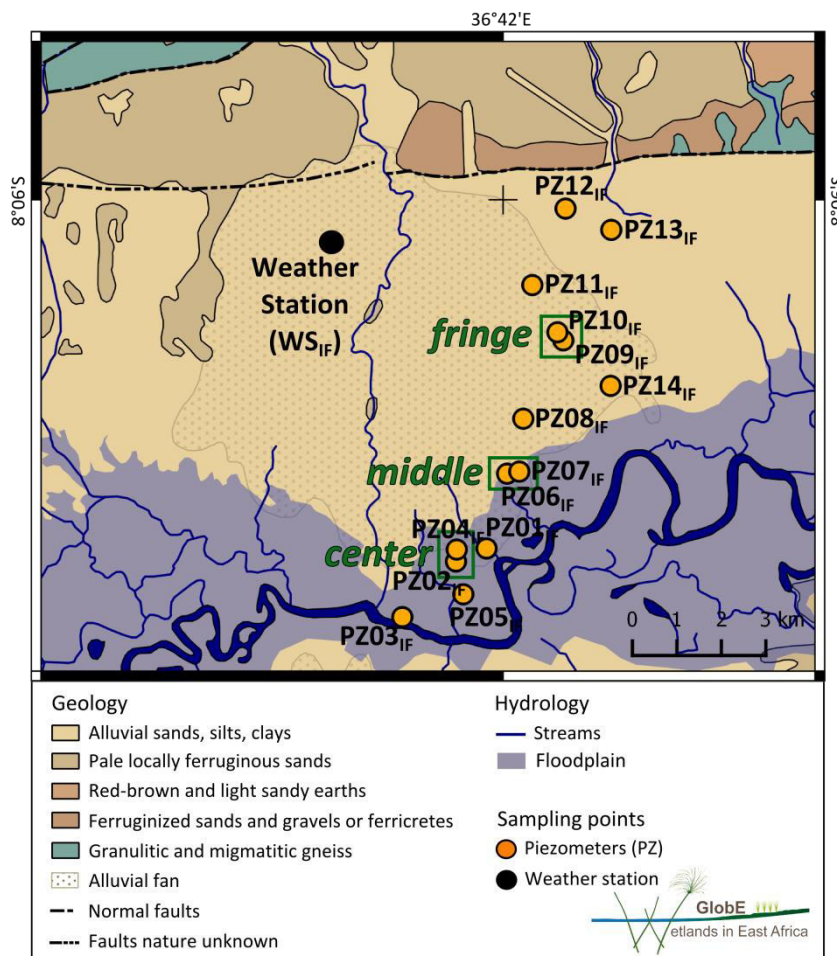


**Fig. 5.1:** Map section of the south central study site showing locations of piezometers and central field trials. Data sources: Geological Survey of Tanganyika (1962) (geology, streams), Jätzold and Baum (1968) (alluvial fan), personal communication with E. Amler (2016) (floodplain) (IF).

**Tab. 5.2:** Detailed descriptions of all used data of aquifer structure and properties (IF).

Data description	Data type	Number of samples/measurements
Outcrop description of hard rocks	Descriptive	7
Striking and dipping of fractures in hard rocks	Numerical	3
Fracture scan windows	Numerical	2
Mineralogical and geochemical composition of rock samples	Numerical	4
Drilling log descriptions (deep)	Descriptive	10
Drilling log descriptions (shallow: piezometers)	Descriptive	14
Pumping test data	Numerical	33
Falling-head permeability test data	Numerical	12
Grain size analyses data of sediment samples	Numerical	16
Mineralogical and geochemical composition of sediment samples	Numerical	20

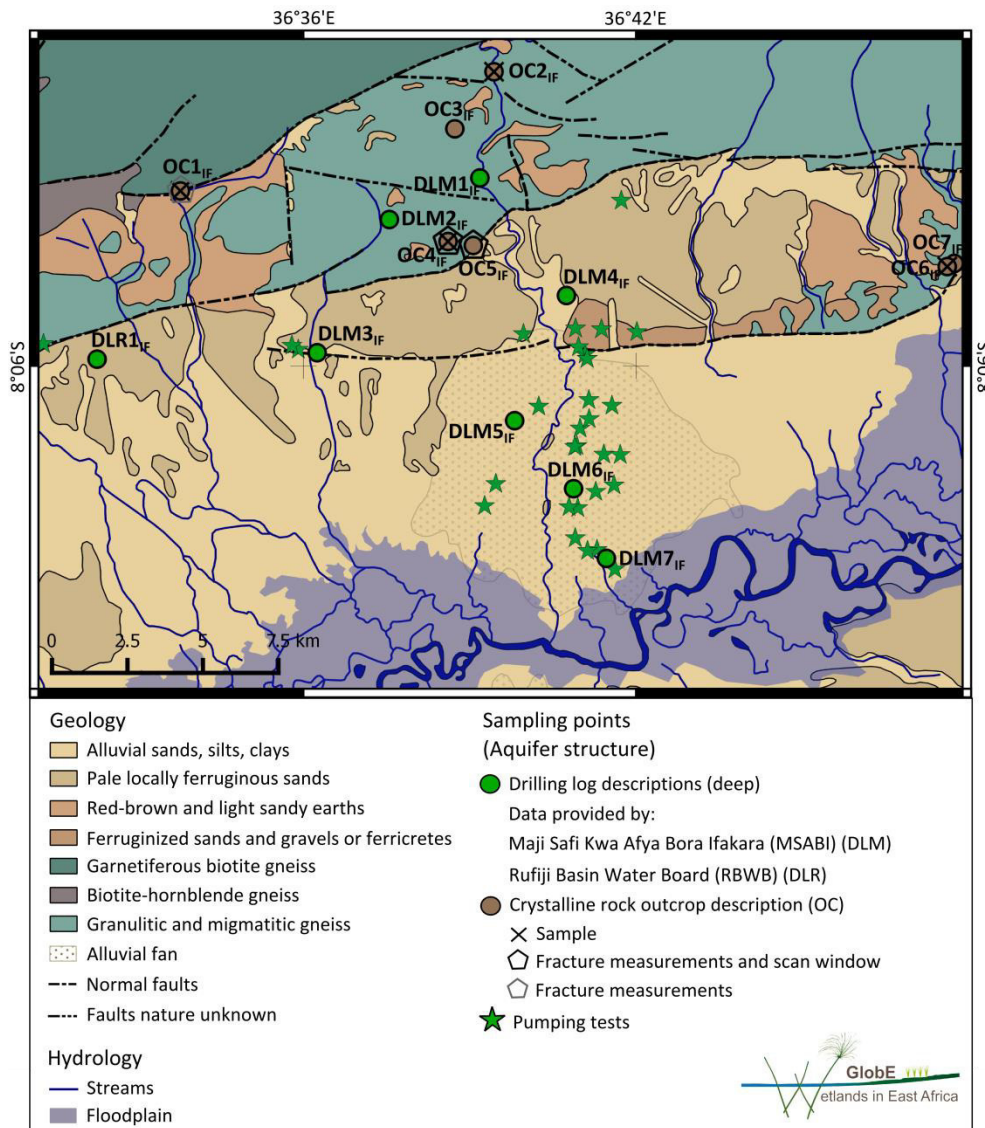


Fig. 5.2: Locations of deep drilling log descriptions, crystalline rock outcrops, and pumping test data. Data sources: Geological Survey of Tanganyika (1962) (geology, streams), Jätzold and Baum (1968) (alluvial fan), personal communication with E. Amler (2016) (floodplain) (IF).

Tab. 5.3: Depths and locations of sediment samples and respective available data (IF).

Sampling point	Sampling depth below surface [m]	Mineralogical / geochemical data	Grain size distribution data	Sampling point	Sampling depth below surface [m]	Mineralogical / geochemical data	Grain size distribution data
PZ02 <sub>IF</sub>	0.8	x	x	PZ07 <sub>IF</sub>	0.3	x	x
	1.7	x	x		1.7	x	-
	3.2	-	x		2.3	x	-
	4.0	x	x		3.9	x	x
PZ04 <sub>IF</sub>	4.1	x	x	PZ09 <sub>IF</sub>	5.4	x	-
PZ06 <sub>IF</sub>	1.0	x	x		5.8	x	x
	3.3	x	x		1.0	x	x
	4.5	x	x		2.9	x	x
PZ10 <sub>IF</sub>	5.5	x	x	4.5	x	x	
				6.0	x	-	
				3.4	x	x	
			3.9	x	-		

### 5.1.2 Groundwater level data (IF)

Groundwater level data were measured on an hourly time resolution in all 14 piezometers, with depths between 3.7 m and 7.4 m, and in eight pumping wells, with depths around 25 m. Data was collected from March 2015 to May 2016. For 13 of the 14 piezometers, the maximum deviation between manual and sensor measurement was smaller than 15 cm. One piezometer (PZ08<sub>IF</sub>) showed random deviations up to 60 cm and was thus discarded from the analyses. For the pumping wells, all deviations were below 50 cm. Groundwater levels within the wells were variable during daytime, due to pumping activities. Manual and sensor measurements were not conducted at the same point of time, explaining higher deviations. For some sensors, data gaps occurred due to technical issues. The hydrographs of four piezometers (PZ04<sub>IF</sub>, PZ05<sub>IF</sub>, PZ11<sub>IF</sub>, PZ12<sub>IF</sub>) and one pumping well showed data gaps that exceeded more than half of the monitoring period. Consequently, those data were discarded from the analyses. Finally, nine hydrographs of piezometers and seven hydrographs of pumping wells are available (Fig. 5.3).

For the creation of piezometric maps, elevation data with a spatial resolution of 30 m was gained from the SRTM 1 Arc-Second Digital Global Elevation Model ([earthexplorer.usgs.gov](http://earthexplorer.usgs.gov)).

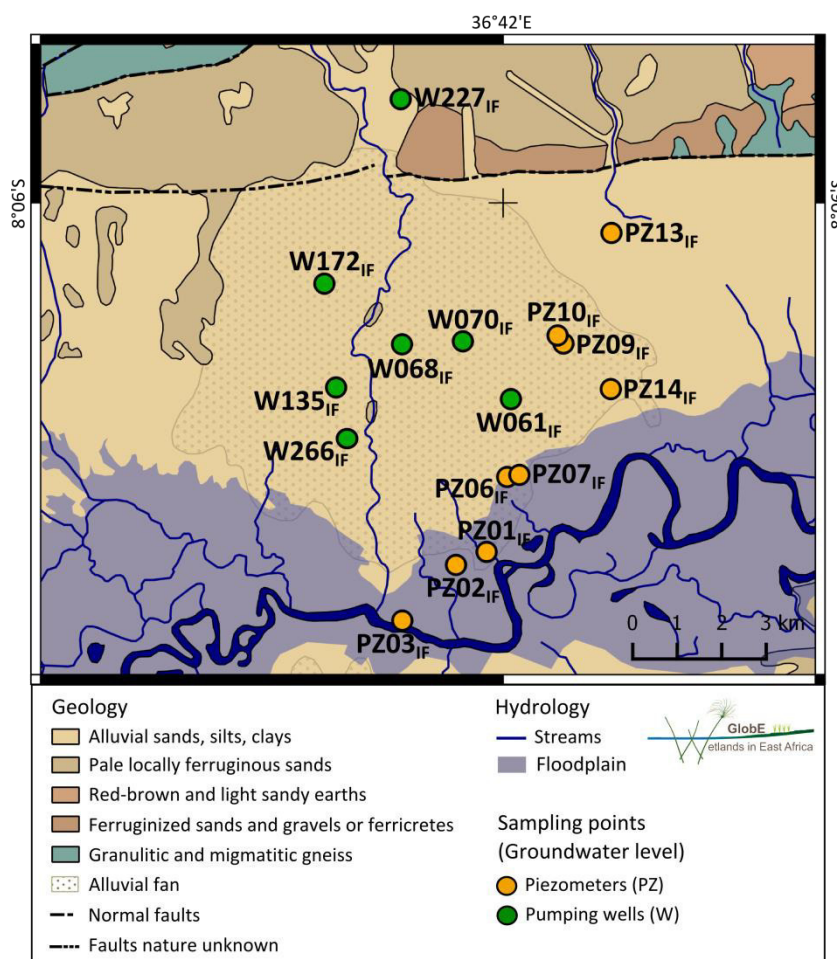


Fig. 5.3: Locations of sampling points related to groundwater level data. Data sources: Geological Survey of Tanganyika (1962) (geology, streams), Jätzold and Baum (1968) (alluvial fan), personal communication with E. Amler (2016) (floodplain) (IF).

### 5.1.3 Hydrochemical and isotopic data (IF)

Hydrochemical and isotopic data of water were collected at 69 water sampling points, including three flooding waters (*center, middle, fringe*), five streams, four shallow draw wells, 45 deep pumping wells, and twelve shallow piezometers (Fig. 5.4). Four snapshot samplings of water representing rainy and dry

seasons were carried out in 2014 and 2015. Rainy season samples were collected during May to June 2014 and May 2015, while dry season samples were collected during October 2014 and October to November 2015. Some sampling points were only sampled once or twice due to accessibility or technical issues.

All in all, 181 water samples were taken and analyzed. Hydrochemical data (EC, pH, Eh,  $O_2^{sat}$ ,  $O_2^{con}$ ,  $T_w$ ,  $T_A$ ,  $HCO_3^-$ ,  $Cl^-$ ,  $SO_4^{2-}$ ,  $NO_3^-$ ,  $NO_2^-$ ,  $Na^+$ ,  $K^+$ ,  $Mg^{2+}$ ,  $Ca^{2+}$ ,  $Fe^{2+}$ ,  $Mn^{2+}$ ,  $Al^{3+}$ ,  $SiO_2$ ,  $CO_2$ ) are available for 165 samples and stable water isotope data ( $\delta^{18}O$ ,  $\delta^2H$ ) are available for 180 samples. Furthermore, analysis results of  $F^-$ ,  $PO_4^{3-}$ , As, Cd, Cr, Cu, Ni, Pb, and Zn are available for all samples collected during rainy season 2014. A detailed distribution of samples collected during the four sampling seasons is displayed in Table 5.4. Flooding water was sampled at *center* and *fringe* in both rainy seasons. In 2014, flooding water at *middle* was sampled for isotopes. While Kilombero (ST1<sub>IF</sub>) and Lumemo (ST2<sub>IF</sub>) rivers were sampled during all four seasons, tributaries were only sampled sporadically, if water was available. Piezometers were solely sampled in 2015. Precipitation was sampled each week, when enough rainfall occurred, from May 2014 to November 2015. All in all 33 precipitation samples were collected and analyzed for stable water isotopes and selected ions (Tab. 5.5).

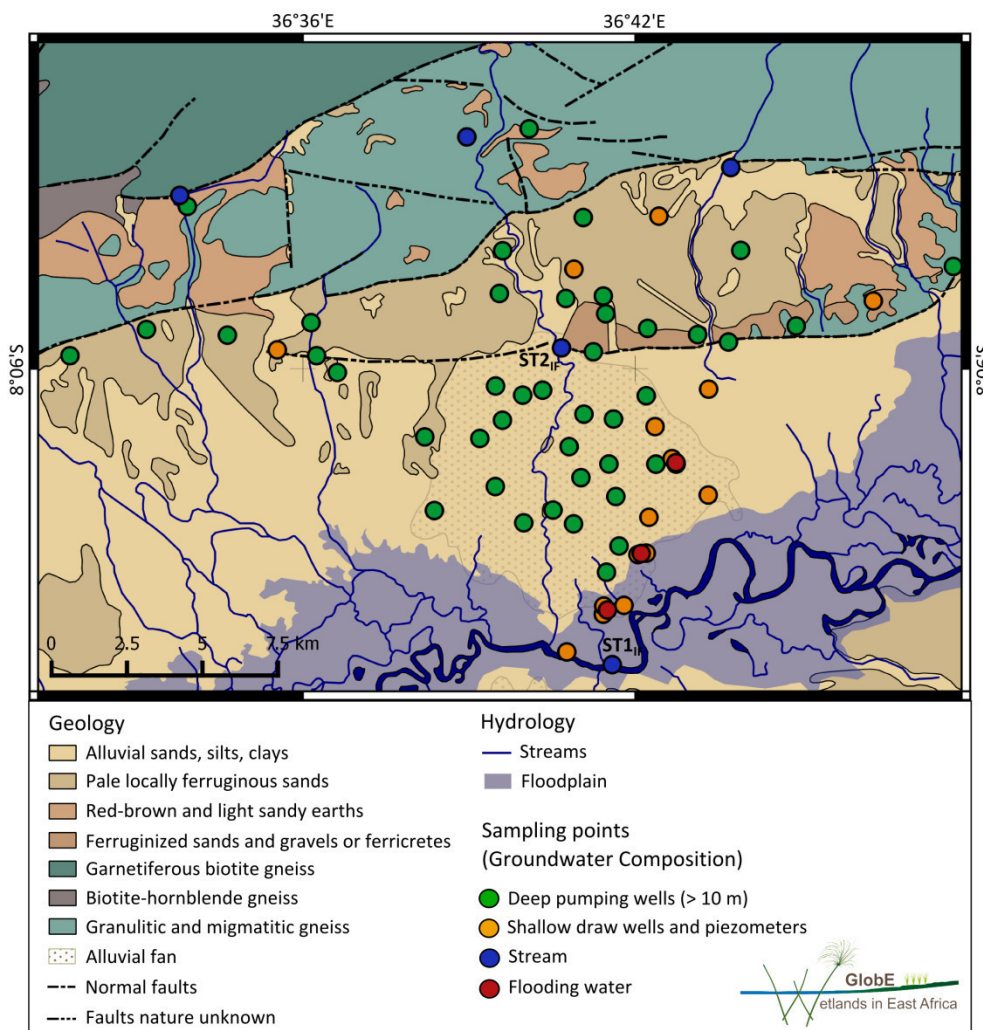


**Fig. 5.4:** Locations of sampling points related to hydrochemical and isotopic data. Data sources: Geological Survey of Tanganyika (1962) (geology, streams), Jätzold and Baum (1968) (alluvial fan), personal communication with E. Amler (2016) (floodplain) (IF).

**Tab. 5.4:** Number of water samples analyzed for hydrochemistry and stable water isotopes during the four snapshot samplings. For the analysis of hydrochemistry, only samples with ion charge balance errors below 10 % are listed (IF).

Data	Season	Flood	Stream	Pumping well	Draw well	Piezometer
Hydrochemistry	Rainy '14	2	5	33	4	-
	Dry '14	-	3	29	3	-
	Rainy '15	2	3	27	3	7
	Dry '15	-	3	26	3	12
Stable water isotopes	Rainy '14	3	4	42	4	-
	Dry '14	-	3	30	3	-
	Rainy '15	2	3	30	3	7
	Dry '15	-	3	26	3	12

**Tab. 5.5:** Number of precipitation samples out of 33 samples in total and respective data availability of different analytes (IF).

Analyte	Number of samples
$\delta^{18}\text{O}$ , $\delta^2\text{H}$	33
$\text{Cl}^-$ , $\text{SO}_4^{2-}$ , $\text{NO}_3^-$	16
$\text{Na}^+$ , $\text{K}^+$ , $\text{Mg}^{2+}$ , $\text{Ca}^{2+}$	3
$\text{SiO}_2$	20

#### 5.1.4 Precipitation data (IF)

Precipitation measurements (10 min time resolution) were obtained from a GlobE weather station located within the study site (Fig. 5.1: WS<sub>IF</sub>). Data gaps in precipitation records were filled with data of an additional tipping bucket located at the CFT *fringe* (Gabiri unpublished).

## 5.2 Data base of the Namulonge study site

Data used for the case study of the Namulonge study site are listed in Table 5.6. Collection of primary data took place between June 2014 and June 2016. Two piezometers each were placed at the CFTs (Fig. 5.5). The two piezometers in each CFT are screened in different depths capturing two water-bearing layers. Hence, they will be referred to as long (L) and short piezometers (S). Another three piezometers were placed along the hydrological gradient at the other side of the stream. Additionally, two other transects perpendicular to the stream, upstream and downstream of the CFTs, were equipped with six piezometers, with three piezometers on each side of the stream (Fig. 5.5). According to the project nomenclature, the three transects are referred to as transects A, C (CFTs), and D in downstream direction.

### 5.2.1 Data of aquifer structure and properties (NA)

Available data of aquifer structure and properties are listed in Table 5.7. Shallow drilling logs were gained during piezometer installation and from additional drilling along prolongations of transects A, C, and D (Fig. 5.6). Additional drilling was conducted in a 10 m distance to the piezometers at transect C. One drilling log each was documented in the wetland of a side-valley in the upper catchment (DU1<sub>NA</sub>), and in the saprolite (SA1<sub>NA</sub>). Sediment and saprolite samples were taken from selected drills focusing on the CFTs and seeking to represent the different transects. The distribution of samples and the respective available data regarding mineralogy, geochemistry, and grain size distribution are listed in Table 5.8. Falling-head permeability tests were conducted at five piezometers in the CFTs (Fig. 5.5: PZ40L<sub>NA</sub>, PZ40S<sub>NA</sub>, PZ42L<sub>NA</sub>, PZ46L<sub>NA</sub>, PZ46S<sub>NA</sub>). Deep drilling log descriptions were provided by the Ministry of Water and Environment, Uganda (MWE) (Fig. 5.6). Chemical compositions of rock samples were adapted from Westerhof et al. (2014), and grain size distribution data of soil up to 1 m depth were provided by the soil research group (personal communication with B. Glasner 2016).

**Tab. 5.6: Data used in the case study of the Namulonge study site (NA).**

<b>Data description</b>	<b>Primary/Secondary</b>	<b>Further description/Source</b>
Altitude	Secondary	SRTM 1 Arc-Second Global Digital Elevation Model – data available from the U.S. Geological Survey (earthexplorer.usgs.gov) Digital Elevation Model based on differential GPS measurements – (Asimwe 2015)
Geology and lithology	Primary/Secondary	Geological map of Uganda, Bombo, 1:100,000 – GTK Consortium (2012) Description of deep drilling logs – data provided by the Ministry of Water and Environment, Uganda (MWE) Description of shallow drilling logs – this study, collected in collaboration with the hydrology research group (Gabiri unpublished)
Catchment	Secondary	Delineation of Nasirye Catchment – personal communication with K. Näschen (2014)
Wetland	Secondary	Delineation of wetland – Beuel et al. (2016) Delineation of Nasirye Stream – Gabiri (unpublished)
Weather	Secondary	Precipitation, temperature (GlobE weather station) – personal communication with V. Ermert (2016) Precipitation – Gabiri (unpublished)
Aquifer properties	Primary/Secondary	Falling head permeability tests, grain size analyses – Heiß (2016), personal communication with B. Glasner (2016), this study
Mineralogy and geochemistry	Primary/Secondary	Mineralogical and geochemical data of rock, saprolite, and sediment samples – Westerhof et al. (2014) (rock samples), Heiß (2016) (saprolite and sediment samples), this study (sediment samples)
Groundwater level	Primary/Secondary	Hourly groundwater level data of piezometers – this study, collected in collaboration with the hydrology research group (Gabiri unpublished) Static groundwater level data of wells – data provided by MWE
Stream level	Secondary	Daily stream level data at the three transects – Gabiri (unpublished)
Hydrochemistry and stable water isotopes	Primary	Hydrochemistry and stable water isotope data of groundwater, soil water, and surface water samples taken during four snapshot samplings – Heiß (2016) (second sampling), this study (all samplings) Monthly hydrochemistry (selected ions) and stable water isotope data of groundwater and surface water – this study Water quality indicators of soil water samples in different treatment plots – this study Weekly stable water isotope data of precipitation – this study



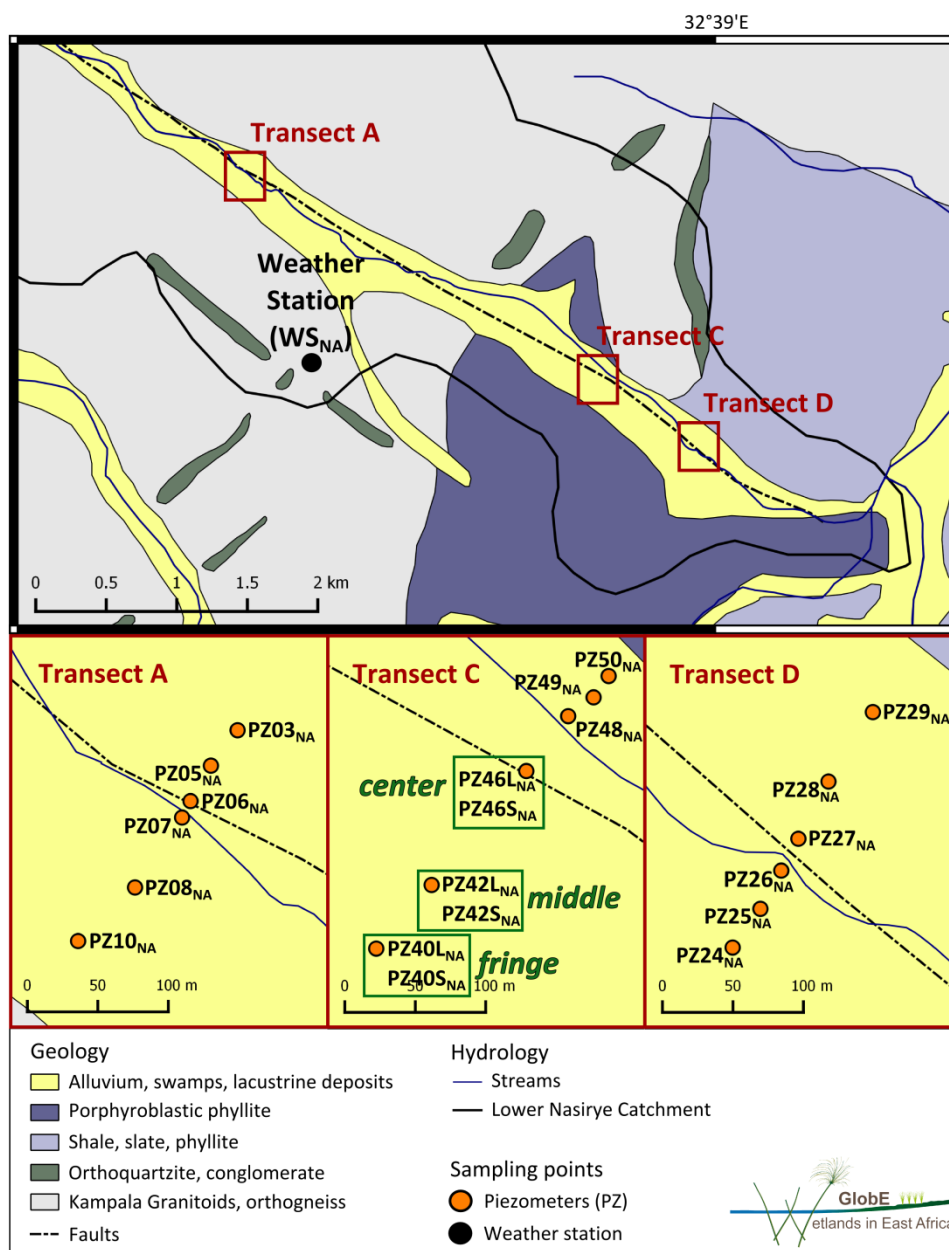


Fig. 5.5: Map section of the south eastern study site showing the three transects A, C, and D including locations of piezometers and central field trials. Data sources: GTK Consortium (2012) (geology, streams), Heiß (2016) (alluvium), Gabiri (unpublished) (Nasirye Stream) (NA).

Tab. 5.7: Detailed descriptions of all used data of aquifer structure and properties (NA).

Data description	Data type	Number of samples/measurements
Mineralogical and geochemical composition of rock samples	Numerical	4
Drilling log descriptions (deep)	Descriptive	14
Drilling log descriptions (shallow: piezometers and additional drillings)	Descriptive	39
Falling head permeability test data	Numerical	5
Grain size analyses data of sediment samples	Numerical	5
Grain size analyses data of soil samples	Numerical	19
Mineralogical and geochemical composition of sediment and saprolite samples	Numerical	43

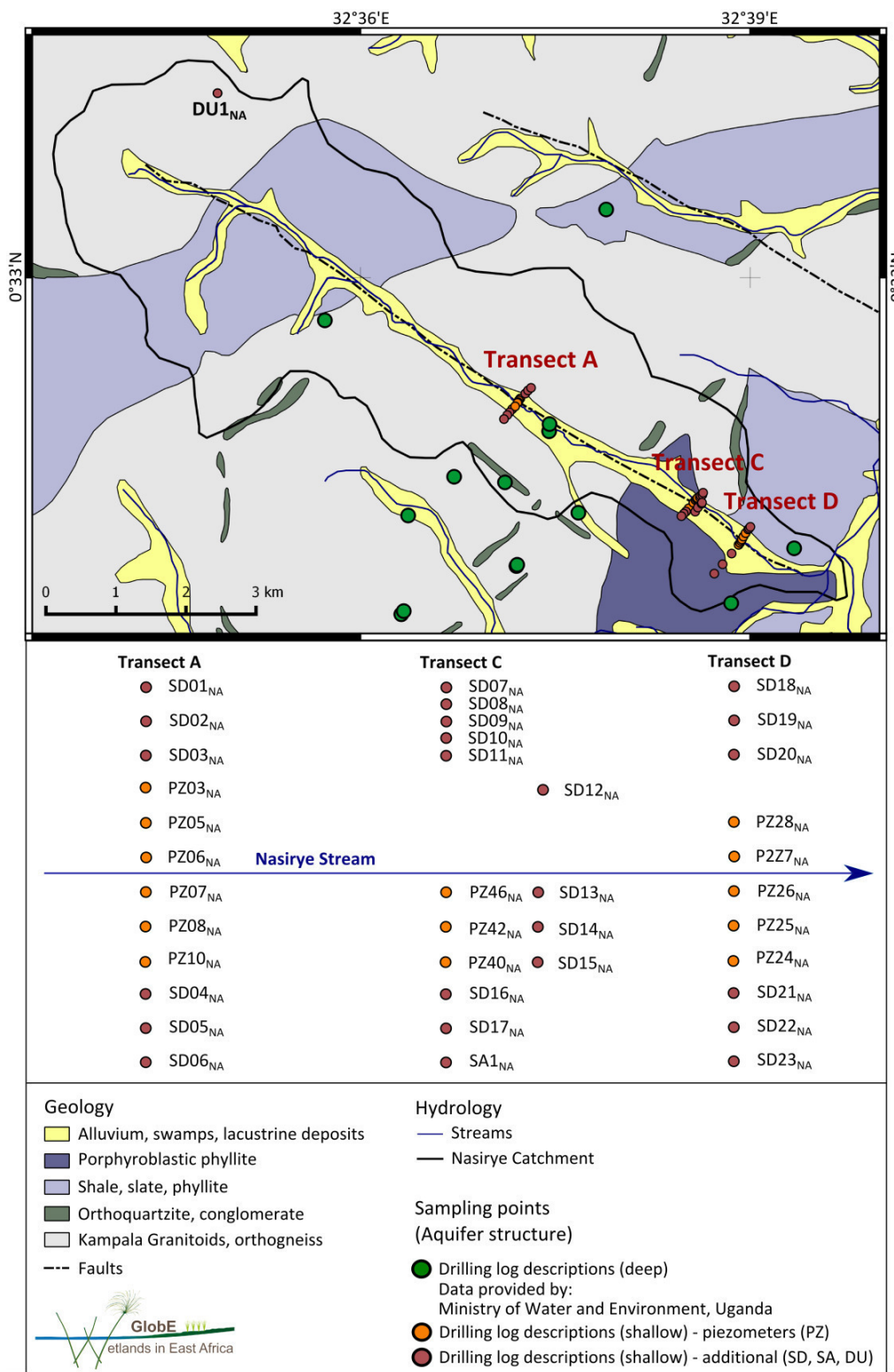


Fig. 5.6: Locations of sampling points related to data of aquifer structure and properties, including a schematic overview of the three transects. Data sources: GTK Consortium (2012) (geology, streams), Heiß (2016) (alluvium), Gabiri (unpublished) (Nasirye Stream) (NA).

Tab. 5.8: Depths and locations of saprolite and sediment samples and respective available data (NA).

Sampling point	Sampling depth below surface [m]	Mineralogical/geochemical data	Grain size distribution data	Sampling point	Sampling depth below surface [m]	Mineralogical /geochemical data	Grain size distribution data
SA1 <sub>NA</sub>	0.5	x		SD14 <sub>NA</sub>	1.6		x
	1.0	x			2.4	x	
	1.9	x			3.0		x
	2.7	x			3.5	x	
	3.6	x			4.0	x	
	4.8	x		PZ46 <sub>NA</sub>	0.2	x	
	5.1	x			0.5	x	
	6.2	x			1.8	x	
	6.8	x			2.2	x	
	7.2	x		SD15 <sub>NA</sub>	1.9		x
					2.9	x	x
PZ03 <sub>NA</sub>	0.8	x		PZ48 <sub>NA</sub>	0.2	x	
PZ05 <sub>NA</sub>	1.4	x			0.5	x	
	2.0	x			PZ49 <sub>NA</sub>	0.2	x
	2.3	x		0.5		x	
PZ10 <sub>NA</sub>	2.1	x		PZ50 <sub>NA</sub>	0.2	x	
PZ40 <sub>NA</sub>	0.2	x			0.5	x	
	0.5	x		SD12 <sub>NA</sub>	2.1	x	x
	2.2	x			SD11 <sub>NA</sub>	1.7	x
	2.9	x		2.9		x	
PZ42 <sub>NA</sub>	0.2	x		3.3	x		
	0.5	x		PZ24 <sub>NA</sub>	2.8	x	
	2.1	x			PZ26 <sub>NA</sub>	2.6	x
			PZ27 <sub>NA</sub>			3.0	x

### 5.2.2 Groundwater level data (NA)

Static groundwater level data of twelve deep pumping wells were provided by the Ministry of Water and Environment, Uganda (Fig. 5.7). Those levels were measured during the installation of the wells. Dynamic groundwater level data were measured on an hourly time resolution in 21 piezometers, with depths between 1.2 m and 3.2 m. Data were collected from November 2014 to August 2016. Two piezometers (PZ03<sub>NA</sub>, PZ24<sub>NA</sub>) were discarded, because the water table did not recover completely after pumping. Three other piezometers (PZ05<sub>NA</sub>, PZ08<sub>NA</sub>, PZ29<sub>NA</sub>) showed huge data gaps or high deviations between manual and sensor measurements, and were thus discarded, too. The remaining 16 piezometers showed deviations between manual and sensor measurements below 15 cm, with most of them showing deviations below 8 cm. Stream level data were gained from Gabiri (unpublished), who reported stream levels from each transect using an installed scale bar.

Elevation data was gained from the SRTM 1 Arc-Second Digital Global Elevation Model (30 m resolution) and from a DEM created based on differential GPS measurements (Asiimwe 2015), which was available for the wetland in the lower Nasirye Catchment. At transect C, the elevation of stream level was referred to heights of piezometers using a water level gauge.

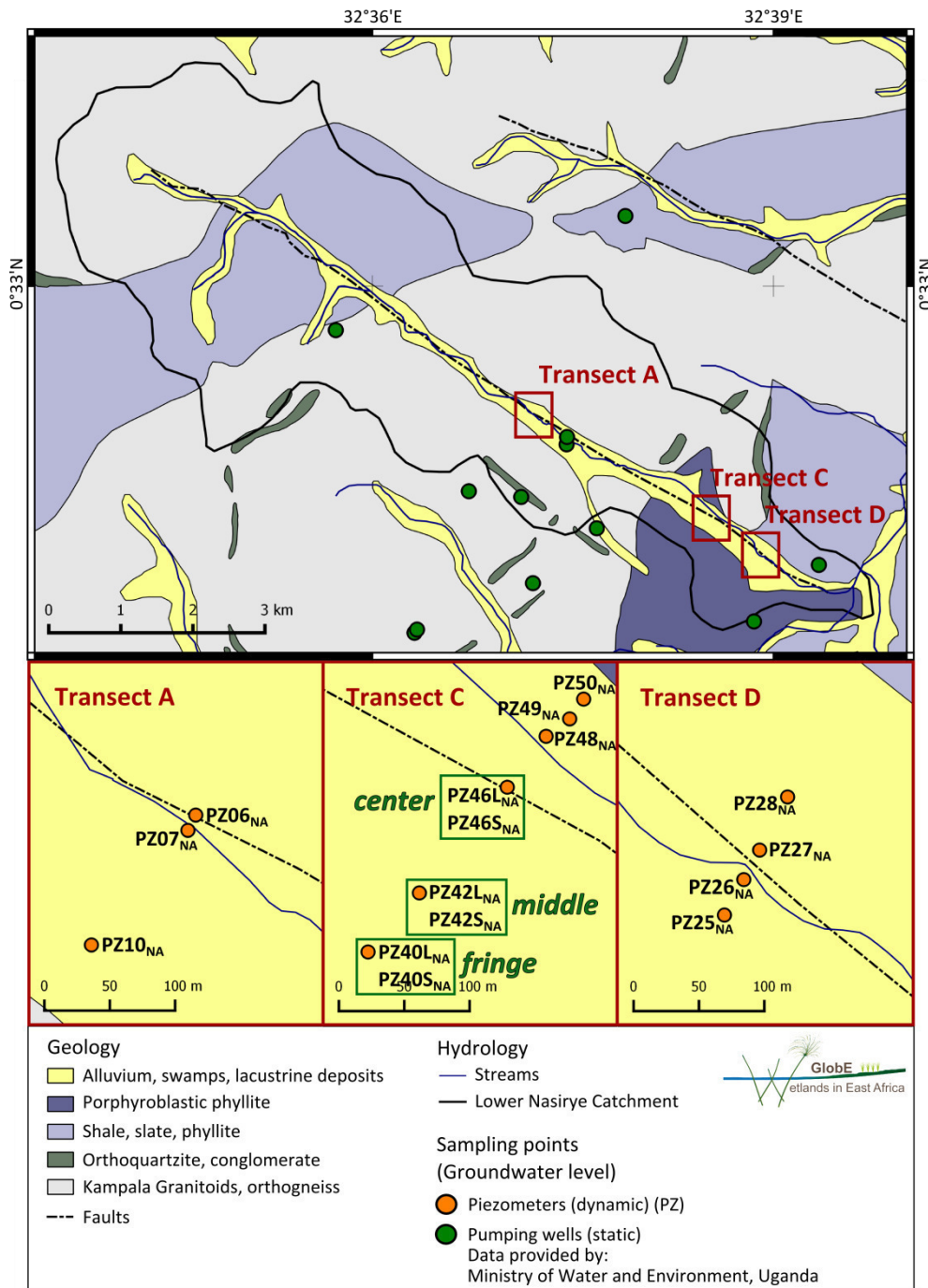


Fig. 5.7: Locations of sampling points related to groundwater level data. Data sources: GTK Consortium (2012) (geology, streams), Heiß (2016) (alluvium), Gabiri (unpublished) (Nasirye Stream) (NA).

### 5.2.3 Hydrochemical and isotopic data (NA)

All in all, 46 water sampling points were sampled including two flooding waters, one stream sampled at eight locations (Nasirye Stream), two springs, 20 shallow piezometers, three deep electrical pumping wells, ten deep hand pumping wells, and one deep open well (Fig. 5.8). Additionally, 33 suction cups were installed and sampled at transect C.

139 samples were collected during four snapshot samplings (Tab. 5.9). Snapshot samplings were carried out during November 2014, April to June 2015, October to November 2015, and June 2016. As rainy and dry seasons were not well marked, snapshot samplings will be referred to as autumn 2014, spring 2015, autumn 2015, and spring 2016. Regarding the snapshot samplings, hydrochemical data (EC, pH, Eh,  $O_2^{sat}$ ,

$O_2^{con}$ ,  $T_w$ ,  $T_A$ ,  $HCO_3^-$ ,  $Cl^-$ ,  $SO_4^{2-}$ ,  $NO_3^-$ ,  $NO_2^-$ ,  $Na^+$ ,  $K^+$ ,  $Mg^{2+}$ ,  $Ca^{2+}$ ,  $Fe^{2+}$ ,  $Mn^{2+}$ ,  $Al^{3+}$ ,  $SiO_2$ ,  $CO_2$ ) are available for 104 samples, and stable water isotope data ( $\delta^{18}O$ ,  $\delta^2H$ ) are available for 126 samples. Moreover, concentrations of  $F^-$ ,  $PO_4^{3-}$ , As, Cd, Cr, Cu, Ni, Pb, and Zn are available for all samples collected during spring 2016.

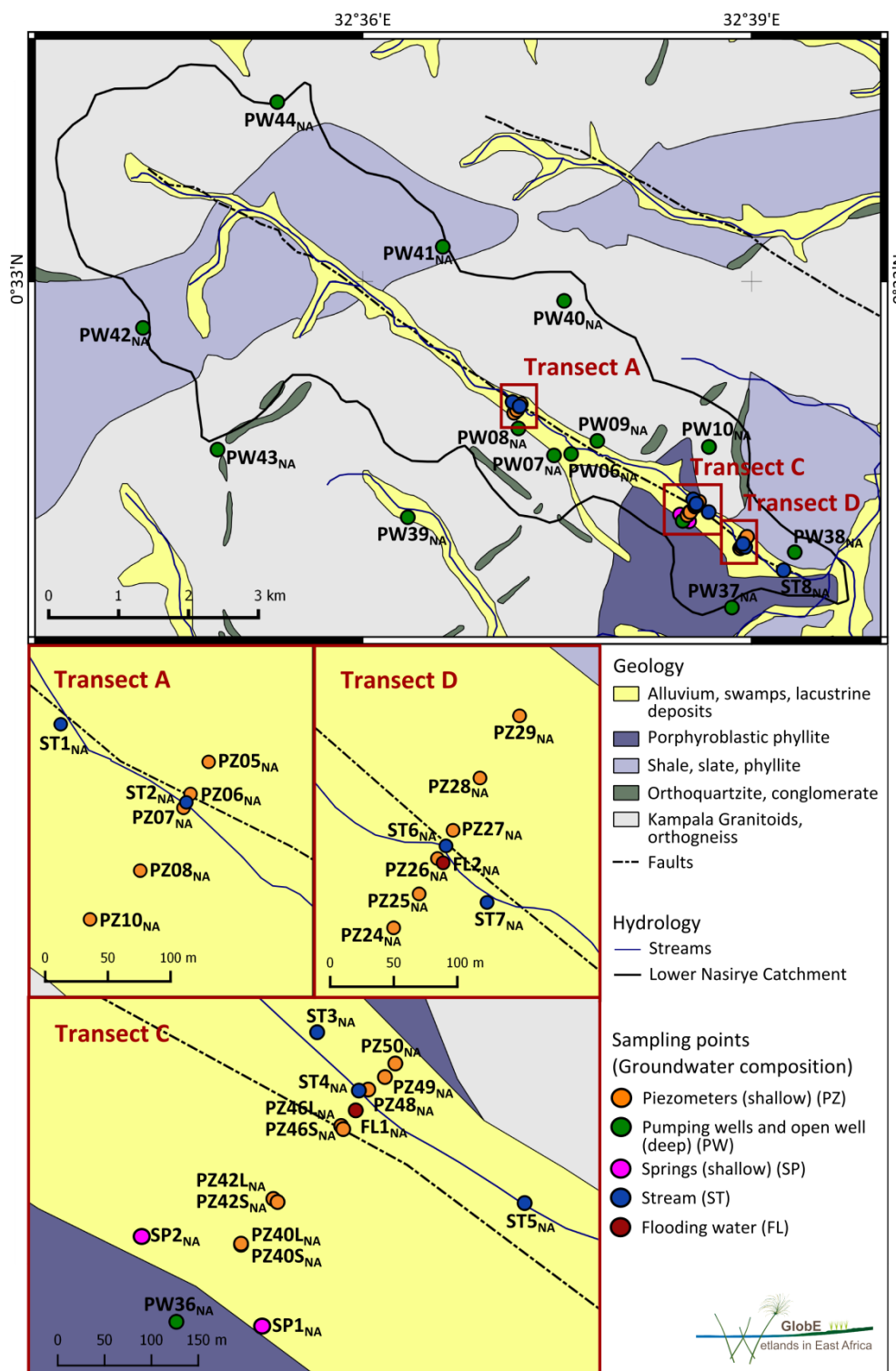


Fig. 5.8: Locations of sampling points related to hydrochemical and isotopic data. Data sources: GTK Consortium (2012) (geology, streams), Heiß (2016) (alluvium), Gabiri (unpublished) (Nasirye Stream) (NA).

**Tab. 5.9: Number of water samples analyzed for hydrochemistry and stable water isotopes during the four snapshot samplings. For the analysis of hydrochemistry, only samples with ion charge balance errors below 10 % are listed (NA).**

Data	Season	Flood	Stream	Pumping well	Piezometer	Spring	Suction cup
Hydrochemistry	Autumn '14	1	4	5	-	1	-
	Spring '15	-	6	12	12	1	-
	Autumn '15	-	3	5	15	1	3
	Spring '16	-	5	9	20	1	-
Stable water isotopes	Autumn '14	1	5	5	12	1	-
	Spring '15	-	6	12	14	1	-
	Autumn '15	1	4	5	20	2	3
	Spring '16	-	5	9	20	1	-

Monthly sampling of 18 selected sampling points was carried out from December 2014 to June 2016 (Tab. 5.10). Data of EC, pH,  $T_w$ ,  $Cl^-$ ,  $SO_4^{2-}$ ,  $NO_3^-$ ,  $Na^+$ ,  $K^+$ ,  $Ca^{2+}$ ,  $Mg^{2+}$ ,  $Fe^{2+}$ ,  $Mn^{2+}$ ,  $Al^{3+}$ , and  $SiO_2$  are available for 239 monthly samples, while data of stable water isotopes are available for 303 monthly samples.

**Tab. 5.10: Sampling points that were monthly sampled and analyzed for selected ions and stable water isotopes (NA).**

Sampling point	Type of sampling point
PZ40L <sub>NA</sub>	Piezometer
PZ40S <sub>NA</sub>	Piezometer
PZ42L <sub>NA</sub>	Piezometer
PZ42S <sub>NA</sub>	Piezometer
PZ46L <sub>NA</sub>	Piezometer
PZ46S <sub>NA</sub>	Piezometer
SP1 <sub>NA</sub>	Spring
ST1 <sub>NA</sub>	Stream
ST3 <sub>NA</sub>	Stream
ST5 <sub>NA</sub>	Stream
ST7 <sub>NA</sub>	Stream
PW07 <sub>NA</sub>	Pumping well
PW36 <sub>NA</sub>	Pumping well

Soil water at transect C near piezometers was sampled at twelve suction cups installed in two different depths (20 cm, 50 cm) in spring 2015. Sampling occurred once a week for six weeks (April to June 2015). Those 48 samples were analyzed for  $\delta^{18}O$  and  $\delta^2H$ . Furthermore, twelve samples of one week were analyzed for EC, pH,  $Na^+$ ,  $K^+$ ,  $Ca^{2+}$ ,  $Mg^{2+}$ ,  $Fe^{2+}$ , and  $SiO_2$ . Additionally, 49 soil water samples were taken from 21 suction cups installed at two different depths (30 cm, 50 cm) in four different treatment plots (Tab. 4.5 p.52: T01, T02, T09, T10) distributed over the three CFTs at transect C in spring 2015 (May) and autumn 2015 (October and November). Sampling in October 2015 occurred three days before and in November three days after the input of NPK-fertilizer in treatments plots T09. Not all suction cups were sampled during all three samplings, as some of them did not always bring water. However, a good coverage of all treatment plots and all CFTs is given. For these soil water samples, indicators of agriculture, such as  $NO_3^-$ ,  $K^+$ , and  $PO_4^{3-}$  were prioritized during water analyses. However, for most of them, data of EC, pH,  $\delta^{18}O$ , and  $\delta^2H$  are available, too. Three soil water samples were analyzed for all major anions and cations as well as for  $SiO_2$ ,  $Fe^{2+}$ , and  $Mn^{2+}$ . Those were included in the snapshot sampling of autumn 2015.

From June 2014 to June 2016, 83 weekly precipitation samples were collected and analyzed (Tab. 5.11).

**Tab. 5.11: Number of precipitation samples out of 83 samples in total and respective data availability of different analytes (NA).**

Analyte	Number of samples
$\delta^{18}\text{O}$ , $\delta^2\text{H}$	83
$\text{Cl}^-$ , $\text{SO}_4^{2-}$ , $\text{NO}_3^-$	61
$\text{Na}^+$ , $\text{K}^+$ , $\text{Mg}^{2+}$ , $\text{Ca}^{2+}$	60
$\text{SiO}_2$	60

#### 5.2.4 Precipitation data (NA)

Precipitation measurements (10 min time resolution) were obtained from a GlobE weather station located within the study site (Fig. 5.5:  $WS_{NA}$ ). Data gaps in precipitation records were filled with data of an additional tipping bucket located at the *fringe* (Gabiri unpublished).

## 6 Case study of the Ifakara study site

In the following section, the results of the Ifakara study site are described, interpreted, and discussed. The results of the analyses of aquifer structure (section 6.1), water dynamics (section 6.2), and water composition (section 6.3) are addressed first. All results are subsequently integrated in a conceptual model (section 6.4). Based on this conceptual model, origin and evolution of flooding water in the wetland are verified and quantified using hydrochemical modeling (section 6.5).

### 6.1 Aquifer structure and properties (IF)

The interpretation of existing geological and geomorphological maps, geological field mappings, and lithological descriptions of drilling logs resulted in a detailed knowledge of the three-dimensional geological setting and thus of the aquifer system. The evaluation of pumping tests, falling-head permeability tests, grain size analyses of sediment samples, and fracture measurements of outcrops allowed a hydrostratigraphic classification of the various geological units (Fig. 6.1).

Both, fractured rock and porous aquifers occur in the study site (Fig. 6.1). The metamorphic crystalline rocks of the Udzungwa Mountains, outcropping in the north (Fig. 2.6 p.15), represent a fractured rock aquifer (Aqf1<sub>IF</sub>). Porous aquifers consist of sediments, which overly the crystalline rocks south of the normal fault system and in small valleys between the hills. According to the lithological descriptions of these sediments, two major porous aquifers were identified, the Quaternary alluvial sediments (Aqp1<sub>IF</sub>) and the Neogene non-alluvial sediments (Aqp2<sub>IF</sub>). As no outcrops of Karoo sediments were observed in the study site and as their occurrence below the Quaternary and Neogene sediments is unproven (Geological Survey of Tanganyika 1962), this unit was not addressed.

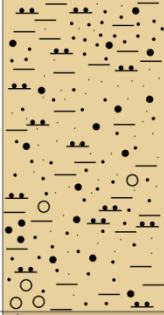
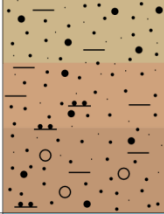


		Lithological unit	Lithological description	Porosity	Hydraulic conductivity [m/s]	Hydrostratigraphy
Quaternary		Alluvial sediments	meandering river deposits: sand, silt, clay (fine-grained overbank deposits and coarser channel deposits) alluvial fan deposits: gravel, sand, silt, clay (dominant grain size decreases from N to S) colluvial deposits: gravel, sand, silt, clay	porous	10 <sup>-6</sup> - 10 <sup>-2 b,c)</sup> highly variable	Aqp1 <sub>IF</sub>
Neogene		Non-alluvial sediments	pale locally ferruginous sands red-brown and light sandy earths ferruginized cemented sands and gravels or ferricretes	porous	10 <sup>-6</sup> - 10 <sup>-3 c)</sup> highly variable	Aqp2 <sub>IF</sub>
Permian/ Triassic		Karoo	sandstones, conglomerates <sup>a)</sup>			
Neo-proterozoic		Crystalline rocks	gneisses, granulites, amphibolites, pegmatites, migmatites	fractured	10 <sup>-7 b)</sup> low	Aqf1 <sub>IF</sub>

Fig. 6.1: Lithological and hydrostratigraphic standard section of the study site showing hydrogeological properties of the different units. Hydraulic conductivities were assigned based on <sup>a)</sup>Geological Survey of Tanganyika (1962), <sup>b)</sup>own data, and <sup>c)</sup>data provided by Rufiji Basin Water Board (RBWB) (IF).



Hereafter, the different hydrostratigraphic units are described in detail in terms of their structural, mineralogical, geochemical, and hydraulic properties (sections 6.1.1, 6.1.2, 6.1.3). Subsequently, the spatial distribution of the respective hydrostratigraphic units is described and discussed (section 6.1.4). This section also includes an evaluation of possible groundwater flow paths and hydraulic connections between aquifers.

### 6.1.1 Crystalline rocks (Aqf1<sub>IF</sub>)

The Neoproterozoic metamorphic crystalline rocks were classified as a fractured rock aquifer. Deep drilling logs located in this unit, as declared by Geological Survey of Tanganyika (1962), showed a porous layer of clay, angular sand, and gravel up to a thickness of 5 m and 15 m, overlying the crystalline rocks themselves (Fig. 5.2 p.56, Appendix A-A<sub>IF</sub>1: DLM1<sub>IF</sub>, DLM2<sub>IF</sub>). This layer was also observed during field mapping. The crystalline rocks only outcrop on top of the hills, at steep slopes, and in river beds. The described sedimentary layer is presumably a saprolite weathering profile, acting as a porous aquifer (section 3.3). Measured water table in the weathering profile was found at 2 m.b.s., indicating groundwater flow and storage in this layer.

The lithologies of the fractured rock aquifer were described at seven outcrops within the study site and four rock samples were taken and analyzed for their mineralogical and geochemical compositions. In accordance with the geological map (Geological Survey of Tanganyika 1962), the metamorphic rocks were mainly described as gneisses. In addition, amphibolites occurred as ligaments and lenses, while pegmatites were present as veins. In some parts, migmatites were observed. The two sampled gneisses consisted of feldspars, quartz, and more or less mica and hornblende (Fig. 6.2). The mineralogical composition of the leucosome within the migmatite was similar to the gneiss samples, whereas the melanosome showed a high content of plagioclases and a considerable amount of hornblende. Pegmatite solely consisted of feldspars and quartz. While Geological Survey of Tanganyika (1962) described the crystalline rocks as pyroxene granulites and gneisses, no pyroxene was found in the analyzed samples. According to the mineralogical compositions, chemical analyses displayed SiO<sub>2</sub> (average: 65 %) and Al<sub>2</sub>O<sub>3</sub> (average: 15 %) as the major oxides. Na<sub>2</sub>O, K<sub>2</sub>O, CaO, and MgO were abundant in variable amounts around 3 %, and Fe<sub>2</sub>O<sub>3</sub> averaged 5 %. Analyses of trace elements showed high amounts of barium, manganese, and strontium.

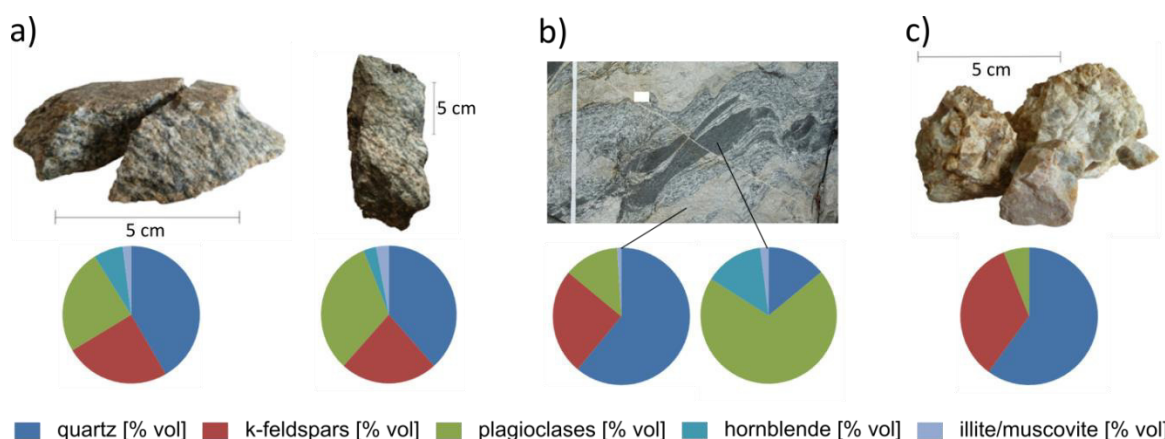


Fig. 6.2: Mineralogical compositions of a) gneisses (OC2<sub>IF</sub>, OC1<sub>IF</sub>), b) leucosome (left) and melanosome (right) of migmatite (OC4<sub>IF</sub>), and c) pegmatite (OC6<sub>IF</sub>) (IF).

Measurements of fracture directions at three points revealed the three major striking directions E-W, NE-SW, and NW-SE, with dipplings between 37° and 85°. These values correspond with those described by Mruma (2002). All described rocks showed negligible primary porosities, but fracture networks. Cal-

culated hydraulic conductivities of the fracture system displayed values of  $4 \times 10^{-7}$  and  $3 \times 10^{-7}$  m/s. Therefore, the fractured rock aquifer is assumed to be of low hydraulic conductivity (Hannappel et al. 2003).

### 6.1.2 Non-alluvial sediments ( $A_{q2_{IF}}$ )

The Neogene non-alluvial sediments represent a porous aquifer. According to Geological Survey of Tanganyika (1962), these sediments can be subdivided into i) pale locally ferruginous sands, ii) red-brown and light sandy earths, and iii) ferruginized cemented sands and gravels or ferricretes (Fig. 2.6 p.15). The two deep drilling logs located in this hydrostratigraphic unit, or rather in the pale locally ferruginous sands, showed alternations of sand and clay (Appendix A-A<sub>IF</sub>.1: DLR1<sub>IF</sub>, DLM3<sub>IF</sub>). The sand was described as rounded or angular with greyish and yellowish color, while the clay was described as sticky clay. Pure clay layers were solely found in the log located in the western study site, whereas mixtures of clay and sand were present in both logs. All in all, the drilling logs indicated a high variability of texture and sedimentological features in horizontal and vertical distribution.

The ferruginous and ferruginized features of the three lithological units (i, ii, iii) indicate an accumulation of iron in the sediments related to the formation of saprolite. This accumulation could have happened *in-situ* during weathering processes within the sediments, or the sediments could represent transported saprolite of the weathering profile that developed on the crystalline rocks. A combination of both processes is most conceivable. The red-brown and light sandy earths (ii) overlie the crystalline rocks in valleys (Geological Survey of Tanganyika 1962). They are probably equivalent to the saprolite overlay of the crystalline rocks (cf. section 6.1.1). Transported saprolite might have accumulated in the valleys. The cemented gravels and sands (iii) are located solely around the outcropping crystalline rocks near the southern fault. Hence, it is most likely that they represent a saprolite overlay, which was not eroded until now. Nevertheless, not enough lithological information is available to determine the exact origin and evolution of the non-alluvial sediments.

Hydraulic conductivities of the non-alluvial sediments were calculated based on transmissivities derived from secondary pumping test data. Five pumping tests were conducted at different boreholes within the pale locally ferruginous sands (i) and four within the ferruginized cemented sands and gravels (iii). Hydraulic conductivities ranged between  $5 \times 10^{-6}$  and  $1 \times 10^{-3}$  m/s in both lithological units, classified as highly variable (Hannappel et al. 2003). This high variability of hydraulic conductivity is consistent with the high variability of texture and sedimentological features, described in the drilling logs.

Even if no mineralogical or geochemical data are available, it is obvious that the three lithological units within this hydrostratigraphic unit differ in terms of their chemical compositions. Ferruginous parts are assumed to contain much more iron than non-ferruginous parts. Thus, a differentiation between ferruginous and non-ferruginous parts would make sense in terms of hydrogeochemistry. It is most likely that the hydraulic conductivity of the ferruginized parts is lower compared to the one of the sands and sandy earths. But a spatial differentiation was difficult, because the pale sands are also locally ferruginous. Consequently, the three lithological units were summarized as one hydrostratigraphic unit (Fig. 6.1).

### 6.1.3 Alluvial sediments ( $A_{q1_{IF}}$ )

The Quaternary alluvial sediments were identified as the main porous aquifer. Geological Survey of Tanganyika (1962) described the Quaternary sediments as alluvial sands, silts, and clays (cf. section 2.3.2). These undifferentiated sediments are composed of river and floodplain deposits, an alluvial fan, and colluvial sediments (Bonarius 1975). Considering recent knowledge about sedimentological structures of

alluvial fans and river deposits, it becomes clear why Geological Survey of Tanganyika (1962) did not differentiate the alluvial sediments. Vertical profiles of alluvial fans are irregular and show no distinct patterns (Einsele 1992). Nevertheless, grain sizes of alluvial fan deposits tend to decrease from proximal to distal zones (Chamley 1990). In the study site, this would result in coarser deposits in the north and finer deposits in the south, near Kilombero River. Meandering river deposits generally comprise fine-grained over-bank deposits and coarse-grained channel deposits (Miall 1996, Nichols 2009). Channel deposits are usually present as lenses and more frequent near the river. Within the study site, this contradicts with the spatial distribution of grain sizes in the alluvial fan and makes a differentiation even more difficult, considering that both units interfinger with each other. Additionally, colluvial sediments, deposited by smaller rivers along the southern normal fault, could show all kinds of grain sizes and maybe interfinger with the other two units as well.

Data regarding the lithology of the alluvial sediments comprise four deep drilling logs and 14 shallow drilling logs recorded during the installation of piezometers. As shallow drilling was done by hand, depths of shallow drilling logs did not exceed eight meters. Nevertheless, these drilling surveys revealed a more detailed description of the sediments.

The deep drilling log located near the mountain fringe, in the proximal parts of the alluvial fan, showed mainly angular stones alternating with layers of sand and clay (Fig. 5.1 p.55, Appendix A-A<sub>IF</sub>1: DLM4<sub>IF</sub>). In contrast, deep drilling logs located further south displayed thick sand layers with small amounts of clay in between overlain by a clay layer of about 10 m thickness (Appendix A-A<sub>IF</sub>1: DLM5<sub>IF</sub>, DLM6<sub>IF</sub>, DLM7<sub>IF</sub>). This clay layer was sometimes interrupted by sand and gravel layers. The drilling log located in the central part of the fan exposed the highest amount of clay within the sand layer. Thus, the deep drilling logs indicated a high spatial variability of the alluvial fan deposits and roughly endorsed the decrease in grain size from proximal to distal parts of the fan. However, finest sediments are rather found in the central alluvial fan than in the south.

Coinciding with the deep drilling logs, shallow drilling logs showed all kind of texture. However, the observed 10 m thick clay layer in the deep drilling logs was not observed in shallow drilling logs, indicating that this layer only exists locally. Thus, it is concluded that the alluvial sediments represent an unconfined aquifer.

All shallow drilling logs located in the floodplain displayed a layer of grey middle and coarse sand in prolonged depths (Fig. 6.3, Appendix A-A<sub>IF</sub>2: PZ01<sub>IF</sub>, PZ03<sub>IF</sub>, PZ05<sub>IF</sub>). This grey sand was also described by Geological Survey of Tanganyika (1962) to be the main deposit within the area. Furthermore, these five drilling logs had a high content of sand in all their layers and only thin layers of clay and silt in between. Thus, it is concluded that these five drilling logs represent channel deposits of the river system. The two drilling logs located north of the alluvial fan, near the southern normal fault, showed solely layers with sand as the dominant grain size (Appendix A-A<sub>IF</sub>2: PZ12<sub>IF</sub>, PZ13<sub>IF</sub>). These sands might be derived from small rivers draining the mountains or from former branches of Kilombero River. All other drilling logs, located within the delineated alluvial fan of Jätzold and Baum (1968), displayed alterations of layers with different grain sizes (Fig. 6.4, Fig. 6.5, Appendix A-A<sub>IF</sub>2: PZ08<sub>IF</sub>, PZ11<sub>IF</sub>, PZ14<sub>IF</sub>). Even two drilling logs within one central field trial showed different sedimentological descriptions of layers (e.g. Fig. 6.5). This indicates the large horizontal heterogeneity within the alluvial sediments, especially within the alluvial fan. It also demonstrates the difficulty to correlate drilling logs with each other.

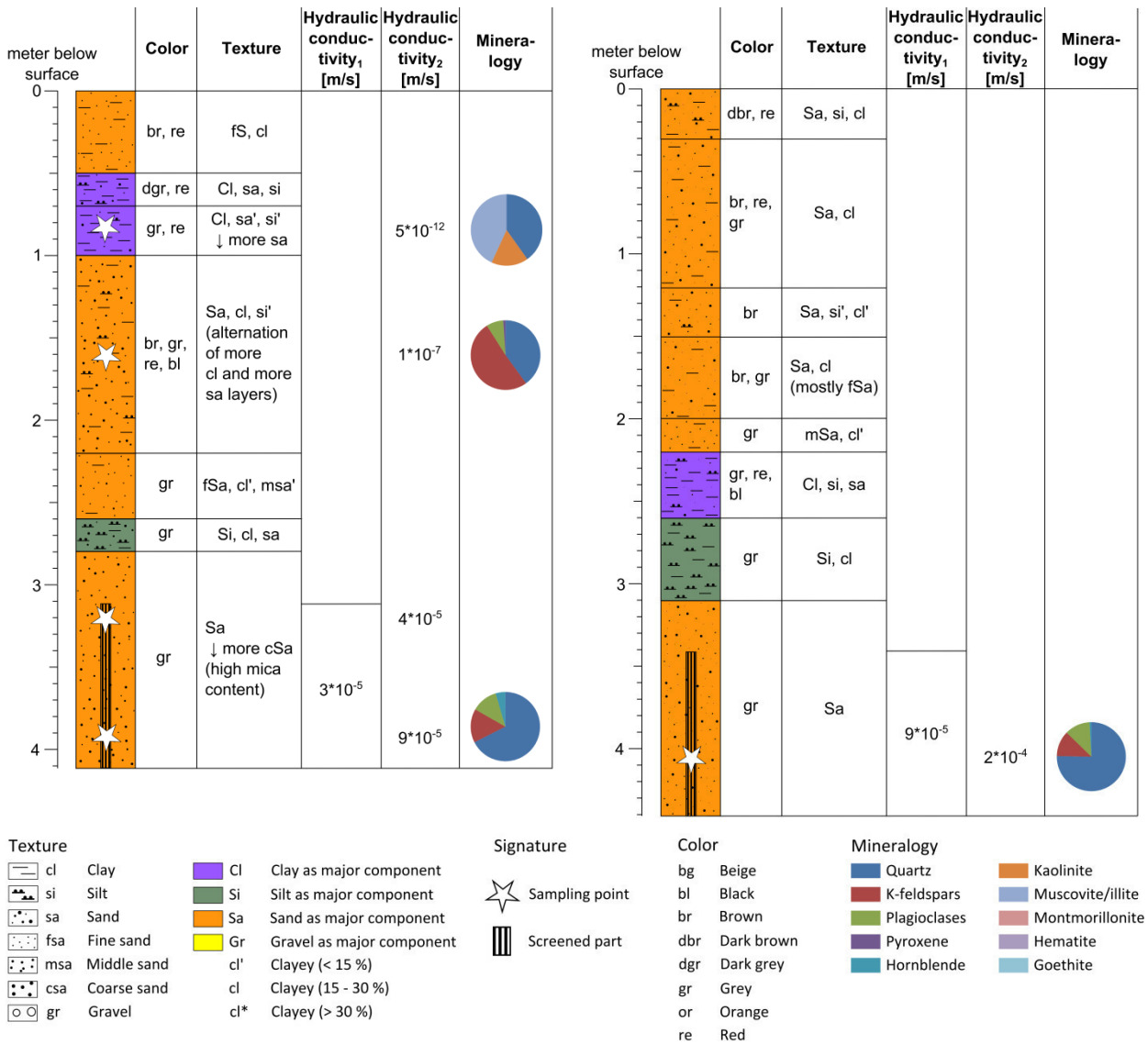


Fig. 6.3: Drilling logs of the two piezometers in the central field trial center (left: PZ02<sub>IF</sub>, right: PZ04<sub>IF</sub>). Hydraulic conductivities were derived from falling-head permeability tests (hydraulic conductivity<sub>1</sub>) and grain size distribution analyses (hydraulic conductivity<sub>2</sub>) (IF).

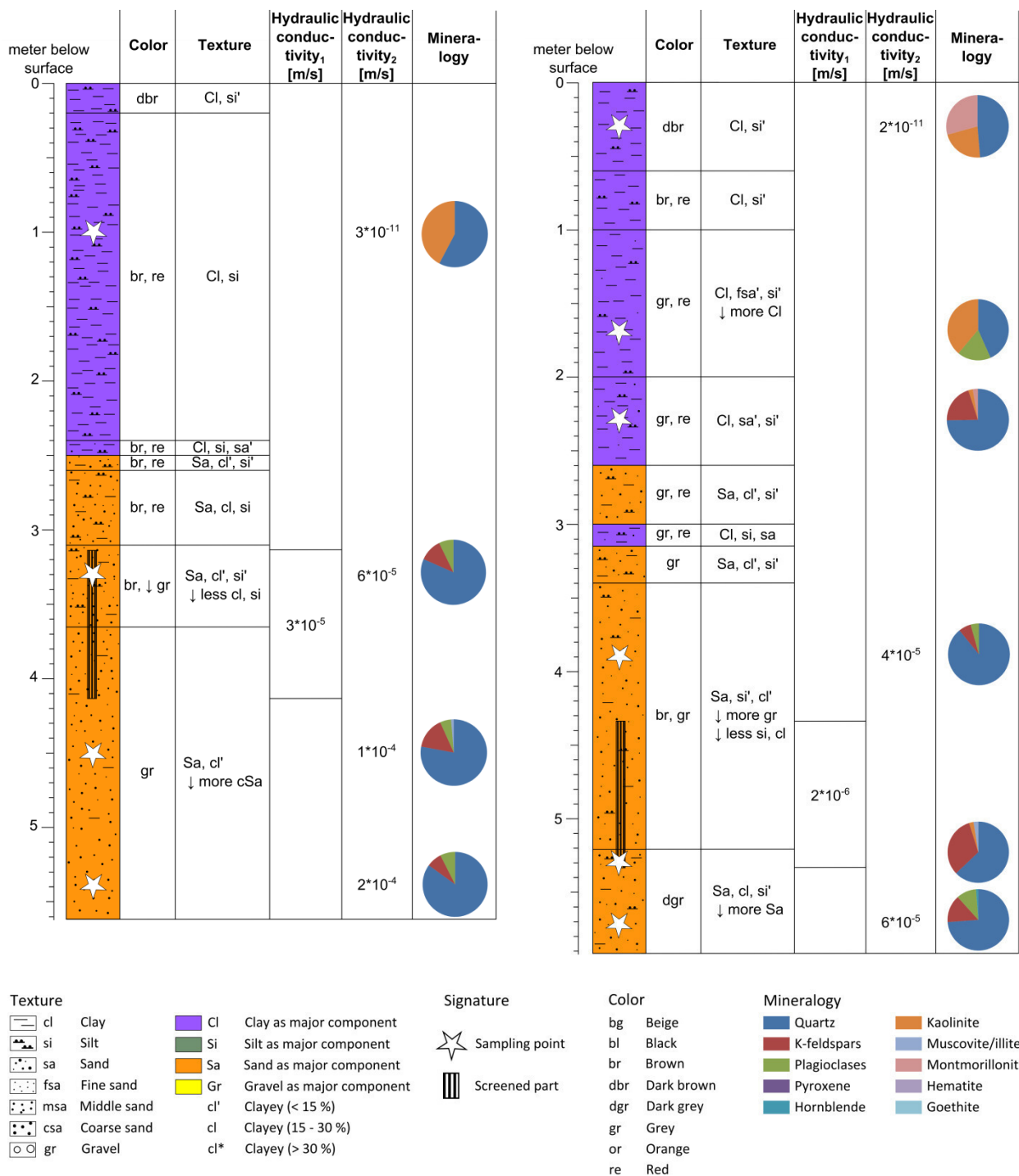
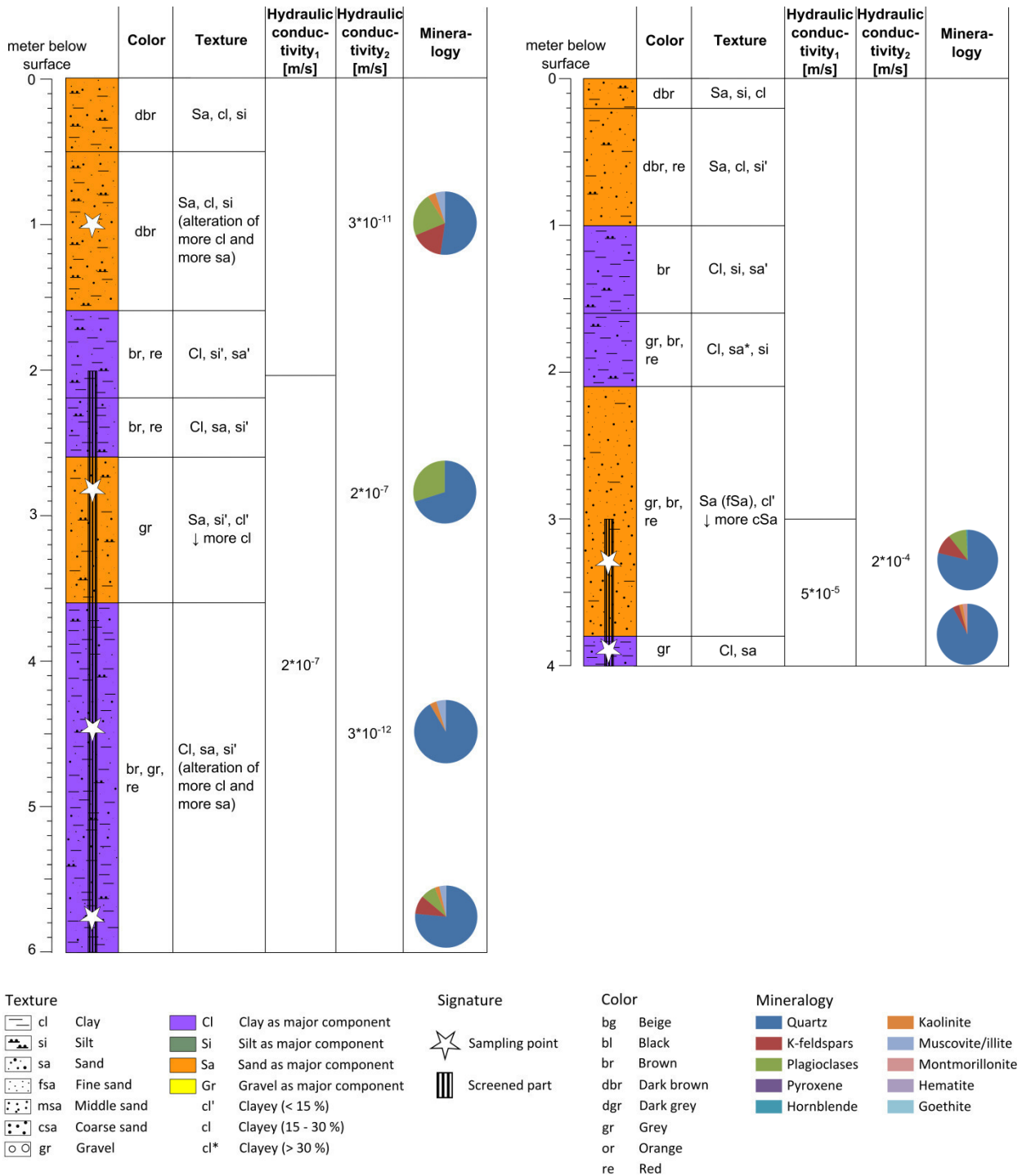


Fig. 6.4: Drilling logs of the two piezometers in the central field trial *middle* (left: PZ06<sub>IF</sub>, right: PZ07<sub>IF</sub>). Hydraulic conductivities were derived from falling-head permeability tests (hydraulic conductivity<sub>1</sub>) and grain size distribution analyses (hydraulic conductivity<sub>2</sub>) (IF).



**Fig. 6.5:** Drilling logs of the two piezometers in the central field trial *fringe* (left: PZ09<sub>IF</sub>, right: PZ10<sub>IF</sub>). Hydraulic conductivities were derived from falling-head permeability tests (hydraulic conductivity<sub>1</sub>) and grain size distribution analyses (hydraulic conductivity<sub>2</sub>) (IF).

The sandy layers were exclusively composed of quartz, k-feldspars, plagioclases, and some hornblende, with quartz being the dominant mineral. Major oxides were SiO<sub>2</sub> (average: 69 %), Al<sub>2</sub>O<sub>3</sub> (average: 15 %). Fe<sub>2</sub>O<sub>3</sub> showed an average of 5 %. Average amounts of all other oxides were below 1 %. Compared to the crystalline rocks, the sediments contained more quartz and less feldspars, but in general the mineralogical compositions were similar. Geochemically, oxides of major cations were depleted in the sediments. The more clayey layers of the alluvial sediments comprised quartz, feldspars, muscovite, and clay minerals, such as kaolinite, illite, and montmorillonite (e.g. Fig. 6.4). These clay minerals probably developed

during *in-situ* silicate weathering. Additionally, the upper layers had higher LOI values compared to the lower layers, indicating the occurrence of organic matter. All sediments were enriched in manganese, barium, and strontium, coinciding with increased trace elements in the crystalline rocks. As most of the crystalline rocks surrounding the Kilombero Valley are composed of rocks similar to those situated in the study site, the chemical composition of crystalline rocks is assumed to represent the chemical source of the valley sediments. This assumption was confirmed by the distribution of samples in a ternary diagram of the trace elements lanthanum (La), scandium (Sc), and thorium (Th) (Fig. 6.6). Those trace elements are suitable indicators of sediment origin, due to their low mobility during weathering (Middelburg et al. 1988, Nyakairu and Koeberl 2002). The ternary diagram shows that most of the sediment samples originated from mixtures of the crystalline rocks.

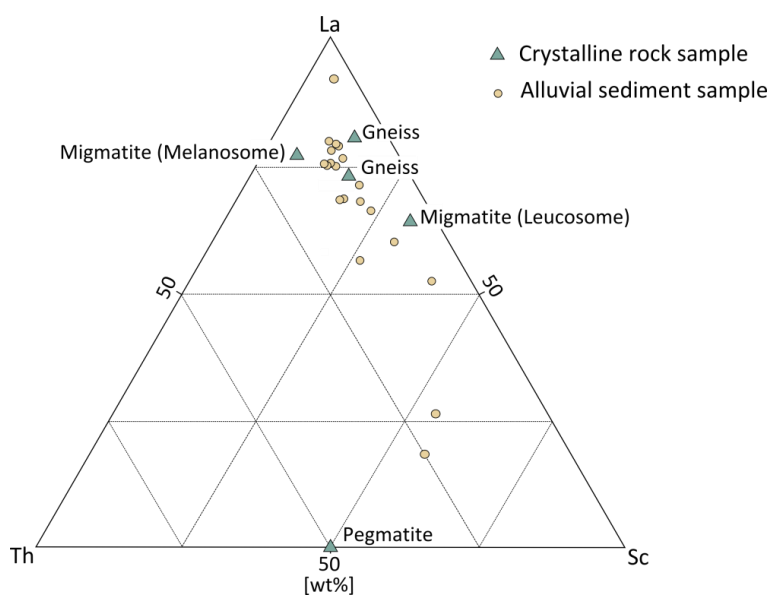


**Fig. 6.6:** Distribution of the crystalline rock and alluvial sediment samples in a ternary diagram of the trace elements lanthanum (La), scandium (Sc), and thorium (Th) (IF).

During weathering of crystalline rocks and the subsequent transport of eroded material, minerals that are more weatherable decrease, while minerals that are less weatherable increase in their relative amount. Following the weatherability of silicate minerals (Goldich 1938, section 3.3.1), quartz weathers much slower than feldspars, pyroxenes, and hornblende. This explains why the sediment samples contained less of the latter ones and more quartz than the crystalline source rocks. The low amounts of major cation oxides in the sediments confirm transportation and weathering. These cations have been removed from the sediments by dissolution and leaching.

Within the alluvial sediments, hydraulic conductivities were determined at three different scales. Data of 24 pumping tests are available (RBWB) (10 m scale). Falling-head permeability tests were conducted at twelve piezometers (m scale), and 16 sediment samples were analyzed for their grain size distributions (cm scale). The pumping tests were conducted at hand pumping wells located in the sediments of the alluvial fan. Calculated hydraulic conductivities ranged from  $3 \times 10^{-6}$  to  $8 \times 10^{-2}$  m/s, indicating a high spatial variability on a large scale. Falling-head permeability tests, conducted at piezometers, revealed hydraulic conductivities between  $2 \times 10^{-7}$  and  $9 \times 10^{-5}$  m/s. These values reflect the hydraulic conductivities of the respective screened layers. While the layer of grey sand had relatively uniform values between  $2 \times 10^{-5}$  and  $9 \times 10^{-5}$  m/s, the other piezometers, located in the alluvial fan and colluvial deposits, showed lower values ranging from  $2 \times 10^{-7}$  to  $2 \times 10^{-5}$  m/s. The calculation of hydraulic conductivity based on grain size distribution analyses resulted in highly variable values. Sediment samples from the

grey sand layer revealed hydraulic conductivities of  $4 \times 10^{-5}$  to  $2 \times 10^{-4}$  m/s, corresponding perfectly with the ones calculated by falling-head permeability tests (Fig. 6.3). The sampled clay layers can be considered nearly impermeable, with hydraulic conductivities around  $10^{-12}$  and  $10^{-11}$  m/s (e.g. Fig. 6.4).

A comparison of the calculated hydraulic conductivities for the three different scales showed that median and minimum values decreased with decreasing scale (Fig. 6.7). Chapuis et al. (2005) and Chesnaux et al. (2011) stated that scale effects of hydraulic conductivity measurements are not expressed in homogeneous porous aquifers. Thus, they are solely related to heterogeneities within the assessed aquifer and not related to skin effects as proposed by other authors before (e.g. Rovey and Niemann 2001). Usually, one would think that the largest scale derives the most reliable values of hydraulic conductivity. Nevertheless, the observed differences between the different methods in this study might be explained by several reasons and are not imperatively related to scaling issues. Pumping tests were solely conducted at pumping wells. These wells were most likely placed in locations with higher hydraulic conductivities than their surroundings. Furthermore, it might be that hydraulic conductivities derived from pumping test data overestimate the actual values, because no information about saturated thickness was available. Therefore, the saturated thickness was calculated based on the bottom of the well, but not based on the base of the entire aquifer. These factors might have induced an overestimation of hydraulic conductivities derived from pumping tests.

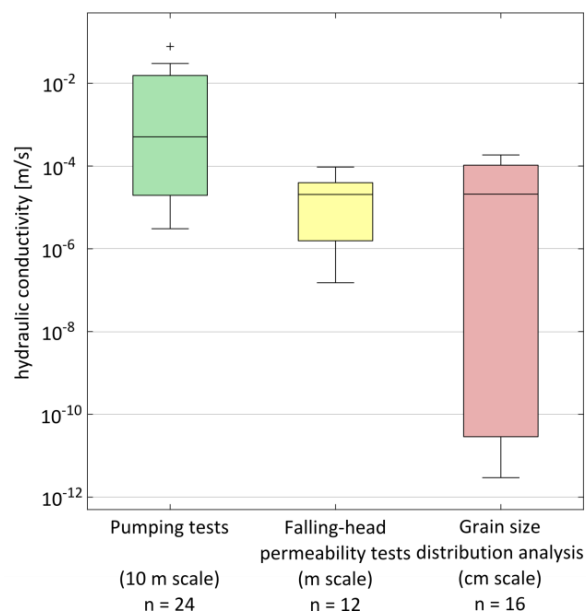


**Fig. 6.7:** Boxplots of hydraulic conductivities of the alluvial sediments determined on three different scales (IF).

Liu et al. (2002) as well as McCloskey and Finnemore (1996) measured maximum hydraulic conductivities of  $10^{-3}$  m/s in alluvial fan deposits. Thus, the very high values determined by pumping tests in this study are assumed to result from errors in saturated thickness values. The very small values determined for some samples on cm-scale are, except for one sample, all related to layers within the first, often clayey meter of depth. These layers are not important in terms of the aquifer and not included in pumping test or falling-head permeability test data, as they fall outside the saturated zone. Hydraulic conductivities derived from grain size distribution analyses and falling-head permeability tests fit well to each other, if the same layer was assessed. This indicates that both methods revealed reliable and plausible results. Nevertheless, the high variability of hydraulic conductivities does not allow the calculation of a lumped hydraulic conductivity for the whole unit of alluvial sediments. Due to the spatial variability, it is also not recommended to assign hydraulic conductivities to different parts of this unit. Thus, the hydrau-



lic conductivity of alluvial sediments was found to be highly variable with plausible values between  $10^{-6}$  and  $10^{-2}$  m/s.

#### 6.1.4 Spatial distribution of aquifers and hydraulic connections (IF)

Based on the geological map and the evaluation of drilling logs, a hydrogeological map (Fig. 6.8) and a schematic hydrogeological cross section, crossing the study site from north to south, were developed (Fig. 6.9).

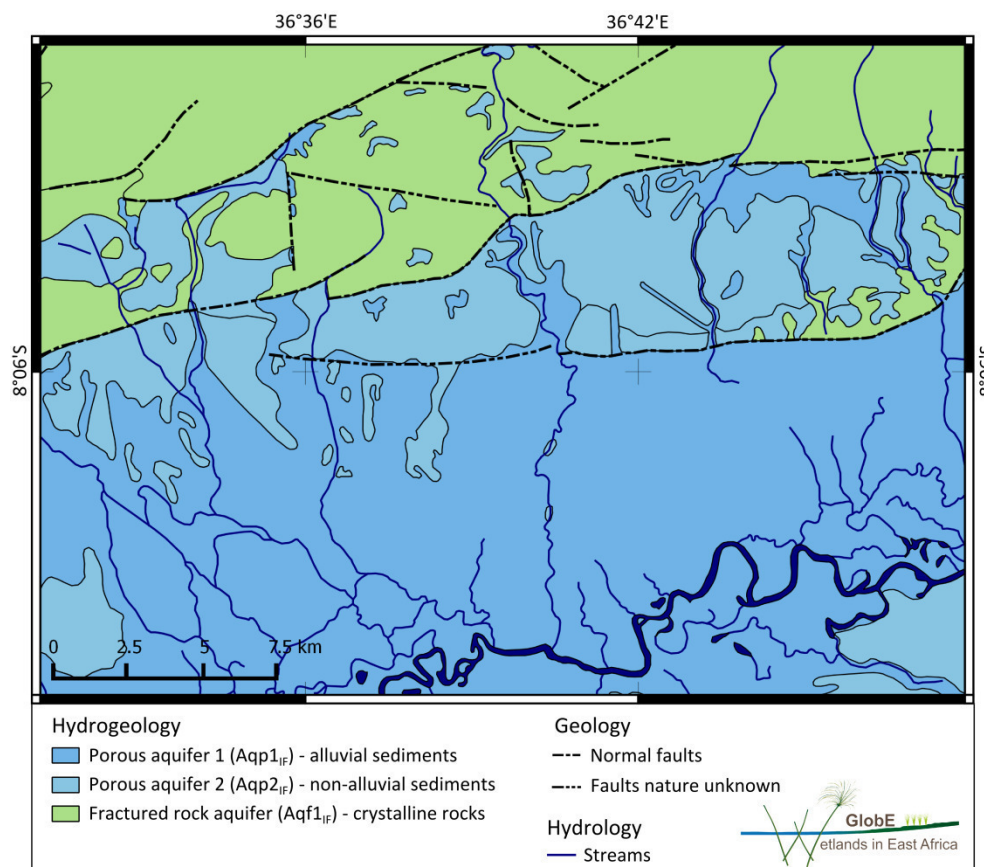


Fig. 6.8: Hydrogeological map of the study site. Units are labeled and colored according to Figure 6.1. Data sources: Geological Survey of Tanganyika (1962) (geology, streams) (IF).

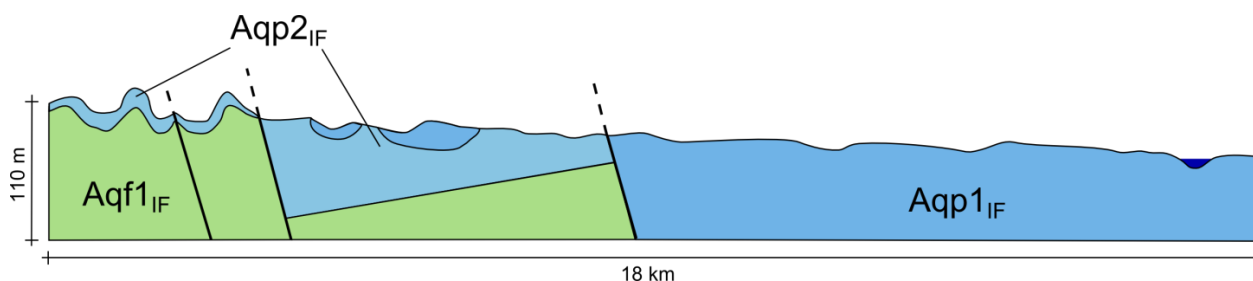


Fig. 6.9: Schematic hydrogeological cross section, crossing the study site from north to south. Units are labeled and colored according to Figure 6.1 (IF).

Main groundwater flow is expected to take place in the porous aquifer, represented by the alluvial sediments (Aqp1<sub>IF</sub>). This aquifer showed a complex structure with high, medium, low permeable, and impermeable zones on large and small scales. Thus, there are zones of mobile and immobile water within the aquifer. It is assumed that the whole alluvial sediments act as one big aquifer, although the occurrence of small perched aquifers is likely as well. The alluvial sediments represent not only the major

aquifer in terms of spatial coverage and thickness, but also in terms of groundwater extraction. Many hand pumping wells are located within this unit, but also bigger electrical pumping wells are found. Considering the relatively permeable parts of this aquifer near Kilombero River, a hydraulic connection between the porous aquifer and the stream bed of Kilombero River is expected.

The fractured rock aquifer (Aqf1<sub>IF</sub>) showed low hydraulic conductivities, indicating a minor role in the entire groundwater flow system. However, this fractured rock aquifer is extensively covered with a saprolite weathering profile, which acts as a porous aquifer. Hence, huge parts of this weathering profile are assumed to be eroded, due to tectonic movements. Parts of the non-alluvial sediments compose of transported saprolite. Hence, reworked and in-situ weathering profile were assigned to the hydrostratigraphic unit of the non-alluvial sediments in the cross section (Fig. 6.9: Aqp2<sub>IF</sub>). The weathering profile acts as a storage layer for infiltrating precipitation, which subsequently percolates into the underlying fractured rock aquifer.

The fractured rock aquifer is separated from the two porous aquifers in the south via a normal fault system. Thus, the tilted block and the down-thrown block of the fractured rock aquifer underlie the non-alluvial sediments and the alluvial sediments, respectively. The thickness of the sediments is unknown. Drilling logs located in the sediments, reaching depths up to 25 m in the non-alluvial sediments and 30 m in the alluvial sediments, did not reach the crystalline rocks. According to Le Gall et al. (2004), the sedimentary infilling of the valley north of Kilombero Valley reaches depths up to 8,000 m, with 3,000 m Neogene sediments and 4,000 to 5,000 m Karoo sediments. Nevertheless, Geological Survey of Tanganyika (1962) supposed a ridge of Precambrian rocks around Ifakara, proven by the occurrence of weathered gneiss at a depth of 2 m.b.s. south of Kilombero River near Ifakara. For the non-alluvial sediments it is most likely that they are lower in thickness compared to the alluvial sediments, because they are located on the tilted block of crystalline rocks.

Hydraulic connections between the different aquifers might occur along the two normal faults. However, in some parts, faults could act as hydraulic barriers between different aquifers. Furthermore, deeper groundwater might rise along the preferential flow paths within the fault system. Groundwater exchange between the fractured rock aquifer and non-alluvial sediments might take place along the northern normal fault. The southern fringe of the tilted block outcrops near the southern normal fault. In those parts, flow between fractured rock aquifer and alluvial sediments might occur as well. However, as fractures of the fractured rock aquifer mainly strike in parallel direction to the fault system, the major flow direction of water is parallel to the fault system, too. Thus, flow of groundwater between the fractured rock aquifer and the porous aquifers is assumed to be small. A hydraulic connection between non-alluvial and alluvial sediments along the southern normal fault is likely. Nevertheless, in those parts, where the crystalline rocks outcrop, they could act as a barrier between the two porous media.

## 6.2 Water dynamics (IF)

The analysis of water dynamics is based on groundwater level measurements conducted in nine piezometers and seven pumping wells in the alluvial sediments (Fig. 5.3 p.57). Unfortunately, no recent data regarding stream level or discharge were available.

Groundwater levels ranged between 8 m below surface in the alluvial fan in dry season (W266<sub>IF</sub>) and 2.5 m above surface in the floodplain in rainy season (PZ02<sub>IF</sub>). In general, groundwater levels increased during rainy season in all wells and piezometers, showing seasonal variations depending on rainfall conditions. All piezometers located in the floodplain showed groundwater levels above surface during rainy seasons, confirming the delineated floodplain (Fig. 5.1 p.55). However, it needs to be considered that

groundwater level above surface measured in the piezometers does not implicitly mean that flooding occurs at the surface. Nevertheless, the unconfined conditions of the aquifer allow the assumption that groundwater levels above surface and flooding at the surface usually occur simultaneously.

Differences between rainy and dry seasons were highest for the piezometer located directly next to Kilombero River (PZ03<sub>IF</sub>) and lowest for a piezometer at *fringe* (PZ10<sub>IF</sub>). Piezometers at *fringe* revealed smallest depths to water table during dry season compared to the other piezometers.

### 6.2.1 Groundwater flow direction (IF)

Groundwater levels above sea level (hydraulic heads) showed high uncertainties, due to high uncertainties in elevation data gained from SRTM DEM. Uncertainties in elevation result from different sources, such as the spatial resolution of the DEM (30 m). Jarvis et al. (2004) stated uncertainties in SRTM elevation of up to 8 m. In order to provide more accurate elevation data, the remote sensing research group of GlobE conducted Unmanned Aerial Vehicle (UAV) surveys. Unfortunately, the digital elevation model, based on these surveys, was not available until end of 2016 and could thus not be used in this study. Therefore, the SRTM DEM values were used, although they are highly uncertain.

Due to the high uncertainties, a numerical interpolation of hydraulic heads in order to create piezometric maps was unrewarding. Nevertheless, the comparison of hydraulic heads was used to provide information about major hydraulic gradients and groundwater flow directions. Data proved a constant groundwater flow direction from NNW to SSE within the study site throughout the whole year, indicating groundwater discharge to Kilombero River. The hydraulic gradient decreased in flow direction. In the northern parts of the alluvial fan (pumping wells), the gradient was relatively steep and thus reliable, as the differences between hydraulic heads of different points were higher than their expected uncertainty. In contrast, within the flat areas of the floodplain and the southern alluvial fan, the uncertainties of hydraulic heads did not allow for a determination of groundwater flow direction. Here, the hydraulic gradient is expected to be flat according to the topography.

### 6.2.2 Groundwater table fluctuations (IF)

In order to get more insights into the groundwater flow regime, hydrographs of groundwater levels below surface are described and discussed. Based on the results of correlation analyses (section 4.2.2), the 16 hydrographs of groundwater levels below surface were divided into seven groups (Tab. 6.1, Fig. 6.10, Appendix B-B<sub>IF</sub>1).

One group solely consists of piezometer PZ03<sub>IF</sub>, which is located in a 50 m distance to Kilombero River (Fig. 6.10). This hydrograph is assumed to represent the water level of Kilombero River (*kr*), which could not be measured directly. Group p1 is represented by all piezometers located in the floodplain. These are the piezometers at *center* (PZ02<sub>IF</sub>) and *middle* (PZ06<sub>IF</sub>, PZ07<sub>IF</sub>), and PZ01<sub>IF</sub>. Group p2 is located within the alluvial fan at *fringe* (PZ09<sub>IF</sub>, PZ10<sub>IF</sub>), and group p3 is located east of the alluvial fan (PZ13<sub>IF</sub>, PZ14<sub>IF</sub>). The three groups of wells (*w1*, *w2*, *w3*) did not show any spatial pattern and are all located within the alluvial fan.

**Tab. 6.1: Pearson’s correlation coefficients of hydrographs of different piezometers and wells. Coefficients equal or higher than 0.95 are marked as bold. Sampling points are sorted and signed to groups based on correlation analyses. Representative hydrographs are marked as bold (IF).**

	kr	p1				p2		p3		w1		w2		w3		
	PZ03 <sub>IF</sub>	PZ01 <sub>IF</sub>	PZ02 <sub>IF</sub>	<b>PZ06<sub>IF</sub></b>	PZ07 <sub>IF</sub>	PZ09 <sub>IF</sub>	<b>PZ10<sub>IF</sub></b>	<b>PZ13<sub>IF</sub></b>	PZ14 <sub>IF</sub>	<b>W061<sub>IF</sub></b>	W135 <sub>IF</sub>	W172 <sub>IF</sub>	W068 <sub>IF</sub>	<b>W266<sub>IF</sub></b>	W070 <sub>IF</sub>	<b>W227<sub>IF</sub></b>
<b>kr</b>	<b>PZ03<sub>IF</sub></b>															
	PZ01 <sub>IF</sub>	0.93														
<b>p1</b>	PZ02 <sub>IF</sub>	0.94	<b>0.99</b>													
	<b>PZ06<sub>IF</sub></b>	0.82	<b>0.98</b>	<b>0.95</b>												
	PZ07 <sub>IF</sub>	0.73	<b>0.97</b>	<b>0.95</b>	<b>1.00</b>											
<b>p2</b>	PZ09 <sub>IF</sub>	0.87	0.59	0.80	0.85	0.59										
	<b>PZ10<sub>IF</sub></b>	0.88	0.78	0.80	0.77	0.75	<b>0.99</b>									
<b>p3</b>	<b>PZ13<sub>IF</sub></b>	0.91	0.93	0.93	0.93	0.92	0.63	0.88								
	PZ14 <sub>IF</sub>	0.93	0.88	0.90	0.86	0.84	0.86	0.94	<b>0.96</b>							
<b>w1</b>	<b>W061<sub>IF</sub></b>	0.47	0.80	0.73	0.87	0.87	0.72	0.45	0.69	0.53						
	W135 <sub>IF</sub>	0.43	0.73	0.66	0.79	0.81	0.68	0.38	0.62	0.45	<b>0.98</b>					
	W172 <sub>IF</sub>	0.33	0.69	0.59	0.75	0.74	0.67	0.24	0.54	0.36	<b>0.97</b>	<b>0.96</b>				
<b>w2</b>	W068 <sub>IF</sub>	0.70	0.89	0.83	0.93	0.93	0.79	0.71	0.87	0.75	0.88	0.89	0.76			
	<b>W266<sub>IF</sub></b>	0.59	0.82	0.73	0.86	0.87	0.81	0.56	0.73	0.59	0.93	0.80	0.70	<b>0.96</b>		
<b>w3</b>	W070 <sub>IF</sub>	0.72	0.91	0.87	<b>0.96</b>	<b>0.95</b>	0.79	0.72	0.89	0.80	0.92	0.87	0.81	0.92	0.89	
	<b>W227<sub>IF</sub></b>	0.84	0.97	0.93	<b>0.98</b>	<b>0.98</b>	0.84	0.82	0.94	0.88	0.84	0.80	0.70	0.93	0.87	<b>0.97</b>

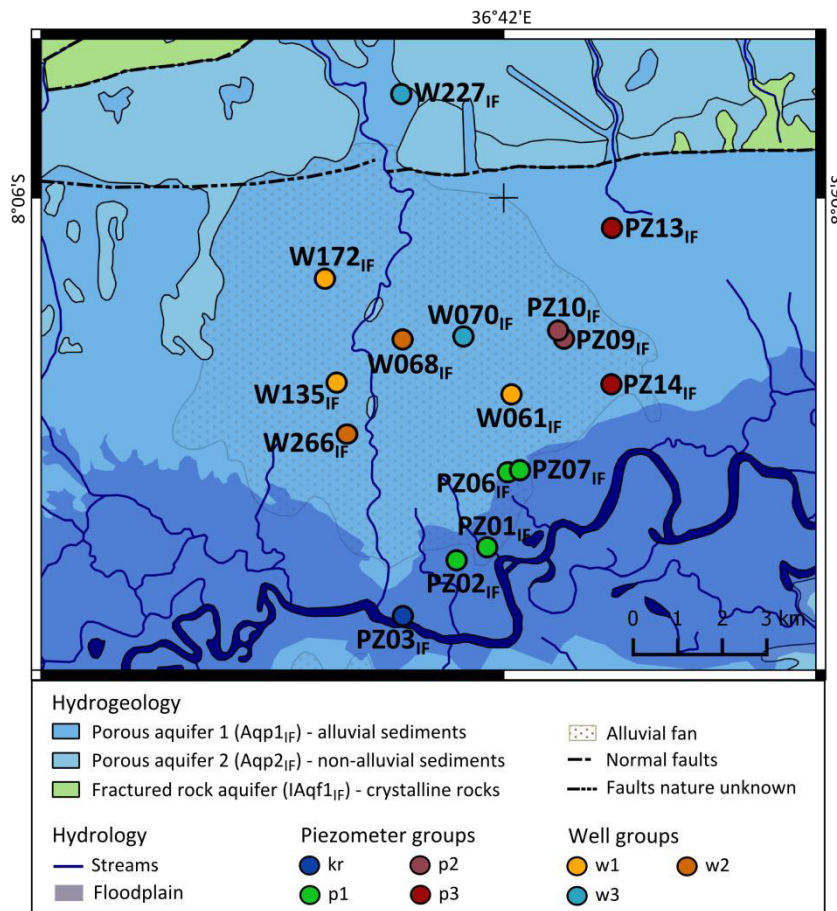


**Fig. 6.10: Spatial distribution of the groups of piezometers and wells based on correlation analyses of hydrographs within the southern study site. Data sources: Geological Survey of Tanganyika (1962) (geology, streams), Jätzold and Baum (1968) (alluvial fan) (IF).**

Group p2 showed clear responses to rainfall events in late 2015 (Fig. 6.11), indicating direct recharge within the study site. At the *fringe*, the location of p2 piezometers, groundwater levels below surface

were shallow (< 1.5 m.b.s.) throughout the whole year. Thus, the unsaturated zone is small in thickness, allowing rapid percolation of infiltrated rainfall to the groundwater table. The other hydrographs did not show such rapid responses to rainfall. Here, thicker unsaturated zones might cause longer percolation times. However, it might also be that no direct recharge occurs in those wells and piezometers.

Hydrographs of p1 and, to a lesser extent, of p3 and w3 showed similar behaviors compared to kr, with rising water levels at the beginning of flooding events (Fig. 6.11). The level of Kilombero River and the amount of precipitation within Kilombero Catchment are most probably correlated. Hence, rises in groundwater level at the beginning of flooding events can be either derived from river bank infiltration or from direct groundwater recharge. Furthermore, groundwater recharge in the north of the study site could lead to an increased southwards flow of groundwater, resulting in rising groundwater levels. This southwards flow was proven based on hydraulic heads, as outlined above.

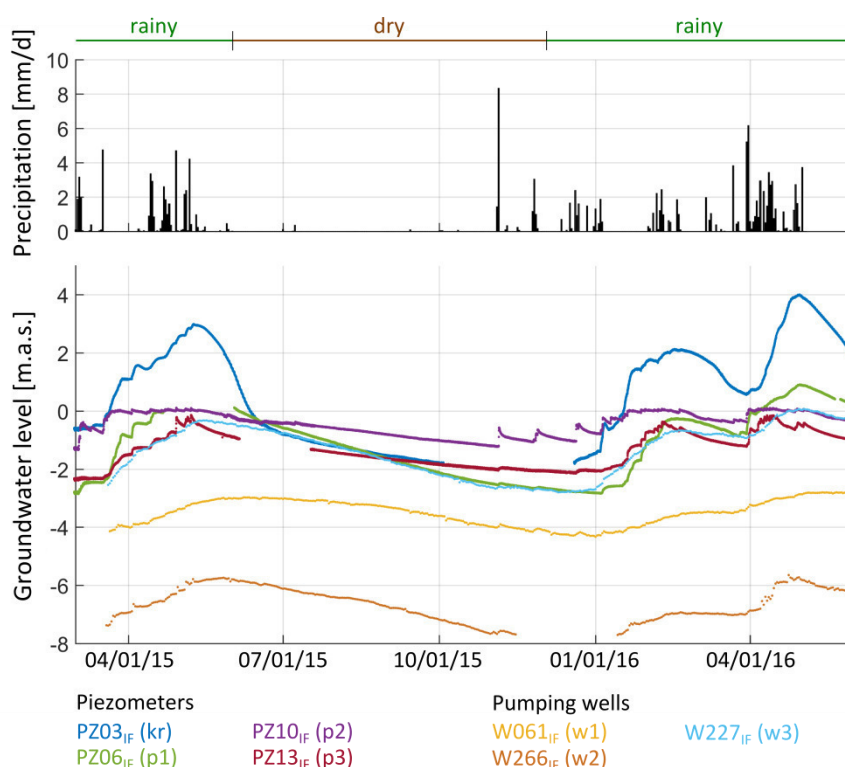


**Fig. 6.11: Comparison of daily precipitation (above) and hydrographs of the representative piezometers and wells that were selected based on correlation analyses (below) (IF).**

During the flooding event in early 2016, the river water started rising at the beginning of January (Fig. 6.11). The groundwater level of PZ06<sub>IF</sub> (p1) started to respond mid of January 2016. This response of PZ06 to the rising river level was most likely induced by lateral river bank infiltration, showing a time offset of around two weeks. This offset occurred to be shorter with decreasing distance of piezometers of p1 to Kilombero River (Appendix B-B<sub>IF</sub>1). Thus, the hydraulic gradient, which is roughly directed towards the river, was inverted near the river during this flooding event. After the mid of January up to late March 2016, the water levels of kr and p1 rose and fell simultaneously. A second, even higher, flooding event started on the 1st of April 2016. Nevertheless, the groundwater level of PZ06 already started rising three days before that date. This shows that the interaction processes between floodplain groundwater and Kilombero River were active in both directions, changing the direction of hydraulic gradient from time to time. Thereby, infiltration, from stream to groundwater, occurs mainly at the beginning of flooding events, when the river level rises fast and induces a hydraulic gradient away from the river. Exfiltration, from groundwater to stream, occurs most probably during the rest of the year, as

indicated by the constant flow direction to Kilombero River in the northern parts of the alluvial sediments.

In contrast, river bank infiltration was disproved for group w3. The hydraulic gradient between W227<sub>IF</sub> (w3) and PZ03<sub>IF</sub> (kr) was reliable and directed to the river. However, W227<sub>IF</sub> might be influenced by the river level of Lumemo River, due to its vicinity to this tributary. Groundwater levels of w3 started rising before p1, indicating that the increase in groundwater level was not induced by lateral river bank infiltration. This is also true for the other sampling points in the alluvial fan, which did not show strong responses to flooding events. For piezometers of p3, which are located in the flat areas east of the alluvial fan, river bank infiltration could neither be proven nor disproven by hydrograph analysis.

Considering the grouping of hydrographs, it becomes clear that all piezometers located in the floodplain (p1) showed temporal influences of river bank infiltration, inverting the hydraulic gradient in the floodplain at the beginning of flooding events. Such a lateral infiltration of river water to groundwater might also occur at the piezometers of p3. Within the alluvial fan, river bank infiltration is not likely, as shown by hydraulic gradients and hydrographs. Nevertheless, as reliable elevation data are lacking, a more detailed assessment of groundwater flow patterns and interactions with Kilombero River is difficult.

### 6.3 Water composition (IF)

The following section gives a detailed overview of the groundwater and surface water composition with respect to temporal and spatial variations. This overview is based on several water samples taken during four snapshot samplings representing rainy and dry season 2014 and 2015. First, hydrochemical compositions of water samples are described. Afterwards, results of multivariate statistical analyses (PCA, HCA) are presented and discussed, and identified cluster groups are interpreted in terms of hydrochemical characteristics and evolution (section 6.3.1). Subsequently, the composition of stable water isotopes within the water samples is outlined (section 6.3.2). Finally, water quality is assessed in terms of human health, acceptability, and agricultural production (section 6.3.3). All hydrochemical and isotopic data are documented in Appendix C-C<sub>IF</sub>.

#### 6.3.1 Hydrochemistry (IF)

Sampled surface waters were stream water of Kilombero River and its tributaries, and flooding water at the central field trials (CFTs) *center*, *middle*, and *fringe*. Groundwater is subdivided into shallow groundwater, sampled at draw wells and piezometers up to 10 m depth, and deep groundwater, sampled at pumping wells between 10 and 100 m depth. While electrical conductivities (ECs) of surface water were low and homogeneous, with values between 40 and 413  $\mu\text{S}/\text{cm}$ , groundwater showed a higher variability of EC, ranging between 20 and 2210  $\mu\text{S}/\text{cm}$  (Fig. 6.12). However, most samples had ECs below 500  $\mu\text{S}/\text{cm}$ . The pH values were neutral to acidic, with lower values for groundwater than for surface water. Oxygen content and redox potential were higher for surface water than for groundwater. However, groundwater samples showed oxidizing conditions as well.

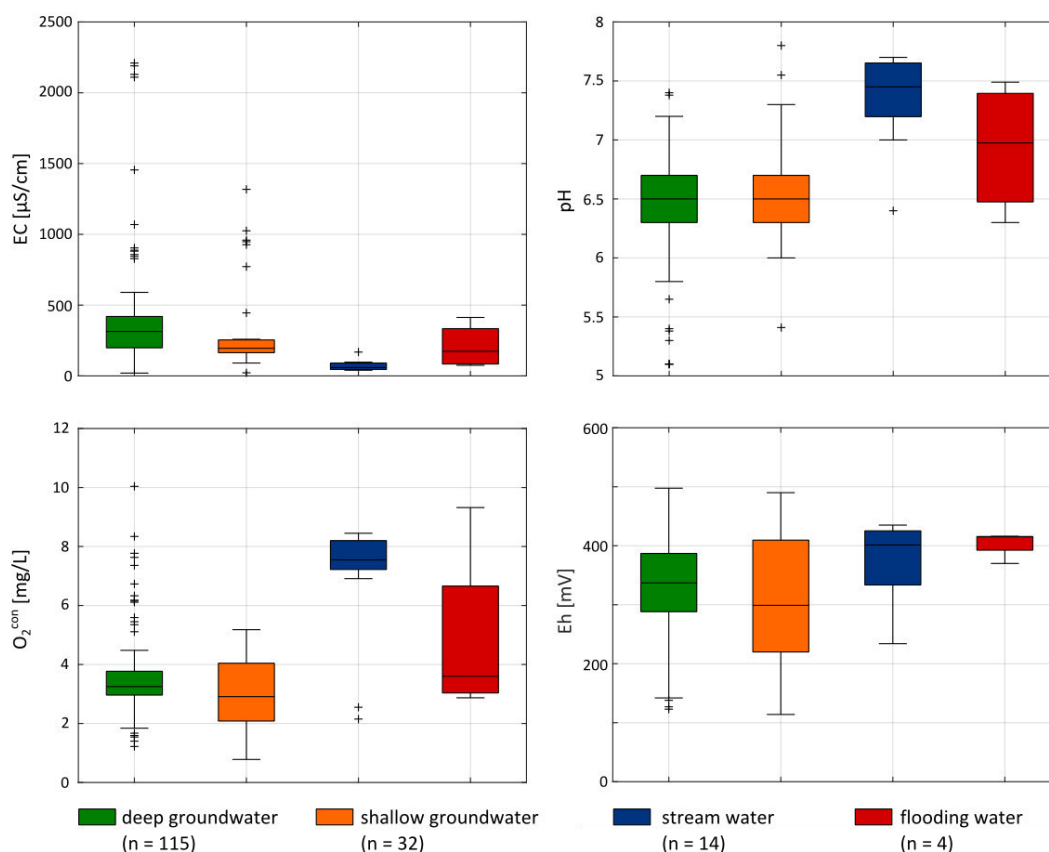


Fig. 6.12: Boxplots of measured *in-situ* parameters (electrical conductivity (EC), pH,  $\text{O}_2^{\text{con}}$ , redox potential (Eh)) of deep and shallow groundwater, stream water, and flooding water (IF).

### 6.3.1.1 Stream water (IF)

ECs of the main stream waters (Kilombero and Lumemo rivers, Fig. 5.4 p.58:  $\text{ST1}_{\text{IF}}$ ,  $\text{ST2}_{\text{IF}}$ ) were similar throughout the seasons with  $42 \pm 1 \mu\text{S}/\text{cm}$  for Kilombero and  $54 \pm 4 \mu\text{S}/\text{cm}$  for Lumemo River. Other stream waters were represented by smaller seasonal streams, draining the mountain range, with ECs ranging between 86 and 196  $\mu\text{S}/\text{cm}$ .

The pH values of Kilombero and Lumemo rivers ranged between 7.3 and 7.7. For Kilombero River, a differentiation in oxygen content was observed. Values were higher in dry seasons (7 mg/L in both years) than in rainy seasons (2 mg/L in both years). Temperatures of Lumemo River were higher in dry than in rainy seasons, whereas temperatures of Kilombero River remained stable throughout the seasons. Hydrochemical composition of stream water did not vary much from season to season (Fig. 6.13). All sampled stream waters fell within the  $\text{Na-HCO}_3$  water type, except for the small tributary Kihogosi River (western study site), which belonged to the  $\text{Ca-HCO}_3$  water type.

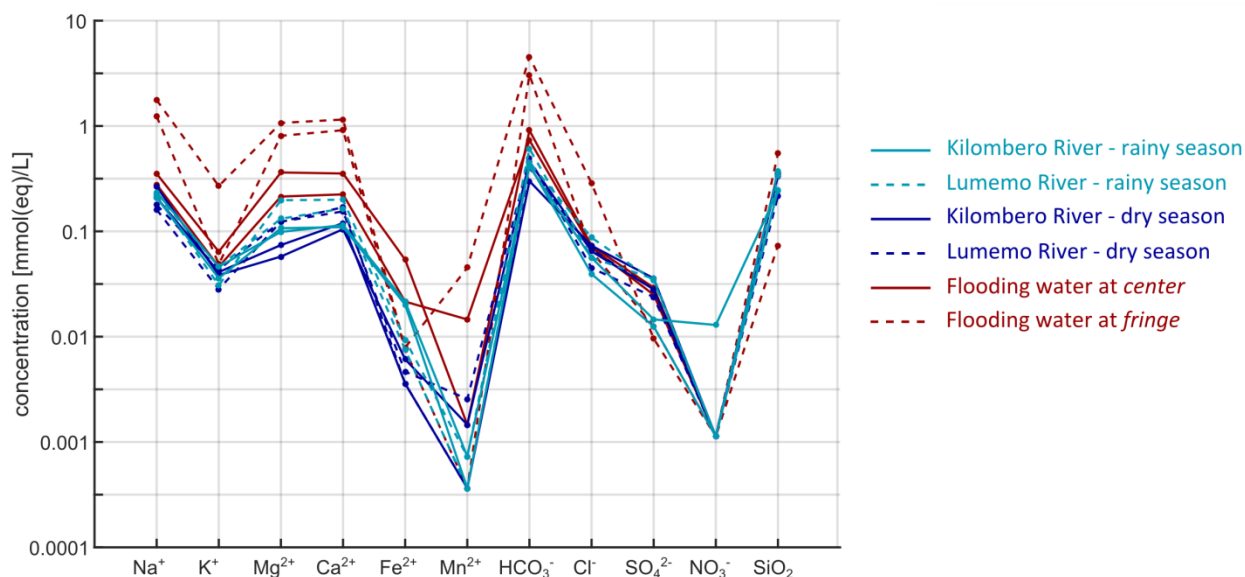


Fig. 6.13: Schoeller diagram of the main stream water samples (Kilombero and Lumemo rivers) and flooding water samples (center and fringe) for 2014 and 2015 (IF).

### 6.3.1.2 Flooding water (IF)

Flooding waters mainly belonged to Na-HCO<sub>3</sub> water type, with flooding water at *center* in 2015 belonging to Mg-HCO<sub>3</sub> water type. ECs, temperatures, and pH-values of flooding water were lower at *center* compared to *fringe* (Tab. 6.2). Redox potential indicated oxidizing conditions for all flooding waters, and oxygen content was higher in 2015 compared to 2014. The two flooding waters at *center* and *fringe* differed strongly from each other in terms of hydrochemistry (Fig. 6.13). Flooding water at *center* showed a similar hydrochemical composition compared to stream water of Kilombero River, while flooding water at *fringe* displayed higher HCO<sub>3</sub><sup>-</sup>, Na<sup>+</sup>, Mg<sup>2+</sup>, and Ca<sup>2+</sup> concentrations than stream water. *In-situ* parameters and hydrochemistry showed that spatial variability of flooding water was more significant than temporal variability.

Tab. 6.2: Measured *in-situ* parameters of flooding water at *center* and *fringe* during rainy seasons 2014 and 2015 (IF).

<i>In-situ</i> parameter	Flooding water at <i>center</i>		Flooding water at <i>fringe</i>	
	2014	2015	2014	2015
Electrical conductivity [ $\mu$ S/cm]	75	93	413	255
Temperature of water [ $^{\circ}$ C]	25.2	27.1	29.2	29.5
pH-value	6.7	6.3	7.5	7.3
Redox potential [mV]	370	416	415	415
Oxygen content [mg/L]	3.2	4.0	2.9	9.3

### 6.3.1.3 Groundwater (IF)

Most of the groundwater samples fell within the Na-HCO<sub>3</sub> water type. Considering that aquifers are made up of silicate minerals, this water type indicates a strong influence of silicate weathering. This influence was confirmed by remarkable concentrations of SiO<sub>2</sub> (13-125 mg/L). Some samples belonged to Ca-HCO<sub>3</sub>, Mg-HCO<sub>3</sub>, or Na-Cl water type. No difference was observed between shallow and deep groundwater in terms of water type and major ion hydrochemistry (Fig. 6.14). Similarly, no relation between water type and hydrostratigraphic or lithological unit was observed. Nevertheless, variability of major ion hydrochemistry and EC (20-2210  $\mu$ S/cm) was high in general.



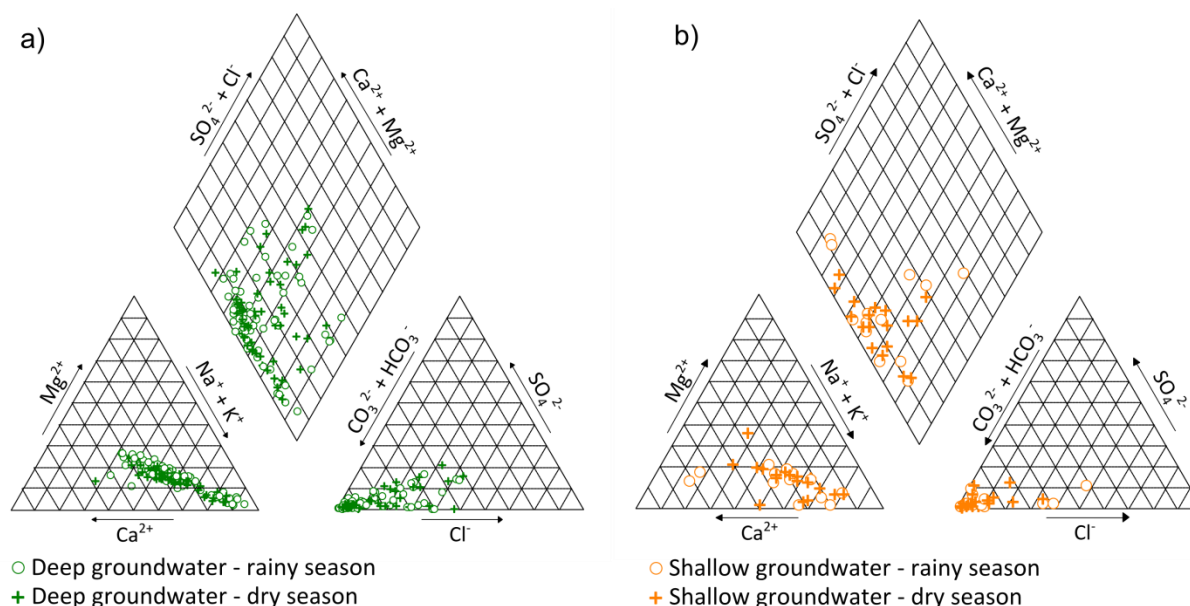


**Fig. 6.14: Piper diagrams of a) deep groundwater samples and b) shallow groundwater samples (IF).**

Temporal variation of hydrochemistry was small (Fig. 6.14). EC stayed almost stable in shallow and deep groundwater during the four snapshot samplings. However, histograms of differences in ECs between rainy and dry seasons showed a trend of decreased ECs during rainy season, although absolute differences remained small (Fig. 6.15). Sign-tests revealed that differences were significant between dry season 2014 and rainy season 2015, and between rainy and dry season 2015. Differences between rainy and dry season 2014 were not significant.

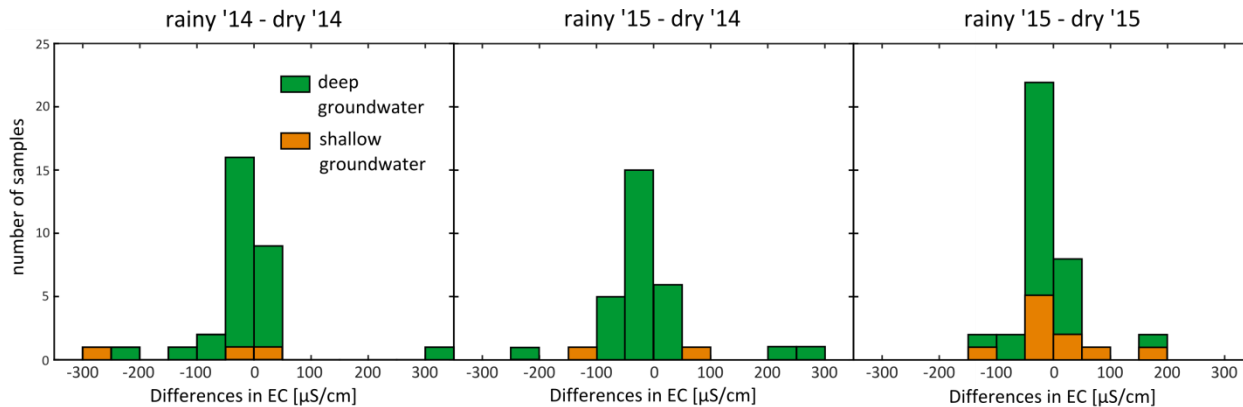


**Fig. 6.15: Histograms showing the distribution of differences in electrical conductivities (ECs) for shallow and deep groundwater between rainy and dry seasons (IF).**

In contrast, spatial variation of EC was higher than temporal. Mineralization, expressed by EC, throughout the whole study site was heterogeneous, and even wells located next to each other could show different values (Fig. 6.16). In general, no clear spatial pattern was observed. However, a hotspot of highest ECs was observed in the western part of the study site. Furthermore, within the alluvial fan, ECs were highest in its central parts. Sampling points located next to Lumemo or Kilombero River were not lower in EC than others, indicating no dilution of groundwater, due to infiltration of stream water.

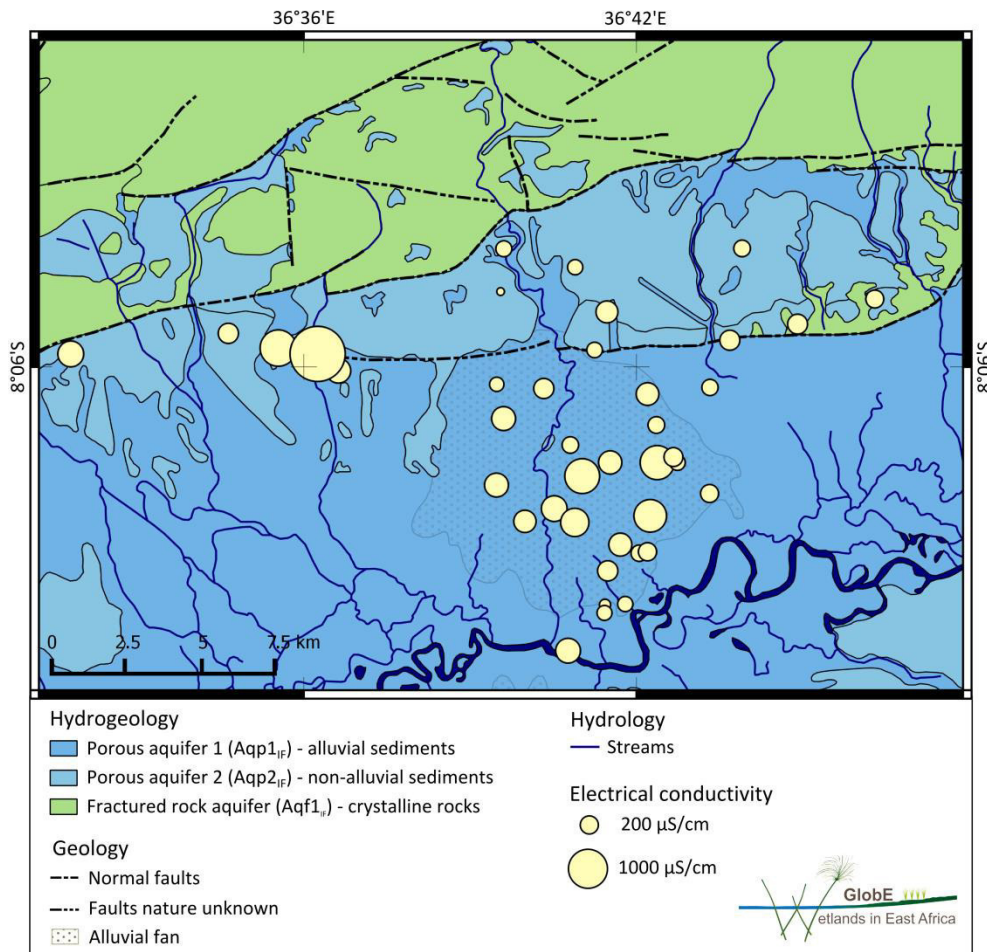


**Fig. 6.16: Spatial distribution of electrical conductivities of groundwater samples in dry season 2015. Data sources: Geological Survey of Tanganyika (1962) (geology, streams), Jätzold and Baum (1968) (alluvial fan) (IF).**

Considering the spatial distribution of temporal variability, no spatial pattern was observed (Fig. 6.17). Sampling points with remarkably higher ECs in dry compared to rainy season were mainly located along the southern normal fault (red points). Wells and piezometers in the flooded areas near Kilombero River did not explicitly show lower ECs in rainy compared to dry season, suggesting that flooding water did not dilute groundwater.

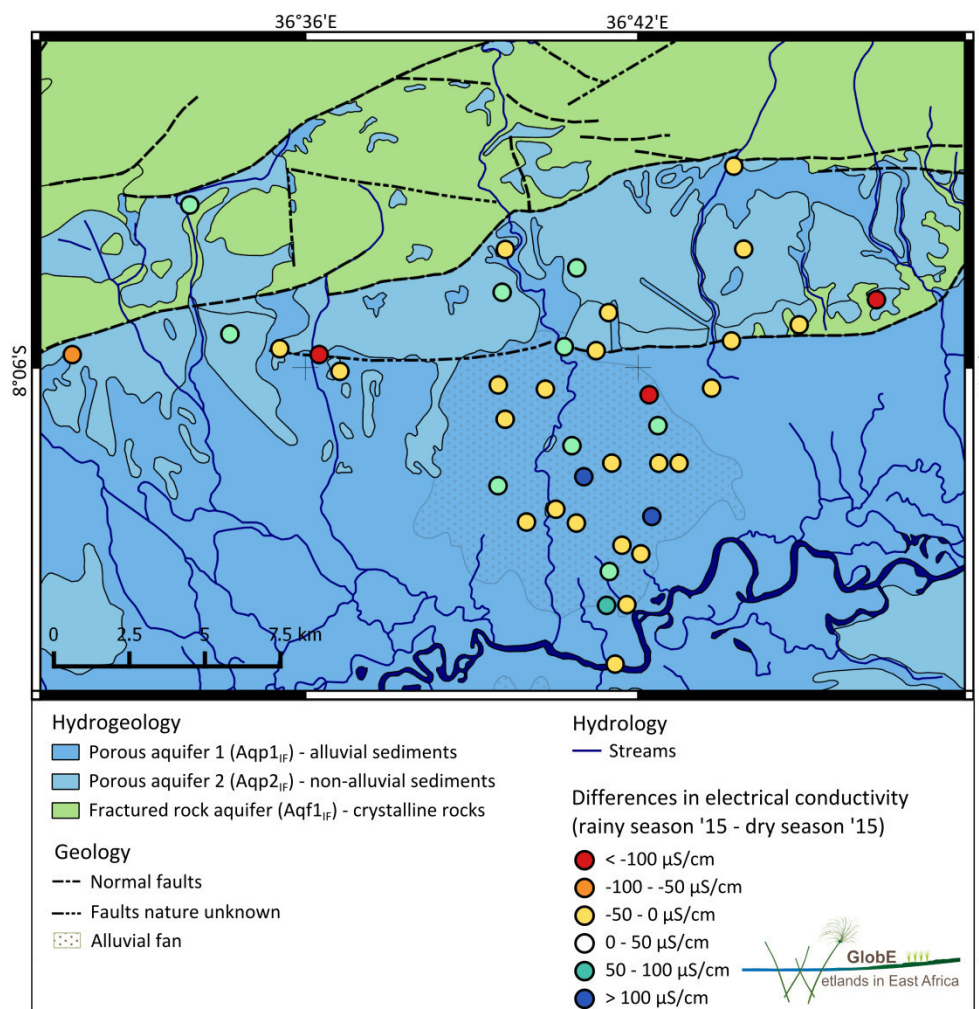


**Fig. 6.17:** Spatial distribution of differences in electrical conductivity of groundwater samples between rainy and dry season 2015. Data sources: Geological Survey of Tanganyika (1962) (geology, streams), Jätzold and Baum (1968) (alluvial fan) (IF).

#### 6.3.1.4 Precipitation (IF)

Concentrations of measured ions in precipitation samples were small in general (Tab. 6.3). Median values of precipitation compositions in nine East African sites (Rodhe et al. 1981 In Johnson 1996) were in the range of measured values in the study site. However, calculated median concentrations of precipitation within the study site were higher compared to median concentrations of the nine East African sites.

**Tab. 6.3:** Minimum, maximum, and median concentrations of different analytes measured in weekly precipitation samples. Median values for East Africa were adopted from Rodhe et al. (1981) (In Johnson 1996) (IF).

Analyte	Minimum [mg/L]	Maximum [mg/L]	Median [mg/L]	Median (East Africa) [mg/L]
Cl <sup>-</sup>	0.3	2.3	0.7	0.30
SO <sub>4</sub> <sup>2-</sup>	0.2	3.7	1.2	0.75
NO <sub>3</sub> <sup>-</sup>	< 0.2	1.7	0.7	0.00
HCO <sub>3</sub> <sup>-</sup>	-	-	-	1.43
Na <sup>+</sup>	0.6	1.6	1.5	0.62
K <sup>+</sup>	0.3	0.6	0.6	0.30
Mg <sup>2+</sup>	< 0.1	0.2	0.1	0.08
Ca <sup>2+</sup>	0.4	0.6	0.6	0.38
SiO <sub>2</sub>	< 0.1	2.0	0.3	-

### 6.3.1.5 Multivariate statistical analyses (IF)

Multivariate statistical analysis was performed for hydrochemical data of the four snapshot samplings. After removing all variables with more than 15 % of values below the LOD (Montcoudiol et al. 2015) and discarding *in-situ* parameters that were vulnerable to errors, the twelve variables EC, pH, Na<sup>+</sup>, K<sup>+</sup>, Mg<sup>2+</sup>, Ca<sup>2+</sup>, Cl<sup>-</sup>, SO<sub>4</sub><sup>2-</sup>, HCO<sub>3</sub><sup>-</sup>, Fe<sup>2+</sup>, Mn<sup>2+</sup>, and SiO<sub>2</sub> were chosen for multivariate statistical analysis. The variables were log transformed before analyses, except for pH and SiO<sub>2</sub>. These two variables showed better normal distributions without log-transformation. All in all, 165 water samples were available for multivariate statistical analysis. Results of Principal Component Analysis (PCA) and Hierarchical Cluster Analysis (HCA) are presented in the following section.

Results of PCA were used to identify major processes controlling the hydrochemistry of water samples (Belkhiri et al. 2011, Moya et al. 2015). The first principal component (PC1<sub>IF</sub>) explained 47 % of the total variance within the dataset, while the second principal component (PC2<sub>IF</sub>) explained another 13 % (Tab. 6.4). Thus, the first two principal components explained 60 % of the total variance, with the first component being much more significant.

**Tab. 6.4: Loadings of variables on the first two principal components (PC1<sub>IF</sub>, PC2<sub>IF</sub>) and the respective explained variance. High factor loadings are marked in grey (IF).**

Variable	PC1 <sub>IF</sub>	PC2 <sub>IF</sub>
Electrical conductivity	0.41	0.01
pH	0.12	0.04
Na <sup>+</sup>	0.38	-0.01
K <sup>+</sup>	0.01	-0.39
Mg <sup>2+</sup>	0.38	0.13
Ca <sup>2+</sup>	0.39	0.00
Cl <sup>-</sup>	0.30	-0.06
SO <sub>4</sub> <sup>2-</sup>	0.22	0.34
HCO <sub>3</sub> <sup>-</sup>	0.39	0.04
Fe <sup>2+</sup>	-0.11	0.64
Mn <sup>2+</sup>	0.18	0.26
SiO <sub>2</sub>	0.21	-0.48
<b>Explained variance</b>	<b>0.47</b>	<b>0.13</b>

EC, Na<sup>+</sup>, Mg<sup>2+</sup>, Ca<sup>2+</sup>, and HCO<sub>3</sub><sup>-</sup> showed high positive loadings to PC1<sub>IF</sub> (Tab. 6.4). These variables are related to the weathering of silicate minerals. During silicate weathering, cations and HCO<sub>3</sub><sup>-</sup> are released to water, resulting in an increased EC (Appelo and Postma 2005).

PC2<sub>IF</sub> was characterized by high positive loadings of Fe<sup>2+</sup> and high negative loadings of K<sup>+</sup> and SiO<sub>2</sub>. The high positive loadings of Fe<sup>2+</sup> might hint at redox processes, such as the reduction of ferric oxyhydroxides (Hem 1985). The high negative loadings of K<sup>+</sup> and SiO<sub>2</sub> might correspond to the weathering of k-feldspar and the precipitation of secondary clay minerals (Appelo and Postma 2005). Additionally, K<sup>+</sup> could be an indicator of overland flow, as it usually gets into solution, if water is in contact with vegetation and soil (King et al. 2014).

It can be concluded that silicate weathering, expressed by PC1<sub>IF</sub> and PC2<sub>IF</sub>, is the major process controlling hydrochemistry of groundwater and surface water. Furthermore, hydrochemistry is, to a lesser extent, influenced by redox processes and biogeochemistry, expressed by PC2<sub>IF</sub>. In contrast, Cl<sup>-</sup> and SO<sub>4</sub><sup>2-</sup> are not responsible for variability within hydrochemistry, indicating only little anthropogenic influence.

Performed HCA, using Ward's linkage method, revealed a clear separation of water samples into four groups (Fig. 6.18). All four cluster groups showed average compositions that are typical for water exposed to silicate rocks (Tab. 6.5, Fig. 6.19).

The plausibility of clustering was confirmed linking the cluster groups to location and type of sampling points (Fig. 6.20). The first separation of samples into two groups was almost identical with the differentiation of samples into surface water ( $C4_{IF}$ ) and groundwater ( $C1_{IF}$ ,  $C2_{IF}$ ,  $C3_{IF}$ ). Cluster group  $C4_{IF}$  is represented by all stream water samples, flooding water at *center*, and few shallow and deep groundwater samples located within the non-alluvial sediments in the northern study site. Samples of this cluster group showed low ECs, and thus low concentrations of all anions and cations, and highly variable pH-values (Tab. 6.5, Fig. 6.19). This group will be referred to as *surface water* in the following.

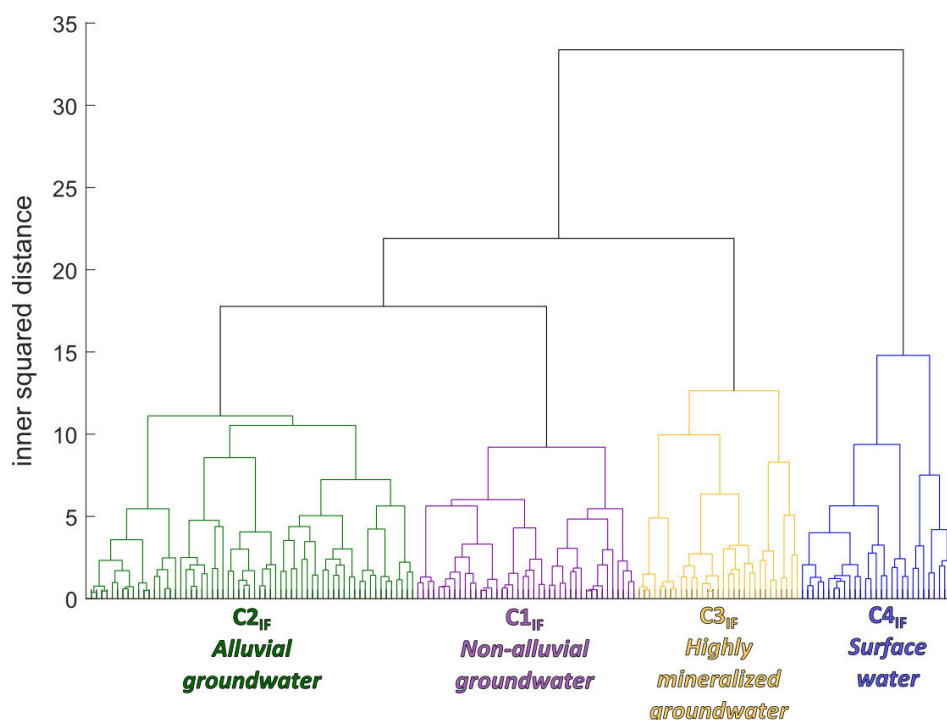


Fig. 6.18: Dendrogram of the Hierarchical Cluster Analysis, performed for 165 water samples using the variables  $\log EC$ ,  $pH$ ,  $\log Na^+$ ,  $\log K^+$ ,  $\log Mg^{2+}$ ,  $\log Ca^{2+}$ ,  $\log Cl^-$ ,  $\log SO_4^{2-}$ ,  $\log HCO_3^-$ ,  $\log Fe^{2+}$ ,  $\log Mn^{2+}$ , and  $SiO_2$  showing the different cluster groups of water samples and their characteristic names (IF).

Tab. 6.5: Means and standard deviations (in brackets) of each variable for all four cluster groups. The amount of samples per group (n) is displayed below the group name (IF).

Group	EC [ $\mu S/cm$ ]	pH [-]	$Na^+$ [mg/L]	$K^+$ [mg/L]	$Mg^{2+}$ [mg/L]	$Ca^{2+}$ [mg/L]	$Cl^-$ [mg/L]	$SO_4^{2-}$ [mg/L]	$HCO_3^-$ [mg/L]	$Fe^{2+}$ [mg/L]	$Mn^{2+}$ [mg/L]	$SiO_2$ [mg/L]
$C1_{IF}$ n=42	287 (102)	6.4 (0.2)	32.5 (19.0)	2.6 (1.8)	7.4 (3.2)	15.2 (5.5)	16.2 (16.5)	1.8 (1.1)	158.7 (60.5)	0.06 (0.08)	0.30 (0.34)	99.0 (13.8)
$C2_{IF}$ n=62	266 (94)	6.5 (0.3)	23.2 (10.2)	1.5 (1.4)	8.6 (3.5)	15.9 (6.9)	14.8 (13.6)	6.2 (6.8)	139.8 (61.6)	3.23 (6.72)	0.46 (0.45)	50.2 (11.3)
$C3_{IF}$ n=31	927 (551)	6.8 (0.4)	119.2 (90.4)	2.4 (2.9)	24.1 (16.4)	47.0 (39.5)	91.8 (139.4)	19.3 (19.3)	413.3 (218.4)	0.07 (0.09)	0.69 (1.20)	62.6 (22.4)
$C4_{IF}$ n=30	78 (46)	6.5 (0.9)	7.9 (4.7)	3.1 (2.4)	1.4 (1.1)	3.9 (2.9)	6.9 (7.2)	1.8 (1.5)	29.8 (14.9)	0.34 (0.53)	0.04 (0.04)	25.5 (8.7)

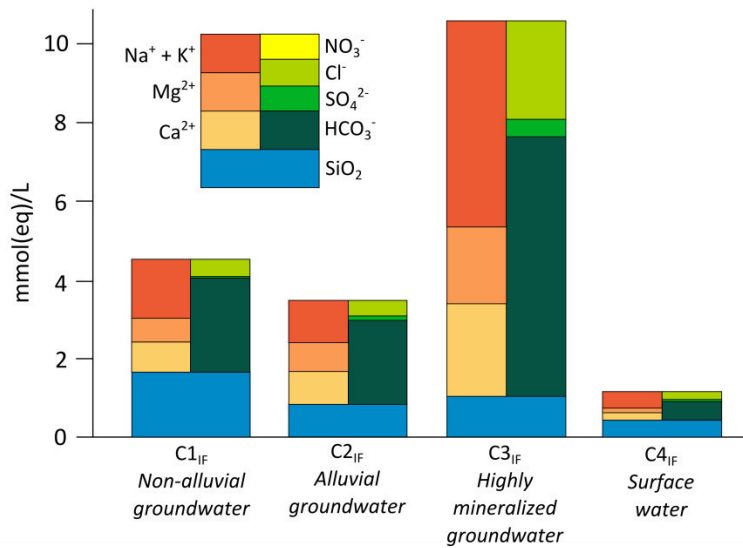


Fig. 6.19: Barcharts of mean hydrochemical compositions of the four groups identified by Hierarchical Cluster Analysis (IF).

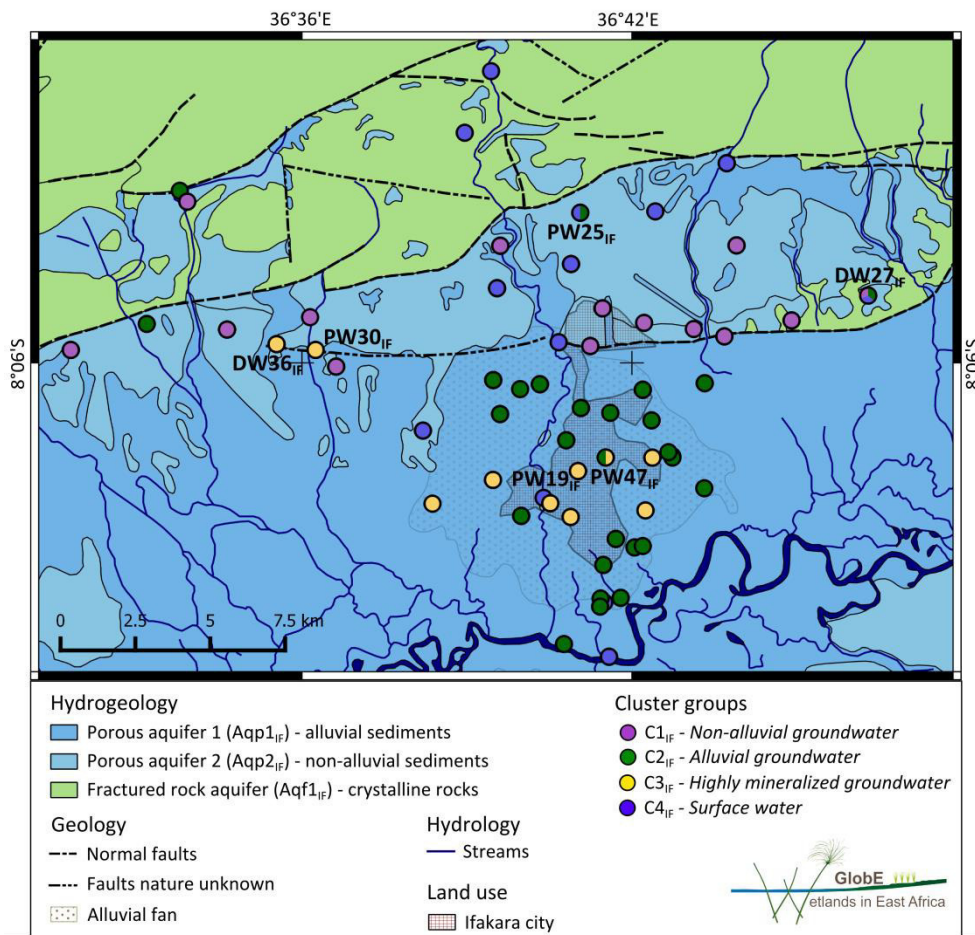


Fig. 6.20: Spatial distribution of the four cluster groups. Data sources: Geological Survey of Tanganyika (1962) (geology, streams), Jätzold and Baum (1968) (alluvial fan), google.com/earth (Ifakara city) (IF).

The other three cluster groups are solely composed of groundwater samples and flooding water at *fringe*. C1<sub>IF</sub> is represented by shallow and deep groundwater samples located along the southern normal fault. Most of these samples fell within the hydrostratigraphic unit of non-alluvial sediments (Aqp2<sub>IF</sub>) (Fig. 6.20). Henceforth, this cluster group will be called *non-alluvial groundwater*. ECs and concentrations of major cations and HCO<sub>3</sub><sup>-</sup> of this groundwater samples were moderate, and concentrations of SiO<sub>2</sub> were high.

In contrast, C2<sub>IF</sub> composes mainly groundwater samples within the alluvial sediments (Aqp1<sub>IF</sub>) (*alluvial groundwater*). The flooding water at *fringe* also belongs to this group, indicating a hydraulic connection between groundwater samples of this group and flooding water at *fringe*. These samples showed similar concentrations of major anions and cations compared to *non-alluvial groundwater*, but lower concentrations of SiO<sub>2</sub> and higher concentrations of Fe<sup>2+</sup> (Tab. 6.5). In terms of Fe<sup>2+</sup>, considerable concentrations were solely found in *alluvial groundwater*.

C3<sub>IF</sub> represents the smallest cluster group of groundwater and contains wells in the city of Ifakara, in the central part of the alluvial fan, and two wells in the western study site. This group differed from the others by higher ECs and higher amounts of all major anions and cations except for K<sup>+</sup>, and will thus be referred to as *highly mineralized groundwater*. In addition, this cluster group showed highest Mn<sup>2+</sup> concentrations.

Almost all water sampling points that were sampled more than once fell within the same cluster group, indicating a low temporal variability of hydrochemistry. Nevertheless, few sampling points belonged to different groups of HCA for different sampling times. One of these exceptions is PW25<sub>IF</sub>, a pumping well located in the non-alluvial sediments (Fig. 6.20). The samples of this well fell in the group of *surface waters* in rainy and in the group of *alluvial groundwater* in dry seasons. This indicates a dilution of this groundwater in rainy season. As this well even fell dry during dry season 2015 and was only 15 m deep (personal communication with local population 2015), it might be screened in the upper part of the saturated zone and thus bring recently infiltrated rainwater during rainy seasons. PW47<sub>IF</sub> fell within the group of *alluvial groundwater* in rainy and in the group of *highly mineralized groundwater* in dry seasons, indicating a dilution, due to direct recharge as well. This well is a pumping well located in the alluvial fan sediments. It was relatively shallow as well, with a depth of only 12 m (personal communication with local population 2015). DW27<sub>IF</sub> is the only sampling point that fell within more than two different groups, showing a high temporal variability. It is a very shallow draw well located near the southern normal fault. Thus, it might be concluded that shallow groundwater becomes locally diluted by direct recharge during rainy seasons.

Returned p-values of Kruskal Wallis tests, which were performed for all variables, indicated the rejection of the null hypothesis that all four cluster groups come from the same distribution at a 1 % significance level for all variables. The returned p-values of followed up multiple comparison tests showed that *non-alluvial* (C1<sub>IF</sub>) and *alluvial groundwater* (C2<sub>IF</sub>) exclusively differed in their K<sup>+</sup>, SO<sub>4</sub><sup>2-</sup>, Fe<sup>2+</sup>, and SiO<sub>2</sub> concentrations (Tab. 6.6). For all other variables, the null hypothesis that both cluster groups come from the same distribution were not rejected, outlining the hydrochemical similarity of *alluvial* and *non-alluvial groundwater*. The other pairs of groups differed significantly in more variables from each other (Tab. 6.6). Furthermore, it became obvious that pH, K<sup>+</sup>, and Mn<sup>2+</sup> were the least important variables in terms of group differences.

Displaying the different cluster groups in a PCA diagram showed the differentiation patterns between the different groups along PC1<sub>IF</sub> and PC2<sub>IF</sub> (Fig. 6.21). The variables EC, Na<sup>+</sup>, Mg<sup>2+</sup>, Ca<sup>2+</sup>, and HCO<sub>3</sub><sup>-</sup> increase along PC1<sub>IF</sub>, as displayed by high positive loadings of these variables to PC1<sub>IF</sub> (Tab. 6.4). Along PC2<sub>IF</sub>, Fe<sup>2+</sup> increases, while K<sup>+</sup> and SiO<sub>2</sub> decrease. The increase in EC, Na<sup>+</sup>, Mg<sup>2+</sup>, Ca<sup>2+</sup>, and HCO<sub>3</sub><sup>-</sup> from *surface water* over *alluvial* and *non-alluvial* to *highly mineralized groundwater* represents increasing mineralization due to silicate weathering. Along PC2<sub>IF</sub>, a difference between *alluvial* and *non-alluvial groundwater* was observed.

**Tab. 6.6:** P-values of multiple comparison tests, following Kruskal-Wallis-tests, for different pairs of cluster groups. Those p-values that indicated a rejection of the null-hypothesis that both cluster groups come from one distribution with respect to a certain variable are marked in grey (level of significance = 1 %) (IF).

Group 1	Group 2	EC	pH	Na <sup>+</sup>	K <sup>+</sup>	Mg <sup>2+</sup>	Ca <sup>2+</sup>	Cl <sup>-</sup>	SO <sub>4</sub> <sup>2-</sup>	HCO <sub>3</sub> <sup>-</sup>	Fe <sup>2+</sup>	Mn <sup>2+</sup>	SiO <sub>2</sub>
C1 <sub>IF</sub>	C2 <sub>IF</sub>	0.89	0.49	0.29	0.00	0.61	0.99	0.96	0.00	0.64	0.00	0.82	0.00
C1 <sub>IF</sub>	C3 <sub>IF</sub>	0.00	0.00	0.00	0.65	0.00	0.00	0.00	0.00	0.00	0.99	0.99	0.00
C1 <sub>IF</sub>	C4 <sub>IF</sub>	0.00	0.27	0.00	0.77	0.00	0.00	0.00	0.97	0.00	0.00	0.00	0.00
C2 <sub>IF</sub>	C3 <sub>IF</sub>	0.00	0.01	0.00	0.13	0.00	0.00	0.00	0.01	0.00	0.00	0.73	0.35
C2 <sub>IF</sub>	C4 <sub>IF</sub>	0.00	0.91	0.00	0.00	0.00	0.00	0.01	0.00	0.00	0.03	0.00	0.00
C3 <sub>IF</sub>	C4 <sub>IF</sub>	0.00	0.17	0.00	0.19	0.00	0.00	0.00	0.00	0.00	0.00	0.00	0.00

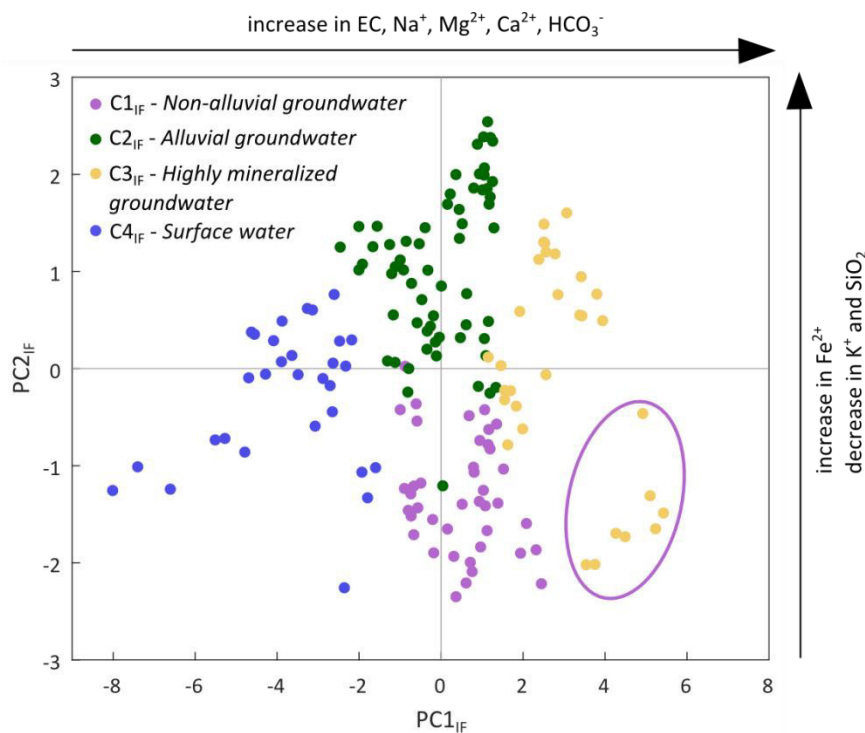


**Fig. 6.21:** Scatterplot of the two principal components (PC1<sub>IF</sub> and PC2<sub>IF</sub>) showing the distribution of water samples. Samples of wells PW30<sub>IF</sub> and DW36<sub>IF</sub>, which are located in the non-alluvial sediments, are encircled (IF).

Samples of *surface water* plot randomly around the negative section of PC1<sub>IF</sub>, indicating the low mineralization, expressed by low values of EC, major cations, and HCO<sub>3</sub><sup>-</sup>. The few groundwater samples that fell within this group were either shallow draw wells or pumping wells with relatively shallow depths. Here, a rapid infiltration of rainfall is expected to be the reason for a dilution leading to low ECs. *Alluvial* and *non-alluvial groundwater* plot around 0 along PC1<sub>IF</sub>, displaying moderate ECs, major cation, and HCO<sub>3</sub><sup>-</sup> concentrations. A differentiation between these two cluster groups is given along PC2<sub>IF</sub>. *Alluvial groundwater* showed higher Fe<sup>2+</sup>, but lower K<sup>+</sup> and SiO<sub>2</sub> concentrations compared to *non-alluvial groundwater*. *Highly mineralized groundwater* is indicated by high values of PC1<sub>IF</sub>. The higher mineralization of these wells might either be derived from longer residence times of groundwater within less permeable zones of the aquifer or from anthropogenic influence, caused by percolation of waste water of Ifakara city. An anthropogenic influence is implied by nitrate concentrations as well, because only samples of this cluster group displayed considerable amounts of NO<sub>3</sub><sup>-</sup>. As *highly mineralized groundwater* includes samples located in the alluvial as well as in the non-alluvial aquifer, it is highly variable along PC2<sub>IF</sub>. It turned out that those wells of *highly mineralized groundwater* that plot in the negative parts of PC2<sub>IF</sub> are located within the non-alluvial sediments (Fig. 6.21). The wells that plot in positive parts of



PC2<sub>IF</sub> are located within the alluvial sediments, respectively. This shows that a clear separation along PC2<sub>IF</sub> is given between groundwater in the alluvial and groundwater in the non-alluvial sediments.

Although Kruskal Wallis tests indicated clear differences between cluster groups, standard deviations and distribution of samples along PC1<sub>IF</sub> and PC2<sub>IF</sub> (Fig. 6.21) displayed wide variabilities within the cluster groups. Variables of samples in different cluster groups can be very different or very similar to each other. The same is true for samples within one cluster group. In general, most samples showed the same pattern of water influenced by silicate weathering, with differing degrees of mineralization.

### 6.3.1.6 Specific ion ratios, saturation indices, and stability diagrams (IF)

All cluster groups indicated clear correlations between EC and HCO<sub>3</sub><sup>-</sup>. Assuming that all HCO<sub>3</sub><sup>-</sup> is derived from silicate weathering, this process was identified as the major source of mineralization (Fig. 6.22). *Surface water* showed lowest degrees of mineralization, while mineralization of groundwater groups was variable. All cluster groups had HCO<sub>3</sub><sup>-</sup>/(Na<sup>+</sup>+2Ca<sup>2+</sup>) ratios around one, suggesting plagioclase weathering (cf. section 3.3.1, Van der Weijden and Pacheco 2007). Feldspar weathering was also indicated by SiO<sub>2</sub>/Na<sup>+</sup> ratios around two (Appelo and Postma 2005). Two pumping wells of the *highly mineralized groundwater* (PW19<sub>IF</sub>, PW30<sub>IF</sub>) revealed different ratios of EC/HCO<sub>3</sub><sup>-</sup>, HCO<sub>3</sub><sup>-</sup>/(Na<sup>+</sup>+2Ca<sup>2+</sup>), and SiO<sub>2</sub>/Na<sup>+</sup> compared to the other samples. Those two samples apparently showed another source of mineralization. Additionally, both wells and another draw well (DW36<sub>IF</sub>) of the *highly mineralized groundwater* had Na<sup>+</sup>/Cl<sup>-</sup> ratios of one, indicating NaCl as a possible source of Na<sup>+</sup>. Compared to the other cluster groups, *surface water* displayed high K<sup>+</sup>/Na<sup>+</sup> ratios together with low ECs, indicating that these waters have been in contact with vegetation and topsoil (King et al. 2014). High amounts of iron were solely detected in *alluvial groundwater*. Those increased iron concentrations were connected to low redox potentials, suggesting the reduction of iron-(hydr)oxides, although the limit of 100 mV was never exceeded (section 3.2, Mitsch and Gosselink 2007).

Most water samples revealed subsaturation with respect to albite and anorthite, but saturation with respect to k-feldspar (Fig. 6.23). In terms of albite and k-feldspar, *non-alluvial groundwater* showed higher saturation indices compared to *alluvial groundwater*. *Surface water* had the lowest saturation indices for all feldspars. Most water samples were supersaturated with respect to secondary clay minerals and iron-(hydr)oxides (Fig. 6.23). Highest saturation indices were observed for kaolinite, and hematite. Quartz showed supersaturation in most samples as well (Fig. 6.24).

Stability diagrams of anorthite and albite showed stability of montmorillonite for all groundwater cluster groups and of kaolinite for *surface water*, coinciding with the high saturation indices of montmorillonite and kaolinite (Fig. 6.24). In terms of k-feldspar-weathering, kaolinite was stable in nearly all water samples.

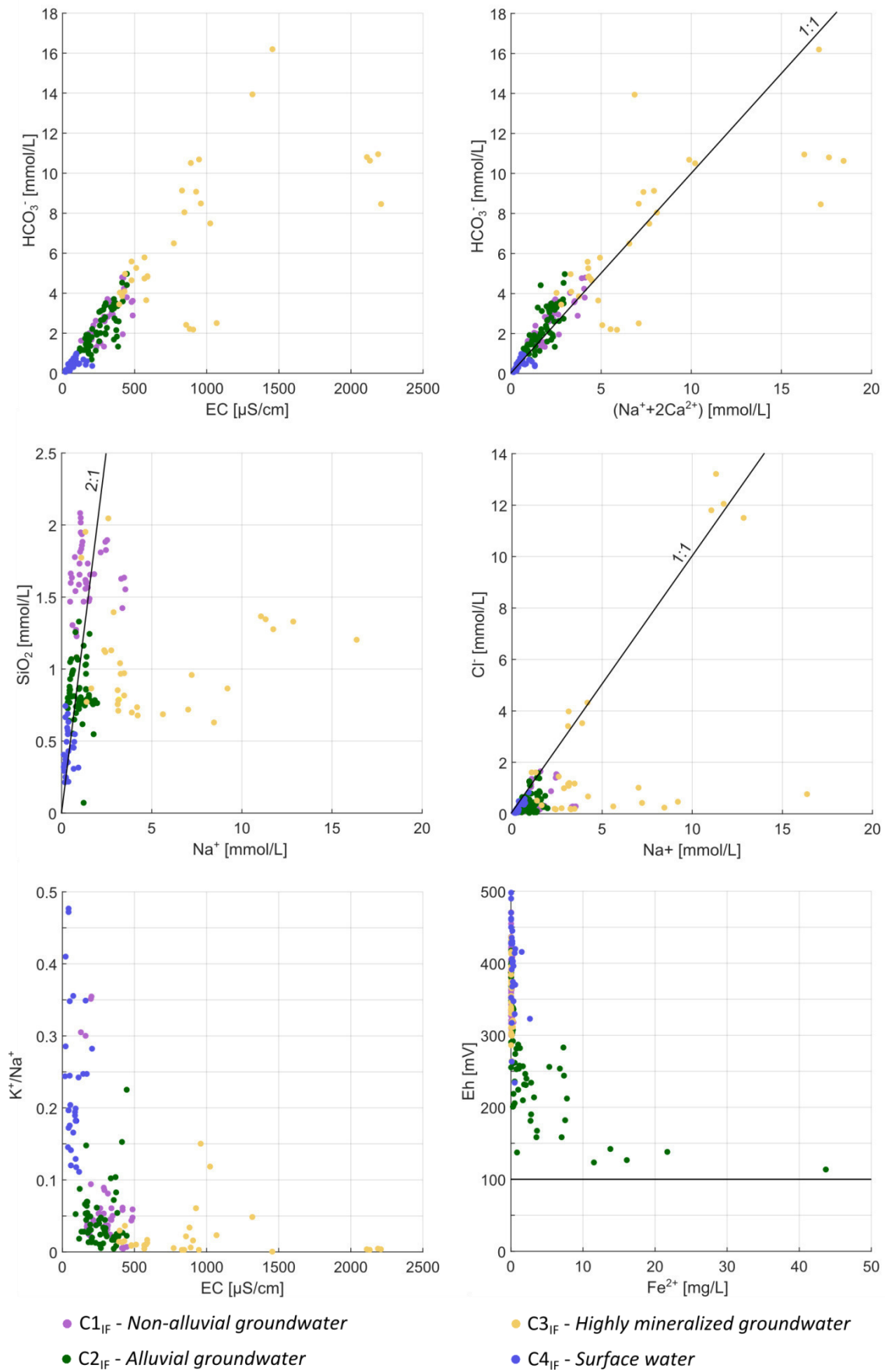


Fig. 6.22: Selected ratios of different hydrochemical parameters for the four cluster groups. Specific ion ratios are illustrated as lines (IF).

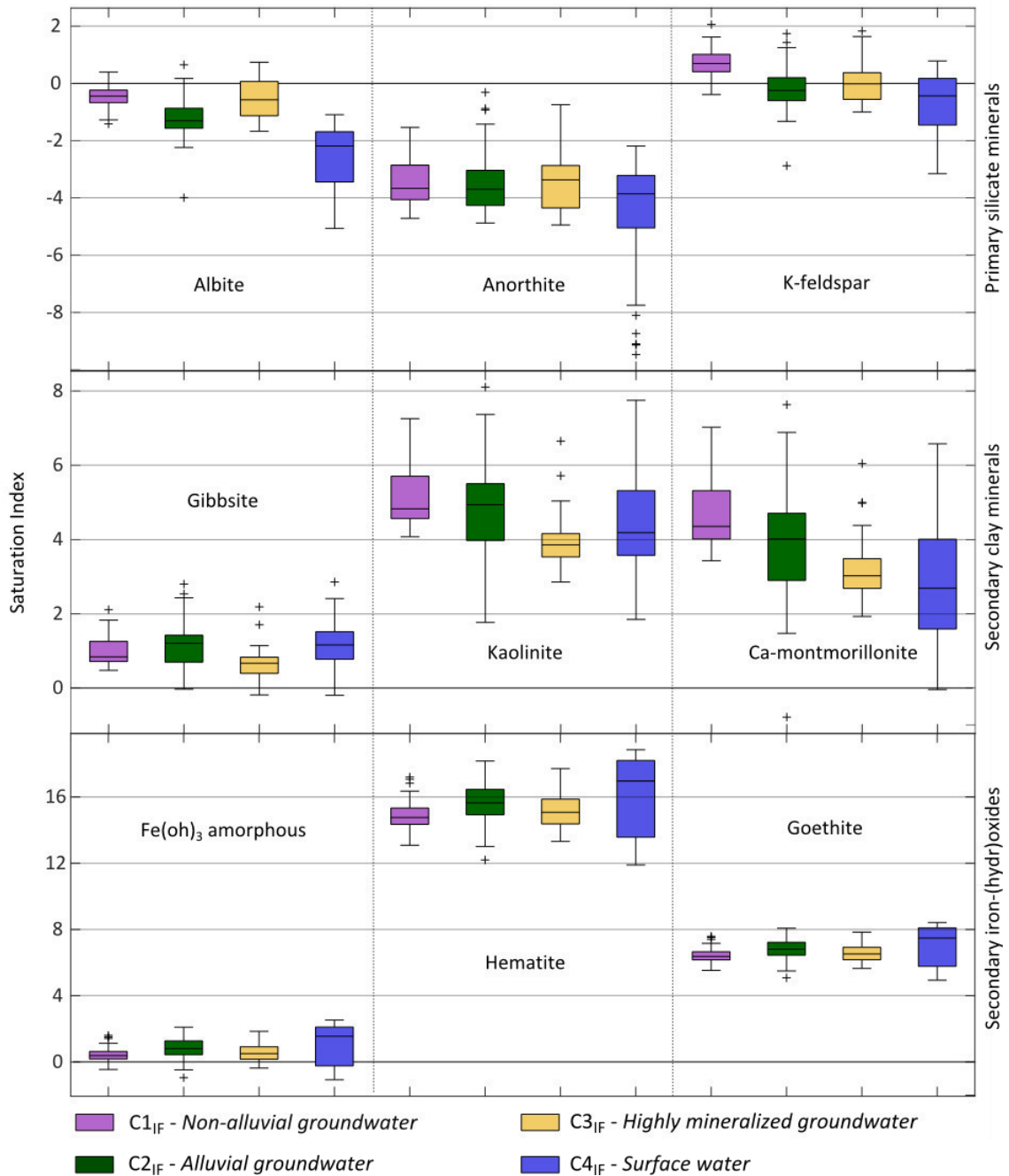
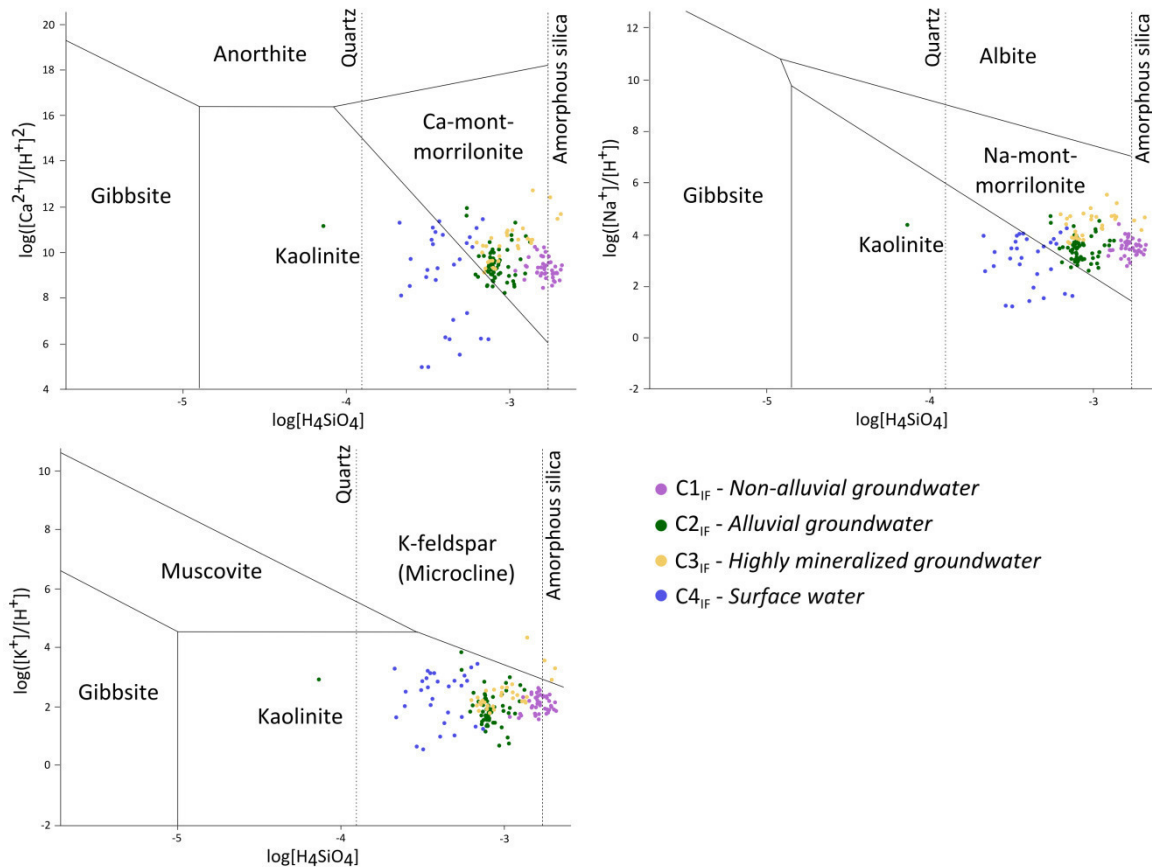


Fig. 6.23: Distribution of saturation indices of primary silicate minerals (feldspars), secondary clay minerals, and secondary iron-(hydr)oxides for the four cluster groups (IF).



**Fig. 6.24:** Stability diagrams of anorthite, albite, k-feldspar (microcline), and their respective weathering products for the four cluster groups (following Tardy 1971) (IF).

The described results show that k-feldspars and plagioclases are dissolved, while secondary clay minerals, such as kaolinite and montmorillonite, and iron-(hydr)oxides, such as hematite and goethite, are precipitated. The dissolution of feldspars is kinetically controlled, while the precipitation of clay minerals and iron-(hydr)oxides already attained equilibrium or even supersaturation (Appelo and Postma 2005). Samples showed saturation or even supersaturation with respect to k-feldspar. It was already observed before that water becomes saturated with respect to k-feldspars before it saturates with plagioclase (Helgeson et al. 1969). The supersaturation with respect to quartz is a consequence of  $\text{SiO}_2$  addition to water during weathering of the above mentioned silicate minerals. In tropical regions, usually gibbsite is formed instead of kaolinite and montmorillonite (Appelo and Postma 2005). The stability of kaolinite and montmorillonite in all samples thus suggests longer residence times of groundwater compared to other tropical regions.

### 6.3.2 Stable water isotopes (IF)

The values of the stable water isotopes  $\delta^{18}\text{O}$  and  $\delta^2\text{H}$  in precipitation ranged from -5.0 to 1.2 ‰ and from -28.1 to 22.5 ‰, respectively. These values are relatively high compared to global meteoric waters reflecting an origin of precipitation in tropical regions (Clark and Fritz 1997). The fitted Local Meteoric Water Line ( $\text{LMWL}_{\text{IF}}$ :  $\delta^2\text{H} = 8.2 \times \delta^{18}\text{O} + 13.5$ ) was almost parallel to the Global Meteoric Water Line (GMWL) (Fig. 6.25). Bohte et al. (2010) determined a LMWL for a catchment in northeastern Tanzania ( $\text{LMWL}_{\text{Bohte}}$ :  $\delta^2\text{H} = 7.9 \times \delta^{18}\text{O} + 11.1$ ), with a comparable equation.

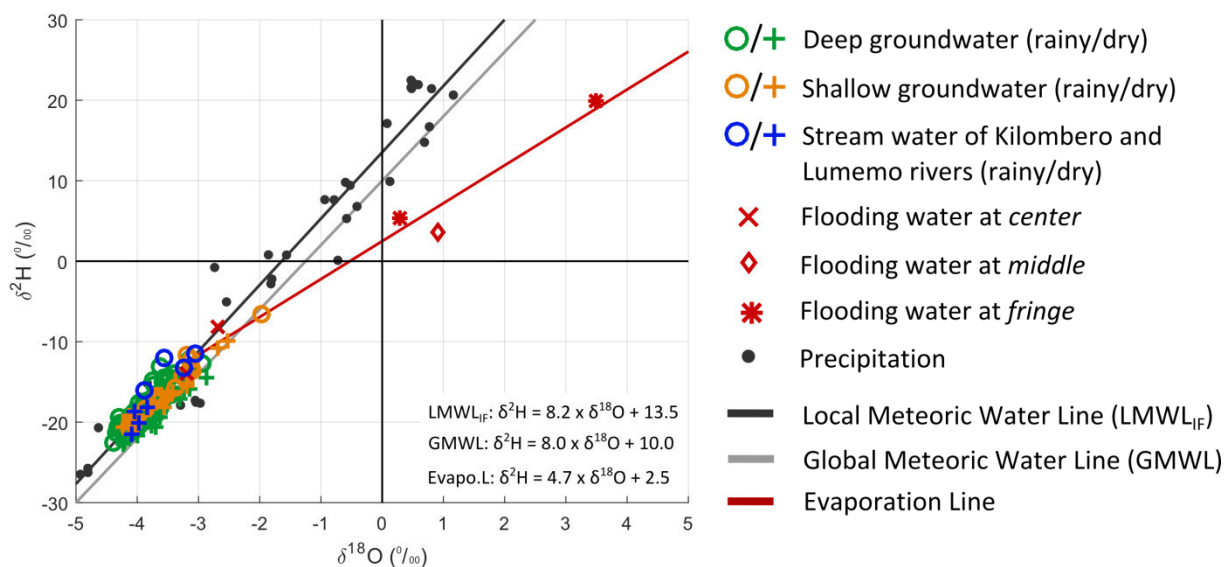


**Fig. 6.25:** Scatterplot of  $\delta^2\text{H}$  against  $\delta^{18}\text{O}$  for deep and shallow groundwater, stream water (Kilombero and Lumemo rivers), flooding water, and precipitation samples (IF).

Temporal variation of isotopes in precipitation showed higher  $\delta^{18}\text{O}$  values in 2014 than in 2015, with a constant decrease from January to May 2015 (Fig. 6.26 a). The same pattern was observed for  $\delta^2\text{H}$ . Nevertheless, a seasonal variation was observed as well. Months with high precipitation amounts were depleted in heavy isotopes compared to those with less precipitation (Fig. 6.26 b). This variation is caused by the amount effect, which leads to a depletion in  $\delta^{18}\text{O}$  of 1.0 to 1.5 ‰ per 100 mm monthly precipitation (Moser 1998). Amount effects are strongest in tropical regions (Lawrence and White 1991). Considering the regression line excluding the three outliers, the presented data showed a higher depletion of around 3.5 ‰  $\delta^{18}\text{O}$  per 100 mm monthly precipitation (Fig. 6.26 b). The three outliers were represented by relatively low  $\delta^{18}\text{O}$  values but almost no amount of precipitation. Here, evaporation of the samples might have altered isotopic composition. Correlation between monthly precipitation and weighted averages of  $\delta^2\text{H}$  showed an increase in  $\delta^2\text{H}$  with increasing precipitation amount as well. The weighted averages of  $\delta^{18}\text{O}$  and  $\delta^2\text{H}$  for the whole measuring period were -2.2 ‰, -3.5‰, and 14.2.

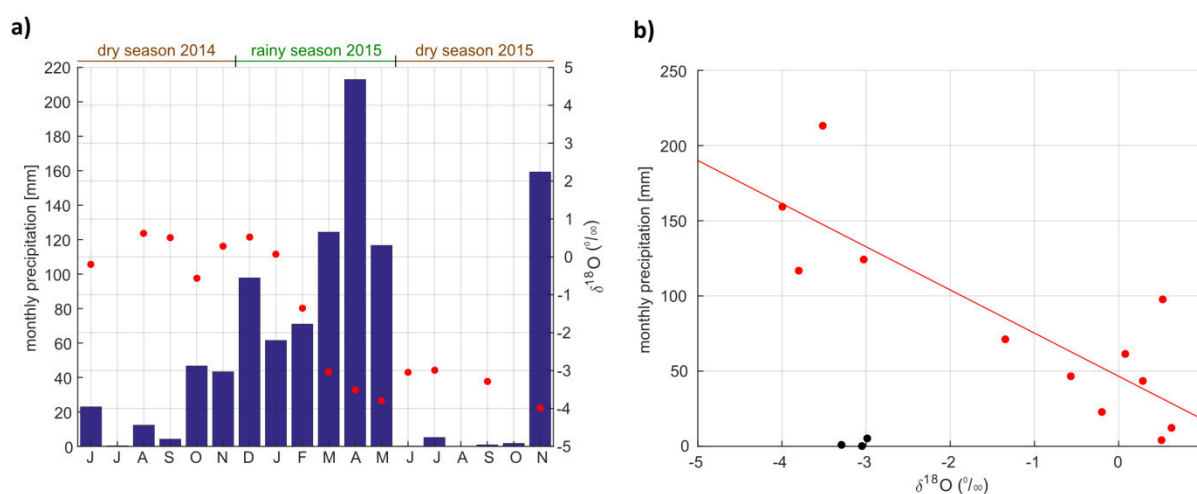


**Fig. 6.26:** Monthly weighted averages of  $\delta^{18}\text{O}$  in precipitation (red points) and monthly amount of precipitation (blue bars) as a) time series (June 2014 to November 2015), and b) correlation graph. The regression line in b) was calculated excluding the three outliers (black points) (IF).

All groundwater and stream water samples plot around the calculated LMWL<sub>IF</sub>, indicating recharge of those waters within the study site or in a similar environment (Fig. 6.25).  $\delta^{18}\text{O}$  values ranged from -4.4 to

-2.0 ‰ and  $\delta^2\text{H}$  values ranged from -22.7 to -6.6 ‰. For stream water of Kilombero River, a clear separation between rainy and dry season was observed (Fig. 6.27). Stream water showed lower values of  $\delta^{18}\text{O}$  and  $\delta^2\text{H}$  in dry season compared to rainy season. In contrast, differences between rainy and dry season were small for groundwater samples and Lumemo River (Fig. 6.27). Most of the sampling points revealed differences in  $\delta^{18}\text{O}$  lower than 0.2 ‰, being close to measurement uncertainties. Furthermore, sign-tests proved that  $\delta^{18}\text{O}$  did not differ significantly between rainy and dry seasons. Thus, it can be concluded that stream water does not contribute to groundwater recharge. In some of the shallow wells, seasonal variability was still observed (Fig. 6.27), indicating some local recharge not fully mixed with the regional groundwater (e.g. DW27<sub>IF</sub>).

While flooding water at *center* had an isotopic composition similar to stream water of Kilombero River, flooding water at *middle* and *fringe* showed clear evaporation effects (Fig. 6.25). The line linking the sampled flooding waters reflects the evaporation line ( $\delta^2\text{H} = 4.7 \times \delta^{18}\text{O} + 2.5$ ). The origin of this line lies close to samples of groundwater and stream water, identifying those two components as possible sources of flooding water. However,  $\delta^{18}\text{O}$  values of precipitation during flooding periods ranged between -3 and -4 ‰ as well, implying that precipitation is a source of evaporated flooding water as well. Because of the absence of evaporation effects in groundwater, infiltration of flooding water at *middle* and *fringe* can be neglected as a potential source of groundwater recharge.

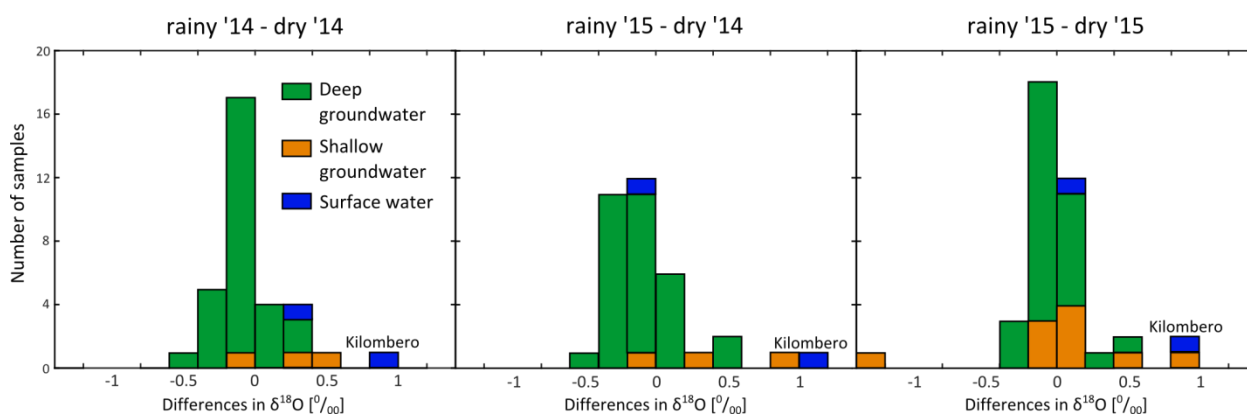


**Fig. 6.27:** Histograms showing the distribution of differences in  $\delta^{18}\text{O}$  for shallow and deep groundwater, and stream water of Kilombero and Lumemo rivers between rainy and dry seasons (IF).

### 6.3.3 Water quality (IF)

Water quality was assessed with regard to human health, acceptability, and irrigation purposes. Groundwater in the study site is used for drinking water and other domestic purposes. Hence, in terms of human health and acceptability, the focus was given to groundwater. In terms of irrigation, all types of water are used and/or will be used in future. Thus, a comprehensive evaluation of all water samples is given here. Finally, the influence of agricultural and other anthropogenic influences on water quality is assessed.

#### 6.3.3.1 Water quality related to human health (IF)

All measured health related dissolved species were compared to the respective guideline value of WHO (2011) (Tab. 4.3 p.50). The health related constituents  $\text{NO}_3^-$ ,  $\text{NO}_2^-$ ,  $\text{Mn}^{2+}$ , and  $\text{Al}^{3+}$  were analyzed for all samples of the four snapshot samplings. The concentrations of  $\text{F}^-$ , and the trace heavy metals As, Cd, Cr, Cu, Ni, Pb, and Zn were determined for all water samples during the first snapshot sampling in rainy season 2014.

In general, only  $\text{NO}_3^-$ ,  $\text{NO}_2^-$ ,  $\text{Mn}^{2+}$ , and  $\text{F}^-$  concentrations in water samples exceeded the guideline values of WHO (2011) (Fig. 6.28).  $\text{NO}_3^-$  and  $\text{NO}_2^-$  concentrations of groundwater, stream water, and flooding water were low. The percentage amount of detectable concentrations in relation to all samples of the four snapshot samplings was 18 % for  $\text{NO}_3^-$  and 3 % for  $\text{NO}_2^-$ . Those samples, where  $\text{NO}_3^-$  was detected, were taken from draw and pumping wells spread over the whole study site. However, groundwater of only two sampling points showed  $\text{NO}_3^-$  concentrations exceeding the guideline value. While the shallow groundwater of DW36<sub>IF</sub> was only affected by  $\text{NO}_3^-$  in rainy season 2014, deep groundwater of PW19<sub>IF</sub> exceeded the guideline value in all seasons except for rainy season 2015.  $\text{NO}_2^-$  concentrations exceeded the guideline value in water of three wells in rainy season 2015 (PW19<sub>IF</sub>, DW36<sub>IF</sub>, PW48<sub>IF</sub>). As during this season no exceeding  $\text{NO}_3^-$  concentrations were measured, a denitrification of  $\text{NO}_3^-$  to  $\text{NO}_2^-$  might have taken place. Redox potential and oxygen saturation of those waters were lower during rainy season compared to dry season, which hints at reducing conditions facilitating denitrification (Mitsch and Gosselink 2007). The absence of  $\text{NO}_3^-$  in flooding water indicates denitrification as well, confirming the water quality function of the wetland in terms of nutrient removal (Hemond and Benoit 1988).

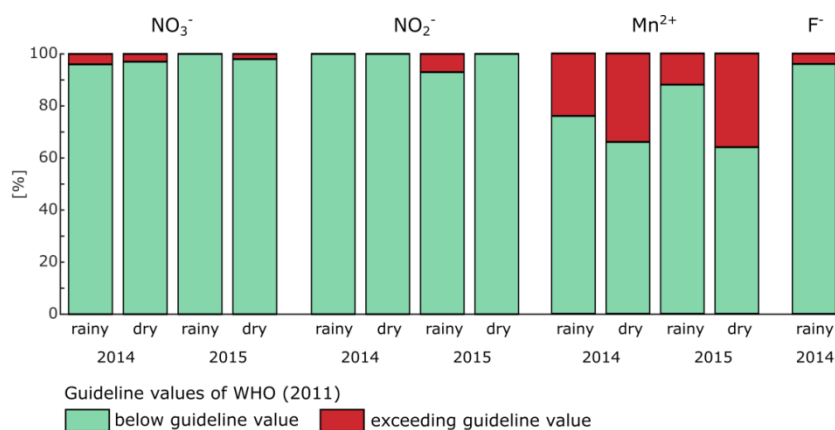


**Fig. 6.28:** Stacked bar charts of the percentage amount of all samples exceeding the guideline values (WHO 2011) of nitrate ( $\text{NO}_3^-$ ), nitrite ( $\text{NO}_2^-$ ), and manganese ( $\text{Mn}^{2+}$ ) for the four snapshot samplings, and of fluoride ( $\text{F}^-$ ) for rainy season 2014 (IF).

Almost all water samples showed detectable concentrations of  $\text{Mn}^{2+}$ . For the different seasons, the health related guideline value was exceeded in 12 to 36 % of all samples, with more exceeded values in dry seasons compared to rainy seasons (Fig. 6.28). Most of the samples that exceeded the guideline value were taken from pumping wells and piezometers, with the exception of one draw well and one flooding water. It was observed that water of some sampling points exceeded the guideline value during all seasons, while others only exceeded them during dry seasons.

The health related guideline value for  $\text{Al}^{3+}$  was not exceeded in any sample. WHO (2011) already stated that those high values usually do not occur in natural waters. Similarly, all amounts of trace heavy metals were below or around the respective limit of detection. Determination of  $\text{F}^-$  turned out to show big uncertainties due to background noise in the chromatograms. A lot of water samples showed increased amounts of  $\text{F}^-$ , and two deep groundwater samples even exceeded the guideline value (PW41<sub>IF</sub>, PW46<sub>IF</sub>). The exact determination of  $\text{F}^-$  concentrations in groundwater within the study site will be addressed by Wieczorek (unpublished).

As shown above, chemical water quality related to drinking water is good in groundwater and surface water of the study site. This coincides with results gained from the whole Rufiji Catchment (Ministry of Water URT 2012a). However, the health related constituents  $\text{NO}_3^-$ ,  $\text{NO}_2^-$ ,  $\text{Mn}^{2+}$ , and  $\text{F}^-$  exceeded the guideline values in certain amounts of samples (Fig. 6.28).

In general, health related water quality was better in the non-alluvial compared to the alluvial sediments (Fig. 6.29). Most sampling points located in the alluvial fan showed DHWQs of one, while most sampling points located in the non-alluvial sediments showed DHWQs of zero. Furthermore, two hotspots with a DHWQ of three were identified (Fig. 6.29: PW19<sub>IF</sub>, DW36<sub>IF</sub>). Only these two and one other well (PW48<sub>IF</sub>) exceeded the guideline values of  $\text{NO}_3^-$  or  $\text{NO}_2^-$ . An anthropogenic contamination is expected here. For the draw well DW36<sub>IF</sub>,  $\text{NO}_3^-$  concentrations were much higher in rainy seasons compared to dry seasons. This indicates a leaching of accumulated  $\text{NO}_3^-$  from soil to groundwater during heavy rainfall events. The pumping well PW19<sub>IF</sub> is located in Ifakara city and lies directly next to a street gutter. Although this gutter is composed of concrete, it might have fissures providing preferential flow paths for waste water to infiltrate into the ground. However, in wide parts of the study site, no effects of drinking water quality due to anthropogenic activities were observed. Nevertheless, it is recommended not to give groundwater to small children, because few hotspots of  $\text{NO}_3^-$  and  $\text{NO}_2^-$  contamination occur. These ions lead to a production of methaemoglobin in the blood, hampering the transport of oxygen (WHO 2011). Bottle-fed infants are at greatest risk, because the intake of water in relation to body weight is high.

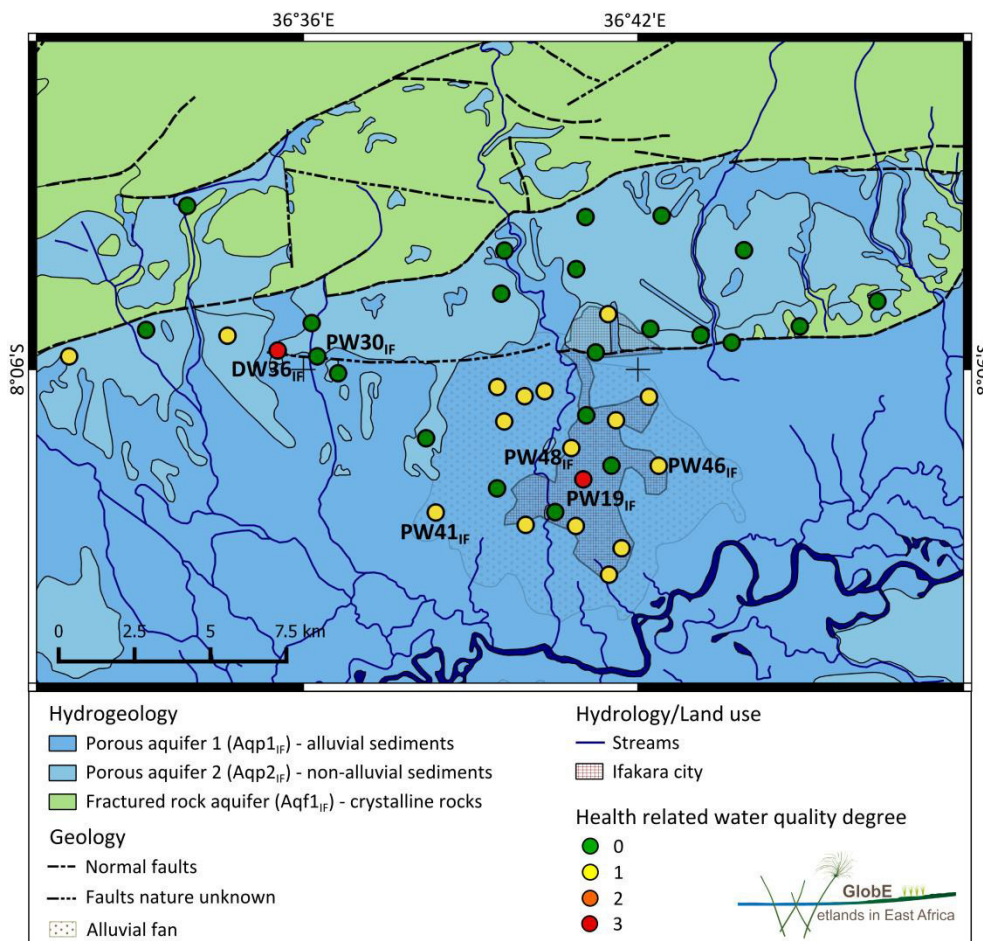


**Fig. 6.29:** Groundwater quality related to human health displayed as Degree of Health related Water Quality (DHWQ). Drinking water quality decreases from 0 (no guideline value exceeded) to 3 (guideline values of three constituents exceeded). Data sources: Geological Survey of Tanganyika (1962) (geology, streams), Jätzold and Baum (1968) (alluvial fan), google.com/earth (Ifakara city) (IF).

Instead, geogenic contamination was identified as the major hazard to drinking water quality. The elevated amounts of  $\text{Mn}^{2+}$  in groundwater are alarming. Manganese is known to cause neurological symptoms, such as muscle weakness and tremor, as well as behavioral symptoms, such as memory loss and cognitive problems (McMillan 1999). More sampling points exceeded the guideline value in dry than in



rainy seasons. Thus, it is most likely that  $Mn^{2+}$  was derived by weathering of manganese containing silicate minerals. Considerable amounts of manganese were found in rock and sediment samples of both crystalline rocks and alluvial sediments (section 6.1). Therefore, a prevention of  $Mn^{2+}$  contamination is not possible. In general, anthropogenic contamination ( $NO_3^-$ ,  $NO_2^-$ ) was higher in rainy seasons, whereas geogenic contamination ( $Mn^{2+}$ ) was higher in dry seasons. Stream water did not show any contamination of the analyzed indicators. However, stream water might show higher bacteriological contaminations, as already outlined by Ministry of Water URT (2012a), and is thus not a good alternative to groundwater in terms of drinking water.

### 6.3.3.2 Water quality related to public acceptability aspects (IF)

Despite the health issues of drinking water quality, the acceptability of water in terms of domestic use was evaluated. Water in the study site is used for domestic purposes, such as laundry cleaning and sanitary purposes. The acceptability related indicators  $Cl^-$ ,  $Na^+$ ,  $SO_4^{2-}$ ,  $Mn^{2+}$ ,  $Fe^{2+}$ ,  $Al^{3+}$ , and pH were analyzed during all four snapshot samplings (Tab. 4.4 p.51). Concentrations of Zn were only analyzed for rainy season 2014.

High concentrations of some major ions give undesirable tastes to drinking water. The  $Na^+$  taste threshold was exceeded in deep groundwater of PW30<sub>IF</sub> during all four seasons and in groundwater of two additional pumping wells in rainy season 2014 (PW41<sub>IF</sub>, PW46<sub>IF</sub>). Furthermore, PW30<sub>IF</sub> appeared to be the only sampling point exceeding the  $Cl^-$  taste threshold in all four seasons.  $SO_4^{2-}$  concentrations were all below the taste threshold. The amounts of Zn ranged between values lower than the limit of detection and 0.2 mg/L, which is far below the taste threshold.

The acceptability thresholds of  $Mn^{2+}$  and  $Fe^{2+}$  were exceeded often (Fig. 6.30). Most of the samples that exceeded thresholds of  $Mn^{2+}$  and  $Fe^{2+}$  were groundwater samples. However, flooding water and stream water sometimes exceeded the thresholds as well. In each season, one deep or shallow groundwater sample exceeded the guideline value of  $Al^{3+}$  except for dry season 2014. While pH values of surface water were almost neutral in most cases, pH values of groundwater were slightly acidic throughout the study site. Around 50 % of all samples fell below the optimum range between 6.5 and 8.5.

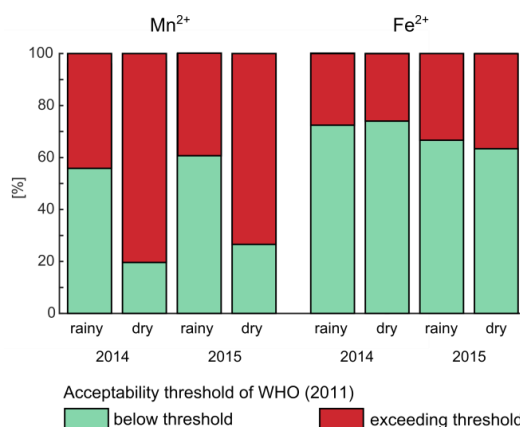


**Fig. 6.30:** Stacked bar charts of the percentage amount of all samples exceeding the acceptability thresholds (WHO 2011) of manganese ( $Mn^{2+}$ ) and iron ( $Fe^{2+}$ ) for the four snapshot samplings (IF).

A few wells provide water that is not good in taste due to major ions. In the case of PW30<sub>IF</sub>, water users already mentioned the salty taste of the water (personal communication with local population 2015). Much more wells showed degraded tastes due to  $Mn^{2+}$  concentrations. Moreover, more than half of the wells displayed problems in terms of discoloration issues due to high  $Mn^{2+}$  and  $Fe^{2+}$  concentrations. This leads to quality degradation in terms of water used for cleaning. Another problem is induced by low pH

vales of groundwater, altering pipes and other parts of the well. This corrosion could lead to a dysfunctionality of the well, which was already observed for some wells during field work. Usually this leads to a decrease in water availability for local communities and, in extreme cases, can cause a complete absence of fresh water for people. However, all of these water quality degradations related to public acceptability are of geogenic origin and cannot be avoided, only treated.

### 6.3.3.3 Water quality related to irrigation purposes and agriculture (IF)

Surface and stream water are already used as irrigation water in the study site and bigger areas of dry land will be irrigated in future (Ministry of Water URT 2012b). Groundwater might be an alternative of irrigation water as well. In terms of salinity, affecting crop water availability, five groundwater samples showed a slight to moderate degree of restriction on use (DRU), while all surface water samples showed no restriction on use (Fig. 6.31). The evaluation of infiltration problems due to low salinity and high SAR revealed different results. Here, higher DRUs were observed. Particularly those wells that showed restrictions on use due to salinity were the only ones that displayed no restriction on use in terms of infiltration (e.g. PW19<sub>IF</sub>, PW30<sub>IF</sub>, DW36<sub>IF</sub>). All other groundwater samples and all surface water samples showed either slight to moderate or severe restrictions on use (Fig. 6.31). No difference was observed between rainy and dry seasons.

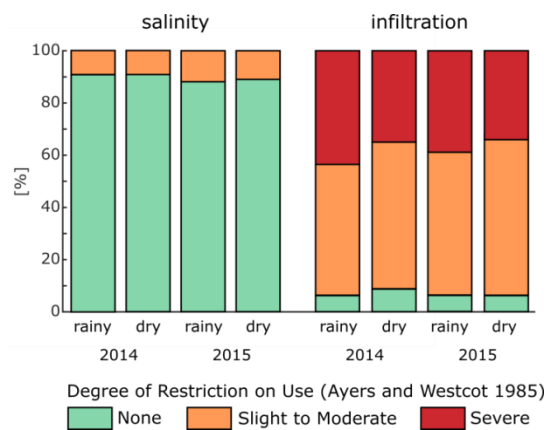


Fig. 6.31: Stacked bar charts of the percentage amount of all samples showing Degrees of Restriction on Use (Ayers and Westcot 1985) related to salinity and infiltration for the four snapshot samplings (IF).

Moderate SARs in combination with low ECs represent the major restrictions on use of water for irrigation. However, the guidelines were developed for arid and semi-arid climates and Ayers and Westcot (1985) state that they are too strict for regions, where more dilution due to precipitation occurs and the water level is shallower. Thus, slight to moderate restrictions on use might not be of big concern. Most stream waters and flooding water at the *center* showed severe restrictions on use, indicating a decrease in permeability of soil due to natural irrigation with those waters. This decrease in permeability is related to the leaching of  $\text{Ca}^{2+}$  from the soil and leads to a decreasing infiltration rate of irrigation water. The negative effects of irrigation water on soil in terms of infiltration should be considered when planning big irrigation schemes. For some crops, even the increased  $\text{Mn}^{2+}$  amounts could be toxic. All other trace elements are not high enough to be toxic in terms of irrigation.

## 6.4 Conceptual model (IF)

The conclusions gained from the described results were summarized and visualized in a conceptual model (Fig. 6.32). The model shows a schematic cross section of the study site from north to south, visualizing groundwater flow paths, hydrochemical evolution of groundwater and surface water, ground-

water-surface water interactions, recharge processes, and the current mutual effects between agricultural production and water quality.

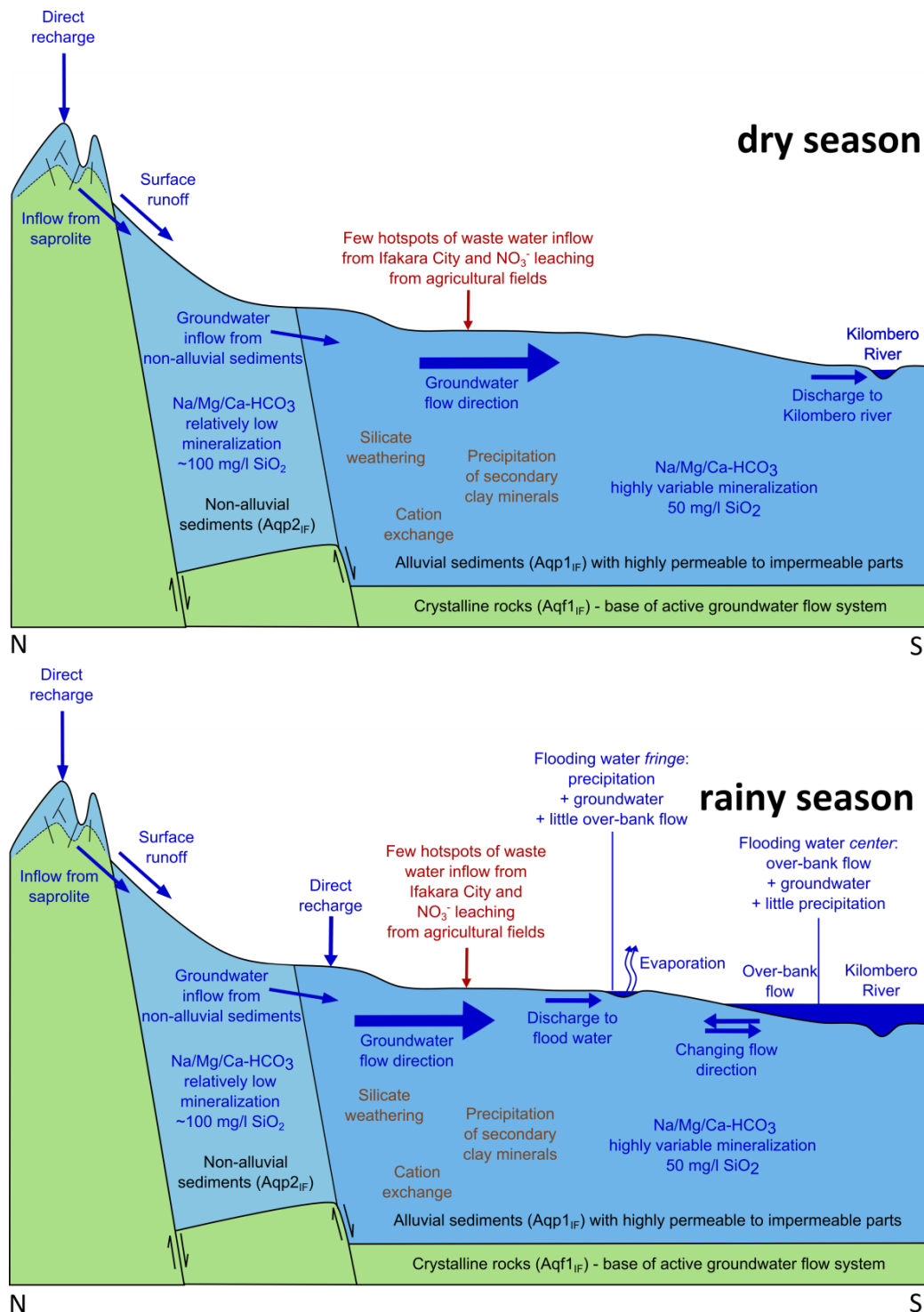


Fig. 6.32: Conceptual hydrogeological wetland model of the Ifakara study site for dry and rainy seasons. Hydrostratigraphic units are colored according to Figure 6.1 (p.68). Water fluxes and compositions are displayed in blue, while hydrochemical processes are displayed in brown. Red texts refer to anthropogenic influences (IF).

#### 6.4.1 Groundwater flow paths (IF)

The study site comprises a fractured rock aquifer that is separated from two porous aquifers via a normal fault system (Fig. 6.1 p.68, Fig. 6.8 p.77, Fig. 6.9 p.77). South of the northern fault, the fractured rock aquifer underlies the porous aquifers in uncertain depths. Due to its low hydraulic conductivity, the

fractured rock aquifer is supposed to build the base of the active groundwater flow system within the southern study site.

As indicated by piezometric data, the hydraulic gradient is directed towards the river (NNW-SSE) during the whole year. Thus, groundwater flows from the mountains to the non-alluvial sediments and from the non-alluvial to the alluvial sediments (N-S) (Fig. 6.32). While only small amounts of groundwater are assumed to flow in the fractured rock aquifer, the weathering profile acts as a porous aquifer contributing flow to the porous aquifers in the south. Additionally, a smaller flow component is directed from the alluvial fan (W) to the floodplain (E). Due to the high variability in texture and hydraulic conductivity within the porous aquifers, groundwater flow paths are quite complex on a small scale and groundwater residence times are variable. Impermeable parts, with stagnant water, coexist with permeable parts, with high flow velocities representing preferential flow paths.

#### 6.4.2 Hydrochemical evolution (IF)

Based on the dominant occurrence of silicate minerals within the crystalline rocks and sediments (Fig. 6.2 p.69, e.g. Fig. 6.3 p.72), as well as on the hydrochemical composition of groundwater (Fig. 6.19 p.90), silicate weathering was identified to be the major process controlling hydrochemistry. The weathering of feldspars, hornblende, and muscovite leads to an addition of  $\text{Na}^+$ ,  $\text{K}^+$ ,  $\text{Mg}^{2+}$ ,  $\text{Ca}^{2+}$ ,  $\text{HCO}_3^-$ , and  $\text{SiO}_2$  to the solution (Appelo and Postma 2005). Silicate weathering occurs within the fractured rock aquifer as well as in the sediments. Major weathering products are kaolinite and montmorillonite, as indicated by sediment mineralogy and water chemistry (e.g. Fig. 6.3 p.72, Fig. 6.24 p.96). As those weathering products usually indicate arid climate, the big influence of dry season climate on hydrochemical processes may be evidenced. To a lesser extent, hydrochemistry is influenced by redox processes, as indicated by high  $\text{Fe}^{2+}$  concentrations in groundwater of the alluvial fan that showed low redox potentials (Fig. 6.22 p.94).

The suggested hydrostratigraphic classification of sediments was fully confirmed by the hydrochemical data. Based on drilling log data and hydraulic conductivity analyses, it was concluded that the alluvial sediments act as one big aquifer system, with high to medium permeable and impermeable zones. This conclusion was confirmed by the results of HCA. HCA provided a clear differentiation between groundwater in the non-alluvial and groundwater in the alluvial sediments (Fig. 6.18 p.89, Fig. 6.20 p.90). However, *highly mineralized groundwater* occurred in both units. Looking closer at this cluster group exhibited that *highly mineralized groundwater* located in the alluvial sediments plots near to *alluvial groundwater* in the PCA plot and *highly mineralized groundwater* located in the non-alluvial sediments plots near to *non-alluvial groundwater* (Fig. 6.21 p.92), confirming a differentiation between those hydrostratigraphic units along  $\text{PC2}_{\text{IF}}$ .

In general, groundwater showed high spatial variabilities of mineralization. Scatter plots of  $\text{EC}/\text{HCO}_3^-$ ,  $\text{SiO}_2/\text{Na}^+$ , and  $\text{HCO}_3^-/(\text{Na}^+ + 2\text{Ca}^{2+})$  as well as saturation indices revealed that all samples of *non-alluvial* and *alluvial groundwater* were predominantly characterized by silicate weathering (Fig. 6.22 p.94, Fig. 6.23 p.95). Hence, the variability in mineralization is determined by water-rock interactions and thus related to the variable permeability of the aquifers. The process of silicate weathering and thus the amount of dissolved ions increases in zones with lower hydraulic conductivities, due to longer residence times of groundwater. In addition, parts in the sediments containing more weatherable minerals lead to higher mineralizations of groundwater as well. All samples of *highly mineralized groundwater*, except for the two wells in the western study site ( $\text{PW30}_{\text{IF}}$ ,  $\text{DW36}_{\text{IF}}$ ) and one well in the alluvial fan ( $\text{PW19}_{\text{IF}}$ ), showed silicate weathering as major source of mineralization as well. In comparison to the other cluster

groups, these samples solely showed higher concentrations of ions, but similar ratios. Thus, they are assumed to be of higher mineralization, due to longer residence times in the aquifers, just like all other groundwater samples. Evaluation of deep drilling logs revealed that the drilling log below the city of Ifakara was more clayey compared to the other parts of the alluvial fan. Lower hydraulic conductivities within this area could explain the longer residence times of *highly mineralized groundwater*. Usually, smallest grain sizes are rather found in the distal zones of alluvial fans than in their central parts (Chamley 1990). However, within the study site, the alluvial fan sediments interfinger with river bed sediments of Kilombero River. Alternating deposition of alluvial fan deposits and river bed sediments, which are more clayey in greater distances to the river, might have induced the observed pattern, with smallest grain sizes and thus lowest hydraulic conductivities in the central parts of the alluvial fan.

The three other wells (PW19<sub>IF</sub>, PW30<sub>IF</sub>, DW36<sub>IF</sub>) showed other sources of mineralization. One of these sources is NaCl, as indicated by Na/Cl ratios (Fig. 6.22 p.94). Furthermore, PW19<sub>IF</sub> and DW36<sub>IF</sub> showed increased NO<sub>3</sub><sup>-</sup> concentrations. For PW19<sub>IF</sub>, NaCl as well as NO<sub>3</sub><sup>-</sup> are probably derived by waste water of Ifakara city, infiltrating through a street gutter. The increased NO<sub>3</sub><sup>-</sup> concentrations in DW36<sub>IF</sub> are most likely derived by the input of fertilizers in agricultural fields around the well. The high NaCl content in PW30<sub>IF</sub> might be explained by either upwelling of deep groundwater, as the well is located near the southern fault, or by evaporites, which might be present in the non-alluvial sediments.

*Alluvial groundwater* mainly differed from *non-alluvial groundwater* by lower SiO<sub>2</sub> and K<sup>+</sup> concentrations and higher Fe<sup>2+</sup> concentrations (Fig. 6.21 p.92). Thus, groundwater becomes depleted in SiO<sub>2</sub> and K<sup>+</sup> and enriched in Fe<sup>2+</sup> along its flow path from the non-alluvial to the alluvial sediments. The decrease in SiO<sub>2</sub> is strongest. Primary silicate minerals, such as feldspars and quartz, as well as amorphous silica are not likely to precipitate, due to kinetic constraints (Appelo and Postma 2005). Hence, it is assumed that SiO<sub>2</sub> and K<sup>+</sup> become decreased due to the precipitation of secondary clay minerals, which was proven to occur based on saturation indices (Fig. 6.23 p.95). Contemporaneously, k-feldspars are no longer dissolved in the alluvial sediments. This was confirmed by the rare occurrence of k-feldspars within the alluvial sediments compared to the crystalline rocks, and the almost attained saturation of *alluvial groundwater* in terms of k-feldspars. If clay minerals, such as montmorillonite and kaolinite, precipitate, SiO<sub>2</sub> is removed from the solution. K<sup>+</sup> becomes decreased, if montmorillonite is transformed to illite (Okrusch and Matthes 2014). This transformation process was proven to occur in the alluvial sediments, as mineralogical analysis showed illite in some sediment samples. Moreover, this was also indicated by the decrease of saturation indices in terms of illite from *non-alluvial* to *alluvial groundwater*. Additionally, cation exchange is expected to take place in the clayey parts of the aquifer. Here, K<sup>+</sup> in solution might be exchanged with Na<sup>+</sup> in the solid phase. Saturation indices of ferric oxyhydroxides such as hematite or goethite showed oversaturation for *alluvial* and *non-alluvial groundwater* indicating the dissolution of iron-bearing silicate minerals and the subsequent precipitation of ferric oxyhydroxides (Appelo and Postma 2005). The occurrence of high iron concentrations in *alluvial groundwater* was related to low redox potentials (Fig. 6.22 p.94), due to the reduction of ferric oxyhydroxides under anoxic conditions (Hem 1985). Lower redox potentials in the alluvial sediments are probably induced by flooding conditions.

#### 6.4.3 Groundwater-surface water interaction and recharge processes (IF)

In terms of interaction and recharge processes the components stream water, flooding water, groundwater, and precipitation are addressed. The interpretation of shallow drilling logs revealed a hydraulic connection between the alluvial sediments and Kilombero River.

The observed variation of  $\delta^{18}\text{O}$  in precipitation between 2014 and 2015 (Fig. 6.26 p.97) was not reflected in stream water of Kilombero and Lumemo rivers. Isotopic compositions of stream water showed only little variations between 2014 and 2015. As precipitation was solely sampled at one point in the study site, it might be not representative for precipitation of the whole Kilombero or Lumemo catchments. Thus, it is rather assumed that stream water originates from precipitation fallen in the whole respective catchment. Even during dry season Kilombero River as well as Lumemo River receive inflow from precipitation, as indicated by similar hydrochemical compositions in rainy and dry seasons (Fig. 6.13 p.84). This precipitation portion might have been fallen in the mountain areas, where rainfall occurs throughout the whole year (personal communication with local population 2014). Furthermore, stream water is derived from base flow of groundwater within the respective catchment. This contribution of groundwater to stream water was proven by the influence of silicate weathering on stream water composition (Fig. 6.19 p.90). For Kilombero River, groundwater discharge within the study site was indicated by the groundwater flow direction. Additionally,  $\text{K}^+/\text{Na}^+$  ratios specified overland flow as another source of stream water (Fig. 6.21 p.92).

The origin of flooding water is variable depending on its location within the study site (Fig. 6.32). Results of HCA showed that flooding water at *center* fell within the group of *surface water*, while flooding water at *fringe* fell within the group of *alluvial groundwater* indicating a significant difference between the origin and hydrochemical evolution of these two flooding waters. During field trips it became obvious that flooding water at *center* was in direct hydraulic connection to the river and derived by over-bank flow. Indeed, hydrochemical composition and isotopic signatures of flooding water at *center* were similar to those of Kilombero River (Fig. 6.13 p.84). However, EC of flooding water was almost two times higher than that of Kilombero River. This increase in EC might have been derived by either evapotranspiration or mixing with another higher mineralized water component. No evaporation effects were observed within the isotopic composition of flooding water at *center* (Fig. 6.25 p.97). However, flooding water is probably transpired by aquatic plants, such as *pistia stratiotes* (personal communication with K. Behn 2017, Kirzhner et al. 2008). After Clark and Fritz (1997) transpiration leads to an increase of EC, but does not alter the isotopic composition. But, looking closer at plant nutrition, transpiration does not explicitly remove pure  $\text{H}_2\text{O}$  from the solution. Plants selectively take up nutrients during transpiration, leading to changes in hydrochemical compositions (Dykyjová 1979). Furthermore, it is assumed that groundwater, which was higher mineralized than stream water, contributes to flooding water at *center*. Such a contribution is likely, because the soil saturates from bottom to top before flooding events (Ziegler 2015), indicating groundwater as the main source of floodplain saturation.

In contrast, flooding water at *fringe* occurred in more isolated parts and is not in direct connection to Kilombero River, although this connection might occur during highest levels of flooding. EC of flooding water was up to ten times higher than that of Kilombero River. Here, isotopic signatures disclosed clear evaporation effects, confirmed by higher temperatures of the water. Again, transpiration might play a role as well. However, isotopic composition does not allow identifying the exact source of this flooding water prior to evapotranspiration. Precipitation fallen before flooding as well as groundwater and stream water of Kilombero River showed isotopic compositions near the origin of the evaporation line (Fig. 6.25 p.97). Thus, all of these components are possible sources of flooding water at *fringe*. Discharge of groundwater to flooding water at *fringe* was also indicated by groundwater level measurements. At *fringe*, groundwater levels ranged around 0 m.b.s., inducing groundwater discharge in small local depressions (Fig. 6.11 p.81). Flooding water at *middle* displayed evaporation effects lower than those of flooding water at *fringe*. This indicates that evaporation effects of flooding water increase with further distance to Kilombero River.

Hydrograph analyses indicated that the hydraulic gradient within the floodplain changes its direction away from the river at the beginning of flooding events. Later on, the gradient changes again in direction to the river. This change in flow direction at the beginning of flooding events induces a groundwater ridge below the floodplain, which was already described by Jung et al. (2004). They proposed that the kinematic wave induced by rising river level operates analogously to piston flow pushing “old” floodplain water ahead. This process was observed here as well, as the groundwater levels within floodplain piezometers rose nearly simultaneously with the river level (Fig. 6.11 p.81). Thus, a dynamic connection between Kilombero River and floodplain groundwater is given, but the amount of stream water entering the aquifer during flooding events is assumed to be small. This was also confirmed by water composition data, as no dilution of groundwater within the floodplain piezometers was observed in rainy season. While groundwater levels below surface showed an influence of flooding events at *center* and *middle*, no influence was observed at *fringe*. But piezometers east of the alluvial fan are maybe influenced by the river level as well.

In the alluvial fan, all wells showed rising water levels at the beginning of flooding events as well. These are most probably induced by groundwater inflow from the north. When the river level rises, the southwards flow velocity of groundwater is lowered, due to the groundwater ridge below the floodplain. This lowering in flow direction leads to increasing groundwater levels.

Based on hydrograph analyses direct recharge could only be proven in piezometers at *fringe*. However, direct recharge was not disproven for the other points of groundwater level measurements. If groundwater is solely derived from direct recharge, it reflects the weighted average composition of stable water isotopes in precipitation (Moser 1998). Such a reflection of direct recharge was not observed within the study site. Groundwater was more depleted in heavy water isotopes compared to the weighted average of precipitation. This might be explained by several reasons. The isotopic composition of precipitation in 2014 might be exceptionally high, and thus not reflect the long term average value. Moreover, recharge could only occur from heavy rainfall events, which are depleted in stable water isotopes. This phenomenon was observed for tropical regions in general by Jasechko and Taylor (2015) and for central Tanzania in particular by Taylor et al. (2013). Furthermore, major recharge could occur in the mountains north of the study site, where the altitude effect leads to depletion as well (Moser 1998).

Temporal variations of EC in groundwater showed little dilution during rainy seasons, indicating little direct recharge (Fig. 6.15 p.85). Few wells distributed over the whole study site pointed to more influence of direct recharge by lower ECs during rainy season and a distinct temporal variability of water composition (PW25<sub>IF</sub>, DW27<sub>IF</sub>, PW47<sub>IF</sub>). Finally, it is concluded that direct recharge occurs during rainy seasons in the study site. Nevertheless, recharge probably occurs in the mountains north of the study site as well.

In terms of indirect recharge, a significant contribution of stream or flooding water to groundwater recharge could be disproven. Firstly, EC of groundwater was not decreased in wells located next to streams or flooding water (Fig. 6.16 p.86). Secondly, no evaporation effects were observed in isotopes of groundwater of wells located next to flooding water at *fringe*, although flooding water itself showed high evaporation effects. Additionally, the isotopic composition of stream water of Kilombero River varied between rainy and dry season, but this variation was not observed in groundwater, except for few shallow wells (Fig. 6.27 p.98). Furthermore, it was shown that infiltration of Kilombero or flooding water solely occurs for short periods of time at the beginning of flooding events in close vicinity to Kilombero River. During rainy season, the pressure gradient of groundwater being recharged in the mountains

north of the study site is high enough in the floodplain to prevent infiltration and percolation of surface water.

#### 6.4.4 Current mutual effects between agricultural production and water quality (IF)

Water quality related to public health was mainly affected by geogenic contamination in terms of  $Mn^{2+}$  (Fig. 6.28 p.99). The  $Mn^{2+}$  elevation is contrary to the former assessments of water quality within the whole Rufiji Basin, where  $Mn^{2+}$  concentrations were generally low (Ministry of Water URT 2012a). In general, groundwater quality was better in the non-alluvial compared to the alluvial sediments (Fig. 6.29 p.100).

Surface water and groundwater did not show any contamination of inorganic components related to agriculture (e.g.  $NO_3^-$ ). Solely two wells showed increased amounts of  $NO_3^-$  of up to 123.6 mg/L. Additionally, those wells were highly mineralized and had different hydrochemical compositions compared to the other samples. One well is located in the western part of the study site, surrounded by agricultural land, and the other well is located in Ifakara city. Thus, these wells are assumed to be affected by anthropogenic contamination in terms of agriculture or waste water input. Nevertheless, water contamination with nutrients derived from anthropogenic sources with respect to drinking water quality was generally very low. However, the discharge of waste water from Ifakara City might become hazardous to groundwater quality in terms of drinking water during the next years. Thus, a proper waste water management of Ifakara City is highly required in order to ensure drinking water quality.

Water quality assessment related to irrigation purposes showed that groundwater as well as surface water had moderate to severe restrictions on use in terms of infiltration. Those restrictions are solely caused by the hydrochemical geogenic background of water. Low mineralized water with relatively high  $Na^+$  concentrations is likely to remove  $Ca^{2+}$  from the soil. This leads to the destruction of soil structure, because finer particles disperse and fill pore spaces (Ayers and Westcot 1985). Hence, infiltration of irrigation water is hampered. In terms of salinity, water showed no restrictions on use except for a few groundwater samples. The high concentrations of  $SiO_2$  are generally promoting for the cultivation of rice, because silicate is essential for rice plants (Scheffer and Schachtschabel 2010).

#### 6.5 Hydrochemical modeling of origin and evolution of flooding water (IF)

Two hydrochemical inverse models were set up using the software PhreeqC, in order to assess the origin and evolution of flooding water at *center* and *fringe*. Modeling was performed for rainy seasons 2014 and 2015.

Flooding water at *center* is derived from over-bank flow of Kilombero River, groundwater discharge, and precipitation (Fig. 6.32 p.103). No evaporation was observed. Thus, Kilombero River, groundwater, and precipitation were set as initial solutions and flooding water at center was set as end solution. In order to include exchange processes with atmosphere and soil, gaseous  $O_2$  and  $CO_2$  were set as phases. Mol balances were required for all major ions ( $Na^+$ ,  $K^+$ ,  $Mg^{2+}$ ,  $Ca^{2+}$ ,  $HCO_3^-$ ,  $Cl^-$ ,  $SO_4^{2-}$ ) and  $SiO_2$ . Uncertainties of chemical constituents in the solutions were set to 20 %. This uncertainty was chosen, considering analytical accuracies as well as possible errors, due to transportation and long storage times of water samples. Furthermore, hydrochemical analyses of low EC water samples usually shows higher uncertainties compared to high EC water samples (Hötzl and Witthüser 1999).

Hydrochemical compositions of Kilombero River and flooding water at *center* were represented by the respective water samples. In contrast, definition of groundwater and precipitation inflow was more complex. Precipitation was only sampled at one location in the study site. However, a spatial variability



of precipitation is most likely. Moreover, precipitation samples were analyzed infrequently for hydrochemical composition. Hence, composition of precipitation was adopted from Rodhe et al. (1981) (In Johnson 1996). Lacking data of SiO<sub>2</sub> concentration was gained from own measurements (Tab. 6.3 p.87). This parametrization of the precipitation solution is highly uncertain. Thus, uncertainties were set to 50 % for the precipitation solution.

Groundwater showed remarkable spatial variabilities, making the definition of the groundwater solution difficult. Therefore, the model was run for different parametrizations of the groundwater solution. According to assumed groundwater inflow patterns to flooding water, three different groundwater solutions were defined:

- 1) Sample composition of the well nearest to the *center* (PW17<sub>IF</sub>)
- 2) Average composition of all *alluvial groundwater* samples
- 3) Average composition of all *alluvial and highly mineralized groundwater* samples (excluding PW30<sub>IF</sub> and DW36<sub>IF</sub>)

Thereby, only those samples were considered that were sampled during the respective season. For groundwater solution 3), those wells were excluded that are located in the western study site. These two wells are not assumed to contribute to flooding water at *center*, due to their spatial distance to the *center*. For rainy season 2014, the inverse modeling code found possible models in all cases. Depending on the parametrization of the groundwater solution, different numbers of models were found (Tab. 6.7). Proportional ratios of stream water, groundwater, and precipitation were similar for all models outlining the robustness of the model against different groundwater solutions. Proportions of Kilombero River were highest followed by groundwater. The input of precipitation was always little or zero, indicating no big influence of the direct input of precipitation. Biogeochemical processes, such as the uptake of nutrients and the transpiration of water by aquatic plants, obviously only played a minor role in flooding water evolution.

**Tab. 6.7:** Results of inverse modeling of the origin and hydrochemical evolution of flooding water at *center* for rainy season 2014 (IF).

Groundwater solution	Proportion of Kilombero River [%]	Proportion of groundwater [%]	Proportion of precip- itation [%]	CO <sub>2</sub> phase mol transfer [mol]
1)	91	9	0	5.8 x 10 <sup>-5</sup>
	91	9	0	0
2)	83	14	3	-8.6 x 10 <sup>-5</sup>
	86	14	0	0
	83	14	3	0
	86	14	0	-9.7 x 10 <sup>-5</sup>
3)	92	7	1	-6.6x 10 <sup>-7</sup>
	93	7	0	0
	92	7	1	0
	93	7	0	-3.5 x 10 <sup>-6</sup>

For rainy season 2015, no possible model was found with the given uncertainties. Thus, it is assumed that further processes occurred during the evolution of flooding water in 2015. Biogeochemical processes within flooding water as well as unknown inputs of fertilizers or detergents to flooding water might have altered hydrochemistry. For instance, aquatic plants selectively remove water and nutrients from the solution (Dykyjová 1979). Furthermore, flooding water was supersaturated with respect to clay minerals, which might precipitate and thus alter water composition as well (Appelo and Postma 2005). Addi-

tionally, diffusion from soil water to flooding water might have changed hydrochemistry. Nevertheless, the failure of the modeling code to find possible models, might also depend on lacking knowledge about the real composition of precipitation, implying that 50 % uncertainty were too small. However, the assumption of a higher uncertainty will lead to highly uncertain model results and was thus not applied.

In terms of flooding water at *fringe*, the conceptual model indicated precipitation, groundwater, and stream water of Kilombero River as possible sources. In addition, flooding water was affected by evaporation. Therefore, precipitation, groundwater, and stream water were set as initial solutions and flooding water at *fringe* was set as end solution. Again, gaseous O<sub>2</sub> and CO<sub>2</sub> were set as phases. In addition, gaseous H<sub>2</sub>O was forced to precipitate, in order to simulate evaporation. Mol balances and uncertainties were set according to the previous model (flooding at *center*). While hydrochemical composition of Kilombero River and flooding water at *fringe* were represented by the respective water samples and composition of precipitation was adopted from Rodhe et al. (1981) (In Johnson 1996), again the model was run for different groundwater solutions:

- 1) Sample composition of the well nearest to the *fringe* (PW43<sub>IF</sub>)
- 2) Average composition of all *alluvial groundwater* samples
- 3) Average composition of all *alluvial* and *highly mineralized groundwater* samples (excluding PW30<sub>IF</sub> and DW36<sub>IF</sub>) in spring 2015

First model calculations revealed that the implementation of sulfur exchange processes was necessary to gain results. The occurrence of sulfur exchange processes in flooding water at *fringe* is realistic, as many exchange processes occur between water and solid phases in wetlands (section 3.2.3). Flooding water at *fringe* was in direct contact to rice fields and partially covered with aquatic plants. Therefore, sulfur was set as an additional phase.

Possible models were found for groundwater solutions 1) and 2) in 2014, indicating that groundwater discharging to flooding water at *fringe* is not influenced by *highly mineralized groundwater*. Cl<sup>-</sup> could not be balanced for groundwater solution 3). Model results showed that flooding water at *fringe* was mainly derived by precipitation, while only little groundwater discharged. A contribution of stream water was only included in two possible models for groundwater solution 1). All other models did not include stream water. Hence, it is concluded that stream water of Kilombero River did not significantly contribute to flooding water at *fringe*. Evaporation rates turned out to be high of up to 96 %. These include the evaporation of the water surface and might also include transpiration from aquatic plants. However, during transpiration plants selectively take up ions, removing not only pure H<sub>2</sub>O from the solution (Dykyjová 1979). Elemental sulfur and oxygen were removed from flooding water in all models. Sulfate removal might have been induced by dissimilatory sulfate reduction under reducing conditions or by assimilatory sulfate-reduction under oxidizing conditions (Faulkner and Richardson 1989). Flooding water at *fringe* showed oxidizing conditions in both years (redox potential: 415 mV, Tab. 6.2 p.84). Nevertheless, reducing conditions might be found in the soil leading to dissimilatory sulfate reduction with flooding water as sulfate source (Faulkner and Richardson 1989). Additionally, measured redox potentials in the field are always difficult to interpret as they often do not show the real redox state (Appelo and Postma 2005). Furthermore, rice is planted in the fields next to flooding water at *fringe*. This crop is known to induce assimilatory sulfate reduction (Lefroy et al. 1992). Based on model results, the flooded areas at *fringe* could be identified as sulfur sinks.

Comparable to flooding water at *center*, no possible model was found for the origin of flooding water at *fringe* in rainy season 2015. This might be explained by the same reasons as outlined above. Moreover, as precipitation is the major component of flooding water, the composition of precipitation is important

for the evolution of flooding water. Obviously, the assumed precipitation composition reflected nature well in 2014, but did not in 2015. Thus, regularly sampling and full analyses of precipitation would help to better define this end-member.

**Tab. 6.8:** Results of inverse modeling of the origin and hydrochemical evolution of flooding water at *fringe* for rainy season 2014 (IF).

Groundwater solution	Proportion of groundwater [%]	Proportion of precipitation [%]	Proportion of Kilombero River [%]	Evaporation rate [%]	CO <sub>2</sub> phase mol transfer [mol]	O redox mol transfer [mol]	S redox mol transfer [mol]
1)	3	95	2	96	$6.7 \times 10^{-4}$	$-6.3 \times 10^{-4}$	$-2.1 \times 10^{-4}$
	3	97	0	96	0	$-7.1 \times 10^{-4}$	$-2.4 \times 10^{-4}$
	3	95	2	96	0	$-6.3 \times 10^{-4}$	$-2.1 \times 10^{-4}$
	3	97	0	96	$8.6 \times 10^{-4}$	$-7.1 \times 10^{-4}$	$-2.4 \times 10^{-4}$
2)	4	96	0	95	$8.3 \times 10^{-4}$	$-6.8 \times 10^{-4}$	$-2.3 \times 10^{-4}$
	4	96	0	95	0	$-6.8 \times 10^{-4}$	$-2.3 \times 10^{-4}$

The inverse modeling of origin and evolution of flooding water at *center* and *fringe* confirmed and quantified processes described in the conceptual models for rainy season 2014. Flooding water at *center* was derived of around 90 % stream water of Kilombero River and 10 % groundwater (Fig. 6.33). Direct precipitation inputs as well as biogeochemical processes only played a minor role. However, in 2015, no possible model was found, indicating a stronger influence of processes not implemented in the model.

Flooding water at *fringe* was derived by precipitation (> 95 %) and groundwater (< 5 %) and showed high evapotranspiration rates of 95 %. This confirms the assumed contribution of groundwater to flooding water, although proportional amounts were smaller than expected. A contribution of stream water of Kilombero River was disproven by inverse modeling. Furthermore, the process of sulfate reduction in flooding water at *fringe* was identified and quantified. Origin and evolution of flooding water in rainy season 2015 was more complex and could not be simulated by the inverse models.

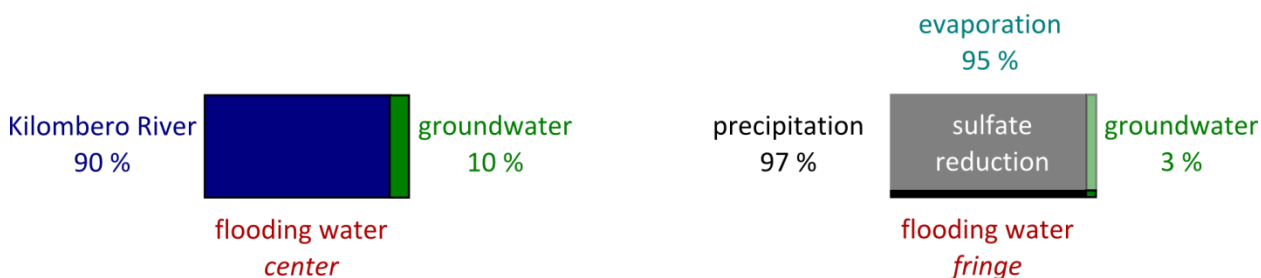


**Fig. 6.33:** Schematic composition and evolution of flooding water at *center* and *fringe* based on hydrochemical modeling (IF).

## 7 Case study of the Namulonge study site

In this section, the results of the Namulonge study site are outlined, and subsequently summarized in a conceptual model. The structure of the text follows the same approach as already applied to the Ifakara study site. In contrast to the Ifakara study site, collected soil water samples in the Namulonge study site allowed a more detailed assessment of the vulnerability of groundwater to different agricultural management options.

### 7.1 Aquifer structure and properties (NA)

The geological map of the study site (GTK Consortium 2012) shows two major lithological units (Fig. 2.11 p.22). Neoproterozoic and Palaeoproterozoic, magmatic and metamorphic crystalline rocks are present in the whole study site, overlain by a weathering profile, as already described for other areas in Uganda (Taylor and Howard 1999). This weathering profile is covered by a unit of Quaternary alluvium, swamps, and lacustrine deposits in valleys, which build the underground of the investigated wetland. These sediments represent a porous aquifer (Aqp1<sub>NA</sub>) in their downer and a porous aquitard (Atp1<sub>NA</sub>) in their upper parts (Fig. 7.1). As the weathering profile is assumed to be deeper in the Namulonge study site compared to the Ifakara study site, it was classified as an own hydrostratigraphic unit. While the weathering profile acts as a porous aquifer (Aqp2<sub>NA</sub>), the crystalline rocks represent a fractured rock aquitard (Atf1<sub>NA</sub>).

		Lithological unit	Lithological description	Porosity	Hydraulic conductivity [m/s]	Hydrostratigraphy
Quaternary		Valley sediments	clayey sediments	porous	10 <sup>-10</sup> - 10 <sup>-8</sup> <sup>a)</sup> very low ultralow	Atp1 <sub>NA</sub>
			interconnected sand and gravel lenses with some clayey parts	porous	10 <sup>-7</sup> - 10 <sup>-5</sup> <sup>b)</sup> low	Aqp1 <sub>NA</sub>
		Weathering profile	Saprolite	porous	10 <sup>-7</sup> - 10 <sup>-4</sup> <sup>c)</sup> highly variable  hydraulic conductivity increases with depth	Aqp2 <sub>NA</sub>
			Saprock			
Palaeoproterozoic	Neoproterozoic	Crystalline rocks	slate, shale, phyllite / granitoids, orthogneiss	fractured	<10 <sup>-7</sup> <sup>d)</sup> very low	Atf1 <sub>NA</sub>

Fig. 7.1: Lithological and hydrostratigraphic standard section of the study site showing hydrogeological properties of the different units. Hydraulic conductivities were assigned based on <sup>a)</sup> personal communication with B. Glasner (2016), <sup>b)</sup> own data, <sup>c)</sup> McFarlane (1992), Taylor and Howard (1996), and <sup>d)</sup> Howard et al. (1992) (NA).

### 7.1.1 Crystalline rocks (Atf1<sub>NA</sub>)

The fractured rock aquitard is represented by unweathered Neoproterozoic granitoids and orthogneisses of the Kampala Suite and Palaeoproterozoic shales, slates, phyllites, porphyroblastic phyllites, and orthoquartzites of the Buganda Group (GTK Consortium 2012).

None of the shallow drilling logs reached the unweathered crystalline rock and no outcrops were found. Secondary data of 14 deep drilling logs showed a layer at the log base, described as hard/fresh/unweathered granite/schist/rock (Fig. 5.6 p.62, Appendix A-A<sub>NA</sub>1). This layer was interpreted to represent the unweathered crystalline rocks. Few layer descriptions were less distinct. But, if no attribute related to weathering was documented, such as weathered or soft, the layer was assumed to be of unweathered character. Even the two logs located in the valley sediments reached the unweathered crystalline rock. The spatial distribution of different lithologies revealed deviations between drilling logs and geological map. Geochemical differences occurred between granitoids and orthogneisses, on one side, and shales, slates, and phyllites, on the other side. Granites of the Kampala Suite as well as slates of the Buganda Group, sampled a few 10 km outside the study site, showed SiO<sub>2</sub> and Al<sub>2</sub>O<sub>3</sub> as major oxides (Westerhof et al. 2014). Granites showed Na<sub>2</sub>O, CaO, K<sub>2</sub>O, and Fe<sub>2</sub>O<sub>3</sub> amounts above 2 %, while slates contained more Fe<sub>2</sub>O<sub>3</sub> and K<sub>2</sub>O, but less Na<sub>2</sub>O and no CaO. MgO ranged around 1 % in all sampled rocks (Westerhof et al. 2014). Considering lithological and mineralogical descriptions (section 2.4.2) as well as geochemistry, no big differences occur between shales, slates, and phyllites of the Buganda Group. Thus, this lithological unit will be referred to as slates in the following. Granitoids and orthogneisses of the Kampala Suite are mainly represented by granites in the study site and its surroundings (Westerhof et al. 2014) and will thus be referred to as granites.

Based on general descriptions of crystalline rocks in tropical Africa (Chilton and Foster 1995, Wright 1992), the matrix permeability is assumed to be negligible, while groundwater flow takes place in fracture networks. Those networks are spatially variable and lumped hydraulic conductivities are usually lower than 10<sup>-7</sup> m/s (Howard et al. 1992), identifying the fractured rock aquitard to be of very low hydraulic conductivity (Hannappel et al. 2003). However, in the study site, almost all documented pumping wells are probably screened in this aquitard, demonstrating that it acts as an aquifer locally. This is consistent with descriptions of Howard and Karundu (1992), who state that the preferred method of well construction in Uganda is to seal the weathering profile and screen the well in fractured parts of the crystalline rocks. It is believed that fracture frequency is highest along valley bottoms (Chilton and Foster 1995). This is consistent with fractures following the valley bottoms delineated in the geological map (GTK Consortium 2012).

Considering available data from drilling logs and literature, a spatial differentiation of different crystalline rocks was unsuccessful. Hence, all types of crystalline rocks were summarized as one hydrostratigraphic unit (Atf1<sub>NA</sub>).

### 7.1.2 Weathering profile of crystalline rocks (Aqp2<sub>NA</sub>)

The weathering profile of crystalline rocks is assumed to be present in the whole study site, either covered with a layer of sediments or not. As outlined in section 2.2.2, this weathering profile acts as a porous aquifer, due to the chemical alteration of fractured crystalline rocks. The weathering profile in the study site was evaluated based on the 14 deep drilling logs. Above the layer of unweathered crystalline rocks, which was described in the latter section, typical descriptions of deep drilling logs showed the following units from top to bottom:

- Soil
- Clay with more or less contents of silt and sand
- Weathered/soft rock/granite/schist

The described lithological units of deep drilling logs were assigned to parts of the typical weathering profile of Chilton and Foster (1995) (Fig. 2.2 p.9), which was confirmed to occur in Uganda (Taylor and Howard 1999) (Tab. 7.1). However, it needs to be considered that boundaries between saprock and saprolite are usually transitional and not distinct, making a differentiation during drilling difficult.

The determined thicknesses of different units (Tab. 7.1) fit to ranges of thickness for tropical weathering profiles provided by Chilton and Foster (1995). Comparisons to thicknesses of weathering profiles in the Aroca Catchment in central Uganda (Taylor and Howard 1999) were difficult, because they used a different classification of the profile. They reported a mean thickness of the “weathered mantle” of 26 m. This “weathered mantle” probably includes saprolite as well as saprock.

**Tab. 7.1: Assignment of drilling log descriptions to lithological units of the typical weathering profile of Chilton and Foster (1995) and thicknesses of the respective units.**

<b>Drilling logs (Ministry of Water and Environment, Uganda)</b>	<b>Typical weathering profile (Chilton and Foster 1995)</b>	<b>Range (median) of thickness [m]</b>
Soil	Residual soil	0.5 – 3 (1)
Clay with more or less contents of silt and sand	Saprolite	17-49 (25)
Weathered/soft rock/granite/schist	Saprock	0-36 (17)

One shallow drilling log was used to describe texture, color, structure, chemistry, and mineralogy of the weathering profile (Fig. 5.6 p.62: SA1<sub>NA</sub>). It was not possible to drill deeper than seven meters, due to technical issues of hand drilling. Considering the median thickness of the saprolite, this drilling log shows only its upper parts and did not reach the saprock. Up to a depth of 6 m.b.s., the main grain size was clay with small amounts of sand and gravel (Fig. 7.2). The lower part of the log was dominated by middle sand. Observed quartz minerals in the profile had angular shapes, indicating an absence of reworking by transport processes (Gilkes et al. 1973). Color of matrix was reddish, changing to orange and beige with increasing depth. Mineralogical composition of the weathering profile mainly comprised quartz, k-feldspar, and kaolinite. Accordingly, major oxides were SiO<sub>2</sub>, Al<sub>2</sub>O<sub>3</sub>, Fe<sub>2</sub>O<sub>3</sub>, and K<sub>2</sub>O. Quartz content decreased, while k-feldspar content increased with depth, confirming increased weathering with nearer distance to the surface. Kaolinite content was highest between 2 and 6 m.b.s. Little amounts of hematite and goethite were abundant up to 5 m.b.s., while Fe<sub>2</sub>O<sub>3</sub> decreased with depth in general.

Mineralogical and geochemical compositions allowed a classification of the weathering profile according to Chilton and Foster (1995). The upper layer of the profile (0-0.4 m.b.s.) represents residual soil, identified by its characteristic dark brown color and root penetration (Fig. 7.2). The residual soil is underlain by saprolite. The upper part of the saprolite (0.6-6.1 m.b.s.) was characterized by a high proportion of secondary clay minerals, especially kaolinite. Furthermore, iron oxides and hydroxides were abundant, indicating prolonged weathering (Appelo and Postma 2005). The abundance or absence of these minerals is responsible for the observed change in color. In contrast, the lower part of the saprolite (deeper than 6.1 m.b.s.) comprised higher amounts of primary minerals, such as k-feldspars, showing a lower weathering degree.

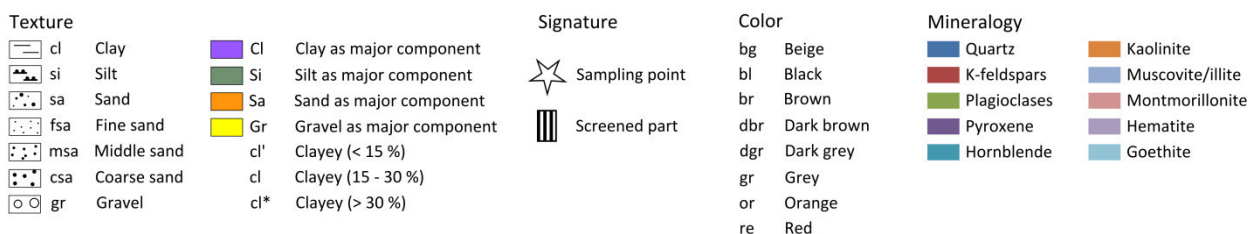
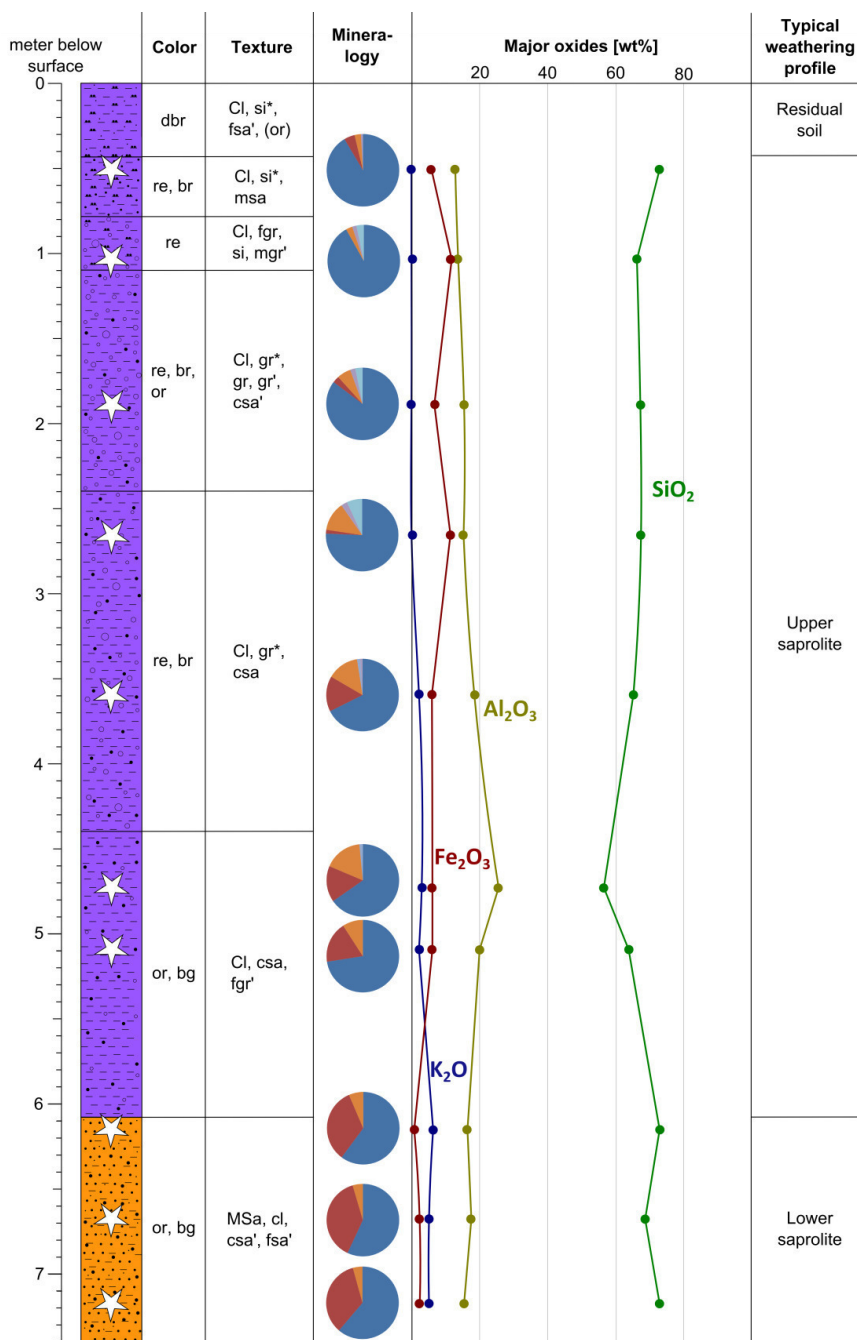


**Fig. 7.2: Drilling log of saprolite weathering profile (SA1<sub>NA</sub>). Typical weathering profile was assigned based on Chilton and Foster (1995) (NA).**

Comparing major oxide concentrations of the weathering profile with those of the different crystalline rocks (Westerhof et al. 2014) showed that both, granites and slates, could be possible crystalline rocks below the weathering profile. However, the high amount of k-feldspars in the weathering profile hint at granites as source rocks (Fig. 7.2). The slates comprise mainly muscovite (Westerhof et al. 2014), which was only observed in small amounts in in the weathering profile. Granite samples (Westerhof et al.

2014) displayed higher amounts of  $\text{NaO}_2$  and  $\text{CaO}_2$  compared to the weathering profile. Thus,  $\text{Na}^+$  and  $\text{Ca}^{2+}$  were leached from the upper seven meters of the weathering profile, due to the weathering of plagioclases. However, according to the geological map (GTK Consortium 2012), the drilling log is located in the slates, showing the uncertainty of lithologies in the geological map (Fig. 5.6 p.62: SA1<sub>NA</sub>).

Drilling log descriptions revealed a clear differentiation in terms of permeability between the upper and lower saprolite. While the upper saprolite showed mainly clay, indicating a very low hydraulic conductivity, the lower saprolite was mainly composed of sand, indicating higher hydraulic conductivities. Therefore, it is assumed that the weathering profile of crystalline rocks acts as a confined or semi-confined aquifer. This was already reported before for central Uganda (Taylor and Howard 1999). However, the upper saprolite might be sandy in some parts as well, and root penetration, cracks, or fractures might provide preferential flow paths. Hence, quantification of hydraulic conductivities is difficult and no general values are available from literature. However, McFarlane (1992) proposed hydraulic conductivities between  $5 \times 10^{-7}$  and  $5 \times 10^{-6}$  m/s for the saprolite and between  $9 \times 10^{-7}$  and  $8 \times 10^{-6}$  m/s for the saprock of a weathering profile in Malawi. Taylor and Howard (1996) measured an average hydraulic conductivity of  $1 \times 10^{-6}$  m/s for the saprolite and of  $1 \times 10^{-4}$  m/s for the saprock in central Uganda. Thus, the weathering profile aquifer is assumed to be of highly variable hydraulic conductivity, ranging from  $5 \times 10^{-7}$  to  $1 \times 10^{-4}$  m/s, with higher values in the lower and lower values in the upper parts.

### 7.1.3 Valley sediments (Aqp1<sub>NA</sub>, Aqt1<sub>NA</sub>)

Although the valley sediments cover just a small area of the study site, they are of major concern for this study, as they underly the wetland. Drilling within the valley sediments in the lower Nasirye Catchment was conducted along three different transects perpendicular to the stream (Fig. 5.6 p.62). Drilling logs along these transects can be divided into 18 logs located at the valley bottom and 19 logs located at the beginning of the valley slopes. Additionally, one drilling log located in the wetland areas of upper Nasirye Catchment was documented. Depths of drilling logs varied between one and four meters below surface (Appendix A-A<sub>NA</sub>2).

Six drilling logs at the slopes showed a layer of soil, followed by saprolite, analogous to the drilling log described in section 7.1.2. Those drilling logs are not included in the following descriptions, as they do not represent the valley sediments. However, they allowed insights into the horizontal extend of the sediments. Other drilling logs at the slopes showed saprolite in different depths, confirming that the weathering profile of crystalline rocks underlies the valley sediments.

Drilling logs in the valley bottom displayed a tendency of fining upwards (Fig. 7.3, Fig. 7.4, Fig. 7.5). This grading was sometimes interrupted by other layers, and texture was usually poorly sorted. Drilling logs located at the slopes showed alternations of clay and sand layers rather than fining upwards. In general, the valley sediments in lower Nasirye Catchment showed layered profiles of highly variable texture, including clay, silt, sand, and gravel.

The upper layer of all drilling logs was identified as an *in-situ* developed organic soil of dark brown color. Texture was described as fine sandy, silty clay. Thicknesses of the soil layer varied between 0.1 and 0.7 m, with a median thickness of 0.2 m. Within the valley bottom, the soil layer was usually underlain by a clay layer containing minor, but highly variable amounts of silt and sand (Fig. 7.6: left). This clay layer showed thicknesses between 0 and 2 m, with a median thickness of 1 m. While the matrix was grey in color, several zones of purple, green, and orange color were observed. This change in color hints at redox processes (Scheffer and Schachtschabel 2010).



A sand layer with thicknesses between 0.4 and 2.9 m, with a median of 1.2 m, was found below the clay layer. The matrix of this layer was grey, but sometimes showed patches of orange color (Fig. 7.6: right). Observed quartz grains in this layer were subangular to rounded in shape, indicating alluvial origin. This sand layer was sometimes interrupted or underlain by more clayey layers. At transects A and C, the sand layer was followed by gravels with a transitional zone (Fig. 7.4, Fig. 7.5). Even this gravel layer contained minor amounts of clay and sand. Gravels were sub-angular to rounded in shape. At the valley slopes, sand and clay layers alternated with each other in varying thicknesses.

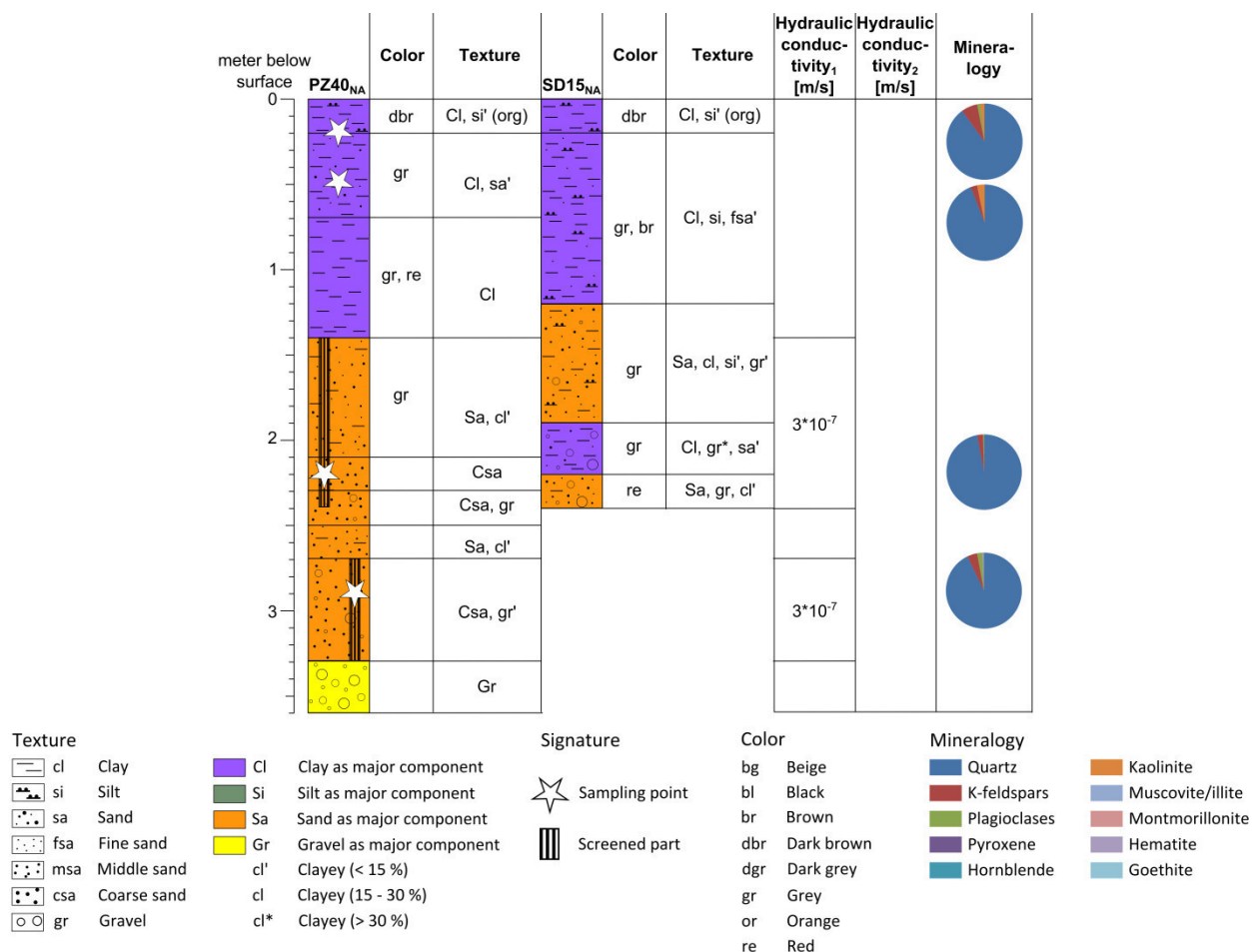


**Fig. 7.3:** Drilling logs of the piezometer in the central field trial *fringe* (PZ40<sub>NA</sub>) and the drilling log next to it (SD15<sub>NA</sub>). Screened parts refer to short and long piezometers (PZ40S<sub>NA</sub>, PZ40L<sub>NA</sub>). Hydraulic conductivities were derived from falling-head permeability tests (hydraulic conductivity<sub>1</sub>) and grain size distribution analyses (hydraulic conductivity<sub>2</sub>) (NA).

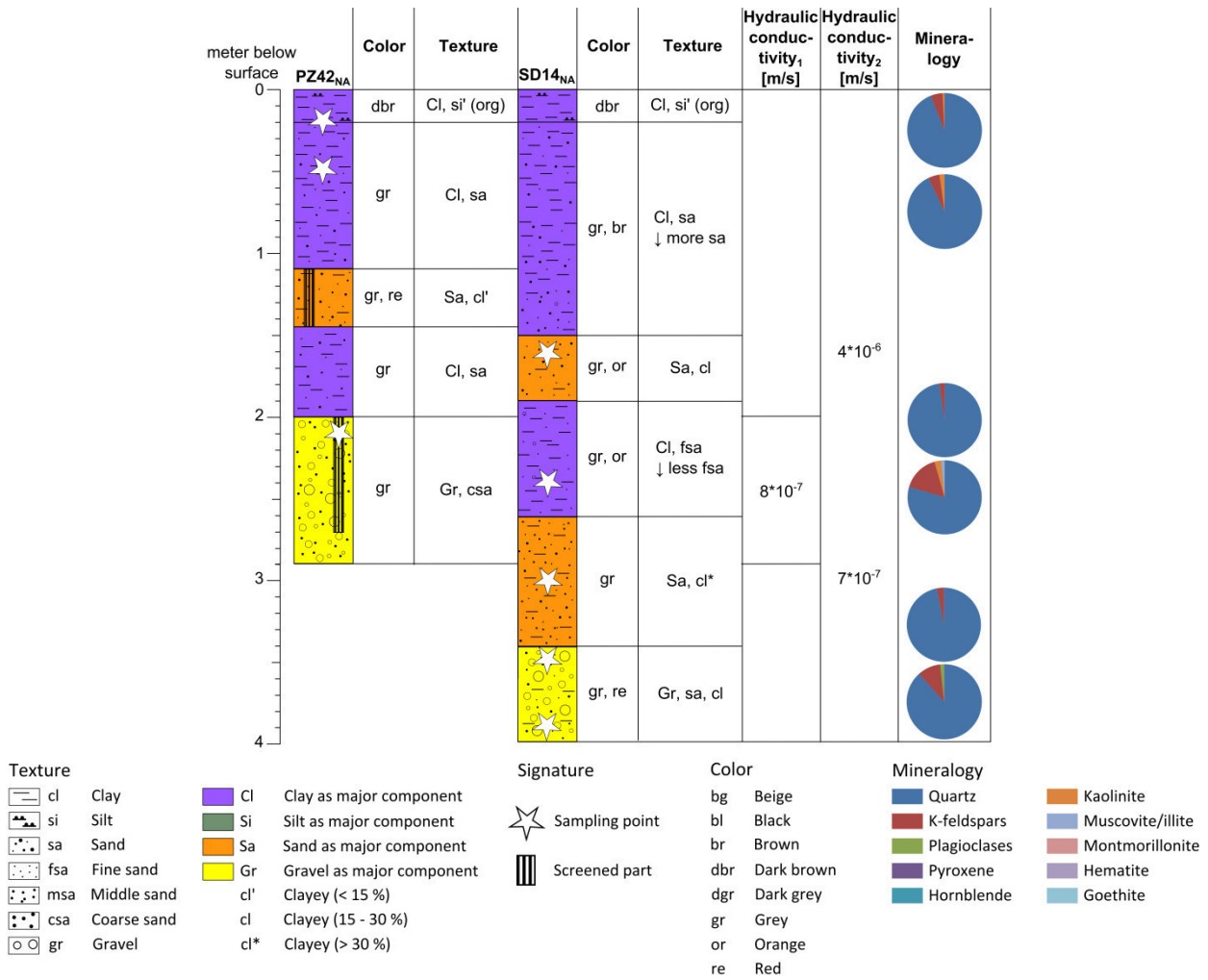


**Fig. 7.4:** Drilling logs of the piezometer in the central field trial *middle* (PZ42<sub>NA</sub>) and the drilling log next to it (SD14<sub>NA</sub>). Screened parts refer to short and long piezometers (PZ42S<sub>NA</sub>, PZ42L<sub>NA</sub>). Hydraulic conductivities were derived from falling-head permeability tests (hydraulic conductivity<sub>1</sub>) and grain size distribution analyses (hydraulic conductivity<sub>2</sub>) (NA).

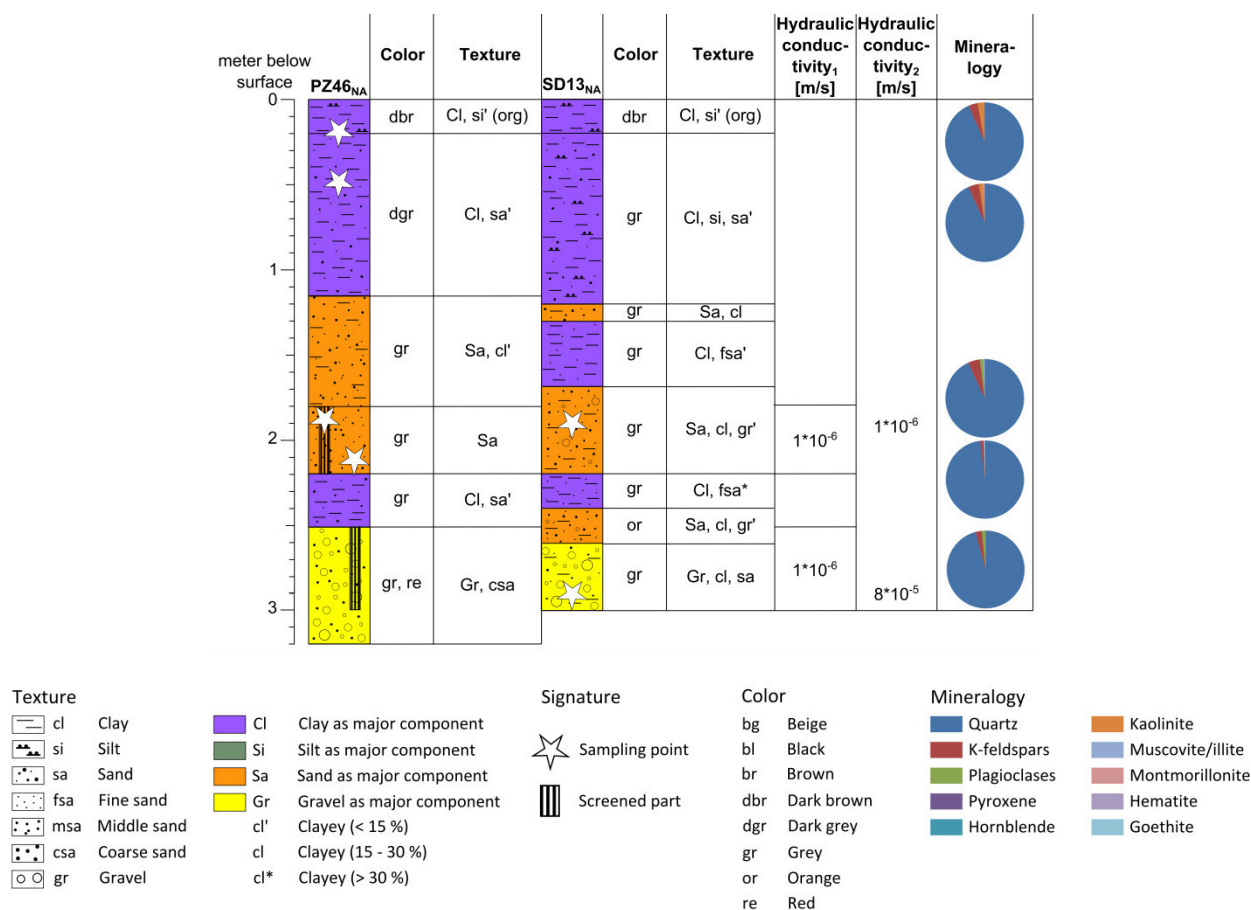


**Fig. 7.5:** Drilling logs of the piezometer in the central field trial center (PZ46<sub>NA</sub>) and the drilling log next to it (SD13<sub>NA</sub>). Screened parts refer to short and long piezometers (PZ46S<sub>NA</sub>, PZ46L<sub>NA</sub>). Hydraulic conductivities were derived from falling-head permeability tests (hydraulic conductivity<sub>1</sub>) and grain size distribution analyses (hydraulic conductivity<sub>2</sub>) (NA).



**Fig. 7.6:** Characteristic grey clay layer (left) and grey sand layer with interbedded orange zones (right) (NA).

The drilling log in a side-valley of the upper Nasirye Catchment showed fining upwards comparable to the lower catchment (Fig. 5.6 p.62: DU1<sub>NA</sub>). However, the clay layer on top of the sequence displayed higher amounts of sand and silt here. Although, this log is not located in the alluvial sediments, as delineated by GTK Consortium (2012), the drilled layers showed indications of valley sediments.

All sampled layers showed quartz as the main mineral, with major or minor amounts of k-feldspar, kaolinite, and plagioclase (Fig. 7.3, Fig. 7.4, Fig. 7.5). Muscovite and montmorillonite were detected in small amounts in the clay layer. Sand and gravel layers comprised minor amounts of hematite and goethite. Accordingly, major oxides were SiO<sub>2</sub>, Al<sub>2</sub>O<sub>3</sub>, and Fe<sub>2</sub>O<sub>3</sub>. Highest values of LOI were found in the soil layer, confirming organic content. The composition of trace elements within the valley sediments indicated

that all crystalline rocks being found in the study site and its surroundings represent possible sources (Fig. 7.7). Most sediments are mixtures of different crystalline rocks, with granites and slates as major sources.

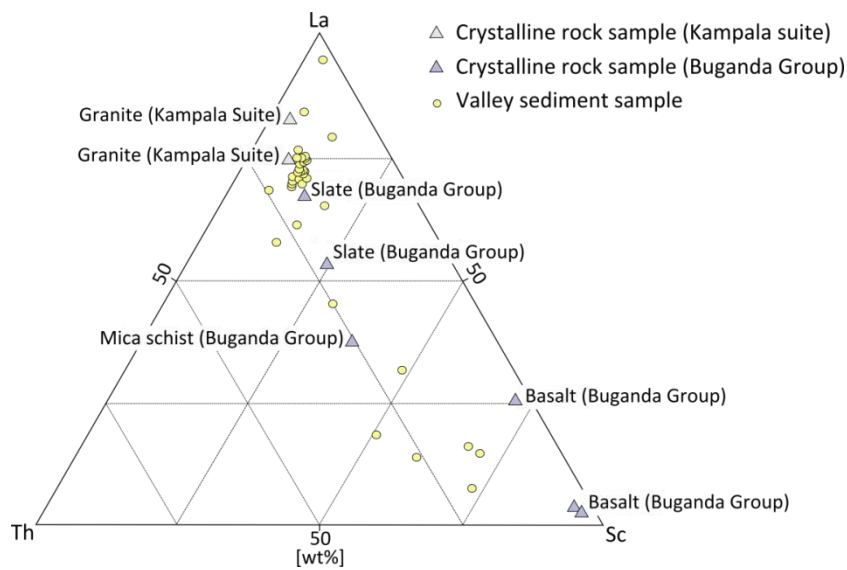


**Fig. 7.7:** Ternary diagram of the trace elements lanthanum (La), scandium (Sc), and thorium (Th) showing crystalline rock (Westerhof et al. 2014) and valley sediment samples (NA).

Considering the hypotheses of wetland sediments on the African weathered surface, valley sediments can be either derived by alluvial deposition, related to stripping, or represent collapsed saprolite, related to deep weathering (McFarlane 1992) (section 3.1.2). Several indicators hint at alluvial deposition as the main source of valley sediments in the Nasirye Catchment. If the valley sediments had developed as collapsed saprolite, no plagioclases would be present. A complete removal of plagioclases during weathering was observed in the upper parts of the saprolite (Fig. 7.2). But valley sediments showed detectable amounts of plagioclase up to 22 %. Additionally, observed quartz minerals were subangular to rounded in shape, indicating transport. The mixture of different crystalline rock end-members, indicated in the sediments, is another proof that the valley sediments have been transported and did not develop *in-situ*. The proposed alluvial origin of the valley sediments fits to the geological map by GTK Consortium (2012). In agreement, Mahan and Brown (2007) identified the sediments in a wetland in central Uganda as alluvial depositions as well. Nevertheless, processes of stripping and deep weathering are not exclusive (McFarlane 1992). Consequently, it is likely that the valley sediments were not solely derived from alluvial deposition, but could also represent *in-situ* saprolite.

Alluvial sediments usually comprise channel sedimentation (lenses) as well as over-bank deposition (Miall 1996). Thickness and expansion of channel lens deposits are determined by width and depth of the channel and by processes of avulsion and lateral migration of the channel (Nichols 2009). Within the study site, the observed sand and gravel layers probably represent channel lenses, while the clayey layers represent over-bank deposition. A vertical connection between channel lenses was observed in some drilling logs, indicating that channel filling (sand and gravel) was more frequent than over-bank deposition (clay). This is usually induced by slow subsidence rates (Nichols 2009). Nevertheless, lenses were not always connected vertically. For instance, at transect C, two aquifer layers were observed interrupted by clay. It is likely that sand and gravel lenses are connected to each other horizontally, allowing lateral groundwater flow from one lens to another.

The sand layers, observed at the valley slopes, are assumed to represent strongly leached parts of the saprolite. In those parts, clay minerals are completely dissociated and solely quartz sand is left (Chilton

and Foster 1995). Furthermore, the sand could represent colluvial transported material of such strongly leached saprolite (Wright 1992).

Hydraulic conductivities of the sand and gravel layers in the valley sediments were determined based on falling-head permeability tests and grain size analyses at transect C. Five falling-head permeability tests revealed low and homogenous hydraulic conductivities between  $3 \times 10^{-7}$  and  $1 \times 10^{-6}$  m/s. Hydraulic conductivities derived from grain size distribution analyses ranged between  $7 \times 10^{-7}$  and  $8 \times 10^{-5}$  m/s, showing a high conformity between the two different scales (e.g. Fig. 7.5). Those values seem low for sand and gravel layers, but are plausible, as significant amounts of smaller grain sizes were observed in all layers. Hydraulic conductivities of the upper soil and clay layers (< 1 m.b.s.) were very low, ranging between  $5 \times 10^{-10}$  and  $6 \times 10^{-8}$  m/s. This confirms that the clay layer acts as a hydraulic barrier, and the sand and gravel layers act as a confined aquifer.

#### 7.1.4 Spatial distribution of aquifers and hydraulic connections (NA)

The weathering profile (Aqp2<sub>NA</sub>) represents the main aquifer, because it covers the whole study site (Fig. 7.8). The weathering profile is composed of saprock overlain by saprolite, being more permeable in its lower than upper parts. Weathering profile aquifers generally show confined to semi-confined conditions (Wright 1992). The basement of this aquifer is made up of different crystalline rocks, representing a fractured rock aquitard (Atf1<sub>NA</sub>). Major groundwater flow is expected to take place in the saprock and in the lower parts of the saprolite. However, groundwater is present in parts of the fractured rock aquitard as well, indicated by pumping wells that are screened in this unit. Within major valleys, the weathering profile aquifer is covered by a porous confined aquifer composed of valley sediments. These are made up of low permeable connected sand and gravel lenses, with minor amounts of silt and clay (Aqp2<sub>NA</sub>), overlain by an almost impermeable clay layer (Atp1<sub>NA</sub>).

The three-dimensional distribution of the weathering profile aquifer depends on several factors. A constant deep weathering without any erosion by stripping would have resulted in similar aquifer thicknesses all over the study site. In this case, the base of the weathering profile aquifer would follow the topography. If weathering occurred, before erosion had formed the recent landscape, the base would rather be flat, and the weathering profile would be thicker on top of hills than in valley bottoms (Dewandel et al. 2006). Furthermore, it could be that weathering is more likely in fracture zones below the valleys (Chilton and Foster 1995). In this case, the weathering profile would be thicker in the valley bottoms than on top of hills. Nevertheless, local differences in crystalline rock lithology might also affect depths of the weathering profile (Dewandel et al. 2006).

With this backdrop, the three-dimensional distribution of the weathering profile aquifer was evaluated based on the deep drilling logs. While thickness of the weathering profile aquifer remained quite stable with varying elevation (Fig. 7.9 a), a correlation was observed between elevation of the surface and elevation of the aquifer base (Fig. 7.9 b). However, this correlation was only observed on a large scale (10 km). Thus, it may be concluded that on a large scale the base of the aquifer is following topographic elevation. The aquifer base dips in southeastern direction. On a small scale, thicknesses differ from hill tops to valley bottoms. Comparing drilling logs located on top of hills and in valley bottoms showed that the weathering profile is slightly thicker on top of hills compared to valley bottoms. This indicates that stripping occurred in the valley bottoms and resulted in the formation of hills and valleys. Stripping was also implied by the alluvial origin of sediments. However, it contradicts the suggested dominance of deep weathering since the Miocene by Taylor and Howard (1998) for the area around the study site (section 2.4.2).

The constant thickness of the weathering profile aquifer on a large scale allows the documentation of an average thickness of this aquifer. Assuming that the weathering profile aquifer is made up of saprolite and saprock, its median thickness is 42 m.

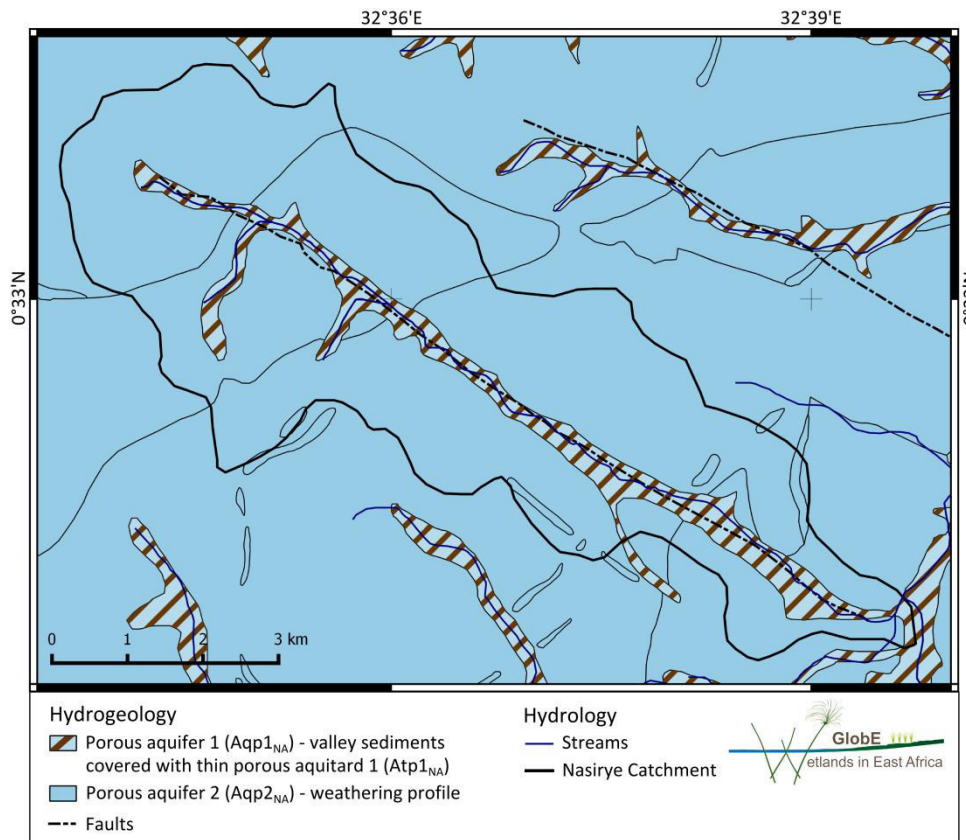


Fig. 7.8: Hydrogeological map of the study site. Units are labeled and colored according to Figure 7.1. Data sources: GTK Consortium (2012) (geology, streams), Heiß (2016) (alluvium), Gabiri (unpublished) (Nasirye Stream) (NA).

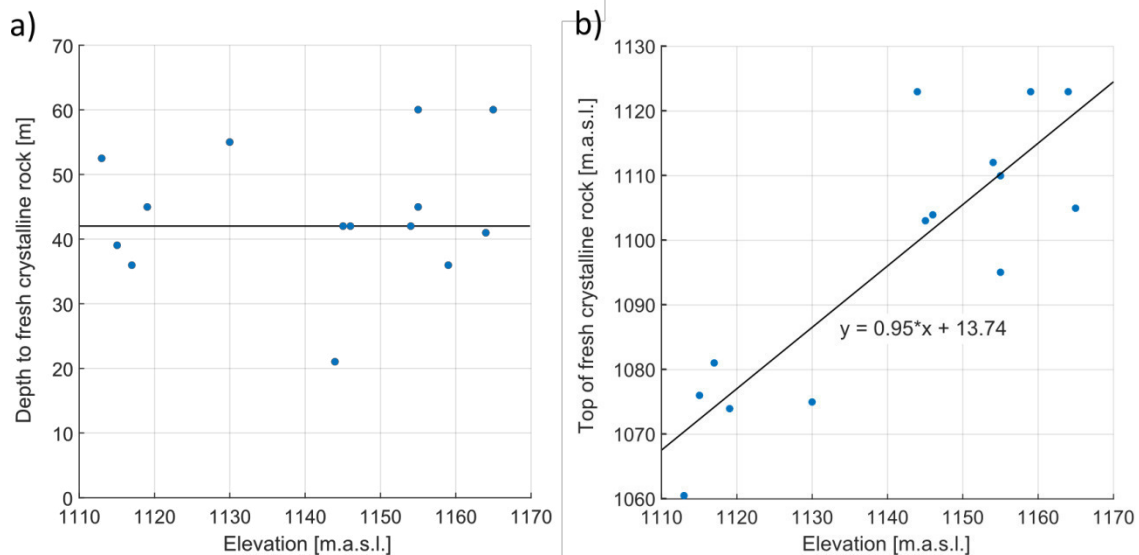
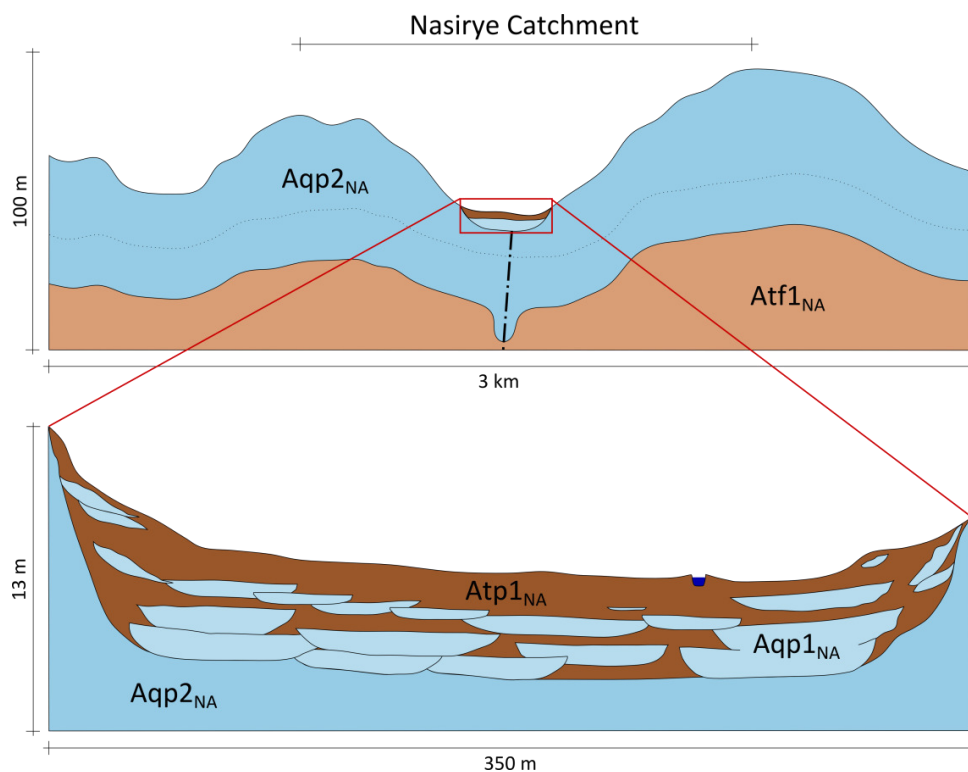


Fig. 7.9: Scatterplots of a) elevation against depth to fresh crystalline rock and b) elevation against top of fresh crystalline rock.

The valley sediment aquifer is small, but of major interest, because it underlies the wetland. The lateral boundary between valley sediments and saprolite was determined and revised in the geological map, based on the shallow drilling logs (Fig. 7.8, Heiß 2016). The actual lateral extend of the sediments is larg-

er than marked on the original map by GTK Consortium (2012). Furthermore, valley sediments are assumed to be present in some side-valleys of Nasirye Catchment, as indicated by one drilling log in the upper catchment.

It was shown that valley sediments are mainly derived from alluvial deposition. Considering this knowledge, a cross section of transect C was developed, showing sandy and gravelly channel lenses (Aqp1<sub>NA</sub>) as well as clayey over-bank deposition (Atp1<sub>NA</sub>) (Fig. 7.10). Lenses are assumed to be connected and build a low permeable aquifer, covered by a layer of almost impermeable clay. In some parts of the wetland, especially in the upper catchment, this clay layer may be permeable due to higher amounts of sand. The draining stream cuts into the clay and in some areas, where the clay is low in thickness, a hydraulic connection with the sand and gravel lenses is possible.



**Fig. 7.10:** Schematic hydrogeological cross section, crossing the study site from southwest to northeast. Units are labeled and colored according to Figure 7.1 (NA).

Comparing the different transects with each other showed that clay sediments were most frequent at transect D. This indicates a reduction in flow energy from upper to lower catchment, resulting in a tendency of larger grain sizes in proximal and smaller grain sizes in distal zones.

Only little connection is expected between valley sediments and weathering profile, because the upper saprolite is of low permeability. However, upper saprolite might have been eroded during stripping in valley bottoms and also show local zones of higher permeability. In these parts, hydraulic connection to the sediments might be favoured.

## 7.2 Water dynamics (NA)

In terms of water dynamics, the weathering profile aquifer together with the crystalline rock aquitard was evaluated based on static water level measurements. The valley sediments aquifer was evaluated based on dynamic water levels measured in piezometers (Fig. 5.7 p.64). Due to the thicknesses and spatial extends of the aquifers, it is assumed that regional groundwater flow takes place in the weathering profile and the underlying crystalline rock, while a local flow system is found in the valley sediments.

Both systems might interact and both influence the wetland. Most pumping wells with groundwater level data are screened in the crystalline rock aquitard, which acts as an aquifer locally and is hydraulically connected to the weathering profile aquifer. Hence, in this section, the aquifer system composed of weathering profile and underlying crystalline rock will be referred to as regional aquifer.

### 7.2.1 Groundwater flow in the regional aquifer (NA)

Static groundwater levels in the regional aquifer ranged between 0.4 and 32.8 m below surface (Fig. 7.11). They were shallowest in valleys and deepest on hilltops and slopes. Calculated isolines of hydraulic head show that groundwater flows roughly from northwest to southeast following the regional relief gradient (Fig. 7.11). On a smaller scale, groundwater flows from the hilltops to the valleys. Thus, it is concluded that groundwater flow follows the relief on different scales. Isolines showed effluent conditions within the Nasirye Catchment, indicating that wetland and stream in the valley drain the groundwater flow system. However, isolines of hydraulic heads are uncertain, because static groundwater levels at different points were not measured simultaneously. Furthermore, uncertainties in hydraulic heads arise from uncertainties in elevation data gained from the DEM. Nevertheless, interpretation of the flow system was more reliable compared to the Ifakara study site, because hydraulic gradients were steeper.

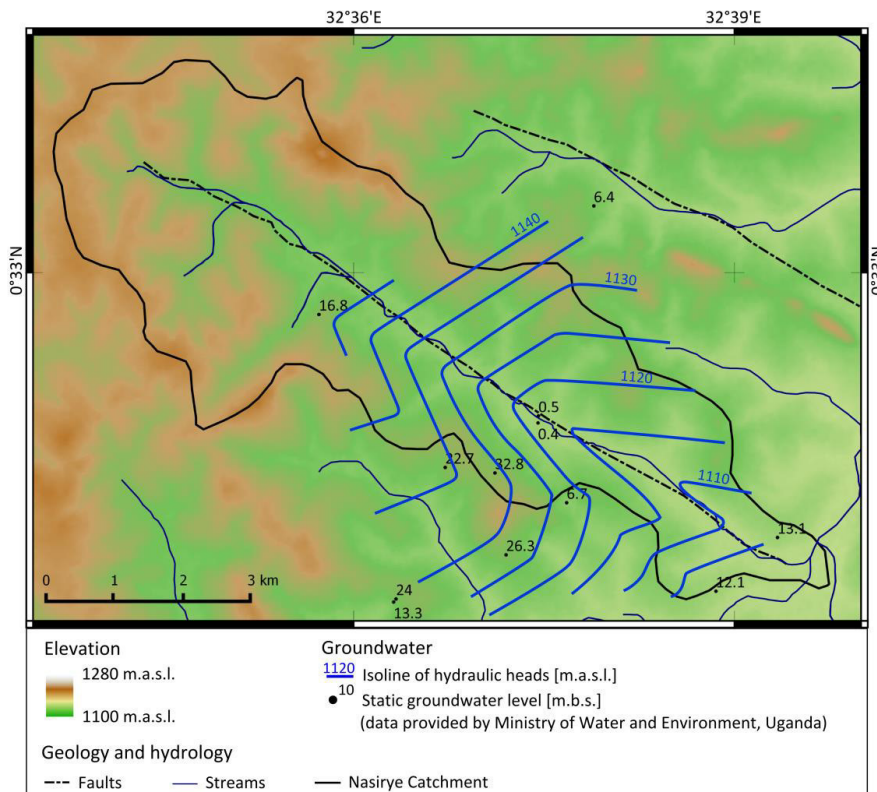


Fig. 7.11: Piezometric map of groundwater in the weathering profile aquifer and crystalline rock aquitard (Aqp2<sub>NA</sub> and Aqf1<sub>NA</sub>), showing isolines of hydraulic heads and point data of static groundwater levels. Data sources: earthexplorer.usgs.gov (elevation), GTK Consortium (2012) (streams), Gabiri (unpublished) (Nasirye Stream) (NA).

### 7.2.2 Groundwater flow in the valley sediment aquifer (NA)

Dynamic groundwater levels in the sedimentary valley aquifer ranged between one meter below surface and one meter above surface (Fig. 7.12). Hence, hydrographs showed a shallow water table within the wetland throughout the year. Groundwater levels were always located in the clay layer, confirming permanently confined conditions. Measured groundwater levels above surface were artesian and did



not represent flooding. In general, groundwater levels in this aquifer were variable and water table fluctuations were often rapid.

In order to compare rainy and dry season flow patterns, two extreme points of time were determined representing dry season (low flow conditions) and rainy season (high flow conditions). These points of time were set to 03/01/15 (dry season) and 12/01/15 (rainy season) (Fig. 7.12).

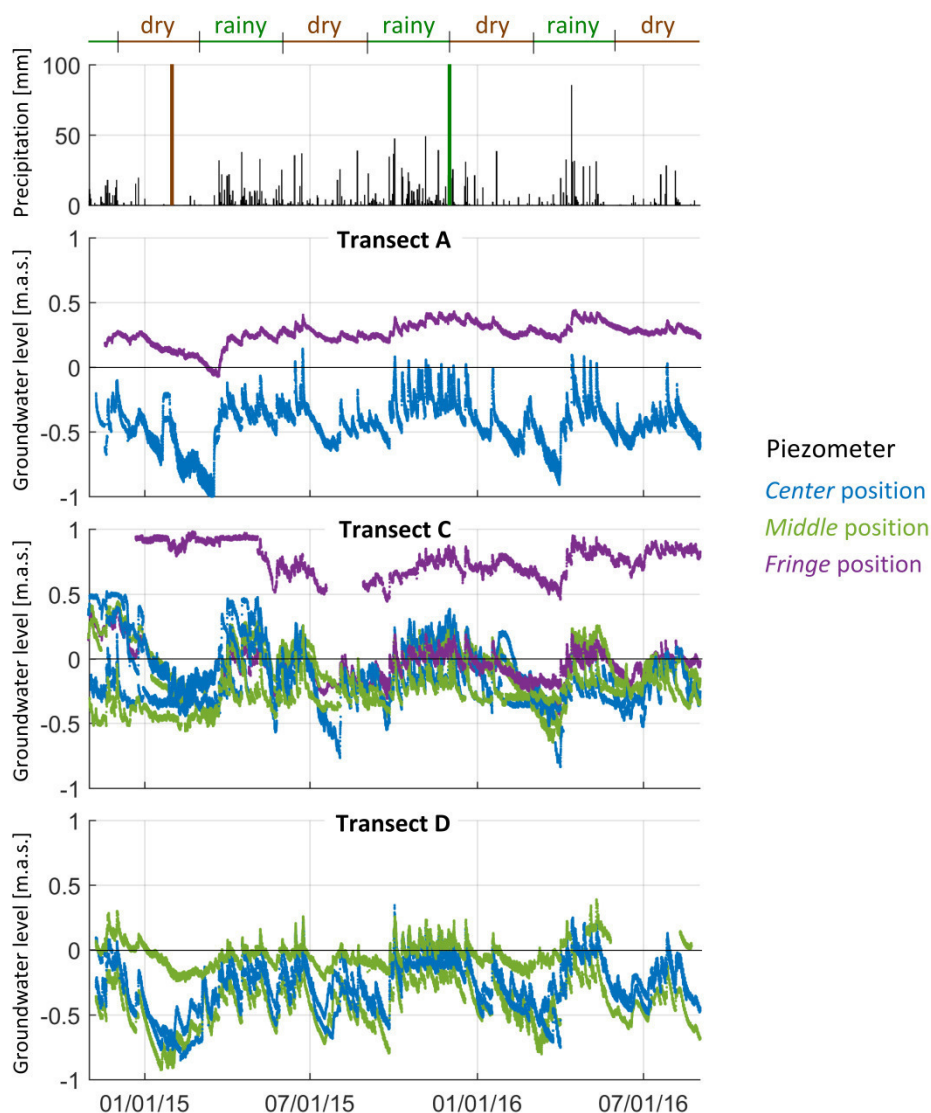


**Fig. 7.12:** Hydrographs of the piezometers at the three transects. Daily precipitation and the two representative points of time for dry (03/01/15) and rainy seasons (12/01/15) are shown above (NA).

Only few groundwater level time series showed high correlations with each other (Appendix B-B<sub>NA</sub>1). Hence, grouping based on correlation analyses was unsuccessful. Considering a threshold of 0.95, solely PZ06<sub>NA</sub> and PZ07<sub>NA</sub>, as well as PZ25<sub>NA</sub> and PZ26<sub>NA</sub>, and PZ46S<sub>NA</sub> and PZ46L<sub>NA</sub> were grouped together, indicating rather similar behaviors in same transects than in same distances to the stream. Lowering the threshold did not give satisfying groups as well. This shows that groundwater level fluctuations were highly diverse within the wetland.

Groundwater levels were highest after periods of high precipitation and lowest after periods of low or without precipitation (Fig. 7.12). In rainy seasons, groundwater levels rose with each precipitation event, while they fell continuously during dry seasons. Comparing water levels at different wetland positions,

piezometers at *center* and *middle* showed rapid responses to rainfall events and high amplitudes (Fig. 7.12). In contrast, piezometers at *fringe* displayed lower amplitudes and smoother behaviors.

Elevation data gained from SRTM DEM were too uncertain to determine groundwater flow directions in the flat valley sediments. But, a rough major groundwater flow direction from northwest to southeast draining the valley bottom in dry season as well as in rainy season was observed in the valley sediments, according to groundwater flow in the weathering profile aquifer. Based on the higher resolved DEM of Asimwe (2015), groundwater flow was evaluated on a smaller scale at transect C. The DEM was developed based on differential GNSS (Global Navigation Satellite System) technology (Asimwe 2015). This method usually shows height accuracies at centimeter level (Paar et al. 2014). However, interpolation of points leads to higher uncertainties at some points (Lee et al. 2005). As the used DEM showed a spatial resolution of 5 m, interpolation uncertainties were assumed to be small. In this study, they were set to 5 cm. Uncertainty of hydraulic heads was calculated using propagation of uncertainties (Taylor 1997), resulting in an uncertainty of 10 cm.

At transect C, groundwater levels were measured in six positions. On the right side of Nasirye Stream, levels were measured in two different depths using long and short piezometers. The long piezometers are screened in the connected sand and gravel lenses and the short piezometers are screened in the upper sand lenses, which are separated from the connected sand and gravel lenses by clay.

Long piezometers revealed a constant flow direction from the slope to the central valley throughout the whole year (Fig. 7.13). However, during rainy season, absolute hydraulic heads were higher compared to dry season. Time series of hydraulic heads at transect C showed that the hydraulic gradient did never change, and hydraulic heads stayed always highest at *fringe* and lowest at *center*. This indicates groundwater recharge at the hilltops and slopes flowing to the valleys. While PZ40<sub>L,NA</sub> showed artesian conditions during rainy and dry season, the other piezometers at transect C were solely artesian during rainy season. During rainy season, the stream level was almost at the same height as hydraulic heads of groundwater. However, as the aquifer is confined and the base of the stream bed is located within the impermeable clay layer, an interaction between shallow groundwater and stream water at transect C is not likely. It is rather assumed that stream level as well as groundwater recharge are correlated to precipitation within Nasirye Catchment.

Groundwater levels of the upper sand lenses, measured in short piezometers, showed different hydraulic heads compared to long piezometers (Fig. 7.3, Fig. 7.4, Fig. 7.5). At *fringe* (PZ40<sub>NA</sub>), the long piezometer displayed significantly higher hydraulic heads than the short one (Fig. 7.14). This indicates an upwards directed pressure gradient, which was already indicated by confined conditions of the aquifer. Hydraulic heads of long and short piezometers showed similar values at *middle* (PZ42<sub>NA</sub>). At *center* (PZ46<sub>NA</sub>), the long piezometer showed lower hydraulic heads than the short one. However, those differences were smaller compared to *fringe*. At *middle* and *center*, differences between hydraulic heads of long and short piezometers were within the range of uncertainties and could thus not be evaluated.

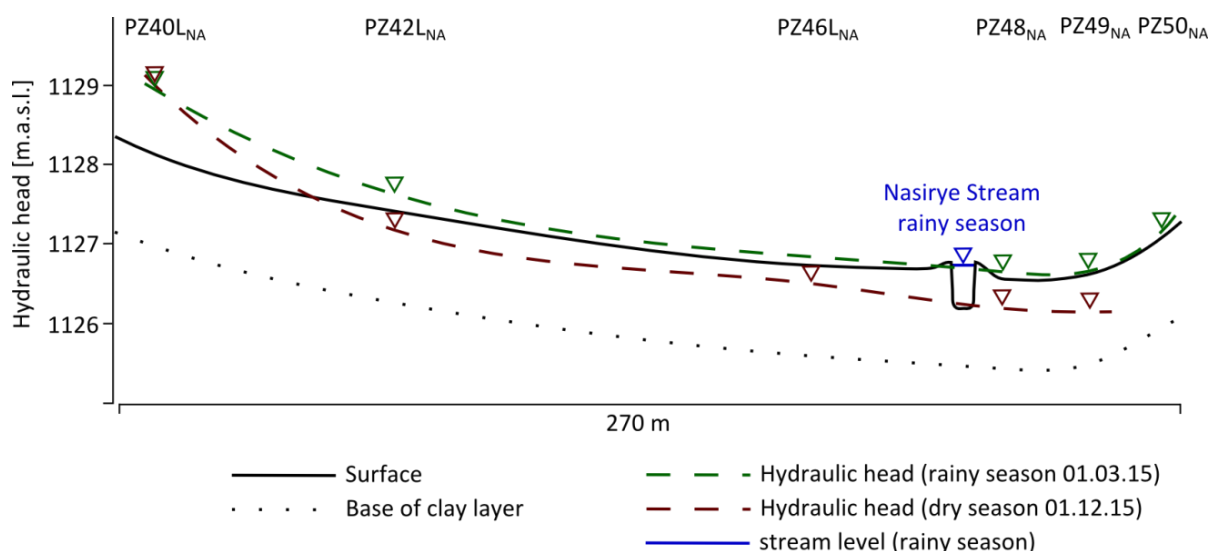


Fig. 7.13: Hydraulic heads of long piezometers at transect C during dry (01.03.15) and rainy (01.12.15) seasons and stream water level during rainy season (01.12.15).

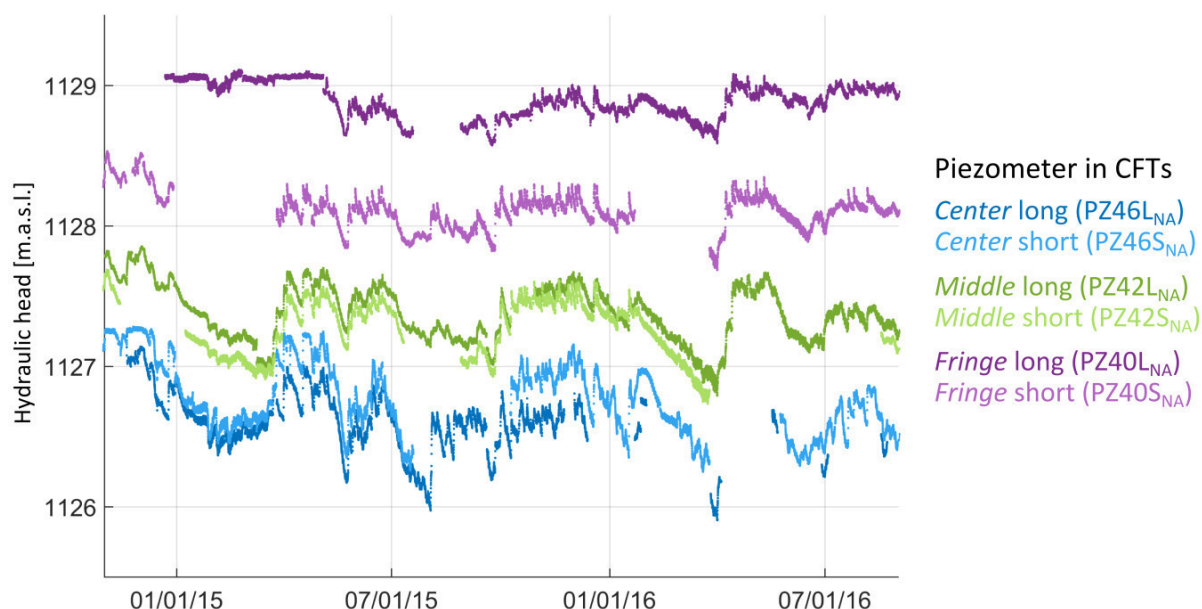


Fig. 7.14: Hydraulic heads of piezometers at transect C in the central field trials *center, middle, and fringe* (NA).

### 7.3 Water composition (NA)

The first three snapshot samplings, autumn 2014, spring 2015, and autumn 2015, fell within rainy season, while the last snapshot sampling, spring 2016, fell within dry season. In addition, monthly samples were selected in between the snapshot samplings, in order to cover the whole range of weather conditions. Sampling points are divided into surface water, including stream water of Nasirye Stream and flooding water, soil water, and groundwater. Deep groundwater was sampled at pumping wells from the crystalline rocks and the weathering profile. Shallow groundwater was sampled at piezometers from the valley sediments and at springs discharging from the upper weathering profile. All hydrochemical and isotopic data are documented in Appendix C-C<sub>NA</sub>.

#### 7.3.1 Hydrochemistry (NA)

ECs of shallow and deep groundwater were similar with low to moderate values (Fig. 7.15). Stream water showed low ECs as well, but a lower variability. Soil water displayed highest ECs. The pH values were

neutral for stream water and slightly acidic for groundwater. Stream water and deep groundwater revealed higher oxygen contents and higher redox potentials than shallow groundwater. This hints at more reducing conditions in shallow groundwater below the wetland. All *in-situ* parameters of flooding water were similar to those of stream water, indicating similar origins of both water components.

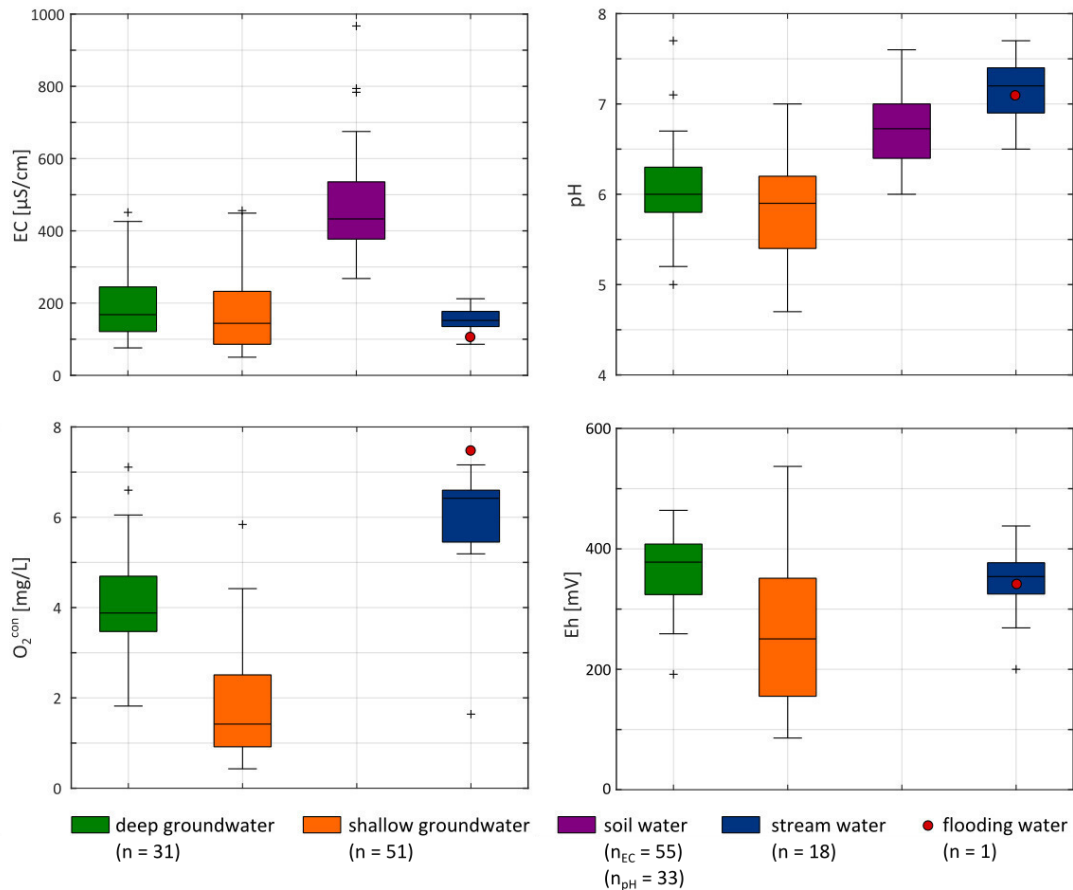
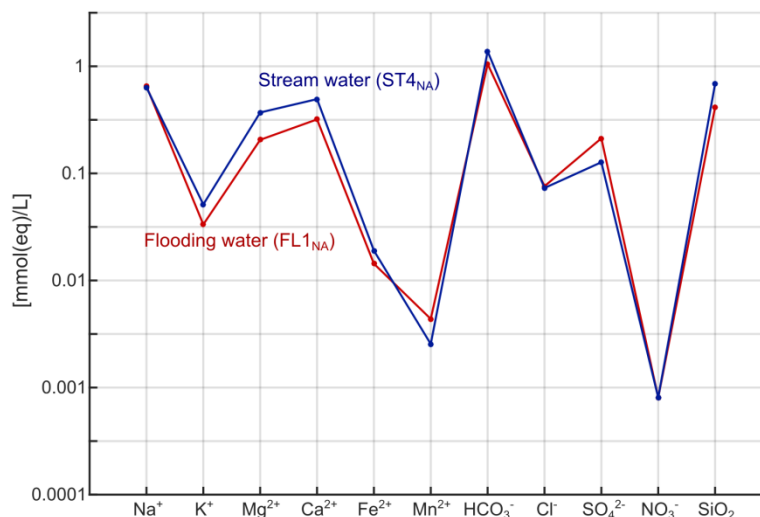


Fig. 7.15: Boxplots of measured *in-situ* parameters (electrical conductivity (EC), pH, O<sub>2</sub>-content (O<sub>2</sub><sup>con</sup>), redox potential (Eh)) of deep and shallow groundwater, soil water, stream water, and flooding water (NA).

### 7.3.1.1 Stream water (NA)

Nasirye Stream was permanently water-bearing, with moderate sediment loads during the whole monitoring period. Stream water showed moderate ECs and pH values ranging between 86 and 231 µS/cm and 6.0 and 8.6, respectively. Redox potentials and oxygen saturations were high in general. Most samples were classified as Na-HCO<sub>3</sub> water types (Fig. 7.16), while few samples in spring 2015 were classified as Na-SO<sub>4</sub> water types. Hydrochemical composition was clearly imprinted by silicate weathering.



**Fig. 7.16:** Schoeller diagram of flooding water and stream water of Nasirye stream (both sampled at transect C in autumn 2014) (NA).

During monthly sampling, stream water was sampled at the inflow into the wetland of lower Nasirye Catchment (ST1<sub>NA</sub>), short before (ST3<sub>NA</sub>) and after the CFT (ST5<sub>NA</sub>) at transect C, and at the outflow from the wetland to a papyrus swamp (ST7<sub>NA</sub>) (Fig. 5.8 p.65). EC of stream water at inflow and outflow showed a higher temporal than spatial variability (Fig. 7.17). Nevertheless, EC at the inlet was often higher than EC at the outlet, indicating nutrient removal during the passage through the wetland. In contrast, pH values were lower at the inlet, due to prolonged exchange with air along the flow path. Time series of stream water, sampled short before and after the CFT, showed similar curves. In general, EC of stream water increased during dry periods (e.g. 01/01/15-03/01/15). At the beginning of rainy periods, EC decreased and subsequently stayed constant throughout the rainy period (Fig. 7.17). This indicates either a higher proportion of direct precipitation and surface runoff in stream water during rainy seasons or influences of evaporation during dry seasons. EC was generally higher in 2015 compared to 2016.

Na<sup>+</sup> concentrations, being an indicator of mineralization, caused by silicate weathering, stayed stable during the measuring period, indicating constant discharge of groundwater influenced by silicate weathering to the stream (Fig. 7.17). In contrast, cumulative concentrations of Cl<sup>-</sup>, SO<sub>4</sub><sup>2-</sup>, and NO<sub>3</sub><sup>-</sup>, being indicators of anthropogenic influence, showed higher variations. EC followed the same trend as the anthropogenic indicators (Fig. 7.17). Thus, it is concluded that anthropogenic influences are a major source of mineralization in stream water. The increase in EC in early 2015 was mainly induced by an increase in SO<sub>4</sub><sup>2-</sup> concentration. This increase might have been derived from intensive inputs of detergents. For example, it was observed during field work that people regularly wash their motorcycles in the stream near the inflow.

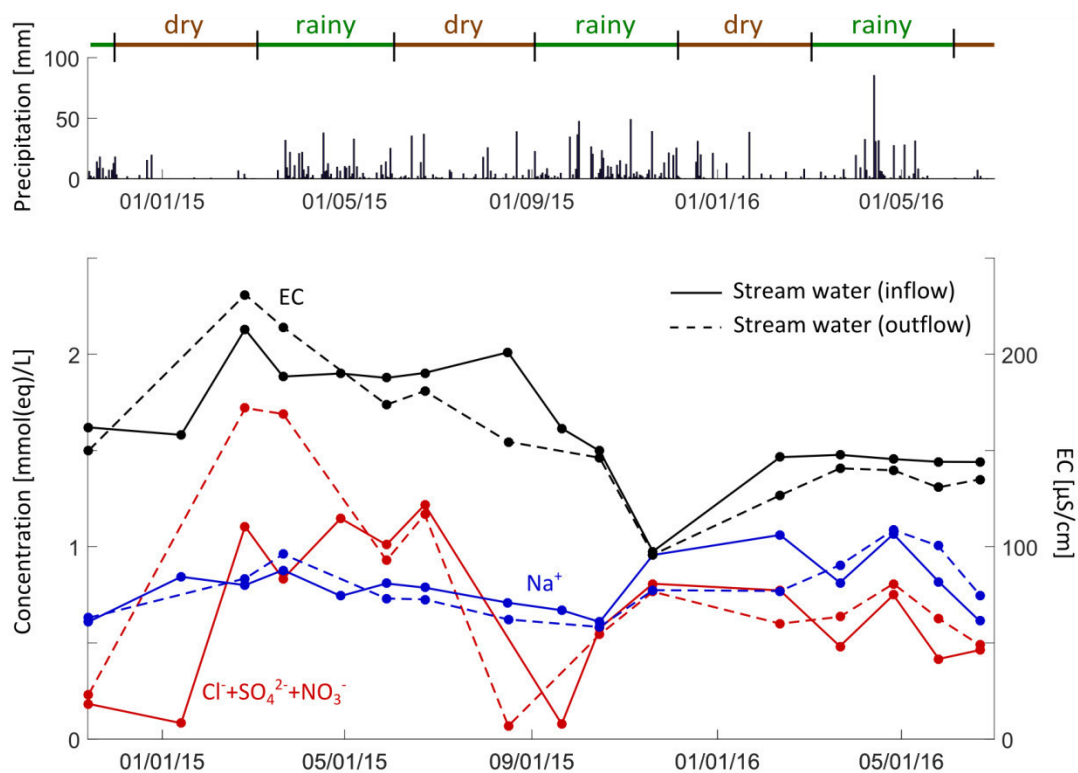


Fig. 7.17: Time series of electrical conductivity (EC), sodium ( $\text{Na}^+$ ) concentrations (indicator of silicate weathering), and cumulative chloride, sulfate, and nitrate ( $\text{Cl}^-$ ,  $\text{SO}_4^{2-}$ ,  $\text{NO}_3^-$ ) concentrations (indicators of anthropogenic influence) of stream water, sampled at the inflow ( $\text{ST1}_{\text{NA}}$ ) and outflow ( $\text{ST7}_{\text{NA}}$ ) of lower Nasirye Catchment. Daily precipitation is shown, and rainy and dry seasons are marked (NA).

### 7.3.1.2 Flooding water (NA)

Flooding occurred sporadically after heavy rainfall events. Flooding water was only sampled once. High sediment loads within the water made a filtration in most cases impossible. The sample was taken at transect C in a treatment plot at *center*. Flooding water belonged to the  $\text{Na-HCO}_3$  water type and showed a similar hydrochemical composition to Nasirye Stream. This indicates over-bank flow of stream water as the major source of flooding water (Fig. 7.15, Fig. 7.16). However, EC of flooding water ( $118 \mu\text{S}/\text{cm}$ ) was lower than EC of stream water ( $155 \mu\text{S}/\text{cm}$ ), suggesting a dilution of flooding water due to precipitation input.

### 7.3.1.3 Groundwater (NA)

Deep groundwater was sampled at hand and electrical pumping wells. Those wells are either screened in the crystalline rock aquitard or in the weathering profile aquifer. Depth information was only available for three of the wells ( $\text{PW37}_{\text{NA}}$ ,  $\text{PW38}_{\text{NA}}$ ,  $\text{PW39}_{\text{NA}}$ ). All of them showed drilling depths far below the boundary between crystalline rock and weathering profile. Thus, they are most probably screened in the crystalline rock aquitard. Deep groundwater displayed hydrochemical compositions imprinted by silicate weathering. Most samples belonged to the  $\text{Na-HCO}_3$ ,  $\text{Ca-HCO}_3$ , or  $\text{Mg-HCO}_3$  water types (Fig. 7.18 a).

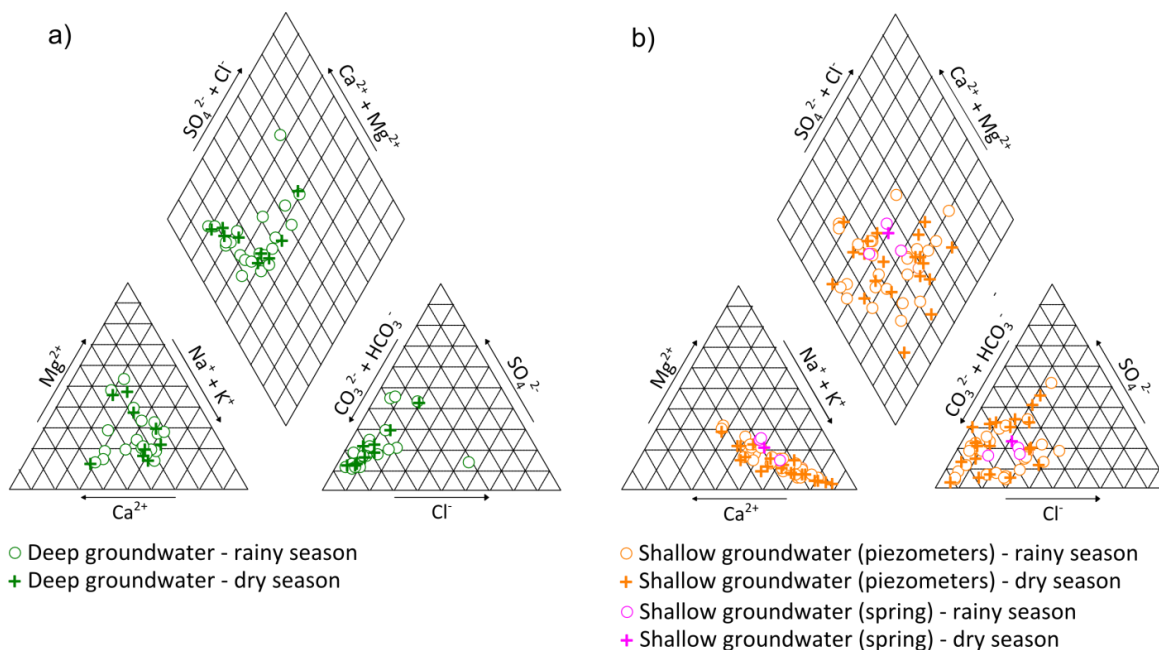


**Fig. 7.18:** Piper diagrams of a) deep groundwater samples and b) shallow groundwater samples (NA).

Water type was related to EC. Groundwater of Na-HCO<sub>3</sub> water type showed lower ECs compared to the other two water types (Fig. 7.19 a). These differences can be explained by the different lithologies of crystalline rocks. Granites contain more weatherable minerals than slates. These minerals are plagioclases as well as biotites, containing Ca and Mg, as indicated by geochemistry (Westerhof et al. 2014). Hence, the higher mineralized Ca/Mg-rich groundwater is related to granites, and the lower mineralized Na-rich groundwater is related to slates. However, based on the geological map, neither water type, nor EC, was related to the lithologies of crystalline rocks (Fig. 7.20). For example, samples of PW07<sub>NA</sub> and PW39<sub>NA</sub> belonged to the low mineralized Na-rich groundwater, although these wells are located in the granite. More leached parts of the granites, which are assumed to be present in the weathering profile, are depleted in highly weatherable minerals. Thus, low mineralized Na-rich groundwater might occur in the weathering profile of granites as well. Additionally, samples of PW36<sub>NA</sub> and PW41<sub>NA</sub> belonged to the higher mineralized Ca/Mg-rich groundwater, although these wells are located in the slates. These discrepancies might hint at errors in the geological map.

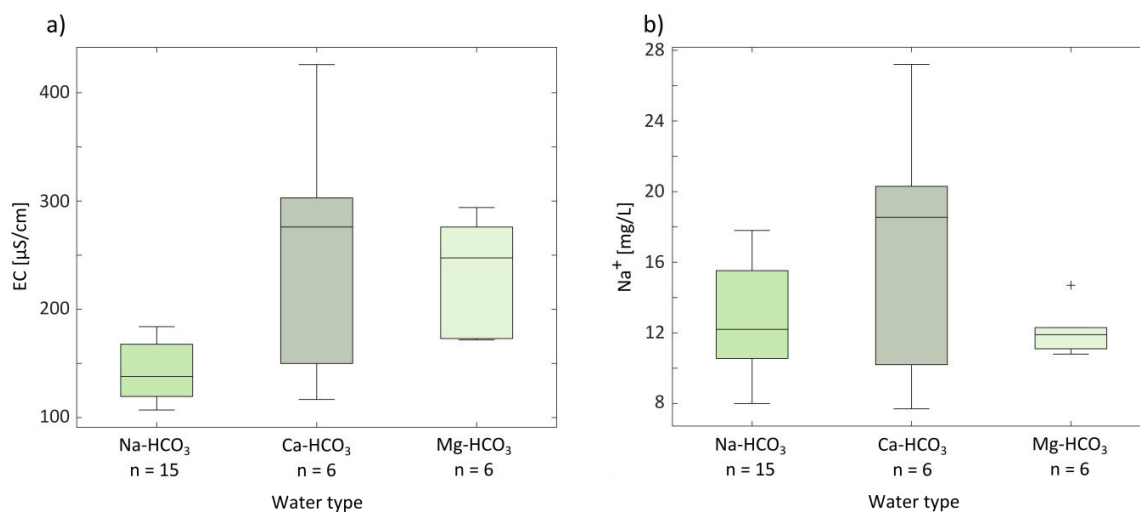


**Fig. 7.19:** Distribution of a) electrical conductivity (EC) and b) sodium (Na<sup>+</sup>) concentrations for different HCO<sub>3</sub> water types of deep groundwater (NA).

Comparing absolute  $\text{Na}^+$  concentrations showed that deep groundwater of  $\text{Ca-HCO}_3$  and  $\text{Mg-HCO}_3$  water types had similar or even higher concentrations compared to  $\text{Na-HCO}_3$  groundwater (Fig. 7.19 b). This indicates that albite weathering, being the major source of  $\text{Na}^+$  during silicate weathering (Appelo and Postma 2005), occurs to similar degrees in all regions of the aquifer.

Groundwater of one well was even characterized as  $\text{Ca-NO}_3$  water type, indicating anthropogenic influence. This water also showed highest mineralization and is located in the upland of the lower Nasirye Catchment (Fig. 7.20:  $\text{PW40}_{\text{NA}}$ ), where agricultural fields are found all over. Groundwater of another well fell within the  $\text{Na-SO}_4$  water type. This well is located in the upper catchment and displayed very low ECs, indicating recently infiltrated precipitation ( $\text{PW44}_{\text{NA}}$ ).

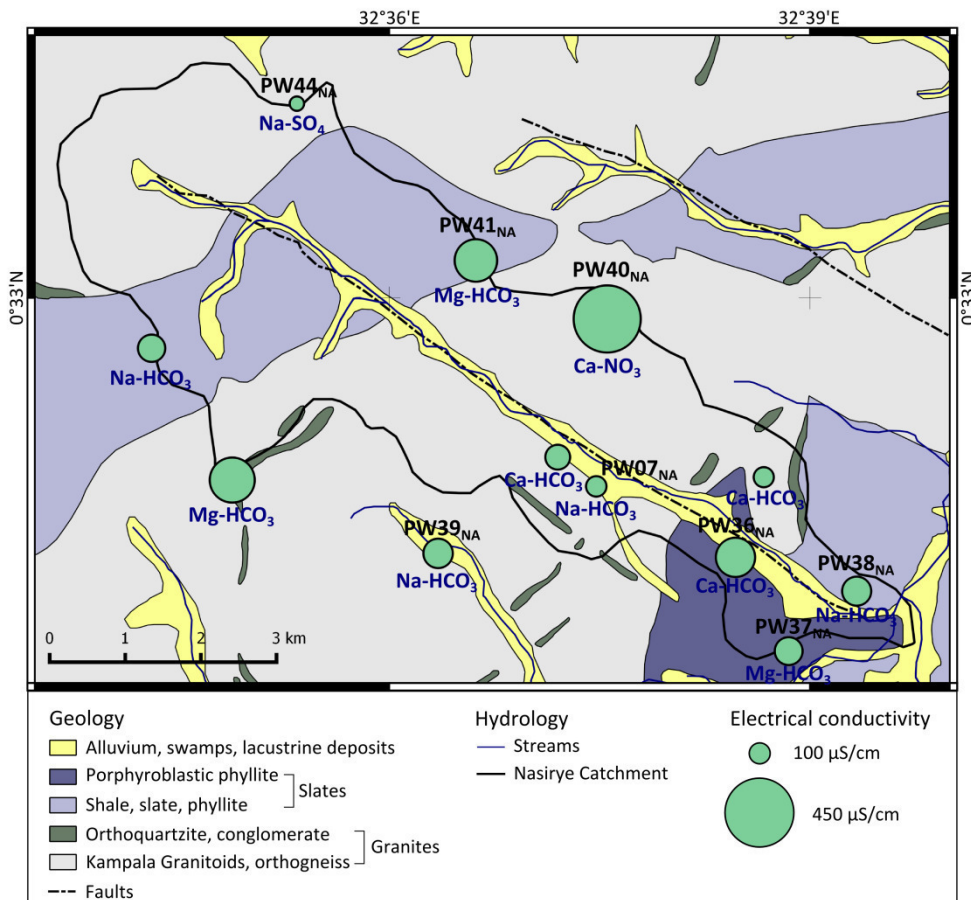


**Fig. 7.20:** Spatial distribution of electrical conductivities and water types of deep groundwater (spring 2015). Data sources: GTK Consortium (2012) (geology, streams), Heiß (2016) (alluvium), Gabiri (unpublished) (Nasirye Stream) (NA).

Temporal variation in deep groundwater chemistry was small (Fig. 7.18 a). This was confirmed by monthly samples of two pumping wells ( $\text{PW07}_{\text{NA}}$ ,  $\text{PW36}_{\text{NA}}$ ). Within each well, neither EC nor indicative ions varied strongly over time (Fig. 7.21). Compared to each other, these two wells showed a remarkable difference in EC. Furthermore, they belonged to different water types. Consequently, Figure 7.21 demonstrates that spatial variability in deep groundwater is more intense than temporal.



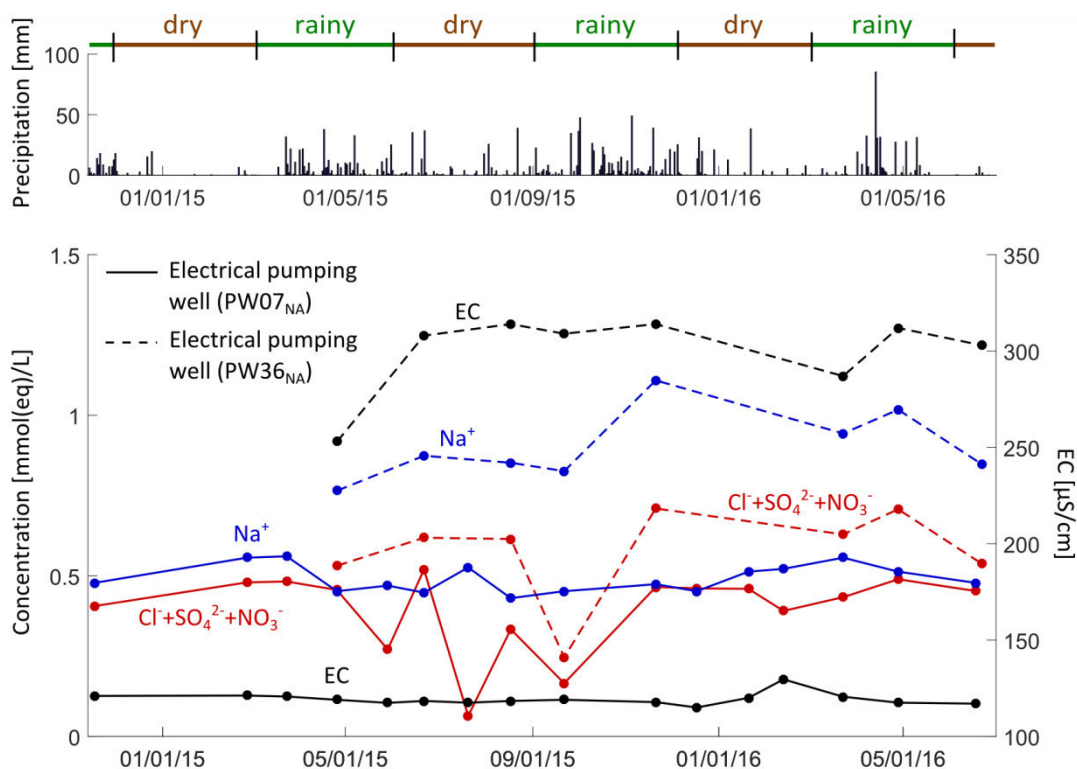


**Fig. 7.21:** Time series of electrical conductivity (EC), sodium ( $\text{Na}^+$ ) concentrations (indicator of silicate weathering), and cumulative chloride, sulfate, and nitrate ( $\text{Cl}^-$ ,  $\text{SO}_4^{2-}$ ,  $\text{NO}_3^-$ ) concentrations (indicators of anthropogenic influence) of deep groundwater at  $\text{PW07}_{\text{NA}}$  and  $\text{PW36}_{\text{NA}}$ . Daily precipitation is shown, and rainy and dry seasons are marked (NA).

Shallow groundwater of the valley sediment aquifer was sampled at piezometers. Furthermore, two springs, discharging at the slope near transect C, were sampled. These springs exist, because local population dug pits at the lower slopes near the wetland. The springs discharge from a sandy layer of the weathering profile at around 0.5 m below surface during the whole year, with higher discharge amounts during rainy season (personal communication with local population 2015).

Most shallow groundwater samples belonged to the  $\text{Na-HCO}_3$  water type (Fig. 7.18 b). Few samples fell within the  $\text{Ca-HCO}_3$ ,  $\text{Na-SO}_4$ , or  $\text{Na-Cl}$  water type. Spring water, discharging from the weathering profile, showed similar compositions to shallow groundwater of the valley sediments, indicating a connection between these two components. In terms of mineralization, shallow groundwater at transect C showed lower ECs compared to the other transects (Fig. 7.22). The higher mineralization in transects A and D is conspicuous, as transect C is located in between. Thus, this difference in mineralization is not related to prolonged weathering along the major flow path from upper to lower valley. It is rather assumed that shallow groundwater at transect C is better drained, due to faster flow velocities promoted by higher hydraulic conductivities, than at the other two transects.

Shallow groundwater flowed from *fringe* to *center* at transect C (cf. section 7.2.2). Here, EC of shallow groundwater increased from *fringe*, over *middle*, to *center* (Fig. 7.23). The same trend was observed for  $\text{Na}^+$  concentrations and pH, demonstrating progressing mineralization due to silicate weathering along the flow path (Tab. 7.2). During silicate weathering  $\text{Na}^+$  is released to the water and pH decreases, due to the consumption of  $\text{H}^+$  (Appelo and Postma 2005).

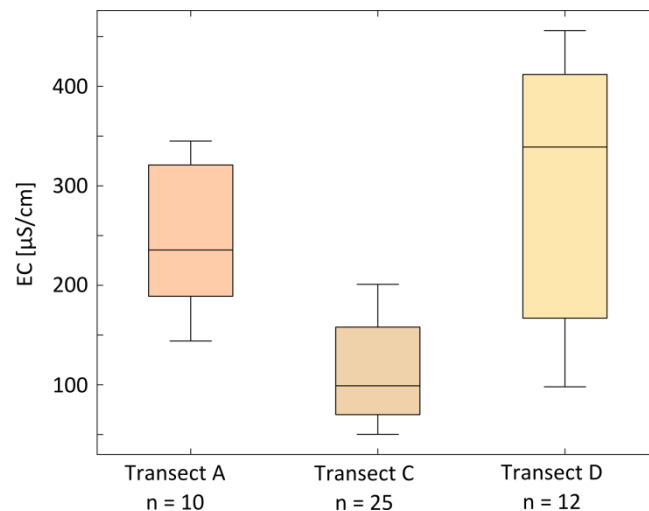


Fig. 7.22: Distribution of electrical conductivity (EC) in shallow groundwater of the valley sediments for the three different transects (NA).

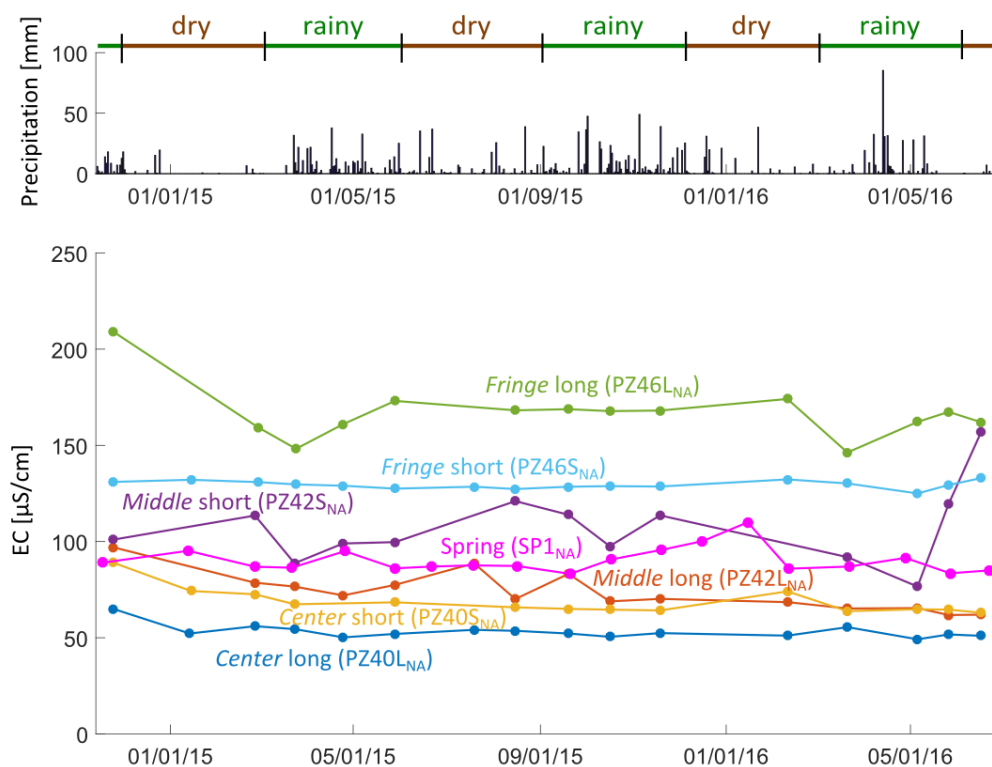


Fig. 7.23: Time series of electrical conductivity (EC) for shallow groundwater from piezometers and the spring at transect C. Daily precipitation is shown and rainy and dry seasons are marked (NA).

The sampled springs are located at the slope near transect C in prolonged flow direction. Thus, spring water, which naturally does not discharge, might flow to shallow groundwater at *fringe*. ECs and pH values of the monthly sampled spring (SP1<sub>NA</sub>) were higher compared to shallow groundwater at *fringe* (Fig. 7.23). However, the other spring (SP2<sub>NA</sub>) showed a lower EC and pH value (Tab. 7.2). Thus, spring water might recharge shallow groundwater of the valley sediments. The spatial differences in EC of spring water highlight the spatial variability in hydrochemistry of shallow groundwater in the weathering profile.

While  $\text{NO}_3^-$  was detected in all spring water samples, it was not observed in shallow groundwater samples of transect C (Fig. 7.23). This is an argument against a flow connection between shallow groundwa-

ter of the weathering profile (springs) and shallow groundwater of the valley sediments. However, denitrification might occur in shallow groundwater of the valley sediments, removing  $\text{NO}_3^-$ . Most redox potentials were below 250 mV, allowing denitrification (Mitsch and Gosselink 2007). Short and long piezometers showed similar hydrochemistry, confirming hydraulic connections between sand and gravel lenses in the valley sediments.

**Tab. 7.2:** Mean values of electrical conductivity (EC), pH value, sodium ( $\text{Na}^+$ ), and nitrate ( $\text{NO}_3^-$ ) concentrations of monthly shallow groundwater samples from spring ( $\text{SP1}_{\text{NA}}$ ) and piezometers at transect C (November 2014 – June 2016). For the second spring ( $\text{SP2}_{\text{NA}}$ ) values of the snapshot sampling in autumn 2015 are displayed (LOD = limit of detection) (NA).

	Spring $\text{SP1}_{\text{NA}}$ ( $\text{SP2}_{\text{NA}}$ )	Fringe		Middle		Center	
		$\text{PZ40L}_{\text{NA}}$	$\text{PZ40S}_{\text{NA}}$	$\text{PZ42L}_{\text{NA}}$	$\text{PZ42S}_{\text{NA}}$	$\text{PZ46L}_{\text{NA}}$	$\text{PZ46S}_{\text{NA}}$
EC [ $\mu\text{S}/\text{cm}$ ]	90 (58)	53	79	74	115	167	129
pH	5.6 (5.1)	4.9	5.4	5.3	5.7	5.8	5.8
$\text{Na}^+$ [mg/L]	7.6 (5.9)	7.9	10.1	15.0	22.8	21.0	16.7
$\text{NO}_3^-$ [mg/L]	9.4 (7.3)	< LOD	< LOD	< LOD	< LOD	< LOD	< LOD

#### 7.3.1.4 Soil water (NA)

Soil water samples of transect C showed variable ECs and relatively neutral pH values (Fig. 7.15). The three fully analyzed soil water samples belonged to the  $\text{Ca-HCO}_3$  water type (Fig. 7.24). Partly analyzed samples showed  $\text{Ca}^{2+}$  to be the dominant cation as well. The dominance of  $\text{Ca}^{2+}$  might be related to desilification in tropical soils, during which  $\text{Ca}^{2+}$  is released to the solution first, followed by other cations (Scheffer and Schachtschabel 2010).

In general, the hydrochemical composition of soil water was typical for water exposed to silicate weathering (Fig. 7.24). However, general mineralization was higher compared to groundwater and stream water. This might be explained by either evapotranspiration of soil water, longer residence times due to low hydraulic conductivities of soil, or fertilizer input. Most conspicuous were the highly variable and sometimes very high iron concentrations, which ranged between 0.04 and 24 mg/L. Those were most likely derived from iron reduction under anoxic conditions within the soil.

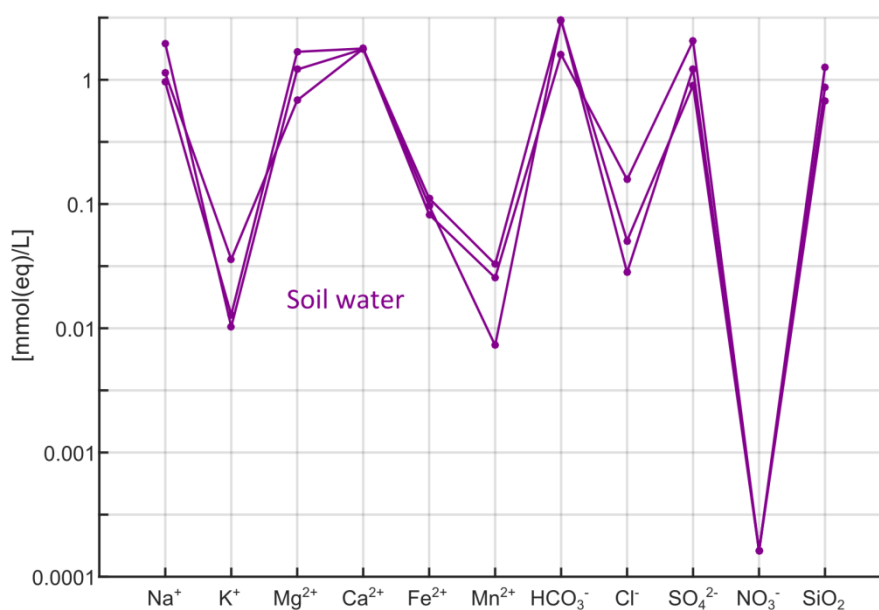


**Fig. 7.24:** Schoeller diagram of the three fully analyzed soil water samples (NA).

### 7.3.1.5 Precipitation (NA)

Precipitation, sampled in Nasiyre Catchment, showed higher median concentrations of most ions compared to East African precipitation, documented by Rodhe et al. (1981) (In Johnson 1996). Variabilities were high, while median concentrations usually were closer to minimum than to maximum concentrations (Tab. 7.3).

**Tab. 7.3: Minimum, maximum, and median concentrations of different analytes measured in weekly precipitation samples. Median values for East Africa were adopted from Rodhe et al. (1981) (In Johnson 1996) (NA).**

Analyte	Minimum [mg/L]	Maximum [mg/L]	Median [mg/L]	Median (East Africa) [mg/L]
Cl <sup>-</sup>	< 0.1	4.9	0.7	0.30
SO <sub>4</sub> <sup>2-</sup>	< 0.2	8.9	1.0	0.75
NO <sub>3</sub> <sup>-</sup>	< 0.1	12.2	0.6	0.00
HCO <sub>3</sub> <sup>-</sup>	-	-	-	1.43
Na <sup>+</sup>	< 0.1	4.6	0.4	0.62
K <sup>+</sup>	< 0.1	5.6	0.5	0.30
Mg <sup>2+</sup>	< 0.1	0.9	0.1	0.08
Ca <sup>2+</sup>	< 0.5	4.9	0.6	0.38
SiO <sub>2</sub>	< 0.1	1.8	0.2	-

### 7.3.1.6 Multivariate statistical analyses (NA)

Multivariate statistical analysis was performed for hydrochemical data of the four snapshot samplings. Furthermore, the three soil water samples, for which all major ions were available, were included in the dataset. Just like in the Ifakara study site, the variables EC, Na<sup>+</sup>, K<sup>+</sup>, Mg<sup>2+</sup>, Ca<sup>2+</sup>, Cl<sup>-</sup>, SO<sub>4</sub><sup>2-</sup>, HCO<sub>3</sub><sup>-</sup>, Fe<sup>2+</sup>, and Mn<sup>2+</sup> were log transformed before analyses, while the variables pH and SiO<sub>2</sub> showed a better normal distribution without log-transformation. All in all, 104 samples were used for multivariate statistical analysis.

The first principal component (PC1<sub>NA</sub>) explained 45 % of the total variance within the dataset, while the second principal component (PC2<sub>NA</sub>) explained another 14 % (Tab. 7.4). Thus, the first two principal components explained 59 % of the total variance. EC, Na<sup>+</sup>, Mg<sup>2+</sup>, Ca<sup>2+</sup>, and HCO<sub>3</sub><sup>-</sup> showed high positive loadings to PC1<sub>NA</sub> (Tab. 7.4). These variables are related to the weathering of silicate minerals (Appelo and Postma 2005, cf. section 6.3.1.5). PC2<sub>NA</sub> was characterized by high positive loadings of Cl<sup>-</sup> and SiO<sub>2</sub> and high negative loadings of pH. The high positive loadings of Cl<sup>-</sup> might correspond to evaporation or anthropogenic influence. Cl<sup>-</sup> is present in most potassium fertilizers (sdnotill.com). In addition, little chloride could be derived by the dissolution of micas, which occur in the phyllites. Increasing SiO<sub>2</sub> is related to silicate weathering. However, these processes are not directly related to low pH-values. Thus, PC2<sub>NA</sub> might not represent a chemical or physical process, but solely reflect coincidences in the dataset.

It can be concluded that silicate weathering is the major process controlling hydrochemistry of groundwater and surface water. Influences of other processes are small or only occur in few samples and were thus not detected by PCA.

Overall, HCA resulted in a separation of water samples into three cluster groups. This grouping can further be subdivided into six sub-cluster groups (Fig. 7.25). The chemical compositions of all sub-cluster groups were imprinted by silicate weathering (Fig. 7.26). In general, compositions of major ions and SiO<sub>2</sub> were similar for the six sub-cluster groups (Fig. 7.26, Tab. 7.5). Nevertheless, Kruskal-Wallis tests revealed significant differences between the six groups (Tab. 7.6).

Tab. 7.4: Loadings of variables on the first two principal components (PC1<sub>NA</sub>, PC2<sub>NA</sub>) and the respective explained variance. High factor loadings are marked in grey (NA).

Variable	PC1 <sub>NA</sub>	PC2 <sub>NA</sub>
Electrical conductivity	0.41	0.00
pH	0.27	-0.39
Na <sup>+</sup>	0.36	0.26
K <sup>+</sup>	-0.10	-0.30
Mg <sup>2+</sup>	0.37	-0.23
Ca <sup>2+</sup>	0.39	-0.11
Cl <sup>-</sup>	0.04	0.42
SO <sub>4</sub> <sup>2-</sup>	0.27	-0.24
HCO <sub>3</sub> <sup>-</sup>	0.40	0.03
Fe <sup>2+</sup>	0.19	0.20
Mn <sup>2+</sup>	0.20	0.17
SiO <sub>2</sub>	0.13	0.57
<b>Explained variance</b>	<b>0.45</b>	<b>0.14</b>

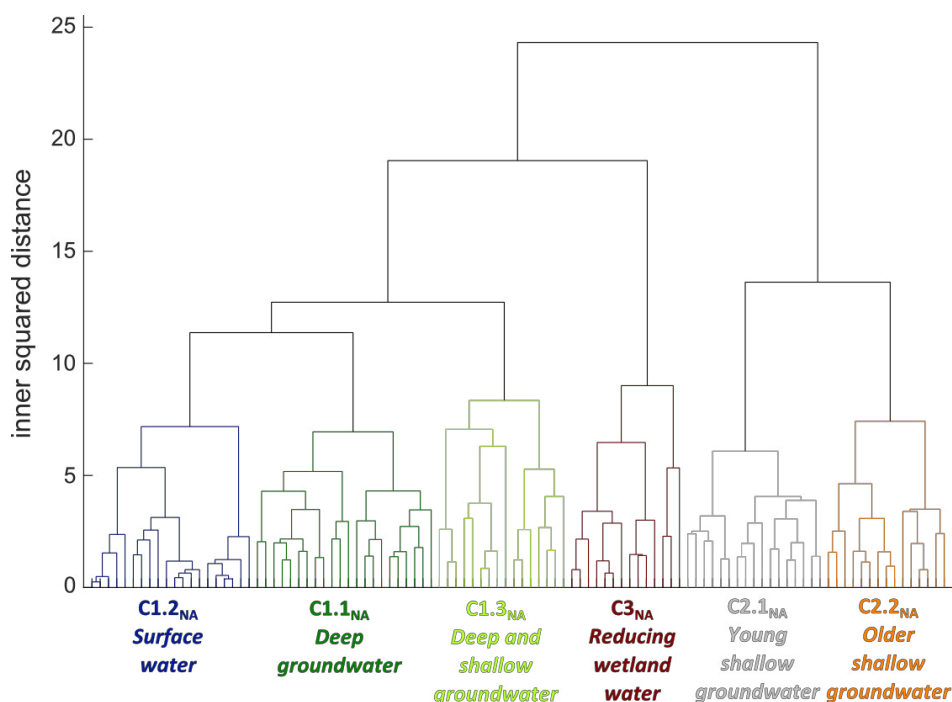


Fig. 7.25: Dendrogram of the Hierarchical Cluster Analysis, performed for 104 water samples using the variables logEC, pH, logNa<sup>+</sup>, logK<sup>+</sup>, logMg<sup>2+</sup>, logCa<sup>2+</sup>, logCl<sup>-</sup>, logSO<sub>4</sub><sup>2-</sup>, logHCO<sub>3</sub><sup>-</sup>, logFe<sup>2+</sup>, logMn<sup>2+</sup>, and SiO<sub>2</sub> showing the different sub-cluster groups of water samples and their characteristic names (NA).

Cluster group C1<sub>NA</sub> is composed of almost all deep groundwater samples, all stream water samples, the flooding water sample, and few shallow groundwater samples from piezometers. This cluster group was divided into three sub-cluster groups. One of these sub-cluster groups (C1.2<sub>NA</sub>) is composed of all stream water samples, the flooding water sample, and one deep groundwater sample. Therefore, this group will be called *surface water*. It is characterized by moderate ECs and neutral pH values.

The deep and shallow groundwater samples build two other sub-cluster groups that differed from each other in their ECs, Na<sup>+</sup>, and Cl<sup>-</sup> concentrations (Tab. 7.6). C1.1<sub>NA</sub> is mainly composed of deep groundwater samples. It contains all low mineralized, Na-HCO<sub>3</sub> deep groundwater samples. Furthermore, all Ca/Mg-HCO<sub>3</sub> deep groundwater samples with lower ECs are part of this group. Thus, this low mineral-

ized group will henceforth be referred to as *deep groundwater*. Samples of this group represent regions of the crystalline rocks dominated by slates and phyllites of the Buganda Group or highly weathered parts in the weathering profile.

In contrast, C1.3<sub>NA</sub>, being composed of eight deep groundwater and eight shallow groundwater samples, showed higher mineralizations. It includes all higher mineralized Ca/Mg-HCO<sub>3</sub> deep groundwater samples. All shallow groundwater samples (piezometers) of this group revealed Na<sup>+</sup> as major cation. No information about depths of pumping wells was available for wells within this group. As the sub-cluster group contains deep and shallow groundwater samples, it will be referred to as *deep and shallow groundwater*. This group showed higher mineralizations compared to *deep groundwater*, due to higher weathering rates in granites, with more weatherable minerals compared to slates. The higher Cl<sup>-</sup> concentrations in samples of this group can be released from micas and feldspars of granites by ion exchange. As shallow and deep groundwater samples fell within this group, a similar hydrochemical evolution of both water components is likely. That does not implicitly mean that both water components are connected, as both aquifers displayed similar mineralogical compositions. Samples of this sub-cluster group were found throughout the study site, demonstrating the spatial variability of mineralization, due to silicate weathering.

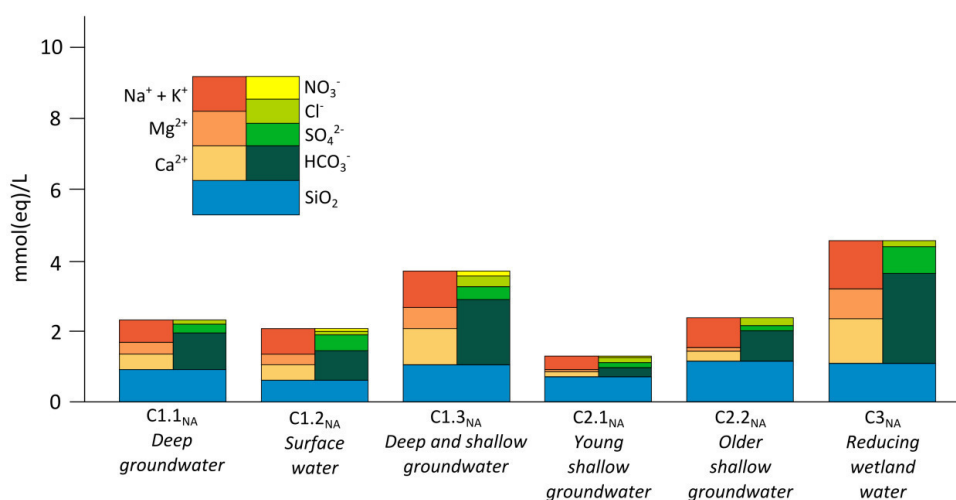


**Fig. 7.26: Barcharts of mean hydrochemical compositions of the six sub-cluster groups identified by Hierarchical Cluster Analysis (NA).**

Both groundwater groups (*deep groundwater*, *deep and shallow groundwater*) showed similar concentrations of most ions compared to *surface water*, indicating a similar origin and evolution (Tab. 7.5). Additionally, both groundwater groups (C1.1<sub>NA</sub>, C1.3<sub>NA</sub>) showed detectable nitrate concentrations, which were not observed in *surface water*.

The second cluster group (C2<sub>NA</sub>) is mainly composed of shallow groundwater samples from piezometers of transect C and springs. However, few samples of piezometers from the other transects fell within this group as well. This cluster group showed low ECs and low pH values, indicating young ages of groundwater. Precipitation that infiltrates into the ground has low ECs and neutral to acidic pH values. During its passage to the groundwater table it becomes more acidic due to the uptake of CO<sub>2</sub> and humin acids from the soil (Appelo and Postma 2005). This cluster group was subdivided into two sub-cluster groups. *Young shallow groundwater* (C2.1<sub>NA</sub>) predominately composed of spring water samples and shallow groundwater samples from *fringe* piezometers. These samples showed lowest ECs and pH-values, indicating recently infiltrated precipitation. *Older shallow groundwater* (C2.2<sub>NA</sub>) is mainly composed of shallow groundwater samples from *middle* and *center* piezometers at transect C. The higher mineralization

of this sub-cluster group confirms that shallow groundwater flows from the *fringe* to the *center* becoming more enriched in major cations, SiO<sub>2</sub>, and HCO<sub>3</sub><sup>-</sup> along its flowpath.

The third cluster group (C3<sub>NA</sub>) is represented by shallow groundwater samples from piezometers of transects A and D and by all soil water samples. This group showed higher ECs than all other samples, but still intermediate mineralizations, averaging 363 μS/cm (Tab. 7.5). Furthermore, this cluster group displayed higher Fe<sup>2+</sup> and Mn<sup>2+</sup> concentrations than the other cluster groups. The high concentrations of Fe<sup>2+</sup> and Mn<sup>2+</sup> indicate reducing conditions within the wetland, confirmed by lowest redox potentials and oxygen saturations in this group, averaging 150 mV and 10 %, respectively. Hence, this group will be referred to as *reducing wetland water*. These samples represent groundwater within less permeable parts of the valley sediments aquifer exposed to flooding or saturation, leading to anoxic conditions. In these parts of the wetland redox processes play an important role and water purification functions are highest.

Tab. 7.5: Means and standard deviations (in brackets) of each variable for all six sub-cluster groups. Nitrate (NO<sub>3</sub><sup>-</sup>) was added for consistency. The amount of samples per group (n) is displayed below the group name (NA).

Group	EC [μS/cm]	pH [-]	Na <sup>+</sup> [mg/L]	K <sup>+</sup> [mg/L]	Mg <sup>2+</sup> [mg/L]	Ca <sup>2+</sup> [mg/L]	Cl <sup>-</sup> [mg/L]	SO <sub>4</sub> <sup>2-</sup> [mg/L]	HCO <sub>3</sub> <sup>-</sup> [mg/L]	Fe <sup>2+</sup> [mg/L]	Mn <sup>2+</sup> [mg/L]	SiO <sub>2</sub> [mg/L]	NO <sub>3</sub> <sup>-</sup> [mg/L]
C1.1 <sub>NA</sub> n=22	150 (36)	6.0 (0.4)	12.8 (3.3)	3.8 (0.8)	4.3 (2.5)	9.1 (2.9)	4.6 (1.8)	12.6 (4.2)	56.4 (21.9)	0.84 (3.06)	0.06 (0.06)	55.9 (13.6)	6.2 (4.5)
C1.2 <sub>NA</sub> n=20	152 (29)	7.1 (0.4)	15.0 (2.1)	2.4 (0.7)	3.9 (1.2)	9.2 (2.3)	4.4 (1.4)	22.2 (17.0)	52.5 (16.9)	0.55 (0.25)	0.18 (0.19)	38.0 (5.7)	0.5 (1.9)
C1.3 <sub>NA</sub> n=16	276 (84)	6.4 (0.5)	22.2 (9.8)	3.2 (1.9)	7.6 (5.7)	21.1 (10.8)	11.3 (8.6)	18.2 (5.9)	113.8 (56.1)	0.98 (2.11)	0.21 (0.37)	63.6 (15.9)	9.9 (31.6)
C2.1 <sub>NA</sub> n=17	73 (14)	5.2 (0.3)	7.7 (1.7)	2.7 (1.2)	1.0 (0.7)	3.2 (1.1)	5.7 (1.7)	6.5 (3.5)	16.6 (5.2)	0.50 (0.82)	0.04 (0.02)	43.0 (11.1)	3.8 (4.7)
C2.2 <sub>NA</sub> n=15	137 (31)	5.9 (0.3)	18.6 (5.8)	1.9 (0.6)	1.4 (0.9)	6.0 (2.9)	8.5 (3.2)	7.8 (6.1)	48.7 (17.8)	0.42 (0.45)	0.10 (0.07)	69.8 (8.0)	0.2 (0.2)
C3 <sub>NA</sub> n=14	363 (73)	6.3 (0.2)	30.8 (10.4)	1.7 (0.9)	10.4 (4.5)	25.6 (8.7)	6.7 (3.4)	37.8 (25.7)	160.7 (36.7)	7.36 (4.34)	0.90 (0.50)	66.0 (17.9)	0.2 (0.4)

Tab. 7.6: P-values of multiple comparison tests, following Kruskal-Wallis-tests, for different pairs of sub-cluster groups. Those p-values that indicated a rejection of the null-hypothesis that both sub-cluster groups come from one distribution with respect to a certain variable are marked in grey (level of significance = 1 %) (NA).

Group 1	Group 2	EC	pH	Na <sup>+</sup>	K <sup>+</sup>	Mg <sup>2+</sup>	Ca <sup>2+</sup>	Cl <sup>-</sup>	SO <sub>4</sub> <sup>2-</sup>	HCO <sub>3</sub> <sup>-</sup>	Fe <sup>total</sup>	Mn <sup>2+</sup>	SiO <sub>2</sub>
C1.1 <sub>NA</sub>	C1.2 <sub>NA</sub>	1.00	0.00	0.76	0.00	1.00	1.00	1.00	0.76	1.00	0.01	0.35	0.01
C1.1 <sub>NA</sub>	C1.3 <sub>NA</sub>	0.01	0.22	0.01	0.14	0.65	0.03	0.00	0.46	0.12	0.46	0.99	0.74
C1.1 <sub>NA</sub>	C2.1 <sub>NA</sub>	0.00	0.01	0.05	0.01	0.00	0.00	0.71	0.06	0.00	0.91	0.99	0.10
C1.1 <sub>NA</sub>	C2.2 <sub>NA</sub>	0.98	1.00	0.12	0.00	0.01	0.42	0.00	0.20	0.99	0.66	0.79	0.10
C1.1 <sub>NA</sub>	C3 <sub>NA</sub>	0.00	0.39	0.00	0.00	0.02	0.00	0.27	0.15	0.00	0.00	0.00	0.65
C1.2 <sub>NA</sub>	C1.3 <sub>NA</sub>	0.01	0.13	0.24	0.79	0.72	0.06	0.00	0.99	0.10	0.81	0.84	0.00
C1.2 <sub>NA</sub>	C2.1 <sub>NA</sub>	0.00	0.00	0.00	1.00	0.00	0.00	0.52	0.00	0.00	0.30	0.16	0.97
C1.2 <sub>NA</sub>	C2.2 <sub>NA</sub>	0.96	0.00	0.82	0.50	0.01	0.31	0.00	0.01	1.00	0.67	0.99	0.00
C1.2 <sub>NA</sub>	C3 <sub>NA</sub>	0.00	0.09	0.00	0.32	0.03	0.00	0.16	0.85	0.00	0.02	0.01	0.00
C1.3 <sub>NA</sub>	C2.1 <sub>NA</sub>	0.00	0.00	0.00	0.98	0.00	0.00	0.06	0.00	0.00	0.97	0.87	0.00
C1.3 <sub>NA</sub>	C2.2 <sub>NA</sub>	0.00	0.12	0.95	0.05	0.00	0.00	0.99	0.00	0.05	1.00	0.99	0.86
C1.3 <sub>NA</sub>	C3 <sub>NA</sub>	0.90	1.00	0.51	0.02	0.61	0.96	0.38	0.99	0.57	0.00	0.00	1.00
C2.1 <sub>NA</sub>	C2.2 <sub>NA</sub>	0.04	0.11	0.00	0.25	0.99	0.43	0.23	1.00	0.01	1.00	0.52	0.00
C2.1 <sub>NA</sub>	C3 <sub>NA</sub>	0.00	0.00	0.00	0.14	0.00	0.00	0.98	0.00	0.00	0.00	0.00	0.00
C2.2 <sub>NA</sub>	C3 <sub>NA</sub>	0.00	0.23	0.11	1.00	0.00	0.00	0.73	0.00	0.00	0.00	0.00	0.94

It becomes obvious that the sub-cluster groups are related to the type of sampled water as well as to the position of sampling points. However, this differentiation is not straight-forward, as temporal and spatial outliers were observed in most sub-cluster groups. Several sampling points fell within different cluster or sub-cluster groups for different sampling times. For instance, two pumping wells once belonged to *deep groundwater* and once to *deep and shallow groundwater*. Another pumping well once fell within *deep groundwater* and three other times within *surface water*. This temporal variability, which did not follow a certain trend regarding rainy or dry seasons, highlights the hydrochemical similarity between all water samples. This is also demonstrated in the PCA plot, where several sub-cluster groups overlap each other (Fig. 7.27). An increase in mineralization was observed from *young shallow groundwater* over *older shallow groundwater*, *deep groundwater*, and *surface water* to *deep and shallow groundwater* and *reducing wetland water* (Fig. 7.27).

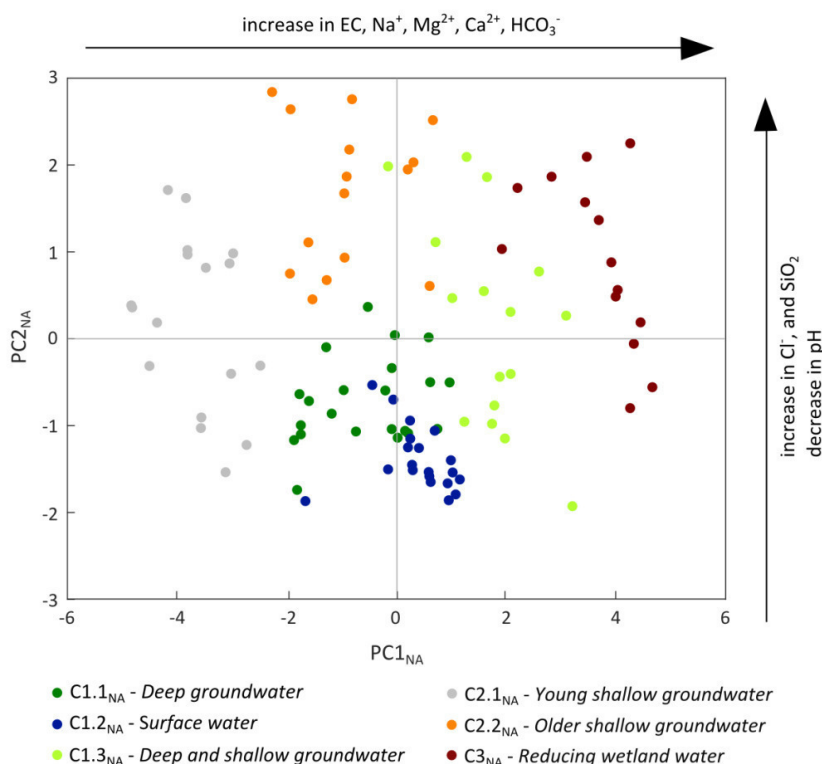


Fig. 7.27: Scatterplot of the two principal components (PC1<sub>NA</sub> and PC2<sub>NA</sub>) showing the distribution of water samples (NA).

### 7.3.1.7 Specific ion ratios, saturation indices, and stability diagrams (NA)

The observed correlation between EC and  $\text{HCO}_3^-$  for all cluster groups confirmed silicate weathering as the major source of mineralization (Fig. 7.28). All cluster groups showed  $\text{HCO}_3^-/(\text{Na}^+ + 2\text{Ca}^{2+})$  ratios around one, indicating the weathering of plagioclases (Van der Weijden and Pacheco 2007). Two sub-cluster groups showed  $\text{SiO}_2/\text{Na}^+$  ratios around two (*deep groundwater*, *young shallow groundwater*), demonstrating feldspar weathering as the dominant source of  $\text{Na}^+$  (Appelo and Postma 2005). In contrast, most samples of *surface water* and *reducing wetland water*, and some samples of *deep and shallow groundwater* and *older shallow groundwater* showed lower  $\text{SiO}_2/\text{Na}^+$  ratios. These might be induced by an increase of  $\text{Na}^+$  during cation exchange or the precipitation of other clay minerals than kaolinite. If, for instance, montmorillonite precipitates instead of kaolinite, more  $\text{SiO}_2$  is retained in the solid solution (Appelo and Postma 2005). While most samples displayed  $\text{Na}^+/\text{Cl}^-$  ratios far above one, few samples of *young shallow groundwater* and *deep and shallow groundwater* showed ratios near one, indicating NaCl as a source of  $\text{Na}^+$ .  $\text{K}^+/\text{Na}^+$  ratios were highest for *deep groundwater* and *young shallow groundwater*



(Fig. 7.29). This might indicate contact with vegetation and soil (King et al. 2014) or high rates of k-feldspar weathering.

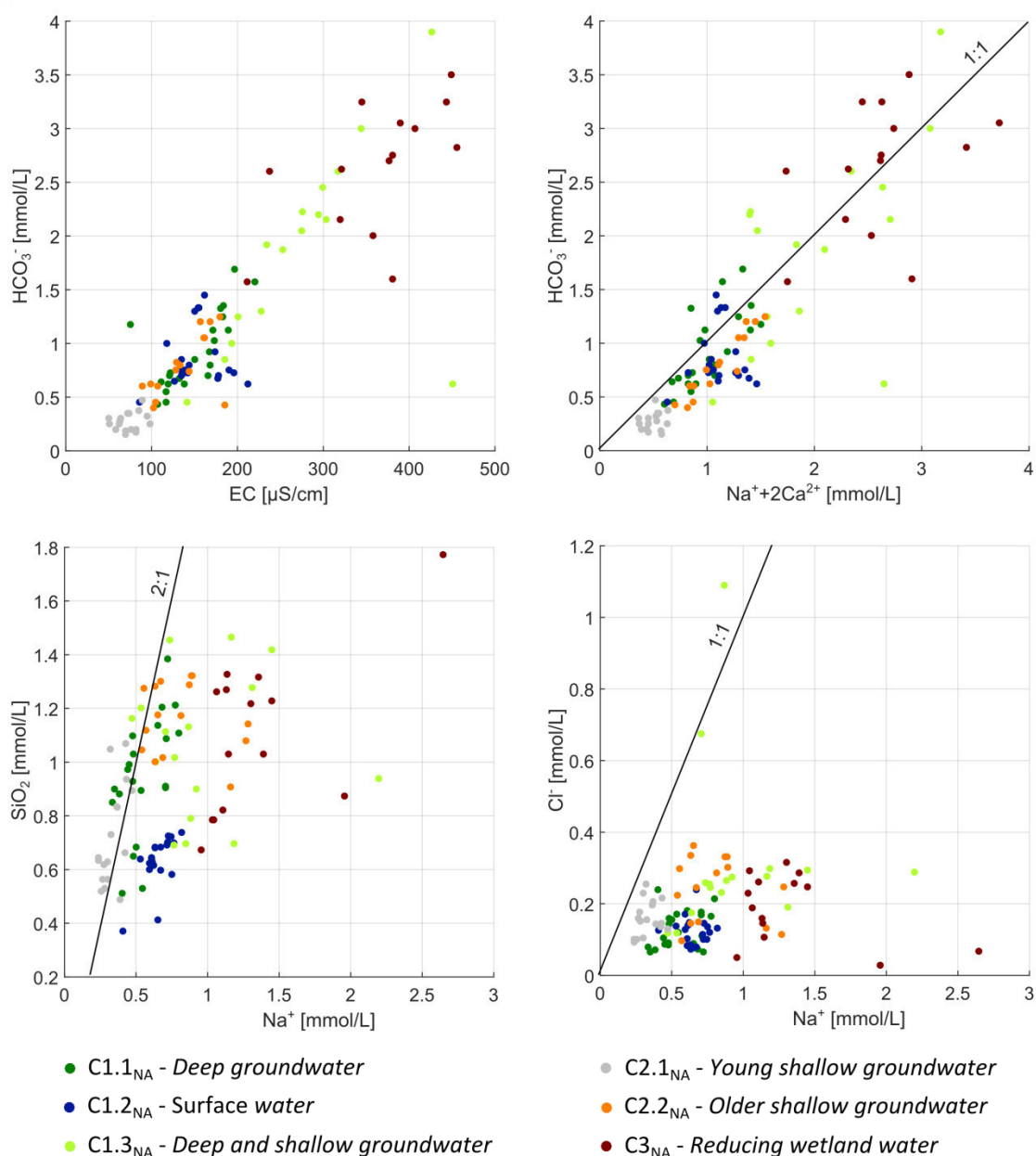


**Fig. 7.28:** Selected ratios of different hydrochemical parameters for the six sub-cluster groups. Specific ion ratios are illustrated as lines (NA).

Concentrations of the redox sensitive species  $\text{NO}_3^-$ ,  $\text{Mn}^{2+}$ , and  $\text{Fe}^{2+}$  were all related to redox potentials (Fig. 7.29). Except for one sample,  $\text{NO}_3^-$  concentrations were solely detected in samples with oxidizing conditions, showing redox potentials above 250 mV. This indicates that existing  $\text{NO}_3^-$  was removed by denitrification in water with lower redox potentials (Mitsch and Gosselink 2007). For instance, *reducing wetland water* did not show any  $\text{NO}_3^-$  concentrations. In general,  $\text{NO}_3^-$  was solely detected in *deep groundwater*, *deep and shallow groundwater*, and *younger shallow groundwater*. High  $\text{Mn}^{2+}$  and  $\text{Fe}^{2+}$  concentrations were observed in all samples of *reducing wetland water* and linked to low redox potentials. These elements were added to the solution during the reduction of iron- and manganese-(hydr)oxides. While highest amounts of  $\text{Mn}^{2+}$  in water were found below 225 mV, redox potential of samples with high  $\text{Fe}^{2+}$  concentrations were higher than the given threshold of 100 mV (Mitsch and

Gosselink 2007). However, determination of redox potentials in the field is difficult and values should always be regarded with caution (Appelo and Postma 2005).

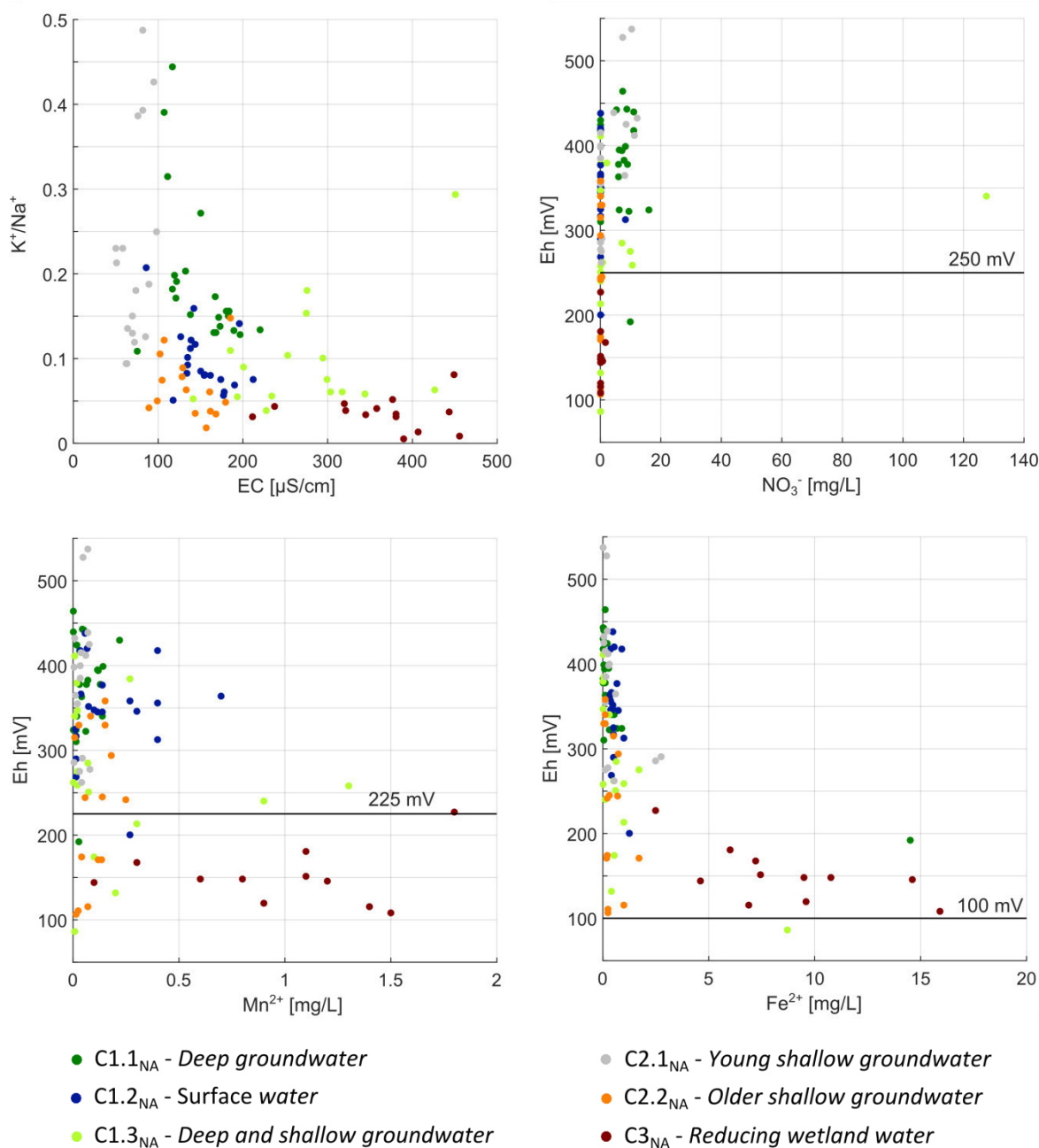
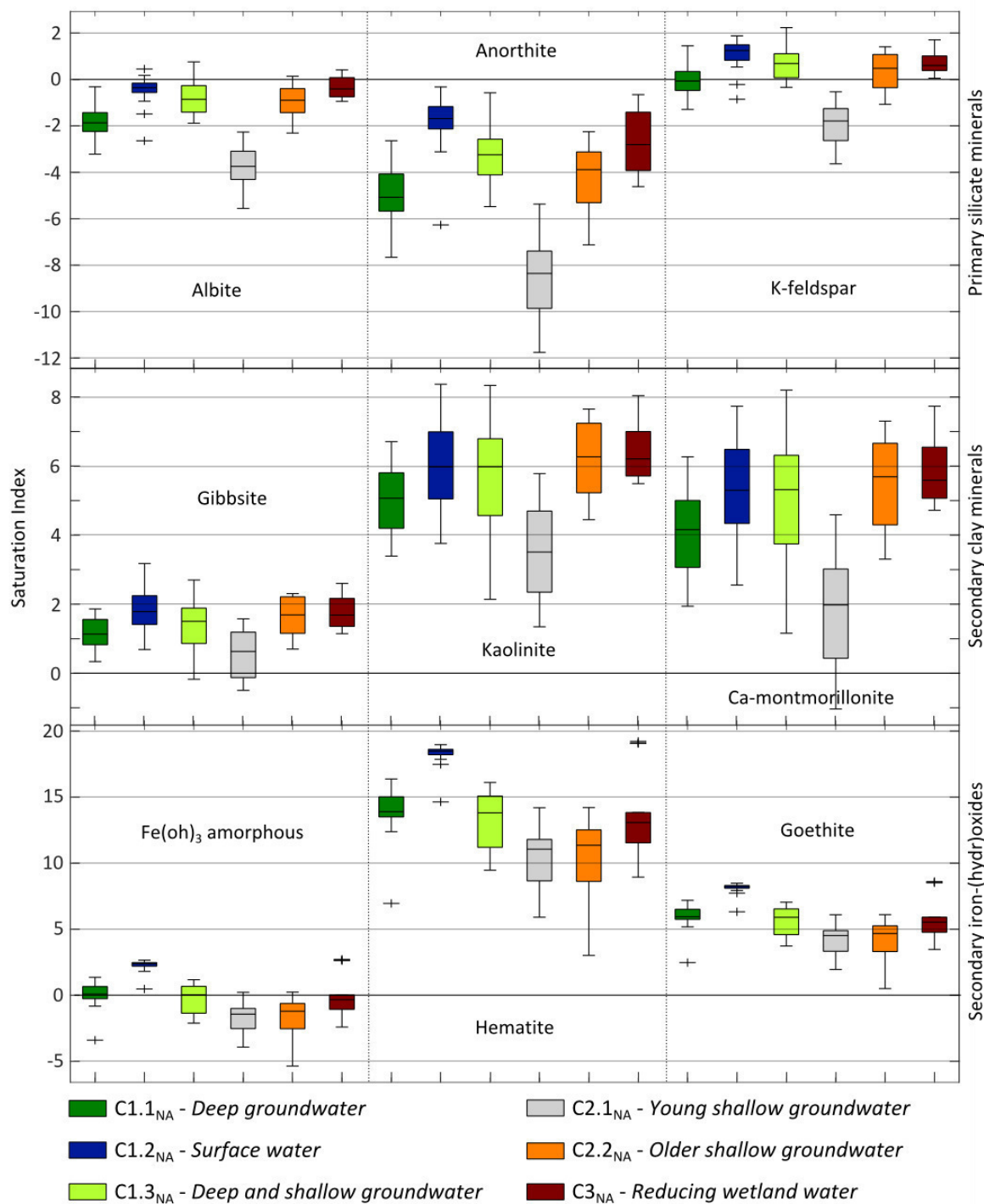


Fig. 7.29: Selected ratios of different hydrochemical parameters for the six sub-cluster groups. Redox potential needed for transformation processes are illustrated as lines (NA).

Water samples were subsaturated to saturated with respect to albite and subsaturated with respect to anorthite (Fig. 7.30). In terms of k-feldspar, saturation to supersaturation was observed. In general, *young shallow groundwater* showed lowest saturation indices followed by *deep groundwater*, confirming the lowest degree of weathering in this sub-cluster groups. All water samples were saturated to supersaturated with respect to secondary clay minerals and most iron-(hydr)oxides (Fig. 7.30). *Young shallow groundwater* had lowest saturation indices for all secondary clay minerals. In terms of iron-(hydr)oxides, *surface water* showed highest saturation indices due to higher pH-values and thus lower solubility of iron (Appelo and Postma 2005).



**Fig. 7.30:** Distribution of saturation indices of primary silicate minerals (feldspars), secondary clay minerals, and secondary iron (hydr)oxides for the six sub-cluster groups (NA).

In terms of plagioclase weathering, *young shallow groundwater* and *deep groundwater*, showed stability of kaolinite, while the other sub-cluster groups showed stability of montmorillonite (Fig. 7.31). Kaolinite was stable in all sub-cluster groups regarding k-feldspar dissolution.

It became obvious that all water samples are strongly influenced by silicate weathering. While feldspars and micas are dissolved, kaolinite, montmorillonite, and iron-(hydr)oxides precipitate (section 6.3.1.6). Although climatic conditions are tropical, montmorillonite is stable in most water samples, indicating prolonged residence times and increased mineralization of water. In contrast, the low saturation state and the stability of kaolinite in *young shallow groundwater* confirm the assumption that these samples

represent recently infiltrated precipitation. The stability of montmorillonite for most sub-cluster groups explains the low  $\text{SiO}_2/\text{Na}^+$  ratios of those groups. If montmorillonite is precipitated instead of kaolinite, more  $\text{SiO}_2$  is retained in the solid phase (Appelo and Postma 2005). Consequently, resulting specific ion ratios in the solution are lower.

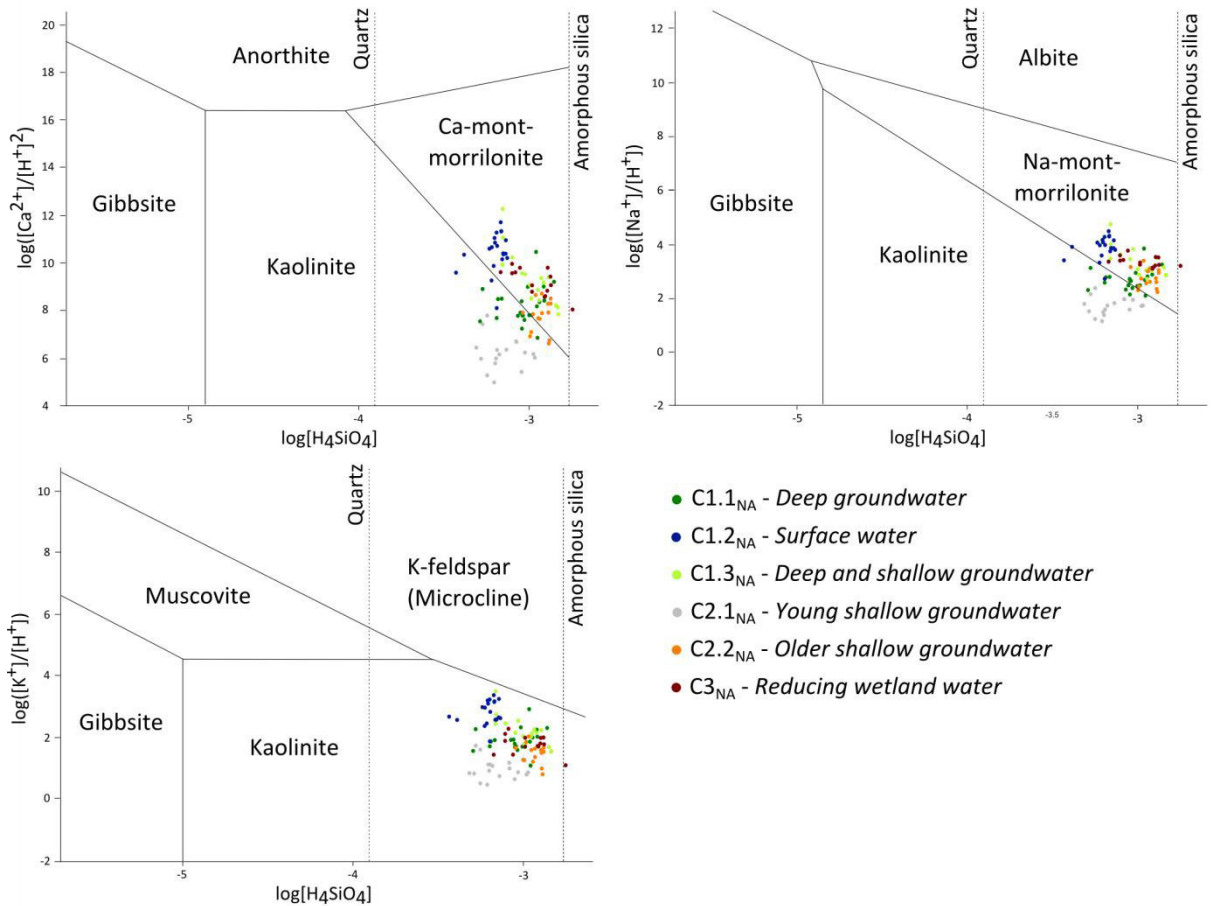


**Fig. 7.31:** Stability diagrams of anorthite, albite, k-feldspar (microcline), and their respective weathering products for the six sub-cluster groups (following Tardy 1971) (NA).

### 7.3.2 Stable water isotopes (NA)

Stable water isotopes in precipitation ranged between  $-8.4$  and  $4.1$  ‰ for  $\delta^{18}\text{O}$  and between  $-55.5$  and  $39.9$  ‰ for  $\delta^2\text{H}$ . The fitted  $\text{LMWL}_{\text{NA}}$  revealed an equation of  $\delta^2\text{H} = 7.0 \times \delta^{18}\text{O} + 9.8$ , being close to the GMWL (Fig. 7.32 a). Temporal variations of isotopic signatures in precipitation showed an influence of the amount effect (Fig. 7.33). Months with high precipitation amounts were more depleted in  $\delta^{18}\text{O}$  than those with small precipitation amounts. This effect was already described for precipitation in tropical regions in general (Jasechko and Taylor 2015), and for precipitation in Uganda in particular (Taylor and Howard 1996). Weighted averages of  $\delta^{18}\text{O}$ ,  $\delta^2\text{H}$ , and d-excess in precipitation for the measuring period were  $-1.7$  ‰,  $-1.7$  ‰, and  $12.0$ .

Almost all water samples of snapshot samplings plot around the  $\text{LMWL}_{\text{NA}}$  (Fig. 7.32 b).  $\delta^{18}\text{O}$  values of deep groundwater ranged between  $-2.9$  and  $-1.9$  ‰, being more depleted than the weighted average of precipitation. This indicates that groundwater recharge mainly occurs from heavy rainfall events, as already described for other tropical regions (Jasechko and Taylor 2015). Values between  $-2.6$  and  $-1.5$  ‰ of shallow groundwater indicate additional recharge by precipitation of rainfall events with smaller amounts. Nevertheless, differences between shallow and deep groundwater were small and some samples showed similar values.

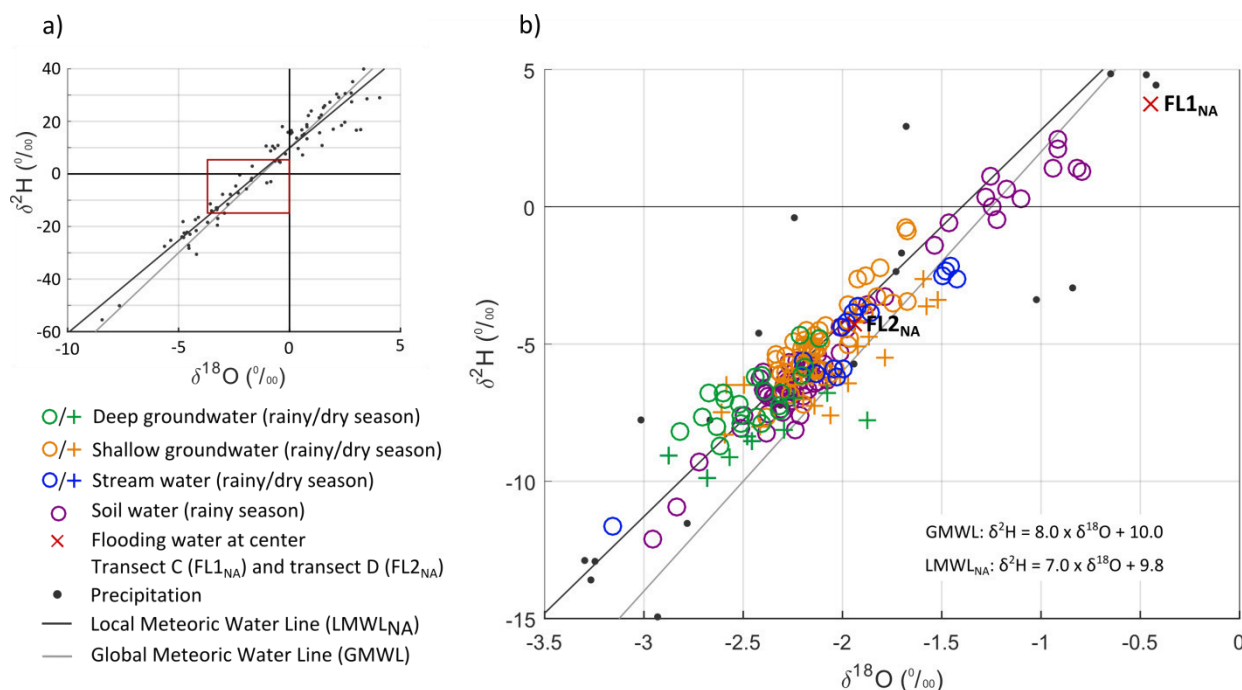


Fig. 7.32: Scatterplot of  $\delta^2\text{H}$  against  $\delta^{18}\text{O}$  for a) precipitation samples and b) deep and shallow groundwater, soil water, stream water, and flooding water (NA).

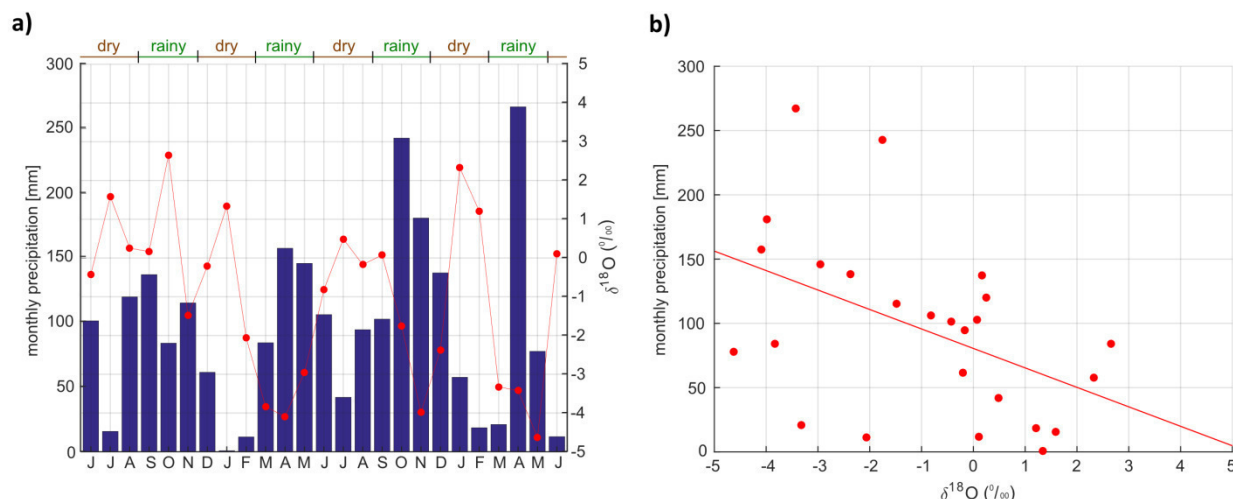
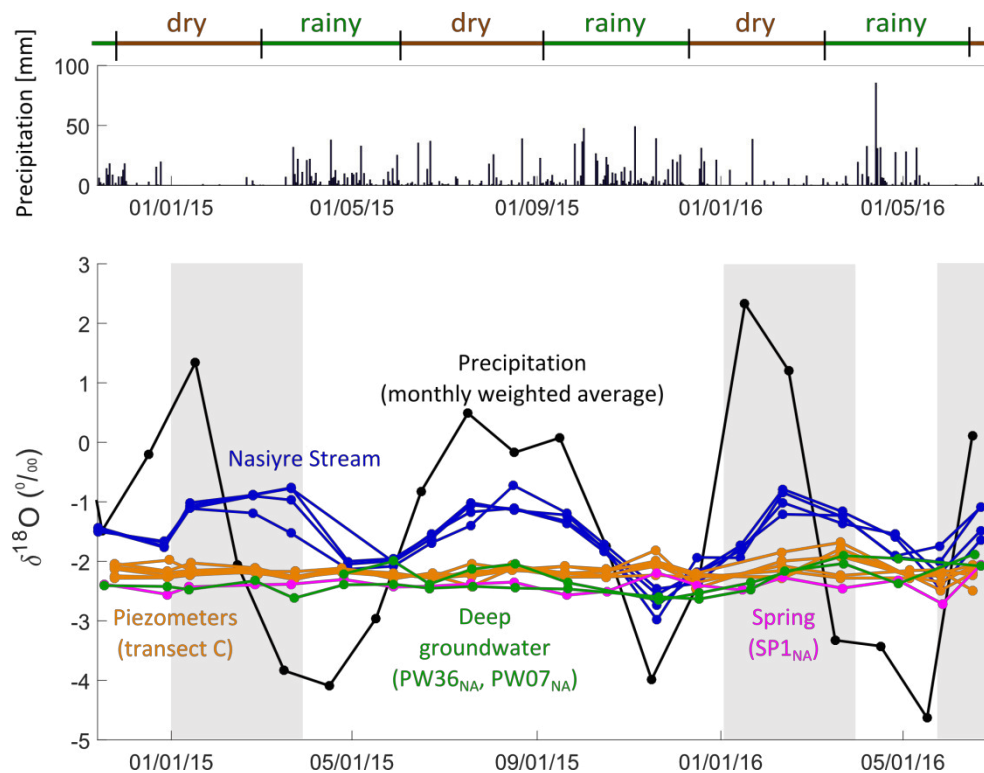


Fig. 7.33: Monthly weighted averages of  $\delta^{18}\text{O}$  in precipitation (red points) and monthly amount of precipitation (blue bars) as a) time series (June 2014 to June 2016), and b) correlation graph (NA).

Monthly samples of shallow and deep groundwater showed no temporal variability (Fig. 7.34). During infiltration and percolation through the unsaturated zone, mixing of infiltrated water occurs, due to the coexistence of slow and fast pathways. This mixing smoothes out the seasonal variations of precipitation during groundwater recharge (Clark and Fritz 1997). Even the spring, which is assumed to represent recently infiltrated precipitation, did not show any temporal variation. This indicates long transit times of spring water and high dispersivities within the unsaturated zone. Absolutely, spring water showed similar isotopic compositions to deep groundwater, suggesting either the same recharge processes for both waters or spring discharge originating from deep groundwater.



**Fig. 7.34:** Time series of  $\delta^{18}\text{O}$  for monthly weighted averages of precipitation, monthly samples of shallow (piezometers, spring) and deep groundwater, and monthly samples of stream water. Daily precipitation is shown and rainy and dry seasons are marked above. Periods with very little precipitation are shaded in grey (NA).

Isotopic composition of stream water showed a higher temporal than spatial variability, as already observed in hydrochemical composition (Fig. 7.34). A seasonal variation in isotopic composition was observed following the same trend as precipitation, but displaying lower amplitudes. This indicates an input of precipitation to stream water. Lower amplitudes in stream water can be explained by the mixing of precipitation in the stream and by a constant input of groundwater, which showed stable isotopic compositions throughout the year (Fig. 7.34). The reflection of seasonal variations of precipitation in stream water is often time shifted, due to transit times of surface and sub-surface runoff derived from precipitation (McGuire and McDonnell 2006). This time shift seemed to be small for Nasiryre Stream. A shift of peaks between stream water and precipitation of more than one month was solely observed in spring 2015. All other peaks of stream water lied close to the peaks of precipitation. This was confirmed based on field observations. After rainfall events, the stream level started rising quickly. Assuming small time shifts, precipitation input to the stream can only occur, when it actually rains. The periods from January to March of both years as well as June and July 2016 where very dry, with only little precipitation. In these periods, an input of precipitation to the stream is unlikely. The increase in heavy isotopes during these time frames can rather be explained by evaporation, as indicated by lower d-excess values (Fig. 7.35).

Soil water plots near shallow groundwater (Fig. 7.32 b). However, some soil water samples were even more enriched in heavy isotopes. The more enriched soil water samples were all taken in autumn 2015, while the more depleted ones were taken in spring 2015. These differences coincide with differences in precipitation fallen before sampling, demonstrating precipitation as the major source of soil water. Surprisingly, no evaporation effects were observed in soil water. In contrast, evaporation effects were observed in flooding water at transect C (Fig. 7.32 b: FL1<sub>NA</sub>). Flooding water at transect D (FL2<sub>NA</sub>) showed similar isotopic compositions to stream water and no evaporation, indicating over-bank flow of stream water as the major source of flooding water.

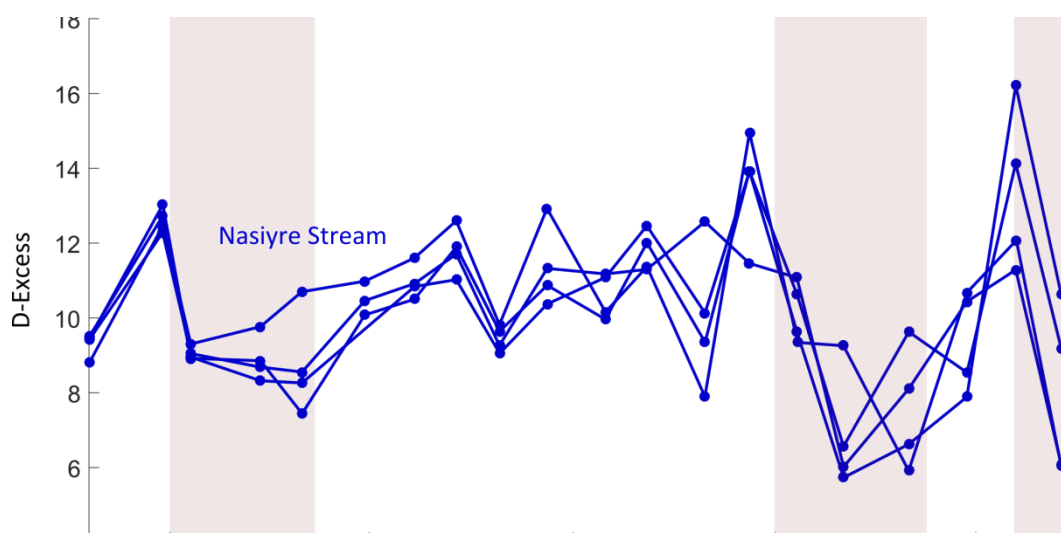


Fig. 7.35: Time series of the D-Excess for monthly samples of stream water. Periods with very little precipitation are shaded in grey (NA).

### 7.3.3 Water quality (NA)

Water quality with regard to human health, acceptability, and irrigation purposes was evaluated based on the snapshot samplings. Additionally, the influences of different agricultural management options on soil water quality were investigated, based on indicator ions of fertilizer input.

#### 7.3.3.1 Water quality related to human health (NA)

The main source of drinking water in the study site is deep groundwater of the crystalline rocks and weathering profile aquifer derived from pumping wells. Moreover, shallow groundwater of the weathering profile, discharging as man-made springs, is used as drinking water.

In general, only few samples exceeded health related guideline values of WHO (2011). Only  $\text{NO}_3^-$ ,  $\text{NO}_2^-$ ,  $\text{Mn}^{2+}$ , and  $\text{F}^-$  showed concentrations above the respective guideline values (Fig. 7.36). Solely one deep groundwater sample displayed a  $\text{NO}_3^-$  concentration of 127.6 mg/L, exceeding the guideline value of 50 mg/L. This sample was taken from a pumping well located in the northcentral catchment. However, this well was only sampled once (PW40<sub>NA</sub>). 36 of the remaining 103 samples showed detectable  $\text{NO}_3^-$  concentrations up to 16 mg/L. These were mainly deep groundwater samples from pumping wells and shallow groundwater samples from springs. Only nine shallow groundwater samples of the valley sediments showed detectable  $\text{NO}_3^-$  concentrations. However, these concentrations were usually below 1 mg/L.  $\text{NO}_2^-$  concentrations were detected in six samples. One deep groundwater sample exceeded the guideline value of 3 mg/L, with a concentration of 8.9 mg/L (PW37<sub>NA</sub>).

$\text{Mn}^{2+}$  was detected in almost all samples. The health related guideline value of  $\text{Mn}^{2+}$  was exceeded in 14 samples, with most of them representing shallow groundwater and soil water of the valley sediments (Fig. 7.36). Although  $\text{Al}^{3+}$  was detected in 90 samples, the guideline value was never exceeded. Furthermore, all concentrations of trace heavy metals were far below the guideline values.  $\text{F}^-$  concentrations exceeding the guideline value were observed in two samples. However, these concentrations need to be regarded with caution, due to high analytical errors (section 6.3.3.1).

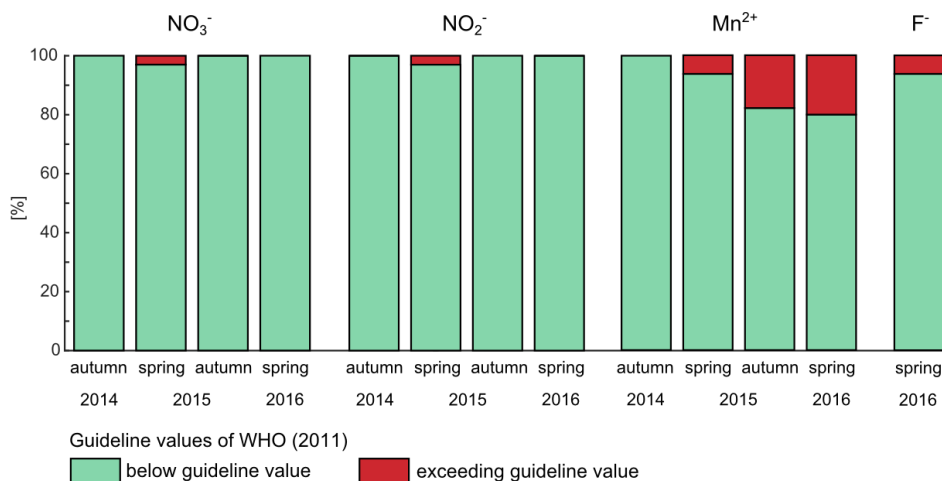


**Fig. 7.36:** Stacked bar charts of the percentage amount of all samples exceeding the guideline values (WHO 2011) of nitrate (NO<sub>3</sub><sup>-</sup>), nitrite (NO<sub>2</sub><sup>-</sup>), and manganese (Mn<sup>2+</sup>) for the four snapshot samplings, and of fluoride (F<sup>-</sup>) for spring 2016 (IF).

It is striking that NO<sub>3</sub><sup>-</sup> concentrations were highest in deep groundwater samples, because this water is the major source of drinking water in the study site. However, not all sampled pumping wells showed detectable NO<sub>3</sub><sup>-</sup> concentrations, and measured concentrations were far below the guideline value except for one sample. NO<sub>3</sub><sup>-</sup> concentrations might have been derived by groundwater recharge from agricultural fields, found all over the study site. In contrast, this is not true for agricultural fields within the wetland. NO<sub>3</sub><sup>-</sup> concentrations of shallow groundwater in the valley sediments were usually below the LOD. This can be explained by the prevention of groundwater recharge in the wetland area, due to the impermeable clay layer.

Monthly sampling of spring and deep groundwater showed remarkable variations in NO<sub>3</sub><sup>-</sup> concentrations throughout the year (Fig. 7.37). NO<sub>3</sub><sup>-</sup> concentrations in spring water were highest after periods of heavy rainfall (e.g. end of 2015) and lowest after periods of no or only little rainfall (e.g. beginning of 2015). This indicates that NO<sub>3</sub><sup>-</sup>, applied to fields on hilltops and slopes by fertilizer, is leached during direct recharge. This NO<sub>3</sub><sup>-</sup> enriched water either discharges as springs or percolates to deep groundwater. Wells without detectable NO<sub>3</sub><sup>-</sup> concentrations (e.g. PW36<sub>NA</sub>) might either be deeper than the others, or NO<sub>3</sub><sup>-</sup> leaching is prevented by impermeable parts of the weathering profile below agricultural fields.

The exceeding Mn<sup>2+</sup> concentrations are not of big concern in terms of drinking water, as they were mainly found in shallow groundwater and soil water of the valley sediments. These waters are usually not used as drinking water. As high Mn<sup>2+</sup> concentrations were related to low redox potentials (Fig. 7.29 p.142), it is assumed that redox processes within the wetland are the source of Mn<sup>2+</sup> in water. This demonstrates that shallow groundwater below the wetland should not be used as drinking water. Deep groundwater showing oxidizing conditions was not contaminated with Mn<sup>2+</sup>.

The DHWQ for all pumping wells was either 0 or 1, highlighting the generally good water quality of deep groundwater (Fig. 7.38). However, it is recommended not to feed infants with the groundwater, in order to avoid methaemoglobinaemia. It should be considered that some samples of soil water and shallow groundwater within the wetland were contaminated with Mn<sup>2+</sup> and should thus not be used as drinking water. The same is temporary true for stream water.



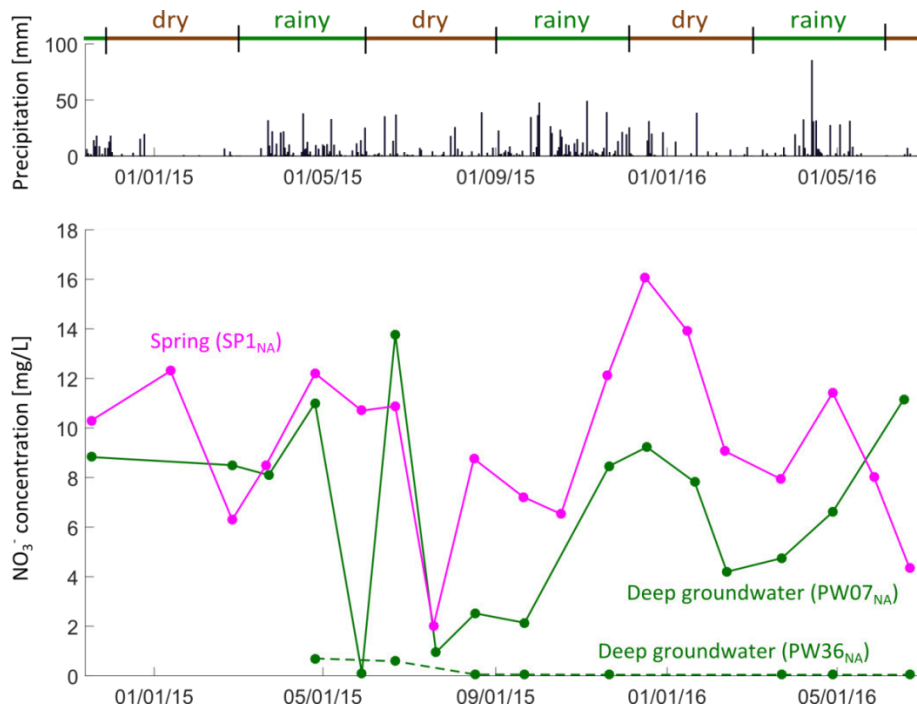


Fig. 7.37: Time series of nitrate (NO<sub>3</sub><sup>-</sup>) concentrations for spring water (SP1<sub>NA</sub>) and deep groundwater (PW07<sub>NA</sub>, PW36<sub>NA</sub>). Daily precipitation is shown and rainy and dry seasons are marked (NA).

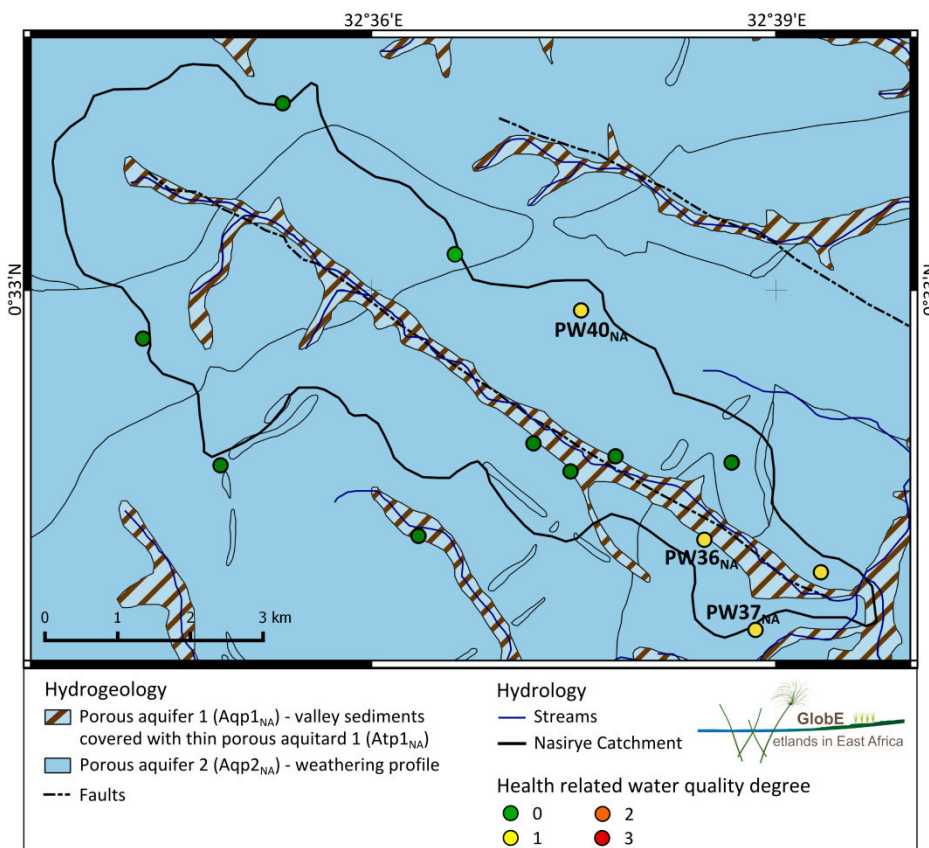


Fig. 7.38: Groundwater quality related to human health displayed as Degree of Health related Water Quality (DHWQ). Drinking water quality decreases from 0 (no guideline value exceeded) to 3 (guideline values of three constituents exceeded). Data sources: GTK Consortium (2012) (geology, streams), Heiß (2016) (alluvium), Gabiri (unpublished) (Nasirye Stream) (NA).

### 7.3.3.2 Water quality related to public acceptability aspects (NA)

Water for domestic purposes is withdrawn from pumping wells, streams, and springs. The taste thresholds for TDS,  $\text{Cl}^-$ ,  $\text{Na}^+$ ,  $\text{SO}_4^{2-}$ , and Zn were never exceeded. However, the acceptability threshold for  $\text{Mn}^{2+}$  was exceeded in 43 samples. All types of water showed such enriched  $\text{Mn}^{2+}$  concentrations. Even more samples exceeded the threshold for  $\text{Fe}^{2+}$  (61 samples). Five samples exceeded the threshold for  $\text{Al}^{3+}$ , with four samples of stream water and one shallow groundwater sample of a piezometer. The contamination with  $\text{Mn}^{2+}$ ,  $\text{Fe}^{2+}$ , and  $\text{Al}^{3+}$  leads to degradations of taste and a discoloration of the water. Most deep groundwater samples displayed pH values below the acceptability range (6.5-8.5). The acidic character of groundwater may lead to pipe corrosion in the wells. Personal communication with local communities revealed that installed plastic pipes were often destroyed by corrosion. Therefore, they were replaced by steal pipes during the last years. Since that time, pumped water showed a brown color in the morning after pumping starts. After some time, the water becomes clear again. This indicates the corrosion of steal pipes and the release of rust particles to water.

In terms of public acceptability, water showed severe problems in terms of discoloration and pipe corrosion. This leads to disacceptance in the population, and, in some cases, to dysfunctionalities of pumping wells.

### 7.3.3.3 Water quality related to irrigation purposes (NA)

All samples showed no restriction on use in terms of salinity (Fig. 7.39). In contrast, most samples showed severe restrictions on use regarding infiltration. The few samples that showed moderate restriction on use were deep and shallow groundwater or soil water samples. All stream water samples showed severe restrictions on use. Nevertheless, stream water is used for irrigation within the study site. Farmers divert the stream during dry seasons to bring water to the fields. This irrigation may lead to a reduction of the infiltration capacity of the soil. Thus, on a long term, the wetland soil might be altered by irrigation water, leading to worse conditions of agricultural production.

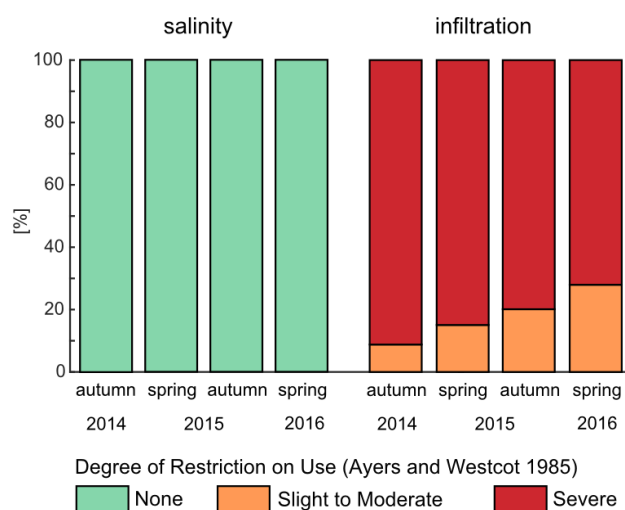


Fig. 7.39: Stacked bar charts of the percentage amount of all samples showing Degrees of Restriction on Use (Ayers and Westcot 1985) related to salinity and infiltration for the four snapshot samplings (NA).

### 7.3.3.4 Effects of agricultural management options on water quality (NA)

Water quality in terms of different agricultural management options was evaluated based on soil water, extracted from different treatment plots. Inorganic fertilizer consisting of Urea-N (46% N), triple superphosphate (45%  $\text{P}_2\text{O}_5$ ), and potash (61%  $\text{K}_2\text{O}$ ) was applied to rice in treatment plots T09 (personal com-

munication with K. Grotelüschen 2015). These fertilizers contain the nutrients N, P, and K as well as the elements Ca, Cl, and S (sdnotill.com). Plots of T10 were fertilized with green manure, including chicken manure.

Samples taken from the four different treatment plots were compared regarding their  $\text{NO}_3^-$ ,  $\text{PO}_4^{3-}$ ,  $\text{K}^+$ ,  $\text{Cl}^-$ , and  $\text{SO}_4^{2-}$  concentrations.  $\text{NO}_3^-$  was solely detected in one sample from T01 in autumn 2015 before fertilization. However, this concentration amounted only 0.2 mg/L. Thus,  $\text{NO}_3^-$ , applied by inorganic and organic fertilizer is probably taken up by crops completely. Furthermore, denitrification is likely to occur in the wetland soil, due to reducing conditions. Denitrification was also indicated to occur in the treatment plots by measurements of gaseous  $\text{N}_2\text{O}$  fluxes (Wagner unpublished).

In terms of  $\text{PO}_4^{3-}$ ,  $\text{K}^+$ , and  $\text{Cl}^-$ , Kruskal Wallis tests revealed no significant differences between the four different treatment plots (Fig. 7.40). For  $\text{SO}_4^{2-}$ , a difference was observed with higher concentrations in T10 compared to T02 and T09. Thus, it is concluded that different management options referring to the four treatment plots did not influence soil water quality significantly. An exception is given for  $\text{SO}_4^{2-}$ . Its enrichment in T10 plots, where green manure was applied, can be explained by sulfur contained in the manure. As sulfur deficiency is known to be a major constraint on agricultural production in tropical soils, the enrichment due to organic manure is beneficial. This was already described as maintaining adequate soil sulfur reserves (Reddy et al. 2002).

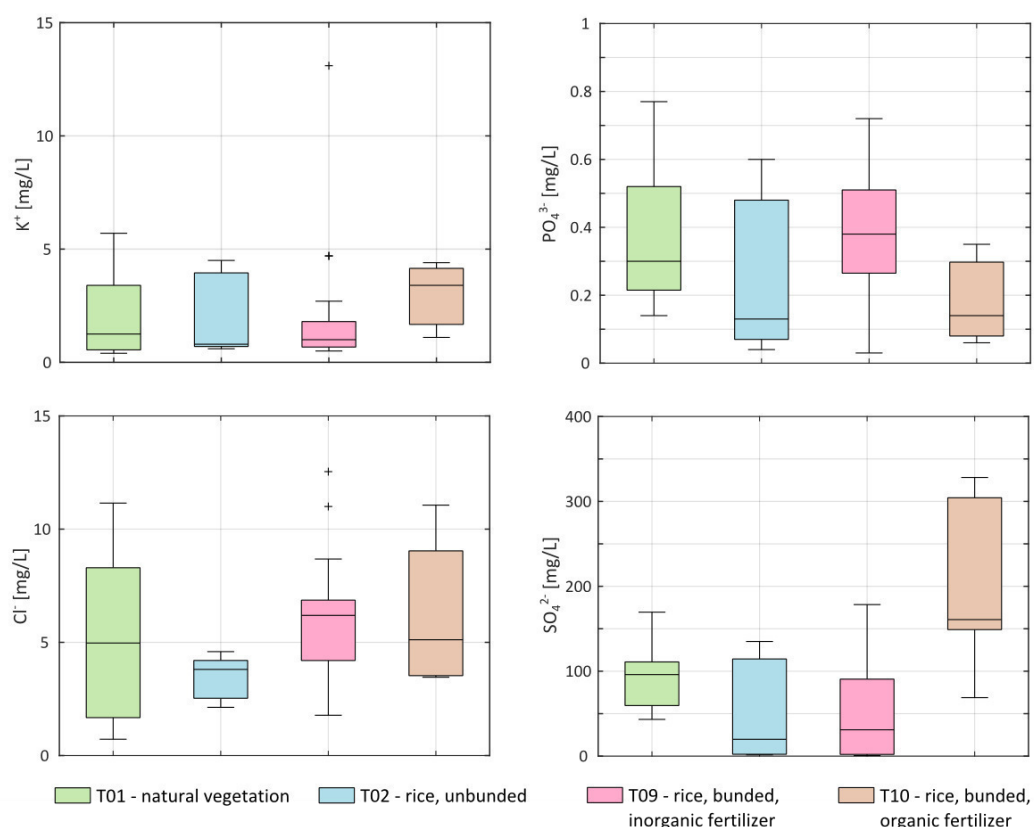


**Fig. 7.40: Concentrations of four indicator ions of fertilizer application, potassium ( $\text{K}^+$ ), phosphate ( $\text{PO}_4^{3-}$ ), chloride ( $\text{Cl}^-$ ), and sulfate ( $\text{SO}_4^{2-}$ ) in soil water samples extracted from the four different treatment plots (NA).**

Soil water in treatment plot T09 was sampled three days before and after fertilization, and analyzed for  $\text{NO}_3^-$ ,  $\text{K}^+$ ,  $\text{Cl}^-$ , and  $\text{SO}_4^{2-}$ . According to the sign-test, no significant differences were observed in samples before and after fertilization with respect to these ions. This might be explained by several reasons. Firstly, nutrients might have been taken up by the rice plants completely, three days after the input of fertilizer. Secondly, soil water was sampled from 20 and 50 cm depths. Due to the low hydraulic conduc-

tivity of the soil, nutrients applied with fertilization might have not reached the suction cups in 20 and 50 cm depths during sampling.

### 7.4 Conceptual model (NA)

The gained results described and discussed above were summarized in a hydrogeological conceptual model (Fig. 7.41). This model visualizes and outlines the hydrogeological setting and processes of the study site on two scales, a) the catchment scale and b) the wetland scale. For both scales, a schematic cross section of the lower catchment from southwest to northeast was developed as a base for the model.

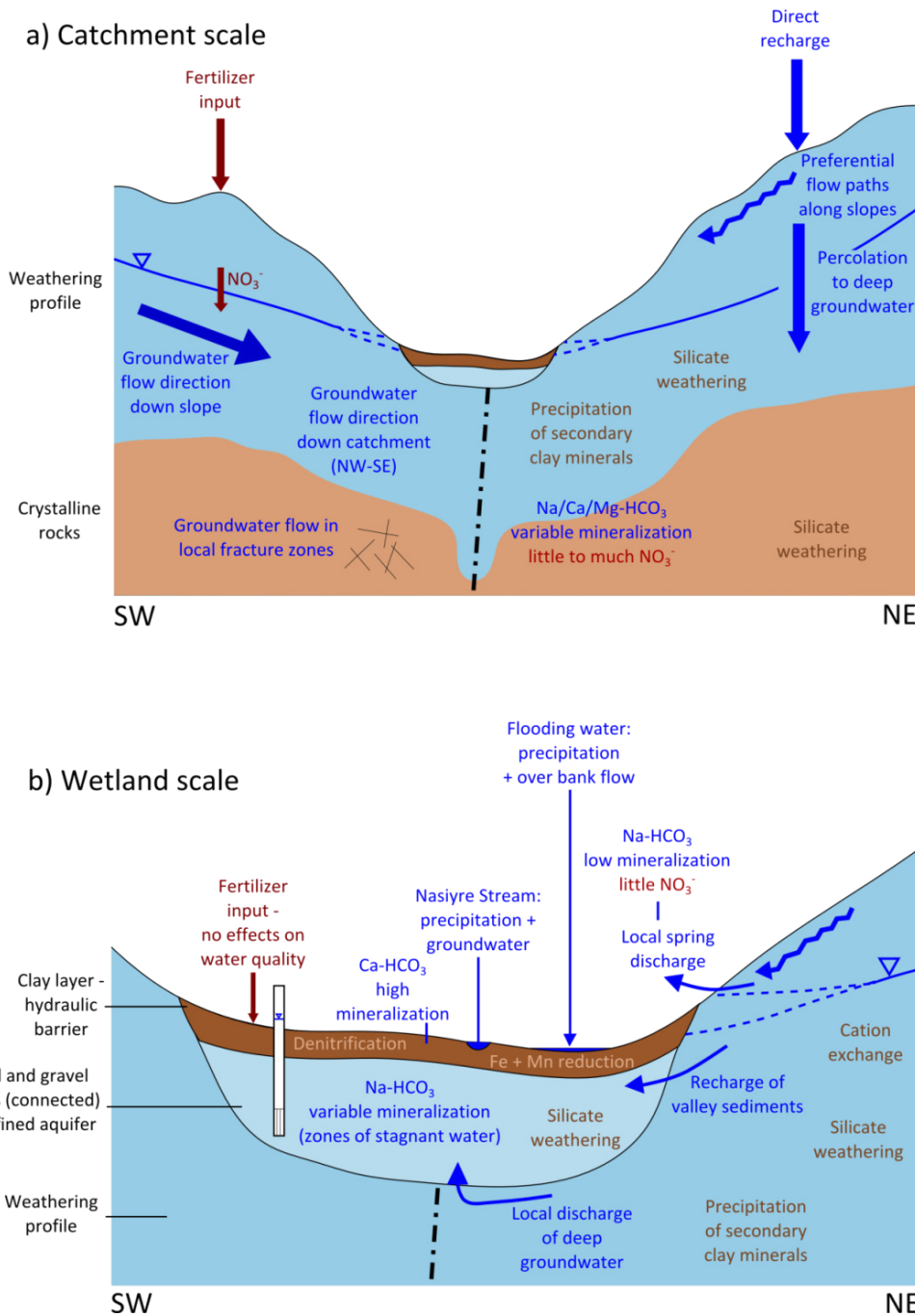


Fig. 7.41: Conceptual hydrogeological model of the Namulonge study site on a) catchment scale and b) wetland scale. Hydrostratigraphic units are colored according to Figure 7.1 (p.112). Water fluxes and compositions are displayed in blue, while hydrochemical processes are displayed in brown. Red texts refer to anthropogenic influences (NA).

#### 7.4.1 Groundwater flow paths (NA)

A regional and a local aquifer coexist in the study site. High spatial heterogeneities of hydraulic conductivity in both aquifers indicate that groundwater flow paths and velocities are spatially variable on all scales (Fig. 7.1 p.112). Regional groundwater flow occurs in the aquifer composed of weathering profile and crystalline rocks (Fig. 7.41 a). The latter one was classified as an aquitard, but acts as an aquifer locally due to fracture networks. This aquitard is hydraulically connected to the weathering profile aquifer (Chilton and Foster 1995). Hydraulic heads of these two units showed a groundwater flow direction from northwest to southeast on a large scale and from hilltops to valleys on a smaller scale (Fig. 7.11 p.124). The regional aquifer is semi-confined, because its upper parts contain a remarkable amount of clay minerals (Fig. 7.2 p. 115).

Local groundwater flow occurs in the valley sediments aquifer, covering the wetland (Fig. 7.41 b). Here, groundwater flows from upper to lower catchment, from northwest to southeast, and from the slopes to the center of the valley as well. The valley sediments aquifer shows confined conditions with artesian character during rainy seasons (Fig. 7.13 p.127).

Based on drilling log data, it was not possible to determine potential hydraulic connections between the weathering profile and the valley sediments. Saprolite was only reached during drilling at the slopes. Within the valley bottom, the gravel layers of valley sediments were too stoney, to be crossed during drilling. As the upper parts of the saprolite are of low hydraulic conductivity, no strong exchange processes are assumed to occur between the two aquifers. Nevertheless, there are parts of the upper saprolite, which are more permeable, showing channels of rapid flow (Wright 1992). These preferential flow paths are probably enhanced along faults zones (McFarlane 1992). Piezometric data of the valley sediments showed the same flow pattern as observed in the regional aquifer. This indicates a hydraulic connection between the two aquifers on catchment scale. Groundwater levels of the regional aquifer were lower than one meter below surface in the valley bottoms, showing a vertical pressure gradient towards the valley sediments. This emphasizes that deep groundwater discharges to shallow groundwater, where hydraulic conductivities of the upper saprolite are high enough to allow water flow. Regarding hydrochemistry, no clear differentiation was given between groundwater of the regional aquifer and the local aquifer. Some shallow groundwater samples from piezometers of transects A and D fell within the same sub-cluster group as deep groundwater from the regional aquifer (*deep and shallow groundwater*). However, a difference was observed between shallow groundwater from piezometers at transect C and deep groundwater. Thus, exchange processes between groundwater of the regional and the local aquifer are assumed to occur locally (Fig. 7.41 b).

#### 7.4.2 Hydrochemical evolution (NA)

Specific ion ratios and saturation indices confirmed silicate weathering as the major source of mineralization for all water samples. HCA and PCA showed that all groups of water samples were similar in their hydrochemical composition, indicating similar hydrochemical evolution of all samples (Fig. 7.26 p.138). In general, saturation indices and stability diagrams showed that feldspars are dissolved, and the clay minerals kaolinite and montmorillonite, as well as the iron-oxide hematite are precipitated (Fig. 7.30 p.143, Fig. 7.31 p.144). However, the major clay mineral in the weathering profile as well as in the valley sediments was kaolinite and only very little montmorillonite was found (Fig. 7.2 p.115, e.g. Fig. 7.3 p.117). This indicates a predominant precipitation of kaolinite. Although the climate is tropical, gibbsite was not stable in any water sample, contradicting theoretical precipitation patterns of clay minerals (Appelo and Postma 2005). However, considering the relatively low hydraulic conductivity of the weath-

ering profile, water has longer residence times compared to other tropical regions, explaining the stability of kaolinite.

Deep groundwater occurs in the crystalline rocks, made up of either unweathered granites or slates, and the weathering profile above these rocks. Granites contain anorthite, albite, k-feldspar, and biotite, and slates contain quartz and muscovite (Westerhof et al. 2014). While quartz, muscovite, and k-feldspar are resistant to chemical weathering, anorthite, albite, and biotite show a higher weatherability (Appelo and Postma 2005). In the weathering profile above crystalline rocks, more weatherable minerals, such as anorthite, albite, and biotite, are almost completely weathered and leached. This was shown in mineralogical data of the upper weathering profile. This differentiation of mineralogy was reflected in hydrochemical compositions of deep groundwater. Deep groundwater samples fell within two sub-cluster groups based on HCA. The deep groundwater samples of *deep and shallow groundwater* showed higher ECs and saturation indices of primary silicate minerals than the group *deep groundwater* (Tab. 7.5 p.139, Fig. 7.30 p.143). Furthermore, *deep and shallow groundwater* had  $Mg^{2+}$  or  $Ca^{2+}$  as the dominant cation. This fact in combination with the higher ECs of this group hints at weathering of highly weatherable minerals, such as anorthite and, to a lesser extent, biotite. Thus, these waters are assumed to be present in the unweathered granites. In contrast, *deep groundwater* is assumed to represent either the unweathered slates or the weathering profile above both, granites and slates. Higher  $K^+/Na^+$  ratios in *deep groundwater* result from k-feldspar (weathering profile granite) or muscovite (slates) weathering in the absence of albite (Fig. 7.29 p.142). However, *deep groundwater* still contained  $Na^+$ , which was confirmed to originate from plagioclase weathering based on ion ratios (Fig. 7.28 p.141). Thus, even in the weathering profile as well as in the slates small amounts of albite occur.

The shallow groundwater samples of *deep and shallow groundwater* showed more  $Na^+$  compared to the deep groundwater samples within this sub-cluster group. This dominance of  $Na^+$  might be related to cation exchange with clay minerals in the valley sediments. Univalent cations are more likely to go into solution than bivalent cations (Carroll 1959). This leads to an addition of  $Na^+$  and a removal of  $Mg^{2+}$  and  $Ca^{2+}$  in the water. Moreover, shallow groundwater samples of this sub-cluster group become mineralized due to silicate weathering in the valley sediments. Thereby, mainly k-feldspars and plagioclases are dissolved.

In general, *young shallow groundwater* revealed least prolonged hydrochemical evolution, expressed by low ECs,  $Na^+$  concentrations, and low pH values (Tab. 7.5 p.139). Hence, it was identified as recently recharged. Older shallow groundwater showed little more prolonged evolution. *Young shallow groundwater* (transect C) as well as *older shallow groundwater* (transect C) differed from shallow groundwater at the other transects (*reducing wetland water, deep and shallow groundwater*). *Young shallow groundwater* is composed of spring and *fringe* piezometer samples, and *older shallow groundwater* is composed of *middle* and *center* piezometer samples at transect C. Thus, these two sub-cluster groups represent water samples along the flow path from the spring over *fringe* to *center*. This is coincident with piezometric data. The increase in mineralization and pH from the *fringe* to the *center* of the wetland is caused by silicate weathering and flow direction. The longer the water is in the system, the more it becomes enriched in major cations and  $HCO_3^-$  and the more  $H^+$  is consumed (Appelo and Postma 2005). Furthermore,  $NO_3^-$  becomes reduced along the flow paths, indicating denitrification (Hemond and Benoit 1988).

In contrast, *reducing wetland water* composed of shallow groundwater at transects A and D as well as soil water at transect C showed highest mineralization. Highest ECs within this group and thus within all samples were observed in soil water. Evaporation as a source of higher EC in soil water was excluded

based on isotopic signatures (Fig. 7.32 p.145). Nevertheless, transpiration of plants might accumulate ions in the soil solution (Clark and Fritz 1997). However, during transpiration, ions in the solution are selectively taken up by plants (Marschner 2012). Moreover, it is concluded that soil water showed increased mineralization due to longer residence times, induced by very low hydraulic conductivities of the soil. Additionally, soil water showed high amounts of redox sensitive species, such as  $\text{Fe}^{2+}$  and  $\text{Mn}^{2+}$ , indicating redox processes under reducing conditions to be another source of mineralization.

The higher proportions of  $\text{Ca}^{2+}$  in soil water compared to all other water samples might be related to the following reasons (Fig. 7.24 p.135). Geochemical analyses of sediment and soil samples showed highest CaO contents in soil (Appendix A-A<sub>NA</sub>5). This increased CaO content might be derived by Ca added to the system with fertilizer. The common phosphorous fertilizer triple superphosphate contains considerable amounts of Ca (sdnotill.com). Moreover,  $\text{Ca}^{2+}$  in soil water might be increased, because this cation is the first to be dissolved during desilification of tropical soils (Scheffer and Schachtschabel 2010).

At transect C, where soil water was sampled, shallow groundwater showed much lower mineralizations, confirming the clay layer to act as a hydraulic barrier. In contrast, shallow groundwater at transects A and D partly fell within the same sub-cluster group as soil water (*reducing wetland water*). A connection between soil water and shallow groundwater only occurs locally, where the clay layer contains more sand and silt. In most parts of the wetland in the lower catchment, the clay layer is thick enough to prevent percolation, and shallow groundwater levels revealed confined conditions, preventing downwards directed flow. Thus, it is assumed that the higher mineralization of shallow groundwater at transects A and D was not induced by mixing with soil water. It was rather induced by prolonged dissolution of silicate minerals in stagnant zones of low permeability as well as by redox processes. High  $\text{Fe}^{2+}$  and  $\text{Mn}^{2+}$  concentrations in these samples were induced by reducing conditions derived from flooding or saturation. While piezometers at transect C were mainly screened in gravel, piezometers at transects A and D were screened in sand, inducing longer residence times. Thus, it is concluded that shallow groundwater at transects A and D shows less rapid flow velocities than at transect C. The rapid flow at transect C avoids reducing conditions and high silicate weathering rates. This outlines the high spatial variability of hydrochemical processes within and below the wetland and their strong relation to soil and sediment characteristics.

### 7.4.3 Groundwater-surface water interaction and recharge processes (NA)

Interactions between groundwater and stream water within the wetland of the lower catchment are very small. The stream bed of Nasirye Stream is made up of a nearly impermeable clay layer, preventing exchange processes between stream water and confined groundwater of the valley sediments (Fig. 7.10 p.123). From a hydrochemical point of view, stream water (*surface water*) was similar to *deep groundwater* and *deep and shallow groundwater*, indicating a connection between these water components. Isotopic composition of stream water showed an influence of groundwater, demonstrating groundwater discharge to the stream (Fig. 7.34 p.146). Furthermore, the stream was always water-bearing during the measuring period, even after periods with no rainfall. The higher pH-values in *surface water* can be explained by the exchange of discharged groundwater with air and thus the degassing of  $\text{CO}_2$ . This was confirmed by lower  $\text{CO}_2$  concentrations in *surface water* compared to *deep groundwater* and *deep and shallow groundwater* (Appendix C-C<sub>NA</sub>1). Groundwater discharge to the stream might occur in the wetland of the upper catchment, where the clay layer is sandier, and from spring discharge at the slopes of the upper catchment. However, the strongest similarity between *surface water* and *deep groundwater* indicates a contribution of deeper rather than shallow groundwater to stream water. This was already concluded for similar wetlands before (McFarlane 1989, McCartney and Neill 1999).

Monthly sampling revealed a slight dilution of stream water during rainfall events, demonstrating an additional contribution of precipitation and surface runoff to stream water (Fig. 7.17 p.130). This was confirmed by isotopic data of stream water, reflecting seasonal variations of precipitation. A constant contribution of groundwater to the stream was indicated by lower amplitudes in isotopic variation of stream water compared to precipitation. Isotopic data further showed evaporation during periods with little precipitation (Fig. 7.35 p.147). Consequently, it is concluded that stream water of Nasirye Stream originates from groundwater and precipitation, with a higher proportion of precipitation during rainy periods. During dry periods, stream water mainly originates from groundwater and becomes evaporated.

Flooding water at transects C and D was mainly derived from over-bank flow of Nasirye Stream, depicted by similar chemical and isotopic compositions to stream water (Fig. 7.16 p.129, Fig. 7.32 p.145). Moreover, stream water and flooding water at transect C fell within the same sub-cluster group (*surface water*). Flooding water at transect C indicated little evaporation effects, which were not observed at transect D (Fig. 7.32 p.145). However, flooding water at transect C showed lower EC compared to stream water, indicating an additional input of precipitation. This was confirmed by field observations, showing that flooding occurs due to the direct input of precipitation. At *fringe*, flooding even occurred due to surface runoff and spring discharge from the slopes. Here, the soil does not dry out as often as at *middle* and *center*.

The gained results confirm all four primary sources of water within the wetland that were summarized for *dambos* by Bullock (1992b) (section 3.1.2). Over-bank flow from the stream and direct precipitation were identified as sources of flooding water at *center*. Soil water in all CFTs was derived from direct precipitation as well. At *fringe*, soil water and flooding water are furthermore derived from subsurface flow and overland flow from the interfluves.

Several conclusions regarding recharge processes were gained from hydrochemical and isotopic data. Direct recharge is the major source of deep groundwater of the crystalline rocks and weathering profile. Deep groundwater showed no seasonal variation in isotopic compositions. In contrast, a strong seasonal variation, induced by the amount effect, was observed in precipitation (Fig. 7.34 p.146). This attenuation of the variation in precipitation is well known and occurs below a critical depth in most aquifers (Clark and Fritz 1997). Due to differential flow paths in the unsaturated zone, mixing of infiltrated water occurs and seasonal variations of precipitation are smoothed out. The high heterogeneity of the residual soil and the upper saprolite in the study site indicate high dispersivities of the unsaturated zone, leading to differential flow paths during recharge. In general,  $\delta^{18}\text{O}$  values of deep groundwater were lower than the weighted mean of precipitation, demonstrating that groundwater recharge mainly occurs during heavy rainfall events, which are depleted in  $\delta^{18}\text{O}$  (Fig. 7.33 p.145). This observation is consistent with general conclusions about groundwater recharge in tropical regions (Jasechko and Taylor 2015) and with other case studies in Uganda (Taylor and Howard 1996, Owor et al. 2009). Although the soil of the weathering profile was described as silty, fine sandy clay, precipitation water infiltrates along preferential flow paths of root zones or highly leached parts. In addition, the soil might be sandier in other parts of the study site. Wright (1992) stated that the collapsed zone of the saprolite, including the residual soil, is typically sandy on hilltops. Thus, major infiltration is assumed to occur on the hilltops. At the slopes, surface runoff is favoured due to relief gradient and lower permeability of the soil.

Spring water, discharging from the weathering profile aquifer, showed similar isotopic signatures to deep groundwater, with no seasonal variation. This indicates the same recharge processes for both waters. The springs discharge from sandy layers at the valley slopes near the valley bottom. These layers



might represent colluvial material that was transported down the slopes (Wright 1992). Furthermore, they could represent strongly leached parts of the saprolite (Chilton and Foster 1995). However, the exact three-dimensional distribution of these sandy parts are not known. Spring water displayed low ECs and pH values, indicating recently infiltrated precipitation. Thus, it is assumed that precipitation, which infiltrates at the hilltops, either percolates and finally recharges deep groundwater or flows along local preferential flow paths down the slopes (Fig. 7.41 b). Eventually, it discharges either as springs or flows to the valley sediments, depending on the respective connection between the sand layer and permeable parts of the valley sediments. At transect C, spring water was hydrochemically similar to shallow groundwater of the valley sediments, indicating a connection here. Accordingly, groundwater flows from *fringe* to *center*, demonstrating recharge from the slopes as well. Thus, it is concluded that the recently infiltrated precipitation flowing down the slopes recharges shallow groundwater at transect C, if it does not discharge as springs. As the valley sediments were identified to be of fluvial origin, shallow groundwater from the slopes should recharge the valley sediments, according to McFarlane (1992). However, few natural springs were observed at the transition zone between valley bottom and slopes, indicating the wetland to be a transition between the two proposed conceptual models of McFarlane (1992). Nevertheless, it is conspicuous that spring water did not show any seasonal variation in isotopic composition. This shows that subsurface flow down the slopes along preferential flow paths is not as rapid as expected. The complete attenuation of the isotopic variability of precipitation in spring water hints at long transit times and high dispersivities in the unsaturated zone. Water that flows along preferential flow paths might also become mixed with water from less permeable zones. Furthermore, the springs discharge the whole year, even after periods with no rainfall. This confirms the long transit times and hints at a storage capacity of the unsaturated zone. Thus, it is concluded that transit times of spring water are long enough to smooth out the isotopic variation. Due to the slow kinetics of silicate weathering, spring water still showed very low ECs and pH values.

Shallow groundwater within the valley sediment aquifer becomes recharged by direct recharge in the upper catchment, where the impermeable clay layer is sandier, and groundwater discharge from the slopes (spring water). Direct recharge is indicated by groundwater level responses to precipitation events. Due to piston flow, the responses induced by direct recharge in the upper catchment are reflected in groundwater levels in the lower catchment (Fig. 7.12 p.125). Isotopic composition of shallow groundwater was slightly higher compared to deep groundwater, indicating that also less heavy rainfall events induce recharge. Nevertheless, the mean  $\delta^{18}\text{O}$  value was still lower than in precipitation, showing that rainfall events with low amounts do not contribute to recharge. As groundwater level fluctuations were less conspicuous at the *fringe* compared to *middle* and *center*, a constant inflow of groundwater from the slopes is expected. This inflow was proven at transect C by hydrochemical data and groundwater flow direction. Furthermore, local discharge of deep groundwater to the valley sediment aquifer is assumed as well. No recharge occurs through the wetland floor in the lower catchment, as already described by McFarlane (1992) for a similar wetland. This was demonstrated by confined conditions of the valley sediment aquifer and completely different hydrochemistry of soil water and shallow groundwater at transect C. However, in some parts, the clay layer is sandier, allowing discharge of shallow groundwater to the wetland. This was for instance observed in one treatment plot at the CFTs, which was always wet, even if the other plots were dried out completely.

#### **7.4.4 Current mutual effects between agricultural production and water quality (NA)**

The whole Nasirye Catchment is used for small-scale agriculture and fertilizers are applied to most fields regularly (personal communication with local population 2015). Assessment of soil water quality in agri-

cultural fields within the wetland showed no influences of inorganic fertilizer application in terms of  $\text{NO}_3^-$ ,  $\text{K}^+$ ,  $\text{Cl}^-$ , and  $\text{SO}_4^{2-}$ . These indicators did not change due to the input of fertilizers, and  $\text{NO}_3^-$  was even not detected at all in soil water (Fig. 7.40 p.151). However, this might be explained by several reasons, as outlined in section 7.3.3.4.

As almost all soil water samples displayed concentrations of  $\text{NO}_3^-$  below the LOD, the wetland was identified as a  $\text{NO}_3^-$  sink. The high influence of denitrification was outlined, because almost all detected  $\text{NO}_3^-$  concentrations of water samples were related to redox potentials above 250 mV. This value represents the threshold for denitrification (Mitsch and Gosselink 2007). However, to assess the processes that lead to the absence of  $\text{NO}_3^-$  in the soil solution in detail, data regarding nitrogen concentrations and other characteristics of the soil are required. The soils of the study site are assessed by Glasner (unpublished).

According to soil water,  $\text{NO}_3^-$  concentrations were very low in shallow groundwater of the valley sediments (Tab. 7.2 p.135). Within the wetland, the clay layer prevents infiltration of contaminated water, and water purification functions, such as denitrification, improve water quality. In contrast, higher concentrations were found in deep groundwater of the crystalline rocks and weathering profile. Spring water represented by shallow groundwater of the weathering profile comprised  $\text{NO}_3^-$  as well (Fig. 7.37 p.149). This indicates that upland agriculture affects water quality more than wetland agriculture. However, both, deep groundwater and spring water, which are used as drinking water, currently showed good water quality in terms of drinking water, except for one sample. An input of  $\text{NO}_3^-$  to the valley sediments with shallow groundwater of the weathering profile is suggested in the conceptual model (Fig. 7.41). However, denitrification has removed all  $\text{NO}_3^-$  from shallow groundwater in the valley sediments.

The plant available water within the wetland is mainly flooding water and soil water. However, soils sometimes dry out completely during dry seasons. Plants with long roots might reach deep enough to reach the lower parts of the clay, which stay wet, due to the capillary rise of water from the confined aquifer below the wetland. All of these plant available water components are of good to moderate quality, in terms of salinity, indicating a good water quality for agricultural production. High  $\text{SiO}_2$  concentrations are promoting for the cultivation of rice (Scheffer and Schachtschabel 2010).

Nevertheless, irrigation with groundwater or stream water, might degrade soils, due to low ECs combined with high  $\text{Na}^+$  contents (Fig. 7.39 p.150). This degradation is related to the leaching of  $\text{Ca}^{2+}$  from the soil, which decreases the permeability of the soil and thus the amount of infiltrated water supplied to crops during irrigation. A leaching of  $\text{Ca}^{2+}$  from the soil was indicated by high  $\text{Ca}^{2+}$  concentrations of soil water. Currently, the wetland is mainly irrigated with stream water, which showed severe restrictions on use regarding infiltration.

## 7.5 Hydrochemical modeling of origin and evolution of flooding water (NA)

The conceptual model displays that flooding water, sampled in a treatment plot of the CFT at *center*, was mainly derived from over-bank flow of Nasirye Stream (Fig. 7.41 p.152). A dilution with precipitation was proposed, based on lower EC of flooding water compared to stream water. Furthermore, isotopic data showed little evaporation effects in flooding water. In order to model the origin of flooding water, stream water of Nasirye Stream and precipitation were set as initial solutions, while flooding water was set as end solution. Exchange processes with the atmosphere, such as evaporation, were implemented, by including the phases  $\text{H}_2\text{O}$  (precip),  $\text{O}_2$ , and  $\text{CO}_2$ . Mol balances were required for  $\text{Na}^+$ ,  $\text{K}^+$ ,  $\text{Mg}^{2+}$ ,  $\text{Ca}^{2+}$ ,  $\text{Cl}^-$ ,  $\text{SO}_4^{2-}$ ,  $\text{HCO}_3^-$ , and  $\text{SiO}_2$ . Uncertainties of chemical compositions were set to 20 %. Compositions of flooding water and stream water were represented by the respective water samples taken in autumn 2014.

For stream water, the sample taken before the passage through transect C was chosen. Regarding precipitation, the model was run for different parameterizations:

- 1) Sample composition of precipitation sampled short before sampling of flooding water (11/24/14)
- 2) Median composition of precipitation sampled during the whole measuring periods
- 3) Median composition of precipitation in East Africa (Rodhe et al. 1981 In Johnson 1996).

Model calculations with all parameterizations revealed that the implementation of sulfur exchange processes were necessary to gain results.

Two possible model solutions each were found for the three parameterizations (Tab. 7.7). All model results were similar. Even if real precipitation showed deviating values, results would be similar, as proven by three different parameterizations. Inverse modeling showed around 30 % precipitation and 70 % stream water as mixing proportions of flooding water (Fig. 7.42). CO<sub>2</sub>, O, and S were more or less added to the system, but never released. The addition of sulfur indicates the mineralization of organic sulfur from the wetland soil (Mitsch and Gosselink 2007). Furthermore, SO<sub>4</sub><sup>2-</sup> might have been added during diffusion processes from soil water to flooding water. Evaporation of flooding water did not occur, following the model results. However, little evaporation effects were observed in isotopic composition.

Tab. 7.7: Results of inverse modeling of the origin and hydrochemical evolution of flooding water at *center* for autumn 2014 (NA).

Precipitation solution	Proportion of precipitation [%]	Proportion of Nasirye Stream [%]	CO <sub>2</sub> phase mol transfer [mol]	O redox mol transfer [mol]	S redox mol transfer [mol]
1)	32.5	67.6	2.01E-04	9.23E-05	6.15E-05
	27.3	72.7		8.78E-05	5.85E-05
2)	32.3	67.8	1.99E-04	8.97E-05	5.98E-05
	31.4	68.6		8.91E-05	5.94E-05
3)	32.4	67.6	2.01E-04	9.11E-05	6.08E-05
	28.1	71.9	0	8.75E-05	5.83E-05



Fig. 7.42: Schematic composition and evolution of flooding water at *center* based on hydrochemical modeling (NA).

## 8 Conclusions and recommendations

The study at hand successfully developed hydrogeological conceptual models, providing the first hydrogeological characterization of the two study sites (Fig. 6.32 p.103, Fig. 7.41 p.152). Groundwater flow paths and hydrochemical evolution processes were described and discussed. The results gave insights into groundwater-surface water interactions and recharge processes in the wetlands and their surroundings. The hydrogeological setting and processes described in the models as well as their relevance for other research activities within GlobE and beyond are concluded and compared in section 8.1 (first research aim). Additionally, the scientific contribution of this study in regards to hydrogeological science is discussed. In this context, constraints regarding the assessments in terms of data scarcity issues are outlined, and recommendations are given for further hydrogeological investigations.

In addition, the study provided a sound overview of the status quo of water quality in the study sites, with respect to drinking water and agricultural use. These results are summarized, and recommendations for water users are made, in terms of drinking water and irrigation purposes in section 8.2 (second research aim). Based on the gained results, the current mutual effects between agricultural production and water quality were outlined and integrated in the conceptual models. With the backdrop of the planned intensification of food production along with population growth, the future mutual effects between agricultural production and water quality are evaluated and discussed in section 8.3 (third research aim). In this context, recommendations are made for stakeholders and scientists. In a further step, these recommendations could be transformed into policy recommendations for wetland users and planners. Finally, the two study sites are integrated into a regional context and their representativity for East African floodplains and valley bottom wetlands is outlined (section 8.4). It is discussed, how the methodology applied in this study can be transferred to other regions in East Africa.

### 8.1 Characterization of hydrogeological setting and processes

The two study sites differ strongly in their hydrogeomorphological settings. While the floodplain wetland of the Ifakara study site is located in a large catchment, the valley bottom wetland of the Namulonge study site is located in a smaller catchment. In terms of precipitation patterns, the Ifakara study site receives almost all annual rainfall during rainy season. This induces an inundation of the floodplain for several weeks or months, once a year. In contrast, rainy and dry seasons are not well marked in the Namulonge study site, and precipitation falls throughout the whole year. Thus, flooding occurs sporadically after heavy rainfall events.

Both study sites are located in Proterozoic orogenic belts surrounding the Tanzanian Craton. Crystalline rocks in both study sites are acidic in character, with higher mafic contents in the Ifakara study site. These rocks are covered with a weathering profile, acting as a porous aquifer. This weathering profile is lower in thickness in the Ifakara study site, due to tectonic activities and subsequent erosion. The wetlands themselves are both located on sediments, building an unconfined aquifer in the Ifakara study site and a confined aquifer in the Namulonge study site. Both sediments are derived from alluvial transported weathered material of crystalline rocks. However, deposition environments and sedimentological features are highly different between the two study sites.

In the Ifakara study site, groundwater flows from the mountains in the north to the alluvial sediments in the south. Finally, groundwater discharges to Kilombero River. Two groundwater flow systems coexist in the Namulonge study site, regional groundwater flow in the crystalline rocks and the weathering profile, and local groundwater flow in the valley sediments. Both aquifers showed groundwater flow directions

down the catchment and from hilltops to valley bottoms. Groundwater of the regional aquifer locally discharges upwards to the local aquifer in the Namulonge study site. Hydrochemistry at both study sites is highly imprinted by silicate weathering, expressed by generally low ECs and high contents of  $\text{HCO}_3^-$  and  $\text{SiO}_2$  (Appelo and Postma 2005). To a lesser extent, redox processes influence hydrochemistry, as already outlined for other wetlands (Mitsch and Gosselink 2007). In general, mineralization of groundwater was higher in the Ifakara study site, indicating longer residence times, which might be related to the larger size of the catchment. However, they can also be explained by a higher amount of weatherable minerals in the crystalline rocks and sediments compared to the Namulonge study site. Nevertheless, general patterns of hydrochemistry were similar in both study sites. Spatial variability of groundwater chemistry was high, but remarkable similarities between the different water components, such as groundwater and surface water, were observed.

In terms of groundwater-surface water interactions, results of this study confirmed the high spatial and temporal variability of groundwater in- and outflow patterns to wetlands (Shedlock et al. 1993, Hunt et al. 1996). In general, both wetlands are rather groundwater discharge than recharge areas. While HCA revealed a clear hydrochemical difference between groundwater and surface water in the Ifakara study site, differences were less distinct in the Namulonge study site. In both study sites, water of the main stream draining the catchment originates from groundwater discharge and precipitation. At Ifakara, groundwater discharge to the stream occurs in the study site itself as well as in the upper catchment. In contrast, at Namulonge, groundwater discharge mainly occurs in the upper catchment, while the stream is separated from the groundwater system in the wetland of the lower catchment by an almost impermeable clay layer.

Flooding water, representing one major source of water for agricultural crop production, indicated similar origins in both study sites. Different sources of flooding water were successfully quantified, using hydrochemical modeling. In the Ifakara study site, flooding water at *center* is mainly derived from over-bank flow of Kilombero River. In contrast, flooding water at *fringe* mainly originates from precipitation. Both flooding waters showed small amounts of groundwater discharge as well. Huge parts of the floodplain are assumed to be already saturated, before flooding induced by over-bank flow of Kilombero River occurs. As outlined by Mertes (1997), this saturation may be induced by precipitation, hillslope seepage, or rising groundwater levels. In the Namulonge study site, flooding water at *center* is also derived from over-bank flow. However, a remarkable amount of precipitation was detected here. No groundwater discharge to flooding water was observed.

The main recharge process in both study sites is direct recharge by precipitation. At Ifakara, direct recharge probably occurs in sediments covering the southern and central study site during rainy seasons and in the mountains north of the study site during the whole year. No indirect recharge by stream or flooding water was observed, coinciding with the proposed saturation of the floodplain prior to inundation. However, at the beginning of flooding events of Kilombero River, the hydraulic gradient becomes directed away from the river. This induces lateral river bank infiltration to floodplain groundwater (e.g. Bates et al. 2000). The hydraulic gradient inverts again after some days. Thus, the amount of water entering the aquifer is small. At Namulonge, direct recharge of the regional aquifer occurs mainly on hilltops. It was proven that only heavy rainfall events contribute significantly to recharge, as common in tropical regions (e.g. Jasechko and Taylor 2015). Infiltrated water either percolates to the regional aquifer or flows down the slopes along preferential flow paths, where it either discharges as springs or recharges groundwater of the local aquifer below the wetland. Local groundwater becomes furthermore

recharged by direct recharge and spring discharge in the upper catchment. No direct recharge occurs through the wetland, due to the clay layer that acts as a hydraulic barrier.

The developed conceptual models represent the first hydrogeological characterizations of the two study sites including the wetlands. Hence, they build the base for any further research related to groundwater in the study sites. It was proven that both studied wetlands interact with groundwater as well as with their respective catchments (e.g. von der Heyden 2004, Acreman and Miller 2007). Again, for the Namulonge study site, the theory of *dambo* wetlands to act as sponges was disproven (Bullock 1992b). It was rather shown that stream discharge during dry seasons mainly originates from deep groundwater, conforming to McFarlane (1989). A direct contribution of groundwater to the wetland was solely observed in the Ifakara study site, where flooding water originates partly from groundwater discharge. However, an indirect contribution of groundwater is present in both study sites. Stream water, which originates partly from groundwater discharge, contributes to flooding water due to over-bank flow, leading to an indirect contribution of groundwater to the wetlands.

The developed conceptual models can furthermore help to find suitable areas for crop cultivation. For instance, in the Ifakara study site, groundwater levels below surface showed lowest fluctuations and smallest depths to water table at *fringe*. Thus, the *fringe* area is maybe most suitable for crop cultivation during dry seasons, because of water availability for crops. Within GlobE, the conceptual models are used to deliver boundary conditions for numerical hydrological models (Näschen unpublished, Gabiri unpublished). Additionally, information about the hydrological regime, based on groundwater level data, can be drawn from the conceptual models. Such information is used in dynamic crop growth models (Grotelüschen unpublished).

Regarding hydrogeological science, the results of this study allowed to make progresses in the understanding of regional hydrogeological systems. It was demonstrated that combining the analyses of aquifer structure, water dynamics, and water composition is feasible to assess hydrogeological systems in data scarce regions. Several studies have already shown that combining quantity and quality assessments of groundwater provides a series of advances. For instance, interactions between groundwater and surface water were successfully identified and quantified based on water level measurements combined with environmental tracer assessments (Lamontagne et al. 2005, Su et al. 2016). King et al. (2014) outlined the importance of combining geological models with hydrochemical analysis, in order to understand hydrogeological systems. The integration of different methods was also shown to be supporting for the development of conceptual models (Girmay et al. 2015, Pétré et al. 2016). This was outlined in this study as well. The analysis of aquifer structure builds the base for the conceptual models. Flow and interaction processes were identified using an iterative process in the interpretation of groundwater level and water composition data. Groundwater levels revealed major flow directions and first implications regarding recharge processes. Hydrochemistry was very efficient for distinguishing between different aquifers, identifying groundwater-surface water interactions, and detecting anthropogenic influences. Combining hydraulic and chemical properties of aquifers and the hydrochemical composition of groundwater allowed the identification of geogenic background concentrations. Furthermore, groundwater flow paths, identified by aquifer structure and water dynamics analyses, were verified and sometimes enhanced by hydrochemistry. However, some results would have been misinterpreted without the supporting or opposing information from stable water isotopes. For instance, hydrochemistry indicated evaporation of flooding water, which was disproven by stable water isotopes. This conclusion emphasizes the importance of multiple tracer approaches, which was already outlined in other studies (Herczeg and Edmunds 2000, Oyarzún et al. 2014, Land and Timmons 2016).

In the context of a multi-methods assessment, the installation of piezometers allowed the application of methods related to all three aspects of the groundwater system. Information about aquifer structure was gained during drilling of the piezometers and from hydraulic tests at the piezometers. Groundwater dynamics were addressed by groundwater level measurements, and groundwater composition was evaluated based on water samples taken from the piezometers. Hence, the relatively low cost method of piezometer installation turned out to be highly relevant for regional studies in data scarce regions. Additionally, it was shown that literature data can help to improve the understanding of hydrogeological systems. These data are often not yet evaluated in detail, although available.

Nevertheless, the hydrogeological characterization was sometimes difficult, because several constraints appeared due to data scarcity issues. The most important constraint was the lacking knowledge of geological structures and features. The exact spatial distribution of sedimentary aquifers remains unknown in both study sites, although this information is crucial to understand groundwater-surface water interactions in wetlands (Hollands 1987). Geoelectrical methods, calibrated and verified with automatic driven drilling surveys, could help to understand the three-dimensional distribution of aquifers (Meju et al. 1999). In addition, these methods could reveal more information about the internal structures of the aquifers (Robineau et al. 2007). In order to set up numerical groundwater flow models, additional information about the spatial distribution of aquifer properties, such as hydraulic conductivities, is needed. In this context, the presented study provides a first dataset of hydraulic conductivities, which can be used as a first approximation. In terms of groundwater flow analysis, a high resolution DEM would be of strong benefit. Without detailed DEMs the hydraulic gradient and thus the groundwater flow direction could not be calculated in flat areas. An UAV survey was carried out in the context of GlobE. Collected data shall be processed to develop a high resolution DEM. However, this DEM was not available, when this study was accomplished. Longer monitoring periods of isotopes in precipitation could help to gain more information about recharge processes in the Ifakara study site. The strong difference in isotopic composition between 2014 and 2015 impeded the sound interpretation of recharge patterns. Due to the high spatial variability in hydrochemistry combined with the similarity between different water components, hydrochemical modeling was challenging. The small and highly uncertain differences in hydrochemical end-members hampered the use of hydrochemical parameters as tracers. This high spatial variability in groundwater chemistry is common in weathered silicate aquifers (Apello and Postma 2005), again emphasizing the need for multi-tracer approaches in such environments.

For further hydrogeological studies of groundwater systems in wetland areas of East Africa, the following recommendations are proposed.

- All available historical and recent literature data should be collected and interpreted.
- Field surveys should be carried out in order to fill knowledge gaps of literature and refine information. The three aspects of the groundwater system aquifer structure, water dynamics, and water composition should be addressed and interpreted iteratively.
- As much methods as possible should be applied seeking to be time and cost efficient (e.g. piezometers) focusing on multiple environmental tracers and groundwater level measurements.

## 8.2 Evaluation of status quo of water quality

Chemical groundwater quality at both study sites was comparatively good in terms of drinking water. However, in the Ifakara study site, a geogenic contamination of groundwater with  $Mn^{2+}$  was observed. Around one third of all groundwater samples showed  $Mn^{2+}$  concentrations, exceeding the guideline value of WHO (2011). In general, groundwater in the non-alluvial sediments of the northern study site

was less contaminated compared to groundwater in the alluvial sediments of the southern study site. In the Namulonge study site, elevated  $Mn^{2+}$  concentrations were mainly found in soil and shallow groundwater, which are not used as drinking water. In both study sites, only few groundwater samples showed elevated  $NO_3^-$  and  $NO_2^-$  concentrations, exceeding the guideline values of WHO (2011). In the Ifakara study site, these constituents are derived from leaching of agricultural used soils as well as from waste water discharge of Ifakara City. In the Namulonge study site, they are predominantly derived from leaching of agricultural used soils. Finally, it can be concluded that groundwater in the two study sites provides a good source of drinking water. However, in the Ifakara study site the contamination of  $Mn^{2+}$  poses health threats to the population. Furthermore,  $NO_3^-$  and  $NO_2^-$  were identified as local hazards to drinking water quality.

The input of  $Mn^{2+}$  to groundwater results from the weathering of manganese-bearing minerals and can thus not be avoided. Such elevated manganese concentrations in drinking water are found in many countries (Frisbie et al. 2012). However, within the whole Rufiji Basin, no elevated  $Mn^{2+}$  concentrations were measured so far (Ministry of Water URT 2012a). This might be explained by the low amount of groundwater samples analyzed and evaluated by Ministry of Water URT (2012a). An increased uptake of  $Mn^{2+}$  with drinking water can cause neurological symptoms as well as memory loss and cognitive problems (McMillan 1999). In terms of  $NO_3^-$  and  $NO_2^-$ , an exposure due to drinking water carries the risk of methaemoglobinaemia, hampering the transport of oxygen in the blood (WHO 2011). This risk is much higher for infants, because the amount of needed drinking water is high compared to their body weight (WHO 2011).

Considering these health effects of contaminated groundwater, it is strongly recommended to inform the local population about water quality. Elevated concentrations of  $Mn^{2+}$  should usually be detectable by taste and color of the water (WHO 2011). Water users should avoid drinking  $Mn^{2+}$  contaminated water, in order to prevent health effects, whenever an alternative is present. The most common treatment method of  $Mn^{2+}$  contaminated water is oxidization and subsequent filtration (Raveendran et al. 2001). However, these methods are not feasible in the Ifakara study site, where water users fetch their water directly from the pumping well. Water purification products, such as water guard and ceramic filters, are accessible for huge parts of the population due to relatively low costs. These products are mainly intended to remove organic contaminants of drinking water, such as bacteria. However, the chlorine contained in water guard solutions might oxidize some of the  $Mn^{2+}$ , which then might be reduced during filtering using a ceramic filter. Therefore, the introduction and sale of such water purification products is highly endorsed by the results of this study. New drinking water wells should rather be placed in the northern parts of the study sites, where  $Mn^{2+}$  concentrations are lower. Nevertheless, this raises the problem of water diversion, as most people are living in the city of Ifakara in the southern study site, outlining the need for drinking water supply there. Regarding the contamination with  $NO_3^-$  and  $NO_2^-$ , water users in both study sites should not give groundwater to infants, whenever an alternative, such as bottled water, is available, in order to avoid the risk of methaemoglobinaemia (WHO 2011). Although only few samples were contaminated with  $NO_3^-$  or  $NO_2^-$ , this precaution should be taken, if no detailed information about those constituents in the water is available.

Population should also be informed about good water quality, because information is the only way to avoid misunderstandings, leading to drastic health problems. For instance, in the Namulonge study site, people were afraid to drink groundwater with high  $Fe^{2+}$  contents, due to its characteristic brownish color. It has been reported that people rather drank surface water instead of brown colored groundwater (NEMA 2008). However, surface water is highly vulnerable to the input of organic pollutants. This con-



tamination, which is not directly visible, is more harmful to human health compared to  $\text{Fe}^{2+}$ , which only degrades taste and color of the water. In the context of this study in collaboration with the public health research group, water quality information sheets were developed, distributed, and explained to population in the Ifakara study site. It is planned to proceed in the same way in the Namulonge study site. Any further research related to water quality should include such dissemination activities.

In terms of irrigation, water in general is low in mineralization and high in  $\text{Na}^+$  content in both study sites, leading to an infiltration problem. This problem is solely induced by geogenic background concentrations of water. Soil that is irrigated with this water can become degraded due to the leaching of  $\text{Ca}^{2+}$ . This destroys the structure of the soil and thus decreases the infiltration capacity (Ayers and Westcot 1985). Hence, infiltration is hampered and the amount of crop available water decreases. If groundwater is considered as irrigation water in the Ifakara study site, an additional problem of  $\text{Mn}^{2+}$  toxicity to crops might occur. However, surface waters in both study sites sometimes showed remarkable concentrations of  $\text{Mn}^{2+}$ , too. Irrigated agriculture should be avoided, whenever it is possible. The choice of irrigation water should be made with caution, integrating water quality aspects. Moreover, proper agricultural management options are required, in order to ensure sufficient yields in irrigated fields. For instance, it is recommended to cultivate crops that are not vulnerable to high  $\text{Mn}^{2+}$  concentrations.

### **8.3 Identification of current and future mutual effects between agricultural production and water quality**

Currently, only little influence of agricultural production on water quality in terms of fertilizer application is recognizable in the two study sites. Groundwater, soil water, and surface water in the wetlands showed generally very low concentrations of nutrients, such as  $\text{NO}_3^-$  or  $\text{PO}_4^{3-}$ . The planned intensification of agricultural production in both wetlands (Paul and Steinbrecher 2013) will most probably include an increased amount of applied agrochemicals, such as fertilizers, and thus a higher potential of water contamination. In addition, in the Ifakara study site, intensification of irrigated upland agriculture is planned in the context of the SAGCOT program (ERM 2013). Considering this scenario, several conclusions can be drawn from the conceptual models, regarding future mutual effects between agricultural production and water quality. Although this study focused on inorganic chemical water quality, some of the following conclusions can also be related to other agrochemicals, such as pesticides.

In the Ifakara study site, an increased input of agrochemicals in the wetland might lead to a contamination of stream and flooding water. Flooding water is in direct contact with cultivated fields and stream water is in direct contact with flooding water. Thus, contaminants might be flushed to downstream areas, leading to an accumulation of nutrients, which might destroy ecosystems in these areas (e.g. Verhoeven et al. 2006). In terms of groundwater and thus drinking water quality, contaminated wetland water might under current conditions only have little influences. Neither stream nor flooding water contributes significantly to groundwater recharge. Therefore, it is most likely that a possible contamination of wetland water will minor affect groundwater quality. However, it remains to be tested, whether an increased abstraction of groundwater for irrigation purposes leads to a higher contribution of surface water to groundwater recharge. In this case, contamination of wetland water would also contaminate groundwater. Furthermore, direct groundwater recharge within the study site might lead to a transport of anthropogenic contaminants to the saturated zone. This is mainly true for upland agriculture, where direct recharge is not hampered by high groundwater levels. An irrigation of upland fields will even cause infiltration, percolation, and thus leaching of nutrients during dry seasons, increasing the leaching potential of nutrients and other pollutants. In addition, it is expected that a contamination of groundwater might influence flooding water and stream water, because groundwater contributes to those surface

waters. Thus, a proper management of groundwater in terms of water quality is recommended. This management should focus on waste water treatment of Ifakara City (e.g. Massoud et al. 2009).

In the Namulonge study site, an intensified agriculture in the wetland might lead to a contamination of soil and flooding water. If fertilizers are applied wisely, the wetland purification functions, including denitrification and uptake by plants or crops, are able to remove enough nutrients. This was proven by measurements of nutrients in soil water of different treatment plots. Nevertheless, long term studies are needed to confirm this snapshot information. In contrast, intensification of fertilizer input at the hilltops and slopes would lead to an increasing inflow of  $\text{NO}_3^-$  to deep groundwater. To a lesser extent,  $\text{NO}_3^-$  leached from the uplands can also enter the wetland as spring discharge or surface runoff. These processes of nitrogen transport into the wetland are assessed more in detail by Schepp (unpublished). Even if soil water in the wetland would contain remarkable amounts of contaminants, these will not percolate to shallow groundwater. This prevention of polluted water to percolate to groundwater due to low permeable wetland soils was already recognized by Hollands (1987). However, contaminated soil or flooding water might be flushed to stream water by overland flow. This might lead to an accumulation of nutrients in downstream areas. Indirect recharge in downstream areas would eventually contaminate groundwater.

It can be concluded that at the moment, water purification functions of the two assessed wetlands are in good working order and able to remove nutrients brought to the system (Fisher and Acreman 2004, Hemond and Benoit 1988). However, increased inputs of nutrients, due to waste water discharge or fertilizer input, might lead to drastic changes in the ecosystem functions, if a certain threshold is exceeded (Verhoeven et al. 2006). Further research is needed on the influence of long term exposure to increased fertilizer applications. In general, agricultural management schemes, such as the SAGCOT program in the Kilombero area (ERM 2013), should always integrate water quality monitoring systems.

The SAGCOT plan of the Kilombero region and the expected agricultural development will probably lead to population growth in the area during the next decades. In turn, Ifakara city will increasingly expand. Given the vulnerability of groundwater to waste water discharge, there is an urgent need for innovative waste water treatment concepts (e.g. WWAP 2017). This is crucial in terms of safe and clean drinking water supply as well as for the functionality of the ecosystem wetland.

Additionally, it is concluded for both wetlands that in terms of groundwater quality, upland agriculture is generally more hazardous to groundwater quality compared to wetland agriculture. However, that does not mean that wetland agriculture will not affect groundwater quality. For instance, in the Namulonge study site, the clay layer, which acts as a hydraulic barrier, should never be penetrated during digging or draining. A penetration would lead to a direct connection between wetland water (soil and flooding water) and shallow groundwater and thus to a contamination of groundwater, if wetland water is contaminated. In the Ifakara study site, increased groundwater abstraction should always be accompanied by groundwater level monitoring. A lowering of the groundwater table may lead to indirect recharge derived from flooding water of the wetland. This might induce groundwater contaminations due to contaminants in flooding water. Furthermore, surface water in the wetland is highly vulnerable to the input of agrochemicals. This surface water might lead to degradation of groundwater quality in downstream areas of the wetlands, endangering drinking water quality there. Additionally, surface water bodies might suffer from high nutrient inputs by streams as well (e.g. Verhoeven et al. 2006).

#### 8.4 Integration of the two study sites into a regional context

In order to upscale results of this study to whole East Africa, it remains to be tested, if the features and processes in the two study sites are representative for floodplains and valley bottom wetlands in East Africa, or if they only show snapshots of a wide variability. It is proposed that at least in terms of hydrochemistry, the two studied wetlands are representative for many East African wetlands. All water components in the study sites were highly imprinted by silicate weathering, due to their location in weathering profile aquifers or sedimentary aquifers derived from weathering profiles. As weathering profile aquifers stretch out through major parts of East Africa (Wright 1992, Chilton and Foster 1995), it is likely that many East African wetlands show similar hydrochemical compositions. Water imprinted by silicate weathering shows generally low mineralization, with  $\text{HCO}_3^-$  as the dominant anion. Major cations are usually distributed equally, except for  $\text{K}^+$ , and remarkable amounts of  $\text{SiO}_2$  are found. The restrictions on use due to low ECs, regarding infiltration problems during irrigation, are probably present in most wetlands of East Africa. It may be concluded that irrigation of upland agriculture with surface or groundwater from wetlands in East Africa is hazardous to soils and therefore not sustainable. Big scale irrigation schemes (ERM 2013) should be planned with caution, considering water quality aspects.

In contrast, flow and interaction processes in East African wetlands strongly depend on topography, climate, and aquifer structure. Hence, the respective results of the two study sites are only valid for other floodplain and valley bottom wetlands in East Africa with identical features. These results highlight the strong need for longer monitoring periods as well as for more case studies of wetlands in different environments. The methodology applied in this study, combining quantity and quality assessments, can be transferred to other wetland systems in East Africa or elsewhere. Piezometer installation, allowing both hydraulic and chemical groundwater investigations using many methods, is feasible in most regions with sedimentary aquifers. The hydrochemical sampling of drinking water wells is possible, whenever such wells exist and accessibility is given. In order to improve the likelihood of accessibility, transparency regarding research activities should be provided to well owners and users. Further research activities regarding hydrogeological systems below wetlands are necessary, because they could help to protect high-sensitive wetland ecosystems as well as groundwater resources, and thus ensure food and drinking water supply in a sustainable way.

## 9 References

- Acreman, M.C. & Miller, F. (2007): Hydrological impact assessment of wetlands. Proceedings of the ISGWAS Conference on Groundwater Sustainability, Spain: 225-255.
- Acres, B.D., Blair Rains, A., King, R.B., Lawton, R.M., Mitchell, A.J.B. & Rackham, L.J. (1985): African dambos: their distribution, characteristics and use. *Zeitschrift Geomorphologie*, 52: 63-86.
- Alibu, S. (unpublished): Maize production in the Namulonge inland valley; Effect of water regime and dropping intensity on crop yield and nutrient flows. PhD thesis, University of Bonn, unpublished.
- Amler, E., Schmidt, M. & Menz, G. (2015): Definitions and mapping of East African wetlands: A Review. *Remote Sensing*, 7: 5256-5282.
- Appelo, C.A.J. & Postma, D. (2005): *Geochemistry, groundwater and pollution*. 2<sup>nd</sup> edition, A.A. Balkema Publishers, Leiden, 649 p.
- Ashley, R.P. & Lloyd, J.W. (1978): An example of the use of factor analysis and cluster analysis in groundwater chemistry interpretation. *Journal of Hydrology*, 39: 355-364.
- Asiimwe, I. (2015): Effect of DEM spatial resolution on hydrologic model output uncertainty. Master thesis, Makerere University, Kampala, 78 p.
- Ayers, R.S. & Westcot, D.W. (1985): *Water quality for agriculture*. FAO Irrigation and Drainage Paper, 29 Rev.1, FAO, Rome, 97 p.
- Balek, J. & Perry, J.E. (1973): Hydrology of seasonally inundated African headwater swamps. *Journal of Hydrology*, 19: 227-249.
- Bates, P.D., Stewart, M.D., Desitter, A., Anderson, M.G. & Renaud, J.P. (2000): Numerical simulation of floodplain hydrology. *Water Resources Research*, 36(9): 2517-2529.
- Beck, A.D. (1964): The Kilombero valley of South-Central Tanganyika. *East African Geographical Review*, 2: 37-43.
- Belkhir, L., Boudoukha, A. & Mouni, L. (2011): A multivariate statistical analysis of groundwater chemistry data. *International Journal of Environmental Research*, 5(2): 537-544.
- Beuel, S., Alvarez, M., Amler, E., Behn, K., Kreye, C., Kotze, D., Leemhuis, C., Wagner, K., Willy, D.K., Ziegler, S. & Becker, M. (2016): A rapid assessment of anthropogenic disturbances in East African wetlands. *Ecological Indicators*, 67: 684-692.
- Beyer, W. (1964): Zur Bestimmung der Wasserdurchlässigkeit von Kiesen und Sanden aus der Kornverteilungskurve. *Wasserwirtschaft-Wassertechnik* 14(6): 165-168.
- Boast, R. (1990): Dambos: a review. *Progress in Physical Geography*, 14: 153-177.
- Böhlke, J.K. (2002): Groundwater recharge and agricultural contamination. *Hydrogeology Journal*, 10: 153-179.
- Bohte, R., Mul, L.M., Bogaard, T.A., Savenije, H.H.G., Uhlenbrook, S. & Kessler, T.C. (2010): Hydrograph separation and scale dependency of natural tracers in a semi-arid catchment. *Hydrology and Earth System Sciences Discussions*, 7: 1343-1372.
- Bonarius, H. (1975): *Physical properties of soils in the Kilombero Valley (Tanzania)*. German Agency for Technical Cooperation Ltd., Eschborn, 35 p.
- Bouwer, H. & Rice, R.C. (1976): A slug test for determining hydraulic conductivity of unconfined aquifers with completely or partially penetrating wells. *Water Resources Research*, 12(3): 423-428.
- Brouwer, P. (2003): *Grundlagen der Röntgenfluoreszenzanalyse. Eine Einführung*. 2. Auflage, PANalytical B.V., Almelo, 66 p.
- Brown, C.E. (1998): *Applied Multivariate Statistics in Geohydrology and Related Sciences*. Springer Verlag, Berlin, 248 p.
- Bullock, A. (1992a): The role of dambos in determining river flow regimes in Zimbabwe. *Journal of Hydrology*, 134: 349-372.
- Bullock, A. (1992b): Dambo hydrology in southern Africa – review and reassessment. *Journal of Hydrology*, 134: 373-396.
- Butturini, A., Bernal, S., Sabater, S. & Sabater, F. (2002): The influence of riparian-hyporheic zone on the hydrological responses on an intermittent stream. *Hydrology and Earth System Sciences*, 6(3): 515-525.
- Carroll, D. (1959): Ion exchange in clays and other minerals. *Geological Society of America Bulletin*, 70(6): 749-779.
- Chamley, H. (1990): *Sedimentology*. Springer-Verlag, Berlin, 258 p.

- Chapuis, R.P., Dallaire, V., Marcotte, D., Chouteau, M., Acevedo, N. & Gagnon, F. (2005): Evaluating the hydraulic conductivity at three different scales within an unconfined sand aquifer at Lachenaie, Quebec. *Canadian Geotechnical Journal* (42): 1212-1220.
- Cheng, S., Grosse, W., Karrenbrock, F. & Thoennesen, M. (2002): Efficiency of constructed wetlands in decontamination of water polluted by heavy metals. *Ecological Engineering*, 18(3): 317-325.
- Chesnaux, R., Baudement, C. & Hay, M (2011): Assessing and comparing the hydraulic properties of granular aquifers on three different scales. *Proceedings of Geohydro*: 28-31.
- Chilton, P.J. & Foster, S.S.D. (1995): Hydrogeological characterisation and water-supply potential of basement aquifers in tropical Africa. *Hydrogeology Journal*, 3(1): 36-49.
- Chilton, P.J. & Smith-Carington, A.K. (1984): Characteristics of the weathered basement aquifer in Malawi in relation to rural water supplies. IAHS Publication no. 144: 57-72.
- Clark, I.D. & Fritz, P. (1997): *Environmental Isotopes in Hydrogeology*. CRC Press, Lewis Publisher, Boca Raton, 353 p.
- Clay, A., Bradley, C., Gerrard, A.J. & Leng, M.J. (2004): Using stable isotopes of water to infer wetland hydrological dynamics. *Hydrology and Earth System Sciences*, 8(6): 1164-1173.
- Cloutier, J., Stevenson, R.K. & Bardoux, M. (2005): Nd isotopic, petrologic and geochemical investigation of the Tulawaka East Gold Deposit, Tanzanian Craton. *Precambrian Research*, 139: 147-163.
- Condie, K.C. (1998): Episodic continental growth and supercontinents: a mantle avalanche connection? *Earth and Planetary Science Letters*, 163: 97-108.
- Cook, P.G. (2003): *A guide to regional groundwater flow in fractured rock aquifers*. CSIRO Australia, Seaview Press, Henley Beach, 108 p.
- Cools, J., Johnston, R., Hattermann, F.F., Douven, W. & Zsuffa, I. (2013): Tools for wetland management: Lessons learnt from a comparative assessment. *Environmental Science & Policy*, 34: 138-145.
- Cooper, H.H.Jr. & Jacob, C.E. (1946): A generalized graphical method for evaluation formation constants and summarizing well-field history. *Transactions, American Geophysical Union*, 27(4): 526-534.
- Craig, H. (1961): Isotopic variations in meteoric waters. *Science*, 133: 1702-1703.
- Cronin, A.A., Breslin, N., Gibson, J., Pedley, S. (2006): Monitoring source and domestic water quality in parallel with sanitary risk identification in Northern Mozambique to prioritise protection interventions. *Journal of Water and Health*, 4(3): 333-345.
- Cui, Q., Wang, W., Li, D. & Guo, X. (2012): An ecosystem health assessment method integrating geochemical indicators of soil in Zoige wetland, southwest China. *Procedia Environ. Sci.*, 13: 1527-1534.
- Dansgaard, W. (1964): Stable isotopes in precipitation. *Tellus XVI*, 4: 436-468.
- Debenham, F. (1948): The water resources of central Africa. *The Geographical Journal*, 111(4/6): 222-233.
- Denny, P. (1993): Eastern Africa. In: Whigham, D.F., Dykyjová, D. & Hejný, S. (eds) (1993): *Wetlands of the world, Volume 1: Inventory, Ecology and Management*. Kluwer Academic Publishers, Dordrecht: 32-46.
- DEV (2009) (Deutsche Einheitsverfahren zur Wasser-, Abwasser- und Schlammuntersuchung): A0-5 Plausibilitätskontrolle von Analysedaten durch Ionenbilanzierung. 74. Lieferung.
- Devito, K.J., Hill, A.R. & Roulet, N. (1996): Groundwater-surface water interactions in headwater forested wetlands of the Canadian Shield. *Journal of Hydrology*, 181: 127-147.
- Devlin, F.J. (2015): HydrogeoSieveXL: an Excel-based tool to estimate hydraulic conductivity from grain-size analysis. *Hydrogeology Journal*, 23: 837-844.
- Dewandel, B., Lachassagne, P., Wyns, R., Maréchal, J.R. & Krishnamurthy, N.S. (2006): A generalized 3-D geological and hydrogeological conceptual model of granite aquifers controlled by single or multiphase weathering. *Journal of Hydrology*, 330: 260-284.
- DIN 4023 (2006): *Geotechnische Erkundung und Untersuchung - Zeichnerische Darstellung der Ergebnisse von Bohrungen und sonstigen direkten Aufschlüssen*.
- Dixon, A.B. (2002): The hydrological impacts and sustainability of wetland drainage cultivation in Illubabor, Ethiopia. *Land Degradation & Development*, 13: 17-31.
- Dixon, A.B. & Wood, A.P. (2003): Wetland cultivation and hydrological management in eastern Africa: Matching community and hydrological needs through sustainable wetland use. *Natural Resources Forum* 27: 117-129.

- Dykyjová, D. (1979): Selective uptake of mineral ions and their concentration factors in aquatic higher plants. *Folia geobotanica & phytotaxonomica*, 14(3): 267-325.
- Dypvik, H., Hankel, O., Nilsen, O., Kaaya, C. & Kilembe, E. (2001): The lithostratigraphy of the Karoo Supergroup in the Kilombero Rift Valley, Tanzania. *Journal of African Earth Sciences*, 32(3): 451-470.
- Dypvik, H. & Nilsen, O. (2002): Rift valley sedimentation and diagenesis, Tanzanian Examples – A review. *South African Journal of Geology*, 105: 93-106.
- Einsele, G. (1992): *Sedimentary Basins, Evolution, Facies and Sediment Budget*. Springer-Verlag, Berlin, 792 p.
- ERM (2013) (Environmental Resources Management): *Southern Agricultural Growth Corridor of Tanzania (SAGCOT): Environmental and Social Management Framework*. Government of Tanzania, 175 p.
- FAO (1960) (Food and Agriculture Organization of the United Nations): *The Rufiji Basin Tanganyika*. FAO Report to the Government of Tanganyika on the preliminary reconnaissance survey of the Rufiji Basin, Volume 2 Hydrology and Water Resources, Part 1 Computation and Analyses, Rome, 1960, 405 p.
- FAO, IFAD & WFP (2015) (Food and Agriculture Organization of the United Nations, International Fund for Agricultural Development & World Food Programme): *The State of Food Insecurity in the World 2015. Meeting the 2015 international hunger targets: taking stock of uneven progress*. Rome, FAO, 62 p.
- Farnham, I.M., Singh, A.K., Stetzenbach, K.J. & Johannessen, K.H. (2002): Treatments of nondetects in multivariate analysis of groundwater geochemistry data. *Chemometrics and Intelligent Laboratory Systems*, 60: 265-281.
- Farnham, I.M., Johannesson, K.H., Singh, A.K., Hodge, V.F. & Stetzenbach, K.J. (2003): Factor analytical approaches for evaluating groundwater trace element chemistry data. *Analytica Chimica Acta*, 490: 123-138.
- Fass, T. (2004): *Hydrogeologie im Aguima Einzugsgebiet in Benin/Westafrika*. PhD thesis, University of Bonn, 137 p.
- Faulkner, R.D. & Lambert, R.A. (1991): The effect of irrigation on dambo hydrology: a case study. *Journal of Hydrology*, 123: 147-161.
- Faulkner, S.P. & Richardson, C.J. (1989): Physical and chemical characteristics of freshwater wetland soils. In: Hammer, D.A. (eds.): *Constructed wetlands for wastewater treatment, municipal, industrial, and agricultural*. Lewis Publishers, Boca Raton, 833 p.
- Fetter, C.W. (1994): *Applied Hydrogeology*. 3<sup>rd</sup> edition, McMillan College Publishing, Prentice Hall, New York, 691 p.
- Fisher, J. & Acreman, M.C. (2004): Wetland nutrient removal: a review of the evidence. *Hydrology and Earth System Sciences Discussions*, 8(4): 673-685.
- Freeze, R.A. & Cherry J.A. (1979): *Groundwater*. Englewood Cliffs, NJ, Prentice Hall, 604 p.
- Frenken, K. & Mharapara, I. (2002): Wetland development and management in SADC countries. Proceedings of a sub-regional workshop held by FAO sub-regional office for East and Southern Africa (SAFR), Harare, Zimbabwe, November 19-23, 2001. *Préci-ex, Les Pailles, Mauritius*, 206 p.
- Frisbie, S.H., Mitchell, E.J., Dustin, H., Maynard, D.M. & Sarkar, B. (2012): World Health Organization discontinues its drinking-water guideline for manganese. *Environmental Health Perspectives*, 120(6): 775-778.
- Gabiri, G. (unpublished): *Modeling wetland surface and subsurface soil water dynamics under different land use and management systems of Uganda and Tanzania, East Africa*. PhD thesis, University of Bonn, unpublished.
- Geißler, T. (2015): *Hydrochemische Charakterisierung des nordöstlichen Kilombero-Einzugsgebietes bei Ifakara, Tansania*. Master thesis, University of Bonn, 104 p.
- Geological Survey of Tanganyika (1962): *Geological Map 1:125,000, Quarter Degree Sheet 235, Ifakara*.
- Geyh, M. (2000): Groundwater – Saturated and unsaturated zone. In: Mook, W.G. (eds.) (2000): *Environmental isotopes in the hydrological cycle*. Technical Document in Hydrology, 39(4), UNESCO, Paris, 200 p.
- Gilkes, R.J., Scholz, G. & Dimmock, G.M. (1973): Lateritic deep weathering of granite. *Journal of Soil Science*, 24: 523-536.
- Girmay, E., Ayenew, T., Kebede, S., Alene, M., Wohnlich, S. & Wisotzky, F. (2015): Conceptual groundwater flow model of the Mekelle Paleozoic-Mesozoic sedimentary outlier and surroundings (northern Ethiopia) using environmental isotopes and dissolved ions. *Hydrogeology Journal*, 23: 649-672.
- Glasner, B. (unpublished): *Changes in soil organic matter content of wetland-soils in East Africa according to land use change*. PhD thesis, University of Mainz, unpublished.
- Glynn, P.D. & Plummer L.N. (2005): Geochemistry and the understanding of ground-water systems. *Hydrogeology Journal*, 13: 263-287.

- Godfray, H.C.J., Beddington, J.R., Crute, L.H., Lawrence, D., Muir, J.F., Pretty, J., Robinson, S., Thomas, S.M. & Toulmin, C. (2010): Food Security: The Challenge of Feeding 9 Billion people. *Science*, 327: 812-818.
- Goldich, S.S. (1938): A study in rock-weathering. *Journal of Geology*, 46:17-58.
- Griffiths, J.F. (1972): Eastern Africa. – In: Lyndolph, P.E. (1972): *World Survey of Climatology: Climates of Africa*. Elsevier Publishing Company, 604 p.
- Grotelüschen, K. (unpublished): Modelling production potentials and constraints of rize and maize cultivation in East African wetlands for the identification of sustainable and applicable agricultural intensification strategies. PhD thesis, University of Bonn, unpublished.
- GTK Consortium (2012): Geological Map of Uganda 1:100,000, Sheet 61, Bombo.
- Güler, C., Thyne, G.D., McCray, J.E. & Turner, A.K. (2002): Evaluation of graphical and multivariate statistical methods for classification of water chemistry data. *Hydrogeology Journal* 10: 455-474.
- Hahn-Weinheimer, P., Hirner, A., Weber-Diefenbach, K. (1995): Röntgenfluoreszenzanalytische Methoden. Grundlagen und praktische Anwendung in den Geo-, Material- und Umweltwissenschaften. 2. Auflage, Vieweg, Braunschweig/Wiesbaden, 283 p.
- Hannappel, S., Fritsche, J.G. & Lessmann, B. (2003): Die Erstellung der hydrogeologischen Übersichtskarte (HÜK 200) in Hessen. *Hessischer Umweltmonitor*, 4/03: 3-9.
- Hayashi, M. & Rosenberry, D.O. (2002): Effects of ground water exchange on the hydrology and ecology of surface water. *Ground Water*, 40(3): 309-316.
- Hazen, A. (1892): Some physical properties of sands and gravels, with special reference to their use in filtration. Massachusetts State Board of Health, vol. 24th annual report: 539-556.
- Hecklau, H. (1989): Ostafrika (Kenya, Tanzania, Uganda). *Wissenschaftliche Länderkunden Band 33*, Wissenschaftliche Buchgesellschaft, Darmstadt, 572 p.
- Heiri, O., Lotter, A.F., Lemcke, G. (2001): Loss on ignition as a method for estimating organic and carbonate content in sediments: reproducibility and comparability of results. *Journal of Paleolimnology*, 25: 101-110.
- Heiß, L. (2016): The alluvium of the Namulonge wetland (Uganda), its contributions to subsurface water dynamics and composition. Master thesis, University of Bonn, 74 p.
- Helgeson, H.C., Garrels, R.M., Mackenzie, F.T. (1969): Evaluation of irreversible reactions in geochemical processes involving minerals and aqueous solutions. *Geochimica et Cosmochimica Acta*, 33: 455-481.
- Helsel, D.R. & Hirsch, R.M. (2002): *Statistical Methods in Water Resources*. Techniques of Water Resources Investigations, Book4, chapter A3, U.S. Geological Survey, 522 p.
- Hem, J. D (1985): *Study and Interpretation of the Chemical Characteristics of Natural Water*. 3rd edition, U.S. Geological Survey Water Supply Paper: 2254, 263 p.
- Hemond, H.F. & Benoit, J. (1988): Cumulative impacts on water quality functions of wetlands. *Environmental management*, 12(5): 639-653.
- Herczeg, A.L. & Edmunds, W.M. (2000): Inorganic ions as tracers. In: Cook, P. & Herczeg, A.L. (2000): *Environmental tracers in subsurface hydrology*, Springer US: 31-77.
- Hijmans, R.J., Cameron, S.E., Parra, J.L., Jones, P.G. & Jarvis, A. (2005): Very high resolution interpolated climate surfaces for global land areas. *International Journal of Climatology*, 25: 1965-1978.
- Hinkle, S.R., Duff, J.H., Triska, F.J., Laenen, A., Gates, E.B., Bencala, K.E., Wentz, D.A. & Silva, S.R. (2001): Linking hyporheic flow and nitrogen cycling near the Willamette River – a large river in Oregon, USA. *Journal of Hydrology*, 244: 157-180.
- Hötzl, H. & Witthüser, K. (1999): *Methoden für die Beschreibung der Grundwasserbeschaffenheit*. DVWK Schriften, 125, Wirtschafts- und Verlagsgesellschaft Gas und Wasser mbH, Bonn, 142 p.
- Hogan, D.M., Jordan, T.E. & Walbridge, M.R. (2004): Phosphorus retention and soil organic carbon in restored and natural freshwater wetlands. *Wetlands*, 24(3): 573-585.
- Hollands, G.G. (1987): Assessing the Relationship of Groundwater and Wetlands. In: Kusler, J.A. & Brooks, G. (eds.): *Proceedings of the National Wetland Symposium: Wetland Hydrology*, Chicago, Illinois: 240-242.
- Howard, K.W.F., Hughes, M., Charlesworth, D.L. & Ngobi, G. (1992): Hydrogeologic evaluation of fracture permeability in crystalline basement aquifers of Uganda. *Applied Hydrogeology*, 1/92: 55-65.
- Howard, K.W.F. & Karundu, J. (1992): Constraints on the exploitation of basement aquifers in East Africa – water balance implications and the role of the regolith. *Journal of Hydrology*, 139: 183-196.

- Hughes, R.H. & Hughes, J.S. (1992): A directory of African wetlands. IUCN - The World Conservation Union, Belhaven, 820 p.
- Hunt, R.J., Krabbenhoft, D.P. & Anderson, M.P. (1996): Groundwater inflow measurements in wetland systems. *Water Resources Research*, 32: 495-507.
- Hunt, R.J., Strand, M. & Walker, J.F. (2006): Measuring groundwater-surface water interaction and its effect on wetland stream benthic productivity, Trout Lake watershed, northern Wisconsin, USA. *Journal of Hydrology*, 320: 370-384.
- Hütter, L.A. (1988): *Wasser und Wasseruntersuchung*. 3th edition, Diesterweg Sauerländer, Frankfurt am Main, 443 p.
- Hvorslev, M.J. (1951): Time lag and soil permeability in ground-water observations. Waterway experiment station, corps of engineers, U.S. Army, Bulletin 36, Vicksburg, Mississippi, 55 p.
- Isaac, R.A. & Kerber, J. D. (1971): Atomic Absorption and Flame Photometry: Techniques und Uses in Soil, Plant and Water Analysis. In: L.M. Walsh (Ed.), *Instrumental Methods for Analysis of Soils and Plant Tissue*. Soil Science Society of America, Madison: 13-37.
- Jätzold, R. & Baum, E. (1968): *The Kilombero Valley*. Weltforum-Verlag GmbH, München, 147 p.
- Jarvis, A., Rubiano, J., Nelson, A., Farrow, A. & Mulligan, M. (2004): Practical use of SRTM data in the tropics - Comparisons with digital elevation models generated from cartographic data. Centro Internacional de Agricultura Tropical (CIAT), Working Document, 198, Cali, 32 p.
- Jasechko, S. & Taylor, R.G. (2015): Intensive rainfall recharges tropical groundwaters. *Environmental Research Letters*, 10: 124015, 8 p.
- Johnston, C.A. (1991): Sediment and nutrient retention by freshwater wetlands: Effects on surface water quality. *Critical Reviews in Environmental Control*, 21: 491-565.
- Johnston, R., Cools, J., Liersch, S., Morardet, S., Murgue, C., Mahieu, M., Zsuffa, I. & Uyttendaele, G.P. (2013): WETwin: A structured approach to evaluating wetland management options in data poor contexts. *Environmental Science and Policy*, 34:3-17.
- Jones, A., Breuning-Madsen, H., Brossard, M., Dampha, A., Deckers, J., Dewitte, O., Gallali, T., Hallet, S., Jones, R., Kilasara, M., Le Roux, P., Micheli, E., Montanarella, L., Spaargaren, O., Thiombiano, L., Van Ranst, E., Yemefack, M. & Zougmore, R. (eds.) (2013): *Soil Atlas of Africa*. European Commission, Publications Office of the European Union, Luxembourg, 176 p.
- Jung, M., Burt, T.P. & Bates, P.D. (2004): Toward a conceptual model of floodplain water table response. *Water Resources Research*, 40: 1-13.
- Moser, H. (1998): Environmental isotopes. In: Käss, W. (1998): *Tracing Technique in Geohydrology*. A.A. Balkema, Rotterdam, 581 p.
- Kangalawe, R.Y.M & Liwenga, E.T. (2005): Livelihoods in the wetlands of Kilombero Valley in Tanzania: Opportunities and challenges to integrated water resource management. *Physics and Chemistry of the Earth*, 30(11): 968-975.
- Kaplan, D., Muñoz-Carpena, R. & Ritter, A. (2010): Untangling complex shallow groundwater dynamics in the floodplain wetlands of a southeastern U.S. coastal river. *Water Resources Research*, 46: W08528, 18 p.
- Kashaigili, J.J. (2010): Assessment of groundwater availability and its current and potential use and impacts in Tanzania. Final report, prepared for the International Water Management Institute (IWMI), Sokoine University of Agriculture, Morogoro, 58 p.
- Kato, F. (2007): Development of a major rice cultivation area in the Kilombero Valley, Tanzania. *African Study Monographs*, 36: 3-18.
- Kazezyilmaz-Alhan, C.M., Medina, M.A.J. & Richardson, C.J. (2007): A wetland hydrology and water quality model incorporating surface water/groundwater interactions. *Water Resources Research*, 43: W04434, 16 p.
- Kebede, S., Travi, Y., Alemayehu, T. & Ayenew, T. (2005): Groundwater recharge, circulation and geochemical evolution in the source region of the Blue Nile River, Ethiopia. *Applied Geochemistry*, 20: 1658-1676.
- Kehew, A.E., Passero, R.N., Krishnamurthy, R.V., Lovett, C.K., Betts, M.A. & Dayharsh, B.A. (1998): Hydrogeochemical interaction between a wetland and an unconfined glacial drift aquifer, southwestern Michigan. *Ground Water*, 36(5): 849-856.



- Key, R.M. (1992): An Introduction to the crystalline basement of Africa. In: Wright, E.P. & Burgess, W.G. (eds.) (1992): *Hydrogeology of Crystalline Basement Aquifers in Africa*. Geological Society Special Publication No 66: 29-57.
- Khan, S., Ahmad, I., Shah, M.T., Rehman, S. & Khaliq, A. (2009): Use of constructed wetland for the removal of heavy metals from industrial wastewater. *Journal of Environmental Management*, 90: 3451-3457.
- King, A.C., Raiber, M. & Cox, M.E. (2014): Multivariate statistical analysis of hydrochemical data to assess alluvial aquifer-stream connectivity during drought and flood: Cressbrook Creek, southeast Queensland, Australia. *Hydrogeology Journal*, 22(2): 481-500
- Kirzhner, F., Zimmels, Y. & Gafni, A. (2008): Effect of Evapotranspiration on the Salinity of Wastewater Treated by Aquatic Plants. *Reviews on Environmental Health*, 23(2): 14-166.
- Klose, S. (2012): Regional hydrogeology and groundwater budget modeling in the arid Middle Drâa Catchment (South-Morocco). PhD thesis, University of Bonn, 266 p.
- Königer, P., Uhlenbrook, S., Leibundgut, C., Jaeger, L. & Mayer, H. (2001): Isotope hydrological investigation on groundwater origin in the floodplain of the Upper Rhine Valley. *New Approaches Characterizing Groundwater Flow*, Seiler & Wohnlich: 363-366.
- Kotze, D.C., Ellery, W.N., Macfarlane, D.M, Jewitt, G.P.W. (2012): A rapid assessment method for coupling anthropogenic stressors and wetland ecological condition. *Ecological Indicators*, 13: 284-293.
- Koutsouris, A.J., Chen, D. & Lyon, S.W. (2016): Comparing global precipitation data sets in eastern Africa: a case study of Kilombero Valley, Tanzania. *International Journal of Climatology*, 36: 2000-2014.
- Kovalevsky, V.S., Krusemann, G.P. & Rushotn, K.R. (eds.) (2004): *Groundwater studies – An international guide for hydrogeological investigations*. IHP-VI, Series on Groundwater, 3, United Nations Educational, Scientific and Cultural Organization (UNESCO), Paris, 430 p.
- Krause, S., Bronstert, A. & Zehe, E. (2007): Groundwater-surface water interactions in a North German lowland floodplain – implications for the river discharge dynamics and riparian water balance. *Journal of Hydrology*, 347: 404-417.
- Krusemann, G.P. & de Ridder, N.A. (2000): *Analysis and evaluation of pumping test data*. 2<sup>nd</sup> edition, International Institute for Land Reclamation and Improvement, Wageningen, 377 p.
- Kulabako, N.R., Nalubega, M. & Thunvik, R. (2007): Study of the impact of land use and hydrogeological settings on the shallow groundwater quality in a peri-urban area of Kampala, Uganda. *Science of the Total Environment*, 81: 180-199.
- Kwesiga, J. (unpublished): Rice production in the Kilombero floodplain, Ifakara, TZ: Effect of water regime and cropping intensity on grain yield and nutrient flows. PhD thesis, University of Bonn, unpublished.
- Laing, G.D., Rinklebe, J., Vandecasteele, B., Meers, E. & Tack, F.M.G. (2009): Trace metal behavior in estuarine and riverine floodplain soils and sediments: A review. *Science of the total environment*, 407: 3972-3985.
- Lambs, L. (2004): Interactions between groundwater and surface water at river banks and the confluence of rivers. *Journal of Hydrology*, 288: 312-326.
- Lamontagne, S., Leaney, F.W. & Herczeg, A.L. (2005): Groundwater-surface water interactions in a large semi-arid floodplain: implications for salinity management. *Hydrological Processes*, 19: 3063-3080.
- Land, L. & Timmons, S. (2016): Evaluation of groundwater residence time in a high mountain aquifer system (Sacramento Mountains, USA): insights gained from use of multiple environmental tracers. *Hydrogeology Journal*, 24: 787-804.
- Langguth, H.R. & Voigt R. (2004): *Hydrogeologische Methoden*. 2nd edition, Springer Verlag, Berlin, Heidelberg, 1005 p.
- Lawrence, J.R. & White, J.W.C. (1991): The elusive climate signal in the isotopic composition of precipitation. In: Taylor, H.P., O'Neil, J.R. & Kaplan, I.R. (eds.): *Stable isotope geochemistry: A tribute to Samuel Epstein*. Special Publication 3, Geochemical Society, San Antonio: 169-185.
- Lazareva, O. & Pichler, T. (2011): Evaluating Complex Hydrogeological Settings in a Constructed Wetland: An Isotopic/Chemical Mass Balance Approach. *Wetlands*, 31(3): 521-534.
- Lee, I., Chang, H.C. & Ge, L. (2005): GPS campaigns for validation of InSAR derived DEMs. *Journal of Global Positioning Systems*, 4(1-2): 82-87.

- Leemhuis, C., Amler, E., Diekkrüger, B., Gabiri, G. & Näschen, K. (2016): East African wetland-catchment data base for sustainable wetland management. *Proceedings of the International Association of Hydrological Sciences*, 374: 123-128.
- Lefroy, R.D.B., Mamaril, C.P., Blair, G.J. & Gonzales, P.J. (1992): Sulphur cycling in rice wetlands. In: Howarth, R.W., Stewart J.W.B. & Ivanov, M.V. (eds.): *Sulphur cycling on the continents: wetlands, terrestrial ecosystems, and associated water bodies*. Scope 48, John Wiley & Sons, New York, 350 p.
- Le Gall, B., Gernigon, L., Ebinger, C., Gloaguen, R., Nilsen, O., Dypvik, H., Deffontaines, B. & Mruma, A. (2004): Neogene-Holocene rift propagation in central Tanzania: Morphostructural and aeromagnetic evidence from the Kilombero area. *Geological Society of America Bulletin*, 116(3-4): 490-510.
- Lehner, B. & Döll, P. (2004): Development and validation of a global database of lakes, reservoirs and wetlands. *Journal of Hydrology*, 296: 1-22.
- Liedtke, K. (2015): *Geochemische und hydrogeologische Charakterisierung des nordöstlichen Kilombero-Einzugsgebietes bei Ifakara, Tansania*. Master thesis, University of Bonn, 72 p.
- Lillesø, J.-P.B., van Breugel, P., Kindt, R., Bingham, M., Demissew, S., Dudley, C., Friis, I., Gachathi, F., Kalema, J., Mbago, F., Minani, V., Moshi, H.N., Mulumba, J., Namaganda, M., Ndangalasi, H.J., Ruffo, C.K., Jamnadass, R. & Graudal, L. (2011): *Potential natural vegetation of Eastern Africa (Ethiopia, Kenya, Malawi, Rwanda, Tanzania, Uganda and Zambia), Volume 1: The Atlas*. Forest and Landscape Working Papers, 61, University of Copenhagen, 155 p.
- Lind, E.M., & Morrison, M.E.S. (1974): *East African vegetation*. Longman, London, UK, 257 p.
- Little, M.G. & Lee, C.T.A. (2006): On the formation of an inverted weathering profile on Mount Kilimanjaro, Tanzania: Buried paleosol or groundwater weathering? *Chemical Geology*, 235: 205-221.
- Liu, C.W., Jang, C.S. & Chen, S.C. (2002): Three-dimensional spatial variability of hydraulic conductivity in the Choushi River alluvial fan, Taiwan. *Environmental Geology*, 43: 48-56.
- Lyon, S.W., Koutsouris, A., Scheibler, F., Jarsjö, J., Mbanguka, R., Tumbo, M., Robert, K.K., Sharma, A.N. & van der Velde, Y. (2015): Interpreting characteristic drainage timescale variability across Kilombero Valley, Tanzania. *Hydrological Processes*, 29: 1912-1924.
- Mahan, S.A. & Brown, D.J. (2007): An optical age chronology of late Quaternary extreme fluvial events recorded in Ugandan dambo soils. *Quaternary Geochronology*, 2: 174-180.
- Marschner, P. (eds.) (2012): *Marschner's Mineral Nutrition of Higher Plants*. 3<sup>rd</sup> edition, Academic Press, Elsevier, London, 672 p.
- Massoud, M.A., Tarhini, A. & Nasr, J.A. (2009): Decentralized approaches to wastewater treatment and management: Applicability in developing countries. *Journal of Environmental Management*, 90: 652-659.
- Master, S., Bekker, A. & Karhu, J.A. (2013): Paleoproterozoic high  $\delta^{13}\text{C}_{\text{carb}}$  marbles from the Ruwenzori Mountains. *Chemical Geology*, 362: 157-164.
- McCarthy, T.S. (2006): Groundwater in the wetlands of the Okavango Delta, Botswana, and its contribution to the structure and function of the ecosystem. *Journal of Hydrology*, 320: 264-282.
- McCartney, M.P. (2000): The water budget of a headwater catchment containing a dambo. *Physics and Chemistry of the Earth*, 25(7-8): 611-616.
- McCartney, M., Butterworth, J., Moriarty, P. & Owen, R. (1998): Comparison of the hydrology of two contrasting headwater catchments in Zimbabwe. *Hydrology, Water Resources and Ecology in Headwaters*, IAHS Publications, 248: 515-522
- McCartney, M.P. & Neill, C. (1999): Water flow pathways and the water balance within a headwater catchment containing a dambo: inferences drawn from hydrochemical investigations. *Hydrology and Earth System Sciences*, 3(4): 581-591.
- McCartney, M.P., Rebelo, L.M., Senaratna Sellamuttu, S. & de Silva, S. (2010): *Wetlands, agriculture and poverty reduction*. International Water Management Institute (IWMI) Research Report, 137, Colombo, 44 p.
- McClanahan, T.R. & Young, T.P. (1996): *East African Ecosystems and their Conservation*. Oxford University Press, Oxford, 452 p.
- McCloskey, T.F. & Finnemore, E.J. (1996): Estimating Hydraulic Conductivities in an Alluvial Basin from Sediment Facies Models. *Ground Water*, 34(6): 1024-1032.
- McConnell, R.B. (1972): Geological Development of the Rift System of Eastern Africa. *Geological Society of America Bulletin*, 83: 2549-2572.

- McFarlane, M.J. (1989): Dambos – Their characteristic and geomorphological evolution in parts of Malawi and Zimbabwe, with particular reference to their role in the hydrogeological regime of surviving areas of African surface. Proceedings of the groundwater exploration and development in crystalline basement aquifers workshop, Commonwealth Science Council Technical Paper, 273 p.
- McFarlane, M.J. (1992): Groundwater movement and water chemistry associated with weathering profiles of the African surface in parts of Malawi. Geological Society Special Publications, no. 66: 101-130.
- McGuire, K.J. & McDonnell, J.J. (2006): A review and evaluation of catchment transit time modeling. *Journal of Hydrology*, 330: 543-563.
- McMillan, D.E. (1999): A brief history of the neurobehavioral toxicity of manganese: some unanswered questions. *Neurotoxicology*, 20(2-3): 499-507.
- Meju, M.A., Fontes, S.L., Oliveira, M.F.B., Lima, J.P.R., Ulugergerli, E.U. & Carrasquilla, A.A. (1999): Regional aquifer mapping using combined VES-TEM-AMT/EMAP methods in the semiarid eastern margin of Parnaiba Basin, Brazil. *Geophysics*, 64(2): 337-356.
- Meng, S.X. & Maynard, J.B. (2001): Use of statistical analysis to formulate conceptual models of geochemical behavior: water chemical data from the Botucatu aquifer in São Paulo state, Brazil. *Journal of Hydrology*, 250: 78-97.
- Merkel, B.J. & Planer-Friedrich, B. (2008): *Grundwasserchemie*. Springer Verlag, Berlin, 242 p.
- Mertes, L.A.K. (1997): Documentation and significance of the perirheic zone on inundated floodplains. *Water Resources Research*, 33(7): 1749-1762.
- Miall, A.D. (1996): *The geology of fluvial deposits*. Springer-Verlag Berlin, Heidelberg, 582 p.
- Middelburg, J.J., Van der Weijden, C.H., & Woittiez, J.R.W. (1988): Chemical processes affecting the mobility of major, minor and trace elements during weathering of granitic rocks. *Chemical Geology*, 68: 253-273.
- Ministry of Water URT (2012a): Rufiji IWRMD Plan Interim Report Volume II, Water Resources Availability Assessment. WREM International, Atlanta, Georgia, USA, 143 p.
- Ministry of Water URT (2012b): Rufiji IWRMD Plan Interim Report, Volume III, Current Water Use and Infrastructure Assessment. WREM International Inc., Atlanta, Georgia, USA, 227 p.
- Mitsch, W.J. & Gosselink, J.G. (2007): *Wetlands*. 4<sup>th</sup> edition, John Wiley & Sons, New Jersey, 582 p.
- Möller, A., Mezger, K. & Schenk, V. (1998): Crustal age domains and the evolution of the continental crust in the Mozambique Belt of Tanzania: Combined Sm-Nd, Rb-Sr, and Pb-Pb isotopic evidence. *Journal of Petrology*, 39(4): 749-783.
- Mombo, F., Speelman, S., Van Huylenbroeck, G., Hella, J., Pantaleo, M. & Moe, S. (2011): Ratification of the Ramsar Convention and sustainable wetlands management: Situation analysis of the Kilombero Valley wetlands in Tanzania. *Journal of Agricultural Extension and Rural Development*, 3(9): 153-164.
- Montcoudiol, N., Molson, J. & Lemieux, J.M. (2015): Groundwater geochemistry of the Outaouais Region (Québec, Canada): a regional-scale study. *Hydrogeology Journal*, 23(2): 377-396.
- Moore, D.M. & Reynolds, R.C. (1997): *X-ray diffraction and the identification and analysis of clay minerals*. 2<sup>nd</sup> edition, Oxford University Press, Oxford, 378 p.
- Moya, C.E., Raiber, M., Taulis, M. & Cox, M.E. (2015): Hydrochemical evolution and groundwater flow processes in the Galilee and Eromanga basins, Great Artesian Basin, Australia: A multivariate statistical approach. *Science of the Total Environment*, 508: 411-426.
- Mruma, A.H. (2002): Structural evolution of the Kilombero Rift Basin in central Tanzania. *Tanzanian Journal of Science*, 28(2): 55-68.
- MWE (Ministry of Water and Environment, Directorate of Water Development, Uganda) (2010): Wakiso District Information. available from [http://www.mwe.go.ug/index.php?option=com\\_docman&view=docman&Itemid=223](http://www.mwe.go.ug/index.php?option=com_docman&view=docman&Itemid=223), 6 p.
- Myamoto, K., Maruyama, A., Haneishi, Y., Matsumoto, S., Tsuboi, T., Asea, G., Okello, S., Takagaki, M. & Kikuchi, M. (2012): NERICA Cultivation and its Yield Determinants: The Case of Upland Rice Farmers in Namulonge, Central Uganda. *Journal of Agricultural Science*, 4(6): 120-135.
- Näschen, K. (unpublished): Regional scale wetland-catchment interactions in East Africa. – PhD thesis, University of Bonn, unpublished.
- Nahlik, A.M. & Mitsch, W.J. (2006): Tropical treatment wetlands dominated by free-floating macrophytes for water quality improvement in Costa Rica. *Ecological Engineering*, 28(3): 246-257.

- Nasir, U.P. & Harikumar, P.S. (2012): Hydrochemical and isotopic investigation of a tropical wetland system in the Indian subcontinent. *Environmental Earth Sciences*, 66: 111-119.
- NEMA (2004) (National Environment Management Authority): State of environment report for Uganda 2004/05. National Environment Management Authority, Kampala, 270 p.
- NEMA (2008) (National Environment Management Authority): State of environment report for Uganda 2008. National Environment Management Authority, Kampala, 265 p.
- Nichols, G. (2009): *Sedimentology and stratigraphy*. 2<sup>nd</sup> edition, Wiley-Blackwell, Oxford, 419 p.
- Nicholson, S.E. (1996): A Review of Climate Dynamics and Climate Variability in Eastern Africa. In: Johnson, T.C. & Odada, E.O. (eds.) (1996): *The Limnology, Climatology and Paleoclimatology of the East African Lakes*. Overseas Publishers Association, Amsterdam, 666 p.
- Nilsen, O., Dypvik, H., Kaaya, C. & Kilembe, E. (1999): Tectono-sedimentary development of the (Permian) Karoo Sediments in the Kilombero Rift Valley, Tanzania. *Journal of African Earth Sciences*, 29(2): 393-409.
- Nsubuga, F.N.W., Olwoch, J.M. & Rautenbach, C.J.W. (2011): Climatic Trends at Namulonge in Uganda: 1947-2009. *Journal of Geography and Geology*, 3(1): 119-131.
- Nsubuga, F.N.W., Namutebi, E.N. & Nsubuga-Ssenfuma, M. (2014): Water resources of Uganda: an assessment and review. *Journal of Water Resource and Protection*, 6: 1297-1315.
- Nyakairu G.W.A. & Koeberl, C. (2002): Variation of Mineral, Chemical, and Rare Earth Element Composition in Size Fractions of Clay-rich Sediments from Kajjansi and Ntawo Clay Deposits, Central Uganda. *Geochemistry*, 62: 73-86.
- Nyarko, B.K., Essumang, D.K., Eghan M.J., Reichert, B., van de Giesen, N. & Vlek, P. (2010): Use of isotopes to study floodplain wetland and river flow interaction in the White Volta River basin, Ghana. – *Isotopes in Environmental and Health Studies*, 46(1): 91-106.
- Okrusch, M. & Matthes S. (2014): *Mineralogie*. 9<sup>th</sup> edition, Spektrum Akademischer Verlag, Heidelberg, 728 p.
- Ollier, C.D. & Galloway, R.W. (1990): The laterite profile, ferricrete and unconformity. *Catena*, 17: 97-109.
- Osborne, P.L. & Totome, R.G. (1994): Long-term impacts of sewage effluent disposal on a tropical wetland. *Water Science and Technology*, 29(4): 111-117.
- Owor, M., Taylor, R.G., Tindimugaya, C. & Mwesigwa, D. (2009): Rainfall intensity and groundwater recharge: empirical evidence from the Upper Nile Basin. *Environmental Research Letters*, 4: 035009, 6 p.
- Owor, M., Taylor, R., Mukwaya, C. & Tindimugaya, C. (2011): Groundwater/surface-water interactions on deeply weathered surfaces on low relief: evidence from Lake Victoria and Kyoga, Uganda. *Hydrogeology Journal*, 19: 1403-1420.
- Oyarzún, R., Barrera, F., Salazar, P., Maturana, H., Oyarzún, J., Aguirre E., Alvarez, P., Jourde, H. & Kretschmer, N. (2014): Multi-method assessment of connectivity between surface water and shallow groundwater: the case of Limarí River basin, north-central Chile. *Hydrogeology Journal*, 22: 1857-1873.
- Paar, R., Novakovic, G. & Kolovrat, D. (2014): Vertical component quality comparison of GPS RTK method in combination with laser system vs. conventional methods for height determination. *INGEO 2014*, April, Prague: 59-66.
- Pallister, J.W. (1971): The tectonics of East Africa. In: UNESCO (1971): *Tectonics of Africa*. UNESCO, Paris, 6: 511-543.
- Parkhurst, D.L. & Appelo, C.A.J. (1999): User's guide to PHREEQC (ver. 2) - A computer program for speciation, batch-reaction, one-dimensional transport, and inverse geochemical calculations. *US Geological Survey Water Resources Investigation Report*, 99-4259, 312 p.
- Paul, H. & Steinbrecher, R. (2013): African Agricultural Growth Corridors and the New Alliance for Food Security and Nutrition. Who benefits, who loses? *EcoNexus Report June 2013*, 17 p.
- Pavelic, P., Giordano, M., Keraita, B., Ramesh, V. & Rao, T. (eds.) (2012): *Groundwater availability and use in sub-saharan Africa: A review of 15 countries*. International Water Management Institute (IWMI), Colombo, 274 p.
- Peel, M.C., Finlayson, B.L. & McMahon, T.A. (2007): Updated world map of the Köppen-Geiger climate classification. *Hydrology and Earth System Sciences*, 11: 1633-1644.
- Pester, M., Knorr, K.H., Friedrich, M.W., Wagner, M. & Loy, A. (2012): Sulfate-reducing microorganisms in wetlands – fameless actors in carbon cycling and climate change. *Frontiers in Microbiology*, 3: 45-64.

- Pétre, M.A., Rivera, A., Lefebvre, R., Henry, M.J. & Fohnagy, A.J.B. (2016): A unified hydrogeological conceptual model of the Milk River transboundary aquifer, traversing Alberta (Canada) and Montana (USA). *Hydrogeology Journal*, 24: 1847-1871.
- Phipps, R.G. (1997): Nitrate removal capacity of constructed wetlands. *Retrospective Theses and Dissertations*, Paper 12024, 68 p.
- Piper, A.M. (1944): A graphic procedure in the geochemical interpretation of water-analyses. *Papers, Hydrology, Transaction, American Geophysical Union*: 914-928.
- Rassam, D.W., Pickett, T. & Knight, J.H. (2009): Incorporating floodplain groundwater interactions in river modeling. 18<sup>th</sup> World IMACS/MODSIM Congress, Cairns, Australia, 37-17 July: 3116-3122.
- Raveendram, R., Ashworth, B. & Chatelier, B. (2001): Manganese removal in drinking water systems. 64<sup>th</sup> Annual Water Industry Engineers and Operators Conference: 92-100.
- Reddy, K.S., Singh, M., Swarup, A., Rao, A.S. & Singh, K.N. (2002): Sulfur mineralization in two soils amended with organic manures, crop residues, and green manures. *Journal of Plant Nutrition and Soil Science*, 165: 167-171.
- Reddy, S.M., Collins, A.S. & Mruma, A. (2003): Complex high strain deformation in the Usagaran Orogen, Tanzania: structural setting of Palaeoproterozoic eclogites. *Tectonophysics*, 375(1-4): 101-123.
- Robineau, B., Join, J.L., Beauvais, A., Parisot, J.C. & Savin, C. (2007): Geoelectrical imaging of a thick regolith developed on ultramafic rocks: groundwater influence. *Australian Journal of Earth Sciences*, 54: 773781.
- Rodenburg, J. (2013): *Inland Valleys: Africa's Future Food Baskets*. Africa Rice Center, Dar es Salaam, 18 p.
- Rodhe, H., Mukolwe, E. & Söderlund, R. (1981): Chemical composition of precipitation in East Africa. *Kenya Journal of Science and Technology (Ser. A) 2*: 3-11. In Johnson, A.I. (1996): *The Limnology, Climatology and Paleoclimatology of the East African Lakes*. Overseas Publishers Association, Amsterdam, 665 p.
- Rovey, C.W. & Niemann, W.L. (2001): Wellskins and slug tests: where's the bias? *Journal of Hydrology*, 243(1-2): 120-132.
- Rozanski, K., Araguás-Araguás, L & Gonfiantini, R. (1993): Isotopic variations in modern global precipitation. *Climate Change in Continental Isotopic Records*, Geophysical Monograph, 78, 36 p.
- Sakané, N., Alvarez, M., Becker, M., Böhme, B., Handa, C., Kamiri, H., Langensiepen, M., Menz, G., Misana, S., Mogha, N., Mösel, B., Mwita, E., Oyieke, H. & Van Wijk, M.T. (2011): Classification, Characterisation, and Use of Small Wetlands in East Africa. *Wetlands*, 31: 1103-1116.
- Sauerbrey, I.I. (1932): On the Problem and Determination of the Permeability Coefficient. *Proceedings VNIIG*, No. 3-5. In Devlin, F.J. (2015): *HydrogeoSieveXL: an Excel-based tool to estimate hydraulic conductivity from grain-size analysis*. *Hydrogeology Journal*, 23: 837-844.
- Scheffer, F. & Schachtschabel, P. (2010): *Lehrbuch der Bodenkunde*. 16<sup>th</sup> edition, Spektrum Akademischer Verlag, Heidelberg, 569 p.
- Schepp, C. (unpublished): Dynamics of matter fluxes in small catchments and their relevance for nitrogen supply in an agriculturally used inland valley wetland in Uganda. PhD thesis, University of Bonn, unpublished.
- Schiff, J.A. & Fankhauser, A. (1981): Assimilatory Sulfate Reduction. In: Bothe, H. & Trebst, A. (eds.): *Biology of Inorganic Nitrogen and Sulfur*. Springer Verlag, Berlin, 384 p.
- Schlüter, T. (1997): *Geology of East Africa*. Gebrüder Borntraeger, Berlin, Stuttgart, 484 p.
- Schlüter, T. (2006): *Geological Atlas of Africa*. Springer-Verlag, Berlin, Heidelberg, 272 p.
- Schoeller, H. (1955): *Geochemie des eaux souterraines*. *Revue de l'Institut Français du pétrole*, 10: 230-44.
- Schreijer, M., Kampf, R., Toet, S. & Verhoeven, J. (1996): The use of constructed wetlands to upgrade treated sewage effluents before discharge to natural surface water in Texel Island, the Netherlands – pilot study. *Water Science and Technology*, 35(5): 231-237.
- Seelig, C. & DeKeyser, S. (2006): *Water quality and wetland function in the northern Prairie Pothole Region*. North Dakota State University, Fargo, 28 p.
- Shedlock, R.J., Wilcox, D.A., Thompson, T.A. & Cohen, D.A. (1993): Interactions between ground water and wetlands, southern shore of Lake Michigan, USA. *Journal of Hydrology*, 141: 127-155.
- Siegel, D.I. (1988): The recharge-discharge function of wetlands near Juneau, Alaska: part 2, geochemical investigations. *Ground Water*, 26(5): 580-586.
- Sikdar, P.K. & Sahu, P. (2009): Understanding wetland sub-surface hydrology using geologic and isotopic signatures. *Hydrology and Earth System Sciences*, 13: 1313-1323.

- Smith, A.G. (1985): Dambos, pediments and fragile equilibria on the Zambian Plateaux. *Zeitschrift für Geomorphologie*, 52: 171-186.
- Sophocleous, M. (2002): Interactions between groundwater and surface water: the state of the science. *Hydrogeology Journal*, 10: 52-67.
- Spieles, D.J. & Mitsch, W.J. (2000): The effects of season and hydrologic and chemical loading on nitrate retention in constructed wetlands: a comparison of low- and high-nutrient riverine systems. *Ecological Engineering*, 14: 7-91.
- Stanford, J.A. & Ward, J.V. (1993): An ecosystem perspective of alluvial rivers: connectivity and the hyporheic corridor. *Journal of the North American Benthological Society*, 12(1): 48-60.
- Steffánson, A. & Arnórsson, S. (2000): Feldspar saturation state in natural waters. *Geochimica et Cosmochimica Acta*, 64: 2567-2584.
- Struckmeier, W.F. & Margat, J. (1995): *Hydrogeological Maps – A Guide and a Standard Legend*. International Contributions to Hydrogeology, Vol. 17, Verlag Heinz Heise, Hannover, 177 p.
- Su, X., Cui, G., Du, S., Yuan, W. & Wang, H. (2016): Using multiple environmental methods to estimate groundwater discharge into an arid lake (Dakebo Lake, Inner Mongolia, China). *Hydrogeology Journal*, 24: 1707-1722.
- Tanner, P.W.G. (1973): Orogenic cycles in East Africa. *Geological Society of America Bulletin*, 84: 2839-2850.
- Tardy, Y. (1971): Characterization of the principle weathering types by the geochemistry of waters from some European and African crystalline massifs. *Chemical Geology*, 7: 253-271.
- Tardy Y., Bocquier, H., Paquet, H., Millot, G. (1973): Formation of clay from granite and its contribution in relation to climate topography. *Geoderma*, 10: 271-284.
- Taylor, J. R. (1997): *An Introduction to Error Analysis – the study of uncertainties in physical measurements*. 2<sup>nd</sup> edition, Sausalito University Science Books, 327 p.
- Taylor, R.G. & Howard, K. (1996): Groundwater recharge in the Victoria Nile basin of East Africa: support for the soil moisture balance approach using stable isotope tracers and flow modelling. *Journal of Hydrology*, 180: 31-53.
- Taylor, R.G. & Howard, K. (1998): Post-palaeozoic evolution of weathered landsurfaces in Uganda by tectonically controlled deep weathering and stripping. *Geomorphology*, 25: 173-192.
- Taylor, R.G. & Howard, K. (1999): Lithological evidence for the evolution of weathered mantles in Uganda by tectonically controlled cycles of deep weathering and stripping. *Catena*, 35: 65-94.
- Taylor, R.G., Todd, M.C., Kongola, L., Maurice, L., Nahozya, E., Sanga, H. & MacDonald, A.M. (2013): Evidence of the dependence of groundwater resources on extreme rainfall in East Africa. *Nature Climate Change*, 3: 374-378.
- Tenczer, V., Fritz, H., Bauernhofer, A. & Hauzenberger, C. (2007): Two orogens – One shear belt: 1 Ga of repeated deformation along the Central Tanzanian Shear Belt. *Journal of structural Geology*, 29: 1632-1649.
- Tindimugaya, C. (2005): Groundwater resources management in urban areas of Uganda: Experiences and challenges. 31<sup>st</sup> WEDC International Conference, Kampala: 311-313.
- Trauth, M.H. (2015): *MATLAB® Recipes for Earth Sciences*. 4<sup>th</sup> Edition, Springer, Heidelberg, 427 p.
- Turyahabwe, N., Kakuru, W., Tweheyo, M. & Tumusiime, D.M. (2013): Contribution of wetland resources to household food security in Uganda. *Agriculture and Food Security*, 2:5, 12 p.
- WWAP (2017) (United Nations World Water Assessment Programme): *The United Nations World Water Development Report 2017. Wastewater: The Untapped Resource*. Paris, UNESCO, 180 p.
- USGS (2005) (U.S. Geological Survey): *Selection of Colors and Patterns for Geologic Maps of the U.S.* Geological Survey. U.S. Geological Survey, Reston, Virginia, 12 p.
- Van der Weijden, C.H. & Pacheco, F.A.L. (2007): From hydrochemistry to chemical weathering: models and problems. *Congress Report, Geochimica XV Semana*: 27-32.
- Verhoeven, J.T.A., Arheimer, B., Yin, C. & Hefting, M.M. (2006): Regional and global concerns over wetlands and water quality. *Trends in Ecology and Evolution*, 21(2): 96-103.
- Von der Heyden, C.J. (2004): The hydrology and hydrogeology of dambos: a review. *Physical Geography*, 28(4): 544-564.
- Wagner, K. (unpublished): Impacts of land use changes on greenhouse gas emissions from wetlands in Uganda and Tanzania. PhD thesis, University of Bonn, unpublished.
- Weiss, J. (1995): *Ion chromatography*. 2<sup>nd</sup> edition, VCH, Weinheim, 465 p.

- Welz, B. (1976): Atomic absorption spectroscopy. 2<sup>nd</sup> edition, Verlag Chemie, Weinheim, 367 p.
- West, A.J., Galy, A. & Bickle, M. (2005): Tectonic and climatic controls on silicate weathering. *Earth and Planetary Science Letters*, 235: 211-228.
- Westerhof, A.B., Härmä, P., Isabirye, E., Katto, E., Koistinen, T., Kuosmanen, E., Lehto, T., Lehtonen, M.I., Mäkitie, H., Manninen, T., Mänttari, I., Pekkala, Y., Pokki, J., Saalman, K. & Virransalo, P. (2014): Geology and Geodynamic Development of Uganda with Explanation of the 1:1,000,000-Scale Geological Map. Geological Survey of Finland, Special Paper 55, 387 p.
- White, D.S. (1993): Perspectives on defining and delineating hyporheic zones. *Journal of the North American Benthological Society*, 12(1): 61-69.
- White, A.F., & Brantley, S.L. (1995): Chemical weathering rates of silicate minerals: an overview. *Chemical Weathering Rates of Silicate Minerals*, 31: 1-22.
- WHO (2011) (World Health Organization): Guidelines for Drinking-water Quality. 4<sup>th</sup> edition, WHO Library Catalogue-in-Publication Data, Gutenberg, Malta, 541 p.
- Wieczorek, M. (unpublished): Spatial distribution and sources of fluoride in groundwater of the north-eastern Kilombero floodplain, Tanzania. Master thesis, University of Bonn, unpublished.
- Winter, T.C. (1999): Relation of streams, lakes, and wetlands to groundwater flow systems. *Hydrogeology Journal*, 7: 28-45.
- Winter, T.C. & Llamas, M.R. (1993): Introduction to the 28<sup>th</sup> international Geological Congress Symposium on the Hydrogeology of Wetlands. *Journal of Hydrology*, 141: 1-3.
- Woessner, W.W. (2000): Stream and Fluvial Plain Ground Water Interactions: Rescaling Hydrogeological Thought. *Ground Water*, 38(3): 423-429.
- Wold, S., Esbensen, K., Geladi, P. (1987): Principal Component Analysis. *Chemometrics and Intelligent Laboratory Systems*, 2: 37-52.
- WRI (2009) (World Resources Institute): Mapping a better future: How spatial analysis can benefit wetlands and reduce poverty in Uganda. World Resources Institute and Wetlands Management Department, Ministry of Water and Environment, Kampala, 39 p.
- Wright, E.P. (1992): The hydrogeology of crystalline basement aquifers in Africa. In: Wright, E.P. & Burgess, W.G. (eds.) (1992): *Hydrogeology of crystalline basement aquifers in Africa*. Geological Society Special Publication No 66: 1-27.
- WTW (2009): SenTIX ORP 900 Operating Manual. WTW GmbH, Weilheim, 39 p.
- Yawson, D.K., Kongo, V.M., & Kachroo, R.K. (2005): Application of linear and nonlinear techniques in river flow forecasting in the Kilombero River basin, Tanzania. *Hydrological Sciences Journal*, 50(5): 37-41.
- Yost, D. & Eswaran, H. (1990): Major land resource areas of Uganda. *World Soil Resources*, Soil Conservation Service, USDA, Washington DC, 218 p.
- Ziegler, M. (2015): Survey and analysis of the soil moisture dynamics in a wetland. Master thesis, University of Applied Sciences Magdeburg-Stendal, 93 p.
- Ziegler, S. (unpublished): Agricultural use of wetlands scrutinized on sustainability and yield potential – Rice production in the Namulonge inland valley: effect of different cropping systems on yield and nutrient flows. PhD thesis, University of Bonn, unpublished.

climate-data.org: <http://de.climate-data.org/location/26417/>; <http://de.climate-data.org/location/785548/> – climate diagrams of the two study sites, latest access October 2016.

earthexplorer.usgs.gov: <http://earthexplorer.usgs.gov> – SRTM 1 Arc-Second Global Digital Elevation Model (data available from the U.S. Geological Survey), latest access January 2014.

esdac.jrc.ec.europa.eu: <http://esdac.jrc.ec.europa.eu/content/generalised-soil-map-intergrated-regional-development-plan-morogoro> – soil map of the Ifakara study site, latest access October 2016.

gadm.org: <http://gadm.org> – Database of Global Administrative Areas version 2.7 – latest access June 2015.

google.com/earth: <http://www.google.com/earth> – Google, Digital Globe, Google Earth 2015, latest access December 2015.

hydrosheds.cr.usgs.gov: <http://hydrosheds.cr.usgs.gov/dataavail.php> – Hydrosheds 30sec river network (data available from U.S. Geological Survey), latest access January 2016.

openlayers.org: <http://openlayers.org/en/latest/examples/bing-maps.html> - Bing Aerial Layer, Rivers, latest access December 2015.

rsis.ramsar.org: <https://rsis.ramsar.org/RISapp/files/RISrep/TZ1173RIS.pdf> – Ramsar Information Sheet, The Kilombero Valley Floodplain, latest access August 2014.

sdnottill.com: <http://www.sdnottill.com/Newsletters/Fertilizer.pdf> – latest access February 2017.

upgmbh.com: <https://www.upgmbh.com/fileadmin/produkte/pdf/07150.pdf> - latest access August 2014.

wetlands-africa.de: <http://www.wetlands-africa.de/wetlands>; <http://www.wetlands-africa.de/project>; <http://www.wetlands-africa.de/region> – latest access March 2017.



## Appendix

### Appendix A – Data of aquifer structure and properties

#### A<sub>IF</sub> – Ifakara study site

A<sub>IF</sub>1 – Deep drilling log descriptions

A<sub>IF</sub>2 – Shallow drilling log descriptions of piezometers

A<sub>IF</sub>3 – Hydraulic conductivities of sediments derived from grain size analysis

A<sub>IF</sub>4 – Hydraulic conductivities of sediments derived from falling-head permeability tests

A<sub>IF</sub>5 – Hydraulic conductivities of sediments derived from pumping tests

A<sub>IF</sub>6 – Geochemical compositions (major oxides) of rock and sediments samples

#### A<sub>NA</sub> – Namulonge study site

A<sub>NA</sub>1 – Deep drilling log descriptions

A<sub>NA</sub>2 – Shallow drilling log descriptions of piezometers and additional drilling logs

A<sub>NA</sub>3 – Hydraulic conductivities of sediments derived from grain size analysis

A<sub>NA</sub>4 – Hydraulic conductivities of sediments derived from falling-head permeability tests

A<sub>NA</sub>5 – Geochemical compositions (major oxides) of saprolite and sediment samples

### Appendix B – Groundwater level data

#### B<sub>IF</sub> – Ifakara study site

B<sub>IF</sub>1 – Hydrographs of groundwater levels

#### B<sub>NA</sub> – Namulonge study site

B<sub>NA</sub>1 – Pearson's correlation coefficients of hydrographs of different piezometers

### Appendix C – Hydrochemical and isotopic data

#### C<sub>IF</sub> – Ifakara study site

C<sub>IF</sub>1 – *In-situ* parameters and HCO<sub>3</sub><sup>-</sup> and CO<sub>2</sub> concentrations of the four snapshot samplings

C<sub>IF</sub>2 – Hydrochemical data of the four snapshot samplings

C<sub>IF</sub>3 – PO<sub>4</sub><sup>3-</sup> and trace heavy metal concentrations of the first snapshot sampling

C<sub>IF</sub>4 – Stable water isotope data of the four snapshot samplings

C<sub>IF</sub>5 – Stable water isotope and hydrochemical data of weekly sampled precipitation

#### C<sub>NA</sub> – Namulonge study site

C<sub>NA</sub>1 – *In-situ* parameters and HCO<sub>3</sub><sup>-</sup> and CO<sub>2</sub> concentrations of the four snapshot samplings

C<sub>NA</sub>2 – Hydrochemical data of the four snapshot samplings

C<sub>NA</sub>3 – PO<sub>4</sub><sup>3-</sup> and trace heavy metal concentrations of the fourth snapshot sampling

C<sub>NA</sub>4 – Stable water isotope data of the four snapshot samplings

C<sub>NA</sub>5 – Stable water isotope and hydrochemical data of weekly sampled precipitation

C<sub>NA</sub>6 – *In-situ* parameters and hydrochemical data of monthly samplings

C<sub>NA</sub>7 – Stable water isotope data of monthly samplings

C<sub>NA</sub>8 – *In-situ* parameters and hydrochemical data of soil water from suction cups

C<sub>NA</sub>9 – Stable water isotope data of soil water from suction cups

### Appendix D – Sampling point locations

#### D<sub>IF</sub> – Ifakara study site

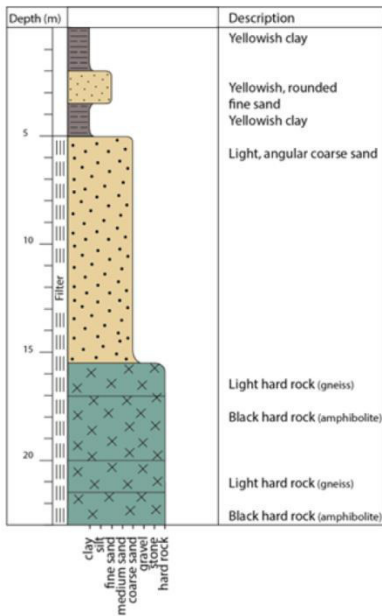
D<sub>IF</sub>1 – Geographic coordinates (WGS84) of all sampling points in the Ifakara study site

#### D<sub>NA</sub> – Namulonge study site

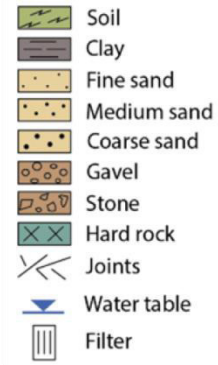
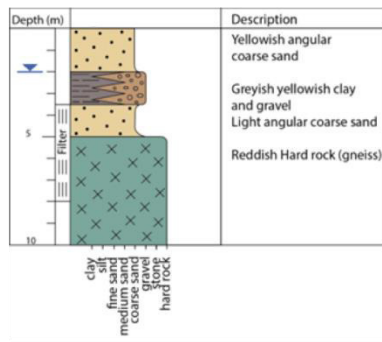
D<sub>NA</sub>1 – Geographic coordinates (WGS84) of all sampling points in the Namulonge study site

**Appendix A-A<sub>IF</sub>1: Deep drilling log descriptions (data provided by RBWB and MSABI, processed and digitized by Liedtke 2015) (IF).**

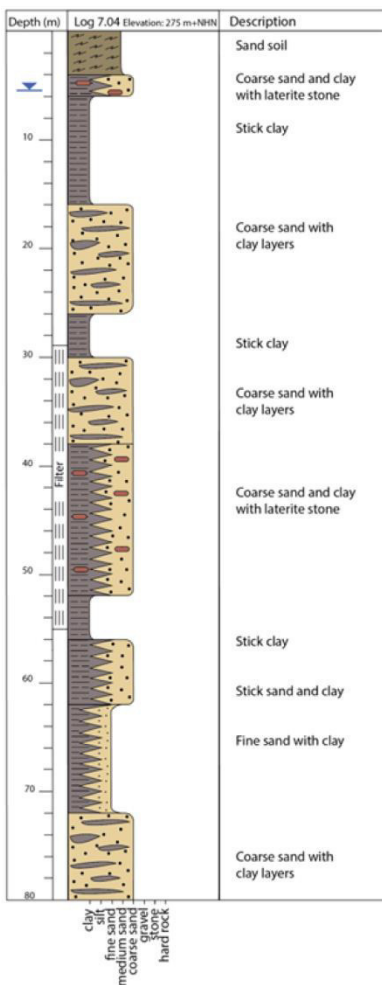
**DLM1<sub>IF</sub>**



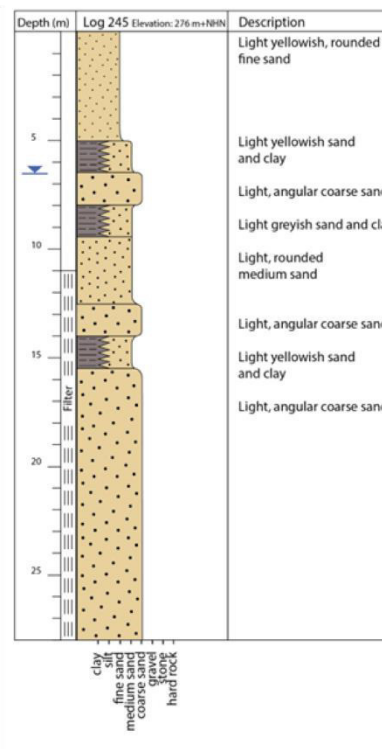
**DLM2<sub>IF</sub>**



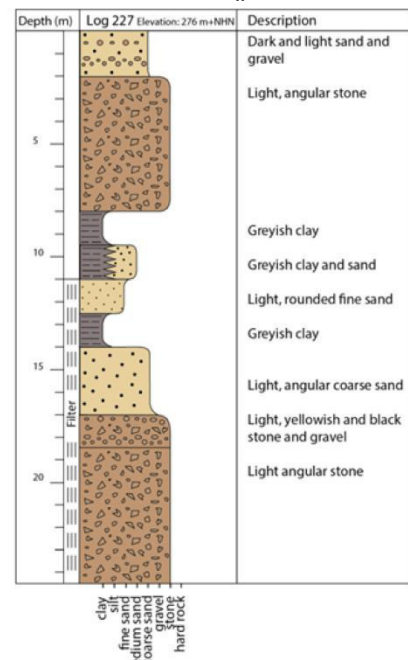
**DLR1<sub>IF</sub>**



**DLM3<sub>IF</sub>**

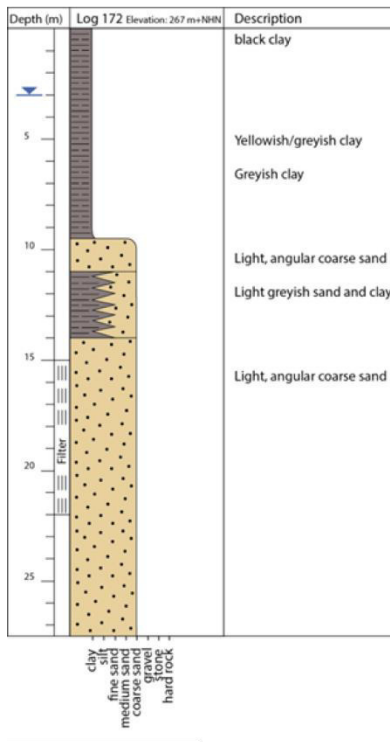


**DLM4<sub>IF</sub>**

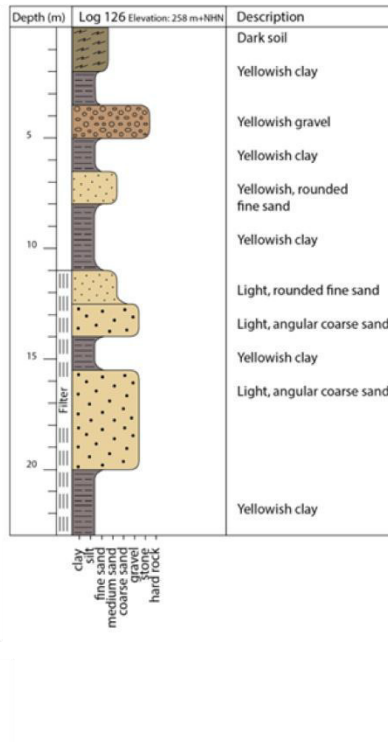


**Appendix A-A<sub>IF</sub>1: Deep drilling log descriptions (data provided by RBWB and MSABI, processed and digitized by Liedtke 2015) (IF).**

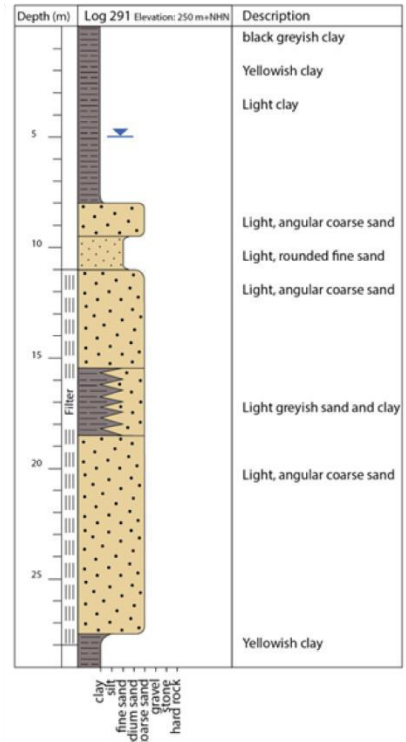
**DLM5<sub>IF</sub>**



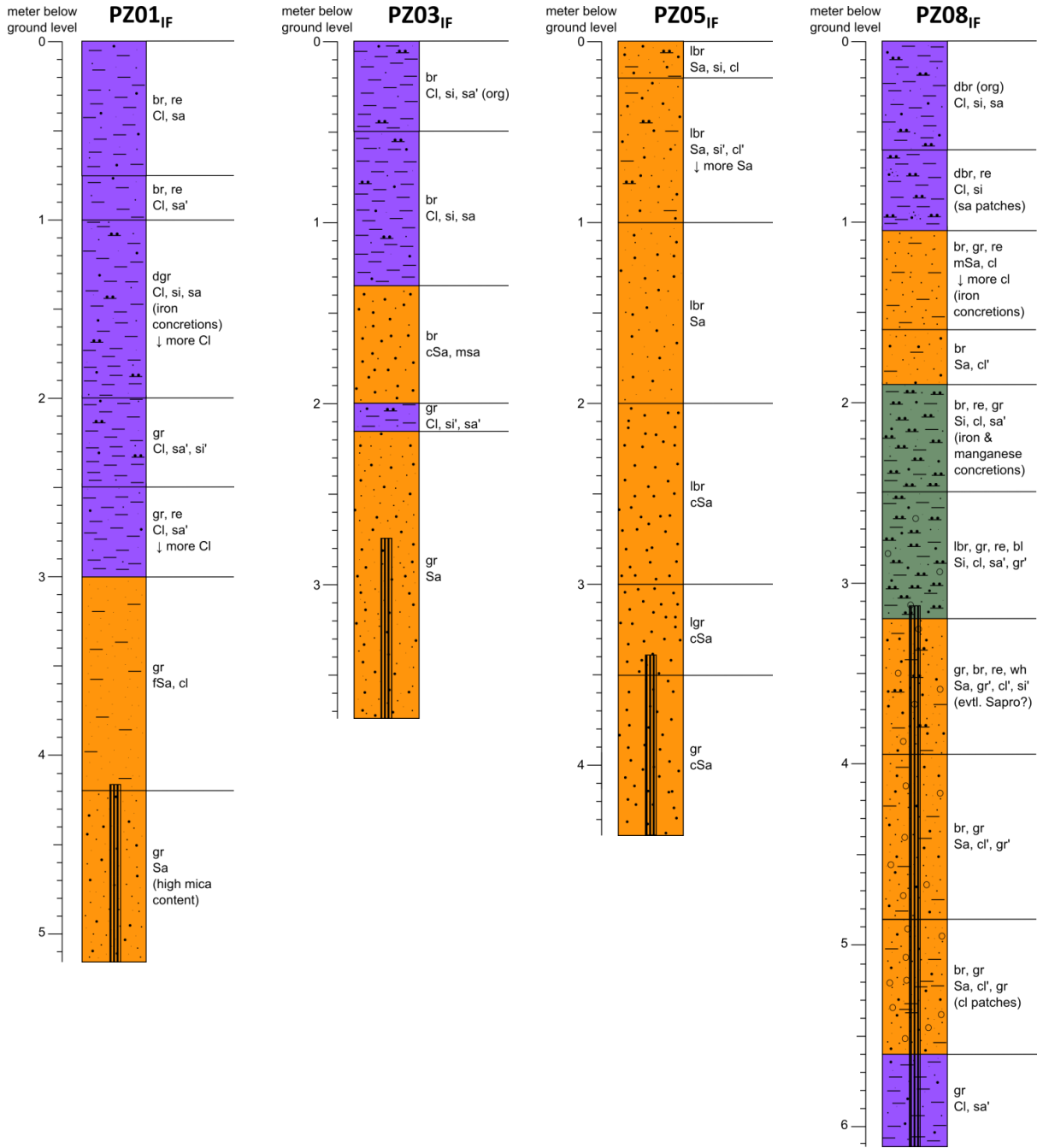
**DLM6<sub>IF</sub>**



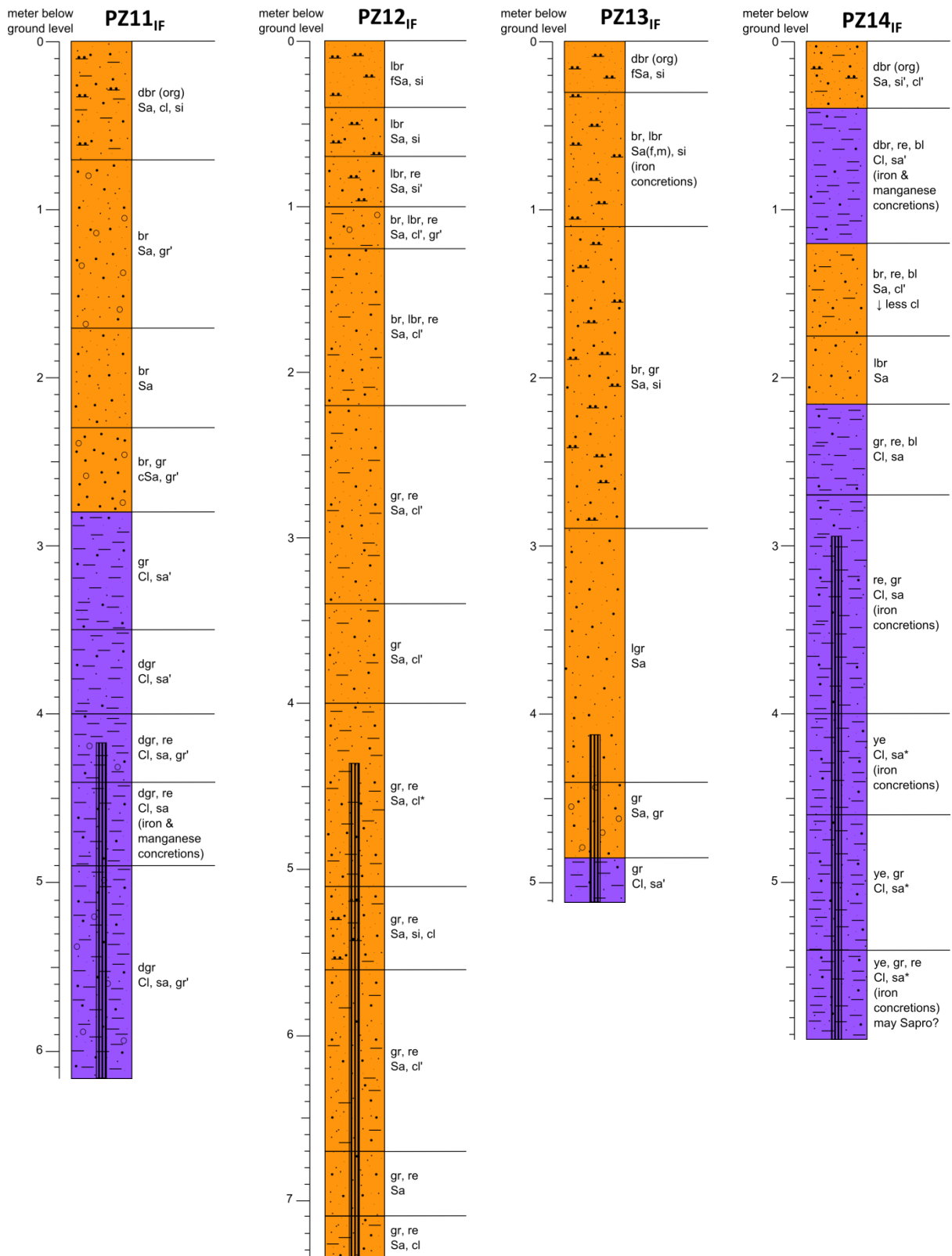
**DLM7<sub>IF</sub>**



**Appendix A-A<sub>IF</sub>2: Shallow drilling log descriptions of piezometers (IF).**



**Appendix A-A<sub>IF</sub>2: Shallow drilling log descriptions of piezometers (IF).  
(Continued)**



**Appendix A-A<sub>IF</sub>3: Hydraulic conductivities of sediments derived from grain size analysis (IF).**

Sampling point	Sampling depth	Hydraulic conductivity following Beyer (1964) [m/s]	Hydraulic conductivity following Hazen (1892) [m/s]	Hydraulic conductivity – average [m/s]
PZ02 <sub>IF</sub>	0.8	$3 \times 10^{-12}$	$6 \times 10^{-12}$	$5 \times 10^{-12}$
	1.7	$1 \times 10^{-07}$	$1 \times 10^{-07}$	$1 \times 10^{-07}$
	3.2	$3 \times 10^{-05}$	$4 \times 10^{-05}$	$4 \times 10^{-05}$
	4.0	$8 \times 10^{-05}$	$1 \times 10^{-04}$	$9 \times 10^{-05}$
PZ04 <sub>IF</sub>	4.1	$2 \times 10^{-04}$	$2 \times 10^{-04}$	$2 \times 10^{-04}$
PZ06 <sub>IF</sub>	1.0	$2 \times 10^{-11}$	$3 \times 10^{-11}$	$3 \times 10^{-11}$
	3.3	$6 \times 10^{-06}$	$5 \times 10^{-06}$	$6 \times 10^{-06}$
	4.5	$1 \times 10^{-04}$	$1 \times 10^{-04}$	$1 \times 10^{-04}$
	5.5	$2 \times 10^{-04}$	$2 \times 10^{-04}$	$2 \times 10^{-04}$
PZ07 <sub>IF</sub>	0.3	$2 \times 10^{-11}$	$3 \times 10^{-11}$	$2 \times 10^{-11}$
	3.9	$4 \times 10^{-05}$	$4 \times 10^{-05}$	$4 \times 10^{-05}$
	5.8	$6 \times 10^{-05}$	$7 \times 10^{-05}$	$6 \times 10^{-05}$
PZ09 <sub>IF</sub>	1.0	$1 \times 10^{-11}$	$5 \times 10^{-11}$	$3 \times 10^{-11}$
	2.9	$2 \times 10^{-07}$	$2 \times 10^{-07}$	$2 \times 10^{-07}$
	4.5	$2 \times 10^{-12}$	$4 \times 10^{-12}$	$3 \times 10^{-12}$
PZ10 <sub>IF</sub>	3.4	$2 \times 10^{-04}$	$2 \times 10^{-04}$	$2 \times 10^{-04}$

**Appendix A-A<sub>IF</sub>4: Hydraulic conductivities of sediments derived from falling-head permeability tests (IF).**

Sampling point	Hydraulic conductivity following Hvorslev (1951) [m/s]
PZ01 <sub>IF</sub>	$2 \times 10^{-05}$
PZ02 <sub>IF</sub>	$3 \times 10^{-05}$
PZ03 <sub>IF</sub>	$5 \times 10^{-05}$
PZ04 <sub>IF</sub>	$9 \times 10^{-05}$
PZ06 <sub>IF</sub>	$3 \times 10^{-05}$
PZ07 <sub>IF</sub>	$2 \times 10^{-06}$
PZ09 <sub>IF</sub>	$2 \times 10^{-07}$
PZ10 <sub>IF</sub>	$5 \times 10^{-05}$
PZ11 <sub>IF</sub>	$2 \times 10^{-05}$
PZ12 <sub>IF</sub>	$5 \times 10^{-07}$
PZ13 <sub>IF</sub>	$2 \times 10^{-05}$
PZ14 <sub>IF</sub>	$8 \times 10^{-07}$

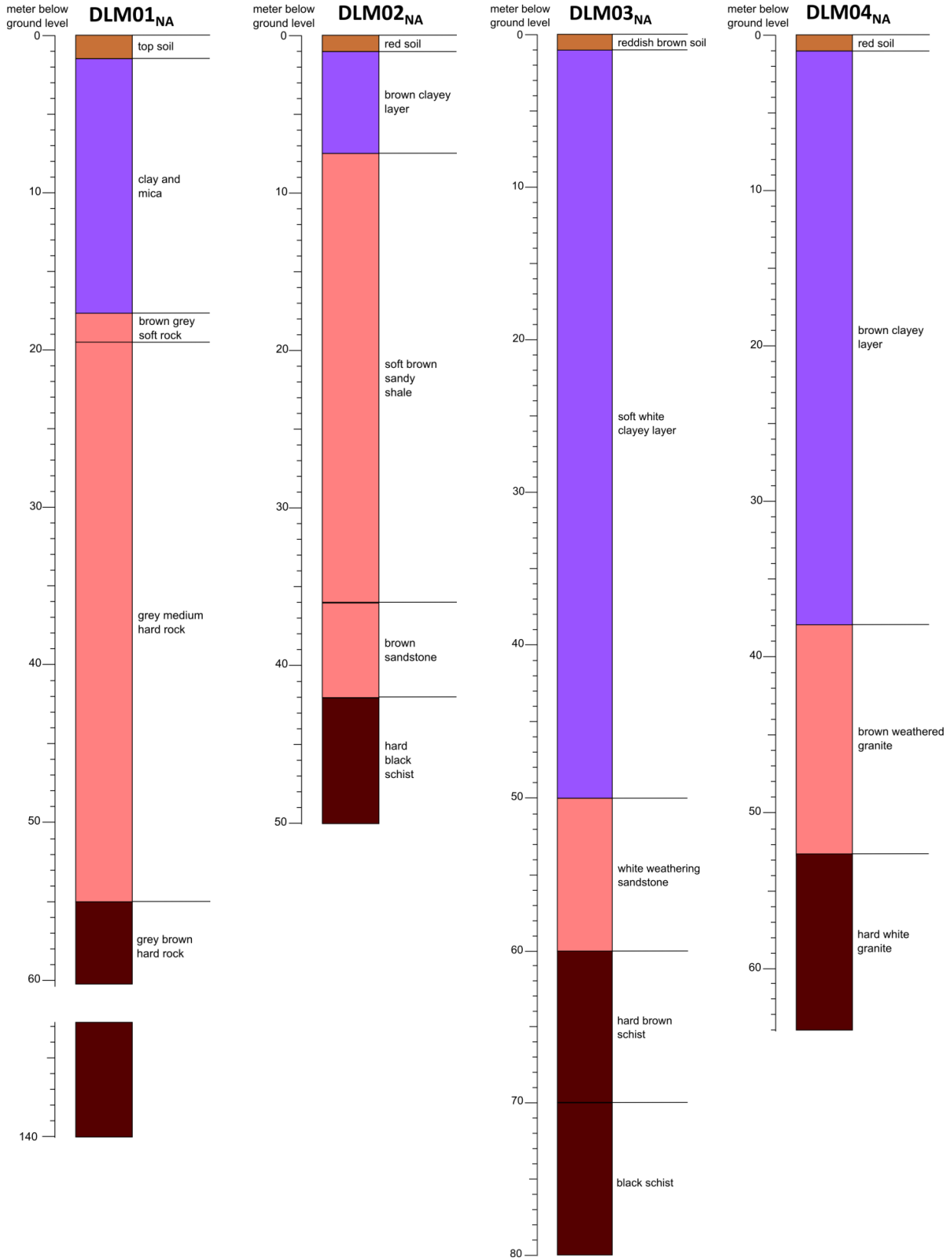
**Appendix A-A<sub>IF</sub>5: Hydraulic conductivities of sediments derived from pumping tests (data provided by RBWB, processed by Liedtke 2015) (IF).**

Sampling point	Hydraulic conductivity following Cooper and Jacob (1946) [m/s]	Sampling point	Hydraulic conductivity following Cooper and Jacob (1946) [m/s]
PT01 <sub>IF</sub>	$2 \times 10^{-02}$	PT18 <sub>IF</sub>	$9 \times 10^{-06}$
PT02 <sub>IF</sub>	$3 \times 10^{-03}$	PT19 <sub>IF</sub>	$9 \times 10^{-04}$
PT03 <sub>IF</sub>	$3 \times 10^{-02}$	PT20 <sub>IF</sub>	$3 \times 10^{-02}$
PT04 <sub>IF</sub>	$2 \times 10^{-05}$	PT21 <sub>IF</sub>	$2 \times 10^{-02}$
PT05 <sub>IF</sub>	$8 \times 10^{-06}$	PT22 <sub>IF</sub>	$8 \times 10^{-01}$
PT06 <sub>IF</sub>	$6 \times 10^{-05}$	PT23 <sub>IF</sub>	$8 \times 10^{-03}$
PT07 <sub>IF</sub>	$5 \times 10^{-05}$	PT24 <sub>IF</sub>	$1 \times 10^{-02}$
PT08 <sub>IF</sub>	$4 \times 10^{-06}$	PT25 <sub>IF</sub>	$1 \times 10^{-03}$
PT09 <sub>IF</sub>	$4 \times 10^{-05}$	PT26 <sub>IF</sub>	$6 \times 10^{-06}$
PT10 <sub>IF</sub>	$2 \times 10^{-02}$	PT27 <sub>IF</sub>	$5 \times 10^{-06}$
PT11 <sub>IF</sub>	$2 \times 10^{-05}$	PT28 <sub>IF</sub>	$1 \times 10^{-03}$
PT12 <sub>IF</sub>	$3 \times 10^{-06}$	PT29 <sub>IF</sub>	$7 \times 10^{-05}$
PT13 <sub>IF</sub>	$7 \times 10^{-05}$	PT30 <sub>IF</sub>	$2 \times 10^{-05}$
PT14 <sub>IF</sub>	$1 \times 10^{-03}$	PT31 <sub>IF</sub>	$6 \times 10^{-06}$
PT15 <sub>IF</sub>	$8 \times 10^{-02}$	PT32 <sub>IF</sub>	$2 \times 10^{-03}$
PT16 <sub>IF</sub>	$4 \times 10^{-06}$	PT33 <sub>IF</sub>	$2 \times 10^{-03}$
PT17 <sub>IF</sub>	$2 \times 10^{-02}$		

**Appendix A-A<sub>IF</sub>6: Geochemical compositions (major oxides) of rock and sediment samples (IF).**

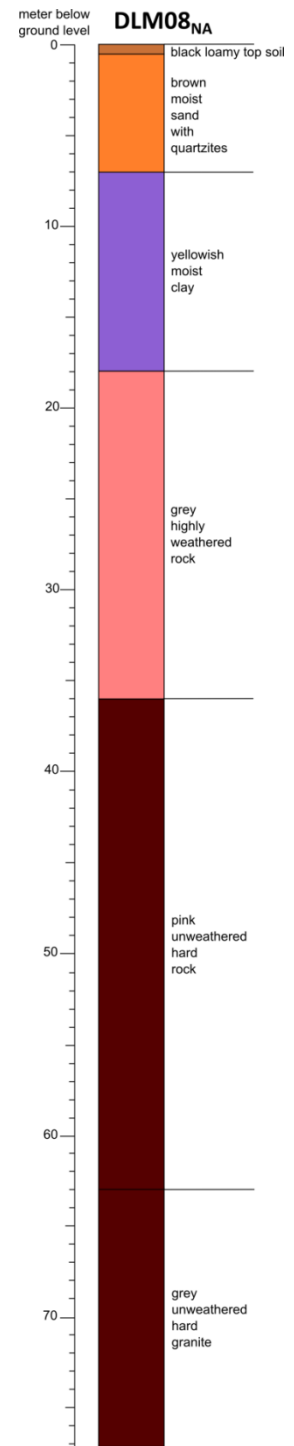
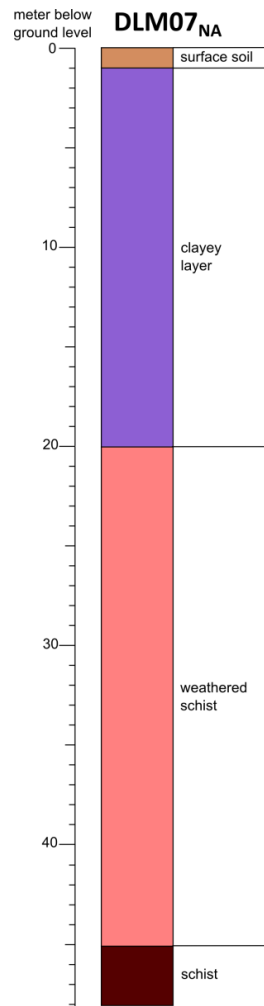
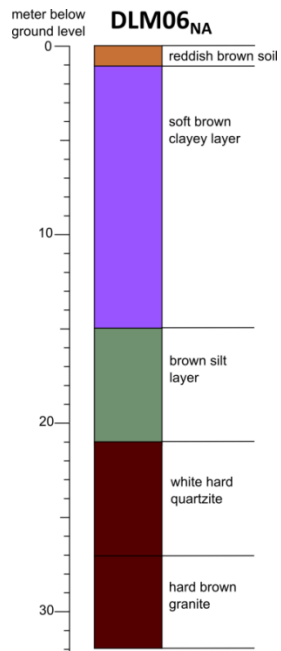
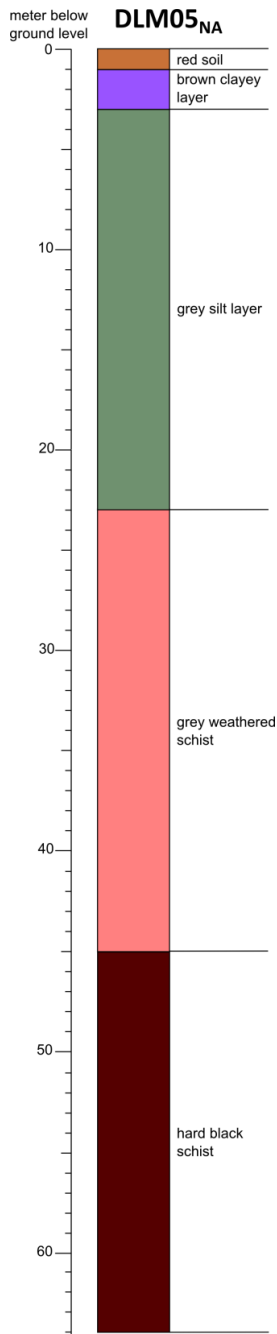
Sampling point	Sampling depth	LOI [%]	SiO <sub>2</sub> [%]	Al <sub>2</sub> O <sub>3</sub> [%]	Fe <sub>2</sub> O <sub>3</sub> [%]	MnO [%]	MgO [%]	CaO [%]	Na <sub>2</sub> O [%]	K <sub>2</sub> O [%]	TiO <sub>2</sub> [%]	P <sub>2</sub> O <sub>5</sub> [%]	SO <sub>3</sub> [%]
PZ02 <sub>IF</sub>	0.8	11.89	51.05	25.59	7.59	0.09	0.70	0.65	0.58	1.43	1.07	0.04	0.08
	1.7	3.42	71.60	14.69	2.63	0.03	0.49	1.33	2.08	3.05	0.45	0.03	0.16
	4.0	0.51	80.30	9.43	2.18	0.03	0.34	1.28	1.83	2.91	0.56	0.01	0.15
PZ04 <sub>IF</sub>	4.1	0.42	85.87	7.24	0.69	0.01	0.13	0.83	1.36	2.61	0.14	0.00	0.06
PZ06 <sub>IF</sub>	1.0	14.48	41.37	28.79	12.09	0.10	0.91	0.39	0.23	1.03	1.31	0.13	0.08
	3.3	2.36	75.28	11.68	4.92	0.04	0.45	1.00	1.34	2.79	1.09	0.05	0.21
	4.5	1.52	80.91	8.92	2.75	0.02	0.20	0.66	1.11	2.86	0.45	0.03	0.01
	5.5	0.43	88.49	5.96	0.65	0.01	0.04	0.53	0.91	2.48	0.12	0.00	0.02
PZ07 <sub>IF</sub>	0.3	14.65	41.25	22.94	15.68	0.11	0.93	0.54	0.17	1.47	1.56	0.38	0.03
	1.7	13.81	43.23	25.18	12.86	0.13	0.79	0.60	0.16	1.05	1.69	0.09	0.01
	2.3	5.87	70.07	16.24	3.01	0.02	0.40	0.64	0.90	2.30	0.60	0.02	0.06
	3.9	1.64	86.63	6.82	0.83	0.01	0.08	0.44	0.70	2.22	0.16	0.00	0.06
	5.4	7.08	62.50	17.31	6.34	0.15	0.87	1.16	1.43	2.61	0.78	0.16	0.21
	5.8	0.65	83.75	8.22	1.41	0.02	0.28	0.93	1.37	2.91	0.24	0.02	0.07
PZ09 <sub>IF</sub>	1.0	7.73	58.72	18.89	7.69	0.07	0.97	1.13	1.30	2.59	0.94	0.22	0.18
	2.9	2.50	74.72	12.74	2.92	0.03	0.50	1.23	1.75	3.01	0.61	0.04	0.19
	4.5	8.45	62.80	18.67	8.32	0.02	0.26	0.32	0.27	0.96	1.02	0.06	0.26
	6.0	6.75	67.43	15.66	6.65	0.07	0.38	0.48	0.50	1.85	1.06	0.03	0.29
PZ10 <sub>IF</sub>	3.4	0.50	79.35	8.30	4.15	0.04	0.28	0.88	1.29	2.97	1.23	0.01	0.14
	3.9	7.06	68.20	16.80	4.79	0.02	0.27	0.35	0.25	1.05	1.12	0.06	0.26
OC1 <sub>IF</sub>	-	0.37	65.47	15.69	4.16	0.05	1.41	3.80	3.90	2.67	0.54	0.17	0.11
OC2 <sub>IF</sub>	-	0.29	61.39	14.91	7.22	0.10	2.09	3.95	3.54	3.53	1.05	0.36	0.21
OC4 <sub>IF</sub>	-	0.24	74.53	12.62	1.51	0.02	0.16	1.30	2.83	5.91	0.28	0.05	< LOD
-	-	0.60	52.94	17.59	8.85	0.20	4.31	6.89	5.04	1.40	0.77	0.14	0.17
OC6 <sub>IF</sub>	-	0.50	74.33	13.36	0.60	0.00	< LOD	0.45	1.90	7.63	0.02	< LOD	< LOD

**Appendix A-A<sub>NA</sub>1: Deep drilling log descriptions (data provided by MWE) (NA).**

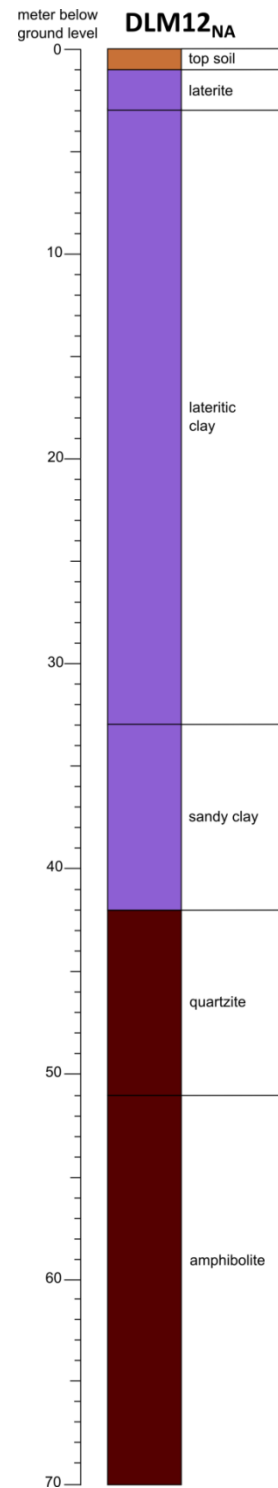
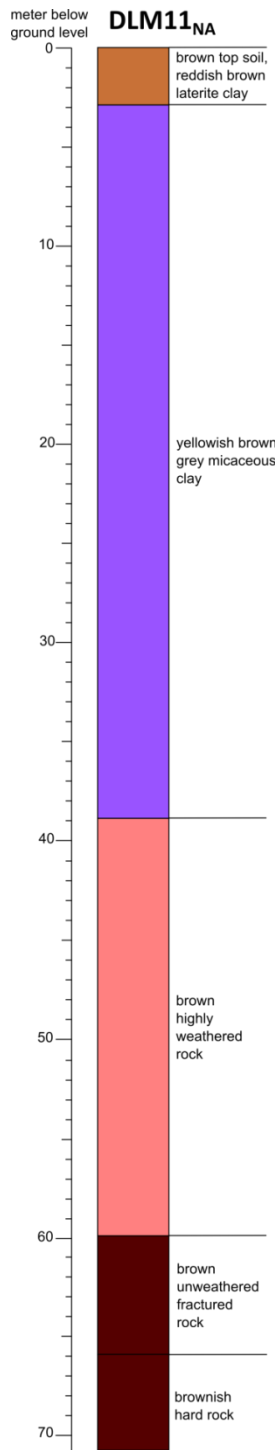
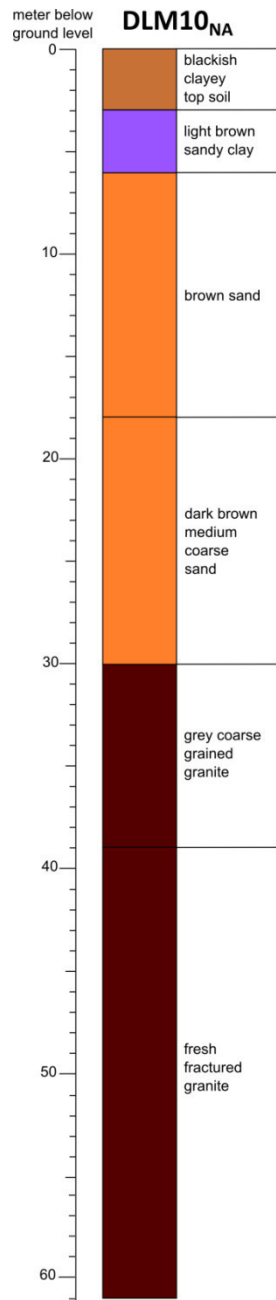
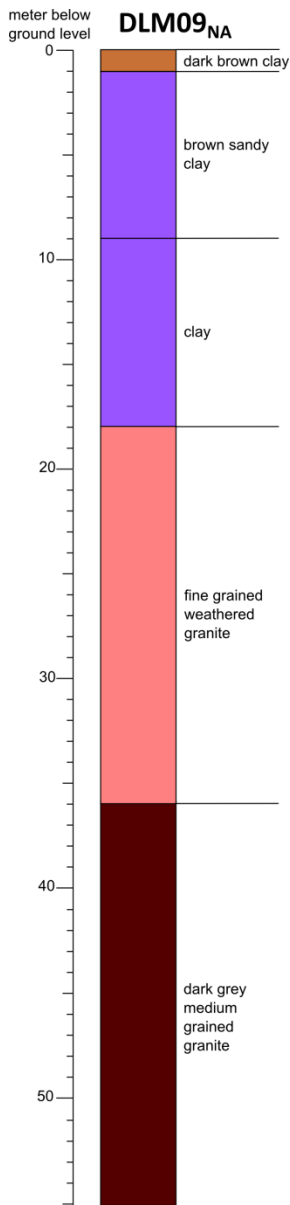




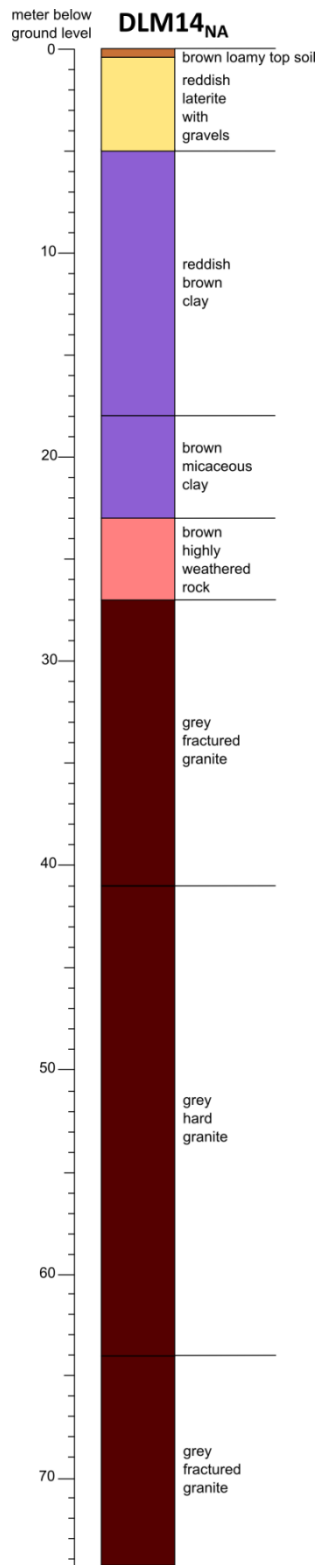
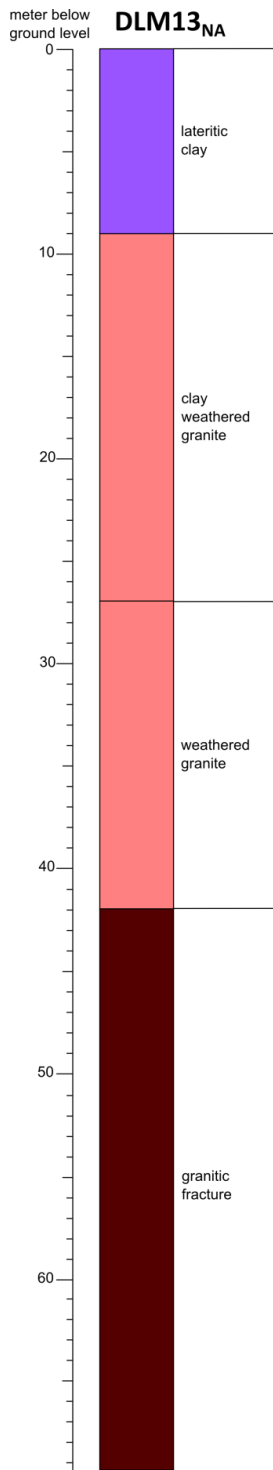
**Appendix A-A<sub>NA</sub>1: Deep drilling log descriptions (data provided by MWE) (NA).  
(Continued)**



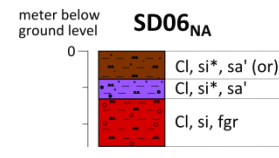
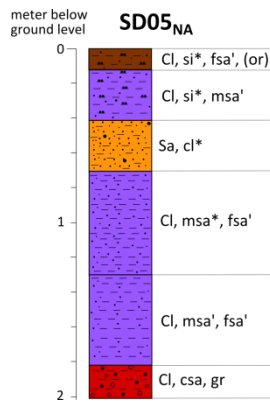
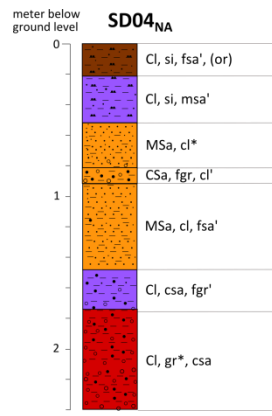
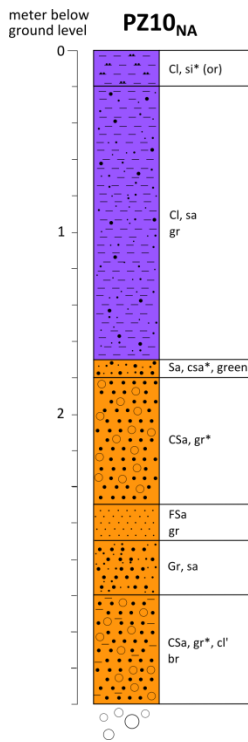
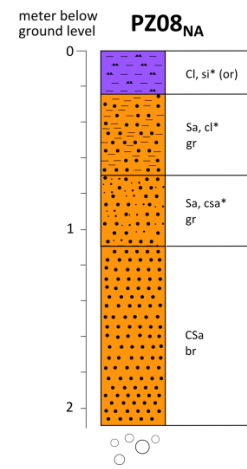
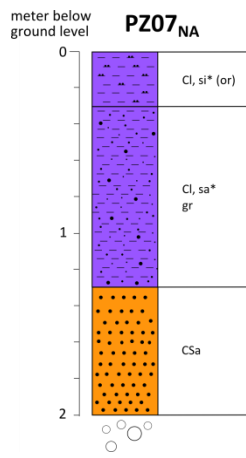
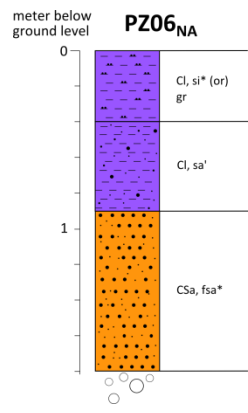
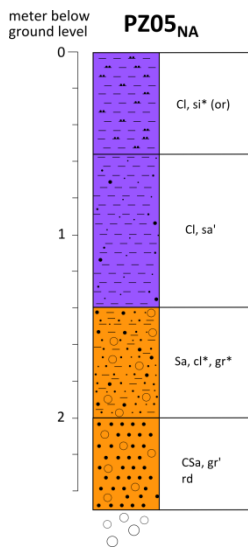
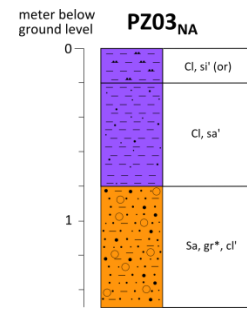
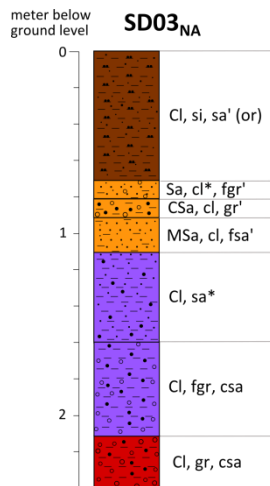
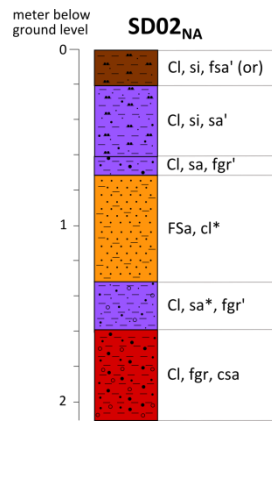
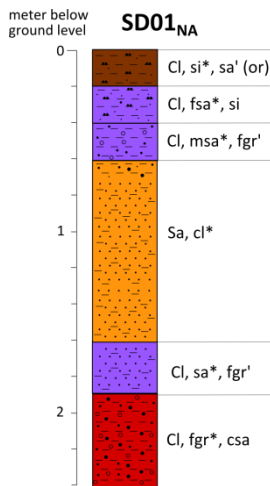
**Appendix A-A<sub>NA</sub>1: Deep drilling log descriptions (data provided by MWE) (NA).  
(Continued)**



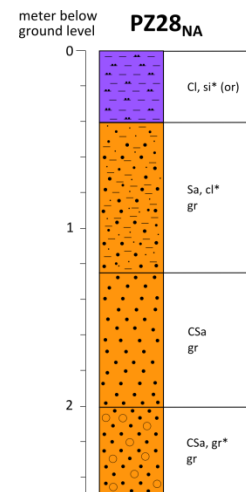
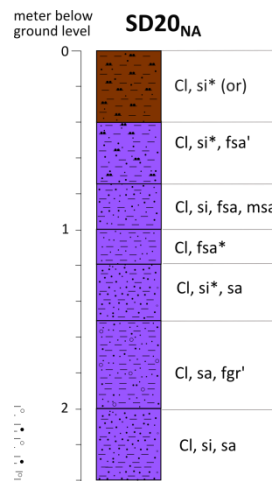
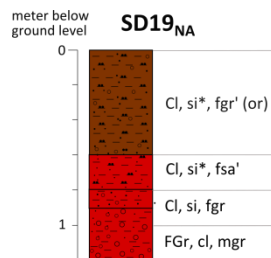
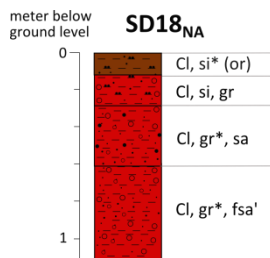
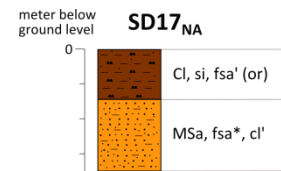
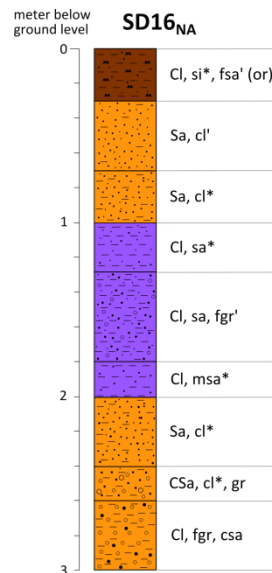
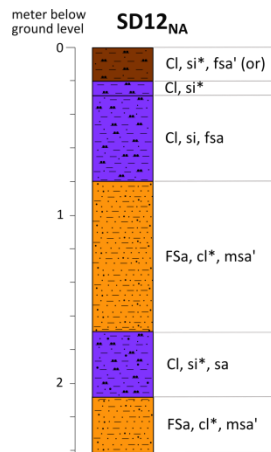
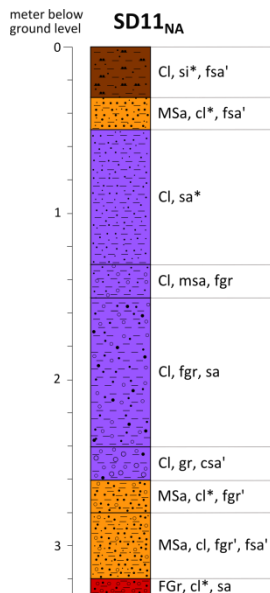
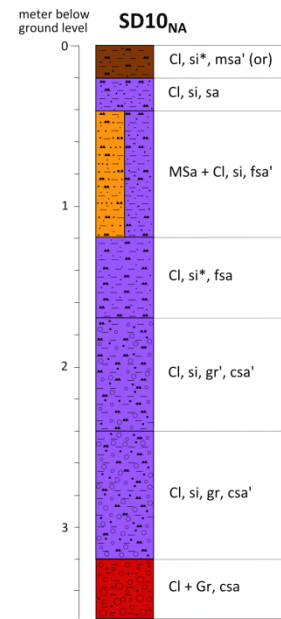
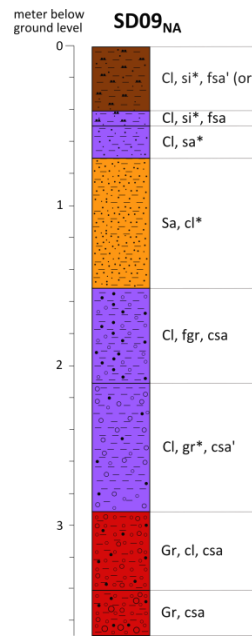
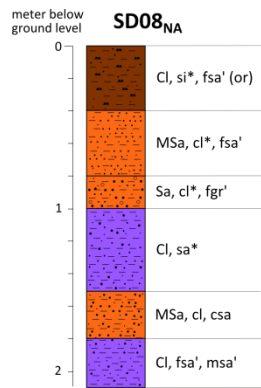
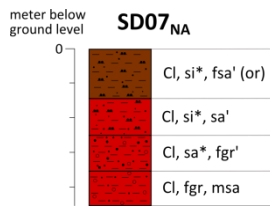
**Appendix A-A<sub>NA</sub>1: Deep drilling log descriptions (data provided by MWE) (NA).  
(Continued)**



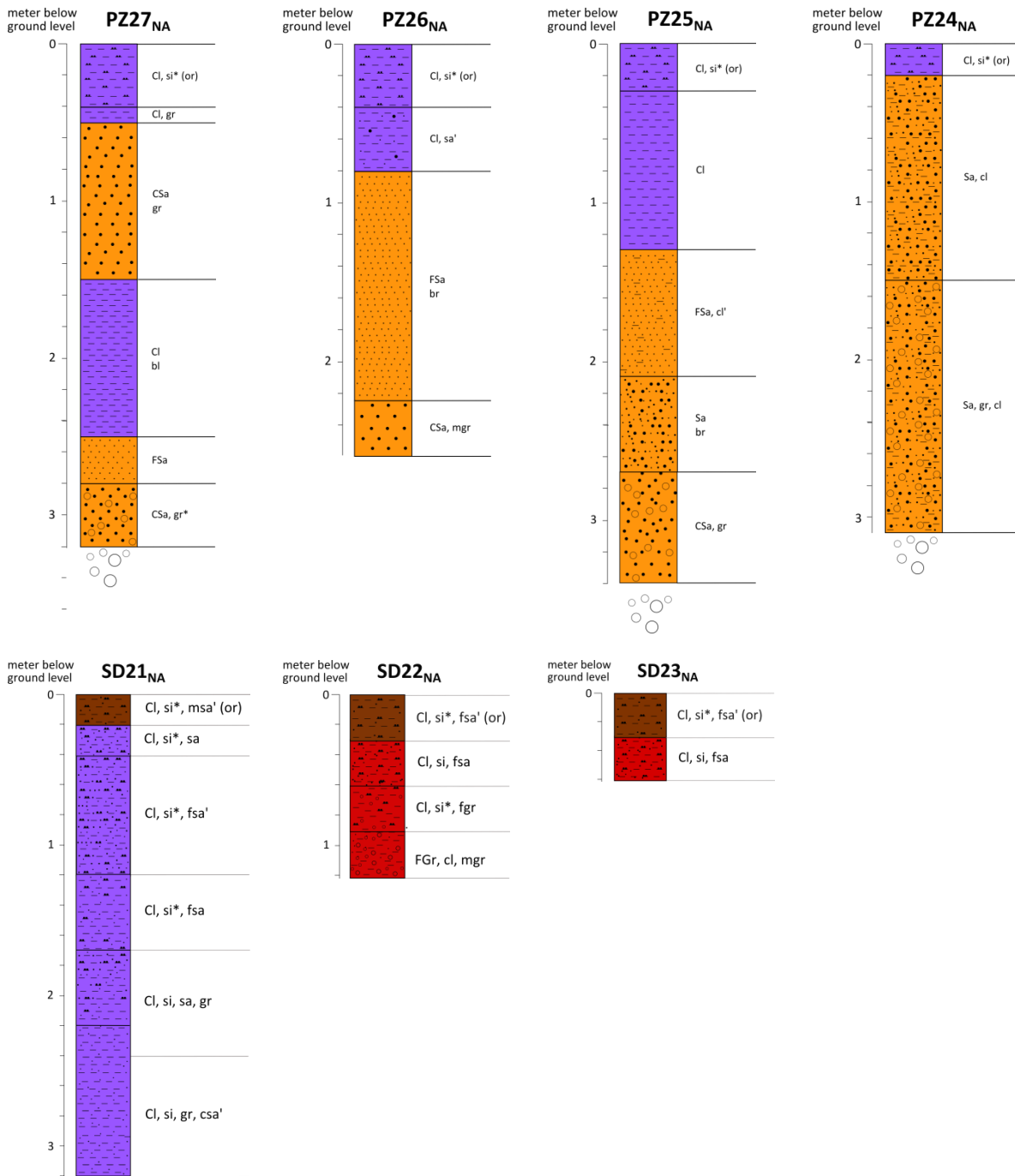
**Appendix A-A<sub>NA</sub>2: Shallow drilling log descriptions of piezometers and additional drilling logs (processed by Heiß 2016) (NA).**



**Appendix A-A<sub>NA</sub>2: Shallow drilling log descriptions of piezometers and additional drilling logs (processed by Heiß 2016)**  
**(Continued) (NA).**



**Appendix A-A<sub>NA</sub>2: Shallow drilling log descriptions of piezometers and additional drilling logs (processed by Heiß 2016) (Continued) (NA).**



**Appendix A-A<sub>NA</sub>3: Hydraulic conductivities of sediments derived from grain size analysis (NA).**

Sampling point	Sampling depth	Hydraulic conductivity following Sauerbrey (1932) [m/s]
SD14 <sub>NA</sub>	1.6	$4 \times 10^{-06}$
	3.0	$7 \times 10^{-07}$
SD15 <sub>NA</sub>	1.9	$1 \times 10^{-06}$
	2.9	$8 \times 10^{-05}$
SD12 <sub>NA</sub>	2.1	$1 \times 10^{-06}$

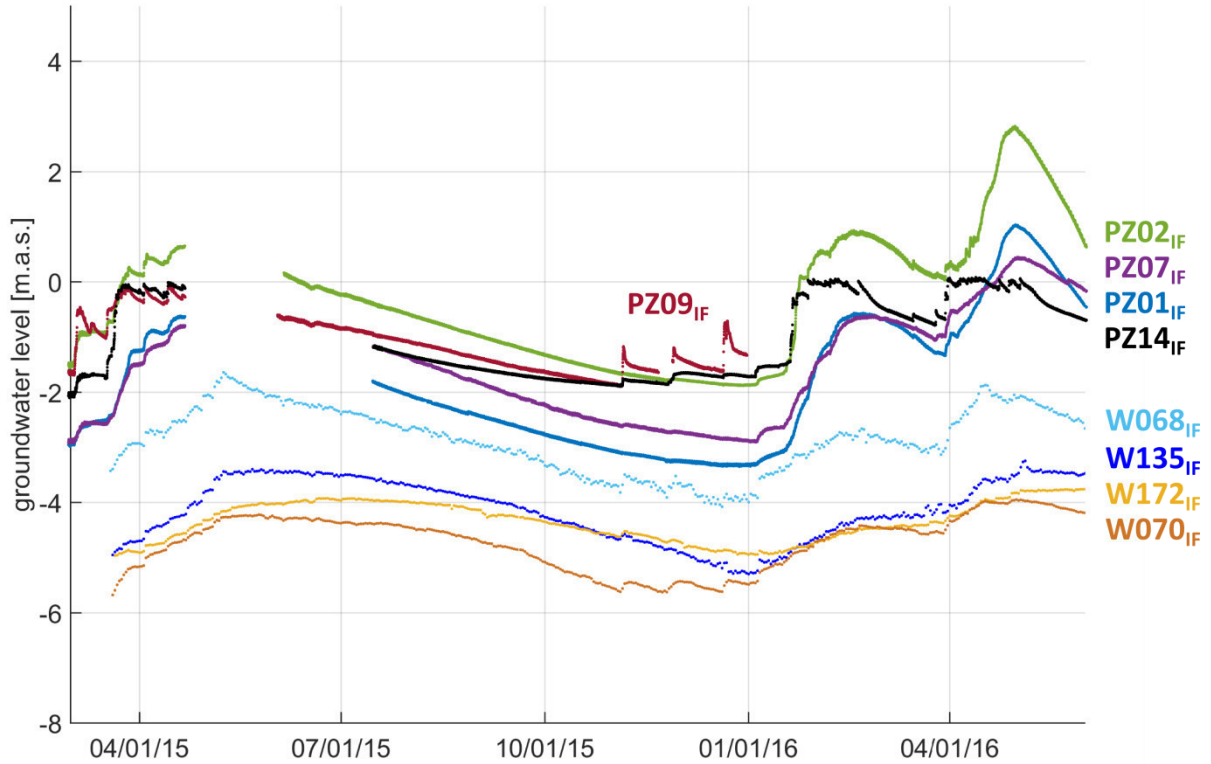
**Appendix A-A<sub>NA</sub>4: Hydraulic conductivities of sediments derived from falling-head permeability tests (NA).**

Sampling point	Hydraulic conductivity following Hvorslev (1951) [m/s]
PZ40L <sub>NA</sub>	$3 \times 10^{-07}$
PZ40S <sub>NA</sub>	$3 \times 10^{-07}$
PZ42L <sub>NA</sub>	$8 \times 10^{-07}$
PZ46L <sub>NA</sub>	$1 \times 10^{-06}$
PZ46S <sub>NA</sub>	$1 \times 10^{-06}$

**Appendix A-A<sub>NA</sub>5: Geochemical compositions (major oxides) of saprolite and sediment samples (LOD = limit of detection) (NA).**

Sampling point	Sampling depth	LOI [%]	SiO <sub>2</sub> [%]	Al <sub>2</sub> O <sub>3</sub> [%]	Fe <sub>2</sub> O <sub>3</sub> [%]	MnO [%]	MgO [%]	CaO [%]	Na <sub>2</sub> O [%]	K <sub>2</sub> O [%]	TiO <sub>2</sub> [%]	P <sub>2</sub> O <sub>5</sub> [%]	SO <sub>3</sub> [%]
SA1 <sub>NA</sub>	0.5	6.82	72.18	12.07	5.69	0.16	0.12	0.17	< LOD	0.71	1.19	0.07	0.31
	1.0	6.40	67.30	13.30	10.97	0.05	0.07	0.13	< LOD	0.46	0.83	0.07	0.26
	1.9	6.57	67.61	15.42	8.06	0.05	0.13	0.23	< LOD	0.54	0.86	0.04	0.21
	2.7	6.40	67.92	14.72	10.79	0.02	0.07	0.11	< LOD	0.34	0.56	0.03	0.16
	3.6	6.95	65.31	19.32	5.54	0.04	0.31	0.11	< LOD	1.81	0.61	0.03	0.17
	4.8	5.97	57.00	25.75	6.10	0.06	0.40	0.06	0.05	3.61	0.69	0.07	0.03
	5.1	6.68	62.98	19.86	6.24	0.03	0.15	0.10	0.03	3.13	0.53	0.05	0.14
	6.2	3.74	71.66	16.60	1.48	0.01	0.03	0.08	0.09	5.65	0.14	0.02	0.06
	6.8	4.49	68.98	17.82	2.39	0.01	0.06	0.09	0.06	5.47	0.25	0.03	0.08
	7.2	3.86	71.91	16.11	1.89	0.02	0.03	0.08	0.06	5.12	0.15	0.03	0.04
PZ03 <sub>NA</sub>	0.8	0.60	96.37	1.44	0.33	< LOD	< LOD	0.09	< LOD	0.09	0.07	< LOD	0.03
PZ05 <sub>NA</sub>	1.4	0.77	93.58	3.49	0.59	< LOD	< LOD	0.12	0.19	1.22	0.10	0.01	0.04
	2.0	3.37	68.14	17.61	2.75	0.02	0.22	0.49	2.40	4.31	0.42	0.05	0.09
	2.3	0.64	73.09	14.76	0.72	0.01	0.04	0.27	3.32	6.81	0.07	< LOD	0.05
PZ10 <sub>NA</sub>	2.1	0.78	94.61	2.59	0.81	0.01	< LOD	0.10	< LOD	0.54	0.20	< LOD	0.06
PZ40 <sub>NA</sub>	0.2	4.10	80.59	6.78	4.58	0.05	0.04	0.14	0.05	1.17	1.35	0.03	0.32
	0.5	3.93	81.47	9.27	1.95	0.03	0.06	0.13	0.02	1.06	1.17	0.01	0.26
	2.2	0.19	95.41	1.81	0.21	0.00	< LOD	0.08	0.04	0.90	0.04	< LOD	0.02
	2.9	0.43	88.20	4.38	1.76	0.02	< LOD	2.82	0.13	0.64	0.26	0.05	0.02
PZ42 <sub>NA</sub>	0.2	5.98	80.65	6.96	1.87	0.03	0.06	0.21	0.10	1.41	0.95	0.05	0.24
	0.5	4.43	79.82	10.39	1.86	0.02	0.11	0.17	0.07	1.26	0.85	0.01	0.23
	2.1	0.42	95.99	1.93	0.34	0.01	< LOD	0.08	0.00	0.69	0.10	< LOD	0.02
SD14 <sub>NA</sub>	2.4	5.18	68.69	13.96	7.86	0.03	0.22	0.24	0.16	2.04	0.82	0.07	0.28
	3.5	2.36	89.78	4.79	1.06	0.04	0.01	0.14	0.03	1.01	0.68	0.02	0.25
	4.0	2.94	81.13	5.23	9.20	0.02	0.01	0.13	0.03	0.93	0.36	0.13	0.16
PZ46 <sub>NA</sub>	0.2	11.32	64.10	15.63	4.29	0.06	0.23	0.63	0.13	1.56	1.27	0.17	0.28
	0.5	3.94	80.66	9.53	2.07	0.02	0.13	0.20	0.08	1.32	0.74	0.02	0.23
	1.8	1.48	89.22	5.44	1.22	0.02	0.04	0.15	0.07	1.41	0.39	0.01	0.16
	2.2	0.32	95.95	1.30	0.26	0.00	< LOD	0.09	< LOD	0.45	0.05	< LOD	0.03
SD15 <sub>NA</sub>	2.9	1.22	90.21	4.43	1.60	0.02	0.01	0.14	0.05	0.95	0.36	0.01	0.05
PZ48 <sub>NA</sub>	0.2	14.74	58.75	16.34	5.40	0.09	0.24	0.52	0.13	1.65	1.19	0.21	0.41
	0.5	7.37	73.90	11.77	2.63	0.08	0.20	0.27	0.16	1.82	0.84	0.05	0.32
PZ49 <sub>NA</sub>	0.2	22.06	50.08	16.88	6.36	0.06	0.22	0.49	0.10	1.32	1.21	0.21	0.70
	0.5	10.77	62.84	16.52	4.39	0.06	0.25	0.42	0.18	2.11	1.36	0.12	0.68
PZ50 <sub>NA</sub>	0.2	19.00	54.94	19.05	6.31	0.06	0.18	0.25	0.06	1.03	1.27	0.24	0.40
	0.5	20.99	48.64	19.45	5.98	0.07	0.19	0.38	0.08	1.16	1.29	0.17	1.30
SD12 <sub>NA</sub>	2.1	2.65	84.43	7.95	1.41	0.02	0.08	0.14	0.09	1.51	0.47	0.02	0.35
SD11 <sub>NA</sub>	1.7	6.10	71.08	16.31	3.76	0.02	0.12	0.12	< LOD	1.06	0.87	0.04	0.21
	2.9	1.81	87.94	6.06	0.71	0.02	< LOD	0.09	0.00	1.27	0.59	0.01	0.18
	3.3	3.94	78.94	11.48	2.60	0.02	0.12	0.12	0.00	1.46	0.71	0.02	0.17
PZ24 <sub>NA</sub>	2.8	0.07	99.69	0.12	0.13	< LOD	< LOD	0.07	< LOD	0.03	0.01	< LOD	< LOD
PZ26 <sub>NA</sub>	2.6	0.18	97.07	1.42	0.21	< LOD	< LOD	0.09	0.01	0.67	0.04	< LOD	< LOD
PZ27 <sub>NA</sub>	3.0	0.16	98.29	0.58	0.19	< LOD	< LOD	0.07	< LOD	0.13	0.02	< LOD	< LOD

Appendix B-B<sub>IF</sub>1: Hydrographs of groundwater levels (IF).



Appendix B-B<sub>NA</sub>1: Pearson's correlation coefficients of hydrographs of different piezometers. Coefficients equal or higher than 0.95 are marked as bold (NA).

	PZ06 <sub>NA</sub>	PZ07 <sub>NA</sub>	PZ10 <sub>NA</sub>	PZ25 <sub>NA</sub>	PZ26 <sub>NA</sub>	PZ27 <sub>NA</sub>	PZ28 <sub>NA</sub>	PZ40L <sub>NA</sub>	PZ40S <sub>NA</sub>	PZ42L <sub>NA</sub>	PZ42S <sub>NA</sub>	PZ46L <sub>NA</sub>	PZ46S <sub>NA</sub>	PZ48 <sub>NA</sub>	PZ49 <sub>NA</sub>	PZ50 <sub>NA</sub>
PZ06 <sub>NA</sub>																
PZ07 <sub>NA</sub>	<b>0.96</b>															
PZ10 <sub>NA</sub>	0.63	0.72														
PZ25 <sub>NA</sub>	0.66	0.72	0.63													
PZ26 <sub>NA</sub>	0.67	0.74	0.64	<b>0.98</b>												
PZ27 <sub>NA</sub>	0.74	0.79	0.68	0.91	0.91											
PZ28 <sub>NA</sub>	0.67	0.73	0.69	0.76	0.77	0.83										
PZ40L <sub>NA</sub>	0.12	0.03	-0.21	0.08	0.02	0.15	0.17									
PZ40S <sub>NA</sub>	0.74	0.80	0.60	0.73	0.75	0.84	0.82	0.76								
PZ42L <sub>NA</sub>	0.70	0.64	0.47	0.56	0.55	0.64	0.65	0.42	0.83							
PZ42S <sub>NA</sub>	0.73	0.74	0.66	0.75	0.73	0.76	0.74	0.20	0.86	0.94						
PZ46L <sub>NA</sub>	0.47	0.40	0.20	0.42	0.39	0.56	0.59	0.60	0.76	0.75	0.57					
PZ46S <sub>NA</sub>	0.54	0.63	0.10	0.55	0.39	0.72	0.79	0.47	0.78	0.84	0.75	<b>0.95</b>				
PZ48 <sub>NA</sub>	0.87	0.74	0.46	0.70	0.75	0.75	0.67	0.45	0.71	0.61	0.69	0.75	0.71			
PZ49 <sub>NA</sub>	0.68	0.77	0.69	0.75	0.79	0.74	0.74	0.49	0.64	0.34	0.64	0.31	0.62	0.92		
PZ50 <sub>NA</sub>	0.86	0.84	0.88	0.90	0.88	0.89	0.79	0.71	0.87	0.83	0.89	0.94	0.77	0.86	0.81	



**Appendix C-C<sub>IF1</sub>: In-situ parameters and HCO<sub>3</sub><sup>-</sup> and CO<sub>2</sub> concentrations of the four snapshot samplings (IF).**

Sampling point	Sampling date	EC [μS/cm]	pH [-]	Eh [mV]	O <sub>2</sub> <sup>sat</sup> [%]	O <sub>2</sub> <sup>con</sup> [mg/L]	T <sub>w</sub> [°C]	HCO <sub>3</sub> <sup>-</sup> [mg/L]	CO <sub>2</sub> [mg/L]
ST3 <sub>IF</sub>	05/17/14	94	7.2	429	92	7.5	23.7	59.4	5.3
ST2 <sub>IF</sub>	05/17/14	60	7.5	427	101	8.5	22.3	34.4	4.4
PW04 <sub>IF</sub>	05/19/14	265	6.5	253	40	3.3	27.2	190.2	25.5
PW05 <sub>IF</sub>	05/19/14	282	6.8	218	55	4.3	27.3	193.9	14.4
PW06 <sub>IF</sub>	05/20/14	127	6.1	364	50	3.8	28.0	99.2	41.4
ST4 <sub>IF</sub>	02/20/14	86	7.1	263	100	8.2	23.6	47.3	4.4
PW09 <sub>IF</sub>	05/20/14	340	6.6	310	42	3.5	28.2	184.0	40.0
PW11 <sub>IF</sub>	05/21/14	184	6.3	319	46	3.5	28.0	120.0	37.8
PW14 <sub>IF</sub>	05/22/14	251	6.2	359	49	3.7	29.2	91.3	36.1
PW17 <sub>IF</sub>	05/23/14	262	6.4	247	50	3.9	27.6	123.1	26.4
PW18 <sub>IF</sub>	05/23/14	590	6.4	312	43	3.3	27.7	293.6	74.4
PW19 <sub>IF</sub>	05/23/14	904	6.2	432	31	2.4	28.7	134.0	58.1
PW21 <sub>IF</sub>	05/27/14	164	6.3	308	39	3.0	27.4	85.3	36.1
PW22 <sub>IF</sub>	05/27/14	169	6.3	320	43	3.2	28.5	106.1	27.7
PW23 <sub>IF</sub>	05/27/14	334	6.7	127	42	3.2	29.0	201.9	54.6
PW24 <sub>IF</sub>	05/27/14	434	6.9	286	44	3.3	28.2	302.3	28.2
PW25 <sub>IF</sub>	05/28/14	20	5.1	498	73	5.5	28.9	3.9	10.6
PW26 <sub>IF</sub>	05/28/14	419	6.2	336	39	3.0	28.7	119.4	58.1
DW27 <sub>IF</sub>	05/28/14	172	6.2	381	45	3.4	27.7	102.1	27.7
PW28 <sub>IF</sub>	05/29/14	112	5.7	427	55	4.2	27.3	28.0	33.4
PW29 <sub>IF</sub>	05/29/14	420	6.5	420	36	2.8	27.6	290.3	59.9
PW30 <sub>IF</sub>	05/29/14	2130	6.7	313	35	2.6	28.3	648.9	44.0
PW31 <sub>IF</sub>	05/29/14	346	6.5	349	38	2.9	27.7	194.3	28.2
PW32 <sub>IF</sub>	05/29/14	480	6.2	389	43	3.3	27.2	216.9	80.1
ST5 <sub>IF</sub>	05/30/14	168	7.7	401	99	8.0	24.4	109.9	9.7
PW34 <sub>IF</sub>	05/30/14	215	6.3	384	59	4.5	27.5	145.0	43.1
PW35 <sub>IF</sub>	05/30/14	314	6.3	343	42	3.2	27.4	211.4	52.8
DW36 <sub>IF</sub>	05/30/14	1025	7.6	432	56	4.3	27.1	457.0	7.0
DW37 <sub>IF</sub>	06/02/14	161	6.2	461	52	3.9	27.5	26.7	9.7
PW38 <sub>IF</sub>	06/02/14	76	5.4	323	45	3.4	28.1	18.3	46.7
PW39 <sub>IF</sub>	06/02/14	119	6.3	257	40	3.3	28.0	75.6	27.3
PW41 <sub>IF</sub>	06/02/14	1455	7.4	436	132	10.0	27.9	988.8	11.4
PW42 <sub>IF</sub>	06/02/14	361	6.5	181	31	2.3	29.1	202.1	35.2
PW43 <sub>IF</sub>	06/03/14	282	6.5	236	35	2.7	26.9	163.9	40.5
PW44 <sub>IF</sub>	06/03/14	298	6.5	258	40	3.1	27.3	214.0	38.3
PW46 <sub>IF</sub>	06/03/14	888	6.9	321	46	3.5	27.8	641.6	32.6
PW47 <sub>IF</sub>	06/03/14	372	6.6	369	73	5.4	29.9	130.7	21.6
PW48 <sub>IF</sub>	06/04/14	200	5.9	402	43	3.1	28.4	42.2	37.8
PW49 <sub>IF</sub>	06/04/14	330	6.5	326	44	3.4	27.0	214.9	44.9
FL1 <sub>IF</sub>	06/05/14	75	6.7	370	40	3.2	25.2	44.8	4.0
FL3 <sub>IF</sub>	06/05/14	413	7.5	415	39	2.9	29.2	276.4	33.4
ST1 <sub>IF</sub>	06/05/14	42	6.4	420	28	2.2	27.6	25.1	6.6
PW52 <sub>IF</sub>	06/07/14	197	6.6	402	45	3.4	28.5	118.5	22.4
DW53 <sub>IF</sub>	06/07/14	22	5.4	490	53	4.2	24.9	10.2	18.5
ST2 <sub>IF</sub>	06/12/14	54	7.6	430	91	7.9	21.0	27.6	4.8
ST2 <sub>IF</sub>	10/15/14	52	7.3	435	94	7.5	25.3	29.9	3.1
PW21 <sub>IF</sub>	10/15/14	159	6.4	303	49	3.7	28.2	70.2	11.4
PW15 <sub>IF</sub>	10/16/14	314	6.5	382	40	3.0	28.3	172.1	21.1
ST1 <sub>IF</sub>	10/18/14	40	7.6	400	95	7.4	27.2	28.1	3.5
PW05 <sub>IF</sub>	10/18/14	298	7.4	261	52	4.0	27.4	208.7	11.4
PW14 <sub>IF</sub>	10/19/14	264	6.4	405	55	4.1	29.1	91.5	28.2
DW27 <sub>IF</sub>	10/19/14	200	6.6	470	68	5.2	27.4	114.1	17.6
DW37 <sub>IF</sub>	10/21/14	146	6.6	450	62	4.7	28.0	42.7	7.0
PW09 <sub>IF</sub>	10/21/14	342	6.8	380	46	3.5	28.3	221.5	20.2
PW22 <sub>IF</sub>	10/21/14	178	6.5	354	42	3.2	28.6	112.3	27.3
PW18 <sub>IF</sub>	10/21/14	587	6.5	319	48	3.6	28.4	296.6	47.5
PW17 <sub>IF</sub>	10/21/14	295	6.6	234	50	3.8	27.7	122.7	25.5
ST4 <sub>IF</sub>	10/22/14	97	7.7	329	104	8.3	24.9	56.4	2.6
PW06 <sub>IF</sub>	10/22/14	160	6.4	402	53	4.0	28.3	94.0	18.5
PW48 <sub>IF</sub>	10/22/14	180	6.2	417	42	3.2	27.9	60.1	29.0
PW19 <sub>IF</sub>	10/22/14	857	6.4	416	39	2.9	28.3	148.3	36.1
PW28 <sub>IF</sub>	10/24/14	115	5.8	368	36	2.7	28.3	29.0	26.4
PW29 <sub>IF</sub>	10/24/14	425	6.5	428	42	3.2	27.8	258.1	43.1
PW30 <sub>IF</sub>	10/24/14	2190	6.7	355	42	3.1	28.5	668.2	46.7
DW36 <sub>IF</sub>	10/24/14	1318	7.3	370	52	4.1	26.7	851.2	15.0

**Appendix C-C<sub>IF</sub>1: *In-situ* parameters and HCO<sub>3</sub><sup>-</sup> and CO<sub>2</sub> concentrations of the four snapshot samplings (IF). (Continued)**

Sampling point	Sampling date	EC [μS/cm]	pH [-]	Eh [mV]	O <sub>2</sub> <sup>sat</sup> [%]	O <sub>2</sub> <sup>con</sup> [mg/L]	T <sub>w</sub> [°C]	HCO <sub>3</sub> <sup>-</sup> [mg/L]	CO <sub>2</sub> [mg/L]
PW35 <sub>IF</sub>	10/24/14	312	6.5	420	42	3.2	27.4	210.5	46.2
PW32 <sub>IF</sub>	10/24/14	486	6.4	437	46	3.5	27.6	221.5	59.0
PW47 <sub>IF</sub>	10/25/14	398	7.0	351	75	5.6	29.1	245.3	17.6
PW46 <sub>IF</sub>	10/25/14	569	6.8	339	56	4.3	28.2	353.3	22.0
PW43 <sub>IF</sub>	10/25/14	358	6.6	232	38	2.9	27.5	197.7	31.7
PW39 <sub>IF</sub>	10/27/14	133	6.4	287	41	3.3	26.5	70.2	19.4
PW23 <sub>IF</sub>	10/27/14	445	6.7	142	43	3.2	29.0	303.9	46.2
PW24 <sub>IF</sub>	10/27/14	430	7.0	337	49	3.7	28.1	249.0	12.3
PW42 <sub>IF</sub>	10/27/14	362	6.8	210	41	3.4	28.7	203.2	19.4
PW25 <sub>IF</sub>	10/28/14	254	6.4	387	82	6.2	28.2	97.6	23.8
PW38 <sub>IF</sub>	10/28/14	42	5.4	396	44	3.4	28.4	17.1	36.1
PW11 <sub>IF</sub>	10/28/14	189	6.5	318	46	3.5	27.7	123.3	33.0
PW34 <sub>IF</sub>	10/29/14	229	6.7	388	79	6.2	26.2	159.3	19.4
PW60 <sub>IF</sub>	10/29/14	510	7.2	390	38	2.9	28.0	321.3	9.7
PW61 <sub>IF</sub>	10/29/14	376	6.4	254	53	4.0	28.1	111.7	44.0
PW2 <sub>IF</sub>	05/15/15	171	6.3	327	41	3.1	28.5	110.4	17.6
PW09 <sub>IF</sub>	05/15/15	332	6.6	307	40	3.0	28.4	216.0	23.8
DW37 <sub>IF</sub>	05/15/15	204	6.5	462	66	4.9	28.7	22.6	8.8
PW21 <sub>IF</sub>	05/16/15	172	6.4	345	52	3.9	28.2	88.5	20.2
PW48 <sub>IF</sub>	05/16/15	229	6.0	386	43	3.2	28.3	69.6	38.7
PW19 <sub>IF</sub>	05/16/15	1069	6.3	384	35	2.6	28.9	153.8	43.1
PW17 <sub>IF</sub>	05/16/15	309	6.5	231	50	3.8	28.0	139.1	21.1
PW18 <sub>IF</sub>	05/16/15	566	6.5	314	48	3.6	28.2	289.2	51.9
PW05 <sub>IF</sub>	05/18/15	293	7.0	202	48	3.7	27.5	205.0	20.2
PW39 <sub>IF</sub>	05/18/15	115	6.4	281	39	3.1	26.9	66.5	26.4
PW23 <sub>IF</sub>	05/18/15	382	6.6	138	45	3.4	29.2	205.0	51.1
PW42 <sub>IF</sub>	05/18/15	357	6.7	214	36	2.7	28.5	212.3	28.2
PW43 <sub>IF</sub>	05/19/15	267	6.6	336	34	2.6	27.4	161.1	28.2
PW47 <sub>IF</sub>	05/19/15	390	6.7	405	86	6.3	29.6	157.4	21.1
PW46 <sub>IF</sub>	05/19/15	828	6.9	365	42	3.2	28.0	556.5	45.8
PW61 <sub>IF</sub>	05/19/15	356	6.0	283	41	3.2	28.2	102.5	45.8
PW15 <sub>IF</sub>	05/20/15	288	6.6	408	43	3.2	28.6	172.1	34.3
PW14 <sub>IF</sub>	05/20/15	259	6.3	373	50	3.7	29.4	95.2	37.0
DW27 <sub>IF</sub>	05/20/15	92	6.0	445	32	2.4	27.6	29.9	22.9
PW12 <sub>IF</sub>	05/20/15	356	6.8	336	45	3.5	27.4	227.0	23.8
PW32 <sub>IF</sub>	05/21/15	419	6.3	388	40	3.1	27.0	245.3	59.0
PW35 <sub>IF</sub>	05/21/15	313	6.4	364	43	3.3	27.5	227.0	44.9
DW36 <sub>IF</sub>	05/21/15	927	7.1	391	38	2.9	27.6	552.8	20.2
PW30 <sub>IF</sub>	05/21/15	2110	6.7	311	42	3.2	28.5	659.0	36.1
ST4 <sub>IF</sub>	05/22/15	86	7.3	234	97	8.2	22.6	48.2	5.3
PW06 <sub>IF</sub>	05/22/15	197	6.3	366	50	3.8	28.2	124.5	36.1
PW60 <sub>IF</sub>	05/22/15	478	7.1	395	97	7.4	28.2	340.5	15.0
PW29 <sub>IF</sub>	05/22/15	415	6.5	381	67	5.1	28.2	292.9	66.0
PW25 <sub>IF</sub>	05/23/15	21	5.1	470	82	6.1	29.0	4.3	11.4
PW38 <sub>IF</sub>	05/23/15	51	5.1	403	43	3.3	28.3	7.9	35.2
PW11 <sub>IF</sub>	05/23/15	181	6.4	345	50	3.8	27.9	121.4	30.8
ST2 <sub>IF</sub>	05/23/15	59	7.7	374	97	8.3	22.1	37.2	2.6
PZ01 <sub>IF</sub>	05/25/15	158	6.3	167	10	0.8	27.8	106.8	-
PZ06 <sub>IF</sub>	05/25/15	186	6.1	282	42	3.3	27.6	99.5	21.1
PZ08 <sub>IF</sub>	05/25/15	948	6.9	264	19	1.5	29.1	651.7	-
FL3 <sub>IF</sub>	05/25/15	255	7.3	415	126	9.3	29.5	186.7	3.5
PZ13 <sub>IF</sub>	05/26/15	179	6.2	244	21	1.6	29.3	117.8	35.2
PZ11 <sub>IF</sub>	05/26/15	205	6.3	399	24	1.8	28.5	135.5	-
ST1 <sub>IF</sub>	05/26/15	42	7.0	414	33	2.6	27.1	26.2	4.4
PZ04 <sub>IF</sub>	05/28/15	163	6.3	212	16	1.3	27.1	117.8	37.8
FL1 <sub>IF</sub>	05/28/15	93	6.3	416	52	4.0	27.1	55.5	10.6
PW29 <sub>IF</sub>	11/13/15	444	6.9	455	101	7.6	28.1	231.9	13.2
DW36 <sub>IF</sub>	11/13/15	959	7.8	413	38	2.9	27.9	518.7	4.0
PW35 <sub>IF</sub>	11/13/15	296	6.3	387	24	1.8	27.8	164.8	29.0
PW32 <sub>IF</sub>	11/13/15	485	6.2	422	33	2.5	28.1	177.0	-
PW30 <sub>IF</sub>	11/13/15	2210	6.6	346	22	1.6	29.7	515.6	39.6
PW22 <sub>IF</sub>	11/14/15	175	6.2	316	28	2.1	28.2	88.5	21.1
PW60 <sub>IF</sub>	11/14/15	480	7.2	330	88	6.7	28.3	283.7	8.8
PW18 <sub>IF</sub>	11/14/15	581	6.3	301	25	1.9	28.2	222.7	51.9
PW17 <sub>IF</sub>	11/14/15	298	6.5	240	42	3.2	28.3	119.0	14.1
PW42 <sub>IF</sub>	11/14/15	361	6.5	190	19	1.4	29.4	167.8	22.0











**Appendix C-C<sub>IF</sub>5: Stable water isotope and hydrochemical data of weekly sampled precipitation (LOD/Q = limit of detection/quantification) (IF).**

Sampling point	Sampling date	Sampling time	$\delta^{18}\text{O}$ [‰]	$\delta^2\text{H}$ [‰]	Cl <sup>-</sup> [mg/L]	SO <sub>4</sub> <sup>2-</sup> [mg/L]	NO <sub>3</sub> <sup>-</sup> [mg/L]	Na <sup>+</sup> [mg/L]	K <sup>+</sup> [mg/L]	Mg <sup>2+</sup> [mg/L]	Ca <sup>2+</sup> [mg/L]	SiO <sub>2</sub> [mg/L]
WS <sub>IF</sub>	05/23/14	10 am	0.08	17.1	-	-	-	-	-	-	-	-
	05/30/14	10 am	1.16	20.6	-	-	-	-	-	-	-	-
	06/17/14	5 pm	-0.52	9.4	-	-	-	-	-	-	-	-
	06/24/14	5 pm	0.77	16.7	-	-	-	-	-	-	-	-
	08/05/14	5 pm	0.13	9.9	-	-	-	-	-	-	-	-
	09/09/14	5 pm	0.69	14.8	-	-	-	-	-	-	-	-
	09/23/14	6 pm	-3.19	-14.2	-	-	-	-	-	-	-	-
	10/21/14	6 pm	-0.58	5.3	-	-	-	-	-	-	-	-
	10/28/14	6 pm	-0.41	6.8	-	-	-	-	-	-	-	-
	11/04/14	6 pm	-0.72	0.1	-	-	-	-	-	-	-	-
	12/23/14	5 pm	0.48	21.5	-	-	-	-	-	-	-	-
	12/30/14	6 pm	0.59	21.9	-	-	-	-	-	-	-	-
	01/06/15	6 pm	-1.56	0.8	1.0	0.9	< LOD	-	-	-	-	0.3
	01/13/15	6 pm	-0.94	7.6	2.3	-	1.6	-	-	-	-	0.5
	01/20/15	6 pm	0.47	21.6	0.7	3.7	1.4	-	-	-	-	0.5
	01/27/15	6 pm	0.50	22.2	0.7	2.4	1.3	-	-	-	-	0.4
	02/03/15	6 pm	0.81	21.4	0.9	1.5	1.3	-	-	-	-	0.5
	02/10/15	6 pm	0.47	22.5	1.1	1.7	1.7	-	-	-	-	0.5
	02/24/15	6 pm	-1.82	-2.8	0.6	0.7	0.5	-	-	-	-	< LOQ
	03/10/15	6 pm	-1.80	-2.2	0.8	3.1	0.7	-	-	-	-	< LOQ
	03/17/15	6 pm	-4.93	-26.5	-	-	-	-	-	-	-	< LOQ
	03/31/15	6 pm	-4.81	-25.7	-	-	-	-	-	-	-	< LOQ
	04/07/15	6 pm	-4.81	-26.3	0.5	0.6	-	-	-	-	-	< LOQ
	04/21/15	6 pm	-4.13	-19.4	< LOQ	1.2	-	-	-	-	-	< LOQ
	04/28/15	6 pm	-2.54	-5.1	0.5	< LOQ	< LOD	-	-	-	-	< LOD
	05/12/15	6 pm	-3.84	-15.2	< LOQ	< LOQ	< LOD	-	-	-	-	< LOQ
	05/26/15	6 pm	-3.96	-16.9	< LOQ	< LOQ	< LOD	-	-	-	-	< LOQ
	06/28/15	6 pm	-3.05	-17.3	-	-	-	-	-	-	-	-
	07/04/15	6 pm	-3.04	-17.5	< LOQ	< LOQ	0.6	0.6	0.3	< LOQ	0.4	1.9
	07/23/15	6 pm	-2.97	-17.6	-	-	-	-	-	-	-	2.0
	09/22/15	6 pm	-3.29	-17.9	-	-	-	-	-	-	-	1.2
	11/03/15	6 pm	-4.03	-18.5	1.3	1.3	0.7	1.6	0.6	0.1	0.6	< LOQ
	11/10/15	6 pm	-4.00	-18.4	1.4	1.4	0.9	1.5	0.6	0.2	0.6	< LOQ

**Appendix C-C<sub>NA</sub>1: In-situ parameters and HCO<sub>3</sub><sup>-</sup> and CO<sub>2</sub> concentrations of the four snapshot samplings (NA).**

Sampling point	Sampling date	EC [μS/cm]	pH [-]	Eh [mV]	O <sub>2</sub> <sup>sat</sup> [%]	O <sub>2</sub> <sup>con</sup> [mg/L]	T <sub>w</sub> [°C]	HCO <sub>3</sub> <sup>-</sup> [mg/L]	CO <sub>2</sub> [mg/L]
ST1 <sub>NA</sub>	11/13/14	162	7.2	200	70	5.4	22.1	88.5	11.4
ST3 <sub>NA</sub>	11/13/14	155	7.5	420	89	6.6	23.9	81.2	3.5
ST5 <sub>NA</sub>	11/13/14	154	7.5	438	89	6.4	25.4	81.2	3.5
ST7 <sub>NA</sub>	11/13/14	150	7.7	352	81	5.6	27.3	79.3	4.4
SP1 <sub>NA</sub>	11/17/14	89	5.9	537	25	1.9	24.1	29.0	68.2
OW06 <sub>NA</sub>	11/17/14	197	6.4	383	30	2.3	21.8	103.1	37.0
PW07 <sub>NA</sub>	11/17/14	121	6.0	443	78	5.3	28.2	42.7	30.8
PW09 <sub>NA</sub>	11/17/14	111	5.9	399	55	4.1	23.7	39.1	-
PW10 <sub>NA</sub>	11/19/14	107	5.6	395	66	4.8	24	26.2	37.0
FL1 <sub>NA</sub>	11/19/14	118	7.1	345	105	7.5	25.8	61.0	3.5
PW08 <sub>NA</sub>	11/20/14	426	7.7	379	96	7.1	24.1	238.0	4.4
PZ40L <sub>NA</sub>	04/24/15	50.2	4.7	398	12	0.9	24.1	18.3	45.8
PZ40S <sub>NA</sub>	04/24/15	72	5.4	286	20	1.4	24.8	21.4	30.8
PZ42S <sub>NA</sub>	04/24/15	99	5.4	107	16	1.2	25.1	38.1	25.5
PZ46L <sub>NA</sub>	04/24/15	161	6.0	244	17	1.2	24.6	64.1	24.6
PZ46S <sub>NA</sub>	04/24/15	129	5.8	330	22	1.6	25	50.3	23.8
PZ40S <sub>NA</sub>	04/24/15	185	6.0	315	19	1.4	24.2	25.9	29.9
PZ50L <sub>NA</sub>	04/24/15	75	5.2	310	36	2.6	24.6	71.7	31.7
ST4 <sub>NA</sub>	04/24/15	212	6.9	269	91	12.3	26	38.1	4.4
PW07 <sub>NA</sub>	04/25/15	119	5.8	440	62	4.2	28	38.1	38.7
PW08 <sub>NA</sub>	04/25/15	150	6.3	442	65	4.7	24.5	51.9	23.8
SP1 <sub>NA</sub>	04/25/15	95	5.7	432	62	4.4	26.1	19.8	30.8
PW36 <sub>NA</sub>	04/25/15	253	6.6	262	26	1.8	26.9	114.4	26.4
ST1 <sub>NA</sub>	04/28/15	190	7.0	325	74	5.7	23.3	45.8	8.8
ST3 <sub>NA</sub>	04/28/15	178	7.0	290	92	6.5	25.9	42.7	6.2
ST5 <sub>NA</sub>	04/28/15	177	7.0	317	93	6.3	27.8	41.2	7.0
PW39 <sub>NA</sub>	05/06/15	183	6.3	464	63	4.7	23.4	76.3	36.1
PW41 <sub>NA</sub>	05/06/15	276	6.4	259	47	3.4	24.3	135.8	48.4



**Appendix C-C<sub>NA</sub>1: *In-situ* parameters and HCO<sub>3</sub><sup>-</sup> and CO<sub>2</sub> concentrations of the four snapshot samplings (NA).  
(Continued)**

Sampling point	Sampling date	EC [μS/cm]	pH [-]	Eh [mV]	O <sub>2</sub> <sup>sat</sup> [%]	O <sub>2</sub> <sup>con</sup> [mg/L]	T <sub>w</sub> [°C]	HCO <sub>3</sub> <sup>-</sup> [mg/L]	CO <sub>2</sub> [mg/L]
PW42 <sub>NA</sub>	05/06/15	168	5.8	340	59	4.3	23.4	48.8	57.2
PW43 <sub>NA</sub>	05/06/15	294	6.3	275	52	3.7	24.3	134.3	56.3
PW44 <sub>NA</sub>	05/06/15	76	5.2	365	59	4.2	24.5	12.2	45.8
PW37 <sub>NA</sub>	05/18/15	171.8	6.1	424	51	3.8	23.2	68.7	45.8
PW38 <sub>NA</sub>	05/18/15	180.4	6.4	192	53	3.8	25	80.9	43.1
PW40 <sub>NA</sub>	05/18/15	451	5.8	341	66	4.9	24.4	38.1	39.6
PW45 <sub>NA</sub>	05/18/15	116.7	5.8	324	69	5.1	24.6	27.5	40.5
PZ07 <sub>NA</sub>	05/25/15	317	6.4	86	12	0.9	25.3	158.7	44.0
PZ10 <sub>NA</sub>	05/25/15	179.4	6.3	115	82	5.8	25.3	76.3	29.0
ST2 <sub>NA</sub>	05/25/15	195.5	7.3	367	85	6.6	22.8	44.2	13.2
PZ25 <sub>NA</sub>	06/03/15	443	6.6	108	8	0.6	24	198.3	84.5
PZ26 <sub>NA</sub>	06/03/15	377	6.2	116	9	0.7	23.9	164.8	102.1
PZ27 <sub>NA</sub>	06/03/15	228	6.0	251	27	1.9	24.2	79.3	55.5
ST6 <sub>NA</sub>	06/03/15	173.7	6.9	418	87	6.6	23.2	56.4	13.2
PZ40L <sub>NA</sub>	10/27/15	82	5.0	400	20	1.4	26.8	12.2	68.7
PZ40S <sub>NA</sub>	10/27/15	74	5.4	291	31	2.2	25.4	21.4	17.6
PZ42L <sub>NA</sub>	10/27/15	64	5.2	355	17	1.2	23.6	18.3	16.3
PZ42S <sub>NA</sub>	10/27/15	89	5.4	111	32	2.2	23.7	36.6	14.1
PZ46L <sub>NA</sub>	10/27/15	168	6.1	171	14	1.0	23.3	73.2	23.8
PZ46S <sub>NA</sub>	10/27/15	128	6.0	340	19	1.4	23.4	45.8	18.5
ST4 <sub>NA</sub>	10/28/15	127	6.5	377	68	5.2	22.2	39.7	6.6
PZ48L <sub>NA</sub>	10/28/15	185	6.2	384	19	1.4	24.2	51.9	14.1
PZ49L <sub>NA</sub>	10/28/15	107	5.8	294	27	2.0	24.7	36.6	14.1
PZ50L <sub>NA</sub>	10/28/15	70	5.1	415	29	2.1	24.9	9.2	20.2
PW36 <sub>NA</sub>	10/30/15	299	6.7	411	81	6.1	23.7	149.5	10.6
PW48 <sub>NA</sub>	10/30/15	58	5.1	528	47	3.5	24.4	12.2	22.9
PZ25 <sub>NA</sub>	10/30/15	449	6.4	146	13	0.9	23.4	213.6	31.4
PZ26 <sub>NA</sub>	10/30/15	320	6.0	151	7	0.5	23.1	131.2	31.7
PZ27 <sub>NA</sub>	11/02/15	193	5.8	213	22	1.7	24.3	61.0	21.1
ST6 <sub>NA</sub>	11/02/15	134	6.8	345	74	5.2	26.9	45.8	6.2
PZ08 <sub>NA</sub>	11/03/15	344	6.5	132	41	2.8	28.2	183.1	11.7
PZ07 <sub>NA</sub>	11/03/15	345	6.4	148	8	0.5	26	198.3	13.2
PZ06 <sub>NA</sub>	11/03/15	237	6.2	168	9	0.7	25.2	158.7	30.8
PW39 <sub>NA</sub>	11/05/15	184	6.0	363	54	3.9	24.9	82.4	22.9
PW07 <sub>NA</sub>	11/05/15	122	5.8	378	57	3.9	27.8	44.2	24.6
PW37 <sub>NA</sub>	11/05/15	132	5.7	378	42	3.1	29.2	41.2	28.2
ST8 <sub>NA</sub>	11/05/15	86	6.8	348	21	1.6	21.4	27.5	7.0
PW38 <sub>NA</sub>	11/05/15	138	5.8	324	43	3.2	24.3	38.1	28.2
S13C50 <sub>NA</sub>	11/06/15	381	6.5	210	-	-	-	97.6	-
S93C30 <sub>NA</sub>	11/06/15	407	6.4	210	-	-	-	183.1	-
S13M50 <sub>NA</sub>	11/06/15	390	6.5	210	-	-	-	186.1	-
PZ40L <sub>NA</sub>	06/16/16	51	4.8	385	35	2.6	23	15.3	60.7
PZ40S <sub>NA</sub>	06/16/16	62	5.3	262	46	3.4	23.4	15.3	37.0
PZ42L <sub>NA</sub>	06/16/16	63	5.3	275	44	3.2	24.7	16.8	37.0
PZ42S <sub>NA</sub>	06/16/16	157	5.9	174	14	1.0	24.7	73.2	32.1
PZ46L <sub>NA</sub>	06/16/16	162	6.2	245	46	3.4	24.6	64.1	20.2
PZ46S <sub>NA</sub>	06/16/16	133	5.8	330	16	1.2	24.7	48.8	30.8
ST4 <sub>NA</sub>	06/16/16	135	7.5	358	95	7.2	22.7	51.9	6.2
PZ48L <sub>NA</sub>	06/16/16	201	6.0	258	8	0.6	23.4	76.3	34.8
PZ49L <sub>NA</sub>	06/16/16	105	5.6	242	7	0.5	23.6	27.5	45.8
PZ50L <sub>NA</sub>	06/16/16	70	4.9	278	19	1.4	24.6	11.4	42.2
PW07 <sub>NA</sub>	06/17/16	117	5.7	418	59	4.4	23.9	33.6	39.2
ST1 <sub>NA</sub>	06/21/16	144	7.3	364	70	5.5	21.4	48.8	7.9
ST3 <sub>NA</sub>	06/21/16	139	7.4	356	86	6.6	21.9	45.8	6.2
ST5 <sub>NA</sub>	06/21/16	138	7.2	418	86	6.6	22	44.2	6.2
SP1 <sub>NA</sub>	06/21/16	85	5.2	439	39	2.9	23.9	22.9	53.7
PW36 <sub>NA</sub>	06/21/16	303	7.1	347	88	6.6	23.2	131.2	11.4
ST7 <sub>NA</sub>	06/21/16	135	7.2	346	85	6.5	22.6	42.7	7.5
PZ10 <sub>NA</sub>	06/22/16	144	6.1	171	46	3.4	24	45.3	19.1
PZ08 <sub>NA</sub>	06/22/16	234	6.5	240	18	1.3	23.8	117.0	22.0
PZ07 <sub>NA</sub>	06/22/16	321	6.2	148	21	1.5	25.1	160.2	47.5
PZ06 <sub>NA</sub>	06/22/16	211	6.2	227	11	0.8	25	96.1	41.4
PZ05 <sub>NA</sub>	06/22/16	189	7.0	430	170	12.5	25	68.7	8.8
PZ24 <sub>NA</sub>	06/22/16	456	5.8	144	8	0.6	24.5	172.4	81.0







**Appendix C-C<sub>NA</sub>4: Stable water isotope data of the four snapshot samplings (NA). (Continued)**

Sampling point	Sampling date	$\delta^{18}\text{O}$ [‰]	$\delta^2\text{H}$ [‰]	Sampling point	Sampling date	$\delta^{18}\text{O}$ [‰]	$\delta^2\text{H}$ [‰]	Sampling point	Sampling date	$\delta^{18}\text{O}$ [‰]	$\delta^2\text{H}$ [‰]
PZ10 <sub>NA</sub>	11/03/15	-2.17	-5.1	PZ42S <sub>NA</sub>	06/16/16	-2.24	-6.5	PZ08 <sub>NA</sub>	06/22/16	-2.42	-8.0
PZ08 <sub>NA</sub>	11/03/15	-2.26	-6.9	PZ46L <sub>NA</sub>	06/16/16	-2.08	-6.5	PZ07 <sub>NA</sub>	06/22/16	-1.86	-4.8
PZ07 <sub>NA</sub>	11/03/15	-1.75	-3.5	PZ46S <sub>NA</sub>	06/16/16	-2.06	-6.1	PZ06 <sub>NA</sub>	06/22/16	-1.79	-5.5
PZ06 <sub>NA</sub>	11/03/15	-1.67	-3.5	ST4 <sub>NA</sub>	06/16/16	-1.32	-3.9	PZ05 <sub>NA</sub>	06/22/16	-1.97	-6.4
PZ05 <sub>NA</sub>	11/03/15	-2.22	-5.8	PZ48 <sub>NA</sub>	06/16/16	-2.01	-6.2	PZ24 <sub>NA</sub>	06/22/16	-1.52	-3.4
PW39 <sub>NA</sub>	11/05/15	-2.20	-6.2	PZ49 <sub>NA</sub>	06/16/16	-1.93	-5.1	PZ25 <sub>NA</sub>	06/22/16	-1.59	-2.6
PW07 <sub>NA</sub>	11/05/15	-2.31	-6.8	PZ50 <sub>NA</sub>	06/16/16	-1.94	-4.2	PZ26 <sub>NA</sub>	06/22/16	-1.58	-3.6
PW37 <sub>NA</sub>	11/05/15	-2.51	-7.6	PW07 <sub>NA</sub>	06/17/16	-1.88	-7.8	PW37 <sub>NA</sub>	06/24/16	-2.29	-8.1
ST8 <sub>NA</sub>	11/05/15	-3.15	-11.6	ST1 <sub>NA</sub>	06/21/16	-1.08	-2.6	PW38 <sub>NA</sub>	06/24/16	-2.57	-9.1
PW38 <sub>NA</sub>	11/05/15	-2.52	-7.2	ST3 <sub>NA</sub>	06/21/16	-1.09	-2.7	PW33 <sub>NA</sub>	06/24/16	-2.61	-7.5
ST13C50 <sub>NA</sub>	11/06/15	-1.53	-1.4	ST5 <sub>NA</sub>	06/21/16	-1.64	-2.5	PW39 <sub>NA</sub>	06/28/16	-2.24	-7.0
ST93C30 <sub>NA</sub>	11/06/15	-1.10	0.3	SP1 <sub>NA</sub>	06/21/16	-2.06	-7.6	PW43 <sub>NA</sub>	06/28/16	-2.68	-9.9
ST13M50 <sub>NA</sub>	11/06/15	-1.18	0.6	PW36 <sub>NA</sub>	06/21/16	-2.08	-6.8	PW42 <sub>NA</sub>	06/28/16	-2.88	-9.1
PZ40L <sub>NA</sub>	06/16/16	-2.49	-6.5	ST7 <sub>NA</sub>	06/21/16	-1.48	-2.7	PW44 <sub>NA</sub>	06/28/16	-2.48	-8.4
PZ40S <sub>NA</sub>	06/16/16	-2.20	-7.0	PZ10 <sub>NA</sub>	06/22/16	-2.30	-6.3	PW41 <sub>NA</sub>	06/28/16	-2.46	-8.6
PZ42L <sub>NA</sub>	06/16/16	-2.15	-6.2								

**Appendix C-C<sub>NA</sub>5: Stable water isotope and hydrochemical data of weekly sampled precipitation (LOD/Q = limit of detection/quantification) (NA).**

Sampling point	Sampling date	Sampling time	$\delta^{18}\text{O}$ [‰]	$\delta^2\text{H}$ [‰]	Cl <sup>-</sup> [mg/L]	SO <sub>4</sub> <sup>2-</sup> [mg/L]	NO <sub>3</sub> <sup>-</sup> [mg/L]	Na <sup>+</sup> [mg/L]	K <sup>+</sup> [mg/L]	Mg <sup>2+</sup> [mg/L]	Ca <sup>2+</sup> [mg/L]	SiO <sub>2</sub> [mg/L]
WS <sub>NA</sub>	06/10/14	12 am	-4.77	-24.2	-	-	-	-	-	-	-	-
	06/17/14	11 am	-0.18	7.6	-	-	-	-	-	-	-	-
	06/23/14	10 am	1.43	22.4	-	-	-	-	-	-	-	-
	06/30/14	10 am	3.49	28.6	-	-	-	-	-	-	-	-
	07/14/14	10 am	1.53	25.2	-	-	-	-	-	-	-	-
	07/21/14	11 am	2.13	30.4	-	-	-	-	-	-	-	-
	08/05/14	11 am	0.79	13.4	-	-	-	-	-	-	-	-
	08/11/14	9 am	0.39	9.7	-	-	-	-	-	-	-	-
	08/18/14	9 am	0.59	7.2	-	-	-	-	-	-	-	-
	08/26/14	9 am	0.05	15.3	-	-	-	-	-	-	-	-
	09/02/14	9 am	-0.42	4.4	-	-	-	-	-	-	-	-
	09/09/14	9 am	-4.19	-30.6	-	-	-	-	-	-	-	-
	09/16/14	9 am	3.21	16.8	-	-	-	-	-	-	-	-
	09/22/14	9 am	2.49	19.7	-	-	-	-	-	-	-	-
	09/29/14	9 am	2.80	27.4	-	-	-	-	-	-	-	-
	10/06/14	9 am	4.06	29.0	-	-	-	-	-	-	-	-
	10/13/14	9 am	1.47	10.8	-	-	-	-	-	-	-	-
	10/20/14	9 am	-0.47	4.8	-	-	-	-	-	-	-	-
	10/27/14	9 am	3.01	16.6	-	-	-	-	-	-	-	-
	11/03/14	9 am	2.34	18.5	-	-	-	-	-	-	-	-
	11/10/14	9 am	1.97	17.0	-	-	-	-	-	-	-	-
	11/17/14	9 am	1.36	15.7	1.4	1.1	1.4	-	-	-	-	< LOQ
	11/24/14	9 am	-2.93	-14.9	1.3	0.5	1.0	0.9	0.8	< LOQ	0.5	< LOD
	12/01/14	9 am	-3.25	-12.9	1.0	< LOQ	1.2	0.6	0.4	< LOQ	< LOQ	< LOQ
	12/08/14	9 am	-2.24	-0.4	< LOQ	< LOQ	< LOQ	0.4	0.6	< LOQ	< LOQ	< LOD
	12/15/14	9 am	0.66	15.2	1.6	1.1	2.8	-	-	-	-	0.3
	01/05/15	9 am	0.98	23.9	1	1.3	2.8	0.3	0.8	0.2	1.1	0.2
	02/20/15	9 am	1.34	21.4	-	-	-	-	-	-	-	< LOD
	03/11/15	9 am	-7.67	-50.1	< LOQ	< LOQ	< LOQ	0.2	0.3	< LOQ	< LOQ	< LOQ
	03/23/15	9 am	-3.30	-12.9	0.6	0.8	0.9	0.3	0.5	< LOQ	0.9	< LOQ
	03/30/15	9 am	-4.24	-17.4	< LOD	0.7	1.3	< LOQ	0.1	< LOQ	< LOQ	0.2
	04/06/15	9 am	-5.35	-25.3	< LOQ	< LOQ	< LOQ	0.2	0.1	< LOQ	< LOQ	< LOQ
	04/13/15	9 am	-4.11	-16.5	0.5	0.8	1.9	0.3	0.5	0.1	< LOQ	< LOQ
	04/20/15	9 am	-3.01	-7.8	< LOD	< LOD	1.9	< LOQ	< LOQ	< LOQ	< LOQ	< LOQ
	04/27/15	9 am	-3.51	-14.0	< LOQ	< LOQ	1.3	0.2	0.3	< LOQ	< LOQ	< LOQ
	05/04/15	9 am	-4.75	-22.5	< LOD	< LOQ	0.8	0.1	0.2	< LOQ	< LOQ	< LOQ
	05/18/15	9 am	-4.20	-21.6	0.9	1.5	3.6	0.3	0.9	0.1	0.6	0.3
	05/25/15	9 am	0.32	13.6	0.7	1.0	3.5	0.4	0.7	0.2	1.5	0.3
	06/15/15	9 am	-1.05	10.6	0.6	0.9	< LOD	0.3	0.4	0.1	1.0	< LOQ
	06/22/15	9 am	-1.68	2.9	< LOQ	1.0	< LOD	0.4	0.3	0.1	1.3	< LOQ
	06/29/15	9 am	-0.32	18.0	< LOQ	0.8	< LOD	0.3	0.2	< LOQ	0.6	< LOQ
	07/06/15	9 am	2.22	29.1	2.0	2.6	10.3	1.0	2.9	0.3	2.2	0.7



















**Appendix D-D<sub>IF</sub>1: Geographic coordinates (WGS84) of all sampling points in the Ifakara study site (IF). (Continued)**

Sampling point	Type of sampling point	Geographic coordinate N	Geographic coordinate E	Sampling point	Type of sampling point	Geographic coordinate N	Geographic coordinate E
PW11 <sub>IF</sub>	Pumping well	-8.06448	36.66012	PW47 <sub>IF</sub>	Pumping well	-8.12869	36.69209
PW12 <sub>IF</sub>	Pumping well	-8.02659	36.83292	PW48 <sub>IF</sub>	Pumping well	-8.12345	36.68011
PW13 <sub>IF</sub>	Pumping well	-8.05358	36.80846	PW49 <sub>IF</sub>	Pumping well	-8.08613	36.60248
PW14 <sub>IF</sub>	Pumping well	-8.08712	36.74842	PW52 <sub>IF</sub>	Pumping well	-8.08973	36.71878
PW15 <sub>IF</sub>	Pumping well	-8.09196	36.72804	PW60 <sub>IF</sub>	Pumping well	-8.14256	36.67528
PW17 <sub>IF</sub>	Pumping well	-8.16127	36.69135	PW61 <sub>IF</sub>	Pumping well	-8.15338	36.69514
PW18 <sub>IF</sub>	Pumping well	-8.14672	36.68145	PZ01 <sub>IF</sub>	Piezometer	-8.17124	36.69662
PW19 <sub>IF</sub>	Pumping well	-8.13279	36.68368	PZ02 <sub>IF</sub>	Piezometer	-8.17390	36.69038
PW20 <sub>IF</sub>	Pumping well	-8.06919	36.79572	PZ03 <sub>IF</sub>	Piezometer	-8.18526	36.67943
PW21 <sub>IF</sub>	Pumping well	-8.11367	36.68457	PZ04 <sub>IF</sub>	Piezometer	-8.17146	36.69054
PW22 <sub>IF</sub>	Pumping well	-8.09489	36.68740	PZ05 <sub>IF</sub>	Piezometer	-8.18060	36.69188
PW23 <sub>IF</sub>	Pumping well	-8.11551	36.66005	PZ06 <sub>IF</sub>	Piezometer	-8.15596	36.70082
PW24 <sub>IF</sub>	Pumping well	-8.13548	36.65791	PZ07 <sub>IF</sub>	Piezometer	-8.15553	36.70331
PW25 <sub>IF</sub>	Pumping well	-8.05447	36.68437	PZ08 <sub>IF</sub>	Piezometer	-8.14473	36.70413
PW26 <sub>IF</sub>	Pumping well	-8.08785	36.70372	PZ09 <sub>IF</sub>	Piezometer	-8.12872	36.71230
PW28 <sub>IF</sub>	Pumping well	-8.12053	36.63669	PZ10 <sub>IF</sub>	Piezometer	-8.12707	36.71110
PW29 <sub>IF</sub>	Pumping well	-8.10112	36.61039	PZ11 <sub>IF</sub>	Piezometer	-8.11743	36.70597
PW30 <sub>IF</sub>	Pumping well	-8.09606	36.60416	PZ12 <sub>IF</sub>	Piezometer	-8.10180	36.71276
PW31 <sub>IF</sub>	Pumping well	-8.08818	36.55298	PZ13 <sub>IF</sub>	Piezometer	-8.10615	36.72209
PW32 <sub>IF</sub>	Pumping well	-8.09607	36.52996	PZ14 <sub>IF</sub>	Piezometer	-8.13802	36.72196
PW34 <sub>IF</sub>	Pumping well	-8.05110	36.56526	ST1 <sub>IF</sub>	Stream	-8.18911	36.69309
PW35 <sub>IF</sub>	Pumping well	-8.08989	36.57732	ST2 <sub>IF</sub>	Stream	-8.09373	36.67782
PW38 <sub>IF</sub>	Pumping well	-8.07734	36.65915	ST3 <sub>IF</sub>	Stream	-8.03021	36.64936
PW39 <sub>IF</sub>	Pumping well	-8.10521	36.65799	ST4 <sub>IF</sub>	Stream	-8.03945	36.72876
PW40 <sub>IF</sub>	Pumping well	-8.12099	36.65325	ST5 <sub>IF</sub>	Stream	-8.04780	36.56300
PW41 <sub>IF</sub>	Pumping well	-8.14269	36.63958	W061 <sub>IF</sub>	Pumping well	-8.14007	36.70158
PW42 <sub>IF</sub>	Pumping well	-8.14639	36.66646	W068 <sub>IF</sub>	Pumping well	-8.12888	36.67937
PW43 <sub>IF</sub>	Pumping well	-8.10814	36.70332	W070 <sub>IF</sub>	Pumping well	-8.12827	36.69178
PW44 <sub>IF</sub>	Pumping well	-8.11515	36.69346	W135 <sub>IF</sub>	Pumping well	-8.13768	36.66592
PW45 <sub>IF</sub>	Pumping well	-8.13847	36.69417	W172 <sub>IF</sub>	Pumping well	-8.11650	36.66353
PW46 <sub>IF</sub>	Pumping well	-8.12874	36.70623	W227 <sub>IF</sub>	Pumping well	-8.07885	36.67910
PW46.1 <sub>IF</sub>	Pumping well	-8.12874	36.70623	WS <sub>IF</sub>	Weather station	-8.10827	36.66549

**Appendix D-D<sub>NA</sub>1: Geographic coordinates (WGS84) of all sampling points in the Namulonge study site (NA).**

Sampling point	Type of sampling point	Geographic coordinate N	Geographic coordinate E	Sampling point	Type of sampling point	Geographic coordinate N	Geographic coordinate E
DLM01 <sub>NA</sub>	Pumping well	0.51977	32.62796	PW41 <sub>NA</sub>	Pumping well	0.55445	32.61030
DLM02 <sub>NA</sub>	Pumping well	0.50672	32.60524	PW42 <sub>NA</sub>	Pumping well	0.54402	32.57177
DLM03 <sub>NA</sub>	Pumping well	0.51291	32.62001	PW43 <sub>NA</sub>	Pumping well	0.52836	32.58135
DLM04 <sub>NA</sub>	Pumping well	0.50814	32.64756	PW44 <sub>NA</sub>	Pumping well	0.57308	32.58903
DLM05 <sub>NA</sub>	Pumping well	0.51520	32.65564	PZ03 <sub>NA</sub>	Piezometer	0.53444	32.62050
DLM06 <sub>NA</sub>	Pumping well	0.51941	32.60612	PZ05 <sub>NA</sub>	Piezometer	0.53422	32.62033
DLM07 <sub>NA</sub>	Pumping well	0.51308	32.62011	PZ06 <sub>NA</sub>	Piezometer	0.53399	32.62020
DLM08 <sub>NA</sub>	Pumping well	0.52440	32.61202	PZ07 <sub>NA</sub>	Piezometer	0.53389	32.62015
DLM09 <sub>NA</sub>	Pumping well	0.53024	32.62421	PZ08 <sub>NA</sub>	Piezometer	0.53344	32.61984
DLM10 <sub>NA</sub>	Pumping well	0.53117	32.62426	PZ10 <sub>NA</sub>	Piezometer	0.53309	32.61948
DLM11 <sub>NA</sub>	Pumping well	0.52367	32.61854	PZ40 <sub>NA</sub>	Piezometer	0.51992	32.64176
DLM12 <sub>NA</sub>	Pumping well	0.50713	32.60556	PZ42 <sub>NA</sub>	Piezometer	0.52036	32.64207
DLM13 <sub>NA</sub>	Pumping well	0.55875	32.63153	PZ46 <sub>NA</sub>	Piezometer	0.52106	32.64272
DLM14 <sub>NA</sub>	Pumping well	0.54450	32.59543	PZ48 <sub>NA</sub>	Piezometer	0.52141	32.64298
FL1 <sub>NA</sub>	Flooding water	0.52121	32.64286	PZ49 <sub>NA</sub>	Piezometer	0.52153	32.64314
FL2 <sub>NA</sub>	Flooding water	0.51617	32.64879	PZ50 <sub>NA</sub>	Piezometer	0.52166	32.64324
PW06 <sub>NA</sub>	Pumping well	0.5278	32.62680	PZ24 <sub>NA</sub>	Piezometer	0.51565	32.64852
PW07 <sub>NA</sub>	Pumping well	0.52761	32.62460	PZ25 <sub>NA</sub>	Piezometer	0.51589	32.64870
PW08 <sub>NA</sub>	Pumping well	0.53108	32.62002	PZ26 <sub>NA</sub>	Piezometer	0.51614	32.64883
PW09 <sub>NA</sub>	Pumping well	0.52948	32.63016	PZ27 <sub>NA</sub>	Piezometer	0.51634	32.64894
PW10 <sub>NA</sub>	Pumping well	0.52871	32.64453	PZ28 <sub>NA</sub>	Piezometer	0.51671	32.64913
PW36 <sub>NA</sub>	Pumping well	0.51918	32.64114	PZ29 <sub>NA</sub>	Piezometer	0.51715	32.64941
PW37 <sub>NA</sub>	Pumping well	0.50804	32.64746	SA <sub>NA</sub>	Additional drilling log	0.57371	32.58169
PW38 <sub>NA</sub>	Pumping well	0.51516	32.65554	SD01 <sub>NA</sub>	Additional drilling log	0.53562	32.62072
PW39 <sub>NA</sub>	Pumping well	0.51965	32.60581	SD02 <sub>NA</sub>	Additional drilling log	0.53541	32.62066
PW40 <sub>NA</sub>	Pumping well	0.54750	32.62590	SD03 <sub>NA</sub>	Additional drilling log	0.53521	32.62054

**Appendix D-D<sub>NA</sub>1: Geographic coordinates (WGS84) of all sampling points in the Namulonge study site (NA).  
(Continued)**

Sampling point	Type of sampling point	Geographic coordinate N	Geographic coordinate E	Sampling point	Type of sampling point	Geographic coordinate N	Geographic coordinate E
SD04 <sub>NA</sub>	Additional drilling log	0.53256	32.61935	SD20 <sub>NA</sub>	Additional drilling log	0.51731	32.64953
SD05 <sub>NA</sub>	Additional drilling log	0.53246	32.61927	SD21 <sub>NA</sub>	Additional drilling log	0.51503	32.64779
SD06 <sub>NA</sub>	Additional drilling log	0.53187	32.61914	SD22 <sub>NA</sub>	Additional drilling log	0.51445	32.64689
SD07 <sub>NA</sub>	Additional drilling log	0.52198	32.64351	SD23 <sub>NA</sub>	Additional drilling log	0.51271	32.64594
SD08 <sub>NA</sub>	Additional drilling log	0.52189	32.64346	SP1 <sub>NA</sub>	Spring	0.51914	32.64196
SD09 <sub>NA</sub>	Additional drilling log	0.52183	32.64335	SP2 <sub>NA</sub>	Spring	0.52000	32.64080
SD10 <sub>NA</sub>	Additional drilling log	0.52177	32.64332	ST1 <sub>NA</sub>	Stream	0.53449	32.61927
SD11 <sub>NA</sub>	Additional drilling log	0.52172	32.64328	ST2 <sub>NA</sub>	Stream	0.53393	32.62017
SD12 <sub>NA</sub>	Additional drilling log	0.52162	32.64331	ST3 <sub>NA</sub>	Stream	0.52196	32.64249
SD13 <sub>NA</sub>	Additional drilling log	0.52099	32.64281	ST4 <sub>NA</sub>	Stream	0.52140	32.64289
SD14 <sub>NA</sub>	Additional drilling log	0.52026	32.64225	ST5 <sub>NA</sub>	Stream	0.52032	32.64448
SD15 <sub>NA</sub>	Additional drilling log	0.51986	32.64186	ST6 <sub>NA</sub>	Stream	0.51623	32.64889
SD16 <sub>NA</sub>	Additional drilling log	0.51978	32.64143	ST7 <sub>NA</sub>	Stream	0.51583	32.64918
SD17 <sub>NA</sub>	Additional drilling log	0.51972	32.64130	ST8 <sub>NA</sub>	Stream	0.51284	32.65410
SD18 <sub>NA</sub>	Additional drilling log	0.51765	32.64975	WS <sub>NA</sub>	Weather station	0.52221	32.62439
SD19 <sub>NA</sub>	Additional drilling log	0.51753	32.64966				